frontiers | Research Topics

Genetic targets for cancer immunotherapy

Edited by
Alip Ghosh, Soma Banerjee, Jaideep Banerjee and Ayan Biswas

Published in
Frontiers in Genetics



FRONTIERS EBOOK COPYRIGHT STATEMENT

The copyright in the text of individual articles in this ebook is the property of their respective authors or their respective institutions or funders. The copyright in graphics and images within each article may be subject to copyright of other parties. In both cases this is subject to a license granted to Frontiers.

The compilation of articles constituting this ebook is the property of Frontiers.

Each article within this ebook, and the ebook itself, are published under the most recent version of the Creative Commons CC-BY licence. The version current at the date of publication of this ebook is CC-BY 4.0. If the CC-BY licence is updated, the licence granted by Frontiers is automatically updated to the new version.

When exercising any right under the CC-BY licence, Frontiers must be attributed as the original publisher of the article or ebook, as applicable.

Authors have the responsibility of ensuring that any graphics or other materials which are the property of others may be included in the CC-BY licence, but this should be checked before relying on the CC-BY licence to reproduce those materials. Any copyright notices relating to those materials must be complied with.

Copyright and source acknowledgement notices may not be removed and must be displayed in any copy, derivative work or partial copy which includes the elements in question.

All copyright, and all rights therein, are protected by national and international copyright laws. The above represents a summary only. For further information please read Frontiers' Conditions for Website Use and Copyright Statement, and the applicable CC-BY licence.

ISSN 1664-8714
ISBN 978-2-8325-2997-3
DOI 10.3389/978-2-8325-2997-3

About Frontiers

Frontiers is more than just an open access publisher of scholarly articles: it is a pioneering approach to the world of academia, radically improving the way scholarly research is managed. The grand vision of Frontiers is a world where all people have an equal opportunity to seek, share and generate knowledge. Frontiers provides immediate and permanent online open access to all its publications, but this alone is not enough to realize our grand goals.

Frontiers journal series

The Frontiers journal series is a multi-tier and interdisciplinary set of open-access, online journals, promising a paradigm shift from the current review, selection and dissemination processes in academic publishing. All Frontiers journals are driven by researchers for researchers; therefore, they constitute a service to the scholarly community. At the same time, the *Frontiers journal series* operates on a revolutionary invention, the tiered publishing system, initially addressing specific communities of scholars, and gradually climbing up to broader public understanding, thus serving the interests of the lay society, too.

Dedication to quality

Each Frontiers article is a landmark of the highest quality, thanks to genuinely collaborative interactions between authors and review editors, who include some of the world's best academicians. Research must be certified by peers before entering a stream of knowledge that may eventually reach the public - and shape society; therefore, Frontiers only applies the most rigorous and unbiased reviews. Frontiers revolutionizes research publishing by freely delivering the most outstanding research, evaluated with no bias from both the academic and social point of view. By applying the most advanced information technologies, Frontiers is catapulting scholarly publishing into a new generation.

What are Frontiers Research Topics?

Frontiers Research Topics are very popular trademarks of the *Frontiers journals series*: they are collections of at least ten articles, all centered on a particular subject. With their unique mix of varied contributions from Original Research to Review Articles, Frontiers Research Topics unify the most influential researchers, the latest key findings and historical advances in a hot research area.

Find out more on how to host your own Frontiers Research Topic or contribute to one as an author by contacting the Frontiers editorial office: frontiersin.org/about/contact

Genetic targets for cancer immunotherapy

Topic editors

Alip Ghosh — University of Maryland, United States

Soma Banerjee — Institute of Post Graduate Medical Education And Research (IPGMER), India

Jaideep Banerjee — Smith & Nephew, United Kingdom

Ayan Biswas — University of Alabama at Birmingham, United States

Citation

Ghosh, A., Banerjee, S., Banerjee, J., Biswas, A., eds. (2023). *Genetic targets for cancer immunotherapy*. Lausanne: Frontiers Media SA. doi: 10.3389/978-2-8325-2997-3

Table of contents

05 Roles of HMGBs in Prognosis and Immunotherapy: A Pan-Cancer Analysis
Tong Lin, Yingzhao Zhang, Zhimei Lin and Lisheng Peng

21 Identification of the Crucial Role of CCL22 in *F. nucleatum*-Related Colorectal Tumorigenesis that Correlates With Tumor Microenvironment and Immune Checkpoint Therapy
Hufei Wang, Kangjia Luo, Zilong Guan, Zhi Li, Jun Xiang, Suwen Ou, Yangbao Tao, Songlin Ran, Jinhua Ye, Tianyi Ma, Tianyu Qiao, Zhiming Zhang, Yinghu Jin, Yanni Song and Rui Huang

34 Identification of Novel Prognostic Biomarkers Relevant to Immune Infiltration in Lung Adenocarcinoma
Zhi Xia, Xueyao Rong, Ziyu Dai and Dongbo Zhou

47 High Expression of DC-STAMP Gene Predicts Adverse Outcomes in AML
Qian Liang, Lele Zhang, Wenjun Wang, Jingyu Zhao, Qiaoli Li, Hong Pan, Zhen Gao, Liwei Fang and Jun Shi

60 Association of a Novel DOCK2 Mutation-Related Gene Signature With Immune in Hepatocellular Carcinoma
Yushen Huang, Wen Luo, Siyun Chen, Hongmei Su, Wuchang Zhu, Yuanyuan Wei, Yue Qiu, Yan Long, Yanxia Shi and Jinbin Wei

78 MCM10 is a Prognostic Biomarker and Correlated With Immune Checkpoints in Ovarian Cancer
Zhenzhen Wu, Yueyuan Wang, Juan Li, Huiling Wang, Xunyuan Tuo and Jing Zheng

90 INSC Is Down-Regulated in Colon Cancer and Correlated to Immune Infiltration
Tao Yu, Dan Li, Zhi Zeng, Xu Xu, Haiming Zhang, Jie Wu, Wei Song and Hua Zhu

102 KIFC3 Promotes Proliferation, Migration, and Invasion in Colorectal Cancer *via* PI3K/AKT/mTOR Signaling Pathway
Huiling Liao, Lan Zhang, Shimin Lu, Wei Li and Weiguo Dong

124 Association Between *GSDMB* Gene Polymorphism and Cervical Cancer in the Northeast Chinese Han Population
Songxue Li, Xiaoying Li, Shuang Zhang, Yanan Feng, Tianshuang Jia, Manning Zhu, Lei Fang, Liping Gong, Shuang Dong, Xianchao Kong, Zhenzhen Wang and Litao Sun

136 Identification and Validation of a Three Pyroptosis-Related lncRNA Signature for Prognosis Prediction in Lung Adenocarcinoma
Jichang Liu, Qiang Liu, Hongchang Shen, Yong Liu, Yadong Wang, Guanghui Wang and Jiajun Du

151 Identification and Validation of an m6A Modification of JAK-STAT Signaling Pathway–Related Prognostic Prediction Model in Gastric Cancer
Fei Jiang, Xiaowei Chen, Yan Shen and Xiaobing Shen

163 Effects of the PLK4 inhibitor Centrinone on the biological behaviors of acute myeloid leukemia cell lines
Xing-Ru Mu, Meng-Meng Ma, Zi-Yi Lu, Jun Liu, Yu-Tong Xue, Jiang Cao, Ling-Yu Zeng, Feng Li, Kai-Lin Xu and Qing-Yun Wu

175 Improving PARP inhibitor efficacy in high-grade serous ovarian carcinoma: A focus on the immune system
Nirashaa T. Bound, Cassandra J. Vandenberg, Apriliana E. R. Kartikasari, Magdalena Plebanski and Clare L. Scott

196 Development and validation of a combined glycolysis and immune prognostic signature for lung squamous cell carcinoma
Qiang Huang, Shan Yang, Hao Yan, Hong Chen, Yuzhu Wang and Yang Wang

frontiers in Genetics

ORIGINAL RESEARCH
published: 29 October 2021
doi: 10.3389/fgene.2021.764245

Roles of HMGBs in Prognosis and Immunotherapy: A Pan-Cancer Analysis

Tong Lin[1], *Yingzhao Zhang*[1], *Zhimei Lin*[1] *and Lisheng Peng*[2]*

[1]The Fourth Clinical Medical School, Guangzhou University of Chinese Medicine, Shenzhen, China, [2]Department of Science and Education, Shenzhen Traditional Chinese Medicine Hospital, Shenzhen, China

Background: High mobility group box (HMGB) proteins are DNA chaperones involved in transcription, DNA repair, and genome stability. Extracellular HMGBs also act as cytokines to promote inflammatory and immune responses. Accumulating evidence has suggested that HMGBs are implicated in cancer pathogenesis; however, their prognostic and immunological values in pan-cancer are not completely clear.

Methods: Multiple tools were applied to analyze the expression, genetic alternations, and prognostic and clinicopathological relevance of HMGB in pan-cancer. Correlations between HMGB expression and tumor immune-infiltrating cells (TIICs), immune checkpoint (ICP) expression, microsatellite instability (MSI), and tumor mutational burden (TMB) in pan-cancer were investigated to uncover their interactions with the tumor immune microenvironment (TIME). Gene set enrichment analysis (GSEA) was conducted for correlated genes of HMGBs to expound potential mechanisms.

Results: HMGB expression was significantly elevated in various cancers. Both prognostic and clinicopathological significance was observed for *HMGB1* in ACC; *HMGB2* in ACC, LGG, LIHC, and SKCM; and *HMGB3* in ESCA. Prognostic values were also found for *HMGB2* in KIRP and MESO and *HMGB3* in BRCA, SARC, SKCM, OV, and LAML. The global alternation of HMGBs showed prognostic significance in ACC, KIRC, and UCEC. Furthermore, HMGBs were significantly correlated with TIIC infiltration, ICP expression, MSI, and TMB in various cancers, indicating their regulations on the TIME. Lastly, results of GSEA-illuminated genes positively correlated with HMGBs which were similarly chromosome components participating in DNA activity-associated events.

Conclusion: This study demonstrated that HMGBs might be promising predictive biomarkers for the prognosis and immunotherapeutic response, also immunotherapy targets of multiple cancers.

Keywords: HMGB, pan-cancer, prognosis, immunotherapy, biomarker

OPEN ACCESS

Edited by:
Ayan Biswas,
University of Alabama at Birmingham, United States

Reviewed by:
Vikash Kansal,
University of Alabama at Birmingham, United States
Puneet Khandelwal,
Johns Hopkins Medicine, United States

***Correspondence:**
Lisheng Peng
pls0556@gzucm.edu.cn

Specialty section:
This article was submitted to Cancer Genetics and Oncogenomics, a section of the journal Frontiers in Genetics

Received: *25 August 2021*
Accepted: *17 September 2021*
Published: *29 October 2021*

Citation:
Lin T, Zhang Y, Lin Z and Peng L (2021) Roles of HMGBs in Prognosis and Immunotherapy: A Pan-Cancer Analysis. Front. Genet. 12:764245. doi: 10.3389/fgene.2021.764245

INTRODUCTION

Immunotherapy has revolutionized the treatment landscape of patients with advanced cancers, especially immune checkpoint inhibitors (ICIs). Immune checkpoints (ICPs), such as programmed death protein 1 (PD-1) and its ligand (PD-L1), are negative modulatory signaling pathways for activation of T cells, which in turn facilitate immune tolerance and promote cancer. ICIs aim to unleash T cells from exhaustion and enhance anticancer immune activity. However, only 20% of patients derive the response to ICIs across all malignancies, which severely limits their clinical benefits (Rameshbabu et al., 2021). Therefore, seeking new immunotherapeutic targets and predictive biomarkers for immunotherapy efficacy for patient selection is a hot issue of the current research (Yi et al., 2018).

The high mobility group box (HMGB) protein family, consisting of HMGB1-4, includes non-histone chromatin components (Rapoport et al., 2020). HMGB1-3 share over 80% identical sequence and structure, comprising two DNA-binding domains and an acidic tail. However, HMGB4 lacks the acidic tail and is not ubiquitously expressed like HMGB1-3 (Taniguchi et al., 2018). This study focused on HMGB1-3. HMGBs are predominantly in the nucleus and act as DNA chaperones, thereby modulating chromosome stabilization, telomerase maintenance, replication, transcription, and DNA repair (Cheng et al., 2020). In the cytoplasmic or extracellular milieu, HMGBs act as chemokines or cytokines to evoke inflammatory and immune responses (Niu et al., 2020).

Accumulating evidence had hinted HMGBs' participation in cancer pathogenesis. First, effective DNA damage repair is indispensable for cancer cells to maintain growth. Second, excessive extracellular HMGBs induce chronic inflammation, which is a hallmark of cancer (Mukherjee and Vasquez, 2020). The overexpression and prognostic relevance of HMGBs had been observed in various cancers, including prostate (Jung et al., 2021), liver (Zhang et al., 2014), cervix (Cheng et al., 2017; Li T. et al., 2020), breast (Fu et al., 2018), stomach (Cui et al., 2019), esophagus (Gao et al., 2015), and hematopoietic malignancies (Yuan et al., 2020). Given the roles of HMGBs in the regulation of inflammation and immunity, they appear to be candidate targets for cancer immunotherapy. However, HMGB1 is double-faced in cancers. HMGB1 can maintain genome stability and interact with tumor suppressor proteins, e.g., Rb, to prevent oncogenesis (Mandke and Vasquez, 2019). Besides, extracellular HMGB1 can stimulate anticancer immune responses during the process called immunogenic cell death (ICD) (Fucikova et al., 2020; Rapoport et al., 2020). Beyond the controversy of HMGB1, the roles of HMGB2/3 in cancers are unclear, especially in the context of the tumor immune microenvironment (TIME).

In this work, we comprehensively analyzed the expression, genetic alternations, clinicopathological and prognostic relevance, and underlying mechanisms of HMGBs in pan-cancer. Since biomarkers reflecting TIME, including tumor immune-infiltrating cells (TIICs) and ICP gene expression, and tumor intrinsic features, including microsatellite instability (MSI) and tumor mutational burden (TMB), may predict immunotherapy efficacy (Duffy and Crown, 2019), correlations between HMGB expression and these factors were investigated. This study may offer novel insights into HMGBs' potential values in cancer immunotherapy.

MATERIALS AND METHODS

Analysis of High Mobility Group Box Genes Expression in Cancers

The differential mRNA expression of HMGBs between human cancers and paired normal controls was analyzed using Oncomine (https://www.oncomine.org) (Rhodes et al., 2007) and Gene Expression Profiling Interactive Analysis 2 (GEPIA2) (http://gepia2.cancer-pku.cn/) (Tang et al., 2017). In the GEPIA2 portal, the data of 33 types of cancers were from the Cancer Genome Atlas (TCGA), and the normal data were combined TCGA and Genotype Tissue Expression (GTEx). The screening criteria were limited to |fold change (FC)| > 2 and a p value <0.01 for both portals.

Analysis of the Prognostic Value of High Mobility Group Box Genes in Cancers

Associations between HMGB expression and overall survival (OS) and relapse-free survival (RFS) of patients with diverse TCGA cancers were evaluated by five databases, Kaplan–Meier (KM) Plotter (http://www.kmplot.com/) (Nagy et al., 2021), Long-term Outcome and Gene Expression Profiling Database of pan-cancers (LOGpc, http://bioinfo.henu.edu.cn/DatabaseList.jsp), SurvExpress (http://bioinformatica.mty.itesm.mx:8080/Biomatec/SurvivaX.jsp) (Aguirre-Gamboa et al., 2013), Tumor IMmune Estimation Resource (TIMER) (http://timer.cistrome.org) (Li Z. et al., 2020), and GEPIA2. Here, patients were divided into high- and low-expression groups by median.

Analysis of the Clinicopathological Relevance of High Mobility Group Box Genes in Cancers

Associations between HMGB expression and clinicopathological features, including major stages and tumor grades of patients with diverse cancers, were explored using TCGA data by UALCAN (http://ualcan.path.uab.edu) (Chandrashekar et al., 2017).

Identification of Genetic Alternations of High Mobility Group Box Genes in Cancers

Genetic alternations of HMGBs including mutations, structural variants, and copy number alterations were analyzed by cBioPortal (http://www.cbioportal.org) (Cerami et al., 2012; Gao et al., 2013), using the "TCGA PanCancer Atlas" datasets. Associations between the global alternation of HMGBs and patient's survivals in pan-cancer were also analyzed; here, samples were split into "altered" and "unaltered" groups.

Analysis of Correlations Between High Mobility Group Box Genes Expression and Immune Infiltrates and Immune Checkpoint Genes in Cancers

Correlations between HMGB expression and the infiltration of diverse TIICs, including CD8 T cells, CD4 T cells, helper T (Th) 1 cells, Th2 cells, regulatory T cells (Tregs), natural killer (NK) cells, global macrophages, M1/M2 macrophages, neutrophils, myeloid dendritic cells (mDCs), B cells, and myeloid-derived suppressor cells (MDSCs), were explored using the TIMER portal. Correlations between HMGB expression and the infiltration of Th17 were assessed using TISIDB (http://cis.hku.hk/TISIDB) (Ru et al., 2019). Forty-three ICP genes were selected incorporating three review articles (Marin-Acevedo et al., 2021b) (Marin-Acevedo et al., 2021a) (Marin-Acevedo et al., 2018); correlations between the expression of HMGBs and these ICP genes were analyzed using TIMER.

Analysis of Correlations Between High Mobility Group Box Genes Expression and Microsatellite Instability and Tumor Mutational Burden in Cancers

The RNA sequence data of 33 kinds of TCGA cancers were downloaded from the Genomic Data Commons (GDC) portal (https://portal.gdc.cancer.gov/). MSI (Bonneville et al., 2017) and TMB (Thorsson et al., 2019) data were derived from two previous studies, respectively. Correlations between HMGB expression and MSI and TMB were analyzed using R software version 4.0.3.

Gene Set Enrichment Analysis for the Correlated Genes of High Mobility Group Box

Correlated genes of *HMGB1* in ACC (n = 79), *HMGB2* in LGG (n = 516), and *HMGB3* in BRAC (n = 1093) were explored using the LinkFinder module of the LinkedOmics platform (Vasaikar et al., 2018). Then, the significantly correlated genes of the *HMGB1/2/3* were respectively sequenced to perform gene set enrichment analysis (GSEA), using Web-based Gene SeT Analysis Toolkit (WebGestalt) (Liao et al., 2019). GSEA was conducted for gene ontology (GO) and Kyoto Encyclopedia of Genes and Genomes (KEGG) pathway categories. GO categories included biological process (BP), cellular component (CC), and molecular function (MF) aspects. The category size was restricted between 5 and 2,000, and the number of permutations was limited up to 1,000. A gene set with a false discovery rate (FDR) < 0.05 was considered significantly enriched.

Statistical Analysis

A comparison of the mRNA expression was performed using Student's t-test (Oncomine and UALCAN) or one-way ANOVA test (GEPIA2). Survival curves were plotted using the Kaplan–Meier method, and the log-rank test was performed to identify differences and calculate p values. Associations between gene expression and survival were estimated using Cox proportional regression to generate the hazard ratio (HR) and 95% confidence interval (CI). Spearman's method was applied to analyze correlations between gene expression and the infiltration level of TIICs, MSI, and TMB. Correlations between any two genes were evaluated using the Pearson test. Correlation strength was measured by correlation coefficient (r) values: 0.00–0.39, 0.40–0.59, and 0.60–1.0 were weak, moderate, and strong, respectively. All tests were two-tailed paired, and p values <0.05 were considered statistically significant.

RESULTS

Expression of High Mobility Group Box Genes in Cancers

Initially, the results from the Oncomine database showed that HMGB1/2/3 were significantly highly expressed in a total of 22, 22, and 51 datasets, whereas they were lowly expressed in two, three, and one datasets of various cancers, respectively, compared with paired normal controls (**Figure 1A**). Except for several datasets of leukemia, lymphoma, and sarcoma, HMGBs were consistently up-expressed in most human cancers.

In the GEPIA2 database, *HMGB1/2/3* were significantly differentially expressed in a total of 8, 14, and 24 types of TCGA cancers, respectively, compared with the corresponding normal controls (**Figures 1B–D**). In detail, *HMGB1/2/3* was uniformly up-expressed in eight kinds of cancers, including colon adenocarcinoma (COAD), lymphoid neoplasm diffuse large B-cell lymphoma (DLBC), glioblastoma multiforme (GBM), brain lower grade glioma (LGG), pancreatic adenocarcinoma (PAAD), rectum adenocarcinoma (READ), stomach adenocarcinoma (STAD), and thymoma (THYM). *HMGB2/3* was highly expressed in four kinds of cancers, including adrenocortical carcinoma (ACC), bladder urothelial carcinoma (BLCA), cervical squamous cell carcinoma and endocervical adenocarcinoma (CESC), and uterine carcinosarcoma (UCS), while they were down-expressed in acute myeloid leukemia (LAML). Besides, *HMGB2* was upregulated in liver hepatocellular carcinoma (LIHC). *HMGB3* was upregulated in 11 other types of cancers, including breast invasive carcinoma (BRCA), esophageal carcinoma (ESCA), head and neck squamous cell carcinoma (HNSC), kidney chromophobe (KICH), kidney renal clear cell carcinoma (KIRC), lung adenocarcinoma (LUAD), lung squamous cell carcinoma (LUSC), ovarian serous cystadenocarcinoma (OV), prostate adenocarcinoma (PRAD), testicular germ cell tumors (TGCT), and uterine corpus endometrial carcinoma (UCEC). To be short, HMGB expression was significantly elevated in most cancers, except that *HMGB2/3* were downregulated in LAML. Moreover, *HMGB3* was the most universally overexpressed among the HMGB family.

Prognostic Significance of High Mobility Group Box Genes in Cancers

In the first step, associations between HMGB expression and OS and RFS of patients with diverse cancers were evaluated

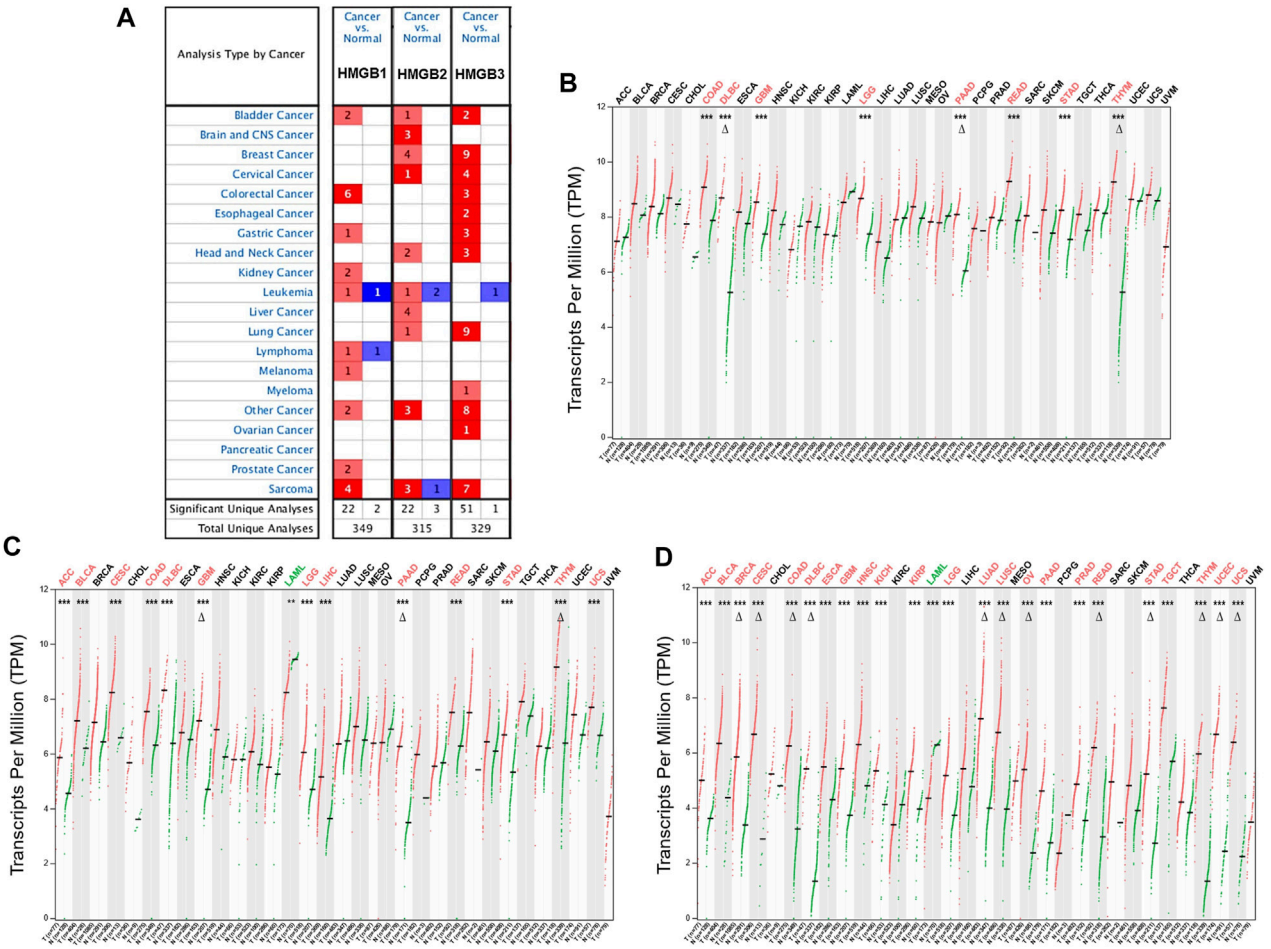


FIGURE 1 | The differential expression of High Mobility Group Box (HMGBs) between cancers and normal controls. **(A)** A summary of the datasets in which HMGBs were significantly up- (red) or down- (blue) expressed in cancers, compared with normal controls (Oncomine). Numbers in cells represent dataset counts. The expression of **(B)** HMGB1, **(C)** HMGB2, and **(D)** HMGB3 in TCGA cancers and paired normal controls (GEPIA2). A black font indicates no significant difference; red or green fonts indicate significant up- or down-expression, respectively, with |fold change (FC)| > 2 and p values <0.01. $^{***}p < 0.001$; $^{\Delta}|FC| > 4$ and $p < 0.01$.

integrating LOGpc, KM Plotter, SurvExpres, and TIMER platforms (**Supplementary Table S1**). We found that a higher expression of *HMGB1* was significantly related with worse OS of patients with ACC (HR = 2.36, p = 0.043) and KICH (HR = 4.75 p = 0.037), whereas a better OS of patients with THYM was found (HR = 0.11, p = 0.011) (**Figure 2A**). An elevated expression of *HMGB2* was significantly linked to shorter OS of patients with ACC (HR = 4.67, p = 0.001), KICH (HR = 6.54, p = 0.004), KIRC (HR = 1.53, p = 0.004), KIRP (HR = 2.20, p = 0.011), LGG (HR = 2.19, p = 9.00E-05), LIHC (HR = 1.85, p = 0.001), and MESO (HR = 2.09, p = 6.72E-06), and a longer OS of patients with SKCM (HR = 0.71, p = 0.013) and THYM (HR = 0.18, p = 0.018) (**Figure 2B**). *HMGB3* overexpression implied unfavorable OS of patients with BRCA (HR = 1.58, p = 0.006), ESCA (HR = 1.64, p = 0.034), KIRC (HR = 1.52, p = 0.006), MESO (HR = 1.66, p = 0.003), SARC (HR = 2.10, p = 2.00E-04), and SKCM (HR = 1.61, p = 0.001), but better OS of patients with LAML (HR = 0.56, p = 0.006), OV (HR = 0.76, p = 0.043), and STAD (HR = 0.71, p = 0.040) (**Figure 2C**).

Apart from several cancer types with insufficient sample size that were not analyzed, we further found that *HMGB1* upregulation was significantly linked with unfavorable RFS of ACC, COAD, PAAD, and READ, but better RFS of LGG (**Figure 2D**). *HMGB2* high expression suggested worse RFS of KIRP, LGG, LIHC, but better RFS of GBM (**Figure 2E**). *HMGB3* up-expression implied better RFS of OV but worse RFS of TGCT (**Figure 2F**).

Second step, heat maps exhibiting HMGBs' prognostic values were generated by GEPIA (**Figures 2G,H**). Here, *HMGB1* high expression indicated both worse OS and RFS of ACC and LUAD; worse RFS of CESC, HNSC, and SARC; and better OS of KIRC. *HMGB2* up-expression suggested both worse OS and RFS of ACC, KIRP, LGG, and LIHC; worse OS of MESO and PAAD; worse RFS of LUAD and PRAD; and better OS of SKCM. *HMGB3* upregulation signified both poorer OS and RFS of ESCA; worse OS of BRCA, LGG, SARC, and SKCM; and better OS and RFS of LAML and OV. We took the intersection of the findings of the two steps of survival

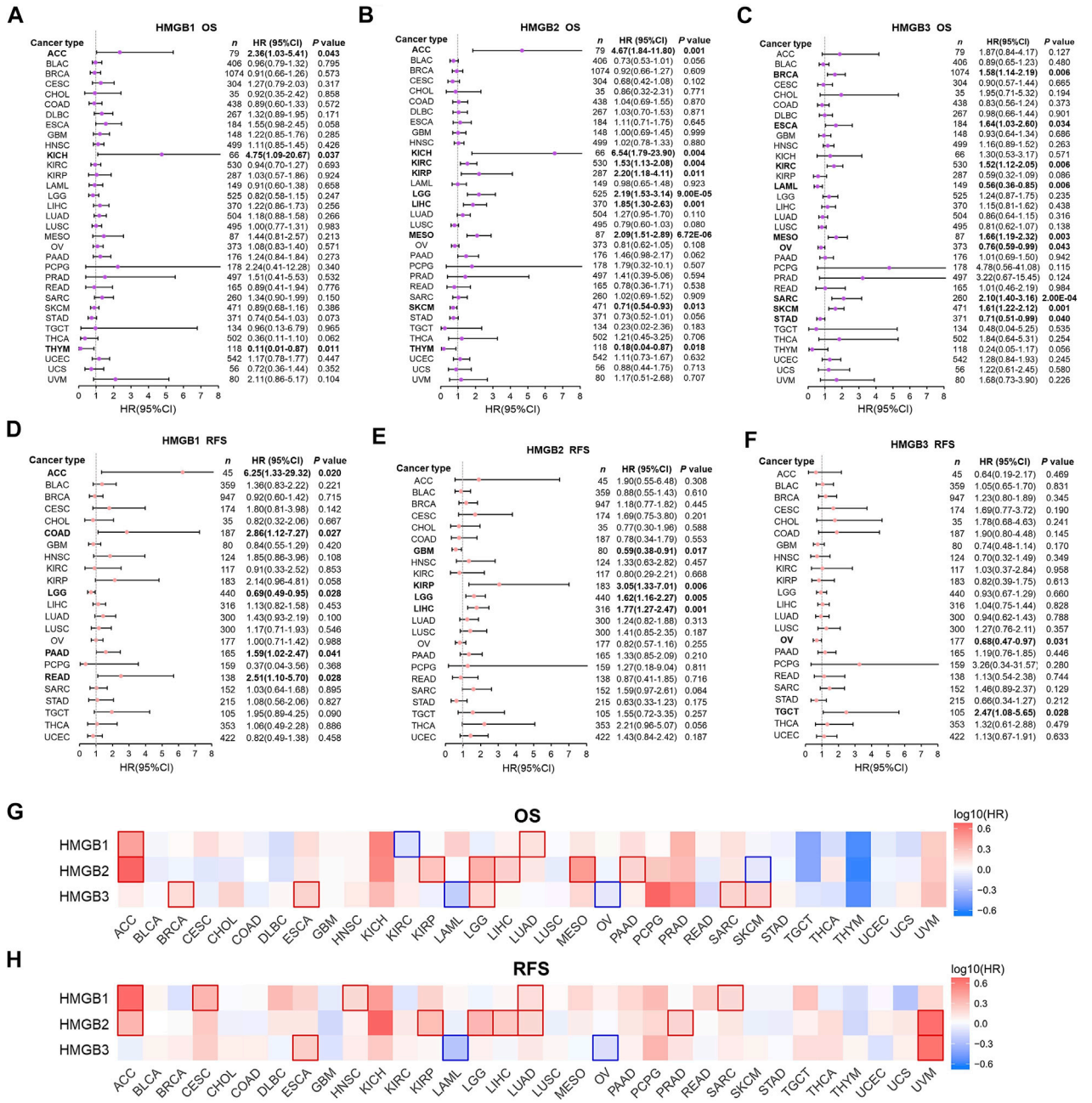


FIGURE 2 | Prognostic significance of High Mobility Group Box (HMGBs) in cancers. Associations between HMGB expression and **(A–C)** OS and **(D–F)** RFS of patients with various cancers. Heat maps showing relations of HMGB expression with **(G)** OS and **(H)** RFS of various cancers (GEPIA2). Results with significance are framed; red or blue frames indicate high or low survival risk, respectively. OS, overall survival; RFS, relapse-free survival; HR, hazard ratio; CI, confidence interval.

analyses to improve the robustness, which was provided in the discussion section.

Clinicopathological Relevance of High Mobility Group Box Genes in Cancers

Subsequently, correlations between HMGB expression and clinicopathological characteristics of diverse cancers were investigated. We found that *HMGB1* expression was elevated with the stage progression of ACC and READ. *HMGB1* expression was significantly higher in Stage-IV ACC and Stage-III READ than in Stage-I/II ACC and Stage-II READ, respectively ($p < 0.05$) (**Figures 3A,B**). *HMGB2* expression was elevated as stages of ACC, KIRC, and LIHC were promoted, while stages of SKCM improved. The expression of *HMGB2* was significantly higher in Stage-IV ACC, Stage-IV

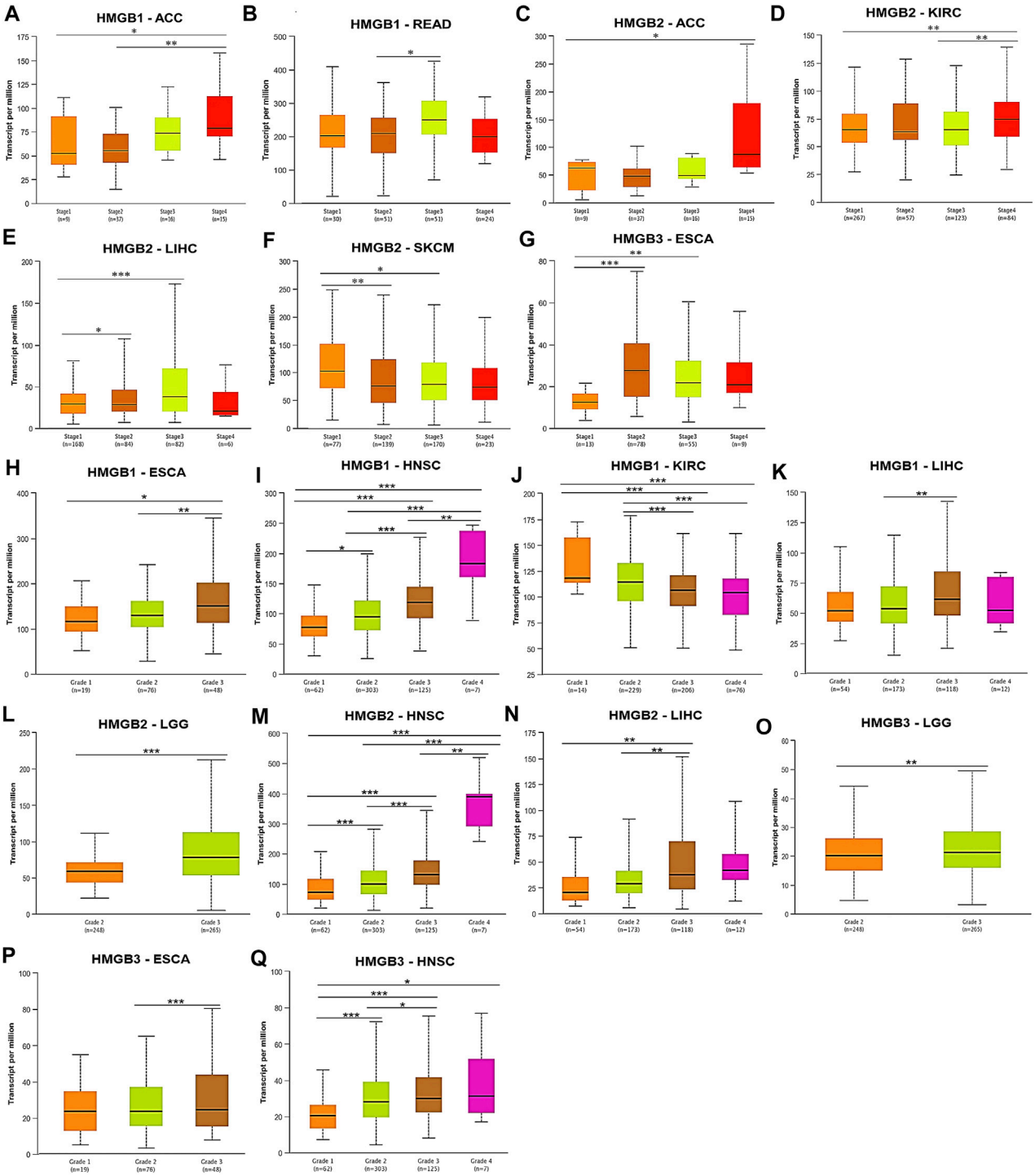


FIGURE 3 | Clinicopathological relevance of High Mobility Group Box (HMGBs) in cancers. Associations of the expression of **(A–B)** HMGB1, **(C–F)** HMGB2, and **(G)** HMGB3 with pathological stages of several cancers. Associations of the expression of **(H–K)** HMGB1, **(L–N)** HMGB2, and **(O–Q)** HMGB3 with tumor grades of several cancers (UALCAN). $^{*}p < 0.05$, $^{**}p < 0.01$, $^{***}p < 0.001$.

KIRC, and Stage-II/III LIHC than in Stage-I ACC, Stage-I/III KIRC, and Stage-I LIHC, respectively. In contrast, *HMGB2* expression was significantly lower in Stage-II/III SKCM, compared to that in Stage-I ones ($p < 0.05$) (**Figures 3C–F**). *HMGB3* expression was elevated in Stage-II/III ESCA, compared with that in Stage-I ones ($p < 0.05$) (**Figure 3G**).

What is more, tumor grades of HNSC were significantly increased with the elevation of HMGB expression (**Figures**

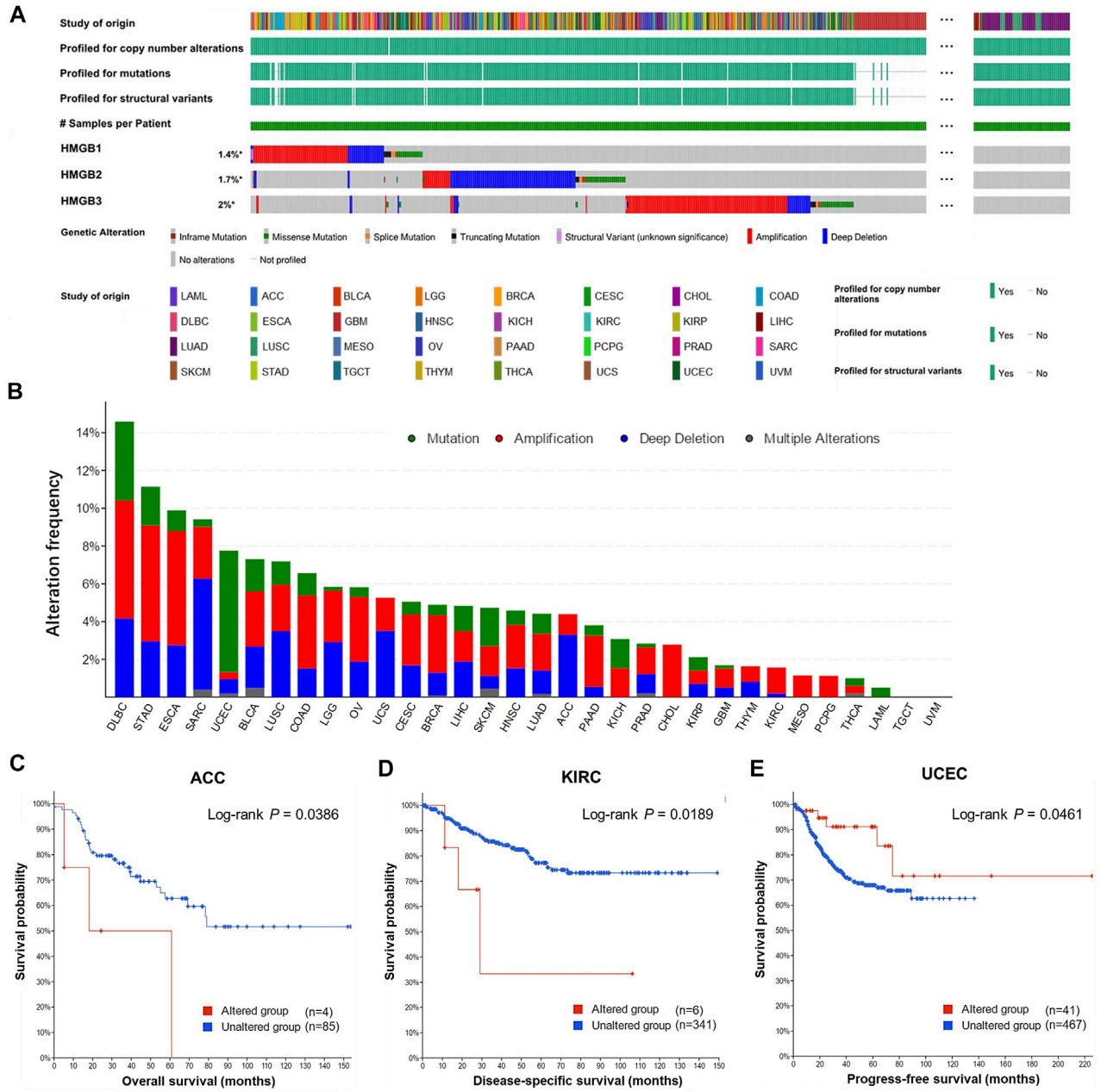


FIGURE 4 | Genetic alternations of High Mobility Group Box (HMGBs) in cancers. **(A)** An overview of the genomic alternations of HMGBs occurred in pan-cancer. **(B)** The alternation frequency of HMGBs in cancers. Associations of HMGBs' global alternation with the survival of patients with **(C)** ACC, **(D)** KIRC, and **(E)** UCEC (cBioPortal).

3I,M,Q), while an opposite trend was observed for *HMGB1* expression in KIRC (**Figure 3J**). Significantly, *HMGB1/2* expression was higher in Grade-3 tumors of LIHC than in Grade-2 (and −1) ones ($p < 0.01$) (**Figures 3K,N**). *HMGB1/3* expression was higher in Grade-3 tumors of ESCA than in Grade-2 (and −1) ones ($p < 0.05$) (**Figures 3H,P**). *HMGB2/3* expression was higher in Grade-3 tumors of LGG than in Grade-2 ones ($p < 0.01$) (**Figures 3L,O**). Collectively, HMGB up-expression indicated the clinicopathological advancement of ACC, ESCA, HNSC, LIHC, LGG, and READ and the alleviation of KIRC and SKCM.

Genetic Alternations of High Mobility Group Box Genes in Cancers

Overall, genetic alternations of HMGBs were identified in a total of 529 (4.83%) out of 10,953 samples, including in-frame mutation, missense mutation, splice mutation, truncating

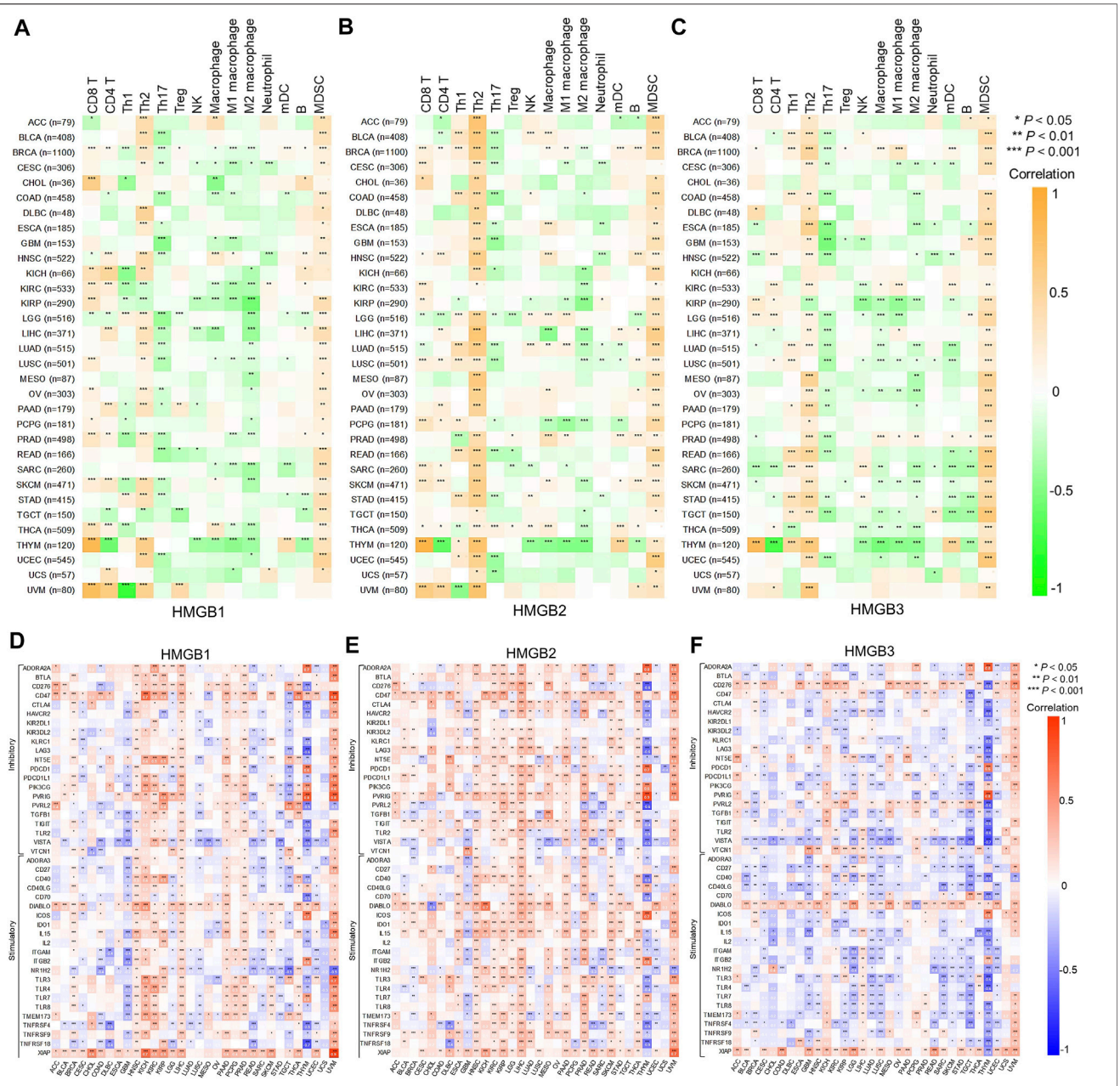


FIGURE 5 | Correlations between High Mobility Group Box (HMGBs) expression and **(A–C)** immune infiltration and **(D–F)** ICP genes expression in cancers. Th, helper T cell; Treg, regulatory T cell; NK cell, natural killer cell; mDC, myeloid dendritic cell; MDSC, myeloid-derived suppressor cell.

mutation, structural variant, amplification, and deep deletion (**Figure 4A**). Among all the cancers, HMGBs altered the most frequently in DLBL, with an incidence rate of 14.58%, followed by STAD (11.14%) and ESCA (9.89%) (**Figure 4B**). *HMGB3* was the most frequently altered one within HMGBs (221 out of 10950 samples).

The occurrence of HMGB alternations was significantly related to poorer OS of ACC (**Figure 4C**) and poorer disease-specific survival of KIRC (**Figure 4D**), but a better progression-free survival of UCEC ($p < 0.05$) (**Figure 4E**). Apart from these, no significant survival relevance was found for other cancer types.

Correlations Between High Mobility Group Box Genes Expression and Immune Infiltrates and Immune Checkpoint Genes in Cancers

Correlations between HMGB expression and infiltration levels of TIICs were investigated integrating TIMER and

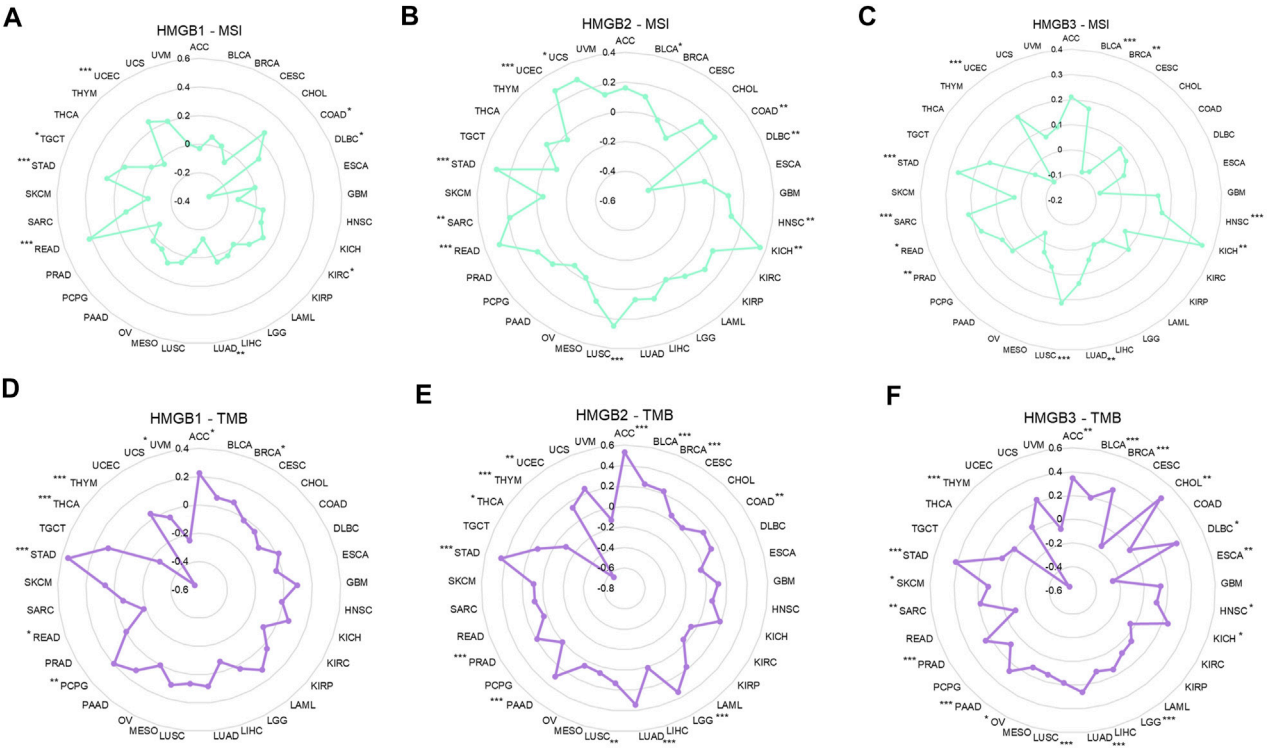


FIGURE 6 | Correlations between High Mobility Group Box (HMGBs) expression and the **(A–C)** MSI and **(D–F)** TMB of cancers. MSI, microsatellite instability; TMB, tumor mutational burden.

TISID. Generally, HMGBs were significantly positively correlated with the infiltration of Th2 cells and MDSCs and negatively correlated with that of Th17 cells in pan-cancer (**Figures 5A–C**). Specifically, *HMGB1* expression showed positive correlations with the infiltration of CD8 and CD4 T cells, but negative ones with that of Th1 cells and macrophages in BRCA, KIRC, KIRP, LIHC, PRAD, SKCM, and THCA. *HMGB2* expression was positively or negatively correlated with the infiltration of diverse TIICs in BRCA, LGG, LUAD, PCPG, and THCA, without a consistent pattern. *HMGB3* expression exhibited negative correlations with the infiltration of macrophage lineages in KIRP, LGG, LUAD, LUSC, OV, SARC, SKCM, TGCT, and THCA. Notably, strong to very strong correlations were observed as follows: HMGB expression and the infiltration of CD8 T cells and (or) Th2 cells in THYM and UVM; *HMGB2* expression and Th2 cell infiltration in ACC, BLCA, LIHC, and MESO; and *HMGB2/3* expression and MDSC infiltration in UCEC.

Inhibitory and stimulatory ICPs regulate immune escape and immune efficacy, respectively. Here, we explored correlations between the expression of HMGBs and 43 ICP genes (21 inhibitory and 22 stimulatory). In general, the relationships between the expression of HMGBs and inhibitory or stimulatory ICP genes were isotropic. To highlight, strong correlations were identified for HMGB expression with many ICP genes of THYM, with mostly negative relations, as well as *HMGB1/2* expression with numerous ICP genes of UVM. Besides, significant positive correlations between the expression of HMGBs and ICP genes were found in the following cancers: *HMGB1* in HNSC, LIHC, PAAD, and PRAD and *HMGB2* in HNSC, KIRC, KIRP, LGG, LIHC, PRAD, THCA, and SKCM. In contrast, significant negative correlations were found as follows: HMGBs in GBM and *HMGB3* in KIRP, LGG, LUAD, LUSC, and TGCT. (**Figures 5D–F**).

Correlations Between High Mobility Group Box Genes Expression and Microsatellite instability and Tumor Mutational Burden in Cancers

Among 33 kinds of cancers, *HMGB1/2/3* expression was significantly positively correlated with the MSI of 6 (18.2%), 10 (30.3%), and 10 (30.3%) types of cancers but negatively correlated with the MSI of 2 (6.0%), 1 (3.0%), and 1 (3.0%) types of cancers respectively (**Figures 6A–C**).

As for the TMB, *HMGB1/2/3* expression was significantly positively correlated with the TMB of 4 (12.1%), 11 (33.3%), and 16 (48.5%) kinds of cancers but negatively correlated with the TMB of 4 (12.1%), 2 (6.0%), and 2 (6.0%) kinds of cancers, respectively (**Figures 6D–F**). Particularly, HMGB expression had almost strong negative correlations with the TMB of THYM. In addition, positive relationships with both MSI and TMB were

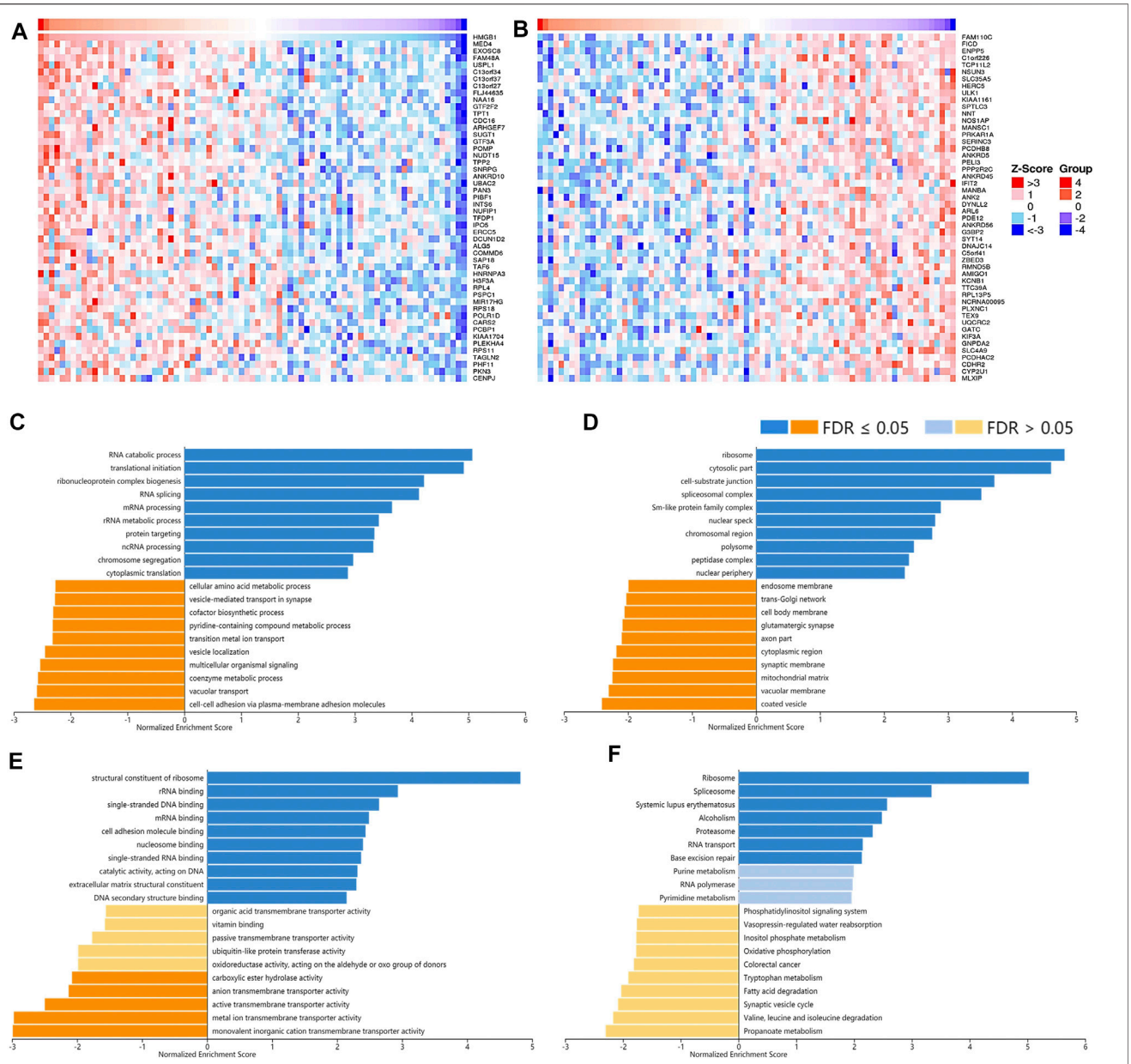


FIGURE 7 | The corrected genes of High Mobility Group Box 1 (HMGB1) in ACC and GSEA results. The top 50 genes significantly **(A)** positively and **(B)** negatively correlated with HMGB1 in ACC (LinkedOmics). The top 20 significantly enriched **(C)** GO-BP, **(D)** GO-CC, **(E)** GO-MF, and **(F)** KEGG pathway terms of HMGB1 correlated genes based on GSEA. A bar represents a normalized enrichment score for a term, which in orange or blue represents negatively or positively enriched, respectively.

identified for *HMGB1* in STAD; *HMGB2* in STAD, BLCA, UCEC, LUSC, and COAD; and *HMGB3* in STAD, LUAD, PRAD, LUSC, BLCA, SAR, HNSC, and KICH.

Potential Functions of the Correlated Genes of High Mobility Group Box Genes

To understand the potential mechanisms behind the differential expression and immunological relevance of HMGBs in different cancer types, we explored correlated genes of *HMGB1/2/3* in three representative cancer types and performed GSEA for them, respectively. A total of 3,452 genes were found significantly correlated with *HMGB1* in ACC, and the top 50 of the positively and negatively correlated ones are shown in **Figures 7A,B** respectively. The results of GSEA illuminated that the positively correlated genes of *HMGB1* in ACC might comprise the ribosome, cytosolic part, cell–substrate junction, etc., and partake in RNA metabolic processes and translation. Signaling pathways of the ribosome, spliceosome, and purine metabolism were involved. Nevertheless, the negatively correlated genes of *HMGB1* might

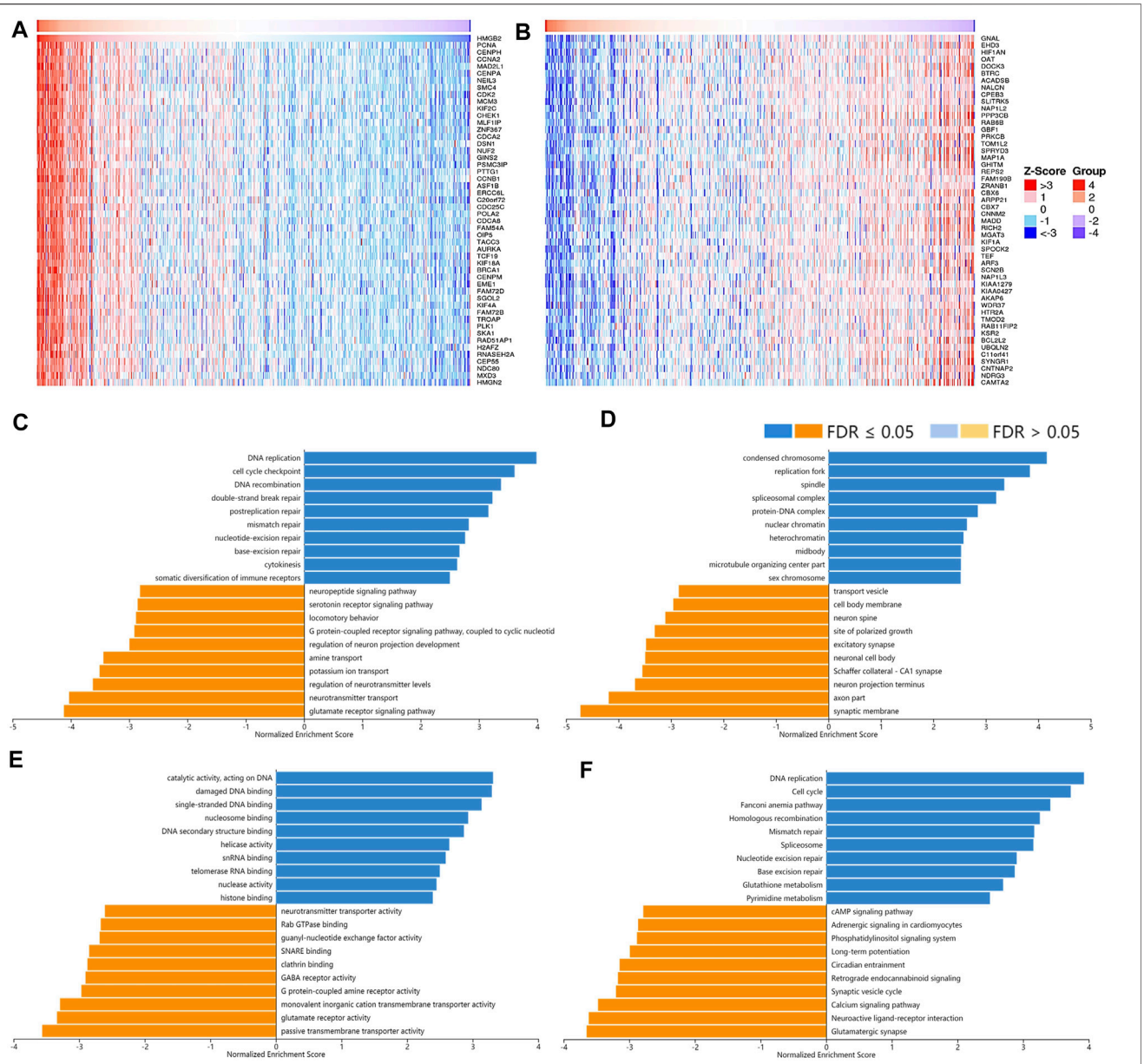


FIGURE 8 | The correlated genes of High Mobility Group Box 2 (HMGB2) in LGG and GSEA results. The top 50 genes significantly **(A)** positively and **(B)** negatively correlated with HMGB2 in LGG (LinkedOmics). The top 20 significantly enriched **(C)** GO-BP, **(D)** GO-CC, **(E)** GO-MF, and **(F)** KEGG pathway terms of HMGB2 correlated genes based on GSEA. A bar represents a normalized enrichment score for a term, which in orange or blue represents negatively or positively enriched respectively.

comprise coated vesicles and vacuolar membranes and be involved in cell–cell adhesion *via* plasma–membrane adhesion molecules and various transmembrane transports (**Figures 7C–F**).

A total of 12,967 genes were found significantly correlated with *HMGB2* in LGG (**Figures 8A,B**). The positively correlated genes of *HMGB2* in LGG might be components of the chromosome, replication fork, and spindle and be responsible for BPs and pathways regulating cell cycle checkpoint, DNA replication, recombination, and damage repair, as well as somatic diversification immune receptors. In contrast, the negatively correlated genes of *HMGB2* might consist of the synaptic membrane, axon part, neuron projection terminus, and transport vesicles and be involved in signaling pathways of glutamate receptor, neurotransmitter transport, G protein-coupled receptor, and cAMP (**Figures 8C–F**).

As for the correlated genes of *HMGB3* in BRAC, 14,028 genes were significantly observed in all (**Figures 9A,B**). Similarly, the positively correlated genes of *HMGB3* in BRAC were generally chromosome structures and partake in BPs and pathways related to replication, DNA repair, and chromatin remodeling. Additionally, pathways of amino acid biosynthesis, carbon metabolism, and citrate cycle were also enriched. The

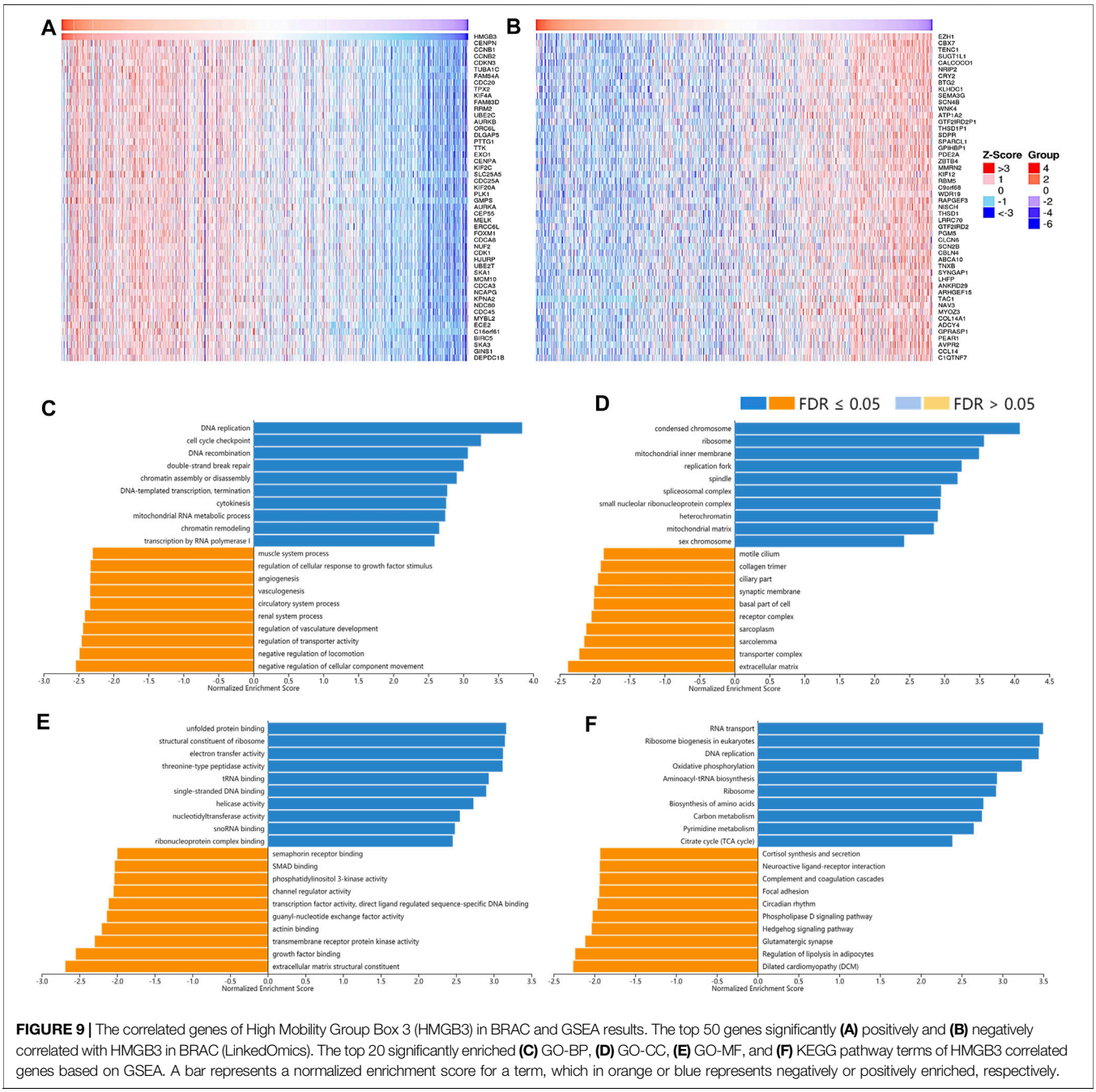


FIGURE 9 | The correlated genes of High Mobility Group Box 3 (HMGB3) in BRAC and GSEA results. The top 50 genes significantly **(A)** positively and **(B)** negatively correlated with HMGB3 in BRAC (LinkedOmics). The top 20 significantly enriched **(C)** GO-BP, **(D)** GO-CC, **(E)** GO-MF, and **(F)** KEGG pathway terms of HMGB3 correlated genes based on GSEA. A bar represents a normalized enrichment score for a term, which in orange or blue represents negatively or positively enriched, respectively.

negatively correlated genes of *HMGB3* might consist of extracellular matrix and transporter complexes, which contributed to angiogenesis and the negative regulation of locomotion. Moreover, the signaling pathways of Hedgehog and focal adhesion were related (**Figures 9C–F**).

DISCUSSION

This study extracted potential values of HMGBs in various cancers, especially in the context of immunotherapy.

From the outset, we found that HMGBs were significantly up-expressed in various TCGA cancers, except that *HMGB2/3* were down-expressed in LAML. Despite that the overexpression of *HMGB1* in cancers was the most prevalently reported (Niu et al., 2020), we found that *HMGB3* was highly expressed in the largest variety of cancers and altered most frequently. Integrating the results of two steps of survival analyses, high expression of HMGBs suggested unfavorable prognosis in the following cancers: *HMGB1* in ACC; *HMGB2* in ACC, KIRP, LGG, LIHC, MESO; and *HMGB3* in BRCA, ESCA, SARC, and SKCM. In contrast, favorable prognostic indications were

found for the up-expression of *HMGB2* in SKCM, as well as *HMGB3* in OV and LAML. By the way, the global alternation of HMGBs was linked with worse outcomes of ACC and KIRC, but a better outcome of UCEC. In addition, elevated HMGB expression indicated clinicopathological advances in these cancers: *HMGB1* in ACC, HNSC, and ESCA; *HMGB2* in ACC, HNSC, KIRC, LGG, and LIHC; and *HMGB3* in ESCA and HNSC. Conversely, the up-expression of *HMGB1* and *HMGB2* suggested clinicopathological alleviation of KIRC and SKCM, respectively.

The findings of some earlier studies were consistent with ours. Nguyen *et al.* reported that HMGB1 was related to the clinical and pathological characteristics of HNSC (Nguyen et al., 2016). Kwon *et al.* stated that HMGB2 overexpression implied the aggressiveness and worse prognosis of LIHC (Kwon et al., 2010). In an experimental study, HMGB2 was observed to be highly expressed in melanoma, whose silence impeded cell proliferation and invasion, yet promoted cell cycle arrest and apoptosis, leading to melanoma regression, indicating that HMGB2 contributed to melanoma promotion (Mo et al., 2019). As for HMGB3, several experiments revealed that it was upregulated by diverse noncoding RNAs, which in turn fomented malignant behaviors and even immune escape of breast cancer cells (Gu et al., 2019; Chen et al., 2021; Yu et al., 2021). A recent study indicated that hypermethylation of the promoter of miR-216a upregulated HMGB3, which then promoted ESCA (Sun et al., 2021). Paradoxically, HMGB3 high expression was shown to facilitate cisplatin resistance of ovarian cancer cells; however, we found it a favorable prognostic indicator of OV (Mukherjee et al., 2019).

It is well known that CD8 T cells, NK cells, and Th1 cells exert anticancer immunity, while TAMs, MDSCs, Tregs, Th2 cells, and tolerogenic mDCs foster pro-cancer immune escape in the TIME (Zhang and Zhang, 2020; Saillard et al., 2021). ICIs can unleash preexisting tumor-infiltrating lymphocytes (TILs) and restore their lethality to cancer cells. Increased density of TILs, particularly CD8 T cells, improved the therapeutic responses and outcomes of patients across various malignancies (Nishino et al., 2017). However, only patients with high ICP expression may benefit from ICI therapy; a most adopted predictor is PD-L1 expression (Randrian et al., 2021). In this study, we investigated correlations between HMGB expression and both immune infiltration and ICP gene expression, to learn their involvements in the TIME and predictive capacities for the response to ICI therapy. Generally, HMGBs were positively or negatively associated with both immune-stimulative TIICs/ICP genes and immunosuppressive TIICs/ICP genes in pan-cancer, suggesting that they might modulate the TIME in both provocative and inhibitory ways. However, we inferred that HMGBs were inclined to induce overall immunosuppression in the TIME, since we found that they had uniformly positive correlations with the infiltration of Th2 cells and MDSCs in pan-cancer. Indeed, interactions between HMGB1 and its receptors are critical for the differentiation and activation of MDSCs (Jin et al., 2020) and Tregs (Wild et al., 2012) and the upregulation PD-L1 in the TIME (Wang et al., 2019). Besides, it was evident that HMGB1 could induce a dominance of Th2-type response in inflammation (Ma et al., 2015).

HMGB expression showed strong correlations with TIICs and ICP genes in THYM and UVM, signifying their outstanding positions in the TIME of the two kinds of cancers. For HNSC, HMGB up-expression suggested increased ICP gene expression and rising density of immune-suppressive Th2 cells, macrophages, and MDSCs, which might contribute to the disease progress. *HMGB2* up-expression indicated elevated infiltration of Th2 cells and MDSCs and (or) ICP gene expression in ACC, KIRP, LGG, LIHC, and MESO, with medium to strong correlation strength, which might partly explain the poor survival of patients with these cancers. Oppositely, *HMGB2* upregulation might benefit SKCM patients through activating CD8 T cells and stimulatory ICPs. In fact, an earlier study indicated that HMGB2 participated in the cytoplasmic chromatin recognition and the subsequent response to anticancer ICP blockade (Zhao et al., 2020). A high *HMGB3* expression was a detrimental prognostic factor for BRCA, ESCA, SARC, and SKCM, which might blame on its negative relationships with various stimulatory ICPs and the infiltration of CD8 T cells but positive interactions with Th2 cells and MDSCs. In contrast, the beneficial role of *HMGB3* in OV might partially be explained by the scarce immunological interactions. All the above manifested HMGBs might partake in the development of these cancers through coordinating TIICs and ICPs, thus potentially serving as immunotherapy targets. Seeing from another angle, HMGBs could also be used as predictive biomarkers for immunotherapeutic response in some cancers. This is because, for a cancer type in which the expression of ICPs and HMGBs was positively correlated, a high HMGB expression might predict a better response to ICI therapy.

Microsatellites are short DNA stretches tandemly repeated throughout the genome, and MSI occurs when the genome gains or loses ≥ one repeat(s). TMB represents the total number of mutations per DNA megabase (Duffy and Crown, 2019). High MSI is an underlying process contributing to high TMB, and higher MSI or TMB levels may generate potent neoantigens for recognition by immune surveillance, thus increasing immunotherapy responses (Duffy and Crown, 2019; Veigas et al., 2021). We found that HMGBs were significantly positively correlated with MSI and (or) TMB in diverse cancers, suggesting that high HMGB expression might predict clinical benefits from immunotherapy for patients with these cancers. Within the HMGB family, *HMGB3* expression was associated with MSI and (or) TMB in most cancer types, consistent with its highest alternation occurrence rate in pan-cancer. Integrating the significance of prognosis, TIICs, ICP genes, and MSI and (or) TMB, we induced that HMGBs might be promising immunological targets for the following cancers: *HMGB1* for ACC and KIRC; *HMGB2* for ACC and LGG; and *HMGB3* for BRAC, SARC, SKCM, and OV.

Genes positively correlated with HMGBs might be their potential co-expressed genes, which were similarly chromosome components regulating DNA replication, transcription, damage repair, chromatin remodeling, and cell cycle. These functions of HMGBs favor cancer cells to maintain their nature of continuous proliferation and protect them from therapy-caused DNA damages (Cámara-Quílez et al.,

2020). What is more, genes positively correlated with HMGB3 in BRAC were also enriched in pathways of amino acids and carbon metabolism, indicating their participation in cancer metabolic alternations. Beyond intracellular functions, HMGBs, especially HMGB1, can be actively secreted by cancer cells *per s*, infiltrating immune cells, and stromal cells, or passively released from necrotic cells into extracellular milieu in response to various stimuli. Upon HMGBs binding to cell-surface receptors or immune receptors, e.g., receptor for advanced glycation end product (RAGE) and toll-like receptors (TLRs), inflammatory and immune responses are amplified *via* a positive feedback loop (Kang et al., 2013; Musumeci et al., 2014). The durable chronic inflammation then activates multiple downstream pathways, e.g., nuclear factor κB (NF-κB), mitogen-activated protein kinase (MAPK), and phosphatidylinositol 3-kinase (PI3K), to promote cancer through modulating apoptosis, autophagy, invasion, metastasis, and angiogenesis (Bianchi et al., 2017; Lee et al., 2019; Mukherjee and Vasquez, 2020). High levels of HMGB1 can recruit MDSCs, macrophages, neutrophils, immature DCs, and Tregs and increase their T cell inhibitory properties to establish a highly immunosuppressive TIME conducive to immune escape (Gorgulho et al., 2019). Furthermore, HMGB1 interacts with immunomodulatory molecules to hinder immune activities, e.g., T-cell immunoglobulin and mucin domain-containing-3 (TIM-3) (Kwak et al., 2020). Paradoxically, HMGB1 also stimulates TILs and produce anticancer immunity as an immunogenic signal during ICD, which is a kind of cell death caused by chemo- or radiotherapies (Apetoh et al., 2007). To summarize, HMGB up-expression is essential for cancer cells to maintain the hallmarks of unlimited proliferation and permanent inflammation, which made them forceful biomarkers of pan-cancer. HMGBs are intertwined in extensive signaling pathways of inflammation and immunity, thus affecting the immune infiltration and ICP expression in the TIME of cancers. Differences between diverse cancer types might attribute to not only the inherent heterogeneity of cancers but also the inflammation level, cytokines, chemokines, inner receptors, targeted cells, and redox states of HMGBs in the tumor sites (Kang et al., 2013). Despite that knowledge about HMGB2/3 is very limited, they might have similar regulatory patterns with HMGB1 based on their high identities. That said, there is still a long way to go to clarify the specific mechanisms.

CONCLUSION

This study observed that HMGBs were significantly differentially expressed in a wide range of cancers. HMGB expression was associated with the prognosis and clinicopathologic characteristics of various cancers, which might be partially explained by their extensive interactions with TIICs and ICPs in the TIME. Besides, HMGB expression was related to MSI and TMB in multiple cancers, which further displayed their potentials as cancer immunotherapy targets and biomarkers for immunotherapeutic response prediction. Therefore, it is necessary to conduct in-depth studies on the immune-related functions of HMGBs, especially HMGB2/3. Besides, we underscored the importance of HMGB1 in ACC and KIRC; HMGB2 in ACC and LGG; and HMGB3 in BRAC, SARC, SKCM, and OV. Although careful validations were warranted, our study might deepen the understanding of the roles of HMGBs in pan-cancer and provide novel insights for future immunotherapy strategies.

DATA AVAILABILITY STATEMENT

The datasets presented in this study can be found in online repositories. The names of the repositories and accession numbers can be found in the article/**Supplementary Material**.

AUTHOR CONTRIBUTIONS

TL designed the study, conducted the analyses, and drafted the original manuscript. YZ reviewed the previous literature and refined the language. ZL edited the figures. LP provided the original idea. All authors have read and contributed to the revision of the manuscript and approved the submitted version.

SUPPLEMENTARY MATERIAL

The Supplementary Material for this article can be found online at: https://www.frontiersin.org/articles/10.3389/fgene.2021.764245/full#supplementary-material

REFERENCES

Aguirre-Gamboa, R., Gomez-Rueda, H., Martínez-Ledesma, E., Martínez-Torteya, A., Chacolla-Huaringa, R., Rodriguez-Barrientos, A., et al. (2013). SurvExpress: An Online Biomarker Validation Tool and Database for Cancer Gene Expression Data Using Survival Analysis. *PLoS One* 8 (9), e74250. doi:10.1371/journal.pone.0074250

Apetoh, L., Ghiringhelli, F., Tesniere, A., Obeid, M., Ortiz, C., Criollo, A., et al. (2007). Toll-Like Receptor 4-Dependent Contribution of the Immune System to Anticancer Chemotherapy and Radiotherapy. *Nat. Med.* 13 (9), 1050–1059. doi:10.1038/nm1622

Bianchi, M. E., Crippa, M. P., Manfredi, A. A., Mezzapelle, R., Rovere Querini, P., and Venereau, E. (2017). High-Mobility Group Box 1 Protein Orchestrates Responses to Tissue Damage via Inflammation, Innate and Adaptive Immunity, and Tissue Repair. *Immunol. Rev.* 280 (1), 74–82. doi:10.1111/imr.12601

Bonneville, R., Krook, M. A., Kautto, E. A., Miya, J., Wing, M. R., Chen, H.-Z., et al. (2017). Landscape of Microsatellite Instability across 39 Cancer Types. *JCO Precision Oncol.* 2017, PO.17.00073. doi:10.1200/PO.17.00073

Cámara-Quílez, M., Barreiro-Alonso, A., Vizoso-Vázquez, Á., Rodríguez-Belmonte, E., Quindós-Varela, M., Lamas-Maceiras, M., et al. (2020). The HMGB1-2 Ovarian Cancer Interactome. The Role of HMGB Proteins and Their Interacting Partners MIEN1 and NOP53 in Ovary Cancer and Drug-Response. *Cancers* 12 (9), 2435. doi:10.3390/cancers12092435

Cerami, E., Gao, J., Dogrusoz, U., Gross, B. E., Sumer, S. O., Aksoy, B. A., et al. (2012). The cBio Cancer Genomics Portal: An Open Platform for Exploring Multidimensional Cancer Genomics Data: Figure 1. *Cancer Discov.* 2 (5), 401–404. doi:10.1158/2159-8290.CD-12-0095

Chandrashekar, D. S., Bashel, B., Balasubramanya, S. A. H., Creighton, C. J., Ponce-Rodriguez, I., Chakravarthi, B. V. S. K., et al. (2017). UALCAN: A Portal for Facilitating Tumor Subgroup Gene Expression and Survival Analyses. *Neoplasia* 19 (8), 649–658. doi:10.1016/j.neo.2017.05.002

Chen, Z., Pei, L., Zhang, D., Xu, F., Zhou, E., and Chen, X. (2021). HDAC3 Increases HMGB3 Expression to Facilitate the Immune Escape of Breast Cancer Cells via Down-Regulating MicroRNA-130a-3p. *Int. J. Biochem. Cel Biol.* 135, 105967. doi:10.1016/j.biocel.2021.105967

Cheng, H., Wang, W., Zhang, Y., Zhang, B., Cheng, J., Teng, P., et al. (2017). Expression Levels and Clinical Significance of Hepsin and HMGB1 Proteins in Cervical Carcinoma. *Oncol. Lett.* 14 (1), 159–164. doi:10.3892/ol.2017.6116

Cheng, K. J., Alshawsh, M. A., Mejia Mohamed, E. H., Thavagnanam, S., Sinniah, A., and Ibrahim, Z. A. (2020). HMGB1: An Overview of its Versatile Roles in the Pathogenesis of Colorectal Cancer. *Cell Oncol.* 43 (2), 177–193. doi:10.1007/s13402-019-00477-5

Cui, G., Cai, F., Ding, Z., and Gao, L. (2019). HMGB2 Promotes the Malignancy of Human Gastric Cancer and Indicates Poor Survival Outcome. *Hum. Pathol.* 84, 133–141. doi:10.1016/j.humpath.2018.09.017

Duffy, M. J., and Crown, J. (2019). Biomarkers for Predicting Response to Immunotherapy with Immune Checkpoint Inhibitors in Cancer Patients. *Clin. Chem.* 65 (10), 1228–1238. doi:10.1373/clinchem.2019.303644

Fu, D., Li, J., Wei, J., Zhang, Z., Luo, Y., Tan, H., et al. (2018). HMGB2 Is Associated with Malignancy and Regulates Warburg Effect by Targeting LDHB and FBP1 in Breast Cancer. *Cell Commun. Signal.* 16 (1), 8. doi:10.1186/s12964-018-0219-0

Fucikova, J., Kepp, O., Kasikova, L., Petroni, G., Yamazaki, T., Liu, P., et al. (2020). Detection of Immunogenic Cell Death and its Relevance for Cancer Therapy. *Cell Death Dis* 11, 1013. doi:10.1038/s41419-020-03221-2

Gao, J., Zou, Z., Gao, J., Zhang, H., Lin, Z., Zhang, Y., et al. (2015). Increased Expression of HMGB3: A Novel Independent Prognostic Marker of Worse Outcome in Patients with Esophageal Squamous Cell Carcinoma. *Int. J. Clin. Exp. Pathol.* 8 (1), 345–352.

Gao, J., Aksoy, B. A., Dogrusoz, U., Dresdner, G., Gross, B., Sumer, S. O., et al. (2013). Integrative Analysis of Complex Cancer Genomics and Clinical Profiles Using the cBioportal. *Sci. Signaling* 6 (269), pl1. doi:10.1126/scisignal.2004088

Gorgulho, C. M., Romagnoli, G. G., Bharthi, R., and Lotze, M. T. (2019). Johnny on the Spot-Chronic Inflammation Is Driven by HMGB1. *Front. Immunol.* 10, 1561. doi:10.3389/fimmu.2019.01561

Gu, J., Xu, T., Huang, Q.-H., Zhang, C.-M., and Chen, H.-Y. (2019). HMGB3 Silence Inhibits Breast Cancer Cell Proliferation and Tumor Growth by Interacting with Hypoxia-Inducible Factor 1α. *Cancer Manag. Res.* 11, 5075–5089. doi:10.2147/CMAR.S204357

Jin, S., Yang, Z., Hao, X., Tang, W., Ma, W., and Zong, H. (2020). Roles of HMGB1 in Regulating Myeloid-Derived Suppressor Cells in the Tumor Microenvironment. *Biomark Res.* 8 (1), 21. doi:10.1186/s40364-020-00201-8

Jung, A. R., Kim, G. E., Kim, M. Y., Ha, U. S., Hong, S. H., Lee, J. Y., et al. (2021). HMGB1 Promotes Tumor Progression and Invasion through HMGB1/TNFR1/NF-Kb Axis in Castration-Resistant Prostate Cancer. *Am. J. Cancer Res.* 11 (5), 2215–2227.

Kang, R., Zhang, Q., Zeh, H. J., Lotze, M. T., and Tang, D. (2013). Hmgb1 in Cancer: Good, Bad, or Both. *Clin. Cancer Res.* 19 (15), 4046–4057. doi:10.1158/1078-0432.CCR-13-0495

Kwak, M. S., Kim, H. S., Lee, B., Kim, Y. H., Son, M., and Shin, J.-S. (2020). Immunological Significance of HMGB1 Post-Translational Modification and Redox Biology. *Front. Immunol.* 11, 1189. doi:10.3389/fimmu.2020.01189

Kwon, J.-H., Kim, J., Park, J. Y., Hong, S. M., Park, C. W., Hong, S. J., et al. (2010). Overexpression of High-Mobility Group Box 2 Is Associated with Tumor Aggressiveness and Prognosis of Hepatocellular Carcinoma. *Clin. Cancer Res.* 16 (22), 5511–5521. doi:10.1158/1078-0432.CCR-10-0825

Lee, J.-J., Park, I. H., Rhee, W. J., Kim, H. S., and Shin, J.-S. (2019). HMGB1 Modulates the Balance between Senescence and Apoptosis in Response to Genotoxic Stress. *FASEB j.* 33 (10), 10942–10953. doi:10.1096/fj.201900288R

Li, T., Fu, J., Zeng, Z., Cohen, D., Li, J., Chen, Q., et al. (2020a). TIMER2.0 for Analysis of Tumor-Infiltrating Immune Cells. *Nucleic Acids Res.* 48 (W1), W509–W514. doi:10.1093/nar/gkaa407

Li, Z., Zhang, Y., Sui, S., Hua, Y., Zhao, A., Tian, X., et al. (2020b). Targeting HMGB3/hTERT Axis for Radioresistance in Cervical Cancer. *J. Exp. Clin. Cancer Res.* 39 (1), 243. doi:10.1186/s13046-020-01737-1

Liao, Y., Wang, J., Jaehnig, E. J., Shi, Z., and Zhang, B. (2019). WebGestalt 2019: Gene Set Analysis Toolkit with Revamped UIs and APIs. *Nucleic Acids Res.* 47 (W1), W199–W205. doi:10.1093/nar/gkz401

Ma, L., Zeng, J., Mo, B., Wang, C., Huang, J., Sun, Y., et al. (2015). High Mobility Group Box 1: A Novel Mediator of Th2-Type Response-Induced Airway Inflammation of Acute Allergic Asthma. *J. Thorac. Dis.* 7 (10), 1732–1741. doi:10.3978/j.issn.2072-1439.2015.10.18

Mandke, P., and Vasquez, K. M. (2019). Interactions of High Mobility Group Box Protein 1 (HMGB1) with Nucleic Acids: Implications in DNA Repair and Immune Responses. *DNA Repair* 83, 102701. doi:10.1016/j.dnarep.2019.102701

Marin-Acevedo, J. A., Dholaria, B., Soyano, A. E., Knutson, K. L., Chumsri, S., and Lou, Y. (2018). Next Generation of Immune Checkpoint Therapy in Cancer: New Developments and Challenges. *J. Hematol. Oncol.* 11 (1), 39. doi:10.1186/s13045-018-0582-8

Marin-Acevedo, J. A., Kimbrough, E. O., and Lou, Y. (2021a). Next Generation of Immune Checkpoint Inhibitors and beyond. *J. Hematol. Oncol.* 14 (1), 45. doi:10.1186/s13045-021-01056-8

Marin-Acevedo, J. A., Kimbrough, E. O., Manochakian, R., Zhao, Y., and Lou, Y. (2021b). Immunotherapies Targeting Stimulatory Pathways and beyond. *J. Hematol. Oncol.* 14 (1), 78. doi:10.1186/s13045-021-01085-3

Mo, Y., Fang, R. H., Wu, J., Si, Y., Jia, S. Q., Li, Q., et al. (2019). MicroRNA-329 Upregulation Impairs the HMGB2/β-catenin Pathway and Regulates Cell Biological Behaviors in Melanoma. *J. Cel. Physiol.* 234 (12), 23518–23527. doi:10.1002/jcp.28920

Mukherjee, A., Huynh, V., Gaines, K., Reh, W. A., and Vasquez, K. M. (2019). Targeting the High-Mobility Group Box 3 Protein Sensitizes Chemoresistant Ovarian Cancer Cells to Cisplatin. *Cancer Res.* 79 (13), 3185–3191. doi:10.1158/0008-5472.CAN-19-0542

Mukherjee, A., and Vasquez, K. M. (2020). Targeting Chromosomal Architectural HMGB Proteins Could Be the Next Frontier in Cancer Therapy. *Cancer Res.* 80 (11), 2075–2082. doi:10.1158/0008-5472.CAN-19-3066

Musumeci, D., Roviello, G. N., and Montesarchio, D. (2014). An Overview on HMGB1 Inhibitors as Potential Therapeutic Agents in HMGB1-Related Pathologies. *Pharmacol. Ther.* 141 (3), 347–357. doi:10.1016/j.pharmthera.2013.11.001

Nagy, Á., Munkácsy, G., and Győrffy, B. (2021). Pancancer Survival Analysis of Cancer Hallmark Genes. *Sci. Rep.* 11 (1), 6047. doi:10.1038/s41598-021-84787-5

Nguyen, A., Bhavsar, S., Riley, E., Caponetti, G., and Agrawal, D. (2016). Clinical Value of High Mobility Group Box 1 and the Receptor for Advanced Glycation End-Products in Head and Neck Cancer: A Systematic Review. *Int. Arch. Otorhinolaryngol.* 20 (4), 382–389. doi:10.1055/s-0036-1583168

Nishino, M., Ramaiya, N. H., Hatabu, H., and Hodi, F. S. (2017). Monitoring Immune-Checkpoint Blockade: Response Evaluation and Biomarker Development. *Nat. Rev. Clin. Oncol.* 14 (11), 655–668. doi:10.1038/nrclinonc.2017.88

Niu, L., Yang, W., Duan, L., Wang, X., Li, Y., Xu, C., et al. (2020). Biological Functions and Theranostic Potential of HMGB Family Members in Human Cancers. *Ther. Adv. Med. Oncol.* 12, 175883592097085. doi:10.1177/1758835920970850

Rameshbabu, S., Labadie, B. W., Argulian, A., and Patnaik, A. (2021). Targeting Innate Immunity in Cancer Therapy. *Vaccines* 9 (2), 138. doi:10.3390/vaccines9020138

Randrian, V., Evrard, C., and Tougeron, D. (2021). Microsatellite Instability in Colorectal Cancers: Carcinogenesis, Neo-Antigens, Immuno-Resistance and Emerging Therapies. *Cancers* 13 (12), 3063. doi:10.3390/cancers13123063

Rapoport, B. L., Steel, H. C., Theron, A. J., Heyman, L., Smit, T., Ramdas, Y., et al. (2020). High Mobility Group Box 1 in Human Cancer. *Cells* 9 (7), 1664. doi:10.3390/cells9071664

Rhodes, D. R., Kalyana-Sundaram, S., Mahavisno, V., Varambally, R., Yu, J., Briggs, B. B., et al. (2007). Oncomine 3.0: Genes, Pathways, and Networks in a Collection of 18,000 Cancer Gene Expression Profiles. *Neoplasia* 9 (2), 166–180. doi:10.1593/neo.07112

Ru, B., Wong, C. N., Tong, Y., Zhong, J. Y., Zhong, S. S. W., Wu, W. C., et al. (2019). TISIDB: An Integrated Repository Portal for Tumor-Immune System Interactions. *Bioinformatics* 35 (20), 4200–4202. doi:10.1093/bioinformatics/btz210

Saillard, M., Cenerenti, M., Romero, P., and Jandus, C. (2021). Impact of Immunotherapy on CD4 T Cell Phenotypes and Function in Cancer. *Vaccines* 9 (5), 454. doi:10.3390/vaccines9050454

Sun, C.-X., Zhu, F., and Qi, L. (2021). Demethylated miR-216a Regulates High Mobility Group Box 3 Promoting Growth of Esophageal Cancer Cells Through Wnt/β-Catenin Pathway. *Front. Oncol.* 11, 622073. doi:10.3389/fonc.2021.622073

Tang, Z., Li, C., Kang, B., Gao, G., Li, C., and Zhang, Z. (2017). GEPIA: A Web Server for Cancer and Normal Gene Expression Profiling and Interactive Analyses. *Nucleic Acids Res.* 45 (W1), W98–W102. doi:10.1093/nar/gkx247

Taniguchi, N., Kawakami, Y., Maruyama, I., and Lotz, M. (2018). HMGB Proteins and Arthritis. *Hum. Cel* 31 (1), 1–9. doi:10.1007/s13577-017-0182-x

Thorsson, V., Gibbs, D. L., Brown, S. D., Wolf, D., Bortone, D. S., Ou Yang, T. H., et al. (2019). The Immune Landscape of Cancer. *Immunity* 51 (2), 411–412. doi:10.1016/j.immuni.2019.08.004

Vasaikar, S. V., Straub, P., Wang, J., and Zhang, B. (2018). Linkedomics: Analyzing Multi-Omics Data within and across 32 Cancer Types. *Nucleic Acids Res.* 46 (D1), D956–D963. doi:10.1093/nar/gkx1090

Veigas, F., Mahmoud, Y. D., Merlo, J., Rinflerch, A., Rabinovich, G. A., and Girotti, M. R. (2021). Immune Checkpoints Pathways in Head and Neck Squamous Cell Carcinoma. *Cancers* 13 (5), 1018. doi:10.3390/cancers13051018

Wang, W., Chapman, N. M., Zhang, B., Li, M., Fan, M., Laribee, R. N., et al. (2019). Upregulation of PD-L1 via HMGB1-Activated IRF3 and NF-Kb Contributes to UV Radiation-Induced Immune Suppression. *Cancer Res.* 79 (11), 2909–2922. doi:10.1158/0008-5472.CAN-18-3134

Wild, C. A., Bergmann, C., Fritz, G., Schuler, P., Hoffmann, T. K., Lotfi, R., et al. (2012). HMGB1 Conveys Immunosuppressive Characteristics on Regulatory and Conventional T Cells. *Int. Immunol.* 24 (8), 485–494. doi:10.1093/intimm/dxs051

Yi, M., Jiao, D., Xu, H., Liu, Q., Zhao, W., Han, X., et al. (2018). Biomarkers for Predicting Efficacy of PD-1/pd-L1 Inhibitors. *Mol. Cancer* 17 (1), 129. doi:10.1186/s12943-018-0864-3

Yu, H., Dong, L., Wang, H., Zhang, Y., Wang, Z., Wang, C., et al. (2021). LINC00504 Promotes the Malignant Biological Behavior of Breast Cancer Cells by Upregulating HMGB3 via Decoying MicroRNA-876-3p. *Cancer Manag. Res.* 13, 1803–1815. doi:10.2147/CMAR.S276290

Yuan, S., Liu, Z., Xu, Z., Liu, J., and Zhang, J. (2020). High Mobility Group Box 1 (HMGB1): A Pivotal Regulator of Hematopoietic Malignancies. *J. Hematol. Oncol.* 13 (1), 91. doi:10.1186/s13045-020-00920-3

Zhang, L., Han, J., Wu, H., Liang, X., Zhang, J., Li, L., et al. (2014). The Association of HMGB1 Expression with Clinicopathological Significance and Prognosis in Hepatocellular Carcinoma: A Meta-Analysis and Literature Review. *PLoS One* 9 (10), e110626. doi:10.1371/journal.pone.0110626

Zhang, Y., and Zhang, Z. (2020). The History and Advances in Cancer Immunotherapy: Understanding the Characteristics of Tumor-Infiltrating Immune Cells and Their Therapeutic Implications. *Cell. Mol. Immunol.* 17 (8), 807–821. doi:10.1038/s41423-020-0488-6

Zhao, B., Liu, P., Fukumoto, T., Nacarelli, T., Fatkhutdinov, N., Wu, S., et al. (2020). Topoisomerase 1 Cleavage Complex Enables Pattern Recognition and Inflammation during Senescence. *Nat. Commun.* 11 (1), 908. doi:10.1038/s41467-020-14652-y

Conflict of Interest: The authors declare that the research was conducted in the absence of any commercial or financial relationships that could be construed as a potential conflict of interest.

Publisher's Note: All claims expressed in this article are solely those of the authors and do not necessarily represent those of their affiliated organizations, or those of the publisher, the editors, and the reviewers. Any product that may be evaluated in this article, or claim that may be made by its manufacturer, is not guaranteed or endorsed by the publisher.

Copyright © 2021 Lin, Zhang, Lin and Peng. This is an open-access article distributed under the terms of the Creative Commons Attribution License (CC BY). The use, distribution or reproduction in other forums is permitted, provided the original author(s) and the copyright owner(s) are credited and that the original publication in this journal is cited, in accordance with accepted academic practice. No use, distribution or reproduction is permitted which does not comply with these terms.

frontiers in Genetics

ORIGINAL RESEARCH
published: 28 February 2022
doi: 10.3389/fgene.2022.811900

Identification of the Crucial Role of CCL22 in *F. nucleatum*-Related Colorectal Tumorigenesis that Correlates With Tumor Microenvironment and Immune Checkpoint Therapy

Hufei Wang[1†], Kangjia Luo[1†], Zilong Guan[1†], Zhi Li[2], Jun Xiang[1], Suwen Ou[1], Yangbao Tao[1], Songlin Ran[1], Jinhua Ye[1], Tianyi Ma[1], Tianyu Qiao[1], Zhiming Zhang[3], Yinghu Jin[1], Yanni Song[4]* and Rui Huang[1]**

[1]Department of Colorectal Cancer Surgery, The Second Affiliated Hospital of Harbin Medical University, Harbin, China, [2]Department of Obstetrics and Gynecology, Second Affiliated Hospital of Harbin Medical University, Harbin, China, [3]Department of Thoracic Surgery, Second Affiliated Hospital of Harbin Medical University, Harbin, China, [4]Department of Breast Surgery, The Third Affiliated Hospital of Harbin Medical University, Harbin, China

Colorectal cancer (CRC) is the third most common malignant cancer worldwide with the second highest mortality. Gut microbiota can educate the tumor microenvironment (TME), consequently influencing the efficacy of immune checkpoint inhibitors (ICIs). Fusobacterium *nucleatum* is one of the most crucial bacteria contributing to colorectal tumorigenesis, but the molecular mechanisms between *F. nucleatum* and TME or ICIs are poorly investigated. In the present study, we firstly analyzed differentially expressed genes and the biological functions between *F. nucleatum*-infected and uninfected CRC cell lines, with the findings that CCL22 mRNA expression was markedly upregulated after *F. nucleatum* infection. Moreover, the survival analysis showed that CCL22 was significantly associated with the overall survival of CRC patients. Gene Ontology and Kyoto Encyclopedia of Genes and Genomes analysis suggested that CCL22 was related to immune-related terms. Furthermore, the ESTIMATE analysis indicated that the high-CCL22-expression subgroup had a higher immune/stromal/estimate score and lower tumor purity. The CIBERSORT analysis indicated that the high-CCL22-expression group had more immune-suppressive cells and less antitumor immune cells. In addition, immune checkpoint genes and cytotoxic genes were positively correlated with CCL22 expression. The immunophenoscore analysis suggested that CCL22 was associated with the IPS-CTLA4 and PD1/PD-L1/PD-L2 score. Interestingly, CCL22 expression in the KRAS and APC mutation groups was markedly reduced compared to that of the wild groups. In summary, our study provided evidence that CCL22 might play a crucial role in *F. nucleatum*-related colorectal tumorigenesis and correlate with TME and ICIs, which deserves further study.

Keywords: *Fusobacterium nucleatum*, tumor microenvironment, immune checkpoint therapy, chemokines, CCL22

OPEN ACCESS

Edited by:
Jaideep Banerjee, Smith & Nephew, United Kingdom

Reviewed by:
Ehsan Nazemalhosseini-Mojarad, Shahid Beheshti University of Medical Sciences, Iran
Graziella Curtale, The Scripps Research Institute, United States

****Correspondence:***
Rui Huang
huangrui2019@163.com
Yanni Song
yannimd@126.com
Yinghu Jin
33887443@qq.com

[†]These authors have contributed equally to this work and share first authorship

Specialty section:
This article was submitted to Cancer Genetics and Oncogenomics, a section of the journal Frontiers in Genetics

Received: *09 November 2021*
Accepted: *11 January 2022*
Published: *28 February 2022*

Citation:
Wang H, Luo K, Guan Z, Li Z, Xiang J, Ou S, Tao Y, Ran S, Ye J, Ma T, Qiao T, Zhang Z, Jin Y, Song Y and Huang R (2022) Identification of the Crucial Role of CCL22 in F. nucleatum-Related Colorectal Tumorigenesis that Correlates With Tumor Microenvironment and Immune Checkpoint Therapy. Front. Genet. 13:811900. doi: 10.3389/fgene.2022.811900

INTRODUCTION

Colorectal cancer (CRC) is the third most common malignant cancer worldwide with the second highest mortality (Siegel et al., 2020a; Siegel et al., 2020b). In order to seek effective treatment options, it is urgent to find new therapeutic targets of CRC.

Fusobacterium nucleatum (*F. nucleatum*), a common member of the oral microbiota known to have a symbiotic relationship with its hosts, has been shown to play a critical role in the development of CRC. Studies have reported that *F. nucleatum* influenced cell metastasis, proliferation, and migration mediated by abnormalities of lncRNA expression, activation of autophagy, and alteration of metabolism (Yang et al., 2017; Yu et al., 2017; Hong et al., 2020). Importantly, *F. nucleatum* can influence colorectal tumorigenesis directly by regulating the tumor microenvironment (TME) *via* increasing myeloid-derived suppressor cells, inhibiting the receptors of natural killer (NK) cells, and controlling T-cell-mediated immune responses (Kostic et al., 2013; Mima et al., 2016; Dong et al., 2020; Serna et al., 2020), which significantly affected the therapeutic response and clinical outcome of patients (Quail and Joyce, 2013; Wood et al., 2014). Hence, dissecting the underlying mechanism of cross-talk between *F. nucleatum* and TME will help search for the potential therapeutic targets.

TME, mainly constituting immune cells and stromal cells (Guo et al., 2018; Stankovic et al., 2018), can shape the development of tumor and impact the response to tumor therapy (Böttcher et al., 2018). Regulating TME is one of the most promising strategies for tumor therapy—for instance, more $CD8^+$ T cell infiltration in CRC was generally associated with a favorable prognosis (Galon et al., 2006; Nazemalhosseini-Mojarad et al., 2019). In addition, studies have shown that TME also influenced the response to immune checkpoint inhibitors (ICIs). Christopher *et al.* found that successful anti-PD-1 immunotherapy required the communication of T cells and dendritic cells, which involves the cytokines (Garris et al., 2018). Another study revealed that the efficacy of anti-CTLA-4 therapy relied on regulatory T cell (Treg) depletion during treatment (Arce Vargas et al., 2018). Yu *et al.* also pointed out that re-modulating the TME enhanced the effect of anti-PD-1 immunotherapy in CRC patients with microsatellite stability (Yu et al., 2019). However, the specific molecular mechanisms underlying the interactions between *F. nucleatum* and the TME or ICIs are poorly understood.

Chemokines, a family of low-molecular-weight proteins, are important parts of the communication of tumor cells and the TME and involved in shaping the immune system in modulating immune cell infiltration (Cabrero-de Las Heras and Martínez-Balibrea, 2018). As a member of the chemokine family, CCL22 was reported to promote Treg communication with dendritic cells to control immunity through their CCR4 receptor in lymph nodes (Rapp et al., 2019). CCL22 also promoted Treg recruitment into the TME and inhibited anticancer immunity in melanoma (Anz et al., 2015; Martinenaite et al., 2016). In addition, some studies showed that CCL22 mRNA expression was significantly higher in tumor tissue compared with paired normal tissue in colorectal adenocarcinomas (Wågsäter et al., 2008; Huang et al., 2015; Heeran et al., 2021). Notably, CCL22 was expressed on exposure to gut microbiota and correlated with Treg and Th1 in CRC (Cremonesi et al., 2018). Wang *et al.* found that the upregulation of CCL22 recruited Th17 cells to promote colon carcinogenesis in miR-34a−/− mice infected by *Citrobacter rodentium* (Wang et al., 2018), which linked the upregulation of CCL22 to the gut microbiota. However, the role of CCL22 in *F. nucleatum*-associated TME has not been well studied.

In this research, we firstly found that the expression of CCL22 was upregulated in CRC cell lines infected by *F. nucleatum* using Gene Expression Omnibus (GEO) datasets. The upregulation of CCL22 was accompanied by an increase in immune score and a decrease in stromal score in patients of The Cancer Genome Atlas (TCGA) colon adenocarcinoma (COAD). A further analysis of the composition of immune cells in the TME showed that the high-CCL22-expression subgroup had more immune-suppressive cells (such as Treg and T follicular helper cells) and less antitumor immune cells (such as activated NK cells). In addition, CCL22 was positively correlated with immune checkpoint genes (BTLA, CTLA4, TIGIT, HAVCR2, CD274, PDCD1, and LAG3) and cytotoxic genes (TNFSF11, GZMA, IFNG, PRF1, GZMK, and GZMM). The IPS-CTLA4 and PD1/PD-L1/PD-L2 score was higher in the high-CCL22-expression subgroup. We also found that the expression of CCL22 was related to overall survival (OS), M stage, APC mutation, and KRAS mutation in TCGA COAD patients. In summary, these results indicated that CCL22 might play a pivotal role in *F. nucleatum*-related colorectal tumorigenesis and correlate with the TME and immune checkpoint therapy.

MATERIALS AND METHODS

Data Source

The RNA expression data of CRC cell lines infected by *F. nucleatum* was downloaded from the GEO database, with accession numbers GEO: GSE141805 (HCT-116) and GSE90944 (HT-29), which respectively contains three pairs of samples (*F. nucleatum vs.* control). In addition, the RNA expression data and clinicopathological information of TCGA COAD were obtained from the TCGA database using the "TCGA-biolinks" package in R Studio (Colaprico et al., 2016). Count value was transformed to transcripts per million (TPM) for further analysis, and GSE39582, with a large sample size and complete survival information, was downloaded as a validation dataset. All data were normalized to ensure standardization. The gene symbols that were detected in more than one probe were kept for further analysis. In total, 20,407 immune-related genes (IRGs) were downloaded from the Molecular Signature Database (MSigDB) C7 immunologic signature gene sets (Subramanian et al., 2005). The detailed information of datasets and online websites used in our study are shown in **Table 1** and **Table 2**.

Differential Gene Analysis

GSE141805 and GSE90944 were used to explore the differentially expressed genes (DEGs) between *F. nucleatum*-infected and uninfected CRC cell lines *via* the R package "edgeR" in R

TABLE 1 | Detailed information of the datasets used in our study.

Data name	Experiment type	Sample	Usage
GSE141805	High-throughput sequencing	*F. nucleatum*-treated HCT-116 colorectal cancer (CRC) cell lines (3)	Differential analysis
		Normal control HCT-116 CRC cell lines (3)	Gene set variation analysis (GSVA)
GSE90944	High-throughput sequencing	*F. nucleatum*-treated HT-29 CRC cell lines (3)	Differential analysis
		Normal control HT-29 CRC cell lines (3)	GSVA
GSE39582	Array	Survival analysis (536)	Survival analysis
TCGA COAD	High-throughput sequencing	Colon cancer samples (480)	Correlation analysis
			Immunophenoscore analysis
		Survival analysis (453)	Survival analysis
		Mutation analysis (399)	Mutation analysis

TABLE 2 | Detailed information of the online websites used in our study.

Website name	Version	Usage	Accession
MSigDB	v7.4	To download immune-related genes from C7	http://gsea-msigdb.org/gsea/msigdb/
		To obtain the reference gene set for gene set variation analysis from C2. kegg	
GEPIA	v1.0	To obtain the top 100 genes with expression similar to CCL22	http://gepia.cancer-pku.cn/
TIMER	v2.0	To analyze the relationships between CCL22 expression and KRAS/APC mutation	http://timer.comp-genomics.org/
TCIA	v1.0	To obtain the immunophenoscore of The Cancer Genome Atlas colon adenocarcinoma that predicts the response to immune checkpoint inhibitors	https://tcia.at/

Studio (Robinson et al., 2010). The cutoff threshold is p-value <.05 and $|\log2FC| \geq 1$. To select the IRGs related to *F. nucleatum* infection, immune-related (IR) DEGs were obtained by intersecting IRGs and DEGs, which were visualized using the "venn" package.

Gene Set Variation Analysis

Gene set variation analysis (GSVA) was performed to investigate the underlying functions and pathways affected by *F. nucleatum* with the "GSVA" package (Hänzelmann et al., 2013). The gene set "c2.cp.kegg.v6.2.symbols.gmt" in MSigDB was selected as the reference gene set. The heat map of enrichment terms was visualized using the "pheatmap" package.

K–M Survival Analysis

To further analyze the prognostic power of the IR DEGs, patients of TCGA-COAD and GSE39582 were divided into high-expression and low-expression subgroups based on the median expression value of each differentially expressed (DE) IRG, and a survival analysis was conducted by the Kaplan–Meier (K–M) method using the "survival" package.

Functional Enrichment Analysis

To explore the potential biological functions related to CCL22, the top 100 genes expressing similarly to CCL22 (Sun et al., 2021), downloaded from GEPIA 1.0 website (Tang et al., 2017), were subjected to Gene Ontology (GO) and Kyoto Encyclopedia of Genes and Genomes (KEGG) analysis using the "clusterProfiler" package (Yu et al., 2012), which was also used for the visualization of enrichment terms. In addition, Gene Set Enrichment Analysis (GSEA) was applied to explore the changed biological functions based on the high- and low-CCL22-expression subgroups in TCGA COAD using the "clusterProfiler" package. The GSEA results of GO and KEGG were respectively calculated based on MSigDB c5.all.v7.0.symbols.gmt and c2.cp.kegg.v7.0.symbols.gmt in R studio, which was visualized using the "enrichplot" package.

Evaluation of Tumor Microenvironment

To dissect the TME associated with CCL22, TCGA-COAD TPM was used to calculate the estimate/immune/stromal score and tumor purity using the "estimate" package based on the high- and low-CCL22-expression subgroups (Yoshihara et al., 2013). Then, the "CIBERSORT" package was used to estimate the proportions of 22 types of immune cells in the TME (Newman et al., 2015).

Immunophenoscore Analysis

Immunophenoscore (IPS), calculated based on the four main types of genes that determine immunogenicity, has the ability to predict the patients' response to ICIs (Charoentong et al., 2017). The IPS range is between 0 and 10. The higher the score, the stronger the immunogenicity and the better the response to ICIs. The IPSs of TCGA COAD patients were downloaded from The Cancer Immunome Atlas (TCIA) (Charoentong et al., 2017).

Mutation Analysis

The mutation data of 399 COAD patients were obtained from the TCGA website, which was analyzed using the "maftools" package in R Studio (Mayakonda et al., 2018). The tumor mutation burden (TMB) was calculated using the formula: (total mutation / total covered bases) × 106. Then, TIMER 2.0 website was used to investigate the CCL22 mutation status in COAD and the correlation between APC/KRAS mutation and CCL22 expression (Li et al., 2020).

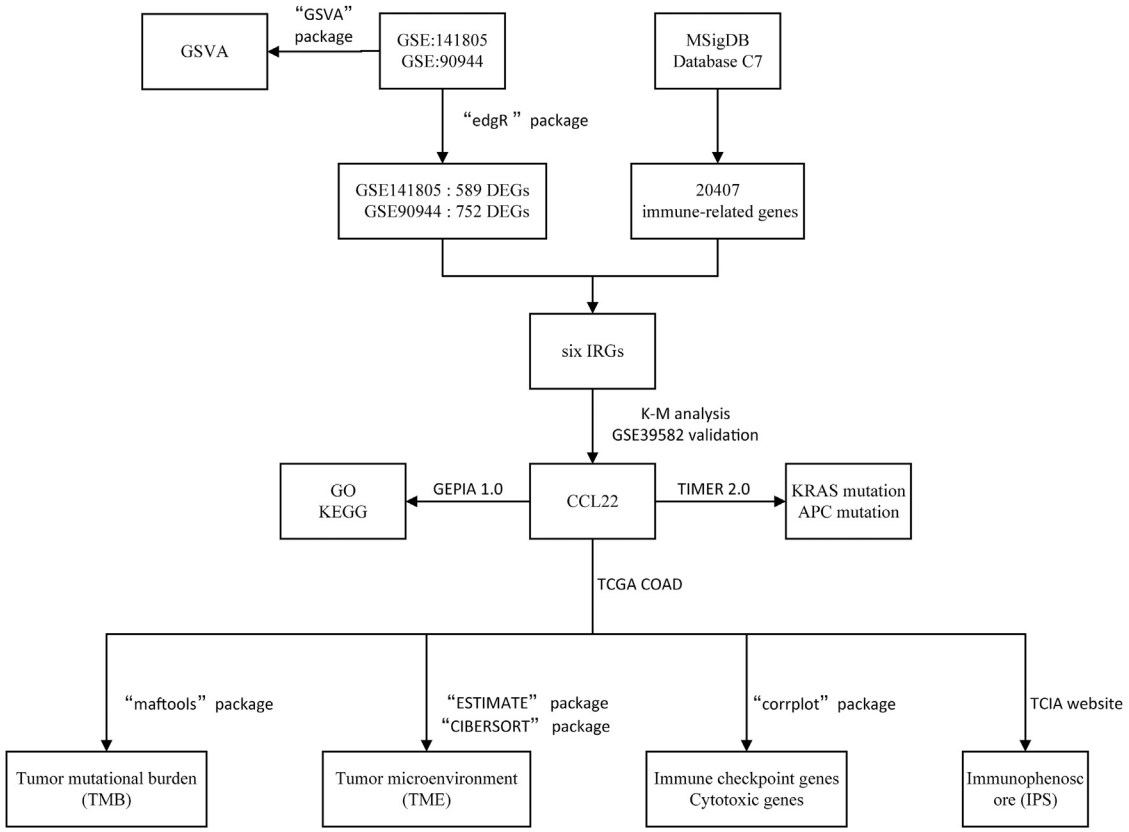


FIGURE 1 | Flow diagram of the present study.

Statistical Analysis

All statistical analyses were performed in R 4.0.3 and its appropriate packages. Data were analyzed with standard statistical tests as appropriate. * represented p <.05, ** represented p <.01, *** represented p <.001, and ns represented no statistical difference.

RESULTS

F. nucleatum Affects Gene Expression and Biological Functions in Colorectal Cancer Cells

The flow diagram of our study is shown in **Figure 1**. Based on p-value <.05 and |log2FC| ≥ 1.0, we respectively obtained 752 DEGs (373 upregulated and 379 downregulated) in GSE90944 and 589 DEGs (260 up upregulated and 329 downregulated) in GSE141805, which were displayed as volcano plots (**Figures 2A,B**). The top 50 DEGs were visualized using heat maps (**Figures 2C,D**). The detailed information of the DEGs is shown in **Supplementary Table S1**. GSVA was used to further investigate the biological function affected by *F. nucleatum* infection. The biological functions were visualized according to p-value <.05 and |log2FC| ≥ 1.0 (**Figures 2E,F**; **Supplementary Table S2**). Surprisingly, there were some biological functions that we were interested in. As shown in **Figure 2E**, we found that "GO_SUCCINATE_METABOLIC_PROCESS" was downregulated and "GO_REGULATION_OF_ACTIVATION_INDUCED_CELL_DEATH_OF_T_CELLS", "GO_REGULATION_OF_MAST_CELL_CYTOKINE_PRODUCTION", and "GO_REGULATION_OF_NK_T_CELL_PROLIFERATION" were upregulated in GSE90944. In GSE141805 (**Figure 2F**), "TIAN_TNF_SIGNALING_VIA_NFKB" and "GO_CCR6_CHEMOKINE_RECEPTOR_BINDING" were upregulated, and "GO_COENZYME_A_METABOLIC_PROCESS" and "GO_CELLULAR_RESPONSE_TO_CISPLATIN" were downregulated. The enrichment biological functions highlighted the crucial role of tumor immunity in *F. nucleatum*-related colorectal cancer.

CCL22 Plays a Crucial Role in Colorectal Cancer Cells Infected by *F. nucleatum*

To explore the relationship between *F. nucleatum* and immunity, we intersected DEGs of the two datasets with IRGs, and a total of six genes remained, including BIRC3, CCL22, CPT1B, ELMO1, PLA2G4C, and SLC25A2 (**Figure 3A**). Among them, CCL22, BIRC3A, and CPT1B were significantly upregulated under *F. nucleatum* treatment in two datasets. To further determine the meaningful genes, we performed K–M analysis according to the

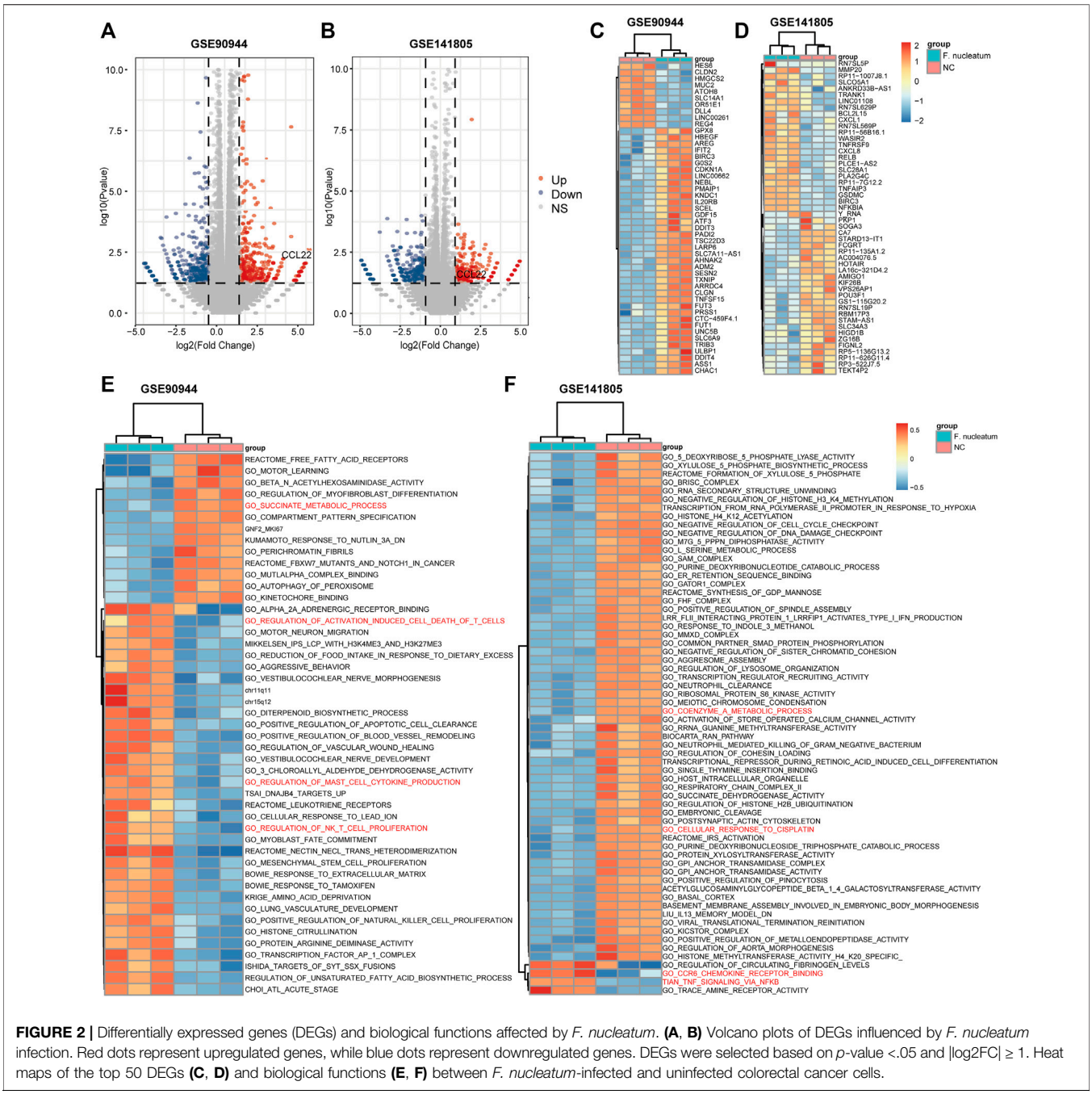


FIGURE 2 | Differentially expressed genes (DEGs) and biological functions affected by *F. nucleatum*. **(A, B)** Volcano plots of DEGs influenced by *F. nucleatum* infection. Red dots represent upregulated genes, while blue dots represent downregulated genes. DEGs were selected based on *p*-value <.05 and |log2FC| ≥ 1. Heat maps of the top 50 DEGs **(C, D)** and biological functions **(E, F)** between *F. nucleatum*-infected and uninfected colorectal cancer cells.

high- and low-expression subgroups of each DE IRG in TCGA (**Figures 3B–G**) and GSE90944 (**Supplementary Figure S1**). Interestingly, CCL22 (p = .011) and CTP1B (p = .021) were selected as meaningful genes in patients of TCGA COAD (**Figures 3B,C**), but only CCL22 was validated in GSE39582 (**Figure 3H**), with p = .014. CCL22 was differentially expressed in the subgroup analyses according to tumor M stage in TCGA COAD (**Figure 3I**). By reviewing the literatures, we found that the upregulation of CCL22 played an important role in bacterial and viral infection-associated tumors (Yang et al., 2012; Wang et al., 2018). Hence, we identified CCL22 for further study.

CCL22 Associated With Immune-Related Biological Functions

To dissect the biological functions of CCL22, we identified the top 100 associated genes of CCL22 in COAD using the GEPIA database, followed by KEGG pathway enrichment analysis and

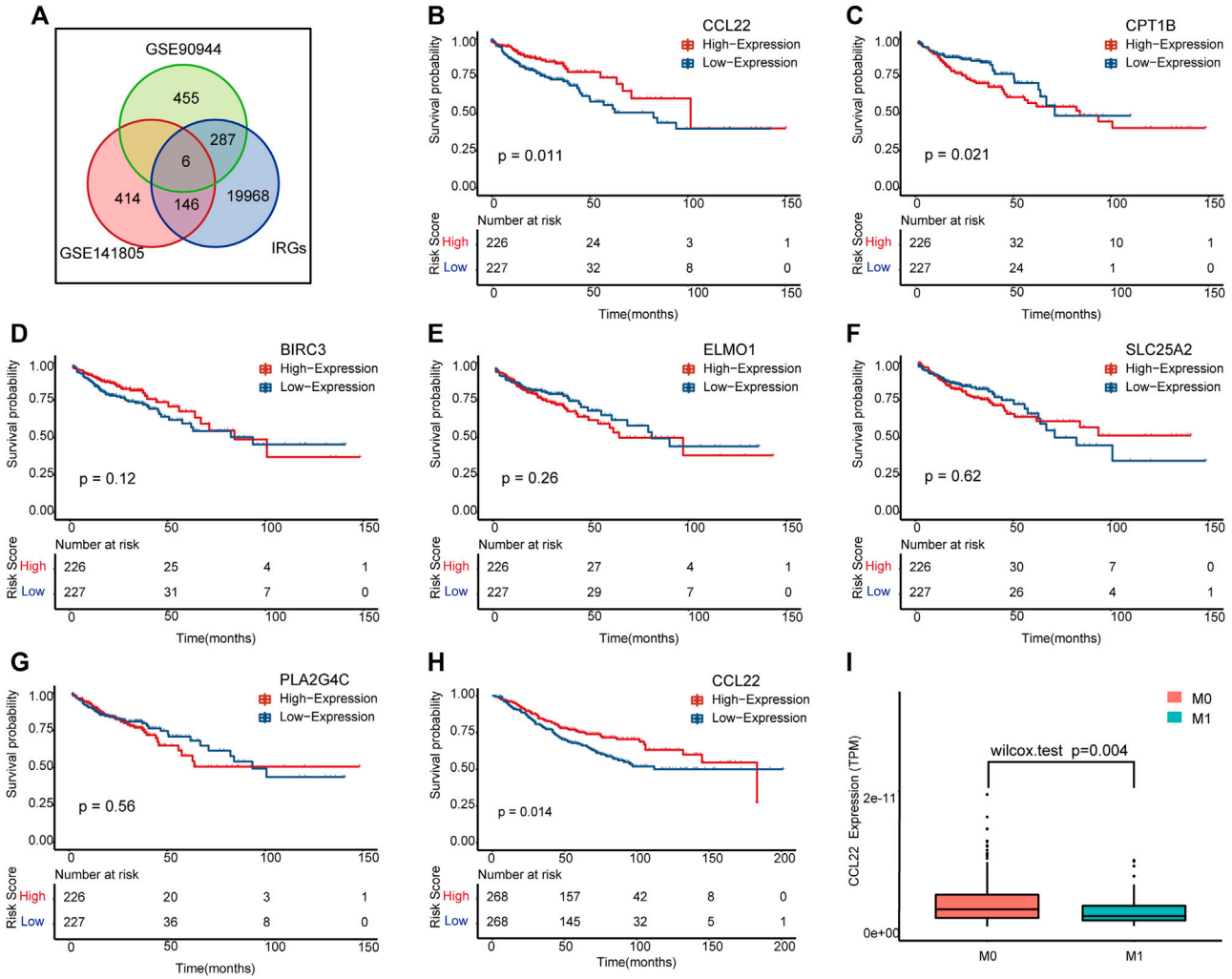


FIGURE 3 | The meaningful immune-related (IR) differentially expressed genes (DEGs) influenced by *F. nucleatum*. **(A)** Venn diagram showing the common genes in GSE90944, GSE141805, and immune-related genes. **(B–G)** Kaplan–Meier survival plots of the IR DEGs in The Cancer Genome Atlas (TCGA) colon adenocarcinoma (COAD). **(H)** Kaplan–Meier survival plot of CCL22 in GSE39582. **(I)** Box plot of CCL22 expression between M0 and M1 stages in TCGA COAD.

GO functional enrichment analysis (**Supplementary Table S3**). As shown in **Figure 4A**, the significantly enriched GO (ALL) terms included "T cell activation", "regulation of leukocyte cell–cell adhesion", and "lymphocyte proliferation", which indicated the role of CCL22 in regulating the immune function. The detailed information of GO (BP, CC, and MF) terms are shown in **Supplementary Figure S2**. The enriched KEGG pathways were as follows: "cytokine–cytokine receptor interaction", "chemokine signaling pathway", "intestinal immune network for IgA production", and "inflammatory bowel disease", indicating the potential role of CCL22 in gastrointestinal diseases (**Figure 4B**). Interestingly, we also found that the "NF-kappa B signaling pathway" was related to CCL22, which suggested a potential relationship among NF-kappa B signaling pathway, *F. nucleatum*, and CCL22. In addition, GSEA revealed that GO functions, such as cell–cell signaling by WNT, B cell differentiation, and chemokine production, were markedly enriched in the high-CCL22-expression subgroup (**Figure 4C**). As for the KEGG pathways, GSEA showed that B cell receptor, chemokine, JAK STAT, and the MAPK signaling pathway were enriched in the high-CCL22-expression subgroup (**Figure 4D**; Supplementary Table S4).

CCL22 Modulates the Tumor Microenvironment in TCGA COAD

Studies have shown that chemokines recruited immune cells into tumor beds and influenced the TME (Marques et al., 2019). To explore whether CCL22 regulated the TME of COAD, ESTIMATE analysis was used to calculate the immune/stromal/estimate score and tumor purity of each patient. We excitedly found that the immune/stromal/estimate scores (**Figures 5A–C**) were significantly higher, while tumor purity (**Figure 5D**) was significantly lower in the high-CCL22-expression subgroup compared to the low-CCL22-expression subgroup, which suggested that CCL22 was closely

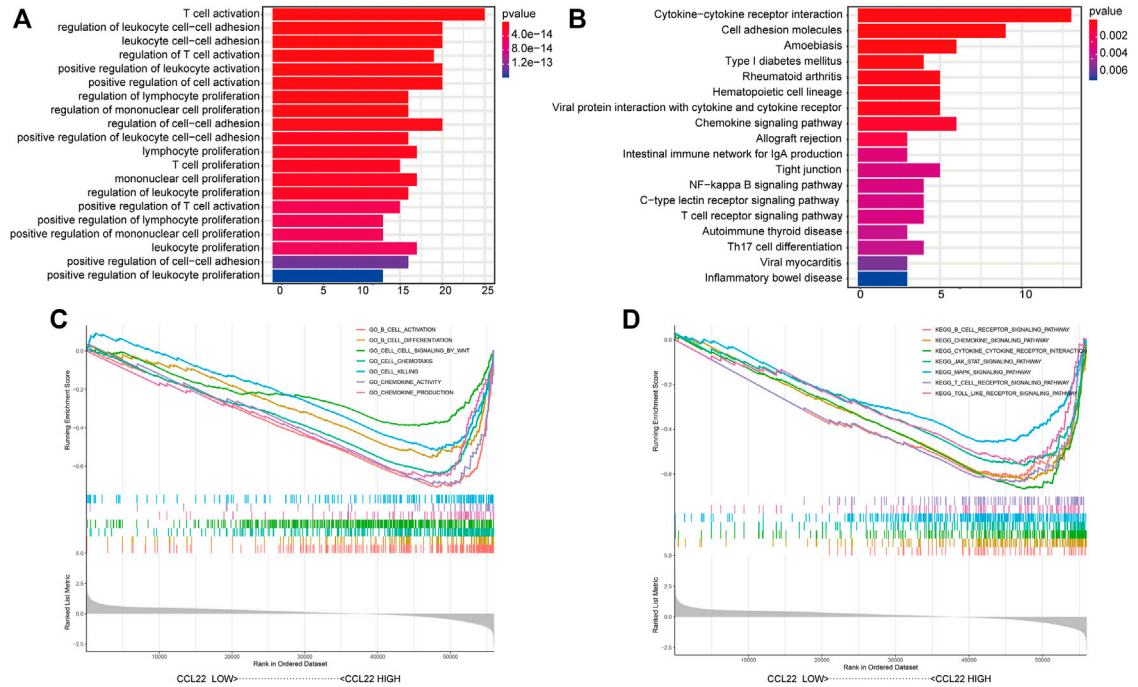


FIGURE 4 | Biological function analysis of CCL22. Representative Gene Ontology (GO) functions **(A)** and Kyoto Encyclopedia of Genes and Genomes (KEGG) pathways **(B)** of the top 100 genes with expression similar to CCL22. Representative Gene Set Enrichment Analysis results of GO functions **(C)** and KEGG pathways **(D)** based on MSigDB.

related to TME. Then, TPM value was applied to the CIBERSORT algorithm to further determine the composition of immune cells in TCGA COAD tissues with a different CCL22 expression status. We found that CCL22 was positively associated with Treg ($p < .001$), naive B cells ($p < .05$), activated dendritic cells ($p < .01$), neutrophils ($p < .01$), and T follicular helper cell ($p < .05$), while it was negatively associated with activated NK cells ($p < .05$) and monocytes ($p < .001$) in COAD, as shown in **Figure 5E**.

CCL22 Related to Immune Checkpoint Therapy

Studies have shown that the TME is closely related to the efficacy of immune checkpoint therapy (Tumeh et al., 2014; Hegde et al., 2016). To explore whether CCL22 was also associated with immune checkpoint therapy in COAD, the correlations between CCL22 and immune checkpoint molecules were analyzed (Kim et al., 2017; Nishino et al., 2017; Zhai et al., 2018). As shown in **Figure 6A**, we found that CCL22 was positively related to BTLA, CTLA4, TIGIT, HAVCR2, CD274, PDCD1, and LAG3 (correlation value = 0.38, 0.54, 0.51, 0.4, 0.24, 0.29, and 0.2; all *p*-value <.05). As shown in **Figure 6B**, CCL22 expression was positively correlated with cytotoxic genes, such as TNFSF11, GZMA, IFNG, PRF1, GZMK, and GZMM (correlation value = 0.31, 0.21, 0.18, 0.23, 0.32, and 0.35; all *p*-value <.05). It has been reported that IPS is a predictor of response to ICIs based on the TCGA data. To explore the relationship between CCL22 and IPS, the IPS of TCGA COAD was downloaded from the TCIA website. Although there was no statistical difference in IPS-PD1/PD-L1/PD-L2 score and IPS-CTLA4 score between the high- and low-CCL22-expression subgroups (**Figures 6D,E**), the high-CCL22-expression subgroup had a statistically higher IPS-CTLA4 and PD1/PD-L1/PD-L2 score (**Figure 6C**).

CCL22 Associated With APC and KRAS Mutation in TCGA COAD

Firstly, we explored the mutation status of CCL22 using the Gene_Mutation module of TIMER 2.0 website. As shown in **Figure 7B**, only 2 of the 406 samples had CCL22 mutation in COAD, much lower than APC mutation (286 of the 406 samples) and KRAS mutation (174 of the 406 samples), which are shown in **Supplementary Figure S3**. The top four mutation genes in COAD were APC, TP53, TTN, and KRAS (**Figure 7A**). The mutation of the above-mentioned genes was closely related to colorectal tumorigenesis. Although there was no difference in TMB between the high- and low-CCL22-expression subgroups (**Figure 7C**), we were surprised to find that the expression of CCL22 was significantly decreased in the APC and KRAS mutation groups in the Gene_Mutation module of TIMER2.0 website (**Figure 7D**). This strongly supported the idea that CCL22 might play an important role in colorectal tumorigenesis.

DISCUSSION

Mounting evidence supports that gut microbiota has a profound influence on the effectiveness of tumor immunotherapy (Vétizou

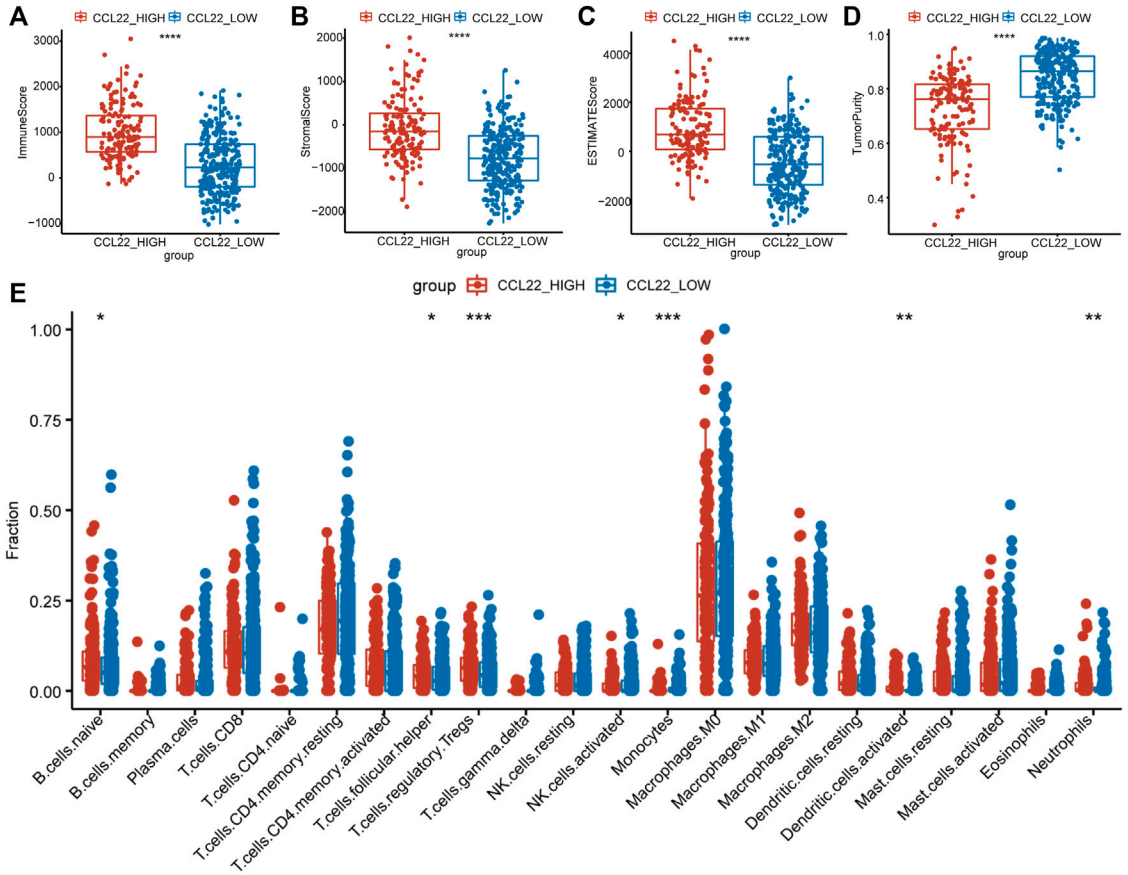


FIGURE 5 | Tumor microenvironment changes associated with CCL22 in The Cancer Genome Atlas colon adenocarcinoma. **(A)** The immune score, **(B)** stromal score, **(C)** estimated score, and **(D)** tumor purity and **(E)** the proportion of 22 types of infiltrating immune cells in high- and low-CCL22-expression subgroups.

et al., 2015; Gopalakrishnan et al., 2018)—for example, *Enterococcus hirae* and *Barnesiella intestinihominis* enhance cyclophosphamide-induced therapeutic immunomodulatory effects (Daillère et al., 2016). Besides this, *Akkermansia muciniphila* can specifically facilitate the effect of PD-1-based immunotherapy by recruiting T lymphocytes into the tumor beds (Routy et al., 2018), thus suggesting the enormous potential of gut microbiota in regulating the TME and influencing antitumor immune. As one of the most crucial bacteria related to CRC, *F. nucleatum* can influence colorectal tumorigenesis directly by increasing myeloid-derived suppressor cells, inhibiting receptors of NK cells, and controlling T-cell-mediated immune responses (Kostic et al., 2013; Mima et al., 2016; Dong et al., 2020; Serna et al., 2020). The molecular mechanisms underlying the interactions between *F. nucleatum* and the TME or immunotherapy are deemed to be further investigated.

In the present research, we firstly analyzed the gene expression and biological functions between *F. nucleatum*-infected and uninfected CRC cell lines. In total, 589 and 752 DEGs were respectively obtained in the GSE141805 and GSE90944 datasets. We found that *F. nucleatum* upregulated "TIAN_TNF_SIGNALING_VIA_NFKB". Studies showed that the activation of NF-kappaB induced by *F. nucleatum* participated in metastasis, proliferation, and chemoresistance to 5-fluorouracil (5-Fu) in CRC (Yang et al., 2017; Zhang et al., 2019; Chen et al., 2020). The downregulation of "GO_CELLULAR_RESPONSE_TO_CISPLATIN" suggested that *F. nucleatum* may contribute to chemoresistance to oxaliplatin in CRC, and Hong *et al.* pointed out that *F. nucleatum* promoted carcinogenesis *via* increasing CRC cell glucose metabolism (Hong et al., 2020). According to our analysis, "GO_COENZYME_A_METABOLIC_PROCESS" and "GO_SUCCINATE_METABOLIC_PROCESS" may also be potential mechanisms of colorectal carcinogenesis induced by *F. nucleatum*. What is more, "GO_REGULATION_OF_ACTIVATION_INDUCED_CELL_DEATH_OF_T_CELLS", "GO_REGULATION_OF_MAST_CELL_CYTOKINE_PRODUCTION", and "GO_REGULATION_OF_NK_T_CELL_PROLIFERATION" were upregulated. The enrichment biological functions also highlighted the crucial role of tumor immunity in *F. nucleatum*-related CRC, which has been validated in many studies (Kostic et al., 2013; Mima et al., 2015; Hamada et al., 2018).

Modulating tumor immunity was considered to be the most promising treatment for tumor, so we further dissected the effect

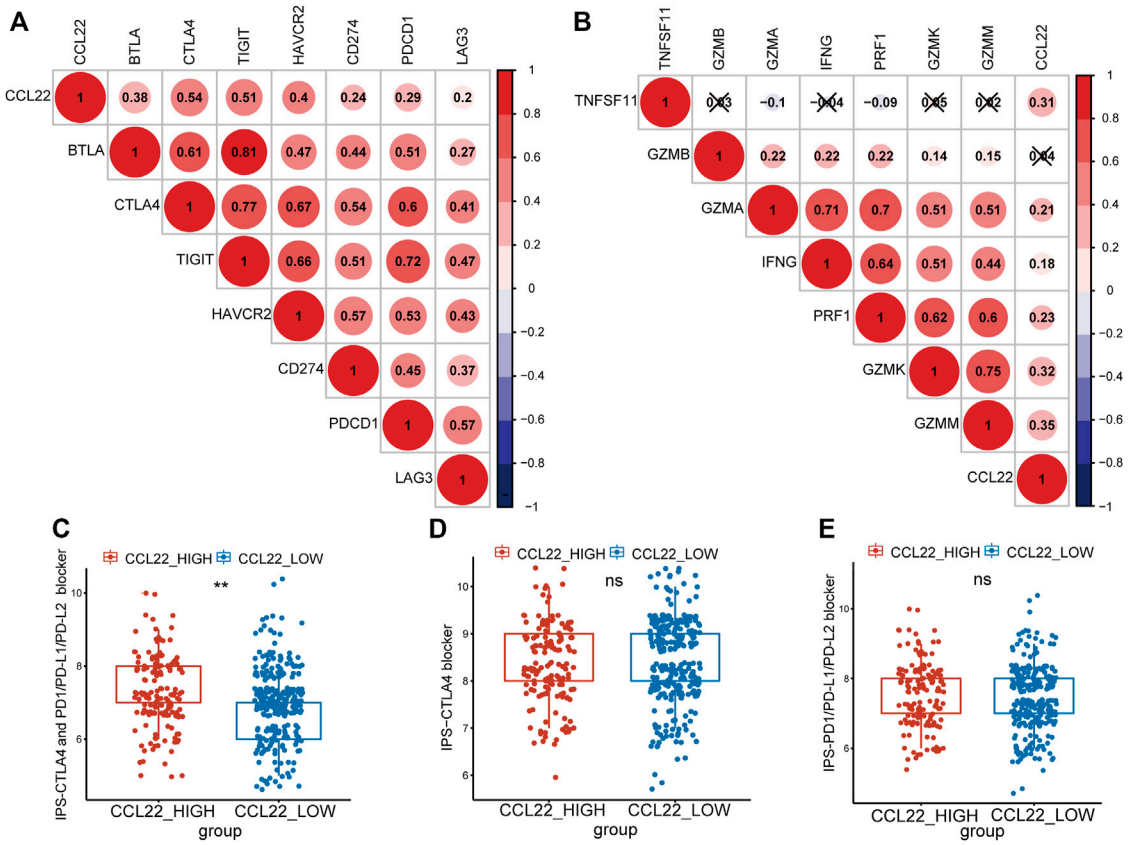


FIGURE 6 | Relationship between CCL22 expression and response to immune checkpoint inhibitors. **(A)** The correlation between CCL22 expression and immune checkpoint genes and **(B)** cytotoxic genes. Red is positive, and blue is negative. The symbol "x" represented a *p*-value >.05, and the circles without "x" meant *p*-value <.05. The numbers in the circle represented the correlation value. Box plots showing the association between **(C)** IPS-CTLA4 and PD1/PD-L1/PD-L2, **(D)** IPS-CTLA4, and **(E)** IPS-PD1/PD-L1/PD-L2 scores and CCL22 expression in patients of The Cancer Genome Atlas colon adenocarcinoma.

of *F. nucleatum* on tumor immunity. By intersecting with IRGs, we finally obtained six DE IRGs, including BIRC3, CCL22, CPT1B, ELMO1, PLA2G4C, and SLC25A2. Surprisingly, BIRC3 was reported to upregulate after *F. nucleatum* infection and promote chemoresistance to 5-Fu in CRC (Zhang et al., 2019), which suggested the reliability of our analysis. Furthermore, the survival analysis showed that CCL22 was significantly related to the OS and M stages of CRC patients in TCGA COAD. The prognostic power of CCL22 was also validated in GSE39582. Hence, we identified CCL22 for further study, and GO and KEGG analysis showed that CCL22 were mainly related to immune-related functions. Interestingly, we found that "NF-kappa B signaling pathway" was related to CCL22, which was also induced by *F. nucleatum* infection. This evidence suggested the potential relationships among NF-kappa B signaling pathway, *F. nucleatum*, and CCL22.

It has been reported that CCL22, a member of the chemokine family, can recruit immune cells to rewire the TME *via* binding to CCR4 (Rapp et al., 2019). Our study found that the high-CCL22-expression subgroup had a higher immune/stromal/estimate score and lower tumor purity. The high-CCL22-expression subgroup with a markedly higher immune score suggested more immune cell infiltration. Further analysis of the proportion of various immune cells indicated that the high-CCL22-expression subgroup had more immune-suppressive cells (such as Tregs and T follicular helper cells) and less antitumor immune cells (such as activated NK cells). It seemed that CCL22 induced the immune-suppressive TME to promote colorectal tumorigenesis, and it might be a potential target for *F. nucleatum* to affect the TME.

Immune checkpoint inhibitors show great potential in multiple cancers, such as melanoma, bladder cancer, and prostate cancer (Topalian et al., 2012). However, in CRC, only MSI-H patients (Ganesh et al., 2019), a small proportion of CRC, benefit from ICIs. Our study discovered that the CCL22 mRNA expression was positively correlated with immune checkpoint molecules and cytotoxic genes (Garzón-Tituaña et al., 2020), which were reported to influence the functions of immunocytes (Garzón-Tituaña et al., 2020; Cao et al., 2021). These clues indicated that high-CCL22-expression patients may have a better response to ICIs. It has been reported that IPS was a predictor of response to ICIs based on the TCGA data. A higher

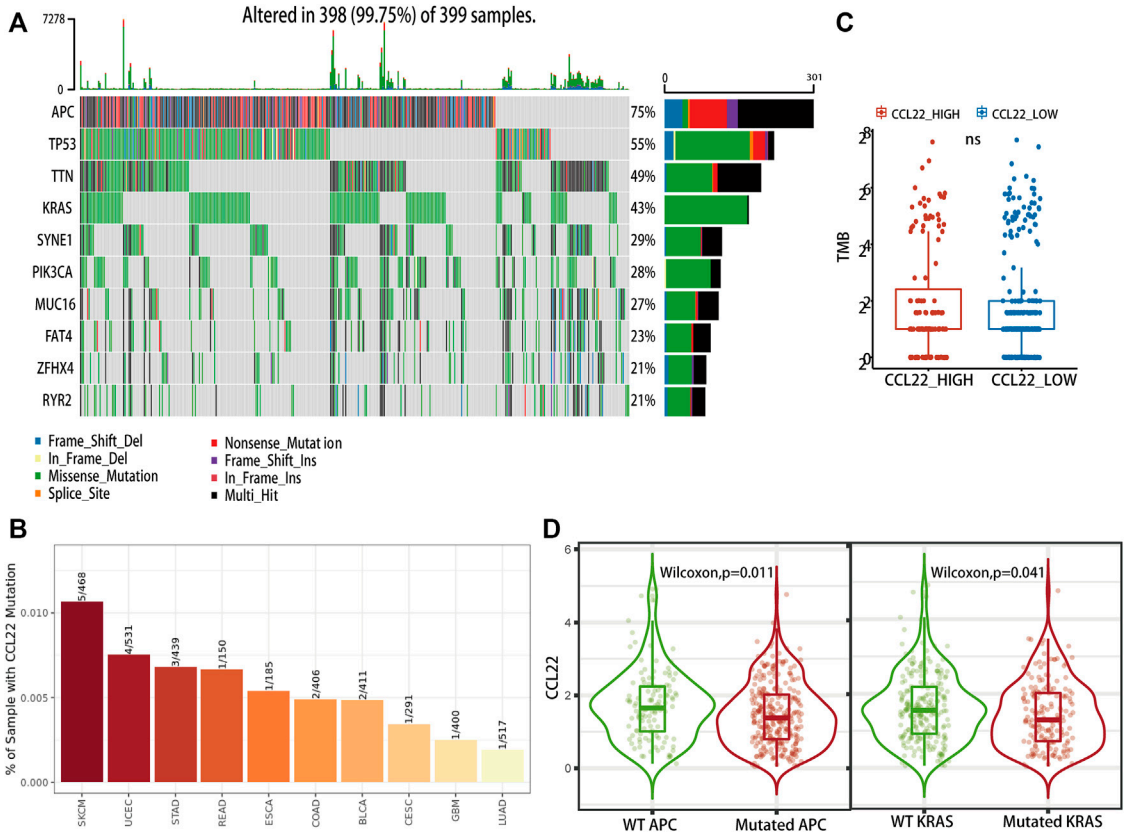


FIGURE 7 | Mutation landscape related to CCL22 in The Cancer Genome Atlas (TCGA) colon adenocarcinoma (COAD). **(A)** Oncoplot showing the top 10 mutational genes in TCGA COAD). **(B)** Mutation status of CCL22 in different cancer types. **(C)** Relationship between CCL22 expression and tumor mutation burden in TCGA COAD. **(D)** Violin plots showing the CCL22 expression in mutant and wild groups of APC and KRAS.

IPS score predicted better response to ICIs (Yan et al., 2021). In the present study, we found that the high-CCL22-expression subgroup had statistically higher IPS-CTLA4 and PD1/PD-L1/PD-L2 scores, which also suggested that high-CCL22-expression patients had a better response to the CTLA4 and PD1/PD-L1/PD-L2 combination therapy. Surprisingly, Rapp *et al.* also pointed out that the CCL22–CCR4 axis may serve as an immune checkpoint and was important for inhibiting T cell immunity (Rapp et al., 2019). Klarquist *et al.* found that the vaccination of CCL22 led to redirecting Treg away from tumors, and the repetitive vaccination with CCL22 sufficiently limited Treg accumulation and tumor growth in animals, which carried the potential of local vaccination of CCL22 to enhance the therapeutic effect of ICIs (Klarquist et al., 2016). All of these highlighted the potential role of CCL22 in ICIs.

TMB, defined as the total number of non-synonymous mutations in the coding regions of genes, has been reported as an effective predictor of response to ICIs (Sen et al., 2019). In patients of TCGA COAD, we did not find a statistically different TMB between the high- and low-CCL22-expression subgroups. However, the expression of CCL22 was higher in the KRAS and APC mutation groups compared to the KRAS and APC wild groups. APC and KRAS are the most predominant mutation genes closely associated with colorectal tumorigenesis (Fearon, 2011). In addition, APC mutation was used to construct a spontaneous tumorigenesis mice model of CRC in biological experiments (Moser et al., 1995; Yamada and Mori, 2007), which implied the potential role of CCL22 in colorectal tumorigenesis.

There were still some limitations in our study. On the one hand, experiments *in vitro* and *in vivo* were lacking, and further QPCR and Western blot were needed to verify the expression of CCL22 as well as of other differentially expressed genes (BIRC3, CPT1B, ELMO1, PLA2G4C, and SLC25A2) in CRC cell lines infected by *F. nucleatum*. The effective impact of *F. nucleatum*-induced expression of CCL22 on colorectal tumorigenesis also needed to be validated in the future. On the other hand, the ability of CCL22 and other differentially expressed genes to predict survival needed to be further validated in multicenter clinical samples. Nevertheless, we found that many literatures have suggested the crucial role of CCL22 in *F. nucleatum*-related colorectal tumorigenesis. First, it has been reported that CCL22 expression is elevated in colorectal cancer (Wågsäter et al., 2008; Huang et al., 2015). Gut microbiota infection can induce the

expression of some chemokines, including CCL22, in colorectal cancer (Cremonesi et al., 2018). What is more, one study showed that the loss of miR-34a can increase CCL22 expression and promote the development of colorectal cancer after an infection by the bacterium *Citrobacter*, while the NF-KB signaling pathway also plays an important role in the development of colorectal cancer (Wang et al., 2018). Our analysis showed that *F. nucleatum* infection could increase CCL22 expression and influence the NF-KB signaling pathway in two kinds of colorectal cancer cells. Moreover, CCL22 was also related to NF-KB signaling pathway in TCGA-COAD. In summary, it is reasonable to conclude that *F. nucleatum* can also increase CCL22 expression, thereby promoting colorectal tumorigenesis, and the NF-KB signaling pathway is a part of its mechanism.

In summary, our study found that CCL22 mRNA expression was upregulated in CRC cell lines infected by *F. nucleatum*. The upregulation of CCL22 was associated with the TME of COAD, in which the high-CCL22-expression subgroup had more immune-suppressive cells and less antitumor immune cells. The high-CCL22-expression subgroup possessed higher IPS-CTLA4 and PD1/PD-L1/PD-L2 scores. This study provides several supporting lines of evidence that highlight the critical role of CCL22 in *F. nucleatum*-related colorectal tumorigenesis and its close relationship with the TME and ICIs, which deserved further cell and animal experiments.

DATA AVAILABILITY STATEMENT

The original data presented in the study are included in GEO and TCGA websites (**Table 1**). Further inquiries can be directed to the corresponding authors.

AUTHOR CONTRIBUTIONS

HW conceived and designed the study, analyzed the data, wrote the manuscript, and generated the figures and tables. KL, ZG, ZL, and JX helped to analyze the data. SO, YT, SR, JY, TM, TQ, and ZZ helped to search for some relevant papers for this research. YJ, YS, and RH guided the research process. All authors reviewed the manuscript.

FUNDING

This work was supported by the National Natural Science Foundation of China (no. 81872034), the Natural Science Foundation of Heilongjiang Province (no. H2017016), the Wu Jieping Medical Foundation (no. 320.6750.19092-41), and the Chen Xiao-ping Foundation for the Development of Science and Technology of Hubei Province (no. CXPJJH12000002-2020025).

ACKNOWLEDGMENTS

We would like to thank everyone who takes part in this study.

SUPPLEMENTARY MATERIAL

The supplementary material for this article can be found online at: https://www.frontiersin.org/articles/10.3389/fgene.2022.811900/full#supplementary-material

REFERENCES

Anz, D., Rapp, M., Eiber, S., Koelzer, V. H., Thaler, R., Haubner, S., et al. (2015). Suppression of Intratumoral CCL22 by Type I Interferon Inhibits Migration of Regulatory T Cells and Blocks Cancer Progression. *Cancer Res.* 75 (21), 4483–4493. doi:10.1158/0008-5472.can-14-3499

Arce Vargas, F., Furness, A. J. S., Litchfield, K., Joshi, K., Rosenthal, R., Ghorani, E., et al. (2018). Fc Effector Function Contributes to the Activity of Human Anti-CTLA-4 Antibodies. *Cancer Cell* 33 (4), 649–e4. doi:10.1016/j.ccell.2018.02.010

Böttcher, J. P., Bonavita, E., Chakravarty, P., Blees, H., Cabeza-Cabrerizo, M., Sammicheli, S., et al. (2018). NK Cells Stimulate Recruitment of cDC1 into the Tumor Microenvironment Promoting Cancer Immune Control. *Cell* 172 (5), 1022–1037. doi:10.1016/j.cell.2018.01.004

Cabrero-de Las Heras, S., and Martínez-Balibrea, E. (2018). CXC Family of Chemokines as Prognostic or Predictive Biomarkers and Possible Drug Targets in Colorectal Cancer. *World J. Gastroenterol.* 24 (42), 4738–4749. doi:10.3748/wjg.v24.i42.4738

Cao, Y., Jiao, N., Sun, T., Ma, Y., Zhang, X., Chen, H., et al. (2021). CXCL11 Correlates with Antitumor Immunity and an Improved Prognosis in Colon Cancer. *Front. Cel Dev. Biol.* 9, 646252. doi:10.3389/fcell.2021.646252

Charoentong, P., Finotello, F., Angelova, M., Mayer, C., Efremova, M., Rieder, D., et al. (2017). Pan-cancer Immunogenomic Analyses Reveal Genotype-Immunophenotype Relationships and Predictors of Response to Checkpoint Blockade. *Cel Rep.* 18 (1), 248–262. doi:10.1016/j.celrep.2016.12.019

Chen, S., Su, T., Zhang, Y., Lee, A., He, J., Ge, Q., et al. (2020). Fusobacterium Nucleatum Promotes Colorectal Cancer Metastasis by Modulating KRT7-AS/KRT7. *Gut Microbes* 11 (3), 511–525. doi:10.1080/19490976.2019.1695494

Colaprico, A., Silva, T. C., Olsen, C., Garofano, L., Cava, C., Garolini, D., et al. (2016). TCGAbiolinks: an R/Bioconductor Package for Integrative Analysis of TCGA Data. *Nucleic Acids Res.* 44 (8), e71. doi:10.1093/nar/gkv1507

Cremonesi, E., Governa, V., Garzon, J. F. G., Mele, V., Amicarella, F., Muraro, M. G., et al. (2018). Gut Microbiota Modulate T Cell Trafficking into Human Colorectal Cancer. *Gut* 67 (11), 1984–1994. doi:10.1136/gutjnl-2016-313498

Daillère, R., Vétizou, M., Waldschmitt, N., Yamazaki, T., Isnard, C., Poirier-Colame, V., et al. (2016). Enterococcus Hirae and Barnesiella Intestinihominis Facilitate Cyclophosphamide-Induced Therapeutic Immunomodulatory Effects. *Immunity* 45 (4), 931–943. doi:10.1016/j.immuni.2016.09.009

Dong, X., Pan, P., Zheng, D. W., Bao, P., Zeng, X., and Zhang, X. Z. (2020). Bioinorganic Hybrid Bacteriophage for Modulation of Intestinal Microbiota to Remodel Tumor-Immune Microenvironment against Colorectal Cancer. *Sci. Adv.* 6 (20), eaba1590. doi:10.1126/sciadv.aba1590

Fearon, E. R. (2011). Molecular Genetics of Colorectal Cancer. *Annu. Rev. Pathol. Mech. Dis.* 6, 479–507. doi:10.1146/annurev-pathol-011110-130235

Galon, J., Costes, A., Sanchez-Cabo, F., Kirilovsky, A., Mlecnik, B., Lagorce-Pagès, C., et al. (2006). Type, Density, and Location of Immune Cells within Human Colorectal Tumors Predict Clinical Outcome. *Science* 313 (5795), 1960–1964. doi:10.1126/science.1129139

Ganesh, K., Stadler, Z. K., Cercek, A., Mendelsohn, R. B., Shia, J., Segal, N. H., et al. (2019). Immunotherapy in Colorectal Cancer: Rationale, Challenges and Potential. *Nat. Rev. Gastroenterol. Hepatol.* 16 (6), 361–375. doi:10.1038/s41575-019-0126-x

Garris, C. S., Arlauckas, S. P., Kohler, R. H., Trefny, M. P., Garren, S., Piot, C., et al. (2018). Successful Anti-PD-1 Cancer Immunotherapy Requires T Cell-Dendritic Cell Crosstalk Involving the Cytokines IFN-γ and IL-12. *Immunity* 49 (6), 1148–1161. doi:10.1016/j.immuni.2018.09.024

Garzón-Tituaña, M., Arias, M. A., Sierra-Monzón, J. L., Morte-Romea, E., Santiago, L., Ramirez-Labrada, A., et al. (2020). The Multifaceted Function of Granzymes in Sepsis: Some Facts and a Lot to Discover. *Front. Immunol.* 11, 1054. doi:10.3389/fimmu.2020.01054

Gopalakrishnan, V., Helmink, B. A., Spencer, C. N., Reuben, A., and Wargo, J. A. (2018). The Influence of the Gut Microbiome on Cancer, Immunity, and Cancer Immunotherapy. *Cancer Cell* 33 (4), 570–580. doi:10.1016/j.ccell.2018.03.015

Guo, X., Zhang, Y., Zheng, L., Zheng, C., Song, J., Zhang, Q., et al. (2018). Global Characterization of T Cells in Non-small-cell Lung Cancer by Single-Cell Sequencing. *Nat. Med.* 24 (7), 978–985. doi:10.1038/s41591-018-0045-3

Hamada, T., Zhang, X., Mima, K., Bullman, S., Sukawa, Y., Nowak, J. A., et al. (2018). Fusobacterium Nucleatum in Colorectal Cancer Relates to Immune Response Differentially by Tumor Microsatellite Instability Status. *Cancer Immunol. Res.* 6 (11), 1327–1336. doi:10.1158/2326-6066.cir-18-0174

Hänzelmann, S., Castelo, R., and Guinney, J. (2013). GSVA: Gene Set Variation Analysis for Microarray and RNA-Seq Data. *BMC Bioinformatics* 14, 7. doi:10.1186/1471-2105-14-7

Heeran, A. B., Dunne, M. R., Morrissey, M. E., Buckley, C. E., Clarke, N., Cannon, A., et al. (2021). The Protein Secretome Is Altered in Rectal Cancer Tissue Compared to Normal Rectal Tissue, and Alterations in the Secretome Induce Enhanced Innate Immune Responses. *Cancers (Basel)* 13 (3)–571. doi:10.3390/cancers13030571

Hegde, P. S., Karanikas, V., and Evers, S. (2016). The where, the when, and the How of Immune Monitoring for Cancer Immunotherapies in the Era of Checkpoint Inhibition. *Clin. Cancer Res.* 22 (8), 1865–1874. doi:10.1158/1078-0432.ccr-15-1507

Hong, J., Guo, F., Lu, S. Y., Shen, C., Ma, D., Zhang, X., et al. (2020). F Nucleatum Targets lncRNA ENO1-IT1 to Promote Glycolysis and Oncogenesis in Colorectal Cancer[J]. *Gut* 70, 2123–2137. doi:10.1136/gutjnl-2020-322780

Huang, Y.-H., Cao, Y.-F., Jiang, Z.-Y., Zhang, S., and Gao, F. (2015). Th22 Cell Accumulation is Associated with Colorectal Cancer Development. *World J. Gastroenterol.* 21 (14), 4216–4224. doi:10.3748/wjg.v21.i14.4216

Kim, J. E., Patel, M. A., Mangraviti, A., Kim, E. S., Theodros, D., Velarde, E., et al. (2017). Combination Therapy with Anti-PD-1, Anti-TIM-3, and Focal Radiation Results in Regression of Murine Gliomas. *Clin. Cancer Res.* 23 (1), 124–136. doi:10.1158/1078-0432.ccr-15-1535

Klarquist, J., Tobin, K., Farhangi Oskuei, P., Henning, S. W., Fernandez, M. F., Dellacecca, E. R., et al. (2016). Ccl22 Diverts T Regulatory Cells and Controls the Growth of Melanoma. *Cancer Res.* 76 (21), 6230–6240. doi:10.1158/0008-5472.can-16-0618

Kostic, A. D., Chun, E., Robertson, L., Glickman, J. N., Gallini, C. A., Michaud, M., et al. (2013). Fusobacterium Nucleatum Potentiates Intestinal Tumorigenesis and Modulates the Tumor-Immune Microenvironment. *Cell Host & Microbe* 14 (2), 207–215. doi:10.1016/j.chom.2013.07.007

Li, T., Fu, J., Zeng, Z., Cohen, D., Li, J., Chen, Q., et al. (2020). TIMER2.0 for Analysis of Tumor-Infiltrating Immune Cells. *Nucleic Acids Res.* 48 (W1), W509–W514. doi:10.1093/nar/gkaa407

Marques, P., Barry, S., Carlsen, E., Collier, D., Ronaldson, A., Awad, S., et al. (2019). Chemokines Modulate the Tumour Microenvironment in Pituitary Neuroendocrine Tumours. *Acta Neuropathol. Commun.* 7 (1), 172. doi:10.1186/s40478-019-0830-3

Martinenaite, E., Munir Ahmad, S., Hansen, M., Met, Ö., Westergaard, M. W., Larsen, S. K., et al. (2016). CCL22-specific T Cells: Modulating the Immunosuppressive Tumor Microenvironment. *Oncoimmunology* 5 (11), e1238541. doi:10.1080/2162402x.2016.1238541

Mayakonda, A., Lin, D.-C., Assenov, Y., Plass, C., and Koeffler, H. P. (2018). Maftools: Efficient and Comprehensive Analysis of Somatic Variants in Cancer. *Genome Res.* 28 (11), 1747–1756. doi:10.1101/gr.239244.118

Mima, K., Nishihara, R., Qian, Z. R., Cao, Y., Sukawa, Y., Nowak, J. A., et al. (2016). Fusobacterium Nucleatumin Colorectal Carcinoma Tissue and Patient Prognosis. *Gut* 65 (12), 1973–1980. doi:10.1136/gutjnl-2015-310101

Mima, K., Sukawa, Y., Nishihara, R., Qian, Z. R., Yamauchi, M., Inamura, K., et al. (2015). Fusobacterium Nucleatumand T Cells in Colorectal Carcinoma. *JAMA Oncol.* 1 (5), 653–661. doi:10.1001/jamaoncol.2015.1377

Moser, A. R., Luongo, C., Gould, K. A., McNeley, M. K., Shoemaker, A. R., and Dove, W. F. (1995). ApcMin: a Mouse Model for Intestinal and Mammary Tumorigenesis. *Eur. J. Cancer* 31A (7-8), 1061–1064. doi:10.1016/0959-8049(95)00181-h

Nazemalhosseini-Mojarad, E., Mohammadpour, S., Torshizi Esafahani, A., Gharib, E., Larki, P., Moradi, A., et al. (2019). Intratumoral Infiltrating Lymphocytes Correlate with Improved Survival in Colorectal Cancer Patients: Independent of Oncogenetic Features. *J. Cel Physiol* 234 (4), 4768–4777. doi:10.1002/jcp.27273

Newman, A. M., Liu, C. L., Green, M. R., Gentles, A. J., Feng, W., Xu, Y., et al. (2015). Robust Enumeration of Cell Subsets from Tissue Expression Profiles. *Nat. Methods* 12 (5), 453–457. doi:10.1038/nmeth.3337

Nishino, M., Ramaiya, N. H., Hatabu, H., and Hodi, F. S. (2017). Monitoring Immune-Checkpoint Blockade: Response Evaluation and Biomarker Development. *Nat. Rev. Clin. Oncol.* 14 (11), 655–668. doi:10.1038/nrclinonc.2017.88

Quail, D. F., and Joyce, J. A. (2013). Microenvironmental Regulation of Tumor Progression and Metastasis. *Nat. Med.* 19 (11), 1423–1437. doi:10.1038/nm.3394

Rapp, M., Wintergerst, M. W. M., Kunz, W. G., Vetter, V. K., Knott, M. M. L., Lisowski, D., et al. (2019). CCL22 Controls Immunity by Promoting Regulatory T Cell Communication with Dendritic Cells in Lymph Nodes. *J. Exp. Med.* 216 (5), 1170–1181. doi:10.1084/jem.20170277

Robinson, M. D., McCarthy, D. J., and Smyth, G. K. (2010). edgeR: a Bioconductor Package for Differential Expression Analysis of Digital Gene Expression Data. *Bioinformatics* 26 (1), 139–140. doi:10.1093/bioinformatics/btp616

Routy, B., Le Chatelier, E., Derosa, L., Duong, C. P. M., Alou, M. T., Daillère, R., et al. (2018). Gut Microbiome Influences Efficacy of PD-1-Based Immunotherapy against Epithelial Tumors. *Science* 359 (6371), 91–97. doi:10.1126/science.aan3706

Sen, T., Rodriguez, B. L., Chen, L., Corte, C. M. D., Morikawa, N., Fujimoto, J., et al. (2019). Targeting DNA Damage Response Promotes Antitumor Immunity through STING-Mediated T-Cell Activation in Small Cell Lung Cancer. *Cancer Discov.* 9 (5), 646–661. doi:10.1158/2159-8290.cd-18-1020

Serna, G., Ruiz-Pace, F., Hernando, J., Alonso, L., Fasani, R., Landolfi, S., et al. (2020). Fusobacterium Nucleatum Persistence and Risk of Recurrence after Preoperative Treatment in Locally Advanced Rectal Cancer. *Ann. Oncol.* 31 (10), 1366–1375. doi:10.1016/j.annonc.2020.06.003

Siegel, R. L., Miller, K. D., Goding Sauer, A., Fedewa, S. A., Butterly, L. F., Anderson, J. C., et al. (2020). Colorectal Cancer Statistics, 2020. *CA A. Cancer J. Clin.* 70 (3), 145–164. doi:10.3322/caac.21601

Siegel, R. L., Miller, K. D., and Jemal, A. (2020). Cancer Statistics, 2020. *CA A. Cancer J. Clin.* 70 (1), 7–30. doi:10.3322/caac.21590

Stankovic, B., Bjørhovde, H. A. K., Skarshaug, R., Aamodt, H., Frafjord, A., Müller, E., et al. (2018). Immune Cell Composition in Human Non-small Cell Lung Cancer. *Front. Immunol.* 9, 3101. doi:10.3389/fimmu.2018.03101

Subramanian, A., Tamayo, P., Mootha, V. K., Mukherjee, S., Ebert, B. L., Gillette, M. A., et al. (2005). Gene Set Enrichment Analysis: A Knowledge-Based Approach for Interpreting Genome-wide Expression Profiles. *Proc. Natl. Acad. Sci.* 102 (43), 15545–15550. doi:10.1073/pnas.0506580102

Sun, H., Wang, Y., Jing, H.-Y., Yang, X.-Y., Shi, X.-X., Zhang, J.-H., et al. (2021). Chaperonin-Containing TCP1 Subunit 6A Is a Prognostic Potential Biomarker that Correlates with the Presence of Immune Infiltrates in Colorectal Cancer. *Front. Genet.* 12, 629856. doi:10.3389/fgene.2021.629856

Tang, Z., Li, C., Kang, B., Gao, G., Li, C., and Zhang, Z. (2017). GEPIA: a Web Server for Cancer and normal Gene Expression Profiling and Interactive Analyses. *Nucleic Acids Res.* 45 (W1), W98–W102. doi:10.1093/nar/gkx247

Topalian, S. L., Hodi, F. S., Brahmer, J. R., Gettinger, S. N., Smith, D. C., McDermott, D. F., et al. (2012). Safety, Activity, and Immune Correlates of Anti-PD-1 Antibody in Cancer. *N. Engl. J. Med.* 366 (26), 2443–2454. doi:10.1056/nejmoa1200690

Tumeh, P. C., Harview, C. L., Yearley, J. H., Shintaku, I. P., Taylor, E. J. M., Robert, L., et al. (2014). PD-1 Blockade Induces Responses by Inhibiting Adaptive Immune Resistance. *Nature* 515 (7528), 568–571. doi:10.1038/nature13954

Vétizou, M., Pitt, J. M., Daillère, R., Lepage, P., Waldschmitt, N., Flament, C., et al. (2015). Anticancer Immunotherapy by CTLA-4 Blockade Relies on the Gut Microbiota. *Science* 350 (6264), 1079–1084. doi:10.1126/science.aad1329

Wågsäter, D., Dienus, O., Löfgren, S., Hugander, A., and Dimberg, J. (2008). Quantification of the Chemokines CCL17 and CCL22 in Human Colorectal Adenocarcinomas. *Mol. Med. Rep.* 1 (2), 211–217. doi:10.3892/mmr.1.2.211

Wang, L., Wang, E., Wang, Y., Mines, R., Xiang, K., Sun, Z., et al. (2018). miR-34a Is a microRNA Safeguard for Citrobacter-Induced Inflammatory colon Oncogenesis[J]. *Elife* 7, e39479. doi:10.7554/elife.39479

Wood, S. L., Pernemalm, M., Crosbie, P. A., and Whetton, A. D. (2014). The Role of the Tumor-Microenvironment in Lung Cancer-Metastasis and its Relationship to Potential Therapeutic Targets. *Cancer Treat. Rev.* 40 (4), 558–566. doi:10.1016/j.ctrv.2013.10.001

Yamada, Y., and Mori, H. (2007). Multistep Carcinogenesis of the colon in ApcMin/+mouse. *Cancer Sci.* 98 (1), 6–10. doi:10.1111/j.1349-7006.2006.00348.x

Yan, T., Ma, G., Wang, K., Liu, W., Zhong, W., and Du, J. (2021). The Immune Heterogeneity between Pulmonary Adenocarcinoma and Squamous Cell Carcinoma: A Comprehensive Analysis Based on lncRNA Model. *Front. Immunol.* 12, 547333. doi:10.3389/fimmu.2021.547333

Yang, P., Li, Q.-J., Feng, Y., Zhang, Y., Markowitz, G. J., Ning, S., et al. (2012). TGF-β-miR-34a-CCL22 Signaling-Induced Treg Cell Recruitment Promotes Venous Metastases of HBV-Positive Hepatocellular Carcinoma. *Cancer Cell* 22 (3), 291–303. doi:10.1016/j.ccr.2012.07.023

Yang, Y., Weng, W., Peng, J., Hong, L., Yang, L., Toiyama, Y., et al. (2017). Fusobacterium Nucleatum Increases Proliferation of Colorectal Cancer Cells and Tumor Development in Mice by Activating Toll-like Receptor 4 Signaling to Nuclear Factor−κB, and Up-Regulating Expression of MicroRNA-21. *Gastroenterology* 152 (4), 851–866. doi:10.1053/j.gastro.2016.11.018

Yoshihara, K., Shahmoradgoli, M., Martínez, E., Vegesna, R., Kim, H., Torres-Garcia, W., et al. (2013). Inferring Tumour Purity and Stromal and Immune Cell Admixture from Expression Data. *Nat. Commun.* 4, 2612. doi:10.1038/ncomms3612

Yu, G., Wang, L.-G., Han, Y., and He, Q.-Y. (2012). clusterProfiler: an R Package for Comparing Biological Themes Among Gene Clusters. *OMICS: A J. Integr. Biol.* 16 (5), 284–287. doi:10.1089/omi.2011.0118

Yu, G., Wu, Y., Wang, W., Xu, J., Lv, X., Cao, X., et al. (2019). Low-dose Decitabine Enhances the Effect of PD-1 Blockade in Colorectal Cancer with Microsatellite Stability by Re-modulating the Tumor Microenvironment. *Cell Mol Immunol* 16 (4), 401–409. doi:10.1038/s41423-018-0026-y

Yu, T., Guo, F., Yu, Y., Sun, T., Ma, D., Han, J., et al. (2017). Fusobacterium Nucleatum Promotes Chemoresistance to Colorectal Cancer by Modulating Autophagy. *Cell* 170 (3), 548–563. doi:10.1016/j.cell.2017.07.008

Zhai, L., Ladomersky, E., Lenzen, A., Nguyen, B., Patel, R., Lauing, K. L., et al. (2018). Ido1 in Cancer: a Gemini of Immune Checkpoints. *Cel Mol Immunol* 15 (5), 447–457. doi:10.1038/cmi.2017.143

Zhang, S., Yang, Y., Weng, W., Guo, B., Cai, G., Ma, Y., et al. (2019). Fusobacterium Nucleatum Promotes Chemoresistance to 5-fluorouracil by Upregulation of BIRC3 Expression in Colorectal Cancer. *J. Exp. Clin. Cancer Res.* 38 (1), 14. doi:10.1186/s13046-018-0985-y

Conflict of Interest: The authors declare that the research was conducted in the absence of any commercial or financial relationships that could be construed as a potential conflict of interest.

Publisher's Note: All claims expressed in this article are solely those of the authors and do not necessarily represent those of their affiliated organizations or those of the publisher, the editors, and the reviewers. Any product that may be evaluated in this article or claim that may be made by its manufacturer is not guaranteed or endorsed by the publisher.

Copyright © 2022 Wang, Luo, Guan, Li, Xiang, Ou, Tao, Ran, Ye, Ma, Qiao, Zhang, Jin, Song and Huang. This is an open-access article distributed under the terms of the Creative Commons Attribution License (CC BY). The use, distribution or reproduction in other forums is permitted, provided the original author(s) and the copyright owner(s) are credited and that the original publication in this journal is cited, in accordance with accepted academic practice. No use, distribution or reproduction is permitted which does not comply with these terms.

frontiers | Frontiers in Genetics

ORIGINAL RESEARCH
published: 27 April 2022
doi: 10.3389/fgene.2022.863796

Identification of Novel Prognostic Biomarkers Relevant to Immune Infiltration in Lung Adenocarcinoma

Zhi Xia[1], *Xueyao Rong*[1], *Ziyu Dai*[1] *and Dongbo Zhou*[1,2]*

[1]*Department of Geriatrics, Xiangya Hospital of Central South University, Changsha, China,* [2]*Xiangya Lung Cancer Center, Xiangya Hospital, Central South University, Changsha, China*

Background: Programmed death ligand-1 (PD-L1) is a biomarker for assessing the immune microenvironment, prognosis, and response to immune checkpoint inhibitors in the clinical treatment of lung adenocarcinoma (LUAD), but it does not work for all patients. This study aims to discover alternative biomarkers.

Methods: Public data were obtained from The Cancer Genome Atlas (TCGA) and Gene Expression Omnibus (GEO). Weighted gene co-expression network analysis (WGCNA) and gene ontology (GO) were used to determine the gene modules relevant to tumor immunity. Protein–protein interaction (PPI) network and GO semantic similarity analyses were applied to identify the module hub genes with functional similarities to PD-L1, and we assessed their correlations with immune infiltration, patient prognosis, and immunotherapy response. Immunohistochemistry (IHC) and hematoxylin and eosin (H&E) staining were used to validate the outcome at the protein level.

Results: We identified an immune response–related module, and two hub genes (PSTPIP1 and PILRA) were selected as potential biomarkers with functional similarities to PD-L1. High expression levels of PSTPIP1 and PILRA were associated with longer overall survival and rich immune infiltration in LUAD patients, and both were significantly high in patients who responded to anti–PD-L1 treatment. Compared to PD-L1–negative LUAD tissues, the protein levels of PSTPIP1 and PILRA were relatively increased in the PD-L1–positive tissues, and the expression of PSTPIP1 and PILRA positively correlated with the tumor-infiltrating lymphocytes.

Conclusion: We identified PSTPIP1 and PILRA as prognostic biomarkers relevant to immune infiltration in LUAD, and both are associated with the response to anti–PD-L1 treatment.

Keywords: lung adenocarcinoma, prognostic biomarkers, immune response, PD-L1, immune infiltration

OPEN ACCESS

Edited by:
Ayan Biswas,
University of Alabama at Birmingham, United States

Reviewed by:
Till Braunschweig,
University Hospital RWTH Aachen, Germany
Lian Xiang Luo,
Guangdong Medical University, China

***Correspondence:**
Dongbo Zhou
zhoudb532311@163.com

Specialty section:
This article was submitted to Cancer Genetics and Oncogenomics, a section of the journal Frontiers in Genetics

Received: *27 January 2022*
Accepted: *28 March 2022*
Published: *27 April 2022*

Citation:
Xia Z, Rong X, Dai Z and Zhou D (2022) Identification of Novel Prognostic Biomarkers Relevant to Immune Infiltration in Lung Adenocarcinoma. Front. Genet. 13:863796. doi: 10.3389/fgene.2022.863796

Abbreviations: CC, cellular component; GO, gene ontology; GSVA, gene set variation analysis; H&E, hematoxylin and eosin; IHC, immunohistochemistry; IFN-γ, interferon-gamma; KEGG, Kyoto Encyclopedia of Genes and Genomes; LUAD, lung adenocarcinoma; MF, molecular function; MM, Module membership; NSCLC, non–small-cell lung cancer; ORRs, objective response rates; PBLs, peripheral blood lymphocytes; PD-L1, programmed death ligand-1; PD1, programmed cell death 1; PILRA, paired Ig-like type 2 receptor alpha; PSTPIP1, proline–serine–threonine phosphatase–interacting protein 1; PPI, protein–protein interactions; SKCM, skin cutaneous melanoma; TCGA, The Cancer Genome Atlas; TILs, tumor-infiltrating lymphocytes; WGCNA, weighted co-expression network analysis.

INTRODUCTION

Lung cancer remains the leading cause of cancer death (Travis, 2011). Lung adenocarcinoma (LUAD) is a predominant subtype of lung cancer, and the majority of LUAD patients are diagnosed at an advanced stage, losing the opportunity for surgery (Siegel et al., 2017). Although chemotherapy and targeted therapy can bring survival benefits to advanced patients, drug resistance is inevitable (Molina et al., 2008). With the rapid development of immunotherapy, programmed cell death 1 (PD1) and its ligand (PD-L1) checkpoint inhibitors have become alternative options for advanced patients, enhancing the anticancer immune response by relaunching T-cell–mediated tumor cell death programs through blocking the interaction between PD1 and PD-L1 (Reck, 2018; Dhillon and Syed, 2019). Both the protein and mRNA of PD-L1 can be used to evaluate the tumor immunophenotype, and a high expression of PD-L1 generally predicts benefits from anti–PD1/PD-L1 therapy, resulting in a better prognosis (Conroy et al., 2019).

Although PD-L1 is a well-validated biomarker for immunotherapy response (Shukuya and Carbone, 2016), its positivity does not indicate a certain response to immune checkpoint inhibitors (ICIs), with the objective response rates (ORRs) fluctuating widely (20%–40%) in PD-L1–positive patients. Meanwhile, a subset of PD-L1–negative patients can acquire a good response (Topalian et al., 2012; Brahmer et al., 2015; Garon et al., 2015; Rizvi et al., 2015; Brahmer et al., 2017; Zhang et al., 2020), suggesting the unstable predictive efficiency of PD-L1. Heterogeneity originating from distinct sub-clonal populations of cells could be an important reason for this, with LUAD showing high heterogeneity in immune molecules. PD-L1 expression is diverse among different tumoral regions, such as primary tumors and metastases, so it is likely that immunohistochemistry fails to assess the true PD-L1 status (Ilie et al., 2016; McLaughlin et al., 2016), thus leading to suboptimal decision-making in clinical treatment. Therefore, calculating the immunophenotype from PD-L1 is oversimple, and several studies have confirmed that the signatures related to intra-tumor immune infiltration can effectively predict the response to immunotherapy (Teng et al., 2015; Ock et al., 2016). The aim of this study was to discover the additional immune response–related biomarkers.

Similar to LUAD, skin cutaneous melanoma (SKCM) has a high ORR in first-line immunotherapy (Brahmer et al., 2015; Garon et al., 2015; Larkin et al., 2015), and a systematic review revealed that both PD-L1–negative and PD-L1–positive patients can benefit from the ICIs (Teng et al., 2018), implying the strong immunogenicity of SKCM. Many publications have indicated shared immune characteristics between LUAD and SKCM, which could effectively influence the immune response. A certain proportion of SKCM and LUAD patients possess a similar immune microenvironment, characterized by a high number of mutations or neoantigens, which benefits the patients in anti–PD-L1/PD1 treatment (Chen et al., 2017). In addition, similar intra-tumor heterogeneity and a high leukocyte fraction between SKCM and LUAD have been confirmed. Heterogeneity is associated with the level of tumor-infiltrating immune cells, while tumor types with high leukocyte fractions are generally the most responsive to ICIs (Morris et al., 2016; Thorsson et al., 2018). These transcriptome-based studies provide evidence for the common immunophenotypic basis between LUAD and SKCM, which indicates that they probably have a wide universality in immune-related biomarkers and clinical evaluation. Given that the preserved pattern of the gene module can convey a similar phenotype (Gustafsson et al., 2014), we presume that there could be core modules related to tumor immunity in SKCM and LUAD, and module hub genes, with functional similarities to PD-L1, might be used as biomarkers to evaluate the immunophenotype. Therefore, the introduction of SKCM to identify the common gene module would enable us to reduce thousands of candidate genes to a small number in specific modules, and we can also verify the prognostic or diagnostic value of the potential genes in both SKCM and LUAD based on their common immunophenotypic basis.

The pipeline is illustrated in **Figure 1**. With RNA expression profiles from The Cancer Genome Atlas (TCGA) and Gene Expression Omnibus (GEO), the present study identified that proline–serine–threonine phosphatase–interacting protein 1 (PSTPIP1) and paired Ig-like type 2 receptor alpha (PILRA) have functional similarities to PD-L1, and both are prognostic biomarkers relevant to immune infiltration and the anti–PD-L1 treatment response.

MATERIALS AND METHODS

Data and Clinical Sample Acquisition

The RNA-sequencing (RNA-seq) data [by expectation maximization (Li and Dewey, 2011), RSEM] were obtained from the TCGA (http://cancergenome.nih.gov) by utilizing cBioPortal (Cerami et al., 2012), namely, SKCM (104 samples of primary solid tumors and 368 samples of metastatic tumors) and LUAD (515 samples of primary solid tumors). Two validation data sets were downloaded from GEO (https://www.ncbi.nlm.nih.gov/geo/), meeting the following criteria: 1) data sets with whole transcriptome data, including RNA microarray or sequence data; 2) data sets with human specimens or tissue samples from animal models; 3) data sets with complete information about the technology, platform, and data processing; 4) data sets with available information about the response to anti–PD-L1/PD1 treatment; and 5) the data sets published within 10 years. We used GSE111414 (the RNA-seq data of $CD8^+$ peripheral blood lymphocytes (PBLs) from LUAD patients treated with nivolumab) and GSE172320 (the RNA microarray data of samples from SKCM mice treated with anti–PD-L1) to determine the implications of PSTPIP1 and PILRA in the anti–PD-L1 treatment response. In addition, GSE68571 (the RNA microarray data of 436 LUAD samples with available differentiation information) was downloaded to explore the association between PSTPIP1/PILRA and LUAD differentiation. Data normalization was performed using the R package "limma."

The LUAD pathological section materials of 18 patients, that is, 9 PD-L1–positive samples and 9 PD-L1–negative samples,

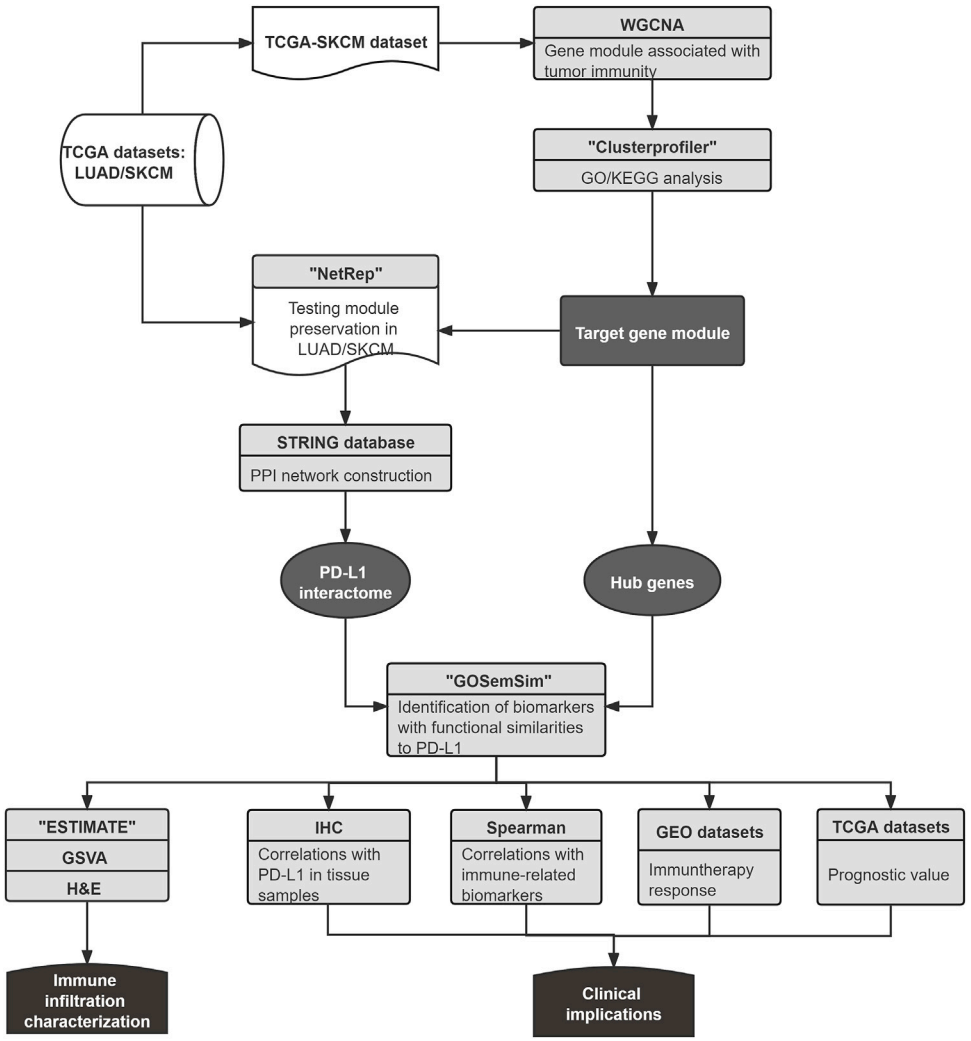


FIGURE 1 | The workflow of this study. First, the shared gene module related to immune regulation of LUAD and SKCM was identified. Next, the PPI network of the gene module was constructed by utilizing the STRING database, and the PD-L1 association network was applied as the PD-L1 interactome, which was used to evaluate the potential biomarkers from the hub genes with functional similarities to PD-L1. Finally, biomarker correlations with patient prognosis, immune biomarkers, immune infiltration, and anti–PD-L1 treatment response were investigated using various approaches.

were acquired from the Department of Pathology, Xiangya Hospital of Central South University, and PD-L1 expression was confirmed by pathologists using the PD-L1 immunohistochemistry (IHC) 22C3 pharmDx assay (Hirsch et al., 2017). The clinicopathological characteristics of the patients are listed in **Supplementary Table S1**. The present study was approved by the ethics committee of Xiangya Hospital of Central South University.

Weighted Gene Co-Expression Network Analysis

WGCNA was performed using the R package "WGCNA" (Langfelder and Horvath, 2008). Modules produced by WGCNA, named by different colors, refer to genes that share a similar connectivity pattern. Module membership (MM) is the relevance of the expression profile to each module eigengene. Hub genes, the central point of the gene module architecture, were defined as those genes with MM > 0.8. The R package "NetRep" was used to evaluate the replication and preservation of the target module from seven module preservation statistics (Ritchie et al., 2016). According to the tutorial, a gene module was considered strongly preserved if the p value was <0.01 for all preservation statistics, weakly preserved if the p value was <0.01 for one or more, but not all, test statistics, and no evidence if no test statistics had a p value < 0.01.

Gene Ontology and Pathway Enrichment Analysis

GlueGO (Bindea et al., 2009) and the R package "Clusterprofiler" (Yu et al., 2012) were applied to the Gene Ontology (GO) and

Kyoto Encyclopedia of Genes and Genomes (KEGG) pathway analysis and outcome visualization. Based on similarly associated genes, GO parent–child terms construct a hierarchy from the global to the specific level. Significant GO terms are summarized into representative terms by the fusion of the GO parent–child terms.

Protein–Protein Interaction Network Construction

The PPI information of the core module was obtained from the STRING database (https://string-db.org/), which offers the most confident interactions among module genes. We constructed a PPI network by using the Cytoscape 3.4.0 software (Shannon et al., 2003). Subsequently, the plug-in Molecular Complex Detection (Bader and Hogue, 2003) and GO analysis were applied to determine the central submodule related to tumor immunity, which helps to identify the core of the immune-related network in the target module (with the parameters: degree cutoff = 2, K-core = 2, and node score cutoff = 0.2).

Gene Ontology Semantic Similarity Analysis

The assessment of GO semantic similarity between genes can predict their relevant functions (Tedder et al., 2010). Based on the PPI information, the protein-coding genes having a connection with PD-L1 were incorporated into the PD-L1 interactome. Using the function "mgeneSim" in the R package "GOSemSim" (Yu et al., 2010), the semantic similarities between each hub gene and the PD-L1 interactome were calculated by taking the molecular function (MF) and cellular component (CC) of the GO topological structure into account. The Wang method was used in this process, which can accurately determine the semantic similarities of genes *via* a graph-based strategy (Wang et al., 2007). We used the geometric mean of semantic similarities in MF and CC to score the functional correlations between each hub gene and the PD-L1 interaction partners. A hub gene with a high score was generally considered to have a high probability of functional similarity to PD-L1, meaning it could be implicated in tumor immune regulation and relevant to the PD-L1 association network. We ranked hub genes by their average functional similarity score, providing an initial evaluation for their functional similarities to PD-L1.

Survival Analysis

Survival analysis was performed using the R packages "survminer" and "survival." Based on the mRNA expression of biomarkers, the samples were divided into two groups to plot Kaplan–Meier survival curves. A high expression was defined as samples with biomarker expression values above the median value, whereas a low expression was defined as samples with biomarker expression values below the median value.

Immune Infiltration Characterization

The R package "ESTIMATE" was used to quantify the total levels of tumor-infiltrating immune cells. Based on the unique properties of the transcriptional profiles, "ESTIMATE" performs a single sample gene set enrichment algorithm, which calculates the strength of the concerted behavior of the immune-related gene sets in each tumor sample (Yoshihara et al., 2013). We further utilized the R package "GSVA" to calculate the enrichment score of each infiltrating lymphocyte. By implementing a nonparametric unsupervised method to score the gene set enrichment in the gene microarray and RNA-seq data, "GSVA" transforms the data from a gene to a gene set by the sample matrix, allowing for the calculation of an enrichment score for each sample without information about explicitly modeling phenotypes (Hänzelmann et al., 2013). According to the median expression value of biomarkers, samples were separated into high expression and low expression groups, and we explored the status of tumor-infiltrating lymphocytes (TILs) in each tissue sample. A list of immune metagenes whose expressions have been shown to accurately predict the infiltration of immune cell populations was utilized as an input object for the "GSVA" (Angelova et al., 2015).

Assay Methods

IHC was used to determine the protein levels of PSTPIP1 and PILRA. LUAD tissue samples were sectioned into 4-mm-thick slices, deparaffinized in xylene and rehydrated in a series of graded alcohols. Antigen retrieval was performed by immersing the slides in sodium citrate. Endogenous peroxidase was blocked by a 10-min incubation with 3% H_2O_2. Next, the slices were incubated with the primary antibodies anti-PSTPIP1 (11951-1-AP, rabbit, polyclonal, dilution 1:50, Proteintech, Wuhan, China), anti-PILRA (orb38981, rabbit, polyclonal, dilution 1:200, Biorbyt, Cambridge, United Kingdom), and PBS (blank control) overnight at 4°C, washed three times with PBS, and incubated with a horseradish peroxidase (HRP)–conjugated secondary antibody (ab205718, Abcam, Cambridge, United Kingdom) for 30 min. Finally, immunostaining was performed with a diaminobenzidine substrate kit (ab64238, Abcam, Cambridge, United Kingdom). According to the outcome of IHC, we equally separated LUAD samples into high- and low-expression groups, and TILs were calculated in hematoxylin and eosin (H&E)–stained sections according to the standardized evaluation of TILs in breast cancer (Salgado et al., 2015). The IHC and H&E staining results were evaluated using the ImageJ software. Three to five typical fields of view per image were measured, and we obtained the mean value. The average optical density (AOD) or stromal TILs were calculated by counting the average of three pathological sections from each sample. The median values of the AOD expressed in each sample were used as the cutoff value, and the samples were divided into the high- or low-expression group.

Statistical Analysis

R statistical software (v.3.6.1) was used for statistical analyses and graphical visualization. The analysis was performed on log2-transformed values. Spearman's correlation test was applied to assess the relationships among biomarkers. The Wilcoxon test was used to compare the distributions of two sets of any continuous variable. The Kruskal–Wallis test was used to compare the distributions of three or more sets of any continuous variable. Null hypotheses were rejected at a two-sided p value lower than 0.05, unless otherwise indicated.

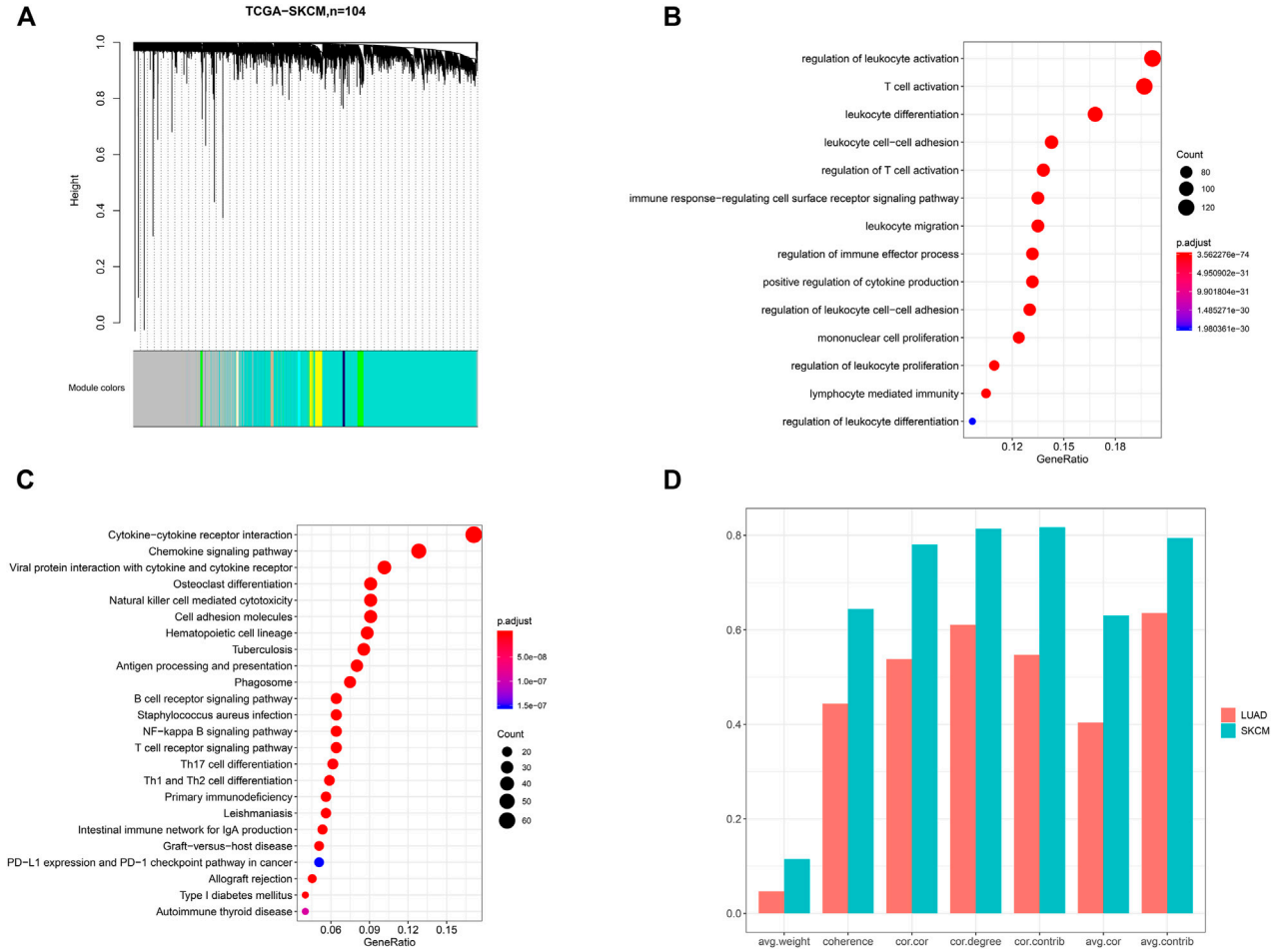


FIGURE 2 | Identification of a gene module associated with tumor immunity. **(A)** Dendrogram of 104 skin cutaneous melanoma (SKCM) samples. The results of **(B)** GO and **(C)** KEGG pathway analyses for the genes belonging to the brown module. **(D)** Assessment of the preservation pattern of the brown module in SKCM and lung adenocarcinomas (LUAD) from seven module preservation statistics, and the bar plots showing the observed value of each module preservation statistic. cor.cor: the concordance of the correlation structure; avg.cor: the average magnitude of the correlation coefficients of the module; avg.weight: the average magnitude of edge weights; cor.degree: the concordance of the weighted degree of nodes; cor.contrib: the concordance of the node contribution; avg.contrib: the average magnitude of the node contribution; coherence: the proportion of variance in the module data explained by the module's summary profile vector.

RESULTS

Identification of the Gene Module Related to Tumor Immunity

To identify the core module, we first performed WGCNA on 104 SKCM samples from primary lesions. The weighted gene co-expression network identified 21 modules (**Figure 2A**). According to the results of the GO and KEGG analyses, we identified the brown module, which consists of 743 protein-coding genes such as PD-L1, involved in tumor immune regulation. The bubble diagram shows the enriched GO terms implicated in the functional regulation of multiple lymphocytes and immune-related processes (**Figure 2B**). KEGG analysis revealed that immune cell–mediated and PD-L1–related pathways were enriched, including the "B-cell receptor signaling pathway," "T-cell receptor signaling pathway," and "PD-L1 expression and PD-1 checkpoint pathway in cancer," which are closely related to tumor immunity and immunotherapy response (**Figure 2C**). Compared to other modules, GO terms associated with immune-related regulation and biological processes were almost concentrated in the brown module, meaning that the module is likely to be in charge of tumor immunity, and thus it is a candidate for the subsequent analysis. Then, we calculated the module's preservation pattern, showing its strong preservation in LUAD and metastatic SKCM, which means that this gene module could be related to the common immunophenotype in SKCM and LUAD (**Figure 2D**).

Construction of the Protein–Protein Interaction Network

A total of 199 hub genes were identified in the brown module. Then, we screened the central submodule in the brown module by

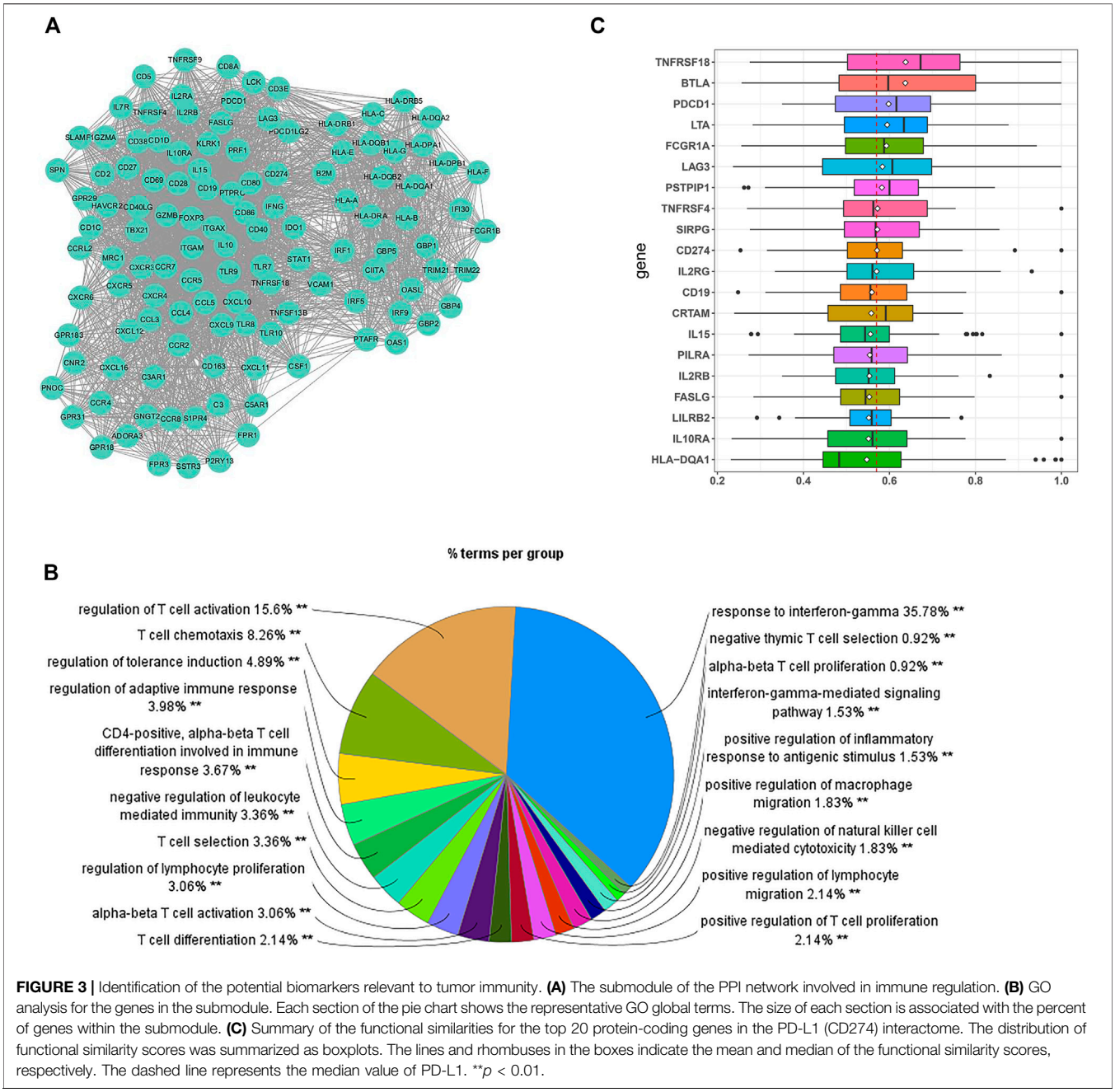


FIGURE 3 | Identification of the potential biomarkers relevant to tumor immunity. **(A)** The submodule of the PPI network involved in immune regulation. **(B)** GO analysis for the genes in the submodule. Each section of the pie chart shows the representative GO global terms. The size of each section is associated with the percent of genes within the submodule. **(C)** Summary of the functional similarities for the top 20 protein-coding genes in the PD-L1 (CD274) interactome. The distribution of functional similarity scores was summarized as boxplots. The lines and rhombuses in the boxes indicate the mean and median of the functional similarity scores, respectively. The dashed line represents the median value of PD-L1. $^{**}p < 0.01$.

constructing the PPI network, and a submodule composed of 119 genes was significantly associated with tumor immunity (**Figure 3A**). In addition to regulating the functions of multiple lymphocytes, most protein-coding genes in the submodule are involved in "T-cell activation" and "response to interferon-gamma (IFN-γ)" (**Figure 3B**). Based on the connections among protein-coding genes provided by the STRING database, we applied the PD-L1 association network as the PD-L1 interactome, which is composed of 83 protein-coding genes, including PD-L1 and its regulators. We utilized the R package "GOSemSim" to score functional similarities between the PD-L1 interactome and 199 hub genes. Genes with high scores are likely to have similar molecular functions to PD-L1. According to the results, we ranked the hub genes by the average functional similarity scores (**Figure 3C**) and found that PD-L1 (namely, CD274, a hub gene of the brown module) had the 10th highest average score among the hub genes, and the average score of the first was significantly higher than that of PD-L1 ($p = 0.0019$). No significant differences were found between the average scores of PD-L1 and the genes ranked second to 19th ($p > 0.05$), while the average score of the genes ranked below the 19th was significantly lower than that of PD-L1 ($p < 0.05$), meaning that the genes ranked second to 19th are most likely to play a similar role to PD-L1 in MF and CC. Except for PSTPIP1

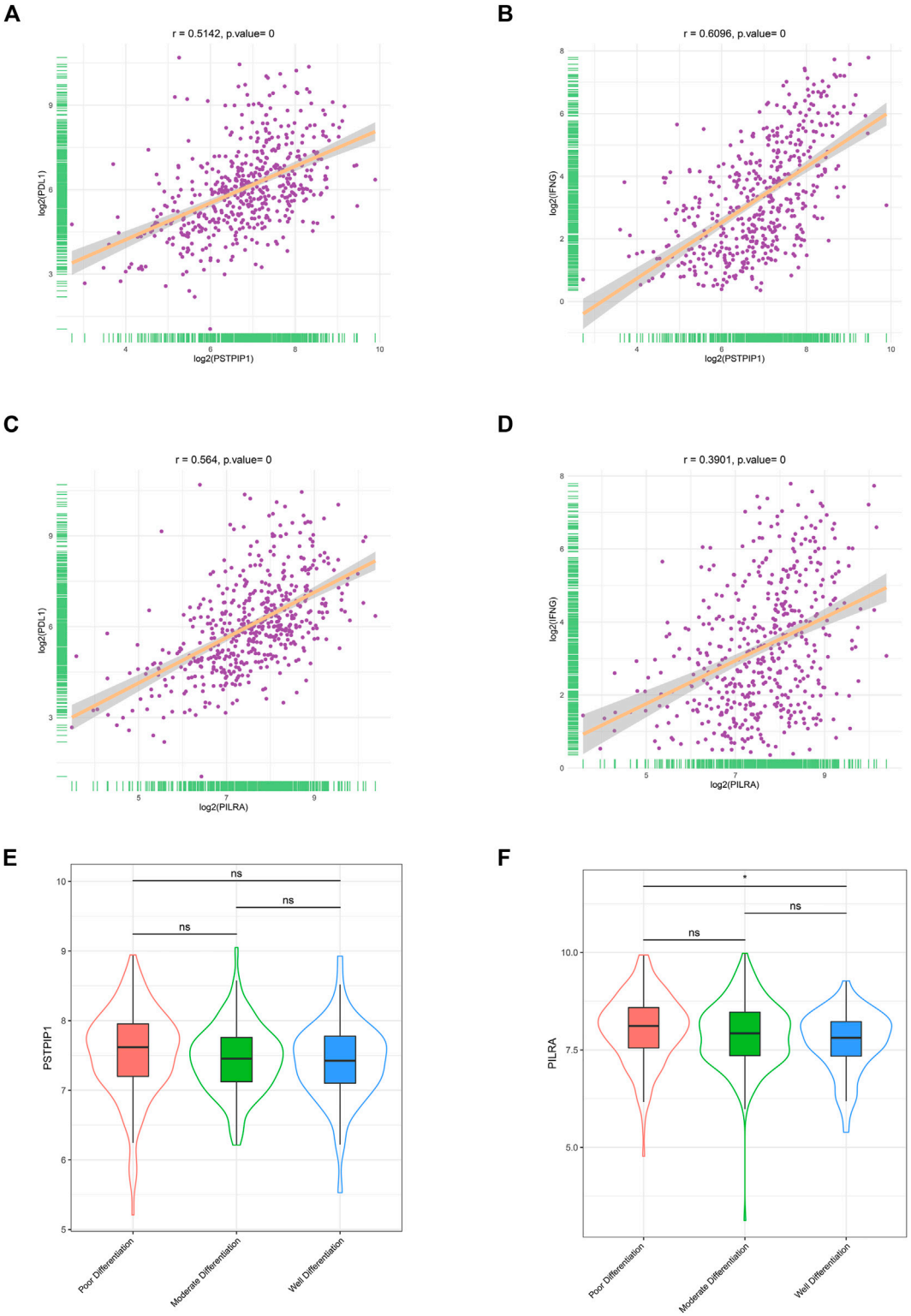


FIGURE 4 | The correlations between PSTPIP1/PILRA and immune biomarkers in LUAD. Scatter plots showing the correlation between **(A)** PSTPIP1 and PD-L1, **(B)** PSTPIP1 and IFN-γ, **(C)** PILRA and PD-L1, and **(D)** PILRA and IFN-γ in the LUAD samples ($n = 515$). Violin plots showing the expression of **(E)** PSTPIP1 and **(F)** PILRA in the LUAD samples with different degrees of differentiation (including 167 with poor differentiation, 209 with moderate differentiation, and 60 with well differentiation). ns indicates $p \geq 0.05$, $^{*}p < 0.05$.

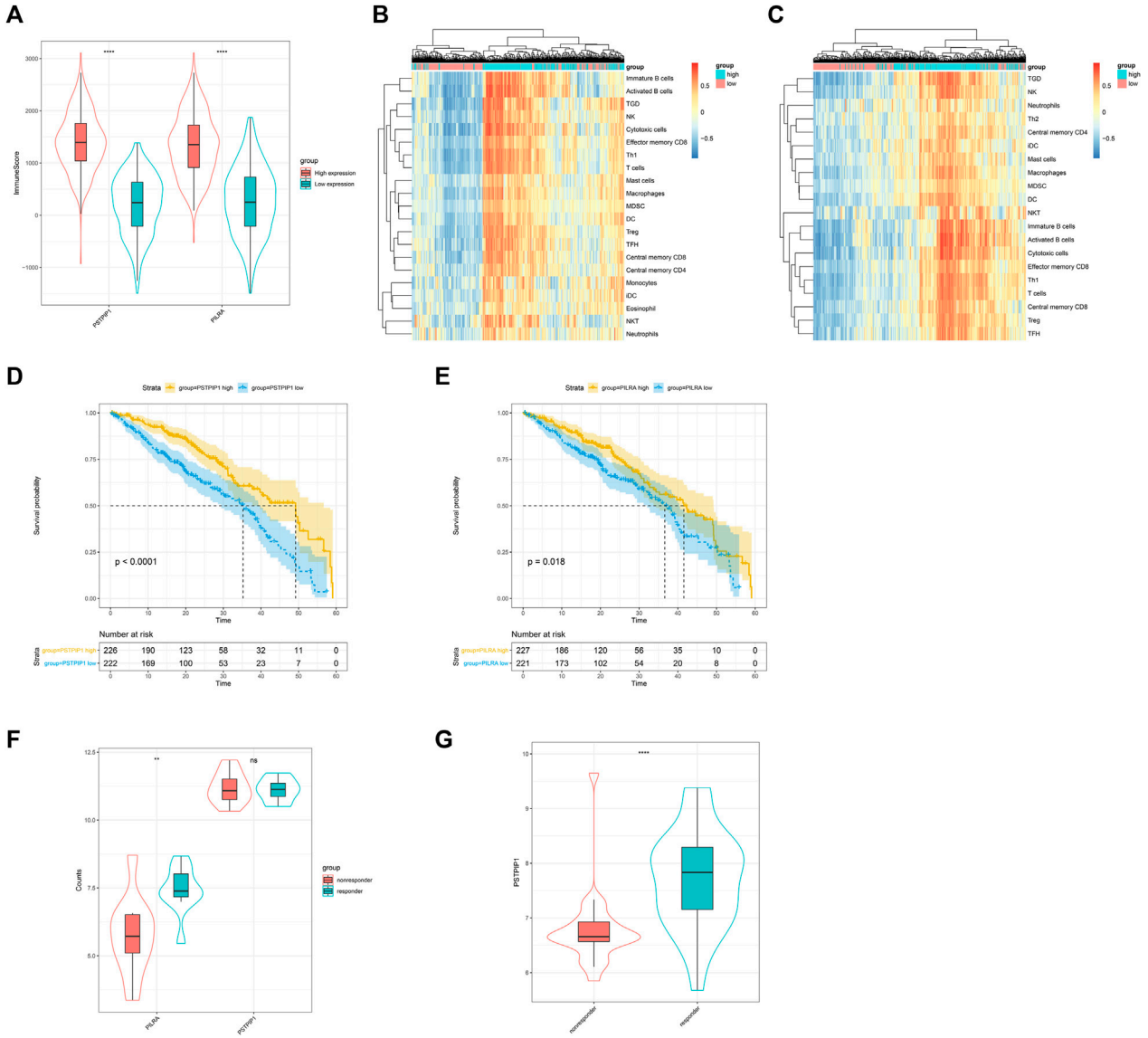


FIGURE 5 | The influence of PSTPIP1 and PILRA on immune infiltration and prognosis in LUAD. Violin plots showing **(A)** the immune score in samples with low or high expression of PSTPIP1 and PILRA. GSVA-derived clustering heat maps of differentially infiltrated immune cell populations between the high and low expression groups of **(B)** PSTPIP1 and **(C)** PILRA. Only lymphocytes with log(fold change) > 0.2 are shown. The influence of **(D)** PSTPIP1 and **(E)** PILRA on the overall survival time of LUAD patients. The yellow line indicates samples with highly expressed genes and the blue line indicates samples with lowly expressed genes. Violin plots showing **(F)** the expression of PSTPIP1 and PILRA in the LUAD patients with different responses to nivolumab (including five responders and five nonresponders) and **(G)** the expression of PSTPIP1 in SKCM mice with different responses to anti–PD-L1 treatment (including 27 responders and 23 nonresponders). ns indicates $p \geq 0.05$, $^{**}p < 0.01$, $^{****}p < 0.0001$.

and PILRA, the other genes with high scores have been identified to have functionally relevant roles in the immune checkpoint, tumoral immune cells, and immune infiltration, while few studies have reported the role of PSTPIP1 and PILRA in tumor immunity.

Implications in Tumor Immunity

We calculated the relationship between PSTPIP1/PILRA and the immune biomarkers, namely, PD-L1 and IFN-γ. We observed a significantly positive correlation between PSTPIP1/PILRA and PD-L1/IFN-γ in the LUAD samples (**Figures 4A–D**), and similar outcomes were observed in SKCM (**Supplementary Figure S1**). Given that LUAD differentiation can influence the expression of PD-L1 (Takada et al., 2016), we further explored the correlation between PSTPIP1/PILRA and tumor differentiation. The results revealed that LUAD tissue samples with distinct differentiation had similar levels of PSTPIP1. Compared with poorly differentiated samples, PILRA decreased in well-differentiated

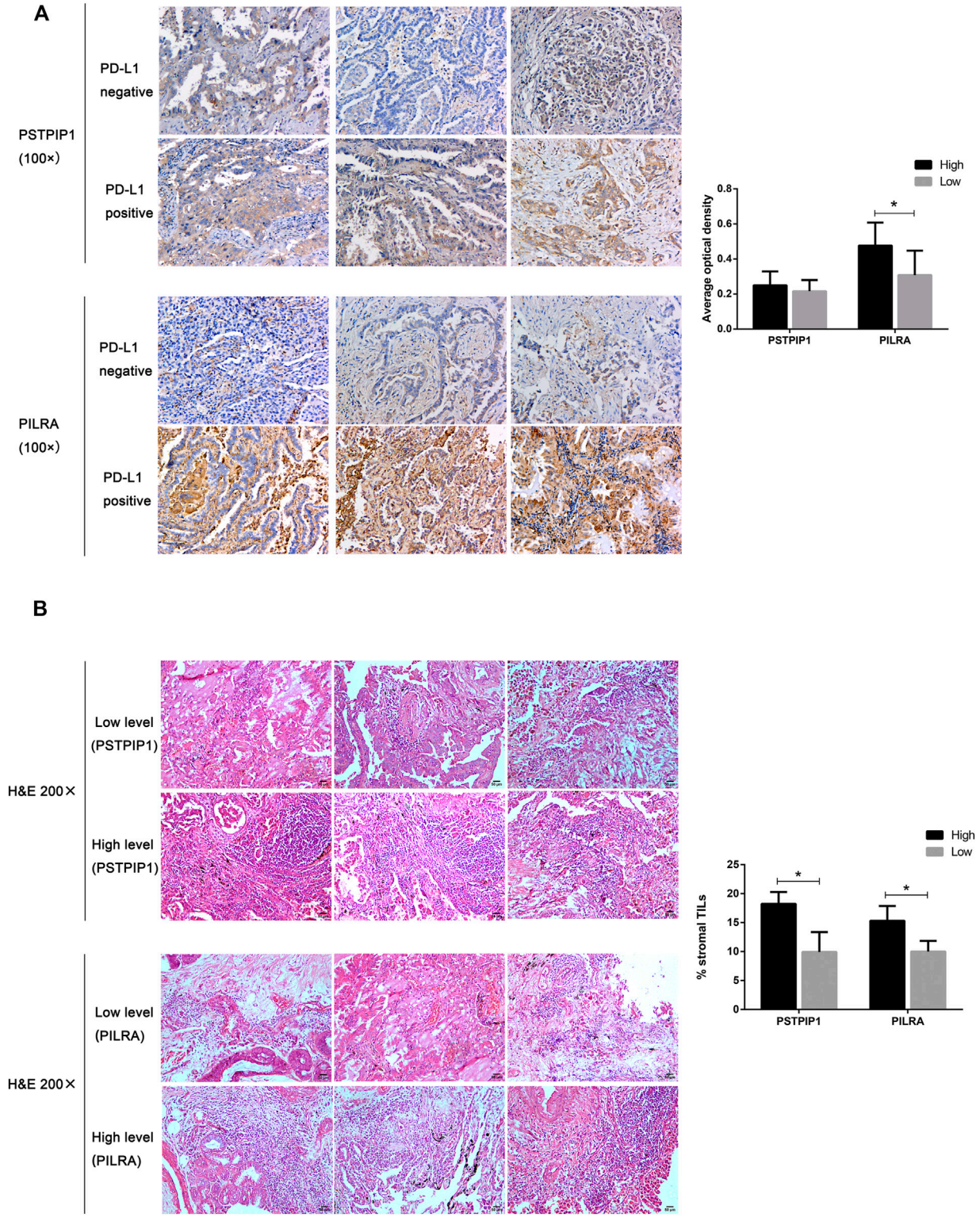


FIGURE 6 | Histopathological examples of PSTPIP1/PILRA expression and tumor-infiltrating lymphocytes (TILs) in LUAD. **(A)** PSTPIP1 and PILRA expression is demonstrated by brown staining, and the bar plot shows the average optical density of PSTPIP1 and PILRA in the PD-L1–positive or PD-L1–negative LUAD tissue samples. **(B)** The TILs are displayed as purple spots in hematoxylin and eosin staining, and bar plots show the stromal TILs in tissue samples with high and low PSTPIP1/PILRA expressions. *$p < 0.05$.

LUAD, but no significant difference was observed between the moderately and well-differentiated samples or between the poorly and moderately differentiated samples (**Figures 4E,F**).

Immune Infiltration and Survival Analysis

We explored the correlation between PSTPIP1/PILRA and TILs. The ESTIMATE immune scores revealed that the LUAD samples with a high expression of PSTPIP1 and PILRA had significantly richer immune infiltration (**Figure 5A**). GSVA confirmed that the high expression of PSTPIP1 and PILRA led to an increased enrichment of multiple lymphocytes (**Figures 5B,C**). We next investigated the prognostic value of PSTPIP1 and PILRA and found that the high expression of PSTPIP1 and PILRA contributed to longer overall survival (OS) (**Figures 5D,E**). Similar results were confirmed in SKCM (**Supplementary Figure S2A–E**). We investigated the correlations between PSTPIP1/PILRA and the anti–PD-L1 treatment response in LUAD patients and found that PILRA mRNA was significantly high in $CD8^+$ PBLs from the patients who responded to nivolumab, but the expression of PSTPIP1 was not different between the responders and nonresponders (**Figure 5F**). However, the significantly increased expression of the PSTPIP1 homologous gene was confirmed in tumor tissues from the SKCM mice that responded to the anti–PD-L1 treatment (**Figure 5G**).

Correlation Between Tumor-Infiltrating Lymphocytes and Biomarkers at the Protein Level

We validated the protein expression of PSTPIP1 and PILRA in the PD-L1–positive and PD-L1–negative LUAD tissue samples. In contrast to the PD-L1–negative samples, we observed that the protein level of PILRA was higher in the PD-L1–positive samples ($p = 0.0174$) (**Figure 6A**). Although PSTPIP1 showed a relatively higher expression in the PD-L1–positive tissues, there was no statistical significance when compared to the PD-L1–negative samples ($p = 0.3355$) (**Figure 6A**). At the same time, both PSTPIP1 and PILRA high expression samples possessed relatively richer TILs, while relatively lower TILs were prone to exist in samples with low PSTPIP1 and PILRA expressions ($p < 0.05$), and stromal TILs tended to exceed 10% in the LUAD samples with a high expression of PSTPIP1 and PILRA (**Figure 6B**).

DISCUSSION

This study applied network analysis methods to transcriptome data to explore the immune basis of LUAD and identified that it shares a strongly preserved immune response–related module with SKCM. The hub genes PSTPIP1 and PILRA are novel prognostic biomarkers positively correlated with TILs, and both could be used to predict immunotherapy response.

TILs are well-validated factors influencing the ICI response (Gibney et al., 2016), and PD-L1–positive SKCM accompanied by high TILs accounts for 40% of cases, which is the favorable immunophenotype for immunotherapy response (Teng et al., 2015). This provides the basis for SKCM patients with an ideal clinical efficacy in various immunotherapeutic approaches (Tsai et al., 2014). Researchers found that some LUAD cases have an immunophenotype similar to that of SKCM (Morris et al., 2016; Chen et al., 2017; Thorsson et al., 2018), which could be explained by the existence of a shared gene module related to tumor immunity. In the present study, we identified this sharing module, and two hub genes were considered to have functional similarities to PD-L1. The PSTPIP1 hub gene was related to T-cell activation, differentiation, and migration, modulating the function of innate immune cells and the innate immune response, and its mutation was confirmed as a crucial driver of immunodeficiency and auto-inflammatory diseases (Holzinger and Roth, 2016; Janssen et al., 2018). The PILRA hub gene was primarily expressed on multiple immune cells (Kogure et al., 2011; Sun et al., 2012), which can trigger increased natural killer cell–mediated IFN-γ secretion by binding to o-glycosylated receptors (Ophir et al., 2016). However, few studies have reported the correlation between these two protein-coding genes and the tumor-related immune response, and we confirmed that they have a relationship with multiple infiltrating lymphocytes and tumor immune regulation.

The majority of module genes are involved in the response to IFN-γ, a well-established biomarker for tumor immunity (Dong et al., 2016). IFN-γ is secreted from the TILs, which compromises antitumor immunity by promoting PD-L1 expression on the surface of tumor and immune cells (Bald et al., 2014; Remon et al., 2016; Ayers et al., 2017). Previous studies have reported a positive association between IFN-γ and PD-L1 at the mRNA level (Hayano et al., 2017), and a high expression of tumoral IFN-γ mRNA was associated with a good response to the PD-L1 inhibitor durvalumab in non–small-cell lung cancer (NSCLC) patients; the ORR in IFN-γ–positive patients reached 33%, while it was 8% in IFN-γ–negative patients, and the highest ORR (46%) was observed in cases with a coexisting positive expression of IFN-γ and PD-L1 (Higgs et al., 2015). Both PSTPIP1 and PILRA were positively associated with PD-L1 and IFN-γ, supporting their influence on the immune response. PILRA was lower in well-differentiated LUAD, which contradicts the widely validated correlations between the high PD-L1 expression and good differentiation. Therefore, to some extent, we can exclude the possibility that PSTPIP1 and PILRA levels are correlated with tumor differentiation rather than immune biomarkers. However, the protein expression of PSTPIP1 was not significantly increased in the PD-L1–positive LUAD tissues, implying that its correlation with PD-L1 might be indirect.

The TILs (mainly $CD8^+$ T cells) are important biomarkers for assessing the immune microenvironment, and both the tumor cell surface PD-L1 and intratumoral IFN-γ are associated with the level of the TILs (Dong et al., 2016; Tang et al., 2016). TIL-derived IFN-γ induces the expression of PD-L1, which in turn suppresses TIL-mediated antitumor immunity (Gowrishankar et al., 2015). We confirmed that TILs were significant in samples with high PSTPIP1 and PILRA levels. Tumors positive for PD-L1 and TILs

are adaptively resistant to elimination by TILs, and this immunophenotype is most likely to respond to anti–PD-L1 therapy (Zhang and Chen, 2016). We found that the LUAD patients who responded to PD-1/PD-L1 blockade treatment tended to have a high expression of PILRA mRNA in $CD8^+$ PBLs. Although PSTPIP1 expression showed no significant difference, we confirmed that significantly increased PSTPIP1 expression was observed in tumor tissues from SKCM mice that responded to anti–PD-L1 treatment. This difference might be derived from a distinctive gene repertoire between $CD8^+$ TILs and PBLs (Mohme et al., 2018). The high expression of PSTPIP1 inhibits CD3-dependent T-cell activation, which is significantly higher in TILs rather than in PBLs (Marcos et al., 2014; Lukesova et al., 2015), leading to adaptive resistance. Therefore, high expression of PSTPIP1 in the TILs could indicate a clinical response after immunotherapy of relaunching T-cell–mediated actions. We presumed that the differential expression of PSTPIP1 between the responders and non-responders might be observed in TILs rather than PBLs. Previous studies have confirmed that subpopulations of TILs, such as effector memory and central memory $CD8^+$ cells, effector memory $CD4^+$ cells, natural killer cells, and activated dendritic cells, are associated with good prognosis (Angelova et al., 2015), leading to an improved survival time in NSCLC patients (Thomas et al., 2013; Teng et al., 2015; Teng et al., 2016). The survival analysis is consistent with these conclusions, and the survival benefits of high PSTPIP1 and PILRA expressions are possibly due to rich TILs, and their influence is also in accord with their positive correlations with PD-L1, which confirms that both the protein and mRNA levels of PD-L1 are associated with increased TILs and OS in NSCLC patients (Velcheti et al., 2014; Ma et al., 2020). In general, PSTPIP1 and PILRA act as biomarkers for TILs and thus have positive correlations with PD-L1 and IFN-γ.

In the present study, we confirmed that PSTPIP1 and PILRA have a relationship with the TILs at both the protein and gene levels. However, selection bias was inevitable because of the small sample sizes, which is the main limitation of this study. Moreover, there was a lack of sufficient available data to firmly validate the conclusions made from the TCGA. Further study is needed to verify the clinical value of PSTPIP1 and PILRA in the additional samples and to explore their molecular functions in tumor immune regulation.

CONCLUSION

In conclusion, the present study demonstrated that PSTPIP1 and PILRA can reflect the status of TILs and work as prognostic biomarkers, and they could act as biomarkers relevant to the anti–PD-L1 treatment response.

DATA AVAILABILITY STATEMENT

The original contributions presented in the study are included in the article/**Supplementary Material**. Further inquiries can be directed to the corresponding author.

ETHICS STATEMENT

The studies involving human participants were reviewed and approved by the Medical Ethics Committee of Xiangya Hospital of Central South University. The ethics committee waived the requirement of written informed consent for participation.

AUTHOR CONTRIBUTIONS

ZX, DZ, XR, and ZD contributed to the study design. ZX analyzed the data and drafted the manuscript. XR contributed to the data acquisition. ZD contributed to experimental verification. DZ, ZX, XR, and ZD have read and approved the final version of the manuscript.

FUNDING

This work was supported by the National Multidisciplinary Cooperative Diagnosis and Treatment Capacity Building Project for Major Diseases (Lung Cancer).

SUPPLEMENTARY MATERIAL

The Supplementary Material for this article can be found online at: https://www.frontiersin.org/articles/10.3389/fgene.2022.863796/full#supplementary-material

Supplementary Figure S1 | Correlations between PSTPIP1/PILRA and immune biomarkers in skin cutaneous melanoma (SKCM). Scatter plots showing the correlations between **(A)** PSTPIP1 and PD-L1, **(B)** PSTPIP1 and IFN-γ, **(C)** PILRA and PD-L1, and **(D)** PILRA and IFN-γ in SKCM samples (n = 472).

Supplementary Figure S2 | The influence of PSTPIP1 and PILRA on immune infiltration and prognosis in SKCM. Violin plots showing **(A)** the immune score in samples with low or high expression of PSTPIP1 and PILRA. GSVA-derived clustering heatmaps of differentially infiltrated immune cell populations between the high and low expression groups of **(B)** PSTPIP1 and **(C)** PILRA. Only lymphocytes with log (fold change) > 0.2 are shown. The influence of **(D)** PSTPIP1 and **(E)** PILRA on the overall survival time of SKCM patients. The yellow line indicates samples with highly expressed genes, and the blue line indicates samples with lowly expressed genes. ****$p < 0.0001$.

Supplementary Table S1 | Clinical and pathological characteristics of lung adenocarcinomas patients.

REFERENCES

Angelova, M., Charoentong, P., Hackl, H., Fischer, M. L., Snajder, R., Krogsdam, A. M., et al. (2015). Characterization of the Immunophenotypes and Antigenomes of Colorectal Cancers Reveals Distinct Tumor Escape Mechanisms and Novel Targets for Immunotherapy. *Genome Biol.* 16 (1), 64. doi:10.1186/s13059-015-0620-6

Ayers, M., Lunceford, J., Nebozhyn, M., Murphy, E., Loboda, A., Kaufman, D. R., et al. (2017). IFN-γ-Related mRNA Profile Predicts Clinical Response to PD-1 Blockade. *J. Clin. Invest.* 127 (8), 2930–2940. doi:10.1172/jci91190

Bader, G. D., and Hogue, C. W. (2003). An Automated Method for Finding Molecular Complexes in Large Protein Interaction Networks. *BMC Bioinformatics* 4, 2. doi:10.1186/1471-2105-4-2

Bald, T., Landsberg, J., Lopez-Ramos, D., Renn, M., Glodde, N., Jansen, P., et al. (2014). Immune Cell-Poor Melanomas Benefit from PD-1 Blockade after Targeted Type I IFN Activation. *Cancer Discov.* 4 (6), 674–687. doi:10.1158/2159-8290.cd-13-0458

Bindea, G., Mlecnik, B., Hackl, H., Charoentong, P., Tosolini, M., Kirilovsky, A., et al. (2009). ClueGO: A Cytoscape Plug-In to Decipher Functionally Grouped Gene Ontology and Pathway Annotation Networks. *Bioinformatics* 25 (8), 1091–1093. doi:10.1093/bioinformatics/btp101

Brahmer, J., Reckamp, K. L., Baas, P., Crinò, L., Eberhardt, W. E. E., Poddubskaya, E., et al. (2015). Nivolumab Versus Docetaxel in Advanced Squamous-Cell Non-Small-Cell Lung Cancer. *N. Engl. J. Med.* 373 (2), 123–135. doi:10.1056/nejmoa1504627

Brahmer, J. R., Rodríguez-Abreu, D., Robinson, A. G., Hui, R., Csőszi, T., Fülöp, A., et al. (2017). Health-Related Quality-Of-Life Results for Pembrolizumab Versus Chemotherapy in Advanced, PD-L1-Positive NSCLC (KEYNOTE-024): A Multicentre, International, Randomised, Open-Label Phase 3 Trial. *Lancet Oncol.* 18 (12), 1600–1609. doi:10.1016/s1470-2045(17)30690-3

Cerami, E., Gao, J., Dogrusoz, U., Gross, B. E., Sumer, S. O., Aksoy, B. A., et al. (2012). The cBio Cancer Genomics Portal: An Open Platform for Exploring Multidimensional Cancer Genomics Data. *Cancer Discov.* 2 (5), 401–404. doi:10.1158/2159-8290.cd-12-0095

Chen, Y.-P., Zhang, Y., Lv, J.-W., Li, Y.-Q., Wang, Y.-Q., He, Q.-M., et al. (2017). Genomic Analysis of Tumor Microenvironment Immune Types across 14 Solid Cancer Types: Immunotherapeutic Implications. *Theranostics* 7 (14), 3585–3594. doi:10.7150/thno.21471

Conroy, J. M., Pabla, S., Nesline, M. K., Glenn, S. T., Papanicolau-Sengos, A., Burgher, B., et al. (2019). Next Generation Sequencing of PD-L1 for Predicting Response to Immune Checkpoint Inhibitors. *J. Immunotherapy Cancer* 7 (1), 18. doi:10.1186/s40425-018-0489-5

Dhillon, S., and Syed, Y. Y. (2019). Atezolizumab First-Line Combination Therapy: A Review in Metastatic Nonsquamous NSCLC. *Targ Oncol.* 14 (6), 759–768. doi:10.1007/s11523-019-00686-w

Dong, Z.-Y., Wu, S.-P., Liao, R.-Q., Huang, S.-M., and Wu, Y.-L. (2016). Potential Biomarker for Checkpoint Blockade Immunotherapy and Treatment Strategy. *Tumor Biol.* 37 (4), 4251–4261. doi:10.1007/s13277-016-4812-9

Garon, E. B., Rizvi, N. A., Hui, R., Leighl, N., Balmanoukian, A. S., Eder, J. P., et al. (2015). Pembrolizumab for the Treatment of Non-Small-Cell Lung Cancer. *N. Engl. J. Med.* 372 (21), 2018–2028. doi:10.1056/nejmoa1501824

Gibney, G. T., Weiner, L. M., and Atkins, M. B. (2016). Predictive Biomarkers for Checkpoint Inhibitor-Based Immunotherapy. *Lancet Oncol.* 17 (12), e542–e551. doi:10.1016/s1470-2045(16)30406-5

Gowrishankar, K., Gunatilake, D., Gallagher, S. J., Tiffen, J., Rizos, H., and Hersey, P. (2015). Inducible but Not Constitutive Expression of PD-L1 in Human Melanoma Cells Is Dependent on Activation of NF-κB. *PLoS One* 10 (4), e0123410. doi:10.1371/journal.pone.0123410

Gustafsson, M., Nestor, C. E., Zhang, H., Barabási, A.-L., Baranzini, S., Brunak, S., et al. (2014). Modules, Networks and Systems Medicine for Understanding Disease and Aiding Diagnosis. *Genome Med.* 6 (10), 82. doi:10.1186/s13073-014-0082-6

Hänzelmann, S., Castelo, R., and Guinney, J. (2013). GSVA: Gene Set Variation Analysis for Microarray and RNA-Seq Data. *BMC Bioinformatics* 14, 7. doi:10.1186/1471-2105-14-7

Hayano, A., Komohara, Y., Takashima, Y., Takeya, H., Homma, J., Fukai, J., et al. (2017). Programmed Cell Death Ligand 1 Expression in Primary Central Nervous System Lymphomas: A Clinicopathological Study. *Anticancer Res.* 37 (10), 5655–5666. doi:10.21873/anticanres.12001

Higgs, B. W., Robbins, P. B., Blake-Haskins, J. A., Zhu, W., Morehouse, C., Brohawn, P. Z., et al. (2015). 15LBA High Tumoral IFNγ mRNA, PD-L1 Protein, and Combined IFNγ mRNA/PD-L1 Protein Expression Associates with Response to Durvalumab (Anti-PD-L1) Monotherapy in NSCLC Patients. *Eur. J. Cancer* 51 (3), S717. doi:10.1016/S0959-8049(16)31937-2

Hirsch, F. R., McElhinny, A., Stanforth, D., Ranger-Moore, J., Jansson, M., Kulangara, K., et al. (2017). PD-L1 Immunohistochemistry Assays for Lung Cancer: Results from Phase 1 of the Blueprint PD-L1 IHC Assay Comparison Project. *J. Thorac. Oncol.* 12 (2), 208–222. doi:10.1016/j.jtho.2016.11.2228

Holzinger, D., and Roth, J. (2016). Alarming Consequences - Autoinflammatory Disease Spectrum Due to Mutations in Proline-Serine-Threonine Phosphatase-Interacting Protein 1. *Curr. Opin. Rheumatol.* 28 (5), 550–559. doi:10.1097/bor.0000000000000314

Ilie, M., Long-Mira, E., Bence, C., Butori, C., Lassalle, S., Bouhlel, L., et al. (2016). Comparative Study of the PD-L1 Status between Surgically Resected Specimens and Matched Biopsies of NSCLC Patients Reveal Major Discordances: A Potential Issue for Anti-PD-L1 Therapeutic Strategies. *Ann. Oncol.* 27 (1), 147–153. doi:10.1093/annonc/mdv489

Janssen, W. J. M., Grobarova, V., Leleux, J., Jongeneel, L., van Gijn, M., van Montfrans, J. M., et al. (2018). Proline-Serine-Threonine Phosphatase Interacting Protein 1 (PSTPIP1) Controls Immune Synapse Stability in Human T Cells. *J. Allergy Clin. Immunol.* 142 (6), 1947–1955. doi:10.1016/j.jaci.2018.01.030

Kogure, A., Shiratori, I., Wang, J., Lanier, L. L., and Arase, H. (2011). PANP Is a Novel O-Glycosylated PILRα Ligand Expressed in Neural Tissues. *Biochem. Biophysical Res. Commun.* 405 (3), 428–433. doi:10.1016/j.bbrc.2011.01.047

Langfelder, P., and Horvath, S. (2008). WGCNA: An R Package for Weighted Correlation Network Analysis. *BMC Bioinformatics* 9, 559. doi:10.1186/1471-2105-9-559

Larkin, J., Chiarion-Sileni, V., Gonzalez, R., Grob, J. J., Cowey, C. L., Lao, C. D., et al. (2015). Combined Nivolumab and Ipilimumab or Monotherapy in Untreated Melanoma. *N. Engl. J. Med.* 373 (1), 23–34. doi:10.1056/nejmoa1504030

Li, B., and Dewey, C. N. (2011). RSEM: Accurate Transcript Quantification from RNA-Seq Data with or without a Reference Genome. *BMC Bioinformatics* 12, 323. doi:10.1186/1471-2105-12-323

Lukesova, S., Vroblova, V., Tosner, J., Kopecky, J., Sedlakova, I., Čermáková, E., et al. (2015). Comparative Study of Various Subpopulations of Cytotoxic Cells in Blood and Ascites from Patients with Ovarian Carcinoma. *Contemp. Oncol. (Pozn)* 19 (4), 290–299. doi:10.5114/wo.2015.54388

Ma, K., Qiao, Y., Wang, H., and Wang, S. (2020). Comparative Expression Analysis of PD-1, PD-L1, and CD8A in Lung Adenocarcinoma. *Ann. Transl Med.* 8 (22), 1478. doi:10.21037/atm-20-6486

Marcos, T., Ruiz-Martín, V., de la Puerta, M. L., Trinidad, A. G., Rodríguez, M. D. C., de la Fuente, M. A., et al. (2014). Proline-Serine-Threonine Phosphatase Interacting Protein 1 Inhibition of T-Cell Receptor Signaling Depends on its SH3 Domain. *FEBS J.* 281 (17), 3844–3854. doi:10.1111/febs.12912

McLaughlin, J., Han, G., Schalper, K. A., Carvajal-Hausdorf, D., Pelekanou, V., Rehman, J., et al. (2016). Quantitative Assessment of the Heterogeneity of PD-L1 Expression in Non-Small-Cell Lung Cancer. *JAMA Oncol.* 2 (1), 46–54. doi:10.1001/jamaoncol.2015.3638

Mohme, M., Schliffke, S., Maire, C. L., Rünger, A., Glau, L., Mende, K. C., et al. (2018). Immunophenotyping of Newly Diagnosed and Recurrent Glioblastoma Defines Distinct Immune Exhaustion Profiles in Peripheral and Tumor-Infiltrating Lymphocytes. *Clin. Cancer Res.* 24 (17), 4187–4200. doi:10.1158/1078-0432.ccr-17-2617

Molina, J. R., Yang, P., Cassivi, S. D., Schild, S. E., and Adjei, A. A. (2008). Non-Small Cell Lung Cancer: Epidemiology, Risk Factors, Treatment, and Survivorship. *Mayo Clinic Proc.* 83 (5), 584–594. doi:10.1016/s0025-6196(11)60735-0

Morris, L. G. T., Riaz, N., Desrichard, A., Şenbabaoğlu, Y., Hakimi, A. A., Makarov, V., et al. (2016). Pan-Cancer Analysis of Intratumor Heterogeneity as a Prognostic Determinant of Survival. *Oncotarget* 7 (9), 10051–10063. doi:10.18632/oncotarget.7067

Ock, C.-Y., Keam, B., Kim, S., Lee, J.-S., Kim, M., Kim, T. M., et al. (2016). Pan-Cancer Immunogenomic Perspective on the Tumor Microenvironment Based on PD-L1 and CD8 T-Cell Infiltration. *Clin. Cancer Res.* 22 (9), 2261–2270. doi:10.1158/1078-0432.ccr-15-2834

Ophir, Y., Duev-Cohen, A., Yamin, R., Tsukerman, P., Bauman, Y., Gamliel, M., et al. (2016). PILRα Binds an Unknown Receptor Expressed Primarily on CD56bright and Decidual-NK Cells and Activates NK Cell Functions. *Oncotarget* 7 (27), 40953–40964. doi:10.18632/oncotarget.8397

Reck, M. (2018). Pembrolizumab as First-Line Therapy for Metastatic Non-Small-Cell Lung Cancer. *Immunotherapy* 10 (2), 93–105. doi:10.2217/imt-2017-0121

Remon, J., Chaput, N., and Planchard, D. (2016). Predictive Biomarkers for Programmed Death-1/Programmed Death Ligand Immune Checkpoint

Inhibitors in Nonsmall Cell Lung Cancer. *Curr. Opin. Oncol.* 28 (2), 122–129. doi:10.1097/cco.0000000000000263

Ritchie, S. C., Watts, S., Fearnley, L. G., Holt, K. E., Abraham, G., and Inouye, M. (2016). A Scalable Permutation Approach Reveals Replication and Preservation Patterns of Network Modules in Large Datasets. *Cel Syst.* 3 (1), 71–82. doi:10.1016/j.cels.2016.06.012

Rizvi, N. A., Mazières, J., Planchard, D., Stinchcombe, T. E., Dy, G. K., Antonia, S. J., et al. (2015). Activity and Safety of Nivolumab, an Anti-PD-1 Immune Checkpoint Inhibitor, for Patients with Advanced, Refractory Squamous Non-Small-Cell Lung Cancer (CheckMate 063): A Phase 2, Single-Arm Trial. *Lancet Oncol.* 16 (3), 257–265. doi:10.1016/s1470-2045(15)70054-9

Salgado, R., Denkert, C., Demaria, S., Sirtaine, N., Klauschen, F., Pruneri, G., et al. (2015). The Evaluation of Tumor-Infiltrating Lymphocytes (TILs) in Breast Cancer: Recommendations by an International TILs Working Group 2014. *Ann. Oncol.* 26 (2), 259–271. doi:10.1093/annonc/mdu450

Shannon, P., Markiel, A., Ozier, O., Baliga, N. S., Wang, J. T., Ramage, D., et al. (2003). Cytoscape: A Software Environment for Integrated Models of Biomolecular Interaction Networks. *Genome Res.* 13 (11), 2498–2504. doi:10.1101/gr.1239303

Shukuya, T., and Carbone, D. P. (2016). Predictive Markers for the Efficacy of Anti-PD-1/PD-L1 Antibodies in Lung Cancer. *J. Thorac. Oncol.* 11 (7), 976–988. doi:10.1016/j.jtho.2016.02.015

Siegel, R. L., Miller, K. D., and Jemal, A. (2017). Cancer Statistics, 2017. *CA: A Cancer J. Clinicians* 67 (1), 7–30. doi:10.3322/caac.21387

Sun, Y., Senger, K., Baginski, T. K., Mazloom, A., Chinn, Y., Pantua, H., et al. (2012). Evolutionarily Conserved Paired Immunoglobulin-Like Receptor α (PILRα) Domain Mediates its Interaction with Diverse Sialylated Ligands. *J. Biol. Chem.* 287 (19), 15837–15850. doi:10.1074/jbc.m111.286633

Takada, K., Okamoto, T., Shoji, F., Shimokawa, M., Akamine, T., Takamori, S., et al. (2016). Clinical Significance of PD-L1 Protein Expression in Surgically Resected Primary Lung Adenocarcinoma. *J. Thorac. Oncol.* 11 (11), 1879–1890. doi:10.1016/j.jtho.2016.06.006

Tang, H., Wang, Y., Chlewicki, L. K., Zhang, Y., Guo, J., Liang, W., et al. (2016). Facilitating T Cell Infiltration in Tumor Microenvironment Overcomes Resistance to PD-L1 Blockade. *Cancer Cell* 29 (3), 285–296. doi:10.1016/j.ccell.2016.02.004

Tedder, P. M. R., Bradford, J. R., Needham, C. J., McConkey, G. A., Bulpitt, A. J., and Westhead, D. R. (2010). Gene Function Prediction Using Semantic Similarity Clustering and Enrichment Analysis in the Malaria Parasite Plasmodium Falciparum. *Bioinformatics* 26 (19), 2431–2437. doi:10.1093/bioinformatics/btq450

Teng, F., Meng, X., Kong, L., Mu, D., Zhu, H., Liu, S., et al. (2015). Tumor-infiltrating Lymphocytes, Forkhead Box P3, Programmed Death Ligand-1, and Cytotoxic T Lymphocyte-Associated Antigen-4 Expressions before and after Neoadjuvant Chemoradiation in Rectal Cancer. *Translational Res.* 166 (6), 721–732. doi:10.1016/j.trsl.2015.06.019

Teng, F., Meng, X., Kong, L., and Yu, J. (2018). Progress and Challenges of Predictive Biomarkers of Anti PD-1/PD-L1 Immunotherapy: A Systematic Review. *Cancer Lett.* 414, 166–173. doi:10.1016/j.canlet.2017.11.014

Teng, F., Meng, X., Wang, X., Yuan, J., Liu, S., Mu, D., et al. (2016). Expressions of CD8+TILs, PD-L1 and Foxp3+TILs in Stage I NSCLC Guiding Adjuvant Chemotherapy Decisions. *Oncotarget* 7 (39), 64318–64329. doi:10.18632/oncotarget.11793

Teng, M. W. L., Ngiow, S. F., Ribas, A., and Smyth, M. J. (2015). Classifying Cancers Based on T-Cell Infiltration and PD-L1. *Cancer Res.* 75 (11), 2139–2145. doi:10.1158/0008-5472.can-15-0255

Thomas, N. E., Busam, K. J., From, L., Kricker, A., Armstrong, B. K., Anton-Culver, H., et al. (2013). Tumor-Infiltrating Lymphocyte Grade in Primary Melanomas Is Independently Associated with Melanoma-Specific Survival in the Population-Based Genes, Environment and Melanoma Study. *J. Clin. Oncol.* 31 (33), 4252–4259. doi:10.1200/jco.2013.51.3002

Thorsson, V., Gibbs, D. L., Brown, S. D., Wolf, D., Bortone, D. S., Ou Yang, T. H., et al. (2018). The Immune Landscape of Cancer. *Immunity* 48 (4), 812–830. doi:10.1016/j.immuni.2018.03.023

Topalian, S. L., Hodi, F. S., Brahmer, J. R., Gettinger, S. N., Smith, D. C., McDermott, D. F., et al. (2012). Safety, Activity, and Immune Correlates of Anti-PD-1 Antibody in Cancer. *N. Engl. J. Med.* 366 (26), 2443–2454. doi:10.1056/nejmoa1200690

Travis, W. D. (2011). Pathology of Lung Cancer. *Clin. chest Med.* 32 (4), 669–692. doi:10.1016/j.ccm.2011.08.005

Tsai, K. K., Zarzoso, I., and Daud, A. I. (2014). PD-1 and PD-L1 Antibodies for Melanoma. *Hum. Vaccin. Immunother.* 10 (11), 3111–3116. doi:10.4161/21645515.2014.983409

Velcheti, V., Schalper, K. A., Carvajal, D. E., Anagnostou, V. K., Syrigos, K. N., Sznol, M., et al. (2014). Programmed Death Ligand-1 Expression in Non-Small Cell Lung Cancer. *Lab. Invest.* 94 (1), 107–116. doi:10.1038/labinvest.2013.130

Wang, J. Z., Du, Z., Payattakool, R., Yu, P. S., and Chen, C.-F. (2007). A New Method to Measure the Semantic Similarity of GO Terms. *Bioinformatics* 23 (10), 1274–1281. doi:10.1093/bioinformatics/btm087

Yoshihara, K., Shahmoradgoli, M., Martínez, E., Vegesna, R., Kim, H., Torres-Garcia, W., et al. (2013). Inferring Tumour Purity and Stromal and Immune Cell Admixture from Expression Data. *Nat. Commun.* 4, 2612. doi:10.1038/ncomms3612

Yu, G., Li, F., Qin, Y., Bo, X., Wu, Y., and Wang, S. (2010). GOSemSim: an R Package for Measuring Semantic Similarity Among GO Terms and Gene Products. *Bioinformatics* 26 (7), 976–978. doi:10.1093/bioinformatics/btq064

Yu, G., Wang, L.-G., Han, Y., and He, Q.-Y. (2012). ClusterProfiler: An R Package for Comparing Biological Themes Among Gene Clusters. *OMICS: A J. Integr. Biol.* 16 (5), 284–287. doi:10.1089/omi.2011.0118

Zhang, S., Bai, X., and Shan, F. (2020). The Progress and Confusion of Anti-PD1/PD-L1 Immunotherapy for Patients with Advanced Non-Small Cell Lung Cancer. *Int. Immunopharmacology* 80, 106247. doi:10.1016/j.intimp.2020.106247

Zhang, Y., and Chen, L. (2016). Classification of Advanced Human Cancers Based on Tumor Immunity in the MicroEnvironment (TIME) for Cancer Immunotherapy. *JAMA Oncol.* 2 (11), 1403–1404. doi:10.1001/jamaoncol.2016.2450

Conflict of Interest: The authors declare that the research was conducted in the absence of any commercial or financial relationships that could be construed as a potential conflict of interest.

Publisher's Note: All claims expressed in this article are solely those of the authors and do not necessarily represent those of their affiliated organizations, or those of the publisher, the editors, and the reviewers. Any product that may be evaluated in this article, or claim that may be made by its manufacturer, is not guaranteed or endorsed by the publisher.

Copyright © 2022 Xia, Rong, Dai and Zhou. This is an open-access article distributed under the terms of the Creative Commons Attribution License (CC BY). The use, distribution or reproduction in other forums is permitted, provided the original author(s) and the copyright owner(s) are credited and that the original publication in this journal is cited, in accordance with accepted academic practice. No use, distribution or reproduction is permitted which does not comply with these terms.

frontiers | Frontiers in Genetics

ORIGINAL RESEARCH
published: 27 April 2022
doi: 10.3389/fgene.2022.876689

High Expression of DC-STAMP Gene Predicts Adverse Outcomes in AML

*Qian Liang, Lele Zhang, Wenjun Wang, Jingyu Zhao, Qiaoli Li, Hong Pan, Zhen Gao, Liwei Fang and Jun Shi**

Regenerative Medicine Clinic, State Key Laboratory of Experimental Hematology, National Clinical Research Center for Blood Diseases, Haihe Laboratory of Cell Ecosystem, Institute of Hematology & Blood Diseases Hospital, Chinese Academy of Medical Sciences & Peking Union Medical College, Tianjin, China

Acute myeloid leukemia (AML) is a genetically heterogeneous hematological malignancy with poor prognosis. We explored the RNA sequence data and clinical information of AML patients from The Cancer Genome Atlas (TCGA) and Genotype-Tissue Expression (GTEx) database to search for the core molecule for prognosis. The *DC-STAMP* expression was significantly higher in AML patients, which was linked to old age, unfavorable cytogenetic risk, and death (all $p < 0.05$). Furthermore, it was revealed that high *DC-STAMP* expression was an independent unfavorable factor for overall survival (OS) by univariate analysis [hazard ratio (HR): 2.683; 95% confidence interval (CI): 1.723–4.178; $p < 0.001$] and multivariate analysis (HR: 1.733; 95% CI: 1.079–2.781; $p = 0.023$). The concordance index (C-index 0.734, 95% CI: 0.706–0.762), calibration curves, and decision curve analysis showed the certain predictive accuracy of a nomogram model based on multivariate analysis for OS. In addition, we found that the differentially expressed gene (DEG) enrichment pathways of high- and low-*DC-STAMP* expression group enrichment pathways were focused on channel activity and platelet alpha granule by the Gene Ontology (GO) and Kyoto Encyclopedia of Genes and Genomes (KEGG), while gene set enrichment analysis (GSEA) pathways were mainly involved in mTORC1 signaling and TNF-α signaling *via* the NF-kB pathway. Moreover, a protein–protein interaction (PPI) network demonstrated that *DC-STAMP* interacted with two hub genes (*PPBP* and *PF4*), which were highly regulated and associated with poor survival. Finally, high *DC-STAMP* expression showed a significantly positive correlation with four immune cell [NK CD56 (dim) cells, macrophages, cytotoxic cells, and CD8 (+) T cells] infiltration and high level of immune checkpoint genes (*PDCD1*, *CD274*, *CTLA-4*, and *TIGIT*). Therefore, our results suggest that high expression of *DC-STAMP* predicts adverse outcomes for AML patients.

Keywords: DC-STAMP, acute myeloid leukemia, prognosis, bioinformatics, TCGA, immune checkpoints

OPEN ACCESS

Edited by:
Ayan Biswas, University of Alabama at Birmingham, United States

Reviewed by:
Ezhilarasi Chendamarai, Washington University in St. Louis, United States
Jing-Dong Zhou, Jiangsu University Affiliated People's Hospital, China

****Correspondence:***
Jun Shi
shijun@ihcams.ac.cn
orcid.org/0000-0002-8531-0483

Specialty section:
This article was submitted to Cancer Genetics and Oncogenomics, a section of the journal Frontiers in Genetics

Received: *15 February 2022*
Accepted: *21 March 2022*
Published: *27 April 2022*

Citation:
Liang Q, Zhang L, Wang W, Zhao J, Li Q, Pan H, Gao Z, Fang L and Shi J (2022) High Expression of DC-STAMP Gene Predicts Adverse Outcomes in AML. Front. Genet. 13:876689. doi: 10.3389/fgene.2022.876689

INTRODUCTION

Acute myeloid leukemia (AML) is a malignant clonal disease originating from hematopoietic stem cells (HSCs) or myeloid progenitors characterized by inhibiting cellular differentiation and proliferation of blast cells (Puram et al., 2016; Assi et al., 2019). Although most patients received traditional chemotherapy and allogeneic hematopoietic stem cell transplantation (allo-HSCT), more than 70% of the patients failed to achieve the desired effects (Chen et al., 2019). Based on some genetic abnormalities, the risk stratification system of AML has been refined and some AML patients

tend to have deeper remission and longer survival through molecular targeted therapy (Estey, 2016; Stone et al., 2017; Kayser and Levis, 2018; DiNardo et al., 2020). However, there are limited numbers of reliable biomarkers for indicating the prognosis of AML and guiding therapy selection (Campos et al., 1993; Tzifi et al., 2012; Fröhling et al., 2002; Patel et al., 2012). Therefore, a much more in-depth and comprehensive research of the molecular abnormalities including genetic mutations and validation would aid in designing effective targeted therapies for AML.

Dendritic cell (DC)-specific transmembrane protein (DC-STAMP), also called TM7SF4, is a seven-transmembrane receptor protein, which is predominantly expressed in myeloid DC, macrophages, and osteoclasts (Hartgers et al., 2000; Yagi et al., 2005). However, DC-STAMP mRNA expression is low in hematopoietic stem and progenitor cells (HSCPs) and monocytes (Eleveld-Trancikova et al., 2008). It plays a role in the limitation of myeloid cell differentiation, regulation of the antigen presentation activity of DC, and maintenance of immune tolerance (Eleveld-Trancikova et al., 2008; Sawatani et al., 2008; Eleveld-Trancikova et al., 2010). A recent study demonstrated that the DC-STAMP was considered as an important molecule promoting the development and progression of multiple myeloma (Silvestris et al., 2011), whereas its role in AML is completely unknown.

In this research, we used not only the cox regression analysis but also a nomogram model, calibration curves, and a decision curve analysis (DCA) to assess the predictive effect of the DC-STAMP on AML patients based on TCGA database. In addition, we performed three types of enrichment analyses, protein–protein interaction (PPI), and a correlation analysis of immune infiltration or immune checkpoints to detect the pathogenic molecular mechanisms of the *DC-STAMP*. Our findings revealed the prognostic value of the DC-STAMP and may provide novel insights into the gene marker of leukemogenesis.

MATERIALS AND METHODS

Data Source

The transcripts per million (TPM) reads format RNA-seq data of TCGA and GTEx were collected by the toil process from the UCSC XENA browser (https://xenabrowser.net/datapages/) (Vivian et al., 2017; Consortium, 2020; Goldman et al., 2020). The data of 173 cases of AML patients and 70 cases of normal people were extracted from TCGA's LAML project and GTEx, respectively. The RNA-seq data of the TPM format was performed for an intrasample comparison after log2 transformation. The clinical data of AML patients were downloaded from TCGA (https://tcga-data.nci.nih.gov/), and 153 patients' data were eligible for inclusion by removing patients without clinical data.

Differential Gene Expression Analysis

We used the median values of DC-STAMP mRNA expression to divide the AML patients into low and high DC-STAMP expression groups. The differentially expressed genes (DEGs) of the aforementioned two groups were identified by comparing the RNA-seq data of the HTSeq-count format by the DESeq2R package (Love et al., 2014). DEGs were defined as an absolute log2 fold change (|log2 FC|) >1.0 with an adjusted p value < 0.05.

Functional and Pathway Enrichment Analysis

The Gene Ontology (GO) functional gene annotation analysis is a common method used for the enrichment analysis of large-scale genes, including the biological process (BP), cellular component (CC), and molecular function (MF) (Gene Ontology Consortium, 2021). The Kyoto Encyclopedia of Genes and Genomes (KEGG) is a widely used database for information storage of genomes, biological pathways, and diseases and drugs (Kanehisa et al., 2021). We performed the GO and KEGG analyses of DEGs in AML using the R package clusterProfiler (Yu et al., 2012).

Gene Set Enrichment Analysis

GSEA is a method that evaluates the correlation between gene expression and phenotype from a pre-defined gene set and determines the relative contribution (Subramanian et al., 2005). We downloaded hallmark gene sets (h.all.v7.2.symbols.gmt) from the MsigDB and utilized the R package clusterProfiler to conduct the GSEA (Yu et al., 2012; Szklarczyk et al., 2019). It was considered a statistical significance when the p value was less than 0.05.

Construction of Protein–Protein Interaction Network

Known proteins and predicted protein–protein interaction were investigated by using the STRING website (https://string-db.org/) (Szklarczyk et al., 2019), which contained 9.6 million proteins and 138 million protein–protein interactions from 2,031 species. In this research, we used the STRING database to construct a PPI network of encoding DEGs, then visualized the results and screened hub genes using the Cytoscape software (version 3.7.1) (Shannon et al., 2003). We further performed the ggplot2 package in R to investigate the association of *DC-STAMP* expression with hub genes by the correlation heatmap.

Correlation Analysis of Immune Infiltration and Immune Checkpoint Genes

We applied the ssGSEA algorithm from the GSVA package (version 1.34.0) to estimate the Pearson correlation coefficient between *DC-STAMP* expression and immune cells and the association of the *DC-STAMP* with the abundance of the 24 types of infiltrated immune cells (Bindea et al., 2013; Hänzelmann et al., 2013). The involved immune cells were activated dendritic cells (aDCs), B cells, CD8 (+) T cells, cytotoxic cells, DCs, eosinophils, immature DCs (iDCs), macrophages, mast cells, neutrophils, NK CD56 (bright) cells, NK CD56 (dim) cells, NK cells, plasmacytoid DCs (pDCs), T cells, T helper cells, T central memory (Tcm) cells, T effector memory (Tem) cells, T

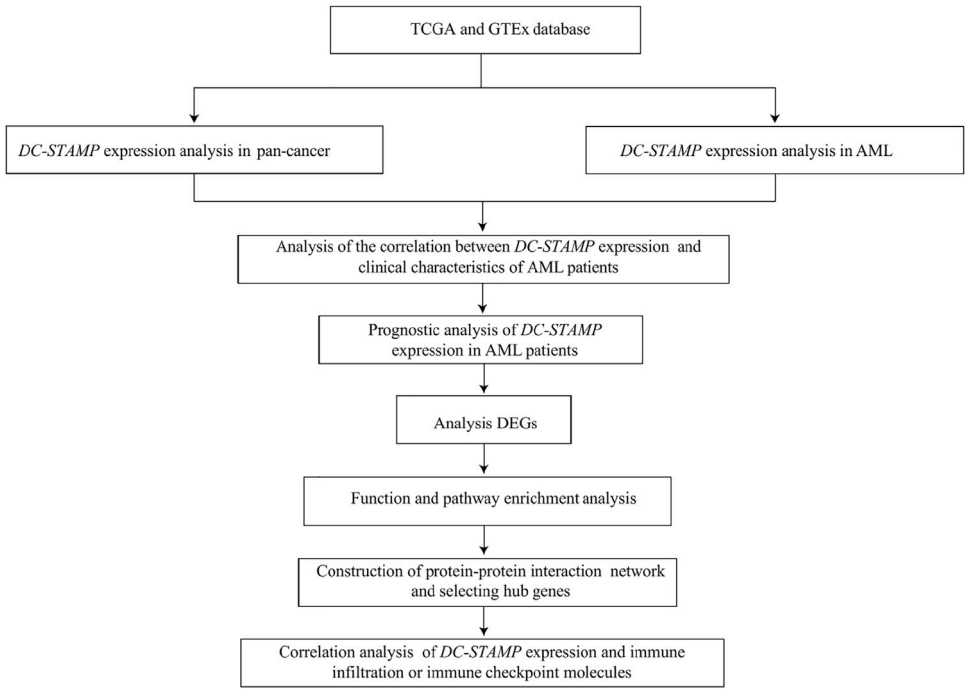


FIGURE 1 | Flowchart of research.

follicular helper (Tfh) cells, T gamma delta (Tgd) cells, Th1 cells, Th17 cells, Th2 cells, and regulatory T (Treg) cells. We next performed the ggplot2 package in R to investigate the association of *DC-STAMP* expression with specific immune cells and widely discussed immune checkpoint genes (*PDCD1*, *CD274*, *CTLA-4*, *LAG-3*, *TIGIT*, and *HAVCR2*) by the scatter plot.

Statistical Methods

All statistical analyses were completed in R programming (https://www.r-project.org/, version 3.6.3). The effectiveness of the *DC-STAMP* in distinguishing AML from normal samples was assessed by the receiver operating characteristic (ROC) curve analysis using the pROC software. The difference between clinical features and *DC-STAMP* expression was detected by Wilcoxon rank sum tests and Kruskal–Wallis tests. The correlation of clinical features between low and high *DC-STAMP* expression was performed by the Pearson χ^2 test. Survival curves were constructed using the Kaplan–Meier (KM) plot. The prognostic risk factors were identified by univariate analyses and the multivariate Cox regression analysis, then, independent factors were recruited for building the final nomogram prognostic model. Additionally, we used calibration and DCA to assess the predictive power of the nomogram model. The nomogram plot and calibration curve were established by using the RMS package in R and the DCA curve was constructed by using the survival package and stdca.R. in R. All tests were two-sided, and $p < 0.05$ was considered to be of statistical significance. The research and analysis flowchart is presented in **Figure 1**.

RESULTS

High Expression of *DC-STAMP* is Linked to Unfavorable Clinical Characteristics in Acute Myeloid Leukemia

We compared the difference in *DC-STAMP* mRNA expression among AML, normal, and other malignancies samples by using the RNA-seq database. Remarkably, *DC-STAMP* expression was upregulated in multiple malignancies (**Figure 2A**), especially in AML ($p < 0.05$, **Figure 2B**). Moreover, the power of the expression difference was 0.672 (95% confidence interval, CI = 0.610–0.735, **Figure 2C**) by the AUC value of the ROC curve analysis. Hence, we are interested in the clinical implications of *DC-STAMP* expression in AML patients. A total of 153 AML patients with clinical information from TCGA were analyzed in the study. As shown in **Figures 2D–G**, *DC-STAMP* expression was associated with old age ($p < 0.01$, **Figure 2D**), unfavorable cytogenetic risk ($p < 0.001$, **Figure 2E**), *NPM1* positive mutation ($p < 0.05$, **Figure 2F**), and death ($p < 0.001$, **Figure 2G**), no association with French-American-British (FAB) classifications (**Supplementary Figure S1**). Furthermore, when patients were grouped by low and high mRNA expression, a strong correlation was found in old age ($p = 0.004$), unfavorable cytogenetic risk category ($p < 0.001$), normal, +8, del (7) karyotype ($p = 0.008$), M2, M5 FAB subtypes ($p = 0.037$), and death ($p = 0.001$, **Table 1**), but no association with gender, white blood cell count, and *FLT3*,

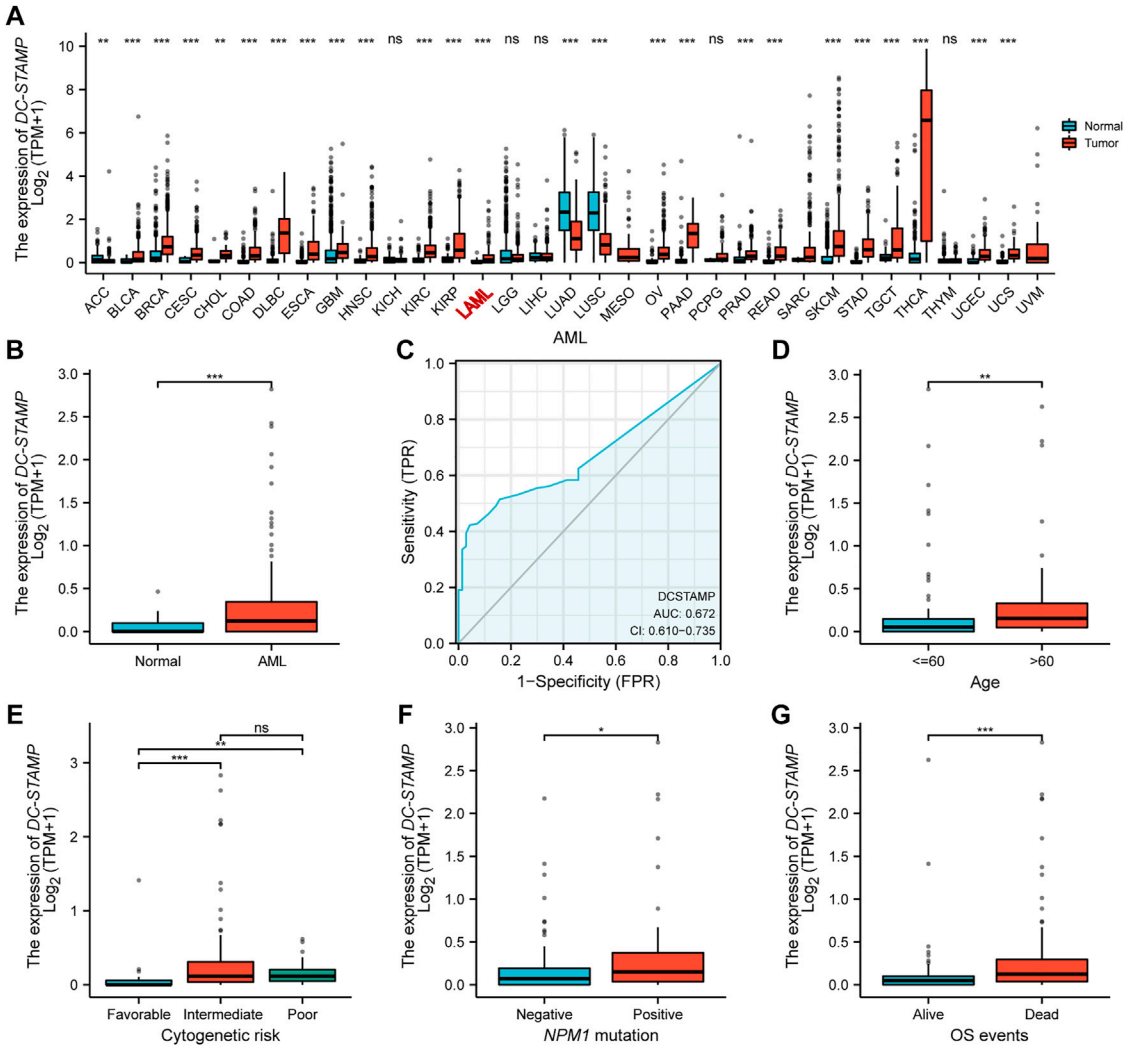


FIGURE 2 | High *DC-STAMP* expression was related with adverse clinical features. **(A)** Level of *DC-STAMP* expression in different tumors from TCGA and GTEx database. **(B)** Expression levels of *DC-STAMP* in AML ($n = 173$) and normal samples ($n = 70$). **(C)** Receiver operating characteristic analysis (ROC) of *DC-STAMP* in AML. Clinical characteristics including **(D)** age, **(E)** cytogenetic risk classification, **(F)** *NPM1* mutation, and **(G)** OS events ($n = 153$). Analysis between two groups of unpaired samples: Wilcoxon rank sum test, analysis among multiple groups of samples: Kruskal–Wallis rank sum test (ns $p \geq 0.05$, *$p < 0.05$, **$p < 0.01$, ***$p < 0.001$).

IDH1, *RAS*, and *NPM1* mutations. Together, high *DC-STAMP* expression was closely related to poor clinical characteristics.

High *DC-STAMP* Expression Predicts Worse Prognosis

We plotted OS curves by the KM method to identify the effect of the *DC-STAMP* on the outcomes in AML patients. Patients with a high expression presented a shorter OS than those with a low expression ($p < 0.001$, **Figure 3A**). We further use the univariate and multivariate Cox regression analyses to identify the value of the *DC-STAMP* for survival. By the univariate analysis, high *DC-STAMP* expression was associated with shorter OS [hazard radio, (HR): 2.683; 95% confidence interval (CI):1.723–4.178; $p < 0.001$, **Supplementary Table S1**]. Simultaneously, both age (HR: 3.333; 95% CI: 2.164–5.134; $p < 0.001$) and unfavorable cytogenetic risk (Intermediate: HR: 2.957; 95% CI; 1.498–5.836; $p = 0.002$, Poor: HR: 4.157; 95% CI: 1.944–8.893; $p < 0.001$) were related with poor OS. Then, we included the aforementioned significant univariable factors ($p < 0.1$) in the multivariate analysis and found that age (HR: 2.548; 95% CI: 1.601–4.055; $p < 0.001$), poor cytogenetic risk (HR: 2.293; 95% CI: 1.024–5.135; $p = 0.044$), and high *DC-STAMP* expression (HR: 1.733; 95% CI: 1.079–2.781; $p = 0.023$) were also independent prognostic factors, respectively. In detail, we drew forest plots to present the aforementioned results of the Cox regression analysis (**Figures 3B,C**, **Supplementary Table S1**).

Furthermore, to provide a quantitative prediction of the outcomes in AML patients, we constructed a nomogram plot using age, cytogenetic risk, and *DC-STAMP* expression (**Figure 3D**). The concordance index (C-index) for predicting the OS was 0.734 (95% CI: 0.706–0.762), indicating that the

TABLE 1 | Clinical characteristics of AML patients with differential *DC-STAMP* expression.

Characteristic	Low expression of *DC-STAMP*	High expression of *DC-STAMP*	*p*
n	75	76	
Age, median (IQR)	51 (39, 62)	61.5 (46.5, 69.25)	0.005[a]
Gender, n (%)			0.084[b]
Female	28 (18.5%)	40 (26.5%)	
Male	47 (31.1%)	36 (23.8%)	
Race, n (%)			1.000[c]
Asian	0 (0%)	1 (0.7%)	
Black or African–American	7 (4.7%)	6 (4%)	
White	67 (45%)	68 (45.6%)	
Age, n (%)			**0.004**[b]
≤60	53 (35.1%)	35 (23.2%)	
>60	22 (14.6%)	41 (27.2%)	
WBC count (x10⁹/L), n (%)			0.255[b]
≤20	34 (22.7%)	43 (28.7%)	
>20	40 (26.7%)	33 (22%)	
Cytogenetic risk, n (%)			< **0.001**[b]
Favorable	26 (17.4%)	5 (3.4%)	
Intermediate	34 (22.8%)	48 (32.2%)	
Poor	15 (10.1%)	21 (14.1%)	
FAB classifications, n (%)			**0.037**[b]
M0	8 (5.3%)	7 (4.7%)	
M1	18 (12%)	17 (11.3%)	
M2	13 (8.7%)	25 (16.7%)	
M3	13 (8.7%)	2 (1.3%)	
M4	16 (10.7%)	13 (8.7%)	
M5	5 (3.3%)	10 (6.7%)	
M6	1 (0.7%)	1 (0.7%)	
M7	0 (0%)	1 (0.7%)	
Cytogenetics, n (%)			**0.008**[b]
Normal	30 (22.2%)	39 (28.9%)	
+8	2 (1.5%)	6 (4.4%)	
del (5)	1 (0.7%)	0 (0%)	
del (7)	2 (1.5%)	4 (3%)	
inv (16)	5 (3.7%)	3 (2.2%)	
t (15; 17)	10 (7.4%)	1 (0.7%)	
t (8; 21)	7 (5.2%)	0 (0%)	
t (9; 11)	1 (0.7%)	0 (0%)	
Complex	12 (8.9%)	12 (8.9%)	
FLT3 mutation, n (%)			0.441[b]
Negative	54 (36.7%)	48 (32.7%)	
Positive	20 (13.6%)	25 (17%)	
IDH1 R132 mutation, n (%)			0.939[b]
Negative	66 (44.3%)	70 (47%)	
Positive	7 (4.7%)	6 (4%)	
IDH1 R140 mutation, n (%)			0.745[b]
Negative	70 (47%)	67 (45%)	
Positive	5 (3.4%)	7 (4.7%)	
IDH1 R172 mutation, n (%)			0.245[c]
Negative	75 (50.3%)	72 (48.3%)	
Positive	0 (0%)	2 (1.3%)	
RAS mutation, n (%)			1.000[c]
Negative	71 (47.3%)	71 (47.3%)	
Positive	4 (2.7%)	4 (2.7%)	
NPM1 mutation, n (%)			0.237[b]
Negative	62 (41.3%)	55 (36.7%)	
Positive	13 (8.7%)	20 (13.3%)	
OS events, n (%)			< **0.001**[b]
Alive	38 (25.2%)	16 (10.6%)	
Dead	37 (24.5%)	60 (39.7%)	

Bold indicates p *value less than 0.05*

[a]*Derived from the Wilcoxon rank sum test.*

[b]*Derived from Pearson's chi-squared test.*

[c]*Derived from Fisher's exact test.*

TABLE 2 | Twenty-eight items of GSEA.

Description	Set size	Enrichment score	NES	p. adjust
HALLMARK_EPITHELIAL_MESENCHYMAL_TRANSITION	195	−0.54676	−2.25033	0.008003
HALLMARK_ESTROGEN_RESPONSE_EARLY	200	−0.54257	−2.23437	0.008003
HALLMARK_MYOGENESIS	196	−0.47064	−1.9364	0.008003
HALLMARK_UV_RESPONSE_DN	142	−0.52416	−2.07013	0.008003
HALLMARK_ANGIOGENESIS	36	−0.55865	−1.75389	0.008003
HALLMARK_MYC_TARGETS_V2	55	0.665077	2.430489	0.008003
HALLMARK_ESTROGEN_RESPONSE_LATE	199	−0.39097	−1.60534	0.008003
HALLMARK_IL6_JAK_STAT3_SIGNALING	87	0.541276	2.153534	0.008003
HALLMARK_UNFOLDED_PROTEIN_RESPONSE	110	0.42742	1.766212	0.008003
HALLMARK_INTERFERON_ALPHA_RESPONSE	83	0.654209	2.566687	0.008003
HALLMARK_SPERMATOGENESIS	123	0.48507	2.043111	0.008003
HALLMARK_ALLOGRAFT_REJECTION	199	0.554861	2.511181	0.008003
HALLMARK_MITOTIC_SPINDLE	180	0.502551	2.25991	0.008003
HALLMARK_COMPLEMENT	187	0.365865	1.643381	0.008003
HALLMARK_E2F_TARGETS	187	0.773265	3.473328	0.008003
HALLMARK_G2M_CHECKPOINT	197	0.75184	3.382364	0.008003
HALLMARK_INFLAMMATORY_RESPONSE	194	0.464461	2.091942	0.008003
HALLMARK_GLYCOLYSIS	186	0.370532	1.661545	0.008003
HALLMARK_INTERFERON_GAMMA_RESPONSE	177	0.588205	2.629924	0.008003
HALLMARK_MTORC1_SIGNALING	196	0.576452	2.590705	0.008003
HALLMARK_MYC_TARGETS_V1	193	0.621926	2.792147	0.008003
HALLMARK_TNFA_SIGNALING_VIA_NFKB	198	0.370429	1.666859	0.008003
HALLMARK_UV_RESPONSE_UP	156	0.359304	1.590277	0.014397
HALLMARK_COAGULATION	136	−0.39733	−1.56144	0.017883
HALLMARK_DNA_REPAIR	136	0.358661	1.537167	0.019802
HALLMARK_BILE_ACID_METABOLISM	99	−0.4003	−1.49457	0.034754
HALLMARK_CHOLESTEROL_HOMEOSTASIS	62	0.396308	1.470851	0.036109

nomogram had a certain predictive accuracy for OS. Additionally, we performed calibration curves and DCA to evaluate the predictive performance of the nomogram model. The calibration curves presented consistency between the predicted OS of the nomogram and the actual proportion of OS at 1-, 3-, and 5-year (**Figure 3E**). Moreover, the DCA curves also verified the clinical utility of the predictive nomogram (**Figures 3F–H**). In summary, this nomogram model had an accurate ability to predict the patients' survival.

Differentially Expressed Gene Enrichment Analysis Reveals the Dysfunctional Signaling Pathway

We further explored the potential mechanisms in AML patients. Firstly, we identified the DEGs between high and low *DC-STAMP* expression. In total, 610 DEGs were obtained and shown in volcano plots (**Figure 4A**), including 260 upregulated genes and 350 downregulated genes ($|\log2FC| > 1$, adjusted p value < 0.05).

Next, we performed the GO and KEGG analyses to investigate the biological function of the aforementioned DEGs and obtained the top 15 GO enrichment items (CC five items, BP five items, and MF five items) and top five KEGG pathways (**Figures 4B,D–F** and **Supplementary Table S2**). Briefly, the channel activity, platelet alpha granule, extracellular structure organization, regulation of ion transmembrane transport, neuroactive ligand-receptor interaction, and extracellular matrix (ECM)–receptor interactions were the most enriched sets.

Moreover, to better understand the mutual connection, we performed an interactive analysis derived from the results of GO and KEGG analyses. It showed that the numbers of enrichment genes were channel activity (counts = 29), passive transmembrane transporter activity (counts = 29), collagen-containing extracellular matrix (counts = 28), substrate-specific channel activity (counts = 28), regulation of ion transmembrane transport (counts = 27), extracellular structure organization (counts = 25), transmembrane transporter complex (counts = 21), ion channel complex (counts = 20), neuroactive ligand-receptor interaction (counts = 19), and skeletal system morphogenesis (counts = 18) (**Figure 4C**).

Finally, the GSEA was used to investigate the enrichment pathway of *DC-STAMP* expression, and a total of 28 significant pathways were enriched (**Table 2**). Interestingly, some pathways, such as IL6-JAK-STAT3 signaling, mTORC1 signaling, TNF-α signaling *via* NF-κB, INF-γ response, glycolysis, and DNA repair (**Figures 4J–L**) were reported to correlate with leukemogenesis (Steelman et al., 2008; Park et al., 2010; Binder et al., 2018; Molina et al., 2018; Gabellier et al., 2020; Grants et al., 2020).

Identification of Hub Genes Connected With *DC-STAMP*

As indicated in **Figure 5A**, the PPI network of 358 encoding DEGs was constructed to determine the hub genes. The top 15 hub genes were selected by the maximum neighborhood component (MNC), density of maximum neighborhood component (DMNC), and maximal clique centrality (MCC) algorithms, respectively (**Figures**

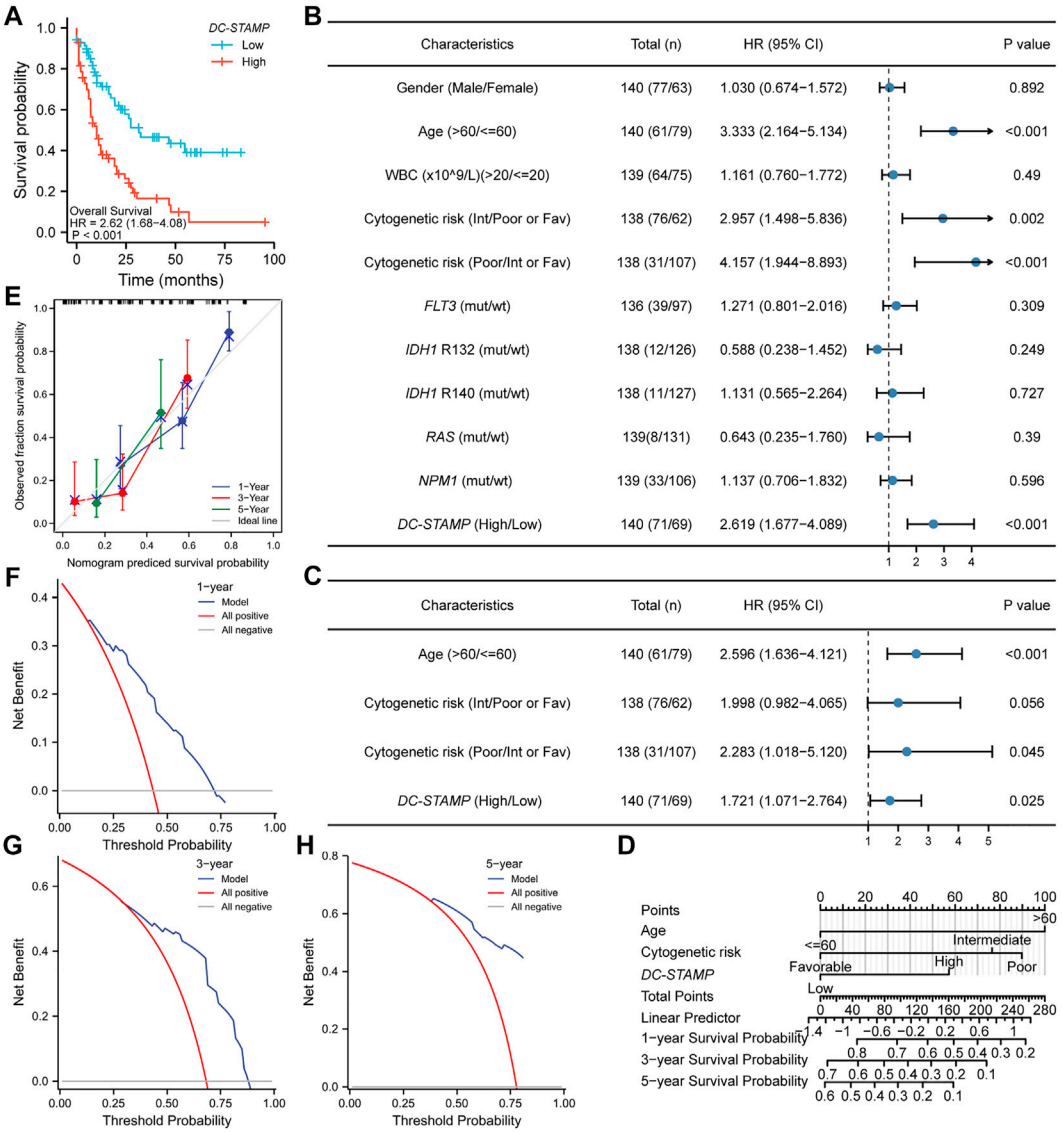


FIGURE 3 | Poor prognostic value of *DC-TAMP* expression in AML. **(A)** KM curve analysis of overall survival (OS) between high and low *DC-STAMP* expression groups. **(B)** Univariate analyses of OS showed by forest plot. **(C)** Multivariate analyses of OS showed by forest plot. **(D)** Nomogram integrates *DC-STAMP* and other prognostic factors in AML. **(E)** Calibration curve of nomogram. The DCA curves of nomogram (F) by 1 year, **(G)** 3 years, and **(H)** 5 years(mut; mutation, wt; wild type, Int; intermediate, Fav; favorable).

5B–D). Therefore, we observed four hub genes (*SELP*, *SERPINE1*, *PF4*, and *PPBP*) shared from the aforementioned three gene lists. We analyzed the association between the *DC-STAMP* and four hub genes. It indicated that the *DC-STAMP* has significant positive correlations with *SELP* ($p < 0.001$, correlation coefficient: 0.364), *PF4* ($p < 0.001$, correlation coefficient: 0.39), and *PPBP* ($p < 0.001$, correlation coefficient: 0.406) (**Figure 5E**). In contrast, the *DC-STAMP* and *SERPINE1* were negatively correlated ($p = 0.005$, correlation coefficient: 0.228) (**Figure 5E**). Finally, an analysis of the relationship between the four hub genes and clinical prognosis in AML patients revealed that only *PF4* and *PPBP* were expressed at a high level, which was associated with poor outcomes (**Figures 5F–I**).

Correlation Analysis Between *DC-STAMP* and Immune Cell or Immune Checkpoint Molecules

To describe the association of *DC-STAMP* expression with immune infiltration in AML, we systematically evaluated 24 kinds of infiltrated immune cells. The result showed that the level of *DC-STAMP* expression had a significant positive correlation with the infiltrating level of NK CD56 (dim) cells, macrophages, cytotoxic cells, and CD8 (+) T cells (**Figure 6A**). The details of a quantified analysis by Spearman's correlation are shown in **Figures 6B–E**. Furthermore, we analyzed the relationship between *DC-STAMP* expressions and widely

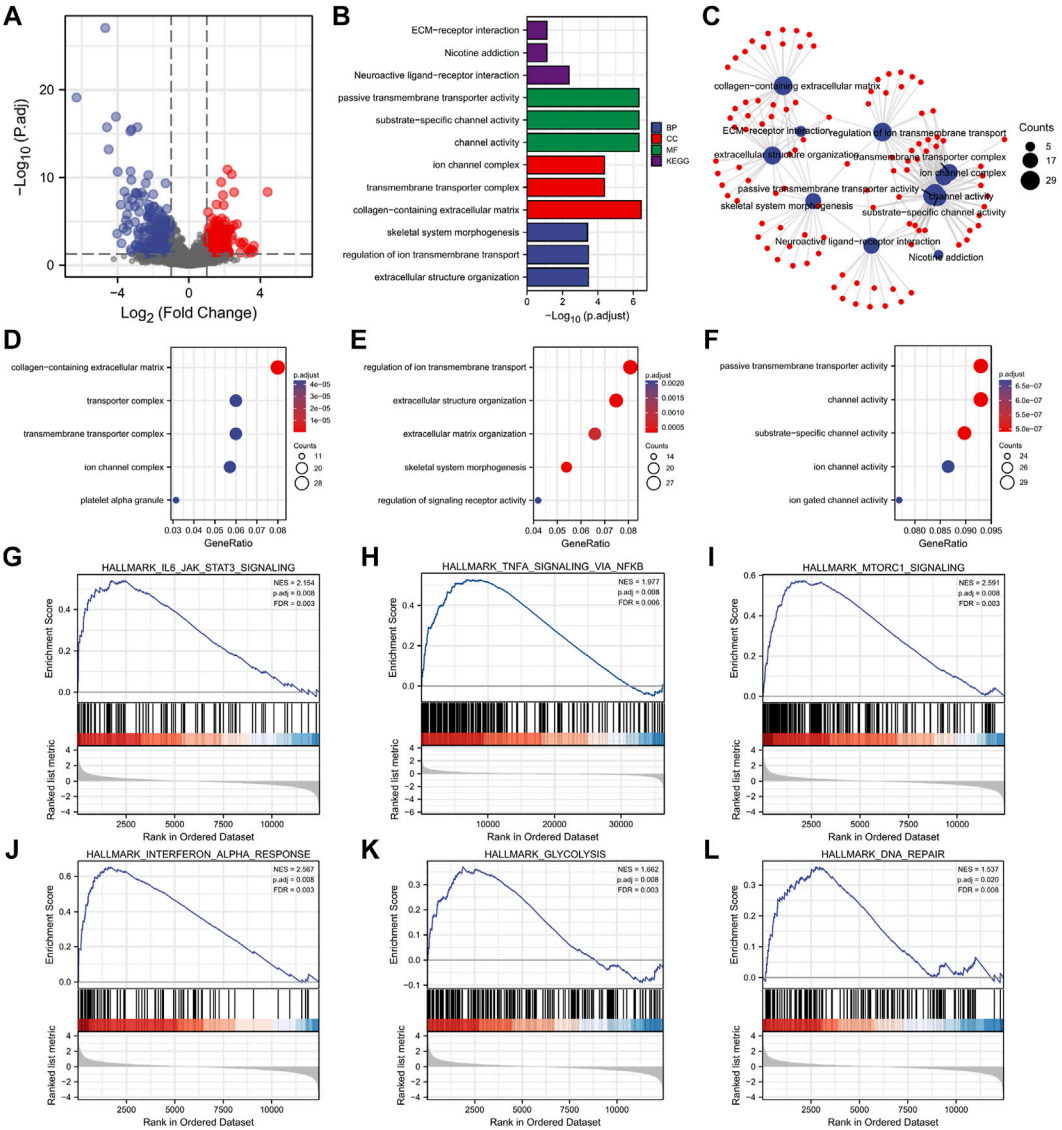


FIGURE 4 | DEG analysis and functional enrichment of high and low *DC-STAMP* expression groups in AML. **(A)** Volcano plot of DEGs. **(B)** GO and KEGG pathway of DEGs. **(C)** Interactive analysis with result of GO and KEGG analyses. **(D–F)** GO enrichment analysis of DEGs. **(G–L)** GSEA of DEGs. **(G)** Enrichment of genes in IL6-JAK-STAT3 signaling pathway. **(H)** Enrichment of genes in inflammatory pathway. **(I)** Enrichment of genes in mTORC1 signaling pathway. **(J)** Enrichment of genes in interferon alpha response pathway. **(K)** Enrichment of genes in glycolysis signaling pathway. **(L)** Enrichment of genes in DNA repair signaling pathway.

discussed immune checkpoint genes (*PDCD1*, *CD274*, *CTLA-4*, *LAG-3*, *TIGIT*, and *HAVCR2*). As shown in **Figure 6F**, the level of *DC-STAMP* gene expression was significantly and positively correlated with *PDCD1*, *CD274*, *CTLA-4*, and *TIGIT*. The specific correlation analysis is shown in **Figures 6G–J**.

DISCUSSION

AML is a hematological neoplastic disease and involves many different molecular genetic abnormalities. The *DC-STAMP* is considered to be a receptor protein, which functions by promoting DC antigen-presentation and osteoclast activation. Only few studies have revealed that overexpression of the *DC-STAMP* would influence the differentiation of myeloid lineage cells (Eleveld-Trancikova et al., 2008). It is also reported that normal HSCPs remain at the low level of the *DC-STAMP* (Eleveld-Trancikova et al., 2008; Eleveld-Trancikova et al., 2010). According to a recent review, a high *DC-STAMP* expression level may have potential pathogenic impacts on myeloid malignancies. However, it is still unknown whether DC-STAMP has an impact on AML.

Based on the aforementioned situation, we first investigated the association between the *DC-STAMP* and clinical features of AML by using TCGA database. As expected, an upregulated *DC-STAMP* expression was observed, and a high level of the *DC-*

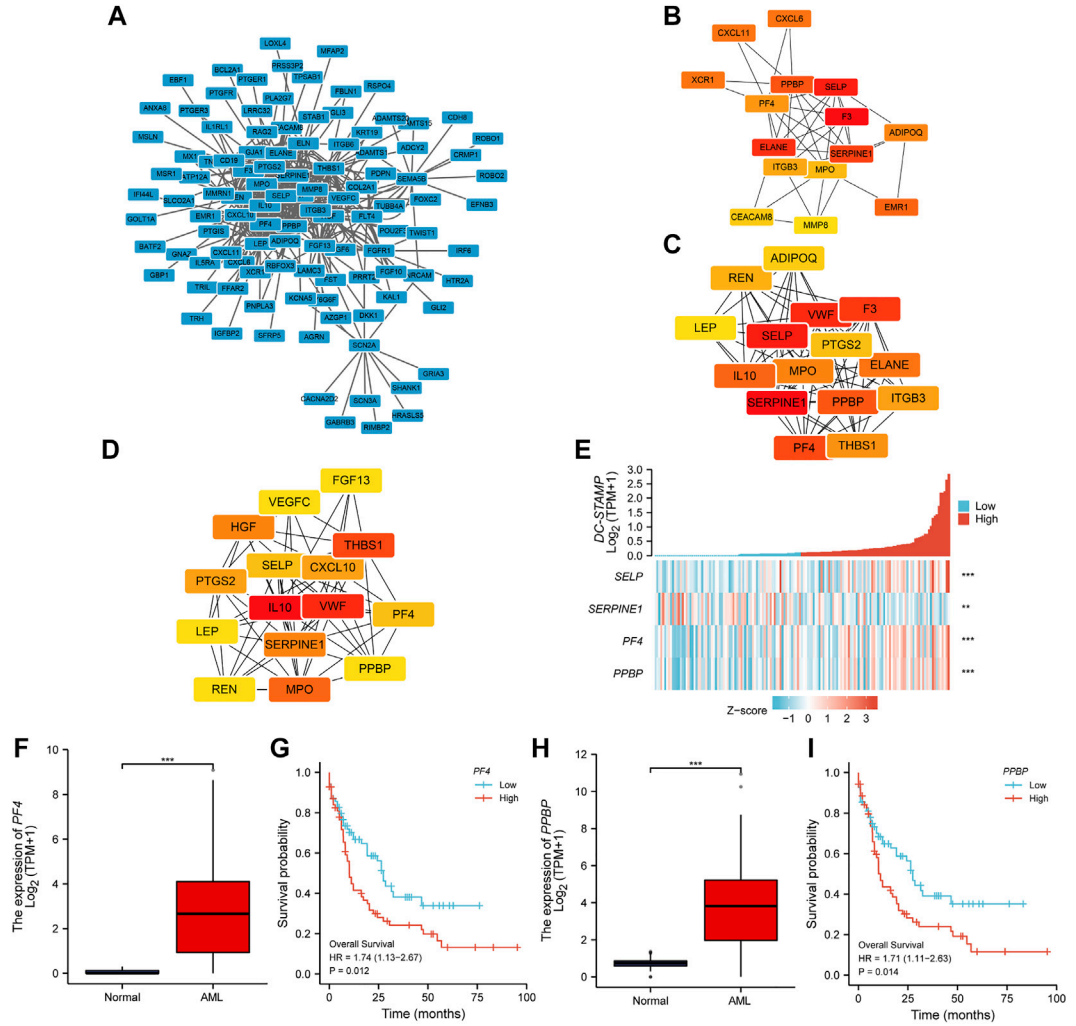


FIGURE 5 | PPI network construction and clinical significance of hub genes. **(A)** The PPI network of 358 encoding DEGs. **(B–D)** Top 15 hub genes were selected respectively by **(B)** MNC, **(C)** DMNC, and **(D)** MCC. **(E)** Association of *DC-STAMP* with four hub genes (*SELP*, *SFRPINE1*, *PF4*, and *PPBP*). **(F)** Expression levels of *PF4* in AML ($n = 173$) and normal subjects ($n = 70$). **(G)** Different OS between high- and low-*PF4* expression levels shown by KM curves. **(H)** Expression levels of *PPBP* in AML ($n = 173$) and normal subjects ($n = 70$). **(I)** Different OS between high- and low-*PPBP* expression levels shown by KM curves. (*$p < 0.05$, **$p < 0.01$, ***$p < 0.001$).

STAMP gene was correlated with adverse clinical characteristics and poor survival. Thus, it was consistent with the hypothesis that an abnormally high level of *DC-STAMP* expression blocked the differentiation of HSCs in AML patients.

Additionally, we preliminarily explored the pathogenic molecular mechanisms of the *DC-STAMP* by using various bioinformatics analyses. Expectedly, we found DEG enrichment pathways were focused on the molecular transport process and platelet alpha granule by GO and KEGG, while GSEA pathways were involved in mTORC1 signaling, TNF-α signaling *via* NF-κB, and inflammatory and DNA repair pathways. A previous research work reported that the activation of mTORC1 signaling promotes the proliferation and survival of the leukemic clones (Steelman et al., 2008; Park et al., 2010) and cytotoxicity in AML cells from the selective AMPK agonist (GSK621) because of mTORC1 activation which was through the eIF2α/ATF4 signaling pathway (Sujobert et al., 2015). Another study also revealed that the mTORC1 pathway had a correlation with easy relapse and disease progression in AML (Oki et al., 2021). Grants et al. (2020) mentioned that NF-κB, IL6, and TNF were a kind of potential drivers of HSC dysfunction, activating inflammatory signaling in myeloid malignancy. As we know, proinflammatory factors were linked to blast cell growth, and the dysregulation of cytokine signaling contributed to a beneficial AML microenvironment (Binder et al., 2018). Therefore, we think that the effect of the *DC-STAMP* on potential pathogens is probably associated with the aforementioned signaling pathways.

Furthermore, we obtained two hub genes (*PF4* and *PPBP*) with poor OS through different PPI calculation methods and survival analyses. It has been reported that *PF4* and *PPBP* belonged to the CXC chemokine family and played roles in platelet activation,

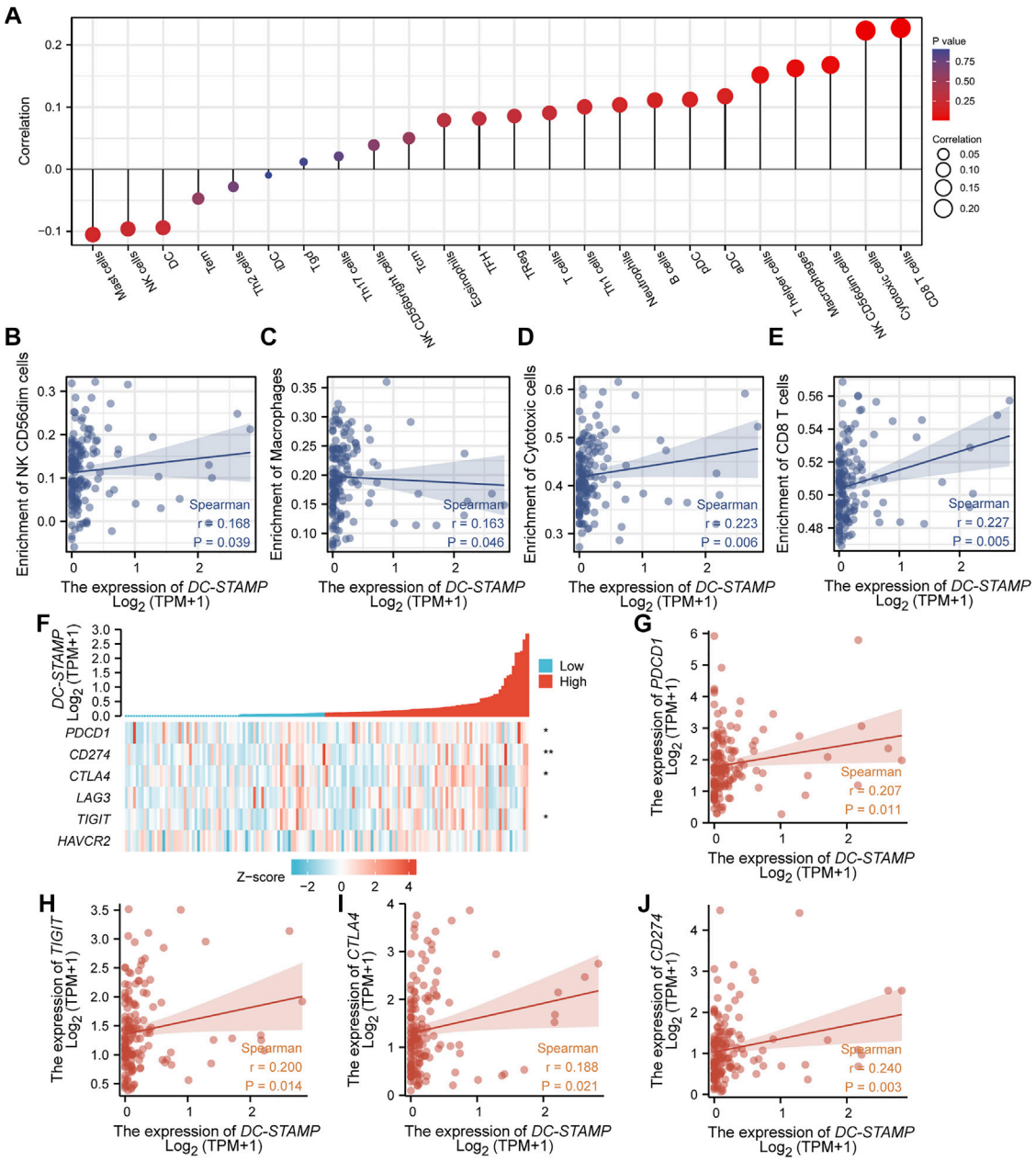


FIGURE 6 | Correlation analysis between the level of *DC-STAMP* gene expression and immune cell infiltration or immune checkpoint molecules. **(A)** Association between *DC-STAMP* expression and 24 kinds of infiltrated immune cells. **(B–E)** Using Spearman's correlation in quantified analysis of the correlation of *DC-STAMP* expression with infiltrating level of (**B**) NK CD56 (dim) cells, **(C)** macrophages, **(D)** cytotoxic cells and **(E)** and CD8 (+) T cells. **(F)** Association of *DC-STAMP* with five immune checkpoint molecules (*PDCD1*, *CD274*, *CTLA-4*, *LAG-3*, *TIGIT*, and *HAVCR2*). **(G–J)** Using Spearman's correlation in quantified analysis of the correlation of *DC-STAMP* expression with (**G**) *PDCD1,* **(H)** *TIGIT,* **(I)** *CTLA-4,* and **(J)** *CD274* (r was Spearman's correlation coefficient) (*$p < 0.05$, **$p < 0.01$, ***$p < 0.001$).

platelet degranulation, immune response to infection, activation of neutrophils and monocytes, and tumorigenesis. (Yan et al., 1994; Martí et al., 2002; Schaffner, 2005; Strieter et al., 2006; Sakurai et al., 2016). These two genes also had been implicated in acute megakaryocytic leukemia, lung adenocarcinoma, gastric cancer, and several autoimmune disorders, including rheumatoid arthritis and Crohn's disease (Ulivi et al., 2013; Pelleri et al., 2014; Takeyama et al., 2015; Pucci et al., 2016; Xia et al., 2017; Wu et al., 2021). Although the *DC-STAMP, PF4,* and *PPBP* had links with tumor-associated immune response, the mechanisms of the synergistic effects of their interaction remain unclear. A more in-depth detection is needed to explore this complex correlation in AML patients in future.

Finally, when analyzing the relationship between *DC-STAMP* expression and immune cell infiltration, we found that the high *DC-STAMP* group was inclined to harbor more immune cells

with cytotoxic effects. As previously demonstrated, the *DC-STAMP* promoted the most efficient CD4 (+) and CD8 (+) T-cell responses *in vitro* (Moulin et al., 2012). Moreover, AML patients had a trend toward increased mature NK cells (NK CD56 (dim) cells) (Tang et al., 2020). We also found *DC-STAMP* expression had a correlation with *PDCD1*, *CD274*, *CTLA-4*, and *TIGIT* which were exhaustion markers of T cells and considered a dysfunction of anti-tumor immunity (Noviello et al., 2019; Wang et al., 2021). A recent study showed that PD1-positive/CD8-positive T cells were higher in relapsed AML patients, compared with newly diagnosed AML patients (Williams et al., 2019). This result may suggest that the *DC-STAMP* was closely related to the immune escape of AML. However, the detailed pathological mechanism of the *DC-STAMP* remains unknown and needs further exploration in the future. The research of *DC-STAMP* expression or the relationship between the *DC-STAMP* and immune checkpoints would be a benefit for the discovery of new immunotherapeutic targets to improve the survival of AML patients.

However, our study still has the following limitations that cannot be ignored. Firstly, we investigate the diagnostic effect of the *DC-STAMP* because of the publicly available TCGA AML database and this observation needs to be subsequently validated in larger independent cohorts. Secondly, although this research comprehensively describes the impact of the *DC-STAMP* level on the survival of AML patients, it lacks the exploration of *DC-STAMP* pathogenic mutations. Lastly, all the interactions between the *DC-STAMP* and AML-associated immune response lack functional validation and detection of the potential molecular mechanisms. Therefore, further laboratory work is required to make up for the aforementioned shortcomings.

CONCLUSION

In this research, it was shown that high expression of *DC-STAMP* has an adverse effect on the overall survival of AML patients and is linked to both AML-associated pathway activation and special immune cells or checkpoints, which suggests that high expression of *DC-STAMP* may be a potential independent prognostic factor and an immunotherapeutic target for AML. This finding could help clinicians decide on optimal regimens and explore new targeted therapies for AML patients.

DATA AVAILABILITY STATEMENT

All data were collected and downloaded from TCGA and GTEx database using the following links: Clinical data of AML was downloaded from TCGA: https://portal.gdc.cancer.gov/projects/TCGA-LAML RNA-seq data of TCGA and GTEx was collected from UCSC XENA browser: https://xenabrowser.net/datapages/.

ETHICS STATEMENT

Written and informed consent was obtained from the individual(s) for the publication of any potential identifiable images or data included in this article.

AUTHOR CONTRIBUTIONS

QL, LZ, WW, and JS conceived the study. QL, LZ, and WW. collected and analyzed the data and wrote the paper. QL, LZ, WW, QL, and LF, contributed to the data collection and analysis. JS designed the research and gave approval of the final manuscript.

FUNDING

This work was supported by the Tianjin Municipal Science and Technology Commission Major Project (18ZXDBSY00070), the National Natural Science Foundation of China (81670120), and CAMS Innovation Fund for Medical Sciences (2021-I2M-1-073).

SUPPLEMENTARY MATERIAL

The Supplementary Material for this article can be found online at: https://www.frontiersin.org/articles/10.3389/fgene.2022.876689/full#supplementary-material

Supplementary Figure S1 | DC-*STAMP* expression has no association with French-American-British (FAB) classifications.

Supplementary Table S1 | Univariate and multivariate Cox regression analyses.

Supplementary Table S2 | GO enrichment analysis and KEGG pathway analysis.

REFERENCES

Assi, S. A., Imperato, M. R., Coleman, D. J. L., Pickin, A., Potluri, S., Ptasinska, A., et al. (2019). Subtype-Specific Regulatory Network Rewiring in Acute Myeloid Leukemia. *Nat. Genet.* 51 (1), 151–162. doi:10.1038/s41588-018-0270-1

Bindea, G., Mlecnik, B., Tosolini, M., Kirilovsky, A., Waldner, M., Obenauf, A. C., et al. (2013). Spatiotemporal Dynamics of Intratumoral Immune Cells Reveal the Immune Landscape in Human Cancer. *Immunity* 39 (4), 782–795. doi:10.1016/j.immuni.2013.10.003

Binder, S., Luciano, M., and Horejs-Hoeck, J. (2018). The Cytokine Network in Acute Myeloid Leukemia (AML): A Focus on Pro- and Anti-Inflammatory Mediators. *Cytokine Growth Factor. Rev.* 43, 8–15. doi:10.1016/j.cytogfr.2018.08.004

Campos, L., Rouault, J., Sabido, O., Oriol, P., Roubi, N., Vasselon, C., et al. (1993). High Expression of Bcl-2 Protein in Acute Myeloid Leukemia Cells Is Associated with Poor Response to Chemotherapy. *Blood* 81 (11), 3091–3096. doi:10.1182/blood.v81.11.3091.3091

Chen, X., Glytsou, C., Zhou, H., Narang, S., Reyna, D. E., Lopez, A., et al. (2019). Targeting Mitochondrial Structure Sensitizes Acute Myeloid Leukemia to Venetoclax Treatment. *Cancer Discov.* 9 (7), 890–909. doi:10.1158/2159-8290.CD-19-0117

Consortium, G. T. (2020). The GTEx Consortium Atlas of Genetic Regulatory Effects across Human Tissues. *Science* 369 (6509), 1318–1330. doi:10.1126/science.aaz1776

DiNardo, C. D., Jonas, B. A., Pullarkat, V., Thirman, M. J., Garcia, J. S., Wei, A. H., et al. (2020). Azacitidine and Venetoclax in Previously Untreated Acute Myeloid Leukemia. *N. Engl. J. Med.* 383 (7), 617–629. doi:10.1056/NEJMoa2012971

Eleveld-Trancikova, D., Janssen, R. A. J., Hendriks, I. A. M., Looman, M. W. G., Moulin, V., Jansen, B. J. H., et al. (2008). The DC-Derived Protein DC-STAMP Influences Differentiation of Myeloid Cells. *Leukemia* 22 (2), 455–459. doi:10.1038/sj.leu.2404910

Eleveld-Trancikova, D., Sanecka, A., van Hout-Kuijer, M. A., Looman, M. W. G., Hendriks, I. A. M., Jansen, B. J. H., et al. (2010). DC-STAMP Interacts with ER-Resident Transcription Factor LUMAN Which Becomes Activated during DC Maturation. *Mol. Immunol.* 47 (11-12), 1963–1973. doi:10.1016/j.molimm.2010.04.019

Estey, E. (2016). Acute Myeloid Leukemia - Many Diseases, Many Treatments. *N. Engl. J. Med.* 375 (21), 2094–2095. doi:10.1056/NEJMe1611424

Fröhling, S., Schlenk, R. F., Breitruck, J., Benner, A., Kreitmeier, S., Tobis, K., et al. (2002). Prognostic Significance of Activating FLT3 Mutations in Younger Adults (16 to 60 years) with Acute Myeloid Leukemia and normal Cytogenetics: A Study of the AML Study Group Ulm. *Blood* 100 (13), 4372–4380. doi:10.1182/blood-2002-05-1440

Gabellier, L., Bret, C., Bossis, G., Cartron, G., and Moreaux, J. (2020). DNA Repair Expression Profiling to Identify High-Risk Cytogenetically Normal Acute Myeloid Leukemia and Define New Therapeutic Targets. *Cancers* 12 (10), 2874. doi:10.3390/cancers12102874

Gene Ontology Consortium (2021). The Gene Ontology Resource: Enriching a GOld Mine. *Nucleic Acids Res.* 49 (D1), D325–D334. doi:10.1093/nar/gkaa1113

Goldman, M. J., Craft, B., Hastie, M., Repečka, K., McDade, F., Kamath, A., et al. (2020). Visualizing and Interpreting Cancer Genomics Data via the Xena Platform. *Nat. Biotechnol.* 38 (6), 675–678. doi:10.1038/s41587-020-0546-8

Grants, J. M., Wegrzyn, J., Hui, T., O'Neill, K., Shadbolt, M., Knapp, D. J. H. F., et al. (2020). Altered microRNA Expression Links IL6 and TNF-Induced Inflammaging with Myeloid Malignancy in Humans and Mice. *Blood* 135 (25), 2235–2251. doi:10.1182/blood.2019003105

Hänzelmann, S., Castelo, R., and Guinney, J. (2013). GSVA: Gene Set Variation Analysis for Microarray and RNA-Seq Data. *BMC Bioinformatics* 14, 7. doi:10.1186/1471-2105-14-7

Hartgers, F. C., Vissers, J. L. M., Looman, M. W. G., Zoelen, C. v., Huffine, C., Figdor, C. G., et al. (2000). DC-STAMP, a Novel Multimembrane-Spanning Molecule Preferentially Expressed by Dendritic Cells. *Eur. J. Immunol.* 30 (12), 3585–3590. doi:10.1002/1521-4141(200012)30:12<3585::aid-immu3585>3.0.co;2-y

Kanehisa, M., Sato, Y., and Kawashima, M. (2021). KEGG Mapping Tools for Uncovering Hidden Features in Biological Data. *Protein Sci.* 31, 47–53. doi:10.1002/pro.4172

Kayser, S., and Levis, M. J. (2018). Advances in Targeted Therapy for Acute Myeloid Leukaemia. *Br. J. Haematol.* 180 (4), 484–500. doi:10.1111/bjh.15032

Love, M. I., Huber, W., and Anders, S. (2014). Moderated Estimation of Fold Change and Dispersion for RNA-Seq Data with DESeq2. *Genome Biol.* 15 (12), 550. doi:10.1186/s13059-014-0550-8

Martí, F., Bertran, E., Llucià, M., Villén, E., Peiró, M., Garcia, J., et al. (2002). Platelet Factor 4 Induces Human Natural Killer Cells to Synthesize and Release Interleukin-8. *J. Leukoc. Biol.* 72 (3), 590–597. doi:10.1189/jlb.72.3.590

Molina, J. R., Sun, Y., Protopopova, M., Gera, S., Bandi, M., Bristow, C., et al. (2018). An Inhibitor of Oxidative Phosphorylation Exploits Cancer Vulnerability. *Nat. Med.* 24 (7), 1036–1046. doi:10.1038/s41591-018-0052-4

Moulin, V., Morgan, M. E., Eleveld-Trancikova, D., Haanen, J. B. A. G., Wielders, E., Looman, M. W. G., et al. (2012). Targeting Dendritic Cells with Antigen via Dendritic Cell-Associated Promoters. *Cancer Gene Ther.* 19 (5), 303–311. doi:10.1038/cgt.2012.2

Noviello, M., Manfredi, F., Ruggiero, E., Perini, T., Oliveira, G., Cortesi, F., et al. (2019). Bone Marrow Central Memory and Memory Stem T-Cell Exhaustion in AML Patients Relapsing after HSCT. *Nat. Commun.* 10 (1), 1065. doi:10.1038/s41467-019-08871-1

Oki, T., Mercier, F., Kato, H., Jung, Y., McDonald, T. O., Spencer, J. A., et al. (2021). Imaging Dynamic mTORC1 Pathway Activity *In Vivo* Reveals Marked Shifts that Support Time-Specific Inhibitor Therapy in AML. *Nat. Commun.* 12 (1), 245. doi:10.1038/s41467-020-20491-8

Park, S., Chapuis, N., Tamburini, J., Bardet, V., Cornillet-Lefebvre, P., Willems, L., et al. (2010). Role of the PI3K/AKT and mTOR Signaling Pathways in Acute Myeloid Leukemia. *Haematologica* 95 (5), 819–828. doi:10.3324/haematol.2009.013797

Patel, J. P., Gönen, M., Figueroa, M. E., Fernandez, H., Sun, Z., Racevskis, J., et al. (2012). Prognostic Relevance of Integrated Genetic Profiling in Acute Myeloid Leukemia. *N. Engl. J. Med.* 366 (12), 1079–1089. doi:10.1056/NEJMoa1112304

Pelleri, M. C., Piovesan, A., Caracausi, M., Berardi, A. C., Vitale, L., and Strippoli, P. (2014). Integrated Differential Transcriptome Maps of Acute Megakaryoblastic Leukemia (AMKL) in Children with or without Down Syndrome (DS). *BMC Med. Genomics* 7, 63. doi:10.1186/s12920-014-0063-z

Pucci, F., Rickelt, S., Newton, A. P., Garris, C., Nunes, E., Evavold, C., et al. (2016). PF4 Promotes Platelet Production and Lung Cancer Growth. *Cel Rep.* 17 (7), 1764–1772. doi:10.1016/j.celrep.2016.10.031

Puram, R. V., Kowalczyk, M. S., de Boer, C. G., Schneider, R. K., Miller, P. G., McConkey, M., et al. (2016). Core Circadian Clock Genes Regulate Leukemia Stem Cells in AML. *Cell* 165 (2), 303–316. doi:10.1016/j.cell.2016.03.015

Sakurai, K., Fujiwara, T., Hasegawa, S., Okitsu, Y., Fukuhara, N., Onishi, Y., et al. (2016). Inhibition of Human Primary Megakaryocyte Differentiation by Anagrelide: A Gene Expression Profiling Analysis. *Int. J. Hematol.* 104 (2), 190–199. doi:10.1007/s12185-016-2006-2

Sawatani, Y., Miyamoto, T., Nagai, S., Maruya, M., Imai, J., Miyamoto, K., et al. (2008). The Role of DC-STAMP in Maintenance of Immune Tolerance through Regulation of Dendritic Cell Function. *Int. Immunol.* 20 (10), 1259–1268. doi:10.1093/intimm/dxn082

Schaffner, A. (2005). Regulated Expression of Platelet Factor 4 in Human Monocytes-Rrole of PARs as a Quantitatively Important Monocyte Activation Pathway. *J. Leukoc. Biol.* 78 (1), 202–209. doi:10.1189/jlb.0105024

Shannon, P., Markiel, A., Ozier, O., Baliga, N. S., Wang, J. T., Ramage, D., et al. (2003). Cytoscape: A Software Environment for Integrated Models of Biomolecular Interaction Networks. *Genome Res.* 13 (11), 2498–2504. doi:10.1101/gr.1239303

Silvestris, F., Ciavarella, S., Strippoli, S., and Dammacco, F. (2011). Cell Fusion and Hyperactive Osteoclastogenesis in Multiple Myeloma. *Adv. Exp. Med. Biol.* 714, 113–128. doi:10.1007/978-94-007-0782-5_5

Steelman, L. S., Abrams, S. L., Whelan, J., Bertrand, F. E., Ludwig, D. E., Bäsecke, J., et al. (2008). Contributions of the Raf/MEK/ERK, PI3K/PTEN/Akt/mTOR and Jak/STAT Pathways to Leukemia. *Leukemia* 22 (4), 686–707. doi:10.1038/leu.2008.26

Stone, R. M., Mandrekar, S. J., Sanford, B. L., Laumann, K., Geyer, S., Bloomfield, C. D., et al. (2017). Midostaurin Plus Chemotherapy for Acute Myeloid Leukemia with a FLT3 Mutation. *N. Engl. J. Med.* 377 (5), 454–464. doi:10.1056/NEJMoa1614359

Strieter, R. M., Burdick, M. D., Mestas, J., Gomperts, B., Keane, M. P., and Belperio, J. A. (2006). Cancer CXC Chemokine Networks and Tumour Angiogenesis. *Eur. J. Cancer* 42 (6), 768–778. doi:10.1016/j.ejca.2006.01.006

Subramanian, A., Tamayo, P., Mootha, V. K., Mukherjee, S., Ebert, B. L., Gillette, M. A., et al. (2005). Gene Set Enrichment Analysis: A Knowledge-Based Approach for Interpreting Genome-wide Expression Profiles. *Proc. Natl. Acad. Sci. U.S.A.* 102 (43), 15545–15550. doi:10.1073/pnas.0506580102

Sujobert, P., Poulain, L., Paubelle, E., Zylbersztejn, F., Grenier, A., Lambert, M., et al. (2015). Co-Activation of AMPK and mTORC1 Induces Cytotoxicity in Acute Myeloid Leukemia. *Cel Rep.* 11 (9), 1446–1457. doi:10.1016/j.celrep.2015.04.063

Szklarczyk, D., Gable, A. L., Lyon, D., Junge, A., Wyder, S., Huerta-Cepas, J., et al. (2019). STRING V11: Protein-Protein Association Networks with Increased Coverage, Supporting Functional Discovery in Genome-Wide Experimental Datasets. *Nucleic Acids Res.* 47 (D1), D607–D613. doi:10.1093/nar/gky1131

Takeyama, H., Mizushima, T., Iijima, H., Shinichiro, S., Uemura, M., Nishimura, J., et al. (2015). Platelet Activation Markers Are Associated with Crohn's Disease Activity in Patients with Low C-Reactive Protein. *Dig. Dis. Sci.* 60 (11), 3418–3423. doi:10.1007/s10620-015-3745-2

Tang, L., Wu, J., Li, C.-G., Jiang, H.-W., Xu, M., Du, M., et al. (2020). Characterization of Immune Dysfunction and Identification of Prognostic Immune-Related Risk Factors in Acute Myeloid Leukemia. *Clin. Cancer Res.* 26 (7), 1763–1772. doi:10.1158/1078-0432.ccr-19-3003

Tzifi, F., Economopoulou, C., Gourgiotis, D., Ardavanis, A., Papageorgiou, S., and Scorilas, A. (2012). The Role of BCL2 Family of Apoptosis Regulator Proteins in Acute and Chronic Leukemias. *Adv. Hematol.* 2012, 524308. doi:10.1155/2012/524308

Ulivi, P., Mercatali, L., Casoni, G.-L., Scarpi, E., Bucchi, L., Silvestrini, R., et al. (2013). Multiple Marker Detection in Peripheral Blood for NSCLC Diagnosis. *PLoS ONE* 8 (2), e57401. doi:10.1371/journal.pone.0057401

Vivian, J., Rao, A. A., Nothaft, F. A., Ketchum, C., Armstrong, J., Novak, A., et al. (2017). Toil Enables Reproducible, Open Source, Big Biomedical Data Analyses. *Nat. Biotechnol.* 35 (4), 314–316. doi:10.1038/nbt.3772

Wang, X., Chen, Y., Li, Z., Huang, B., Xu, L., Lai, J., et al. (2021). Single-Cell RNA-Seq of T Cells in B-ALL Patients Reveals an Exhausted Subset with

Remarkable Heterogeneity. *Adv. Sci.* 8 (19), 2101447. doi:10.1002/advs.202101447

Williams, P., Basu, S., Garcia-Manero, G., Hourigan, C. S., Oetjen, K. A., Cortes, J. E., et al. (2019). The Distribution of T-cell Subsets and the Expression of Immune Checkpoint Receptors and Ligands in Patients with Newly Diagnosed and Relapsed Acute Myeloid Leukemia. *Cancer* 125 (9), 1470–1481. doi:10.1002/cncr.31896

Wu, F., Chen, C., and Peng, F. (2021). Potential Association between Asthma, *Helicobacter P* Infection, and Gastric Cancer. *Front. Oncol.* 11, 630235. doi:10.3389/fonc.2021.630235

Xia, W., Wu, J., Deng, F.-Y., Wu, L.-F., Zhang, Y.-H., Guo, Y.-F., et al. (2017). Integrative Analysis for Identification of Shared Markers from Various Functional Cells/Tissues for Rheumatoid Arthritis. *Immunogenetics* 69 (2), 77–86. doi:10.1007/s00251-016-0956-4

Yagi, M., Miyamoto, T., Sawatani, Y., Iwamoto, K., Hosogane, N., Fujita, N., et al. (2005). DC-STAMP Is Essential for Cell-Cell Fusion in Osteoclasts and Foreign Body Giant Cells. *J. Exp. Med.* 202 (3), 345–351. doi:10.1084/jem.20050645

Yan, Z., Zhang, J., Holt, J., Stewart, G., Niewiarowski, S., and Poncz, M. (1994). Structural Requirements of Platelet Chemokines for Neutrophil Activation. *Blood* 84 (7), 2329–2339. doi:10.1182/blood.v84.7.2329.2329

Yu, G., Wang, L.-G., Han, Y., and He, Q.-Y. (2012). ClusterProfiler: An R Package for Comparing Biological Themes Among Gene Clusters. *OMICS* 16 (5), 284–287. doi:10.1089/omi.2011.0118

Conflict of Interest: The authors declare that the research was conducted in the absence of any commercial or financial relationships that could be construed as a potential conflict of interest.

Publisher's Note: All claims expressed in this article are solely those of the authors and do not necessarily represent those of their affiliated organizations, or those of the publisher, the editors, and the reviewers. Any product that may be evaluated in this article, or claim that may be made by its manufacturer, is not guaranteed or endorsed by the publisher.

Copyright © 2022 Liang, Zhang, Wang, Zhao, Li, Pan, Gao, Fang and Shi. This is an open-access article distributed under the terms of the Creative Commons Attribution License (CC BY). The use, distribution or reproduction in other forums is permitted, provided the original author(s) and the copyright owner(s) are credited and that the original publication in this journal is cited, in accordance with accepted academic practice. No use, distribution or reproduction is permitted which does not comply with these terms.

frontiers | Frontiers in Genetics

ORIGINAL RESEARCH
published: 10 May 2022
doi: 10.3389/fgene.2022.872224

Association of a Novel DOCK2 Mutation-Related Gene Signature With Immune in Hepatocellular Carcinoma

*Yushen Huang[1†], Wen Luo[2†], Siyun Chen[1†], Hongmei Su[1], Wuchang Zhu[1], Yuanyuan Wei[1], Yue Qiu[1], Yan Long[1], Yanxia Shi[1] and Jinbin Wei[1]**

[1]Pharmaceutical College, Guangxi Medical University, Nanning, China, [2]Department of Gastrointestinal Surgery, The Fourth Affiliated Hospital of Guangxi Medical University, Liuzhou, China

Hepatocellular carcinoma (HCC) is a malignant tumor with high morbidity and mortality worldwide. Many studies have shown that dedicator of cytokinesis 2 (DOCK2) has a crucial role as a prognostic factor in various cancers. However, the potentiality of DOCK2 in the diagnosis of HCC has not been fully elucidated. In this work, we aimed to investigate the prognostic role of DOCK2 mutation in HCC. The Cancer Genome Atlas (TCGA) and the International Cancer Genome Consortium (ICGC) cohorts were utilized to identify the mutation frequency of DOCK2. Then, univariate Cox proportional hazard regression analysis, random forest (RF), and multivariate Cox regression analysis were performed to develop the risk score that was significantly related to DOCK2 mutation. Moreover, Gene Set Enrichment Analysis (GSEA), Gene Set Variation Analysis (GSVA), and immune correlation analysis were conducted for an in-depth study of the biological process of DOCK2 mutation involved in HCC. The results revealed that the mutation frequency of DOCK2 was relatively higher than that in non-cancer control subjects, and patients with DOCK2 mutations had a low survival rate and a poor prognosis compared with the DOCK2-wild group. In addition, the secretin receptor (SCTR), tetratricopeptide repeat, ankyrin repeat and coiled-coil domain-containing 1 (TANC1), Alkb homolog 7 (ALKBH7), FRAS1-related extracellular matrix 2 (FREM2), and G protein subunit gamma 4 (GNG4) were found to be the most relevant prognostic genes of DOCK2 mutation, and the risk score based on the five genes played an excellent role in predicting the status of survival, tumor mutation burden (TMB), and microsatellite instability (MSI) in DOCK2 mutant patients. In addition, DOCK2 mutation and the risk score were closely related to immune responses. In conclusion, the present study identifies a novel prognostic signature in light of DOCK2 mutation-related genes that shows great prognostic value in HCC patients; and this gene mutation might promote tumor progression by influencing immune responses. These data may provide valuable insights for future investigations into personalized forecasting methods and also shed light on stratified precision oncology treatment.

Keywords: hepatocellular carcinoma, DOCK2, prognosis, biomarker, immune

OPEN ACCESS

Edited by:
Ayan Biswas,
University of Alabama at Birmingham, United States

Reviewed by:
Vikash Kansal,
Emory University, United States
Ka Wu,
Nanning Second People's Hospital, China

****Correspondence:***
Jinbin Wei
wjbguangxi@sina.cn

[†]These authors have contributed equally to this work and share first authorship

Specialty section:
This article was submitted to Cancer Genetics and Oncogenomics, a section of the journal Frontiers in Genetics

Received: *09 February 2022*
Accepted: *08 April 2022*
Published: *10 May 2022*

Citation:
Huang Y, Luo W, Chen S, Su H, Zhu W, Wei Y, Qiu Y, Long Y, Shi Y and Wei J (2022) Association of a Novel DOCK2 Mutation-Related Gene Signature With Immune in Hepatocellular Carcinoma. Front. Genet. 13:872224. doi: 10.3389/fgene.2022.872224

INTRODUCTION

Hepatocellular carcinoma (HCC), one of the most common forms of cancer, ranks as the second leading cause of cancer death in the world (Zhao et al., 2018; Roderfeld et al., 2020). At present, the treatments for HCC mainly include liver resection, hepatic transplantation, ablation, and transarterial chemoembolization (TACE) (Chen et al., 2020). Nevertheless, due to the high metastasis and recurrence rate after surgery, the overall prognosis of HCC patients remains poor (Li et al., 2021). Usually, liver cancer is not diagnosed until its advanced stage, which makes the fact that most patients receive either no treatment or only palliative treatment (Mittal et al., 2016), indicating that delayed diagnosis results in low patient survival rates. Although alpha-fetoprotein (AFP) is commonly applied as a tumor indicator for the diagnosis of HCC, its low specificity and accuracy are its shortage, which leads to patients missing the best treatment period (Liang Y. et al., 2021). Thus, there is an urgent need to discover new biomarkers to facilitate early detection and prognostic evaluation of HCC.

Dedicator of cytokinesis 2 (DOCK2), originally known as KIAA0209, encodes CDM protein and has been discovered to be linked with a prognostic factor in various cancers (Chen et al., 2018). Recent research exhibited that a high expression level of DOCK2 conferred a good prognosis of acute myeloid leukemia (Hu et al., 2019). In prostate cancer, many specifically hypermethylated genes were found, including DOCK2, GRASP, HIF3A, and PKFP, among which DOCK2 is the candidate marker with the greatest potentiality (Bjerre et al., 2019). In addition, lower DOCK2 expression was related to a poorer prognosis in colorectal cancer, which was attributed to the regulation of canonical and noncanonical Wnt signaling (Yu et al., 2015). Moreover, the DOCK2 genetic variant caused decreased DOCK2 mRNA transcript levels and might be a prognostic biomarker of non-small-cell lung cancer survival (Du et al., 2021). Notably, the mutation of DOCK2 was discovered to correlate with a high risk of HCC (Huang T. et al., 2021). However, the potentiality of DOCK2 in the diagnosis of HCC has not been fully elucidated.

In this work, we intended to investigate the prognostic role of DOCK2 mutation in HCC. First, The Cancer Genome Atlas (TCGA) and the International Cancer Genome Consortium (ICGC) cohorts were utilized to identify the mutation frequency of DOCK2. After clarifying the characteristic genes that are most related to DOCK2 mutation, the risk score was developed, which played an excellent role in predicting the status of survival, tumor mutation burden (TMB), and microsatellite instability (MSI) in DOCK2 mutant patients. Furthermore, for an in-depth study of the biological processes involved in HCC, Gene Set Enrichment Analysis (GSEA), Gene Set Variation Analysis (GSVA), and immune correlation analysis of DOCK2 were performed. Our findings may identify a novel risk score related to DOCK2 mutation for the prognosis of HCC, contributing to early diagnosis, targeted therapy, and prognostic assessment of HCC.

TABLE 1 | Summary of patient data sets.

Variable	TCGA set (*n* = 353)	ICGC set (*n* = 258)
Age (years)	—	—
≤55	119	29
>55	234	229
Gender	—	—
Female	116	67
Male	237	191
Histologic grade	—	—
G1	52	39
G2	171	116
G3	113	80
G4	12	23
TNM stage	—	—
I/II	247	N/A
III/IV	85	N/A
Family history	—	—
No	199	164
Yes	106	77

MATERIALS AND METHODS

Data Processing

In this study, The Cancer Genome Atlas (TCGA, http://cancergenome.nih.gov/) (Tomczak et al., 2015) and the International Cancer Genome Consortium (ICGC, www.icgc.org) (Zhang et al., 2019) were used to download somatic mutation data (MAF files) of TCGA-LIHC cohort and the LIRI-JP cohort. The primary objective of the ICGC database was to provide a comprehensive elucidation of genome changes in multiple cancers that result in human disease burden. Among the ICGC database, the tumor data from different cancer types (or subtypes) were collected, including abnormal gene expression, somatic mutation, epigenetic modification, and clinical data. The ICGC database contains 25,000 tumor genomes. Meanwhile, the clinicopathologic characteristics and the prognostic information of the patients in TCGA-LIHC cohort, such as gender, age, and clinical stage, were obtained from the UCSC Xena website (http://xena.ucsc.edu/) (Goldman et al., 2019). Moreover, RNA sequencing data (count value), containing mutation data and survival data of 353 patient samples (TCGA-LIHC), were downloaded from TCGA database for subsequent analysis and were annotated by the annotation file of the GRCh38 version from the Ensembl database (http://ftp.ensembl.org/pub/current_gtf) (Howe et al., 2021). In addition, the copy number variations data were obtained from TCGA database. The clinical characteristics of patients are listed in **Table 1**.

Mutation Analysis

With the development of tumor genomics, the mutation annotation format (MAF) is being widely accepted and used to store detected somatic mutations. In this study, the maftools package (Mayakonda et al., 2018) and the GenVisR package (Skidmore et al., 2016) were utilized to visualize the somatic mutation data downloaded from TCGA; meanwhile, the GenVisR package was also used to visualize the somatic mutation data obtained from ICGC. Moreover, the mutation of DOCK2 was revealed by the G3viz package (Guo et al., 2019).

Additionally, to evaluate whether the genes have copy number variation in liver cancer, GISTIC2.0 in the Genepattern (https://cloud.genepattern.org/) cloud analysis platform was used to analyze the copy number variation data of liver cancer in TCGA database (M. et al., 2006).

Construction of Dedicator of Cytokinesis 2 Mutation Prediction Model

The liver cancer patients were divided into mutation group (DOCK2-MUT) and wild group (DOCK2-WT) according to the DOCK2 mutation status of the gene expression data downloaded from TCGA. A survival analysis was performed based on the DOCK2 mutation and prognosis information of liver cancer patients, thus investigating the prognostic difference between the DOCK2 mutation group and the wild group. Moreover, the patients' data obtained from TCGA was randomly divided into a training set ($N = 264$) and a testing set ($N = 89$) at a ratio of 7:3. The DOCK2 mutation prediction model was conducted using the random forest (RF) method (Yperman et al., 2019) in the training set, and the model performance was quantified via the receiver operating characteristic (ROC) curve.

Construction of the Prognostic Model

The prognostic model was built in light of the gene expression data of 28 DOCK2 mutant liver cancer patients with clinical information. First, univariate Cox proportional hazard regression analysis was performed to initially identify overall survival (OS)-related genes (p-value<0.05). Next, RF and multivariate Cox regression analyses were conducted to construct a prognostic model. The formula for calculating the risk score is risk score = exp gene 1 × β gene 1 + exp gene 2 × β gene 2 + exp gene 3 × β gene 3 + . . . exp gene n × β gene n (exp gene n indicates the expression level of gene n; β gene n indicates the regression coefficient of gene n calculated by multivariate Cox regression). Moreover, correlation analysis was performed between the DOCK2 mRNA expression and the risk score, as well as between the DOCK2 mRNA expression and the characteristic genes mRNA expression in the model.

Assessment of the Prognostic Model

The liver cancer patients in the DOCK2 mutant group with clinical information were divided into high-risk groups and low-risk groups in light of the median risk score. The OS analysis was performed using the Kaplan–Meier (KM) survival curve and time-dependent ROC, thus evaluating the prediction accuracy of the model. Then, the univariate Cox regression analysis and the multivariate Cox regression analysis were conducted in light of the age, gender, clinical stage, tumor stage, and risk score in DOCK2 mutant liver cancer patients. Meanwhile, the risk score and clinical characteristics were analyzed using correlation analysis.

Tumor Mutation Burden and Microsatellite Instability Analysis

Given that different DOCK2 mutation types may have different effects on tumorigenesis, the expression data of liver cancer patients were divided into two subgroups: inactivated mutation subgroup and other non-silent mutation subgroups. The two subgroups were assessed *via* the KM survival curve and time-dependent ROC.

Tumor mutation burden (TMB) refers to the total number of somatic mutations in the exon coding region of the genome that have substitutions, insertions, or deletions per Mb base in a tumor sample. The TMB score of each liver cancer sample is the total number of somatic mutations (including non-synonymous point mutations, insertions, and deletions in the coding region of exons)/target region size, and the unit is mutations/Mb (Chan et al., 2019). Microsatellite (MS) is defined as a short tandem repeat (STR) in the human genome including single-nucleotide repeats, dinucleotide repeats, and even more nucleotide repeats; microsatellite instability (MSI) refers to the change of any length of microsatellites due to the insertion or deletion of repeat units in tumor tissues compared to normal tissues (Hile et al., 2013). MSI is calculated as the number of insertions or deletions in gene repeats. In this study, the relationship between the risk score and TMB and the correlation between the risk score and MSI were analyzed, respectively.

Differential Analysis

In order to assess the impact of gene expression value on the DOCK2 mutant type compared to the DOCK2 wild type, the limma R package (Ritchie et al., 2015) was used to conduct the discrepant analysis between the DOCK2 mutant group and DOCK2 wild-type group. The absolute value of log fold change (logFC) > 0.5 and p-value <0.05 were set as the threshold for differentially expressed genes. Among them, the genes with logFC > 0.5 and p-value <0.05 were considered upregulated differential genes, while the genes with logFC < −0.5 and p-value <0.05 were regarded as downregulated differential genes, and the aforementioned results were displayed with heat maps and volcano maps.

Gene Functional and Pathway Enrichment Analysis

Gene Ontology (GO) enrichment analysis is a common method for large-scale functional enrichment studies of genes in different dimensions and levels and generally includes three aspects: biological process (BP), molecular function (MF), and cellular component (CC) (Ashburner et al., 2000). The Kyoto Encyclopedia of Genes and Genomes (KEGG) (Ogata et al., 1999) is a widely applied database that stores numerous data about genomes, biological pathways, diseases, and drugs. Additionally, the clusterProfiler R package (Yu et al., 2012) was applied to identify significantly enriched biological processes and pathways by GO functional annotation and KEGG biological pathway enrichment analysis. A p-value <0.05 was considered statistically significant.

Gene Set Enrichment Analysis and Gene Set Variation Analysis

Gene Set Enrichment Analysis (GSEA) is a calculation method to assure whether a set of predefined genes show statistical

differences between two biological states, generally applied to estimate changes in the pathway and bioprocess activity in sample expression datasets (Subramanian et al., 2005). Based on the gene expression profile data of DOCK2 mutant group and DOCK2 wild-type group patients in TCGA-LIHC dataset and the reference gene sets "c5.go.v7.4.entrez.gmt" and "c2.cp.kegg.v7.4.entrez.gmt" downloaded from the MSigDB database (Liberzon et al., 2015), the GSEA method included in the clusterProfiler R package was used to conduct enrichment analysis of TCGA-LIHC gene expression profile data, thus studying the differences in the biological processes of genes between the DOCK2 mutant group and DOCK2 wild group. A p-value <0.05 was considered statistically significant.

Gene Set Variation Analysis (GSVA) (Hnzelmann et al., 2013; Liberzon et al., 2015), a nonparametric unsupervised analysis method, is widely utilized in the evaluation of metabolic pathways enriched in different samples by converting the expression matrix of genes between different samples into the expression matrix of gene sets between samples. To study the biological process variation of the DOCK2 mutant group compared with the DOCK2 wild group, the "GSVA" R package (Hnzelmann et al., 2013; Liberzon et al., 2015) was used to perform gene set variation analysis, and the enrichment scores of each sample in each pathway in the reference gene set "h.all.v7.4.symbols.gmt" were downloaded from the MSigDB database. Moreover, the GSVA results were also analyzed for correlation with the risk scores.

Immunoassay

The immune microenvironment is a comprehensive LoAD system, which is mainly composed of immune cells, inflammatory cells, fibroblasts, interstitial tissues, and various cytokines and chemokines. The infiltration analysis of immune cells in tissues has an important guiding role in disease research and treatment prognosis.

ESTIMATE analysis, an algorithm that quantifies the immune activity (immune infiltration level) in tumor samples on the basis of gene expression data, can reflect the richness of the gene characteristics of the matrix and immune cells. The content of stromal cells and immune cells in TCGA-LIHC was calculated by an ESTIMATE R package (Yoshihara et al., 2013). The correlation between the ESTIMATE score and the expression level of characteristic genes and DOCK2 in the prognostic model was also evaluated.

CIBERSORT is an algorithm that deconvolves the expression matrix of immune cell subtypes in light of the principle of linear support vector regression, making use of RNA-Seq data to assess the abundance of immune cells in the tissue. In this study, the proportion of 22 immune cell subtypes in TCGA-LIHC immune microenvironment was calculated by the CIBERSORT algorithm (Newman et al., 2019) in the R package. The number of permutations was 1,000, and a p-value <0.05 was considered accurate for calculating the content of immune cells. Based on Pearson correlation analysis, the correlation between the expression levels of characteristic genes and DOCK2 in the prognostic model and 22 types of immune cells in liver cancer was calculated.

To test the biological processes and cell signal transduction pathways that the characteristic genes of the prognostic model may be involved in, an immune gene set was obtained from the ImmPort database (Bhattacharya et al., 2014) (https://www.immport.org), and the relationship between the characteristic genes and DOCK2 in the prognostic model and immune genes was determined. The correlation between the expression of the HLA family and the risk score of the prognostic model was also conducted.

Statistical Analysis

All data calculations and statistical analysis were performed using R programming (https://www.r-project.org/, version 3.6.3). Multiple testing corrections were determined using the Benjamini–Hochberg (BH) method, and FDR correction was conducted using multiple tests to reduce the false-positive rate. For the comparison of two groups of continuous variables, the statistical significance of normally distributed variables was estimated by independent Student's t test, and the differences between non-normally distributed variables were analyzed by using the Mann–Whitney U test (the Wilcoxon rank-sum test). The survival R package (Durisová and Dedík, 1993) was utilized in the survival analysis. The Kaplan–Meier survival curve was used to reveal differences in survival, and the significance of the difference in survival time between the two groups of patients was assessed via a log-rank test. Univariate and multivariate Cox analyses were applied to determine independent prognostic factors. As for assessing the accuracy of the risk score to estimate the prognosis, the receiver operator characteristic (ROC) curve was drawn by the pROC package and ROCR package, and the area under the curve (AUC) was calculated (Sing et al., 2005; Robin et al., 2011). All p-values reported from statistical tests were two-sided, and a p-value <0.05 was considered statistically significant.

RESULTS

Genes With High-Frequency Mutations in HCC

First, 54 genes with mutation frequencies greater than 6% in TCGA-LIHC patients obtained from TCGA were identified (**Figure 1A**). Moreover, the 54 genes were further confirmed using the data downloaded from the ICGC database (**Figure 1B**). Among them, the mutation frequency of DOCK2 was relatively high, and the DOCK2 mutation was visualized (**Figures 1C, D**). GISTIC 2.0 was utilized to analyze copy number variation data in TCGA, identifying obviously amplified or deleted genes, and the results showed that DOCK2 had no significant amplification or deletion (**Figures 1E, F**).

Construction of Dedicator of Cytokinesis 2 Mutation Prediction Model

Survival analysis was conducted based on the DOCK2 mutation data and prognostic information of liver cancer patients, and the results revealed that the mutation of DOCK2 had an essential

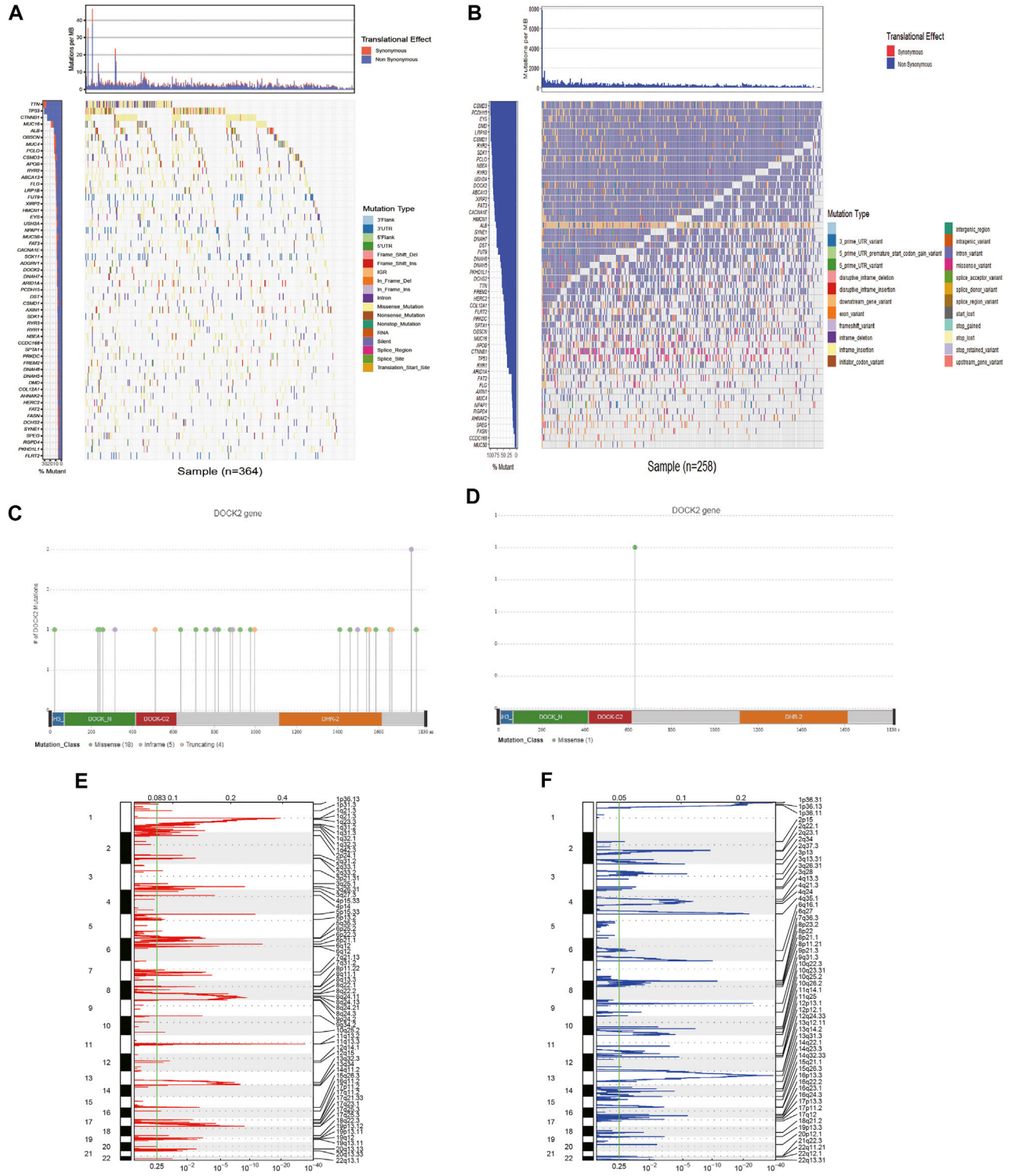


FIGURE 1 | Analysis of somatic mutation and copy number variation in patients with HCC. **(A)** 54 genes with the highest mutation frequency in LIHC patients in TCGA cohort. **(B)** Mutations of 54 genes in ICGC. The panels on the left of the two waterfall charts show genes with high-frequency mutations in different cohorts, and the order was based on their mutation frequency; The panels on the right side of the two waterfall charts reveal different types of mutations represented by various color modules. **(C)** DOCK2 mutation in TCGA cohort. **(D)** DOCK2 mutation in the ICGC cohort. **(E,F)** Identification of significantly amplified and deleted genes. The mRNA located at the focal CNA peak was related to LIHC. The false discovery rate (Q value) and the change score of GISTIC2.0 (x-axis) corresponded to the genome position (y-axis). The dotted line indicates the centromere. The green line represents the significant cutoff (q value of 0.25).

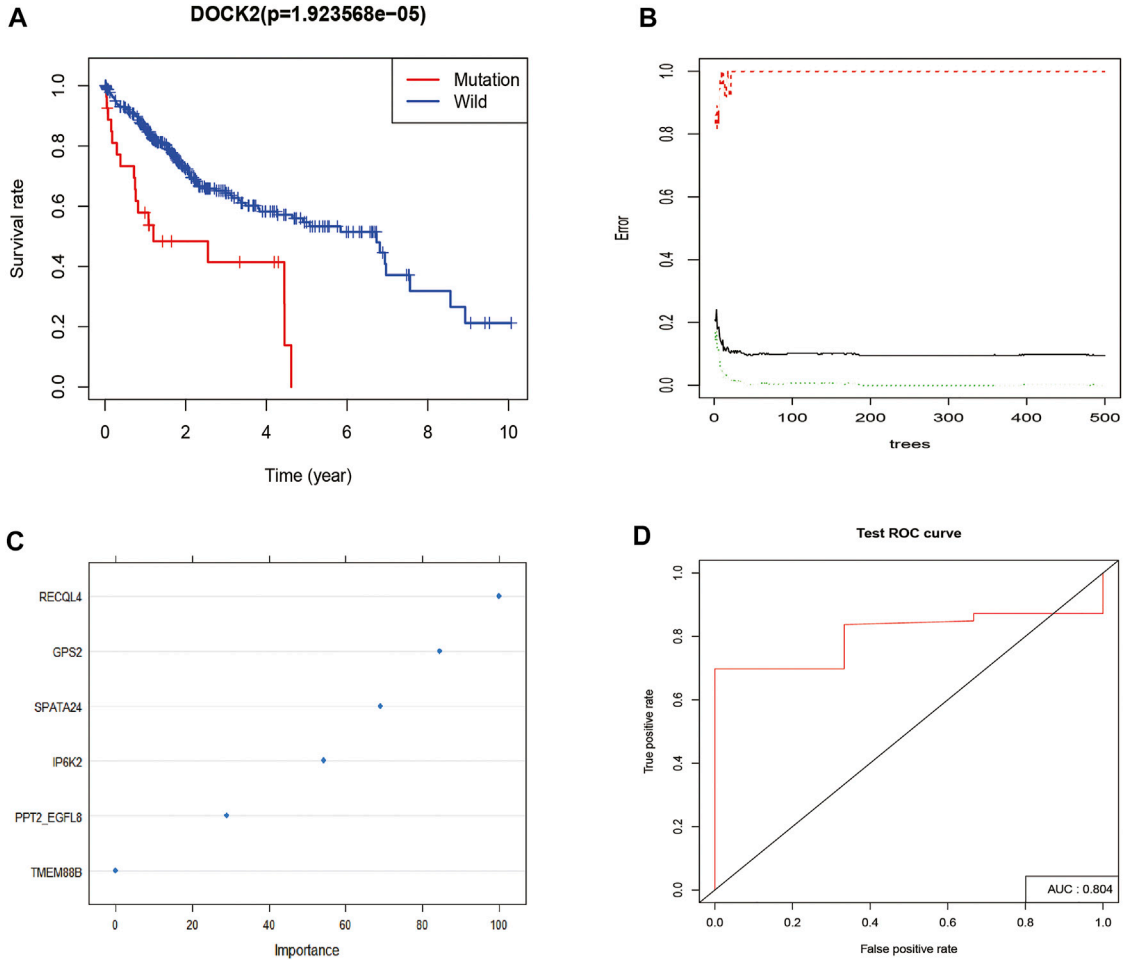


FIGURE 2 | DOCK2 mutation survival analysis and model construction. **(A)** Effect of DOCK2 mutation on OS and its significance. Blue indicates the DOCK2 wild type; red indicates the DOCK2 mutant type. **(B)** Relationship between the model error and the number of decision trees. **(C)** Importance of DOCK2 mutation model variables. **(D)** Performance of the DOCK2 mutation model in the test set.

impact on the prognosis and survival of patients (**Figure 2A**). In the training set, the RF method was used to construct a DOCK2 mutation prediction model in the mRNA data (**Figures 2B, C**). The ROC curve was used to evaluate the performance of the model, and AUC scores close to 1 indicated that the model had high sensitivity under a very low false-positive rate. The model AUC value in the training cohort was 1.00 and that in the validation cohort was 80.4% (**Figure 2D**), which demonstrated that the performance of this model was sufficient to effectively predict DOCK2 mutation in other transcription cohorts.

Construction of the Prognostic Model

Univariate Cox proportional hazard regression analysis was carried out in the gene expression data of 28 DOCK2 mutant LIHC patients with clinical information and 641 genes related to OS were discovered (p-value <0.05) (**Figure 3A**). Then, we conducted the RF method to find out the most important features connected with prognosis, and 15 genes were screened out (**Figure 3B**). Finally, a multivariate Cox proportional hazard regression analysis identified the five genes associated with OS, which are secretin receptor (SCTR), tetratricopeptide repeat, ankyrin repeat and coiled-coil domain-containing 1 (TANC1), Alkb homolog 7 (ALKBH7), FRAS1-related extracellular matrix 2 (FREM2), and G protein subunit gamma 4 (GNG4). Cox regression coefficients of the characteristic genes were calculated, and the risk score of each sample was defined as the sum of the expression of each characteristic gene multiplied by its regression coefficient. To assess the predictive power of the prognostic model, the risk scores of DOCK2 mutant and DOCK2 wild-type patients were calculated and ranked, the survival status of each patient was displayed on the dot chart, and the expression of characteristic genes was shown on the heat map (**Figures 3C, D**). Meanwhile, the correlation between DOCK2 expression and risk score and characteristic gene expression was analyzed, respectively. The expression of DOCK2 was dramatically negatively correlated with the risk score (**Figure 3E**). DOCK2 expression was significantly positively correlated with SCTR (r = 0.293, p-value = 9.6e-10),

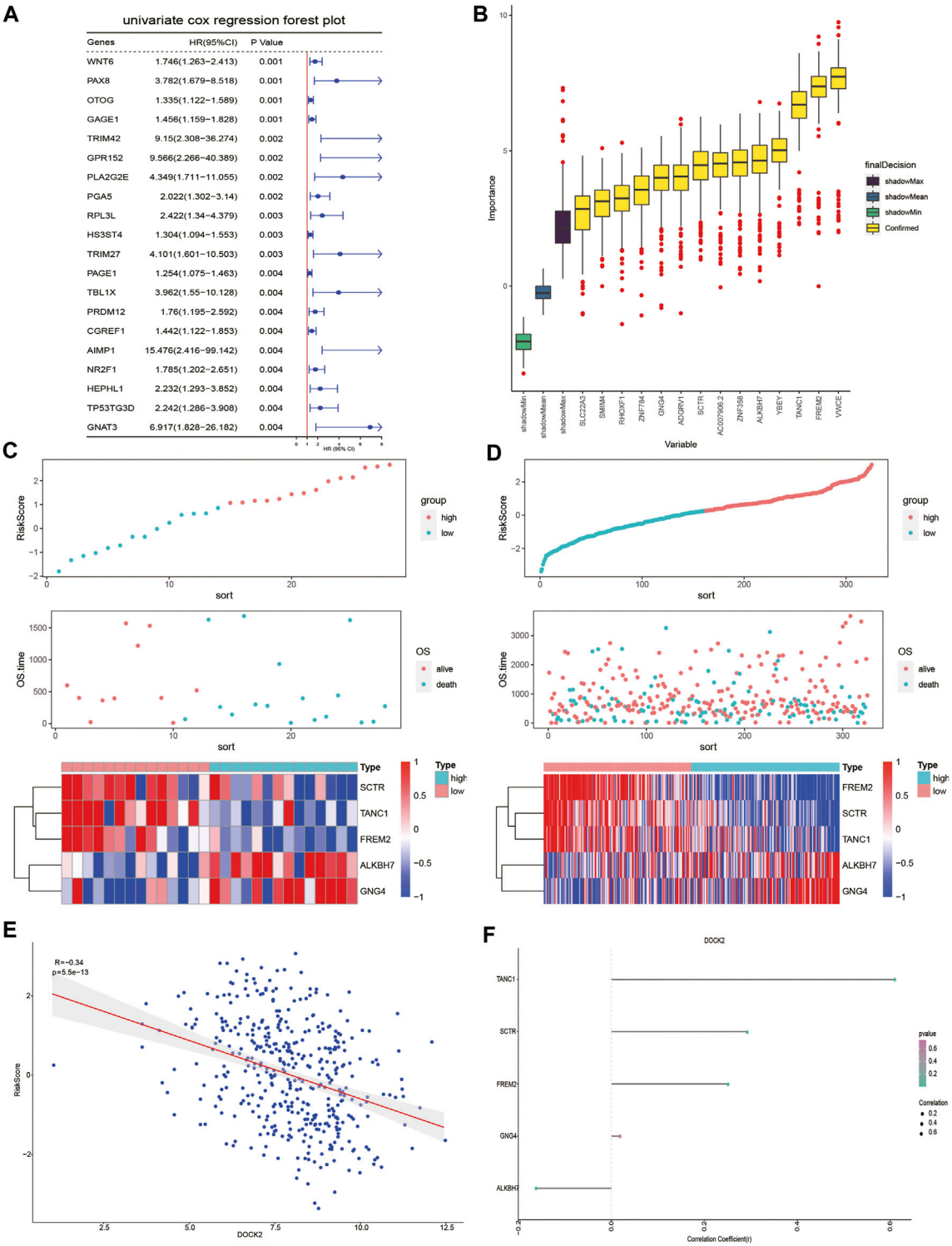


FIGURE 3 | DOCK2 mutation prognostic model. **(A)** Forest plot of the top 20 prognostic-related genes obtained by univariate regression analysis. The left side of the vertical red line is the protective gene, and the right side is the dangerous gene. **(B)** 14 important features selected based on RF. **(C,D)** Risk score, survival status, and characteristic gene expression of DOCK2 mutant and DOCK2 wild type, respectively. **(E)** Scatter plot of the correlation between DOCK2 expression and risk score. **(F)** Correlation between DOCK2 and characteristic genes. The size of the dot represents the strength of the correlation between DOCK2 and the characteristic gene; the size of the point is proportional to the correlation. The color of the dot represents the *p*-value; the greener the color, the smaller the *p*-value, and the pinker the color, the greater the *p*-value. *p*-value ≤ 0.05 was considered statistically significant.

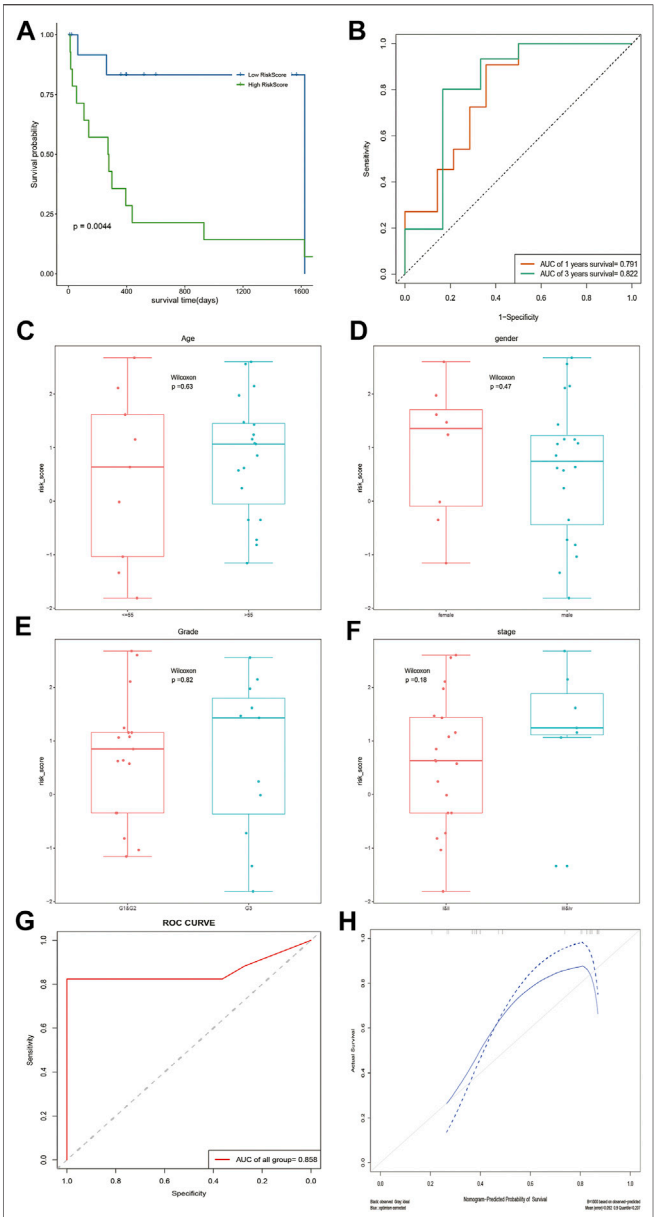


FIGURE 4 | Analysis of the prognostic model and clinical prediction model. **(A)** The impact of risk score on patients' OS and its significance. Blue meant a low-risk score, and green meant a high-risk score. **(B)** Time-dependent ROC analysis of risk score. **(C–F)** Correlation analysis of risk score with age, gender, tumor stage, and clinical stage. **(G)** ROC curve of a clinical prediction model in 28 DOCK2 mutant samples. **(H)** Calibration curve of the clinical prediction model. The X-axis was the outcome probability predicted by the model. The Y-axis was the value obtained by actual observation, and the calculation was repeated 1,000 times. The blue solid line is the calibration curve, and the diagonal line is the ideal curve. The closer the calibration curve was to the ideal curve, the better the predictive ability of the model.

TANC1 (r = 0.607, *p*-value = 1.8e-43), and FREM2 (r = 0.252, *p*-value = 1.8e-07), whereas the expression of DOCK2 had a significant negative correlation with ALKBH7(r = −0.162, *p*-value = 0.0009) (**Figure 3F**).

Assessment of the Prognostic Model

According to the median risk score, DOCK2 mutant liver cancer patients with clinical information were divided into the high-risk group and low-risk group. The results of survival analysis showed that there was a significant difference in OS between the two risk groups of 28 DOCK2 mutant samples (**Figure 4A**). The 1- and 3-year AUCs on the basis of the risk score obtained by the prognostic model were 0.791 and 0.822, respectively (**Figure 4B**). Additionally, the correlation analysis results of the risk score and the clinical characteristics of 28 DOCK2 mutant samples revealed that there were no significant differences in risk scores, different ages, genders, clinical stages, and tumor stages (**Figures 4C–F**). Then, univariate Cox analysis and multivariate Cox analysis were performed based on the age, gender, clinical stage, tumor stage, and risk score of DOCK2 mutant liver cancer patients, thus building a clinical prediction model, the efficacy of which in 28 DOCK2 mutant samples was 85.8% (**Figure 4G**). Meanwhile, the calibration curve showed both good discrimination ability and calibration (**Figure 4H**).

Tumor Mutation Burden and Microsatellite Instability Analysis

Given that different DOCK2 mutation types may have different effects on the occurrence of liver cancer, this study further divided the gene expression data of 28 DOCK2 mutant LIHC patients into two subgroups: the inactivated mutation subgroup (n = 8, containing nonsense mutation and silent mutation) and other non-silent mutation subgroups (n = 20). Survival analysis showed that significant differences in OS were observed between the two risk groups of samples in other non-silent mutation subgroups (**Figures 5A, B**). The time-dependent ROC analysis showed that in the subgroup of inactivated mutations, the 1- and 3-year AUCs of the risk score were both 0.833 (**Figure 5C**); moreover, in other subgroups of non-silent mutations, the 1- and 3-year AUCs of risk scores were 0.651 and 0.665, respectively (**Figure 5D**), suggesting that the risk score could still maintain good predictive performance in subgroups with different mutation types. After acquiring the total number of mutations to obtain TMB and assessing the relationship between the risk score and the TMB, we found that there were obvious differences in TMB between samples with different risk scores (p-value < 0.05) (**Figure 5E**). In addition, MSI between samples with different risk scores also had a significant difference (p-value < 0.05) (**Figure 5F**).

Differential Analysis and Functional Enrichment

To analyze the effect of gene expression values on the DOCK2 mutant samples compared with the DOCK2 wild-type samples, we conducted a limma discrepant analysis to obtain differentially expressed genes. The gene expression profile data of 28 DOCK2 mutant samples and 325 DOCK2 wild-type samples were included in TCGA-LIHC, from which 12 upregulated differential genes (p-value <0.05, logFC > 0.5) and 4

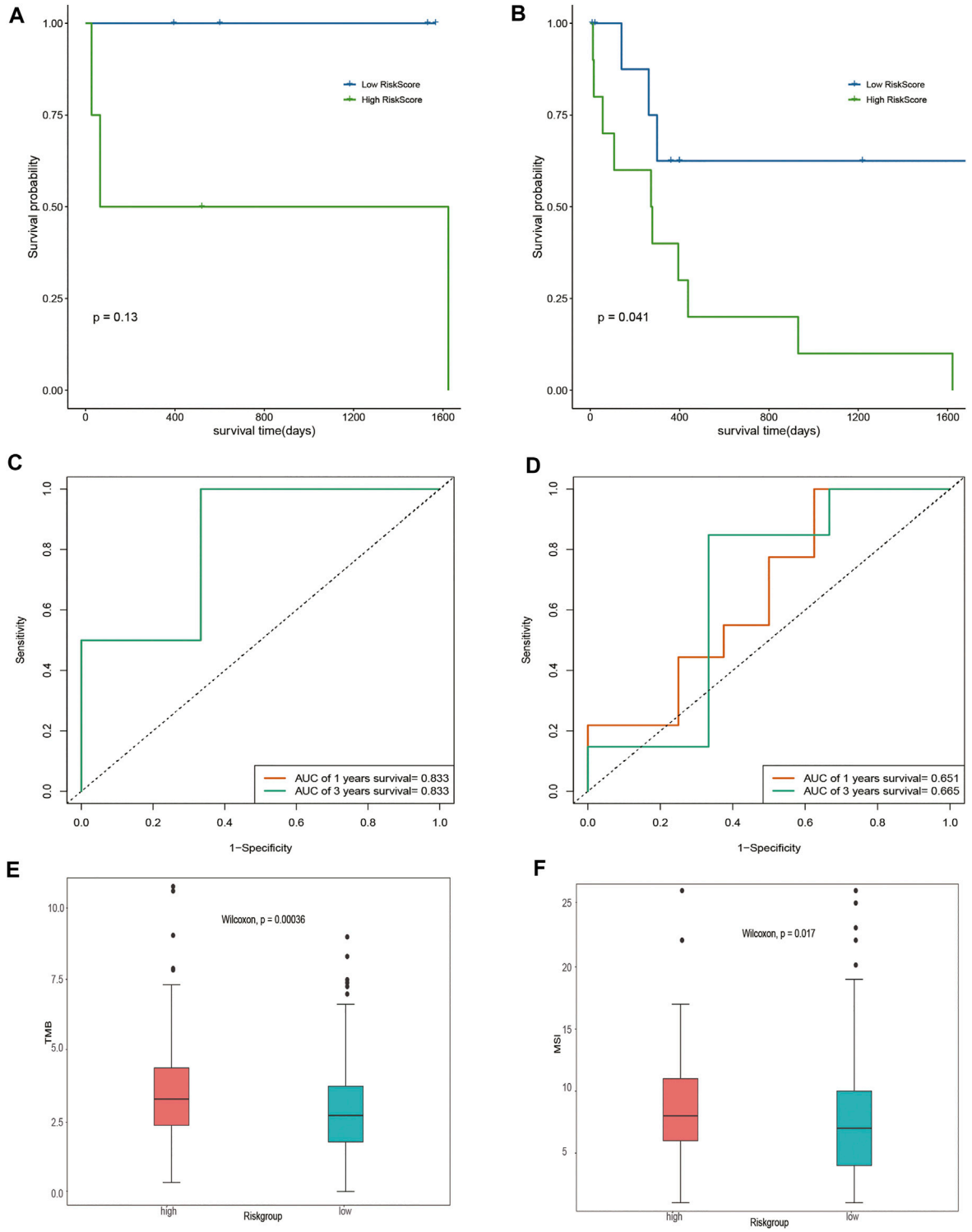


FIGURE 5 | Assessment of risk score. **(A,B)** Impact of risk score on OS in the subgroup of inactivated mutations and other subgroups of non-silent mutations and its significance, respectively. Blue means a low-risk score, and green means a high-risk score. **(C,D)** Time-dependent ROC analysis of the risk score in the subgroup of inactivated mutations and other subgroups of non-silent mutations. **(E)** Analysis of the correlation between TMB and risk score. Pink represents the high-risk group, and green represents the low-risk group. **(F)** Correlation analysis between MSI and risk score. Pink represents the high-risk group, and green represents the low-risk group.

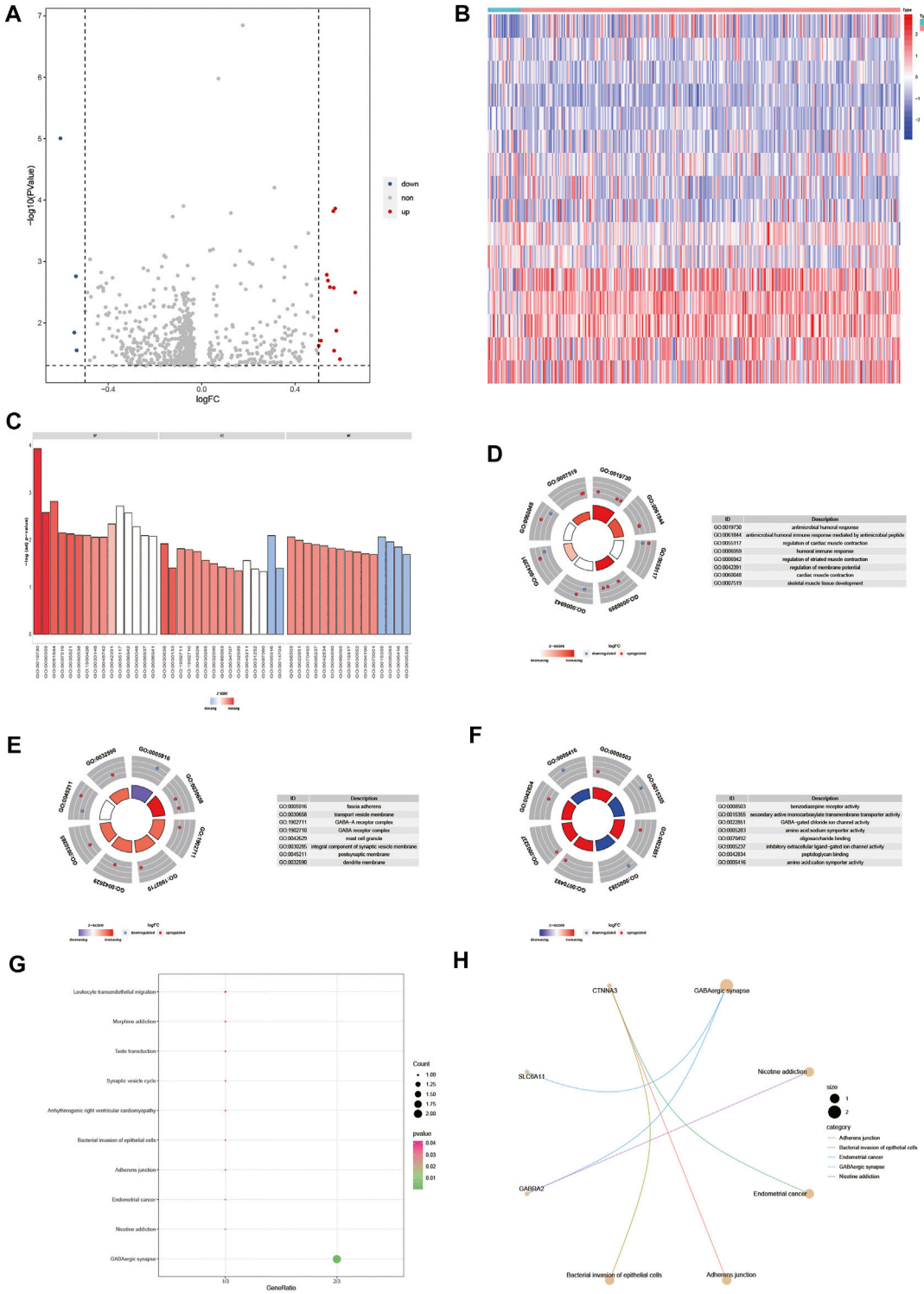


FIGURE 6 | Differential gene and its functional enrichment analysis. **(A)** Abscissa is log2FoldChange, and the ordinate is –log10 (adjust *p*-value). The red nodes indicates upregulation, the blue nodes indicate downregulation, and the gray nodes represent insignificant expression. **(B)** Abscissa is the patient ID, and the ordinate is the differential gene. Red represents high gene expression, and blue represents low gene expression. The green comment bar indicates the DOCK2 mutant sample, while the red comment bar indicates the DOCK2 wild-type sample. **(C–F)** GO function enrichment analysis of differential genes and display of BP, MF, and CC. **(D–F)** Color of the node indicates the level of gene expression value. Blue represents that the expression value was downregulated, and red indicates that the expression value was upregulated. The middle quadrilateral represents the effect of genes on the enriched GO terms. Light color means inhibition; dark color means activation. **(G)** KEGG pathway enrichment analysis. The abscissa is the gene ratio, and the ordinate is the pathway name. The size of the node indicates the number of genes enriched in the pathway, and the color of the node indicates –log10 (*p*-value). **(H)** Display of the first five items in the KEGG enrichment analysis of differential genes.

TABLE 2 | GO enrichment analysis.

Ontology	ID	Description	*p*-value
BP	GO:0019730	Antimicrobial humoral response	0.00011696
BP	GO:0061844	Antimicrobial humoral immune response mediated by antimicrobial peptides	0.001532039
BP	GO:0055117	Regulation of cardiac muscle contraction	0.001927973
BP	GO:0006959	Humoral immune response	0.002637965
BP	GO:0006942	Regulation of striated muscle contraction	0.002684261
BP	GO:0042391	Regulation of membrane potential	0.004609488
BP	GO:0060048	Cardiac muscle contraction	0.005272199
BP	GO:0007519	Skeletal muscle tissue development	0.007122358
BP	GO:0035821	Modification of morphology or physiology of other organisms	0.007470229
BP	GO:0060538	Skeletal muscle organ development	0.007915771
BP	GO:1900426	Positive regulation of defense response to bacterium	0.008007218
BP	GO:0006937	Regulation of muscle contraction	0.0080973
BP	GO:0006941	Striated muscle contraction	0.008373123
BP	GO:0033148	Positive regulation of intracellular estrogen receptor signaling pathway	0.008804639
BP	GO:0048742	Regulation of skeletal muscle fiber development	0.008804639
CC	GO:0005916	Fascia adherens	0.008087095
CC	GO:0030658	Transport vesicle membrane	0.012058338
CC	GO:1902711	GABA-A receptor complex	0.015313019
CC	GO:1902710	GABA receptor complex	0.016112846
CC	GO:0042629	Mast cell granule	0.017710673
CC	GO:0030285	Integral component of synaptic vesicle membrane	0.027246665
CC	GO:0045211	Postsynaptic membrane	0.027593411
CC	GO:0032590	Dendrite membrane	0.031982049
CC	GO:0098563	Intrinsic component of synaptic vesicle membrane	0.037479348
CC	GO:0030133	Transport vesicle	0.039367589
CC	GO:0014704	Intercalated disc	0.039826362
CC	GO:0,034,707	Chloride channel complex	0.039826362
CC	GO:0031252	Cell leading edge	0.041396752
CC	GO:0032589	Neuron projection membrane	0.045281879
CC	GO:0097060	Synaptic membrane	0.04693445
MF	GO:0008503	Benzodiazepine receptor activity	0.008670141
MF	GO:0015355	Secondary active monocarboxylate transmembrane transporter activity	0.008670141
MF	GO:0022851	GABA-gated chloride ion channel activity	0.010239011
MF	GO:0005283	Amino acid:sodium symporter activity	0.011022581
MF	GO:0070492	Oligosaccharide binding	0.011805575
MF	GO:0005237	Inhibitory extracellular ligand-gated ion channel activity	0.012587993
MF	GO:0042834	Peptidoglycan binding	0.013369837
MF	GO:0005416	Amino acid:cation symporter activity	0.014151105
MF	GO:0004890	GABA-A receptor activity	0.014931799
MF	GO:0099095	Ligand-gated anion channel activity	0.015711918
MF	GO:0016917	GABA receptor activity	0.017270437
MF	GO:0030552	cAMP binding	0.018048836
MF	GO:0004190	Aspartic-type endopeptidase activity	0.019603918
MF	GO:0005328	Neurotransmitter:sodium symporter activity	0.020380602
MF	GO:0070001	Aspartic-type peptidase activity	0.020380602

downregulated differential genes (p-value <0.05, logFC < −0.5) were screened out, and the volcanic map and heat map of the differential genes were shown in **Figures 6A,B**. To determine the value of the differential genes, the biological processes, the cellular components, and the molecular functions were performed. GO functional enrichment analysis was first assessed on the 16 differential genes (**Figure 6C** and **Table 2**), and the results showed that these genes were mainly enriched in biological processes such as antimicrobial humoral response, antimicrobial humoral immune response mediated by antimicrobial peptides, regulation of cardiac muscle contraction, humoral immune response, regulation of striated muscle contraction, regulation of membrane potential, cardiac muscle contraction, and skeletal muscle tissue development (**Figure 6D**); in cellular components including fascia adherens, transport vesicle membrane, GABA-A receptor complex, GABA receptor complex, mast cell granule, integral component of synaptic vesicle membrane, postsynaptic membrane, and dendrite membrane (**Figure 6E**); and in molecular functions including benzodiazepine receptor activity, secondary active monocarboxylate transmembrane transporter activity, GABA-gated chloride ion channel activity, amino acid:sodium symporter activity, oligosaccharide binding, inhibitory extracellular ligand-gated ion channel activity, peptidoglycan binding, and amino acid:cation symporter activity (**Figure 6F**). Then, pathways significantly affected by 16 differential genes were also performed (**Figure 6G** and **Table 3**), and the data revealed that the 16 differential genes were involved in

TABLE 3 | KEGG enrichment analysis.

Ontology	ID	Description	*p*-value
KEGG	hsa04727	GABAergic synapse	0.000356208
KEGG	hsa05033	Nicotine addiction	0.014756278
KEGG	hsa05213	Endometrial cancer	0.021348965
KEGG	hsa04520	Adherens junction	0.026092015
KEGG	hsa05100	Bacterial invasion of epithelial cells	0.028275936
KEGG	hsa05412	Arrhythmogenic right ventricular cardiomyopathy	0.028275936
KEGG	hsa04721	Synaptic vesicle cycle	0.028639606
KEGG	hsa04742	Taste transduction	0.031545693
KEGG	hsa05032	Morphine addiction	0.033359051
KEGG	hsa04670	Leukocyte transendothelial migration	0.041671347

GABAergic synapse, nicotine addiction, endometrial cancer, adherens junction, and bacterial invasion of epithelial cells (**Figure 6H**).

Gene Set Enrichment Analysis and Gene Set Variation Analysis

GSEA biological function enrichment analysis of DOCK2-MUT and DOCK2-WT genes was performed, and the results showed that the genes in DOCK2-MUT and DOCK2-WT were enriched in biological processes including coagulation and regulation of cytosolic calcium ion concentration (**Figures 7A, B** and **Table 4**).

Next, the results of GSEA biological pathway enrichment analysis suggested that biological pathways such as complement and coagulation cascades, glycosphingolipid biosynthesis, and ganglio series were identified among the targets in DOCK2-MUT and DOCK2-WT (**Figures 7C, D** and **Table 4**).

Furthermore, in order to comprehensively evaluate the roles of the targets in DOCK2-MUT and DOCK2-WT in liver cancer, the GSVA was conducted. The data showed three hallmarks: reactive_oxygen_species_pathway, spermatogenesis, and uv_response_dn (**Figure 7E**). Among them, spermatogenesis was significantly negatively correlated with risk score (p-value <0.05); uv_response_dn was obviously positively related with risk score (p-value <0.05); however, reactive_oxygen_species_pathway had no significant correlation with risk score (**Figures 7F–H**).

Immunoassay

As liver cancer is considered an immunogenic tumor, the relationship between the expression of DOCK2, SCTR, TANC1, ALKBH7, FREM2, and GNG4 and the levels of immune cells and stromal cells was assessed (**Figures 8A, B**). The data showed a positive correlation between stromal cells and DOCK2, SCTR, TANC1, and FREM2, and a negative correlation between stromal cells and ALKBH7 and GNG4. Moreover, immune cells had a positive correlation with DOCK2 and TANC1 and a negative correlation with ALKBH7 (p-value <0.05).

In addition, the six target genes, DOCK2, SCTR, TANC1, ALKBH7, FREM2, and GNG4, were significantly correlated with specific immune-related genes. For example, DOCK2 was significantly related to the immune gene of SEMA3F; SCTR was correlated with SEMA3F and FGR; and the same situation occurred between GNG4 and SEMA3F and NFYA, FREM2 and FGR, NFYA and MPO, ALKBH7 and SEMA3F, FGR, NFYA and CALCR (p-value <0.05) (**Figure 8C**).

More importantly, the six target genes were obviously interrelated with the infiltration of numerous immune cells. DOCK2 gene expression was distinctly related to the infiltration of 11 immune cells; SCTR gene expression was dramatically correlated with the infiltration of 7 immune cells; TANC1 gene expression was obviously interrelated with the infiltration of 10 immune cells; FREM2 gene expression was distinctly related to the infiltration of one immune cell; ALKBH7 gene expression was dramatically correlated with the infiltration of 4 immune cells; GNG4 gene expression was markedly interrelated with the infiltration of 7 immune cells (p-value <0.05) (**Figure 8D**). Furthermore, the expression value of HLA-DOA was statistically significant in different risk groups (**Figure 8E**).

DISCUSSION

It is worth noting that genetic mutation plays an essential role in HCC. Some reports showed that the genetic mutation of some important genes, including TP53, CTNNB1, and AXIN1, was relevant to poor outcomes for patients with HCC (Zhan et al., 2013; Schulze et al., 2015). It is suggested that exploring genomic instability is a great way to discover promising prognostic biomarkers for the treatment of HCC. DOCK2 has been discovered to be linked with a prognostic factor in various cancers such as acute myeloid leukemia, prostate cancer, colorectal cancer, and non-small-cell lung cancer (Du et al.; Yu et al., 2015; Bjerre et al., 2019; Hu et al., 2019). Nevertheless, research on the diagnosis ability of DOCK2 in HCC remains insufficient. In the present study, a high mutation of DOCK2 was found in TCGA-LIHC cohort, which was further verified in the LIRI-JP cohort, indicating that DOCK2 mutation was significantly frequent in HCC. Moreover, survival analysis showed that patients with DOCK2 mutation had a low survival rate and a poor prognosis compared with the DOCK2 wild-type group, suggesting that DOCK2 might exhibit a great value in the prognosis of HCC.

Given the frequency of DOCK2 mutation in HCC, it is essential to conduct an in-depth study of an effective method

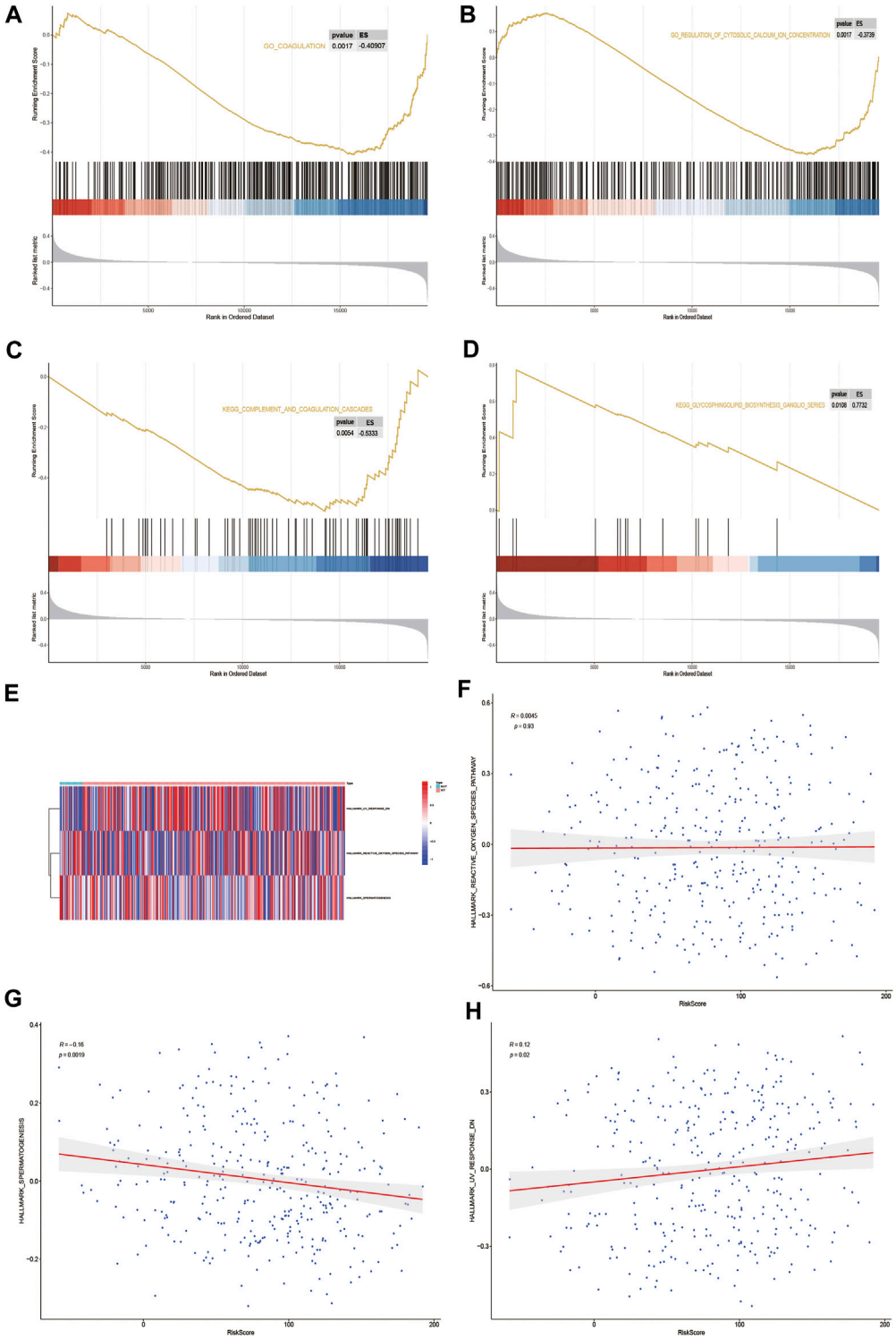


FIGURE 7 | GSEA and GSVA. **(A,B)** Results of GSEA biological function enrichment. **(C,D)** Results of biological pathway enrichment. **(E)** Heat map of the significant hallmark analyzed by GSVA. **(F,H)** Scatter plot of correlation between significant hallmark and risk score.

for predicting the prognosis of DOCK2 mutant HCC patients. Thus, we calculated the risk score on the basis of the five most relevant prognostic genes including SCTR, TANC1, ALKBH7, FREM2, and GNG4. The risk score exhibited great predictive ability in different DOCK2 mutation statuses, risks, and types. Moreover, the risk score showed an excellent correlation with

TABLE 4 | GSEA.

ID	Description	ES	*p*-value
go_coagulation	go_coagulation	–0.409069157	0.001672241
go_regulation_of_cytosolic_calcium_ion_concentration	go_regulation_of_cytosolic_calcium_ion_concentration	–0.373853775	0.001692047
go_ventricular_cardiac_muscle_cell_action_potential	go_ventricular_cardiac_muscle_cell_action_potential	–0.635035665	0.001769912
go_cell_cell_adhesion_via_plasma_membrane_adhesion_molecules	go_cell_cell_adhesion_via_plasma_membrane_adhesion_molecules	–0.432720305	0.00177305
go_negative_regulation_of_execution_phase_of_apoptosis	go_negative_regulation_of_execution_phase_of_apoptosis	-0.756145207	0.001785714
go_negative_regulation_of_myoblast_differentiation	go_negative_regulation_of_myoblast_differentiation	–0.729056439	0.001785714
go_regulation_of_execution_phase_of_apoptosis	go_regulation_of_execution_phase_of_apoptosis	–0.642047088	0.001785714
go_regulation_of_inflammatory_response_to_antigenic_stimulus	go_regulation_of_inflammatory_response_to_antigenic_stimulus	-0.726196139	0.001798561
go_negative_regulation_of_synapse_organization	go_negative_regulation_of_synapse_organization	-0.72808206	0.001801802
go_negative_regulation_of_inflammatory_response_to_antigenic_stimulus	go_negative_regulation_of_inflammatory_response_to_antigenic_stimulus	–0.827265127	0.001805054
go_lipid_translocation	go_lipid_translocation	–0.601531891	0.001808318
go_cytokine_receptor_activity	go_cytokine_receptor_activity	–0.540903843	0.001828154
go_blood_microparticle	go_blood_microparticle	-0.531068688	0.001838235
go_homophilic_cell_adhesion_via_plasma_membrane_adhesion_molecules	go_homophilic_cell_adhesion_via_plasma_membrane_adhesion_molecules	–0.531976492	0.001848429
go_complement_activation	go_complement_activation	–0.566062924	0.001865672
go_immune_receptor_activity	go_immune_receptor_activity	–0.526876463	0.001872659
go_organophosphate_ester_transport	go_organophosphate_ester_transport	–0.455964352	0.001879699
go_dna_replication_independent_nucleosome_organization	go_dna_replication_independent_nucleosome_organization	0.584583627	0.002118644
go_odorant_binding	go_odorant_binding	0.524374367	0.002132196
go_digestion	go_digestion	0.456798178	0.002145923
go_diencephalon_development	go_diencephalon_development	0.542992829	0.002159827
go_ear_morphogenesis	go_ear_morphogenesis	0.482732218	0.002164502
go_neuron_fate_commitment	go_neuron_fate_commitment	0.623987975	0.002164502
go_endocrine_system_development	go_endocrine_system_development	0.486005649	0.002169197
go_appendage_morphogenesis	go_appendage_morphogenesis	0.489850317	0.002178649
go_keratinization	go_keratinization	0.454250476	0.002178649
go_cornification	go_cornification	0.531790615	0.002188184
go_embryonic_skeletal_system_development	go_embryonic_skeletal_system_development	0.503417996	0.002188184
go_skeletal_system_morphogenesis	go_skeletal_system_morphogenesis	0.440722934	0.002188184
go_embryonic_appendage_morphogenesis	go_embryonic_appendage_morphogenesis	0.475526703	0.002192982
go_cell_fate_specification	go_cell_fate_specification	0.504467657	0.002197802
go_divalent_inorganic_anion_homeostasis	go_divalent_inorganic_anion_homeostasis	0.825664161	0.002202643
go_embryonic_skeletal_system_morphogenesis	go_embryonic_skeletal_system_morphogenesis	0.578909723	0.002207506
go_anterior_posterior_pattern_specification	go_anterior_posterior_pattern_specification	0.475479352	0.002222222
go_proximal_distal_pattern_formation	go_proximal_distal_pattern_formation	0.65212998	0.002227171
go_appendage_development	go_appendage_development	0.473257146	0.002247191
go_cornified_envelope	go_cornified_envelope	0.629843229	0.002252252
go_hindlimb_morphogenesis	go_hindlimb_morphogenesis	0.642853948	0.002252252
go_negative_regulation_of_response_to_extracellular_stimulus	go_negative_regulation_of_response_to_extracellular_stimulus	0.795788231	0.002252252
go_muscle_cell_fate_commitment	go_muscle_cell_fate_commitment	0.824992566	0.002277904
go_neuron_fate_specification	go_neuron_fate_specification	0.68805324	0.00228833
go_cell_fate_commitment	go_cell_fate_commitment	0.400964549	0.002309469
go_monovalent_inorganic_anion_homeostasis	go_monovalent_inorganic_anion_homeostasis	0.667695897	0.002309469
go_sensory_organ_morphogenesis	go_sensory_organ_morphogenesis	0.430365367	0.002309469
go_embryonic_organ_morphogenesis	go_embryonic_organ_morphogenesis	0.424037318	0.002364066
kegg_complement_and_coagulation_cascades	kegg_complement_and_coagulation_cascades	–0.533293095	0.001824818
kegg_glycosphingolipid_biosynthesis_ganglio_series	kegg_glycosphingolipid_biosynthesis_ganglio_series	0.773222168	0.004329004
kegg_propanoate_metabolism	kegg_propanoate_metabolism	–0.574271735	0.018248175
kegg_renin_angiotensin_system	kegg_renin_angiotensin_system	–0.660325041	0.023897059

(Continued on following page)

TABLE 4 | (*Continued*) GSEA.

ID	Description	ES	*p*-value
kegg_natural_killer_cell_mediated_cytotoxicity	kegg_natural_killer_cell_mediated_cytotoxicity	−0.4049327	0.024822695
kegg_ribosome	kegg_ribosome	0.412873966	0.041942605
kegg_peroxisome	kegg_peroxisome	−0.435572819	0.042628774
kegg_primary_bile_acid_biosynthesis	kegg_primary_bile_acid_biosynthesis	−0.639717566	0.043478261
kegg_hematopoietic_cell_lineage	kegg_hematopoietic_cell_lineage	−0.426295539	0.045207957

TMB and MSI. Moreover, the clinical prediction model based on age, gender, clinical stage, tumor stage, and risk score revealed both good discrimination ability and calibration, suggesting that these clinical features could independently predict the prognosis of patients with HCC. In addition to providing prognostic information, these five genes can also be used in precise oncology as biomarkers to guide targeted therapy.

SCTR, encoding the protein named G protein-coupled receptor, belongs to the glucagon–VIP–secretin receptor family (Bayliss and Starling, 1902). It has been reported that in colorectal cancer, hypermethylation of SCTR had a diagnostic value (Li et al., 2020). Moreover, SCTR was also found to be a predictor of the risk for breast cancer and pancreatic ductal adenocarcinoma (Zheng et al., 2018; Park et al., 2020). TANC1 has an ankyrin repeat (AR) domain that participates in many cell functions, especially tumorigenesis (Yang et al., 2019). Through Ingenuity Pathway Analysis (IPA), genes regulated by TANC1 were enriched in hepatic inflammation and HCC (Wu et al., 2021). ALKBH7, a mitochondrial ketoglutarate dioxygenase, decreases ROS formation to regulate programmed necrosis (Meng et al., 2019; Kulkarni et al., 2020). A single-nucleotide polymorphism (SNP) of ALKBH7 was clarified as a new prostate cancer biomarker in 2017 (Walker et al., 2017). FREM2 belongs to an extracellular matrix protein located in the dense layer of the epithelial basement membrane (Wang et al., 2021). In prostate adenocarcinoma, FREM2 was found to be one of the most recurrently mutated genes (Zhao et al., 2019). Upregulated FREM2 protein expression was demonstrated in glioblastomas compared to normal samples (Jovcevska et al., 2019). GNG4 is one of the fourteen γ-subunit proteins of the G protein-coupled receptor (Kishibuchi et al., 2020). As a tumor suppressor gene, abnormal expression of GNG4 was reported in multiple cancers containing colorectal cancer, bladder cancer, and glioblastoma (Pal et al., 2016; Zhang et al., 2018; Liang L. et al., 2021). To sum up, evidence has shown that the five genes clarified in this work all have essential roles in malignant development, indicating that developing corresponding targeted therapies for high-risk DOCK2-mutant HCC was feasible.

To understand the role of DOCK2 mutation in HCC from multiple angles, its potential mechanism in this disease should be focused on. Through the analysis of GO, KEGG, GSEA, and GSVA, we found that DOCK2 mutation could influence humoral immune response, transport vesicle membrane, mast cell granule, adherens junction, complement and coagulation cascades, and reactive oxygen species pathway. More importantly, these biological processes and pathways are closely correlated with immune function. Immunity plays an essential role in tumor development including tumor proliferation, invasion, and metastasis. A significantly important reason for tumor initiation and progression is that the tumor microenvironment (TME) changes from immune activation to immune suppression, thereby avoiding immune surveillance (Han et al., 2019). In addition, increasing evidence showed that genetic mutation was not adequate to start tumors, and TME acted as the second hit that might be needed to drive tumor development

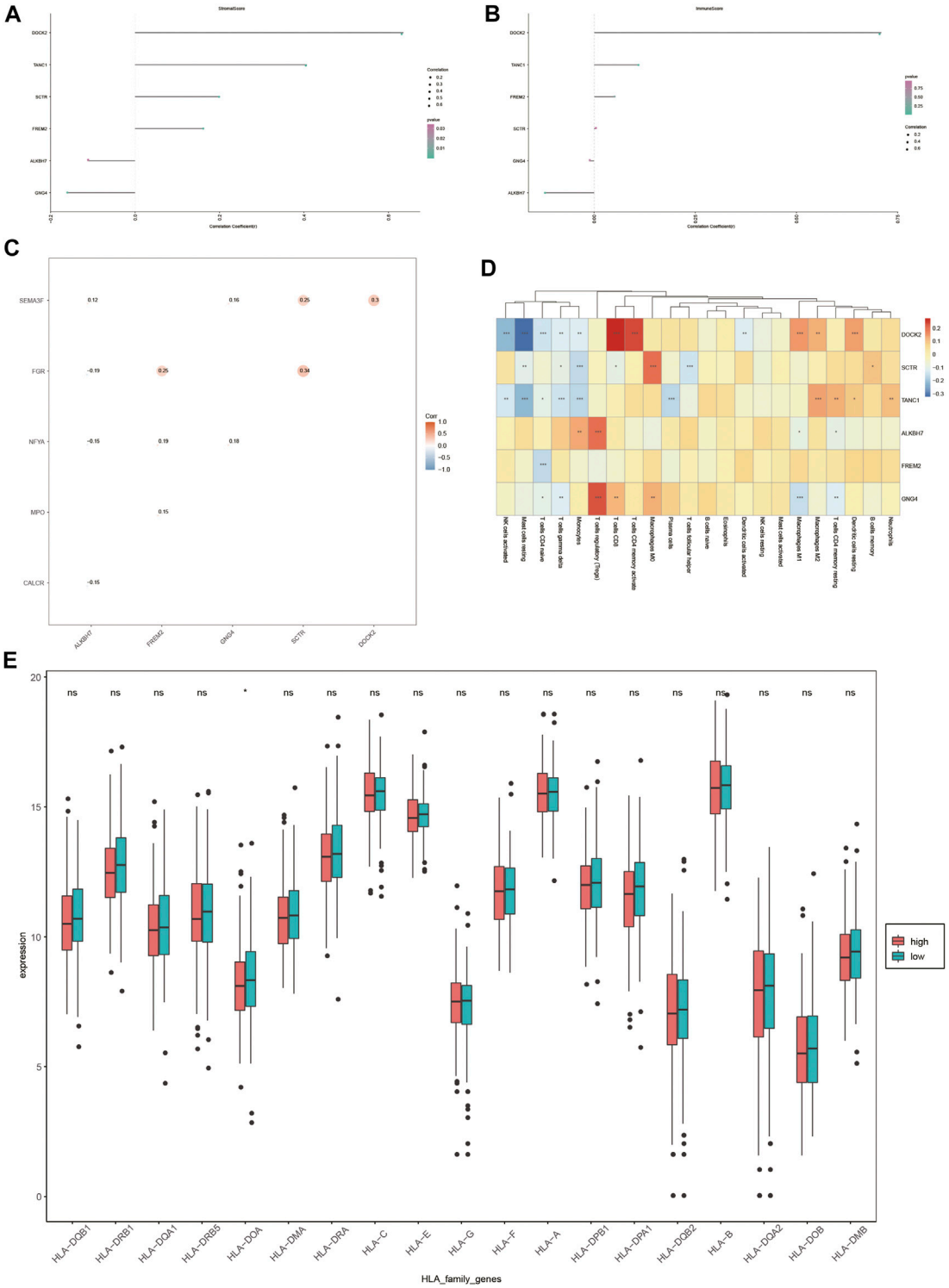


FIGURE 8 | Immune correlation analysis. **(A,B)** Correlation of DOCK2 and characteristic genes with the content of immune cells and stromal cells. **(C)** Correlation between DOCK2 and characteristic genes and immune genes. **(D)** Correlation of DOCK2 and characteristic gene expression with immune cell infiltration. **(E)** Correlation between HLA family expression and the risk score.

(Sahoo et al., 2018). The TME consists of the stromal and immune cells (Huang H. et al., 2021). Both stromal cells and immune cells were found to be significantly correlated with DOCK2 and the characteristic genes of the prognostic model, indicating that DOCK2 might regulate the immune process to promote the development of HCC. There are many immune cells

involved in tumorigenesis and progression. For the in-depth investigation, SEMA3F, FGR, NFYA, MPO, and CALCR showed a high correlation with DOCK2 and its characteristic genes. In addition, the expression level of HLA-DOA revealed a significant difference in different DOCK2 risk groups. Thus, the six immune genes, namely, SEMA3F, FGR, NFYA, MPO, CALCR, and HLA-DOA, might be the targets of DOCK2 immune-related treatments in the future.

Although the current work sheds new light on the relationship between DOCK2 and HCC, there were still some limitations. First of all, the number of cohorts with both TCGA-LIHC and LIRI-JP was restricted, and multi-center large sample research is needed. Second, given that the data were obtained from public resources, the bias of the analyzed profile could not be ignored. Finally, all the results in this work came from *in silico* analyses, and further clinical validations and experiments are required to promote the clinical application of our findings, which will be our next research content in the near future.

In conclusion, the present study identifies a novel prognostic signature based on DOCK2 mutation-related genes that shows great prognostic value in HCC patients, and this gene mutation might promote tumor progression by influencing immune responses. These data provide valuable insights for future investigations into personalized forecasting methods and also shed light on stratified precision oncology treatment.

DATA AVAILABILITY STATEMENT

The datasets presented in this study can be found in online repositories. The names of the repository/repositories and accession number(s) can be found in the article/ Supplementary Material.

AUTHOR CONTRIBUTIONS

JW, YH, WL, and SC designed the study. WL, YW, YQ, YL, and YS analyzed the data. YH and WL made the relative statistics and pictures. YH, HS, and WZ drafted the manuscript and collected the references. JW and SC revised the manuscript. All authors have read and approved the final manuscript.

FUNDING

This work was supported by the National Natural Science Foundation of China (No. 81960767).

REFERENCES

Ashburner, M., Ball, C. A., Blake, J. A., Botstein, D., Butler, H., Cherry, J. M., et al. (2000). Gene Ontology: Tool for the Unification of Biology. *Nat. Genet.* 25 (1), 25–29. doi:10.1038/75556

Bayliss, W. M., and Starling, E. H. (1902). The Mechanism of Pancreatic Secretion. *J. Physiol.* 28, 325–353. doi:10.1113/jphysiol.1902.sp000920

Bhattacharya, S., Andorf, S., Gomes, L., Dunn, P., Schaefer, H., Pontius, J., et al. (2014). ImmPort: Disseminating Data to the Public for the Future of Immunology. *Immunol. Res.* 58 (2-3), 234–239. doi:10.1007/s12026-014-8516-1

Bjerre, M. T., Strand, S. H., Nørgaard, M., Kristensen, H., Rasmussen, A. K., Mortensen, M. M., et al. (2019). Aberrant DOCK2, GRASP, HIF3A and PKFP Hypermethylation Has Potential as a Prognostic Biomarker for Prostate Cancer. *Int. J. Mol. Sci.* 20 (5), 1173. doi:10.3390/ijms20051173

Chan, T. A., Yarchoan, M., Jaffee, E., Swanton, C., Quezada, S. A., Stenzinger, A., et al. (2019). Development of Tumor Mutation burden as an Immunotherapy Biomarker: Utility for the Oncology Clinic. *Ann. Oncol.* 30 (1), 44–56. doi:10.1093/annonc/mdy495

Chen, Y., Meng, F., Wang, B., He, L., Liu, Y., and Liu, Z. (2018). Dock2 in the Development of Inflammation and Cancer. *Eur. J. Immunol.* 48 (6), 915–922. doi:10.1002/eji.201747157

Chen, Z., Xie, H., Hu, M., Huang, T., Hu, Y., Sang, N., et al. (2020). Recent Progress in Treatment of Hepatocellular Carcinoma. *Am. J. Cancer Res.* 10 (9), 2993–3036.

Du, H., Liu, L., Liu, H., and Luo, S. (2021). Wei Q Genetic Variants of DOCK2, EPHB1 and VAV2 in the Natural Killer Cell-Related Pathway Are Associated with Non-small Cell Lung Cancer Survival. *Am. J. Cancer Res.* 11 (5), 2264–2277.

Durisová, M., and Dedík, L. (1993). SURVIVAL--an Integrated Software Package for Survival Curve Estimation and Statistical Comparison of Survival Rates of Two Groups of Patients or Experimental Animals. *Methods Find Exp. Clin. Pharmacol.* 15 (8), 535–540.

Goldman, M. J., Craft, B., Hastie, M., Repeka, K., Mcdade, F., Kamath, A., et al. (2019). Visualizing and Interpreting Cancer Genomics Data via the Xena Platform. *Nat. Biotechnol.* 38, 675–678. doi:10.1038/s41587-020-0546-8

Guo, X., Zhang, B., Zeng, W., Zhao, S., and Ge, D. (2019). G3viz: an R Package to Interactively Visualize Genetic Mutation Data Using a Lollipop-Diagram. *Bioinformatics* 36 (3), 928–929. doi:10.1093/bioinformatics/btz631

Han, Q., Zhao, H., Jiang, Y., Yin, C., and Zhang, J. (2019). HCC-derived Exosomes: Critical Player and Target for Cancer Immune Escape. *Cells* 8 (6), 558. doi:10.3390/cells8060558

Hile, S. E., Shabashev, S., and Eckert, K. A. (2013). Tumor-Specific Microsatellite Instability: Do Distinct Mechanisms Underlie the MSI-L and EMAST Phenotypes? *Mutat. Research/Fundamental Mol. Mech. Mutagenesis* 743-744 (Complete), 67–77. doi:10.1016/j.mrfmmm.2012.11.003

Hnzelmann, S., Castelo, R., and Guinney, J. (2013). GSVA: Gene Set Variation Analysis for Microarray and RNA-Seq Data. *Bmc Bioinformatics* 14 (1), 7. doi:10.1186/1471-2105-14-7

Howe, K. L., Achuthan, P., Allen, J., Allen, J., Alvarez-Jarreta, J., Amode, M. R., et al. (2021). Ensembl 2021. *Nucleic Acids Res.* 49 (D1), D884–D891. doi:10.1093/nar/gkaa942

Hu, N., Pang, Y., Zhao, H., Si, C., Ding, H., Chen, L., et al. (2019). High Expression of DOCK2 Indicates Good Prognosis in Acute Myeloid Leukemia. *J. Cancer* 10 (24), 6088–6094. doi:10.7150/jca.33244

Huang, H., Hu, Y., Guo, L., and Wen, Z. (2021a). Integrated Bioinformatics Analyses of Key Genes Involved in Hepatocellular Carcinoma Immunosuppression. *Oncol. Lett.* 22 (6), 830. doi:10.3892/ol.2021.13091

Huang, T., Yan, T., Chen, G., and Zhang, C. (2021b). Development and Validation of a Gene Mutation-Associated Nomogram for Hepatocellular Carcinoma Patients from Four Countries. *Front. Genet.* 12, 714639. doi:10.3389/fgene.2021.714639

Jovcevska, I., Zottel, A., Samec, N., Mlakar, J., Sorokin, M., Nikitin, D., et al. (2019). High FREM2 Gene and Protein Expression Are Associated with Favorable Prognosis of IDH-WT Glioblastomas. *Cancers (Basel)* 11 (8), 1060. doi:10.3390/cancers11081060

Kishibuchi, R., Kondo, K., Soejima, S., Tsuboi, M., Kajiura, K., Kawakami, Y., et al. (2020). DNA Methylation of GHSR, GNG4, HOXD9 and SALL3 Is a Common Epigenetic Alteration in Thymic Carcinoma. *Int. J. Oncol.* 56 (1), 315–326. doi:10.3892/ijo.2019.4915

Kulkarni, C. A., Nadtochiy, S. M., Kennedy, L., Zhang, J., Chhim, S., Alwaseem, H., et al. (2020). ALKBH7 Mediates Necrosis via Rewiring of Glyoxal Metabolism. *Elife* 9, e58573. doi:10.7554/eLife.58573

Li, C., Pan, X. Y., Ma, M., Zhao, J., Zhao, F., and Lv, Y. P. (2021). Astragalus Polysacharin Inhibits Hepatocellular Carcinoma-like Phenotypes in a Murine HCC Model through Repression of M2 Polarization of Tumour-Associated Macrophages. *Pharm. Biol.* 59 (1), 1533–1539. doi:10.1080/13880209.2021.1991384

Li, D., Zhang, L., Fu, J., Huang, H., Sun, S., Zhang, D., et al. (2020). SCTR Hypermethylation Is a Diagnostic Biomarker in Colorectal Cancer. *Cancer Sci.* 111 (12), 4558–4566. doi:10.1111/cas.14661

Liang, L., Huang, J., Yao, M., Li, L., Jin, X. J., and Cai, X. Y. (2021a). GNG4 Promotes Tumor Progression in Colorectal Cancer. *J. Oncol.* 2021, 9931984. doi:10.1155/2021/9931984

Liang, Y., Wang, S., Huang, X., Chai, R., Tang, Q., Yang, R., et al. (2021b). Dysregulation of Circadian Clock Genes as Significant Clinic Factor in the Tumorigenesis of Hepatocellular Carcinoma. *Comput. Math. Methods Med.* 2021, 8238833. doi:10.1155/2021/8238833

Liberzon, A., Birger, C., Thorvaldsdóttir, H., Ghandi, M., Mesirov, J. P., and Tamayo, P. (2015). The Molecular Signatures Database Hallmark Gene Set Collection. *Cel Syst.* 1 (6), 417–425. doi:10.1016/j.cels.2015.12.004

Mayakonda, A., Lin, D. C., Assenov, Y., Plass, C., and Koeffler, H. P. (2018). Maftools: Efficient and Comprehensive Analysis of Somatic Variants in Cancer. *Genome Res.* 28 (11), 1747–1756. doi:10.1101/gr.239244.118

Meng, S., Zhan, S., Dou, W., and Ge, W. (2019). The Interactome and Proteomic Responses of ALKBH7 in Cell Lines by In-Depth Proteomics Analysis. *Proteome Sci.* 17, 8. doi:10.1186/s12953-019-0156-x

Mittal, S., Kanwal, F., Ying, J., Chung, R., Sada, Y. H., Temple, S., et al. (2016). Effectiveness of Surveillance for Hepatocellular Carcinoma in Clinical Practice: A United States Cohort. *J. Hepatol.* 65 (6), 1148–1154. doi:10.1016/j.jhep.2016.07.025

Newman, A. M., Steen, C. B., Liu, C. L., Gentles, A. J., Chaudhuri, A. A., Scherer, F., et al. (2019). Determining Cell Type Abundance and Expression from Bulk Tissues with Digital Cytometry. *Nat. Biotechnol.* 37 (7), 773–782. doi:10.1038/s41587-019-0114-2

Ogata, H., Goto, S., Sato, K., Fujibuchi, W., Bono, H., and Kanehisa, M. (1999). KEGG: Kyoto Encyclopedia of Genes and Genomes. *Nucleic Acids Res.* 27 (1), 29–34. doi:10.1093/nar/27.1.29

Pal, J., Patil, V., Mondal, B., Shukla, S., Hegde, A. S., Arivazhagan, A., et al. (2016). Epigenetically Silenced GNG4 Inhibits SDF1α/CXCR4 Signaling in Mesenchymal Glioblastoma. *Genes Cancer* 7 (3-4), 136–147. doi:10.18632/genesandcancer.105

Park, S. B., Hwang, K.-T., Chung, C. K., Roy, D., and Yoo, C. (2020). Causal Bayesian Gene Networks Associated with Bone, Brain and Lung Metastasis of Breast Cancer. *Clin. Exp. Metastasis* 37 (6), 657–674. doi:10.1007/s10585-020-10060-0

Reich, M., Liefeld, T., Gould, J., Lerner, J., Tamayo, P., and Mesirov, J. P. (2006). GenePattern 2.0. *Nat. Genet.* 38 (5), 500–501. doi:10.1038/ng0506-500

Ritchie, M. E., Phipson, B., Wu, D., Hu, Y., Law, C. W., Shi, W., et al. (2015). Limma powers Differential Expression Analyses for RNA-Sequencing and Microarray Studies. *Nucleic Acids Res.* 43 (7), e47. doi:10.1093/nar/gkv007

Robin, X., Turck, N., Hainard, A., Tiberti, N., Lisacek, F., Sanchez, J.-C., et al. (2011). pROC: an Open-Source Package for R and S+ to Analyze and Compare ROC Curves. *Bmc Bioinformatics* 12 (1), 77. doi:10.1186/1471-2105-12-77

Roderfeld, M., Padem, S., Lichtenberger, J., Quack, T., Weiskirchen, R., Longerich, T., et al. (2020). Schistosoma Mansoni Egg-Secreted Antigens Activate Hepatocellular Carcinoma-Associated Transcription Factors c-Jun and STAT3 in Hamster and Human Hepatocytes. *Hepatology* 72 (2), 626–641. doi:10.1002/hep.30192

Sahoo, S. S., Zhang, X. D., Hondermarck, H., and Tanwar, P. S. (2018). The Emerging Role of the Microenvironment in Endometrial Cancer. *Cancers (Basel)* 10 (11), 408. doi:10.3390/cancers10110408

Schulze, K., Imbeaud, S., Letouzé, E., Alexandrov, L. B., Calderaro, J., Rebouissou, S., et al. (2015). Exome Sequencing of Hepatocellular Carcinomas Identifies New Mutational Signatures and Potential Therapeutic Targets. *Nat. Genet.* 47 (5), 505–511. doi:10.1038/ng.3252

Sing, T., Sander, O., Beerenwinkel, N., and Lengauer, T. (2005). ROCR: Visualizing Classifier Performance in R. *Bioinformatics* 21 (20), 3940–3941. doi:10.1093/bioinformatics/bti623

Skidmore, Z. L., Wagner, A. H., Lesurf, R., Campbell, K. M., Kunisaki, J., Griffith, O. L., et al. (2016). GenVisR: Genomic Visualizations in R. *Bioinformatics* 32 (19), 3012–3014. doi:10.1093/bioinformatics/btw325

Subramanian, A., Tamayo, P., Mootha, V. K., Mukherjee, S., Ebert, B. L., Gillette, M. A., et al. (2005). Gene Set Enrichment Analysis: A Knowledge-Based Approach for Interpreting Genome-wide Expression Profiles. *Proc. Natl. Acad. Sci. U.S.A.* 102 (43), 15545–15550. doi:10.1073/pnas.0506580102

Tomczak, K., Czerwińska, P., and Wiznerowicz, M. (2015). The Cancer Genome Atlas (TCGA): An Immeasurable Source of Knowledge. *Contemp. Oncol. (Pozn)* 19 (1A), A68–A77. doi:10.5114/wo.2014.47136

Walker, A. R., Silvestrov, P., Müller, T. A., Podolsky, R. H., Dyson, G., Hausinger, R. P., et al. (2017). ALKBH7 Variant Related to Prostate Cancer Exhibits Altered Substrate Binding. *Plos Comput. Biol.* 13 (2), e1005345. doi:10.1371/journal.pcbi.1005345

Wang, L., Sun, X., Jin, C., Fan, Y., and Xue, F. (2021). Identification of Tumor Microenvironment-Related Prognostic Biomarkers for Ovarian Serous Cancer 3-Year Mortality Using Targeted Maximum Likelihood Estimation: A TCGA Data Mining Study. *Front. Genet.* 12, 625145. doi:10.3389/fgene.2021.625145

Wu, D., Li, Y., Ren, Q., Pei, S., Wang, L., Yang, L., et al. (2021). TANC1 Methylation as a Novel Biomarker for the Diagnosis of Patients with Anti-tuberculosis Drug-Induced Liver Injury. *Sci. Rep.* 11 (1), 17423. doi:10.1038/s41598-021-96869-5

Yang, Q., Liu, H., Li, Z., Wang, Y., and Liu, W. (2019). Purification and Mutagenesis Studies of TANC1 Ankyrin Repeats Domain Provide Clues to Understand Mis-Sense Variants from Diseases. *Biochem. Biophysical Res. Commun.* 514 (2), 358–364. doi:10.1016/j.bbrc.2019.04.151

Yoshihara, K., Shahmoradgoli, M., Martínez, E., Vegesna, R., Kim, H., Torres-Garcia, W., et al. (2013). Inferring Tumour Purity and Stromal and Immune Cell Admixture from Expression Data. *Nat. Commun.* 4, 2612. doi:10.1038/ncomms3612

Yperman, J., Becker, T., Valkenborg, D., Popescu, V., Hellings, N., Wijmeersch, B. V., et al. (2019). Machine Learning Analysis of Motor Evoked Potential Time Series to Predict Disability Progression in Multiple Sclerosis. *BMC Neurol.* 20 (1), 105. doi:10.1186/s12883-020-01672-w

Yu, G., Wang, L.-G., Han, Y., and He, Q.-Y. (2012). clusterProfiler: an R Package for Comparing Biological Themes Among Gene Clusters. *OMICS: A J. Integr. Biol.* 16 (5), 284–287. doi:10.1089/omi.2011.0118

Yu, J., Wu, W. K. K., Li, X., He, J., Li, X.-X., Ng, S. S. M., et al. (2015). Novel Recurrently Mutated Genes and a Prognostic Mutation Signature in Colorectal Cancer. *Gut* 64 (4), 636–645. doi:10.1136/gutjnl-2013-306620

Zhan, P., Ji, Y. N., and Yu, L. K. (2013). TP53 Mutation Is Associated with a Poor Outcome for Patients with Hepatocellular Carcinoma: Evidence from a Meta-Analysis. *Hepatobiliary Surg. Nutr.* 2 (5), 260–265. doi:10.3978/j.issn.2304-3881.2013.07.06

Zhang, J., Bajari, R., Andric, D., Gerthoffert, F., Lepsa, A., Nahal-Bose, H., et al. (2019). The International Cancer Genome Consortium Data PortalIdentification of Core Genes and Key Pathways via Integrated Analysis of Gene Expression and DNA Methylation Profiles in Bladder Cancer. *Nat. Biotechnol.* 37, 367–369. doi:10.1038/s41587-019-0055-9

Zhao, X., Lei, Y., Li, G., Cheng, Y., Yang, H., Xie, L., et al. (2019). Integrative Analysis of Cancer Driver Genes in Prostate Adenocarcinoma. *Mol. Med. Rep.* 19 (4), 2707–2715. doi:10.3892/mmr.2019.9902

Zhao, Y., Chen, J., Wei, W., Qi, X., Li, C., and Ren, J. (2018). The Dual-Inhibitory Effect of miR-338-5p on the Multidrug Resistance and Cell Growth of Hepatocellular Carcinoma. *Sig Transduct Target. Ther.* 3, 3. doi:10.1038/s41392-017-0003-4

Zheng, B., Peng, J., Mollayup, A., Bakri, A., Guo, L., Zheng, J., et al. (2018). Construction of a Prognostic Prediction System for Pancreatic Ductal Adenocarcinoma to Investigate the Key Prognostic Genes. *Mol. Med. Rep.* 17 (1), 216–224. doi:10.3892/mmr.2017.7850

Conflict of Interest: The authors declare that the research was conducted in the absence of any commercial or financial relationships that could be construed as a potential conflict of interest.

Publisher's Note: All claims expressed in this article are solely those of the authors and do not necessarily represent those of their affiliated organizations, or those of the publisher, the editors, and the reviewers. Any product that may be evaluated in this article, or claim that may be made by its manufacturer, is not guaranteed or endorsed by the publisher.

Copyright © 2022 Huang, Luo, Chen, Su, Zhu, Wei, Qiu, Long, Shi and Wei. This is an open-access article distributed under the terms of the Creative Commons Attribution License (CC BY). The use, distribution or reproduction in other forums is permitted, provided the original author(s) and the copyright owner(s) are credited and that the original publication in this journal is cited, in accordance with accepted academic practice. No use, distribution or reproduction is permitted which does not comply with these terms.

frontiers | Frontiers in Genetics

ORIGINAL RESEARCH
published: 19 May 2022
doi: 10.3389/fgene.2022.864578

MCM10 is a Prognostic Biomarker and Correlated With Immune Checkpoints in Ovarian Cancer

Zhenzhen Wu[1†], *Yueyuan Wang*[2†], *Juan Li*[1], *Huiling Wang*[3], *Xunyuan Tuo*[3] *and Jing Zheng*[1*]

[1]Department of Gynecology, Gansu Provincial Maternity and Child-Care Hospital, Lanzhou, China, [2]Department of Pathology, Gansu Provincial Maternity and Child-Care Hospital, Lanzhou, China, [3]Department of Gynecological Oncology, Gansu Provincial Maternity and Child-Care Hospital, Lanzhou, China

Background: Microchromosome maintenance protein 10 (MCM10) is required for DNA replication in all eukaryotes, and it plays a key role in the development of many types of malignancies. However, we currently still do not know the relationship between MCM10 and ovarian cancer (OV) prognosis and immune checkpoints.

Methods: The Gene Expression Profiling Interactive Analysis and Tumor Immunology Estimation Resource (TIMER) databases were used to investigate MCM10 expression in Fan cancer. The Kaplan-Meier Plotter and PrognoScan were used to assess the relationship between MCM10 and OV prognosis. The LinkedOmics database was used to analyze the MCM10 co-expression network and explore GO term annotation and the KEGG pathway. The relationship between MCM10 expression and immune infiltration in OV was investigated using the Tumor Immunology Estimation Resource database. cBioPortal database was used to explore the relationship between MCM10 expression and 25 immune checkpoints. Finally, quantitative real-time polymerase chain reaction (qRT-PCR) was performed to detect MCM10 expression. The prognosis was also analyzed by distinguishing between high and low expression groups based on median expression values.

Results: The results of the three data sets (220,651_s_at, 222,962_s_at and 223,570_at) in KM Plotter all indicated that the overall survivalof the high MCM10 expression group was lower than that of the low expression group OV, and the results of GSE9891 also reached the same conclusion. The expression level of MCM10 was negatively correlated with B cells and CD8+T cells, and positively correlated with CD4+T Cells and Macrophages. GO term annotation and KEGG pathway analysis showed that the co-expressed genes of MCM10 were mainly enriched in cell cycle and DNA replication. The alterations in MCM10 coexisted statistically with the immune checkpoints CTLA4, TNFSF4, TNFSF18, CD80, ICOSLG, LILRB1 and CD200. PCR results displayed that MCM10 was highly expressed in OV tissues, and the increased expression of MCM10 was significantly associated with poor overall survival.

Conclusion: These results demonstrated that high expression of MCM10 was associated with poor prognosis in OV and correlated with immune checkpoints.

Keywords: ovarian cancer, Mcm10, bioinformatics, prognosis biomarkers, immune checkpoints

OPEN ACCESS

Edited by:
Alip Ghosh,
University of Maryland, United States

Reviewed by:
Sriram Vijayraghavan,
MUSC Health, United States
Debanjali Dasgupta,
Mayo Clinic, United States

***Correspondence:**
Jing Zheng
394146806@qq.com

[†]These authors have contributed equally to this work

Specialty section:
This article was submitted to Cancer Genetics and Oncogenomics, a section of the journal Frontiers in Genetics

Received: *28 January 2022*
Accepted: *02 May 2022*
Published: *19 May 2022*

Citation:
Wu Z, Wang Y, Li J, Wang H, Tuo X and Zheng J (2022) MCM10 is a Prognostic Biomarker and Correlated With Immune Checkpoints in Ovarian Cancer. Front. Genet. 13:864578. doi: 10.3389/fgene.2022.864578

INTRODUCTION

Ovarian cancer (OV) is a common but fatal gynaecological malignancy. Although the mortality rate from OV has declined over the past 40 years as medical care has improved, it still remains the second leading cause of death from gynaecological cancers in women and the eighth leading cause of death in women (Irusta, 2021). The current treatment for OV is mainly surgical resection and platinum-based chemotherapy, the combination of which usually brings good outcomes, with the addition of anti-angiogenic agents usually for poorly operated and stage IV patients (Lheureux et al., 2019). Despite many efforts to treat OV, the prognosis still remains poor due to the recurrence and metastasis of OV. Thus, identifying novel regulators as diagnostic and therapeutic targets for OV is still urgently required.

Minichromosome maintenance (MCM) proteins are essential for the initiation of DNA replication, and it has been detected to be overexpressed in various cancer tissues, including lung squamous cell carcinoma (Wu et al., 2018), breast cancer (Juríková et al., 2016), glioma (Cai et al., 2018), hepatocellular carcinoma (Liu et al., 2018), etc. As an important player in the initiation pathway of DNA replication, Minichromosome maintenance 10 (MCM10) was first identified in a yeast genetic screen and only presents in eukaryotes (Aves et al., 1998). At the same time, the involvement of MCM10 has also been found in DNA elongation, bolstering the activity of the CMG helicase on bypassing replication blocks (Langston et al., 2017; Lõoke et al., 2017) and promotion of replication fork progression and stability (Baxley and Bielinsky, 2017). In addition to the above group roles, MCM10, like other MCM family proteins, is abnormally expressed in various tumors and associated with prognosis. The overexpression of MCM10 is thought to promote the abnormal proliferation of prostate cancer (PC) cells and associated with poor prognosis of PC (Cui et al., 2018). Meanwhile, it is positively related to poor prognosis in breast cancer (Yang and Wang, 2019). In glioma, the knockdown of MCM10 in glioma cells resulted in decreased cell proliferation, migration and invasion (Kang et al., 2020). However, we have not found many articles on the relationship between MCM10 and OV. Based on the close relationship between MCM10 and various malignant tumors, we have reasons to believe that MCM10 is a potential prognostic marker.

Increasing research results proved that immunotherapy is a very promising therapeutic method in the treatment of malignant tumors, among which the blockade of immune checkpoints has displayed significant efficacy in various types of tumors (Topalian et al., 2016). Interfering with Cytotoxic T lymphocyte (CTLA-4) and ProgrammedDeath-1 (PD-1) reportedly has clinical benefits in several human cancers (Odunsi, 2017), so the characterizing associations between MCM10 and immune checkpoints will potentially enhance OV treatment.

In this study, the online tools TIMER and GEPIA were used to explore the expression of MCM10 in various malignancies. The prognostic value of MCM10 expression in OV was determined using the Kaplan-Meier Plotter and PrognoScan databases. LinkedOmics database was used to view genes and pathways associated with MCM10. The cBioPortal database was used to visualize and compare genetic alterations and explore the association between MCM10 and 25 immune checkpoints. Finally, qRT-PCR was used to detect the expression of MCM10 and analyze the relationship between its expression and prognosis. Our findings revealed an significant role for MCM10 in OV expression and prognosis, and also elucidated the relationship between MCM10 and multiple immune checkpoints.

MATERIALS AND METHODS

Tissue Samples

A total of 22 cancerous and 50 paracancerous ovarian tissue samples were obtained during surgery. The study was approved by the jurisdictional clinical research ethics committees. All patients consented to the study.

qRT-PCR

Frozen tissues (100 mg) were ground into powder in liquid nitrogen, and then suspended in 1 ml TRIZOL Reagent (Invitrogen, United States of America), Total RNA was extracted using TRIZOL reagent. RNA was quantified using a spectrophotometer (Beckman, United States of America). RNA template and random primers were incubated at 70°C for 10 min to melt the secondary structure within the template, and cooled on ice for more than 2 min. Then the complete reaction mixture was incubated at 30°C for 10 min, 42°C for 60 min and 70°C for 15 min. PCR was performed in a total volume of 25 μl containing 1 μl of reverse-transcribed cDNA. After an initial incubation at 94°C for 5 min, the reaction mixtures were subjected to 35 cycles of amplification using the following protocols: 94°C for 45 s, 55°C for 45 s and 72°C for 45 s, followed by a final extension step at 72°C for 7 min. PCR products were analyzed by 1.2% agarose gel electrophoresis and stained with GoldView nucleic acid dye. Real-time RT-PCR was performed using ABI PRISM 7500 Sequence Detection System instrument and software (Applied Biosystems, United States). The relative expression level of MCM10 was measured using SYBR Green I dye-based method. The results were normalized to the expression of glyceraldehyde-3-phosphate dehydrogenase (GAPDH). The Ct values of the amplified products were used in conjunction with the $2^{-\Delta\Delta Ct}$ method to analyze the data (Schmittgen and Livak, 2008; Zhang et al., 2010). The primers used were GAPDH: 5′-AGAAGGCTG GGGCTCATTTG-3′ (F), 5′-AGGGGCCATCCACAGTCTTC-3′ (R); MCM10:5′-CACAGAAATGAACAAGAA-3′(F),5′-AATAAGAACAAGGACACA-3′(R) ; Primers were synthesized by BGI Company.

GEPIA Database Analysis

GEPIA (http://gepia.cancer-pku.cn/index.html) is a recently developed bioinformatics platform that incorporates genotype tissue expression data from 9,736 tumors and 8,587 normal samples. In the current study, the "Expression DIY" component was used to analyze the EFNA1 expression levels in a variety of cancers and adjacent tissues, and $p < 0.05$ was used as the screening threshold significance level (Tang et al., 2017).

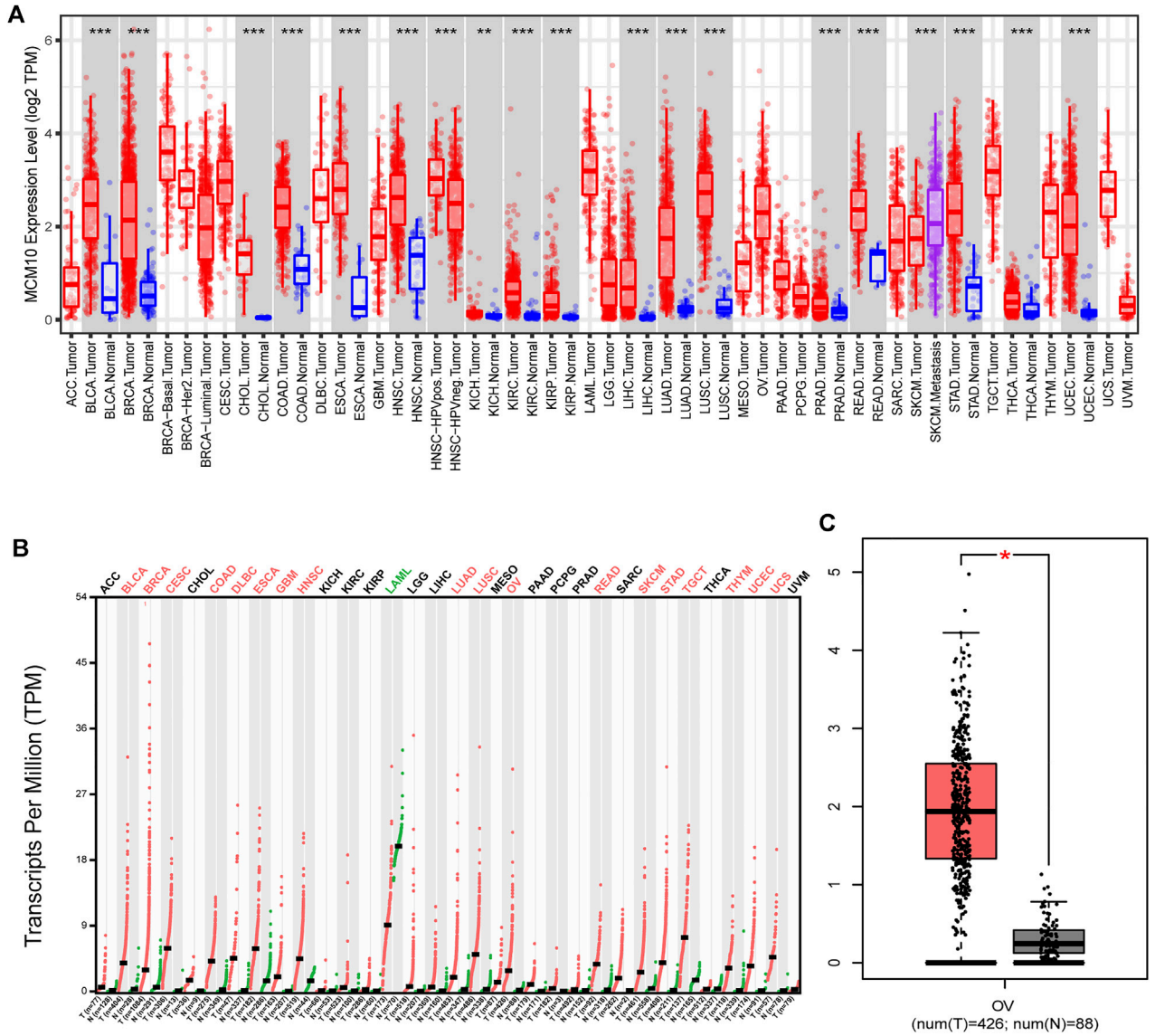


FIGURE 1 | MCM10 expression levels in different types of human cancers. **(A)** MCM10 expression in different tumor types in TIMER. **(B)** MCM10 expression in different tumor types in GEPIA. **(C)** Box plots comparing MCM10 expression in OV and unpaired normal tissues in GEPIA based on analysis of variance method (TCGA tumor versus TCGA normal + GTEx normal).*$p < 0.05$, **$p < 0.01$, ***$p < 0.001$.

TIMER Database

TIMER (https://cistrome.shinyapps.io/timer/) is a tumor immunity database, including 10,897 cancer samples from the TCGA database, together with an abundance of tumor-infiltrating immune cells (TIICs) based on a deconvolution method from gene expression profiles. In the present study, the "Gene" module was applied to analyze the correlations between EFNA1 expression and immune cell infiltration. The immune cells analyzed included $CD4^+$ T cells, $CD8^+$ T cells, B cells, neutrophils, macrophages, and dendritic cells (DCs). The "Correlation" module of TIMER was used to analyze the associations between EFNA1 and other prognosis-related immune cell markers, including $CD8^+$ T cells, all T cells collectively, B cells, monocytes, tumor-associated macrophages (TAMs), M1 and M2 macrophages, neutrophils, natural killer (NK) cells, and DCs (Li et al., 2017).

Survival Analysis and Prognostic Evaluation

Kaplan–Meier Plotter (http://kmplot.com/analysis/) and PrognoScan (http://dna00.bio.kyutech.ac.jp/PrognoScan/index.html) were used for prognostic analyses. Kaplan–Meier Plotter evaluated the prognostic significance of MCM10 mRNA expression in OV. Patients' samples were divided into two groups based on the median MCM10 expression level, and the overall survival (OS) of patients with OV was analyzed. The examination probe ID was used for MCM10 was 220,651_s_at,

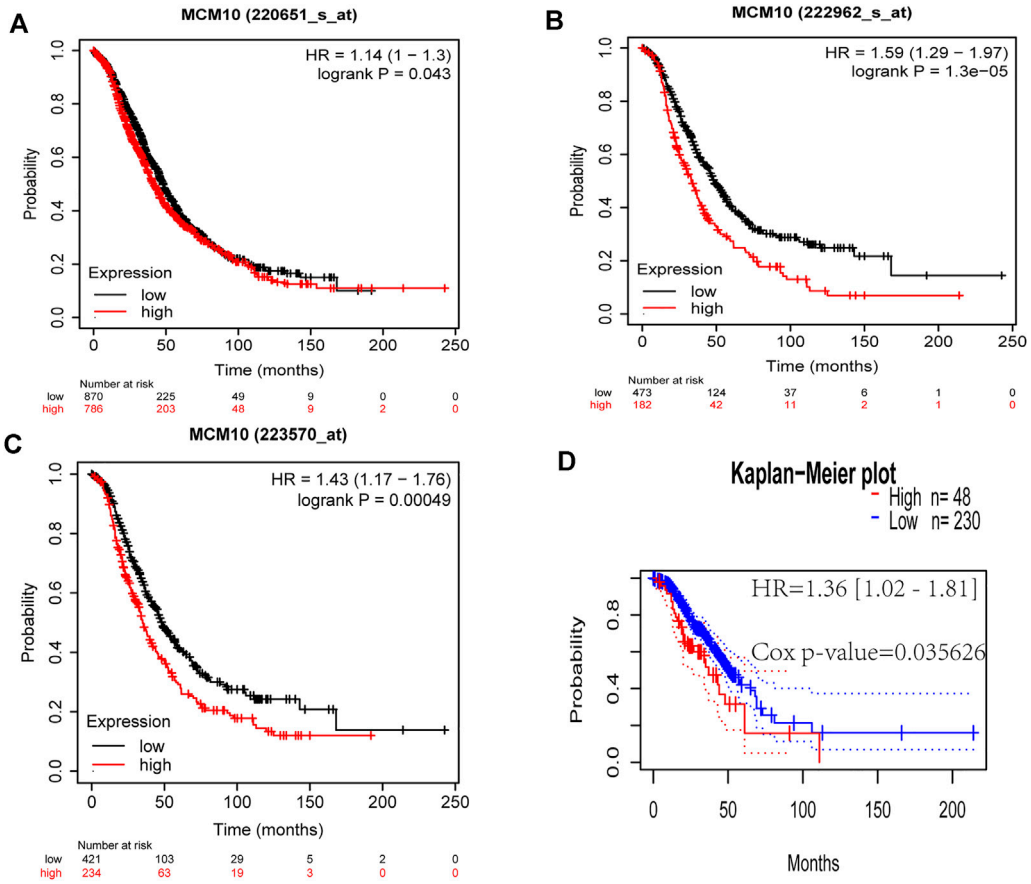


FIGURE 2 | Correlations between MCM10 expression and prognostic indicators in OV. **(A–C)** Correlations between MCM10 and OV prognoses in the Kaplan–Meier Plotter database from different expression callers (220,651_s_at,222,962_s_at, 223,570_at). **(D)** Survival curve from PrognoScan analysis for OS of patients with OV. HR = hazard ratio.

222,962_s_at and 223,570_at. The log-rank *p*-value and hazard ratio (HR) with 95% confidence intervals were calculated. The PrognoScan database mainly collects clinical prognostic information derived from 14 cancers from GEO (Gene Expression Omnibus) and various laboratories, and then applies a minimum *p* value approach in analyses. In the current study, it was used to analyze the prognostic value of MCM10 in OV and adjust the threshold to a Cox *p* value (Mizuno et al., 2009; Lánczky and Győrffy, 2021).

cBioPortal Database

cBioPortal for Cancer Genomics (http://cbioportal.org) is a large repository of genomics datasets. In the present study, cBioPortal was used to visualize and compare the changes in EFNA1 and immune checkpoints in OV. The correlations between MCM10 and immune checkpoints were also investigated. The immune checkpoints analyzed included PD-L1 (CD274), PD-L2 (PDCD1LG2), CD80, CD86, VTCN1, VSIR, HHLA2, TNFRSF14, PVR, CTL4, CD112 (NECTIN2), CD200, LGALS9, ICOSLG, TNFSF9, TNFSF4, CD70, TNFSF18, CD48, CTLA4, CD276, LILRB1, LILRB2, HAVCR2, CD47 and TNFRSF9(CD137) (Wu et al., 2019).

COSMIC Database Analysis of MCM10 Mutations in OV

The Catalogue of Somatic Mutations in Cancer (COSMIC) (https://cancer.sanger.ac.uk) is the most detailed and comprehensive resource to explore the effects of somatic mutations in human cancer. COSMIC database Contains 6 million coding mutations (Tate et al., 2019). Ovary in the"tissue distribution"and "mutation distribution"were chosen.

LinkedOmics Database Analysis of MCM10-Related Pathways

The LinkedOmics (http://www.linkedomics.org) database includes 32 cancer types from TCGA project and 11,158 patients with multiple omics and clinical data. It is also the first multi-omics database that integrates mass spectrometry–based global proteomics data generated by the Clinical Proteomics Cancer Analysis Alliance on selected TCGA tumor samples (Vasaikar et al., 2018). The differentially expressed genes related to MCM10 were screened from the TCGA OV cohort through the LinkFinder module in the database, and the correlations of the results were presented in volcano plots and heat maps, respectively, by Pearson

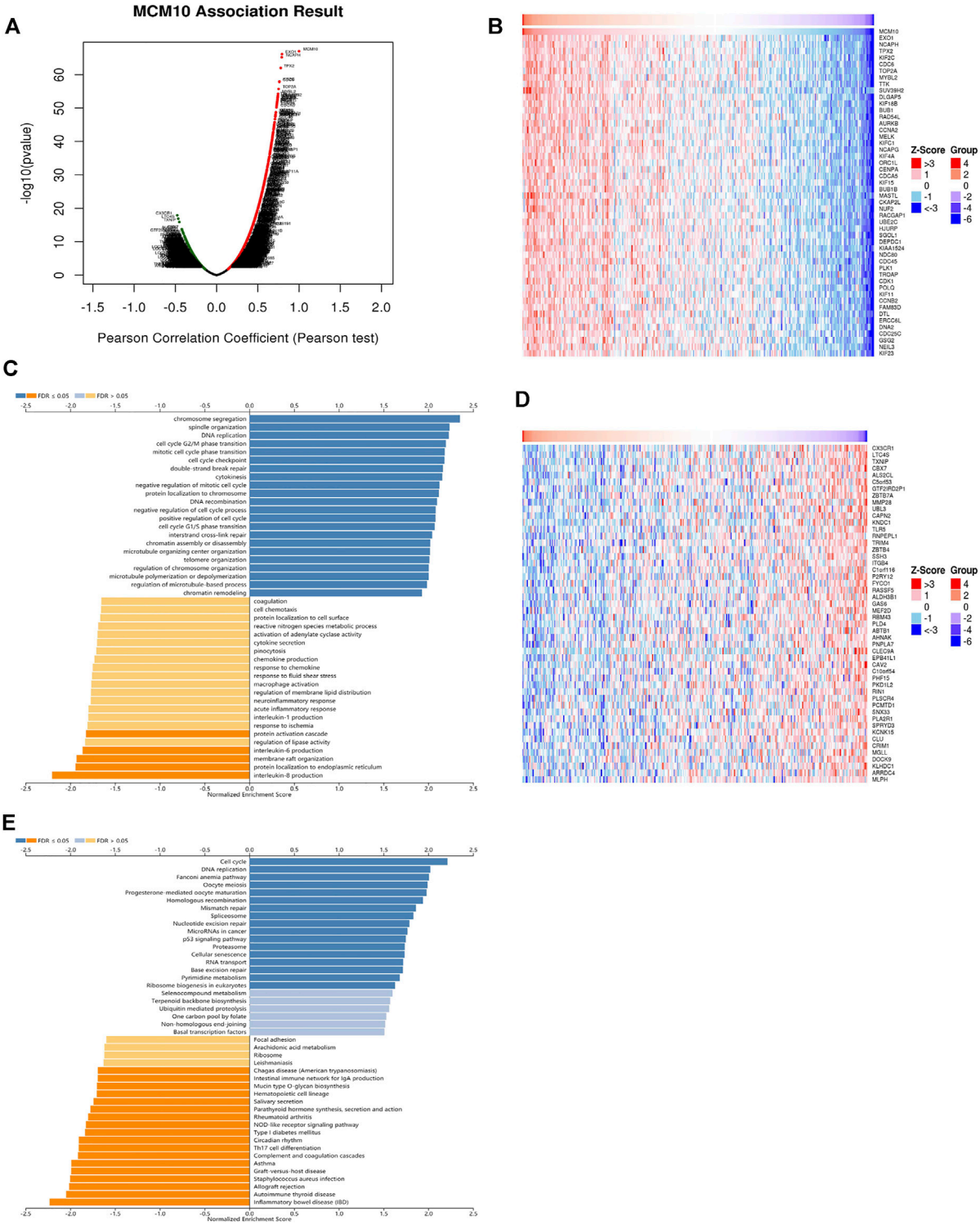


FIGURE 3 | The co-expression genes with MCM10 from the LinkedOmics database in OV. **(A)** The whole significantly associated genes with MCM10 distinguished in OV cohort. **(B–D)** Top 50 genes positively and negatively related to MCM10 in OV **(C,E)** GO annotations and KEGG pathways of CLEC10A in LUAD cohort.

correlation coefficient test. Gene Set Enrichment Analysis (GSEA) in the LinkInterpreter module performed functional module analysis of the Gene Ontology Biological Process (GO_BP), Kyoto Encyclopedia of Genes and Genomes (KEGG) pathways. And 0.05 was considered as the *p*-value cutoff and the Spearman correlation test was conducted to analyze the results statistically.

Statistical Analysis

All data were expressed as means and standard deviations, and SPSS 19.0 software (SPSS Inc. Chicago, IL, United States) was the statistical analysis tool used. The student's *t*-test and one-way analysis of variance were carried out to analyze the differences between groups. $p < 0.05$ was deemed to indicate the statistical significance. All experiments were conducted in triplicate as a minimum. The Kaplan–Meier Plotter and GEPIA results are presented as hazard ratios (HRs) and *p* values, and PrognoScan results are presented as Cox *p* values.

RESULTS

mRNA Expression Levels of MCM10 in Different Types of Human Cancers

To evaluate the differences of MCM10 expression in tumor and normal tissues, the MCM10 mRNA levels in tumor and normal tissues of patients with multiple types of cancer were analyzed using the GEPIA and TIMER database. MCM10 expression was higher in BLCA, BRCA, CHOL, COAD, HNSC, KICH, KIRC, KIRP, LIHC, LUAD, PRAD, READ, STAD, THCA, and UCEC, compared with normal tissues in TIMER (**Figure 1A**). In GEPIA, high expression in BLCA, BRCA, CESC, COAD, DLBC, ESCA, GBM, HNSC, LUAD, LUSC, OV, READ, SKCM, STAD, TGCT, THYM, UCEC and UCS was observed. In addition, lower expression was observed in LAML (**Figure 1B**). MCM10 was highly expressed in OV (**Figure 1C**).

Relationships Between MCM10 and the Prognosis of OV

The prognostic value of MCM10 expression in OV was evaluated using Kaplan-Meier plots and PrognoScan. The expression of MCM10 was significantly associated with the prognosis of OV patients. In analyses with the Kaplan-Meier plots, the OS 220651_s_at [HR = 1.14 (1 -1.3), $p = 0.043$], 222,962_s_at [HR = 1.59 (1.29 -1.97), $p = 1.3e\text{-}05$] and 223,570_at [HR = 1.43 91.17 -1.760, $p = 0.00049$] of OV patients with high MCM10 expression (**Figures 2A–C**) values were significantly lower than those of patients with low MCM10 expression. In PrognoScan database analysis of the prognostic potential of MCM10 in OV, high MCM10 expression in the GSE9891 cohort was associated with poor OS [HR = 1.36 (1.02 -1.810, $p = 0.035626$] (**Figure 2D**).

MCM10 Co-Expression Network in OV

To understand the biological function of MCM10 in OV, the LinkFinder module in the LinkedOmics portal was used to examine the co-expression pattern of MCM10 in TCGA-OV. As shown in **Figure 3A** genes positively correlated with MCM10 were dark red dots, and 3,613 genes negatively correlated with MCM10 were dark green dots. **Figures 3B–D** represents the top 50 genes associated and negatively associated with the MCM10 signature, respectively. GO term annotation proved that the co-expressed genes of MCM10 join mainly in chromosome segregation, spindle organization, DNA replication, cell cycle G2/M phase transition, mitotic cell cycle phase transition, cell cycle checkpoint, double-strand break repair, cytokinesis, negative regulation of mitotic cell cycle and protein localization to chromosome, etc (**Figure 3C**). KEGG pathway analysis indicated the enrichment in Cell cycle, DNA replication, Fanconi anemia pathway, Oocyte meiosis, Progesterone-mediated oocyte maturatio, Homologous recombination, Mismatch repair, Asthma, Graft-versus-host disease, and *Staphylococcus aureus* infection, etc (**Figure 3C**). It was found that GO terms and KEGG pathways were more concentrated in cell cycle and DNA replication.

Mutation of MCM10 in OV

The cBioPortal was used to explore the mutation status of MCM families (MCM2, MCM3, MCM4, MCM5, MCM6, MCM7, MCM8, MCM9, MCM10 and MCMBP). Totally, 30.87% (96/311) of patients had genetic alterations (**Figure 4A**), of which MCM10 accounted for 6.43% (20/311), and the amplification was the most frequent mutation (**Figure 4B**). In COSMIC, we further assessed the mutation type of MCM10, Missense substitutions occurred in approximately 21.43% of the samples, synonymous substitutions occurred in 3.57% of the samples, and nonsense substitutions occurred in 3.57% of the samples (**Figure 4C**). The substitution mutations mainly occurred at A > G (25.00%) and G > T (25.00%), followed by A > T (12.50%), C > A (12.50%), C > G (12.50%), and G > A (12.50%) (**Figure 4D**).

Correlation of MCM10 With Immune Infiltration and Immune Checkpoints

The presence of immune infiltration within tumors can generate important biomarkers to predict the prognosis of tumor patients, with impacts on radiotherapy, chemotherapy and therapy. Therefore, it is cardinal to study the relationship between MCM10 and immunity. We used the "Gene" module in TIMER for database search, entered the target gene MCM10, and selected OV. This module displays infiltration results, including TIMER, EPIC, MCP-COUNTER, CIBERSORT, CIBERSORT-ABS, QUANTISEQ, XCELL, QUANTISE and TIDE. The expression of MCM10 was positively correlated with CD4+T Cells (cor = 0.109, $p = 0.0166$) and Macrophages (cor = 0.101,$p = 0.0275$), and was positively correlated with B cells(cor = -0.1,$p = 0.0288$) and CD8+T Cells(cor = -0.139, $p = 0.00223$) (**Figure 5A**). The relationship between genetic changes in the MCM10 gene and 25 immune checkpoints was explored. Three datasets (MSK, TCGA and MSKCC), including 612 samples, were selected, and genomic studies revealed that MCM10 was involved in the alteration of OV immune checkpoints. The alterations of MCM10 and immune checkpoints in OV were visualized in a compact manner. In OV, the Genetic Alteration of MCM10 was 5% and mainly concentrated in Amplification. There was a part of Missense Mutation, second only to 6% of the immune checkpoint CD47, which was equal to HHLA2 and CD200. This indicated that MCM10 had a high mutation rate during the progression of OV (**Figure 5B**). Then, the association between MCM10 and each immune checkpoint was examined. Notably, the alterations in MCM10 showed statistically significant coexistence rather than rejection with the immune checkpoints CTLA4, TNFSF4, TNFSF18, CD80, ICOSLG, LILRB1 and CD200 (**Table 1**). These findings strongly suggested that MCM10 is a potential co-regulator of the OV immune checkpoint.

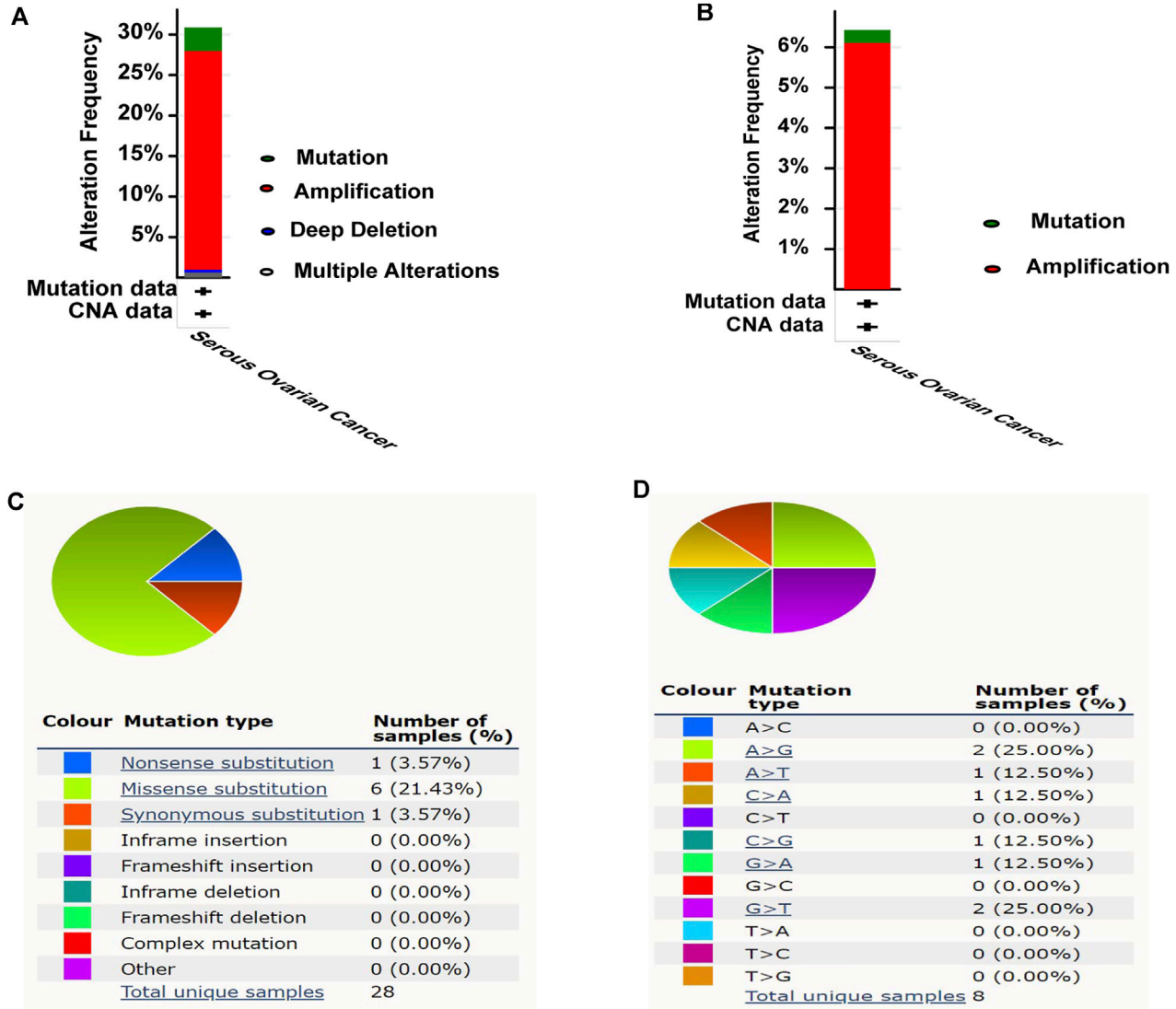


FIGURE 4 | Mutation analysis of MCM10 in OV. **(A)** Mutation frequency of MCM10. **(B)** Mutation frequency of MCM10. **(C–D)** The mutation types of MCM10 in OV by Catalogue of Somatic Mutations in Cancer (COSMIC) database.

Validation of MCM10 in OV Tissues

To explore the expression of MCM10 in OV, qRT-PCR validation was chosen. The results suggested that the expression of MCM10 was elevated in OV (**Figure 6A**). According to the median value of expression, the patients were divided into high and low expression groups to judge the prognosis of patients (**Figure 6B**). The results illustrated that OV patients with high MCM10 had a worse prognosis.

DISSCUSSION

One of the characteristics of tumor cells is unlimited proliferation. Therefore, many proteins related to DNA replication have been considered as potential cancer biomarkers, including MCM protein (Yu et al., 2020). MCM protein has been considered as a biomarker of dysplasia and tumor (Wang et al., 2020). There are several hypotheses about the mechanism of MCM dysregulation leading to tumorigenesis. The first is genomic instability (GIN), because the formation of cancer cells is caused by the accumulation of mutations in oncogenes and tumor suppressor genes. In many studies, GIN caused by MCM mutation has been proved to be related to the occurrence of malignant tumors. (Chuang et al., 2010). Secondly, damage to MCM induces replicative stress, a critical step in the initiation of the oncogenic process (Gaillard et al., 2015). Finally, the study found that MCM family proteins participate in the progression of cell cycle pathways. For example, knockdown of MCM2 reduces the expression of cyclinD1, cyclinA and CDK4, knockdown of MCM3 reduces the expression of cyclinA, knockdown of MCM6 causes CyclinA, CyclinB1,CyclinD1, silencing of MCM7 reduces cyclinD1, cyclinE2 and CDK2, and down-regulation of cyclinD1

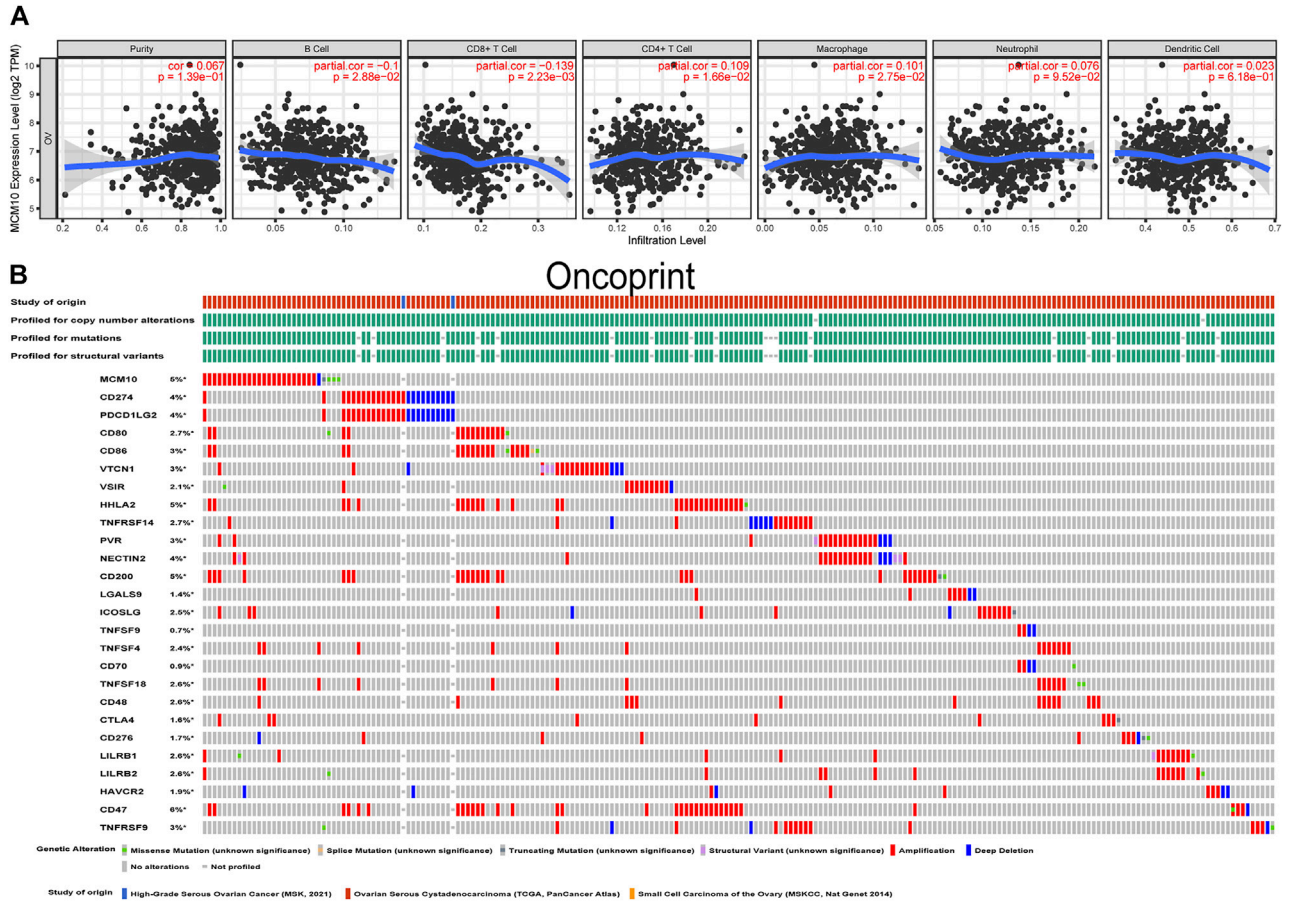


FIGURE 5 | Correlation of MCM10 with immune infiltration and immune checkpoints. **(A)** the correlations between MCM10 and immune cell infiltrations from TIMER. **(B)** Landscape of MCM10 and immune checkpoint alteration in OV from cBioPortal.

in breast cancer cells with MCM10 knockdown (Zhang et al., 2015; Qiu et al., 2017; Liu et al., 2018; Yang and Wang, 2019). These results all suggest that mutations in MCM proteins cause changes in various cyclins, and ultimately aberrant cell cycle progression leads to tumorigenesis. There are few studies on MCM10 in the MCM protein family, especially its relationship with OV, so this study focused on this gene, which has not received much attention but is extremely significant. MCM10 acts as an vital scaffold for DNA replication and protection against replication stress under normal conditions. However, under pathological conditions, MCM10 is frequently deregulated, and gene amplification and overexpression are very common in cancer (Baxley and Bielinsky, 2017). Our results also demonstrated that the changes of the MCM10 gene in OV are mainly concentrated in the amplification, and it was discovered that most of the mutations in MCM10 are missense mutations (93%), and the rest are roughly divided into splicing mutations (3.7%) and nonsense mutations (3.2%) (Gao et al., 2013; Kang et al., 2013), which is consistent with our findings. The mechanism by which MCM10 causes OV, in addition to the aforementioned, may also be related to the specific relationship between MCM10 and female ovaries, where MCM10 is highly expressed in adult female ovaries (Graveley et al., 2011). Based on this, Reubens et al. conducted further research and believed that MCM10 plays a unique biological role in the development or maintenance of the female germline (Reubens et al., 2015). So the mutation of MCM10 may be another cause of OV progression. These data clearly indicated that MCM10 changes in the cancer genome, but whether these changes are the causes or the results of OV still needs further studies to confirm.

Our results proved that the expression of MCM10 in various malignant tumors is different from that in normal tissues, except for the low expression of LAML in the GEPIA database, because the data in the TIMER database are all from TCGA, and normal control samples of some malignant tumors are insufficient, but MCM10 is highly expressed in malignant tumors with differential expression. Since we only obtained high expression of MCM10 in OV from GEPIA, we further verified the expression of MCM10 in OV by qRT-PCR, and it was found that the expression of MCM10 in OV was higher than that in normal ovarian tissue. Subsequently, the relationship between the expression of MCM10 and the prognosis of OV patients was examined in four databases, and it was obvious that the prognosis of OV patients with high expression of MCM10 was worse. After being

TABLE 1 | Mutual-exclusivity analysis between MCM10 and multiple-immune checkpoints in ovarian cancer.

A	B	Neither	A not B	B not A	Both	Log2 Odds ratio	*p*-value	q-value	Tendency	Significant
MCM10	CTLA4	477	25	6	3	>3	0.01	0.154	Co-occurrence	MCM10
MCM10	TNFSF4	474	25	9	3	2.66	0.023	0.329	Co-occurrence	MCM10
MCM10	TNFSF18	473	25	10	3	2.505	0.029	0.379	Co-occurrence	MCM10
MCM10	CD80	472	25	11	3	2.364	0.036	0.401	Co-occurrence	MCM10
MCM10	ICOSLG	472	25	11	3	2.364	0.036	0.401	Co-occurrence	MCM10
MCM10	LILRB1	472	25	11	3	2.364	0.036	0.401	Co-occurrence	MCM10
MCM10	CD200	461	24	22	4	1.804	0.047	0.506	Co-occurrence	MCM10
MCM10	NECTIN2	465	25	18	3	1.632	0.101	0.819	Co-occurrence	MCM10
MCM10	LILRB2	472	26	11	2	1.723	0.156	0.928	Co-occurrence	MCM10
MCM10	CD86	467	26	16	2	1.167	0.258	0.928	Co-occurrence	MCM10
MCM10	PVR	467	26	16	2	1.167	0.258	0.928	Co-occurrence	MCM10
MCM10	CD274	465	26	18	2	0.991	0.301	0.928	Co-occurrence	MCM10
MCM10	PDCD1LG2	465	26	18	2	0.991	0.301	0.928	Co-occurrence	MCM10
MCM10	HAVCR2	475	27	8	1	1.137	0.4	0.928	Co-occurrence	MCM10
MCM10	HHLA2	460	26	23	2	0.621	0.404	0.928	Co-occurrence	MCM10
MCM10	VSIR	473	27	10	1	0.809	0.465	0.928	Co-occurrence	MCM10
MCM10	CD276	473	27	10	1	0.809	0.465	0.928	Co-occurrence	MCM10
MCM10	TNFRSF14	472	27	11	1	0.668	0.495	0.928	Co-occurrence	MCM10
MCM10	CD47	454	26	29	2	0.268	0.519	0.928	Co-occurrence	MCM10
MCM10	CD48	471	27	12	1	0.54	0.524	0.928	Co-occurrence	MCM10
MCM10	TNFRSF9	469	27	14	1	0.311	0.576	0.928	Co-occurrence	MCM10
MCM10	LGALS9	475	28	8	0	<-3	0.635	0.928	Mutual exclusivity	MCM10
MCM10	VTCN1	465	27	18	1	-0.064	0.72	0.928	Mutual exclusivity	MCM10
MCM10	CD70	478	28	5	0	<-3	0.754	0.928	Mutual exclusivity	MCM10
MCM10	TNFSF9	479	28	4	0	<-3	0.798	0.928	Mutual exclusivity	MCM10

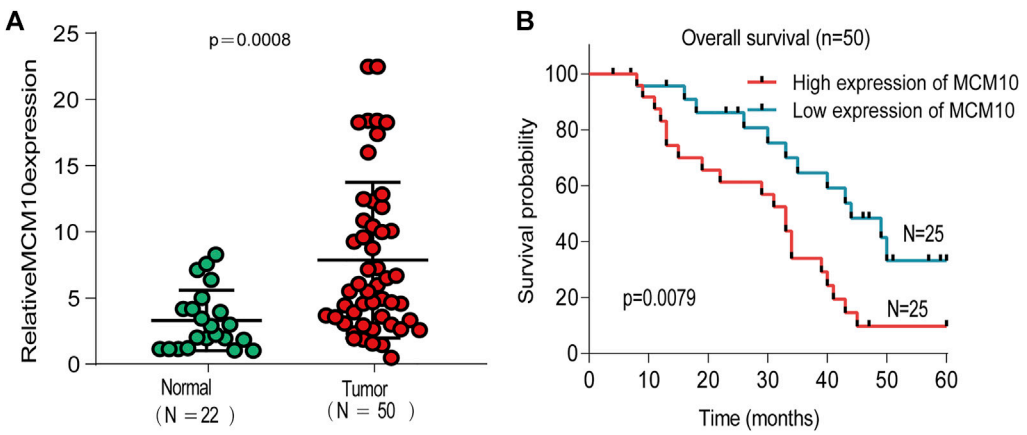


FIGURE 6 | Expression of MCM10 in Independent OV Cohorts. **(A)** qRT-PCR showed that MCM10 expression was up-regulated in OV tissues. **(B)** High MCM10 expression have worse prognosis in OV patients.

divided into high and low expression, the patients in the high expression group also had a poor prognosis. These findings all demonstrated that MCM10, as a promising prognostic biomarker, is increased in OV.

Having verified the differential expression and prognostic potential of MCM10 in OV, in order to better serve the clinic, we next explored the possible pathogenic mechanism of MCM10. In order to test our previous speculation about the pathogenic mechanism of MCM10, the effects of MCM10 changes in OV on the transcriptome were explored, and it was found that 4,297 positively correlated genes and 3,613 negatively correlated genes were changed accordingly, which suggested that the alterations in MCM10 have broad impacts on the transcriptome. The analysis results of GO and KEGG both illustrated that the pathway enrichment of other gene changes caused by MCM10 changes mainly concentrated in the related pathways of cell cycle and DNA replication. Since MCM10 itself participates in DNA replication, it is not surprising that the changes are mainly concentrated in DNA replication. However, the changes of MCM10 are closely related to the cell cycle, which may be closely related to the cell cycle, because the DNA replication process depends on the

regulation of the cell cycle (Tachibana et al., 2005). Previous studies suggested that MCM10 may be part of a high-priority group of genes that may promote cell cycle-related processes in cancer cells (Cerami et al., 2012). A series of cell cycle checkpoint inhibitors targeting OV are already under development or clinical trials (Pujade-Lauraine, 2017). For example, cells initiate multiple responses to protect the genome and ensure survival against DNA damage, and unsuccessful DNA damage repair can lead to mitotic abnormalities and cell death (Lin et al., 2017). High-grade serous ovarian cancer (HGSOC) relies heavily on G2 checkpoint blockade to promote DNA damage repair, which is a process that opens up a new perspective for the treatment of OV (Haynes et al., 2018). If blocking MCM10 can affect both DNA replication and cell cycle, why not? Therefore, the combined treatment of DNA replication and cell cycle intervention may benefit OV patients.

People who care about OV treatment know that OV treatment cannot be cured by single-agent therapy because the results of single-agent studies on OV so far have been disappointing (Disis et al., 2019). The results of the drug combination may have some benefit, but the results are not better than the historical control (Lee et al., 2019). Therefore, it is necessary to explore a new combination therapy method. Tumor immunotherapy is considered as a new and potential tumor treatment method. The infiltration state of tumor-associated immune cells *in vivo* together constitutes the immune microenvironment of tumor cells, and these immune cells may have tumor antagonism or tumor promotion (Jain, 2021). Our results demonstrated that the expression level of MCM10 is negatively correlated with B cells and CD8+T Cells, and positively correlated with CD4+T Cells and Macrophages. This suggests that MCM10 plays a particular role in the immune infiltration of OV. In addition to the critical role of the immune microenvironment in anticancer immunity, another most popular approach in immunotherapy is immune checkpoint blockade (Huang et al., 2020). PD-1/PD-L1 and CTLA-4 are considered as the most principal immune checkpoints at present. In the past decade, great progress has been made in the field of immune checkpoint-related researches. immune checkpoint blockade (ICB) has been very successful in this type of cancer (Havel et al., 2019). However, since the current FAD-approved immune checkpoint inhibitors (ICI) are all monoclonal antibodies (mAbs), there are many shortcomings. Therefore, the therapeutic effects of ICB on OV are still limited. The study on small molecule inhibitors to eliminate the limitations of mAbs is a new direction for ICB therapy (Zhang et al., 2020; Zhang et al., 2021). More and more evidence showed that small molecule inhibitors that target oncogenic play a role far beyond the biological behavior of tumors. Some studies have found that some small molecule inhibitors directly participate in mediating the tumor microenvironment and promoting tumor cell death (Chen et al., 2019; Ziogas et al., 2021). For example, the inhibitors of CDK4/6 can synergize with PD-1 blockade and benefit the treatment of OV (Zhang et al., 2020). It has been revealed that the matrix metalloproteinases (MMPs) inhibitor, SB-3CT, can enhance the effects of PD-1 and CTLA-4 blockade in primary and metastatic tumors in studies (Ye et al., 2020). Small-molecule inhibitor JQ1 targeting BET bromodomains reduces PD-L1 expression, while attenuating progression in PC models (Mao et al., 2019). All of the above studies have proved that ICI combined with small molecule inhibitors is an effective way to address the shortcomings of current ICIs such as low oral availability, long tissue retention time and poor membrane permeability. Changes in seven ICIs occurred simultaneously, and considering that MCM10 is a member of a high-priority gene, the combination of its small-molecule inhibitor and ICI greatly benefits OV patients.

In our study, the expression and prognosis of MCM10 in OV were analyzed by bioinformatics methods, and the related pathways of MCM10 that were related to immune infiltration and immune checkpoints were analyzed. However, inevitably, our tests have certain limitations. Firstly, the number of patients enrolled in our validation experiment is relatively small, and we will update the number of patients in the later stage. Secondly, we only propose possible pathogenic pathways, and further experimental verification is needed, for example, we could test the effects of an artificial knockdown of MCM10 expression on tumor size and progression in cell models, validate qPCR results from tumor samples with Western blots, test for differences between MCM10 expression in CD8 mutant backgrounds and check if MCM10 expression differences cause differences in replication timing, genome stability or cell cycle defects. Finally, we need animal experiments and long-term clinical experiments for MCM10 small-molecule inhibitors, and then apply them to patients and use them in combination with ICI. Most importantly, we will solve these problems slowly, and our efforts have also achieved certain results. Therefore, future researches on Mcm10's relationship to cancer development and progression may lead to discoveries with momentous prognostic and even therapeutic value.

DATA AVAILABILITY STATEMENT

The datasets presented in this study can be found in online repositories. The names of the repository/repositories and accession number(s) can be found in the article/Supplementary Material.

ETHICS STATEMENT

The studies involving human participants were reviewed and approved by the Ethics Committee of Gansu Provincial Maternity and Child-Care Hospital. The patients/participants provided their written informed consent to participate in this study.

AUTHOR CONTRIBUTIONS

JZ and ZW designed the study. YW and JL analyzed the data and wrote the manuscript. HW and XT revised manuscript. All authors have read and approved the final manuscript.

FUNDING

This study was supported by the Gansu Province Health Industry Research Plan (grant number GSWSKY 2020-16).

REFERENCES

Aves, S. J., Tongue, N., Foster, A. J., and Hart, E. A. (1998). The Essential *Schizosaccharomyces pombe* Cdc23 DNA Replication Gene Shares Structural and Functional Homology with the *Saccharomyces cerevisiae* DNA43 (MCM10) Gene. *Curr. Genet.* 34 (3), 164–171. doi:10.1007/s002940050382

Baxley, R., and Bielinsky, A.-K. (2017). Mcm10: A Dynamic Scaffold at Eukaryotic Replication Forks. *Genes.* 8 (2), 73. doi:10.3390/genes8020073

Cai, H.-Q., Cheng, Z.-J., Zhang, H.-P., Wang, P.-F., Zhang, Y., Hao, J.-J., et al. (2018). Overexpression of MCM6 Predicts Poor Survival in Patients with Glioma. *Hum. Pathol.* 78, 182–187. doi:10.1016/j.humpath.2018.04.024

Cerami, E., Gao, J., Dogrusoz, U., Gross, B. E., Sumer, S. O., Aksoy, B. A., et al. (2012). The cBio Cancer Genomics Portal: An Open Platform for Exploring Multidimensional Cancer Genomics Data. *Cancer Discov.* 2 (5), 401–404. doi:10.1158/2159-8290.cd-12-0095

Chen, S., Song, Z., and Zhang, A. (2019). Small-Molecule Immuno-Oncology Therapy: Advances, Challenges and New Directions. *Ctmc* 19 (3), 180–185. doi:10.2174/1568026619666190308131805

Chuang, C.-H., Wallace, M. D., Abratte, C., Southard, T., and Schimenti, J. C. (2010). Incremental Genetic Perturbations to MCM2-7 Expression and Subcellular Distribution Reveal Exquisite Sensitivity of Mice to DNA Replication Stress. *PLoS Genet.* 6 (9), e1001110. doi:10.1371/journal.pgen.1001110

Cui, F., Hu, J., Ning, S., Tan, J., and Tang, H. (2018). Overexpression of MCM10 Promotes Cell Proliferation and Predicts Poor Prognosis in Prostate Cancer. *Prostate* 78 (16), 1299–1310. doi:10.1002/pros.23703

Disis, M. L., Taylor, M. H., Kelly, K., Beck, J. T., Gordon, M., Moore, K. M., et al. (2019). Efficacy and Safety of Avelumab for Patients with Recurrent or Refractory Ovarian Cancer: Phase 1b Results From The JAVELIN Solid Tumor Trial. *JAMA Oncol.* 5 (3), 393–401. doi:10.1001/jamaoncol.2018.6258

Gaillard, H., García-Muse, T., and Aguilera, A. (2015). Replication Stress and Cancer. *Nat. Rev. Cancer* 15 (5), 276–289. doi:10.1038/nrc3916

Gao, J., Aksoy, B. A., Dogrusoz, U., Dresdner, G., Gross, B., Sumer, S. O., et al. (2013). Integrative Analysis of Complex Cancer Genomics and Clinical Profiles Using the cBioPortal. *Sci. Signal.* 6 (269), pl1. doi:10.1126/scisignal.2004088

Graveley, B. R., Brooks, A. N., Carlson, J. W., Duff, M. O., Landolin, J. M., Yang, L., et al. (2011). The Developmental Transcriptome of *Drosophila melanogaster*. *Nature* 471 (7339), 473–479. doi:10.1038/nature09715

Havel, J. J., Chowell, D., and Chan, T. A. (2019). The Evolving Landscape of Biomarkers for Checkpoint Inhibitor Immunotherapy. *Nat. Rev. Cancer* 19 (3), 133–150. doi:10.1038/s41568-019-0116-x

Haynes, B., Murai, J., and Lee, J.-M. (2018). Restored Replication Fork Stabilization, a Mechanism of PARP Inhibitor Resistance, Can Be Overcome by Cell Cycle Checkpoint Inhibition. *Cancer Treat. Rev.* 71, 1–7. doi:10.1016/j.ctrv.2018.09.003

Huang, X., Tang, T., Zhang, G., Hong, Z., Xu, J., Yadav, D. K., et al. (2020). Genomic Investigation of Co-targeting Tumor Immune Microenvironment and Immune Checkpoints in Pan-Cancer Immunotherapy. *npj Precis. Onc.* 4 (1), 29. doi:10.1038/s41698-020-00136-1

Irusta, G. (2021). Roads to the Strategic Targeting of Ovarian Cancer Treatment. *Reprod. Camb. Engl.* 161 (1), R1–R11. doi:10.1530/REP-19-0593

Jain, K. K. (2021). Personalized Immuno-Oncology. *Med Princ Pract Int. J. the Kuwait Univ. Health Sci. Centre* 30 (1), 1–16. doi:10.1159/000511107

Juríková, M., Danihel, Ľ., Polák, Š., and Varga, I. (2016). Ki67, PCNA, and MCM Proteins: Markers of Proliferation in the Diagnosis of Breast Cancer. *Acta Histochem.* 118 (5), 544–552. doi:10.1016/j.acthis.2016.05.002

Kang, G., Hwang, W. C., Do, I.-G., Wang, K., Kang, S. Y., Lee, J., et al. (2013). Exome Sequencing Identifies Early Gastric Carcinoma as an Early Stage of Advanced Gastric Cancer. *PloS one* 8 (12), e82770. doi:10.1371/journal.pone.0082770

Kang, P., Han, Z., Liao, Z., Zhang, H., Jia, W., and Tian, Y. (2020). Knockdown of MCM10 Gene Impairs Glioblastoma Cell Proliferation, Migration and Invasion and the Implications for the Regulation of Tumorigenesis. *J. Mol. Neurosci.* 70 (5), 759–768. doi:10.1007/s12031-020-01486-y

Lánczky, A., and Győrffy, B. (2021). Web-Based Survival Analysis Tool Tailored for Medical Research (KMplot): Development and Implementation. *J. Med. Internet Res.* 23 (7), e27633. doi:10.2196/27633

Langston, L. D., Mayle, R., Schauer, G. D., Yurieva, O., Zhang, D., Yao, N. Y., et al. (2017). Mcm10 Promotes Rapid Isomerization of CMG-DNA for Replisome Bypass of Lagging Strand DNA Blocks. *eLife* 6, e29118. doi:10.7554/eLife.29118

Lee, J. M., Minasian, L., and Kohn, E. C. (2019). New Strategies in Ovarian Cancer Treatment. *Cancer* 125 (Suppl. 24), 4623–4629. doi:10.1002/cncr.32544

Lheureux, S., Braunstein, M., and Oza, A. M. (2019). Epithelial Ovarian Cancer: Evolution of Management in the Era of Precision Medicine. *CA Cancer J. Clin.* 69 (4), 280–304. doi:10.3322/caac.21559

Li, T., Fan, J., Wang, B., Traugh, N., Chen, Q., Liu, J. S., et al. (2017). TIMER: A Web Server for Comprehensive Analysis of Tumor-Infiltrating Immune Cells. *Cancer Res.* 77 (21), e108–e110. doi:10.1158/0008-5472.can-17-0307

Lin, A. B., McNeely, S. C., and Beckmann, R. P. (2017). Achieving Precision Death with Cell-Cycle Inhibitors that Target DNA Replication and Repair. *Clin. Cancer Res.* 23 (13), 3232–3240. doi:10.1158/1078-0432.ccr-16-0083

Liu, Z., Li, J., Chen, J., Shan, Q., Dai, H., Xie, H., et al. (2018). MCM Family in HCC: MCM6 Indicates Adverse Tumor Features and Poor Outcomes and Promotes S/G2 Cell Cycle Progression. *BMC cancer* 18 (1), 200. doi:10.1186/s12885-018-4056-8

Lõoke, M., Maloney, M. F., and Bell, S. P. (2017). Mcm10 Regulates DNA Replication Elongation by Stimulating the CMG Replicative Helicase. *Genes. Dev.* 31 (3), 291–305. doi:10.1101/gad.291336.116

Mao, W., Ghasemzadeh, A., Freeman, Z. T., Obradovic, A., Chaimowitz, M. G., Nirschl, T. R., et al. (2019). Immunogenicity of Prostate Cancer Is Augmented by BET Bromodomain Inhibition. *J. Immunother. cancer* 7 (1), 277. doi:10.1186/s40425-019-0758-y

Mizuno, H., Kitada, K., Nakai, K., and Sarai, A. (2009). PrognoScan: a New Database for Meta-Analysis of the Prognostic Value of Genes. *BMC Med. Genomics* 2, 18. doi:10.1186/1755-8794-2-18

Odunsi, K. (2017). Immunotherapy in Ovarian Cancer. *Ann. Oncol.* 28 (Suppl. l_8), viii1–viii7. doi:10.1093/annonc/mdx444

Pujade-Lauraine, E. (2017). New Treatments in Ovarian Cancer. *Ann. Oncol.* 28 (Suppl. l_8), viii57–viii60. doi:10.1093/annonc/mdx442

Qiu, Y.-T., Wang, W.-J., Zhang, B., Mei, L.-L., and Shi, Z.-Z. (2017). MCM7 Amplification and Overexpression Promote Cell Proliferation, Colony Formation and Migration in Esophageal Squamous Cell Carcinoma by Activating the AKT1/mTOR Signaling Pathway. *Oncol. Rep.* 37 (6), 3590–3596. doi:10.3892/or.2017.5614

Reubens, M. C., Biller, M. D., Bedsole, S. E., Hopkins, L. T., Ables, E. T., and Christensen, T. W. (2015). Mcm10 Is Required for Oogenesis and Early Embryogenesis in Drosophila. *Mech. Dev.* 138, 291–299. doi:10.1016/j.mod.2015.09.002

Schmittgen, T. D., and Livak, K. J. (2008). Analyzing Real-Time PCR Data by the Comparative C(T) Method. *Nat. Protoc.* 3 (6), 1101–1108. doi:10.1038/nprot.2008.73

Tachibana, K.-e. K., Gonzalez, M. A., and Coleman, N. (2005). Cell-cycle-dependent Regulation of DNA Replication and its Relevance to Cancer Pathology. *J. Pathol.* 205 (2), 123–129. doi:10.1002/path.1708

Tang, Z., Li, C., Kang, B., Gao, G., Li, C., and Zhang, Z. (2017). GEPIA: a Web Server for Cancer and Normal Gene Expression Profiling and Interactive Analyses. *Nucleic acids Res.* 45 (W1), W98–W102. doi:10.1093/nar/gkx247

Tate, J. G., Bamford, S., Jubb, H. C., Sondka, Z., Beare, D. M., Bindal, N., et al. (2019). COSMIC: the Catalogue of Somatic Mutations in Cancer. *Nucleic acids Res.* 47 (D1), D941–D947. doi:10.1093/nar/gky1015

Topalian, S. L., Taube, J. M., Anders, R. A., and Pardoll, D. M. (2016). Mechanism-driven Biomarkers to Guide Immune Checkpoint Blockade in Cancer Therapy. *Nat. Rev. Cancer* 16 (5), 275–287. doi:10.1038/nrc.2016.36

Vasaikar, S. V., Straub, P., Wang, J., and Zhang, B. (2018). LinkedOmics: Analyzing Multi-Omics Data within and across 32 Cancer Types. *Nucleic acids Res.* 46 (D1), D956–D963. doi:10.1093/nar/gkx1090

Wang, Y., Chen, H., Zhang, J., Cheng, A. S. L., Yu, J., To, K. F., et al. (2020). MCM Family in Gastrointestinal Cancer and Other Malignancies: From Functional Characterization to Clinical Implication. *Biochimica Biophysica Acta (BBA) - Rev. Cancer* 1874 (2), 188415. doi:10.1016/j.bbcan.2020.188415

Wu, P., Heins, Z. J., Muller, J. T., Katsnelson, L., de Bruijn, I., Abeshouse, A. A., et al. (2019). Integration and Analysis of CPTAC Proteomics Data in the Context of Cancer Genomics in the cBioPortal. *Mol. & Cell. Proteomics* 18 (9), 1893–1898. doi:10.1074/mcp.tir119.001673

Wu, W., Wang, X., Shan, C., Li, Y., and Li, F. (2018). Minichromosome Maintenance Protein 2 Correlates with the Malignant Status and Regulates Proliferation and Cell Cycle in Lung Squamous Cell Carcinoma. *Ott* 11, 5025–5034. doi:10.2147/ott.s169002

Yang, W. D., and Wang, L. (2019). MCM10 Facilitates the Invaded/migrated Potentials of Breast Cancer Cells via Wnt/β-Catenin Signaling and Is Positively Interlinked with Poor Prognosis in Breast Carcinoma. *J. Biochem. Mol. Toxicol.* 33 (7), e22330. doi:10.1002/jbt.22330

Ye, Y., Kuang, X., Xie, Z., Liang, L., Zhang, Z., Zhang, Y., et al. (2020). Small-molecule MMP2/MMP9 Inhibitor SB-3CT Modulates Tumor Immune Surveillance by Regulating PD-L1. *Genome Med.* 12 (1), 83. doi:10.1186/s13073-020-00780-z

Yu, S., Wang, G., Shi, Y., Xu, H., Zheng, Y., and Chen, Y. (2020). MCMs in Cancer: Prognostic Potential and Mechanisms. *Anal. Cell. Pathol. Amst.* 2020, 3750294. doi:10.1155/2020/3750294

Zhang, F., Wang, Z.-m., Liu, H.-y., Bai, Y., Wei, S., Li, Y., et al. (2010). Application of RT-PCR in Formalin-Fixed and Paraffin-Embedded Lung Cancer Tissues. *Acta Pharmacol. Sin.* 31 (1), 111–117. doi:10.1038/aps.2009.178

Zhang, J., Zhang, Y., Qu, B., Yang, H., Hu, S., and Dong, X. (2021). If Small Molecules Immunotherapy Comes, Can the Prime Be Far behind? *Eur. J. Med. Chem.* 218, 113356. doi:10.1016/j.ejmech.2021.113356

Zhang, Q.-F., Li, J., Jiang, K., Wang, R., Ge, J.-l., Yang, H., et al. (2020). CDK4/6 Inhibition Promotes Immune Infiltration in Ovarian Cancer and Synergizes with PD-1 Blockade in a B Cell-dependent Manner. *Theranostics* 10 (23), 10619–10633. doi:10.7150/thno.44871

Zhang, X., Teng, Y., Yang, F., Wang, M., Hong, X., Ye, L.-G., et al. (2015). MCM2 Is a Therapeutic Target of Lovastatin in Human Non-small Cell Lung Carcinomas. *Oncol. Rep.* 33 (5), 2599–2605. doi:10.3892/or.2015.3822

Ziogas, D. C., Konstantinou, F., Bouros, S., Theochari, M., and Gogas, H. (2021). Combining BRAF/MEK Inhibitors with Immunotherapy in the Treatment of Metastatic Melanoma. *Am. J. Clin. Dermatol* 22 (3), 301–314. doi:10.1007/s40257-021-00593-9

Conflict of Interest: The authors declare that the research was conducted in the absence of any commercial or financial relationships that could be construed as a potential conflict of interest.

Publisher's Note: All claims expressed in this article are solely those of the authors and do not necessarily represent those of their affiliated organizations, or those of the publisher, the editors and the reviewers. Any product that may be evaluated in this article, or claim that may be made by its manufacturer, is not guaranteed or endorsed by the publisher.

Copyright © 2022 Wu, Wang, Li, Wang, Tuo and Zheng. This is an open-access article distributed under the terms of the Creative Commons Attribution License (CC BY). The use, distribution or reproduction in other forums is permitted, provided the original author(s) and the copyright owner(s) are credited and that the original publication in this journal is cited, in accordance with accepted academic practice. No use, distribution or reproduction is permitted which does not comply with these terms.

frontiers | Frontiers in Genetics

ORIGINAL RESEARCH
published: 19 May 2022
doi: 10.3389/fgene.2022.821826

INSC Is Down-Regulated in Colon Cancer and Correlated to Immune Infiltration

Tao Yu[1]†, Dan Li[2†], Zhi Zeng[3], Xu Xu[4], Haiming Zhang[1], Jie Wu[2], Wei Song[2] and Hua Zhu[5]**

[1]Department of Oncology, Integrated Chinese and Western Medicine, The Central Hospital of Wuhan, Tongji Medical College, Huazhong University of Science and Technology, Wuhan, China, [2]Department of Pharmacy, Renmin Hospital of Wuhan University, Wuhan, China, [3]Department of Pathology, Renmin Hospital of Wuhan University, Wuhan, China, [4]Department of Geriatrics, Renmin Hospital of Wuhan University, Wuhan, China, [5]Department of Neurosurgery, Renmin Hospital of Wuhan University, Wuhan, China

Background: Previous studies have verified that Inscuteable Spindle Orientation Adaptor Protein (INSC) can regulate cell proliferation and differentiation in the developing nervous system. It also plays an important role in spindle orientation during mitosis and asymmetric division of fibroblasts and participates in the process of stratification of the squamous epithelium. The role and potential mechanism of INSC in the development of colonic adenocarcinoma (COAD) have not been fully understood. This study aimed at exploring the prognostic value of INSC in COAD and the correlation of its expression with immune infiltration.

Methods: The Cancer Genome Atlas (TCGA), Genotype-Tissue Expression (GTEx) project, Gene Expression Profiling Interactive Analysis (GEPIA), and Gene Expression Omnibus (GEO) database were used to analyze the expression of INSC in COAD. The INSC protein expression level was analyzed by immunohistochemistry staining and the Human Protein Atlas (HPA) database. The diagnostic and prognostic values of INSC in COAD patients were analyzed using receiver operating characteristic (ROC) and Kaplan–Meier (KM) survival curves. In order to understand whether INSC is an independent prognostic factor, we used univariable and multivariate Cox analyses to analyze INSC expression and several clinical characteristics with survival. We use STRING analysis to find INSC-related proteins and related biological events analyzed by Gene Ontology (GO) annotation and Kyoto Encyclopedia of Genes and Genomes (KEGG) analysis. At last, GEPIA and the Tumor Immune Estimation Resource (TIMER) were employed to explore the relationship between INSC and immune infiltrates and its marker gene set.

Results: INSC was lower expressed in COAD tissues than in normal colon tissues, which was correlated with tumor stage. Patients with lower expression of INSC had shorter overall survival (OS). Moreover, univariable Cox analysis demonstrated that high expression of INSC was an independent prognostic factor for COAD. ROC analysis showed INSC was an accurate marker for identifying tumors from normal colon tissue, and the AUC of the curve was 0.923. Significant GO term analysis by GSEA showed that genes correlated with INSC were found to be enriched in several immune-related pathways.

OPEN ACCESS

Edited by:
Ayan Biswas,
The University of Alabama at Birmingham, United States

Reviewed by:
Vikash Kansal,
Emory University, United States
Rolando Garcia-Milian,
Yale University, United States

***Correspondence:**
Tao Yu
yutao1986cn@163.com
Hua Zhu
zhuhuawhu@163.com

†These authors have contributed equally to this work

Specialty section:
This article was submitted to Cancer Genetics and Oncogenomics, a section of the journal Frontiers in Genetics

Received: *24 November 2021*
Accepted: *04 April 2022*
Published: *19 May 2022*

Citation:
Yu T, Li D, Zeng Z, Xu X, Zhang H, Wu J, Song W and Zhu H (2022) INSC Is Down-Regulated in Colon Cancer and Correlated to Immune Infiltration. Front. Genet. 13:821826. doi: 10.3389/fgene.2022.821826

Specifically, INSC expression showed significant negative correlations with infiltration levels of B cells, $CD4^+$ T cells, macrophages, DCs, and their marker sets in COAD.

Conclusion: INSC was provided with prognostic value in COAD and related to immune invasion.

Keywords: INSC, immune cell infiltrates, prognosis, colon cancer, bioinformatics analysis

1 INTRODUCTION

Colonic adenocarcinoma (COAD) is one of the most prevalent digestive tract cancers, with a significant fatality rate (Sanoff et al., 2007). Worryingly, the rates of recurrence and death of COAD are rising (Bray et al., 2018). Despite recent advancements in therapy, the 5-year survival rate has not increased appreciably. As a result, finding gene signatures or biomarkers to detect the intrinsic genetic and epigenetic heterogeneity of COAD, as well as developing prognostic models to guide therapy, is critical.

In terms of morbidity, colon cancer, a malignancy of the alimentary canal, ranks third among malignant tumors globally (Bray et al., 2018). According to recent research, more than one million people are diagnosed with colon cancer each year, with a disease-specific death rate of over 33% in industrialized nations (Ferlay et al., 2015). Colon cancer mortality is on the rise as a result of dietary and lifestyle changes (Mcguire, 2016). Despite significant improvements in colon cancer treatment choices, the 5-year survival rate remains poor. As a result, we must seek novel biomarkers to aid in the correct and early diagnosis of COAD, as well as identify effective targets to increase the treatment impact.

INSC (INSC Spindle Orientation Adaptor Protein) is a protein-coding gene according to previous studies. Apico-basal polarity in epithelial stem cells is produced by apical enrichment of the polarity proteins Par3: Par6: aPKC, which can recruit an adaptor called Inscuteable at the apical membrane. INSC codes for a conserved 35-residue peptide (INSC PEPT hereon) that binds to the N-terminal TPR domain of LGN/dLGN with nanomolar affinity 10, 11, and 19 (Culurgioni et al., 2018).

The INSC-dependent system, which includes INSC, BAZ, and PINS, is active throughout mitosis, whereas the cryptic INSC-independent pathway is functional only late in mitosis (anaphase and telophase) and is essential for telophase rescue (Wang et al., 2006). The mitotic spindle is also directed to align along the polarity axis by INSC (Bowman et al., 2008). Current findings in the mouse *epidermis* reveal that the protein INSC plays a critical function in appropriate spindle orientation as both an instructional and regulatory signal (Poulson and Lechler, 2010), which keeps the polarity of the Par complex and the neuroblast (Schober et al., 1999). A genome-wide association study identified INSC gene was associated with Alzheimer's disease-related cognitive phenotypes (Wang et al., 2021). However, the role of the INSC gene in COAD malignancy has not been reported.

In the present study, public databases such as The Cancer Genome Atlas (TCGA) and Gene Expression Omnibus (GEO) were used to comprehensively investigate the relationship between INSC and the prognosis of COAD. TIMER was employed to assess the correlation between INSC and tumor immune cell infiltration. The results provided new insights into the function of INSC and novel targets for the COAD diagnosis and prognosis.

2 METHODS

2.1 RNA-Sequencing Data and Bioinformatic Analysis

Expression data of INSC gene and clinical information of COAD patients were collected from The Cancer Genome Atlas (TCGA, https://tcga.xenahubs.net), Genotype-Tissue Expression (GTEx) project (https://gtexportal.org/) (GTEx Consortium, 2020), and Gene Expression Omnibus (GEO) (http://www.ncbi.nlm.nih.gov/geo/) database (Barrett et al., 2013). The data of 521 samples, including 41 para-cancerous tissues and 480 tumor tissues, from TCGA were extracted. There were 308 normal colonic tissues obtained from GTEx. Additionally, the INSC expression data were obtained from GSE44076 and GSE39582 datasets in the GEO database to verify the INSC expression level in tumor and non-tumor tissues. The boxplot was realized by using the R software package "ggplot2."

2.2 Protein Expression Analysis

The human protein atlas (HPA) database (https://www.proteinatlas.org/) (Uhlén et al., 2015) was applied to determine INSC protein expression levels through immunohistochemistry (IHC) staining (antibody HPA039769). We obtained the INSC IHC photographs of COAD patients from the HPA database.

In order to further confirm the expression of INSC in the colon and COAD tissues, 82 paired normal and COAD tissues (49 men and 33 women, average age of 63 ± 13 years old) were enrolled and determined by IHC staining (Li et al., 2021a). Briefly, deparaffinized and rehydrated sections were subjected to 3% H_2O_2 and then antigen retrieval by citric acid buffer (pH 6.0). After sealing at room temperature for 20 min with 5% bovine serum albumin, the slices are incubated overnight (16–18 h) at 4°C with primary anti-INSC antibody (1:50 dilution for colon tissues, HPA039769, Atlas Antibodies AB, Sweden). Then, the sections were incubated with biotinylated-linked antibodies and peroxidase-labeled streptavidin (UltraSensitive™ SP (Mouse/Rabbit) IHC Kit-9710; Maixin Bio, Fujian, China) for 15 min at room temperature. Then, the reaction products were stained with 3,3′-diaminobenzidine (DAB) and lightly counterstained

with hematoxylin. The sections with PBS instead of primary antibody served as a negative control. The INSC expression levels were evaluated according to the average score of two independent pathologists' evaluations who were unaware of the diagnosis outcome. INSC expression in tumor cells was classified based on a four-tier grading system (scores: 0 = absent, 1 = weak, 2 = moderate, and 3 = strong staining). Generally, a score less than 1 was considered negative, and a score more than 1 was considered positive.

2.3 Prognosis Analysis of Inscuteable Spindle Orientation Adaptor Protein Expression in Colonic Adenocarcinoma

First, we applied the KM survival and receiver operating characteristic (ROC) curves to assess the prognostic values of INSC in patients with COAD. Second, we performed univariate and multivariate regression analyses to evaluate the relationship between the expression of INSC and the overall survival (OS) of patients with COAD as we previously reported (Zhu et al., 2021a; Li et al., 2021b). The forest realized through the "forestplot" R package was applied to display the *p*-value, hazard ratio (HR), and 95% confidence interval (CI) of each variable.

2.4 Functional Analysis of Inscuteable Spindle Orientation Adaptor Protein in Colonic Adenocarcinoma

The (protein–protein interaction) PPI network of INSC was conducted by the Search Tool for the Retrieval of Interacting Genes/Proteins (STRING) (version: 11.5, https://cn.string-db.org/) database. The minimum required interaction score was set as medium confidence 0.400. The max number of interactors to show is as follows: first shell: no more than 10 interactors; second shell: none. We use the R packs such as clusterProfiler [version 3.14.3] and Org Hs. Eg.db [version 3.10.0] to perform the Gene Ontology (GO) and the Kyoto Encyclopedia of Genes and Genomes (KEGG) pathway enrichment analysis of the obtained genes, and the *p*-value is set to be less than 0.05. The results are visualized and displayed in a bubble chart with the ggplot2 package [version 3.3.3].

We further used LinkOmics (http://www.linkedomics.org/login.php) (Vasaikar et al., 2018) to conduct the GO and KEGG pathway enrichment analysis. The cancer type: TCGA_COADREAD; data type: RNAseq; platform: HiSeq RNA; and target dataset: (data type: RNAseq; platform: HiSeq RNA).

2.5 Association Between Immune Cell Infiltration and Inscuteable Spindle Orientation Adaptor Protein in Colonic Adenocarcinoma

We used Tumor Immune Estimation Resource (TIMER) (https://cistrome.shinyapps.io/timer/) and Gene Expression Profiling Interactive Analysis (GEPIA) (http://gepia.cancer-pku.cn/api.html) to investigate the correlations between INSC and tumor-infiltrating immune cells (TIIC). Spearman correlation analysis and the CIBERSORT method were further employed to evaluate the correlation between INSC and TIIC and their corresponding molecular markers.

2.6 Statistical Analysis

The data analysis and mapping involved in this study are completed by R software (version 3.6.3) and R language package ggplot2 (version 3.3.3). RNAseq data were converted into TPM (transcripts per million reads) format, and log2 conversion is performed. For the comparison between groups, the normality test should be conducted first. If the samples do not meet the normality test ($p < 0.05$), then the Mann Whitney *U* test (Wilcoxon rank sum test) will be selected. The chi-square test was used to analyze the correlation of INSC expression with the clinicopathological factors of COAD. The Kaplan–Meier method was used to calculate the relationship between INSC expression and prognosis of COAD. Univariate and multivariate Cox regression analyses were conducted to assess the effect of INSC on the prognosis of COAD. The "survival" package (3.2-10 version) was applied for statistical analysis of survival data, and the "survminer" package (0.4.9 version) was employed for mapping survival curves. The forest was applied to show the *p*-value, HR, and 95% CI of each variable. Spearman correlation analysis was used for genetic correlation. $p \leq 0.05$ was considered to be statistically significant.

3 RESULTS

3.1 Association Between the Expression of Inscuteable Spindle Orientation Adaptor Protein and Clinicopathological Features in Colonic Adenocarcinoma Patients

The clinicopathological features of 478 COAD patients were extracted from TCGA, including age, gender, TNM stage, pathologic stage, and CEA level. According to the expression level of INSC, we divided all samples into high expression and low expression INSC groups by median. Detailed clinical information was shown in **Supplementary Table S1**.

3.2 Expression of Inscuteable Spindle Orientation Adaptor Protein mRNA in Colonic Adenocarcinoma

We investigated numerous sets of data from different databases in order to better understand INSC expression in tumors and normal tissues. The GEPIA database was used to validate INSC mRNA expression. The data are presented as a body heat map (**Supplementary Figure S1**). The color red denotes cancerous tissue, whereas the color green denotes normal tissue. The higher the intensity of expression, the darker the hue. The region around the large intestine is brightly colored, showing that INSC is abundantly expressed in a healthy large intestine. The differential expression of INSC mRNA in pan-cancer cells was next investigated. **Figures 1A and B** show the data from TCGA

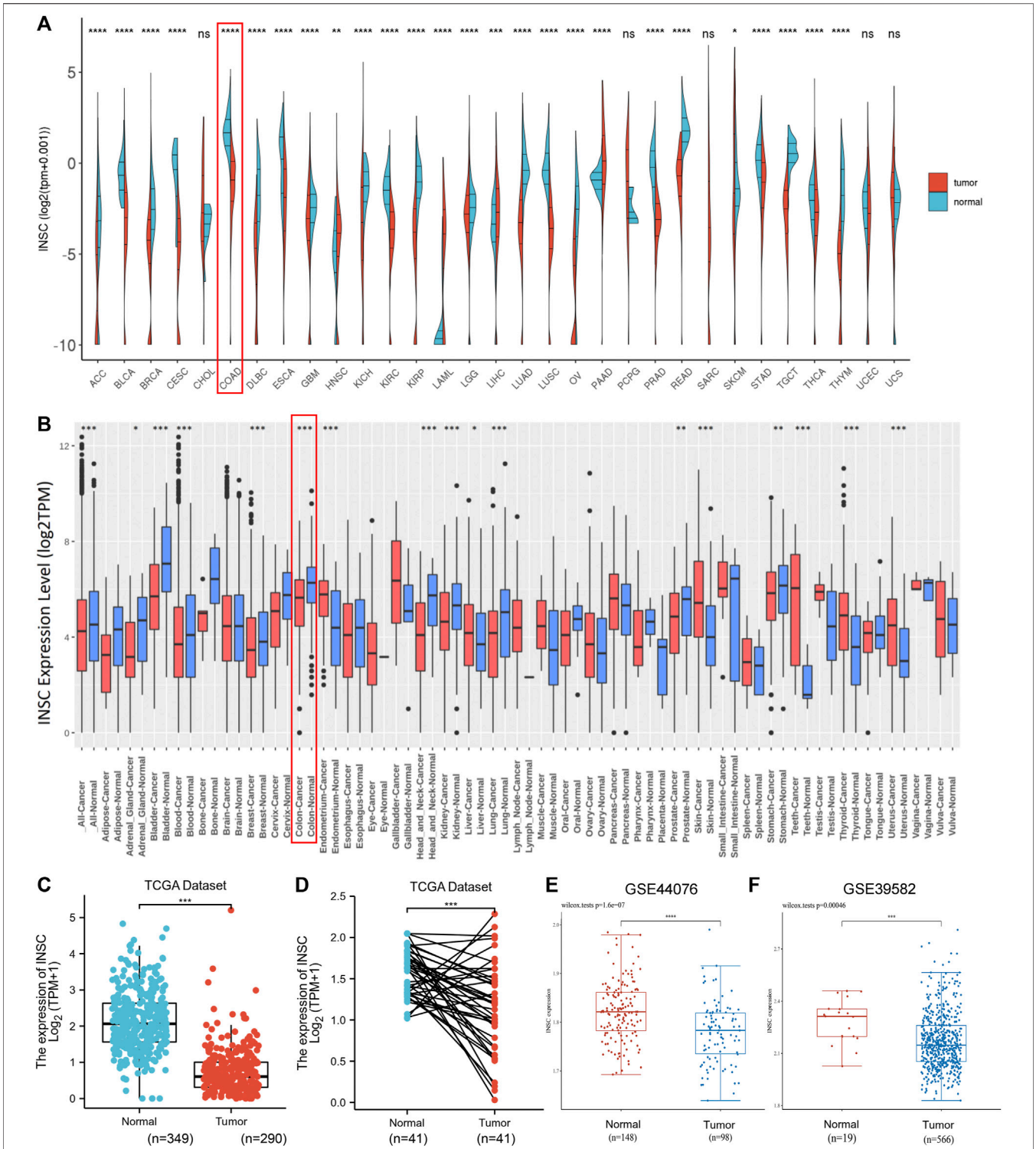


FIGURE 1 | INSC expression levels in cancers. **(A–B)** The expression levels of INSC were different in pan-cancer tissues compared to those in normal tissues according to TCGA datasets **(A)** and GEO datasets **(B)**, respectively. **(C–D)** Compared to the normal colon tissue, the expression level of INSC was significantly decreased in COAD tissues (p <0.001). **(C)** Unpaired samples in TCGA datasets and GTEx datasets. **(D)** Paired samples in only TCGA datasets. The expression of INSC from GSE44076 **(E)** and GSE39582 **(F)** in GEO datasets (*p < 0.05, **p <0.01, ***p < 0.001, ****p < 0.0001).

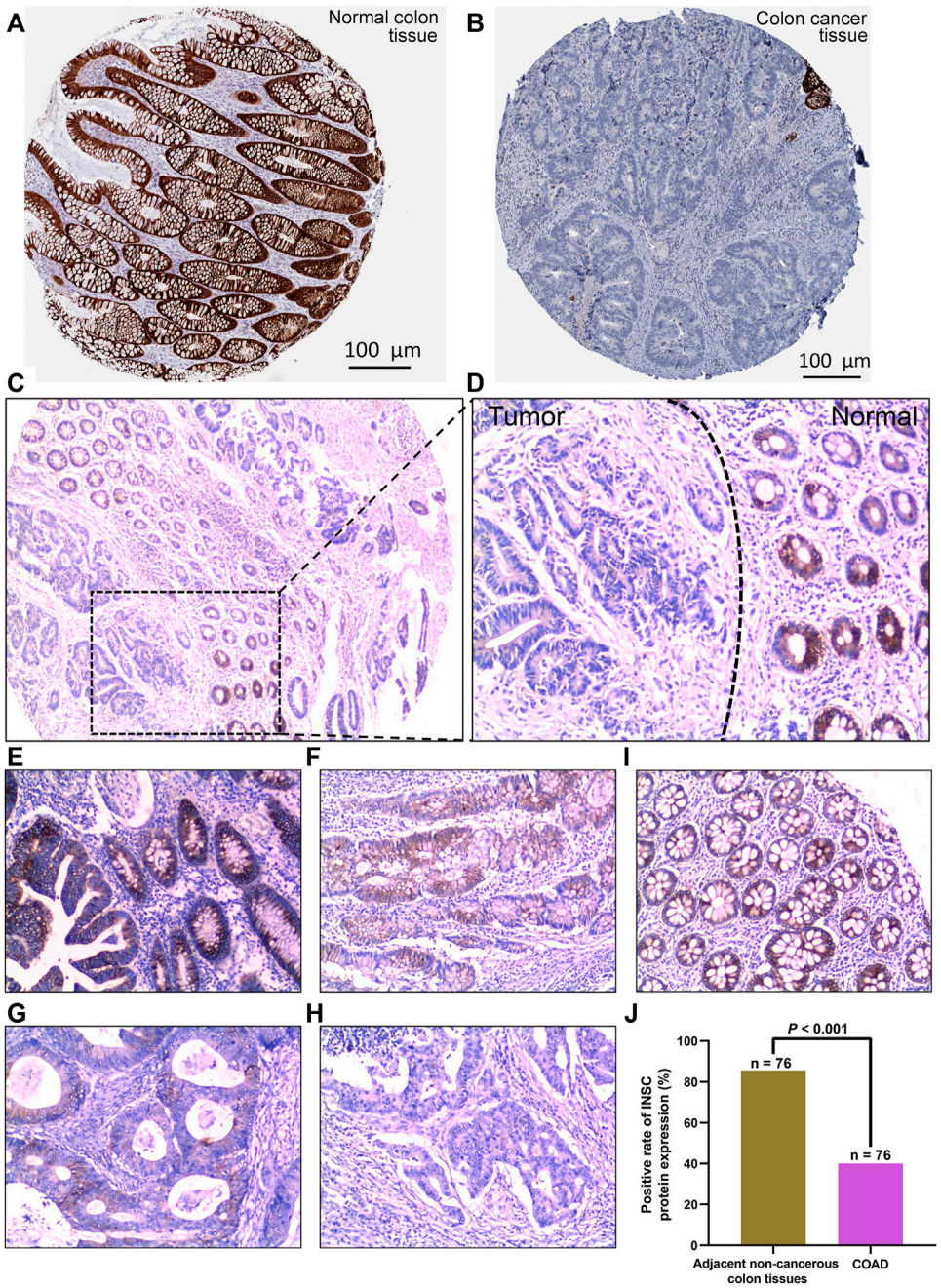


FIGURE 2 | INSC expression in normal colon and COAD tissues was determined by immunohistochemistry. The level of INSC protein in COAD **(A)** and normal tissues **(B)** (Antibody HPA039769) form the HPA database; **(C)** INSC protein expression in COAD and non-cancerous colon tissues and its immunohistochemical staining in representative tissue specimens. Original magnification, ×40; **(D)** immunohistochemical staining of INSC proteins in representative COAD and non-cancerous colon specimens. The left side represents cancer tissues and the right side represents non-cancer tissues. Original magnification, ×100; **(E–H)** the score of INSC expression in representative tumor cells of COAD ((E) score = 3, **(F)** score = 2, **(G)** score = 1, and **(H)** score = 0); magnification, ×100; **(I)** expression of INSC in representative normal colon cells ((I) score = 3); magnification, ×100; **(J)** positive rate of INSC protein expression in adjacent non-cancerous colon tissues and COAD tissues (p <0.001, cancer *vs*. non-cancerous tissues, chi-squared test), n = 82, and six samples were lost.

and GEO, respectively. It was found that in adrenocortical carcinoma, breast cancer, bladder cancer, colon cancer, head and neck cancer, kidney cancer, stomach adenocarcinoma, prostate cancer, lung cancer, and COAD, the INSC mRNA expression was lower in tumors than in normal tissues. **Figures 1C–F** illustrate the mRNA expression of INSC in COAD from TCGA and GEO. INSC expression was considerably lower in COAD tissues than in normal tissues (p < 0.001).

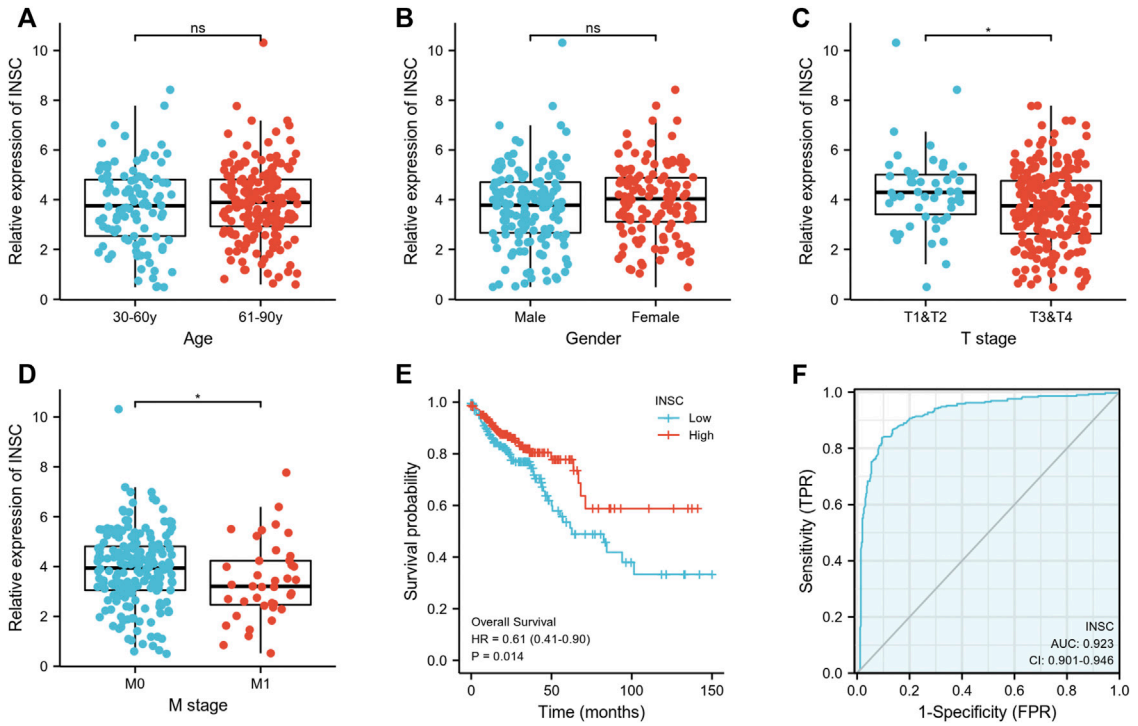


FIGURE 3 | (A,B) Association between INSC expression and clinical features such as age and gender in COAD. **(C,D)** The association between INSC expression and clinical features such as T and M stages in COAD. Lower INSC expression was related to higher T and M stages (*$p < 0.05$). **(E)** The KM survival curve displayed a low level of INSC with a poor prognosis for COAD patients. **(F)** ROC analysis illustrated that INSC was an accurate marker to distinguish tumor from normal tissue. The AUC was 0.923.

3.3 Protein Expression of Inscuteable Spindle Orientation Adaptor Protein in Colon Normal and Cancer Tissues

The protein expression of INSC was analyzed by immunohistochemical staining images obtained from HPA. INSC protein was highly expressed in colonic mucosal glandular epithelial cells located in cytoplasmic and membranous (**Figure 2A**). On the contrary, there was less expression of INSC protein in COAD tissue (**Figure 2B**). To further investigate the protein expression of INSC in non-cancerous colon and COAD tissues, the INSC protein expression was detected in a larger size of 76 COAD tissues and its adjacent non-cancerous colon tissues by IHC staining. The results showed that non-cancerous colon tissues had stronger IHC staining than COAD tissues (**Figures 2C, D**). The scores of INSC protein expression ranging from 3, 2, 1, and 0 in representative COAD tissue specimens were presented in **Figures 2E–H**. The representative IHC staining of non-cancerous colon tissue with a score of 3 was shown in **Figure 2I**. It was also found that the positive expression rate of INSC was higher in normal colon tissues (85.53%) than that in COAD tissues (40.00%) ($p < 0.001$, **Figure 2J**).

3.4 Prognostic Potential of Inscuteable Spindle Orientation Adaptor Protein in Colonic Adenocarcinoma

First, we explored the association of INSC with clinical manifestation in COAD. Lower INSC expression was shown to be related to greater T and M stages (p <0.05) but not age and gender (**Figures 3A–D**). The connection between INSC expression and survival outcomes was assessed by the KM survival curve. The median was used as the cutoff value for the high and low INSC expression groups. OS was shown to be longer in patients with increased INSC expression (log-rank test, $p = 0.014$) (**Figure 3E**). The ROC curve results were reported as AUC scores (area under the ROC curve) (**Figure 3F**). The AUC in this trial was 0.923 (CI: 0.901–0.946). INSC was able to discriminate between normal and malignant tissues according to these findings. **Figures 4A, B** showed a univariable and multivariable Cox regression analysis of INSC and clinical data that might be linked to OS. In the univariate Cox model, a low INSC level ($p = 0.028$) was linked with age and pathologic TNM stage in OS occurrences ($p < 0.01$). Age and pathologic TNM stage were independent variables associated with OS in COAD (p <0.01) in the multivariate Cox model.

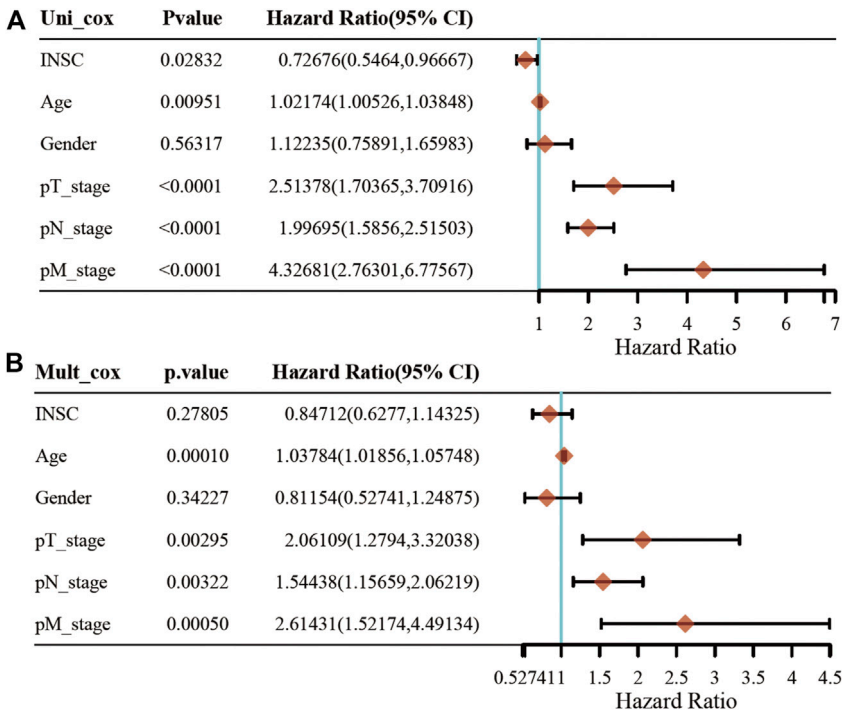


FIGURE 4 | Univariate and multivariate Cox regression of the INSC gene and other five clinical characteristics. **(A)** The forest plot of univariate regression analysis. **(B)** The forest plot of multivariate regression analysis.

3.5 Protein–Protein Interaction Networks and Enrichment Analyses of Inscuteable Spindle Orientation Adaptor Protein-Related Genes

In order to study the functional network of INSC-related genes in COAD, we first identified INSC-related genes with the STRING webtool. INSC-related genes included NAGLU, NUMBL, PCP2, PARD3B, PROX1, PARD3, NUMB, and TTC28 (**Figure 5A**). Their annotation and combined scores are presented in **Figure 5C**. Combined with the GO/KEGG enrichment analysis, we found that genes correlated with INSC were located mainly in the apical part of the cell ($p < 0.001$), cell–cell adherens junction ($p < 0.001$), and bicellular tight junction ($p = 0.023$). They were involved in the biological process of forebrain generation of neurons, lateral ventricle development and neuronal stem cell division. KEGG pathway analysis showed they were enriched in the Notch signaling pathway and glycosaminoglycan degradation (**Figure 5B**). The top 50 positively and negatively correlated genes with INSC were presented in **Figures 5D, E**. We further assessed the GO biological process and KEGG pathway analysis from LinkedOmics. The results showed that INSC was related to several immunological processes and pathways. The GO biological process analysis revealed that INSC was related to leucocyte cell–cell adhesion, B cell activation, negative regulation of cell activation, myeloid dendritic metabolic process, mast cell activation, regulation of leukocyte activation, and adaptive immune response (**Figures 6A,C**). The KEGG pathway analysis showed that INSC was associated with the IL-17 pathway, drug metabolism, and Notch signaling pathway (**Figures 6B, C**).

3.6 Association Between Inscuteable Spindle Orientation Adaptor Protein Expression and Immune Cell Infiltration in Colonic Adenocarcinoma

To further explore how the INSC gene affects tumor progression, the TIMER database was employed to analyze whether INSC expression was associated with TIIC in COAD. The results indicated that the expression of INSC was significantly related to the major immune cell infiltrates, such as B cells and macrophages (**Figure 7A**). INSC copy number variation (CNV) was correlated with the infiltration levels of B cells, $CD8^+$ T cells, and dendritic cells (**Figure 7B**). There was a positive correlation between INSC and B cell markers, CD19, and CD79A (**Figure 7C**). In addition, the CIBERSORT method was further used to assess the cellular composition of TIIC in COAD. It suggested statistical significance between INSC and B cells, $CD4^+$ T cells, macrophages, and dendritic cells ($p < 0.05$) (**Figure 7D**). These results suggest that INSC played a critical role in regulating TIIC infiltration in COAD.

3.7 Correlation of Inscuteable Spindle Orientation Adaptor Protein Expression With Immune Marker Sets

We focused on the association of INSC with marker genes of diverse immune cells, including $CD8^+$ T cells, T cells (normal), B cells, monocytes, TAMs, macrophages M1 and M2, neutrophils, NK cells, and DC, in order to further validate the link between

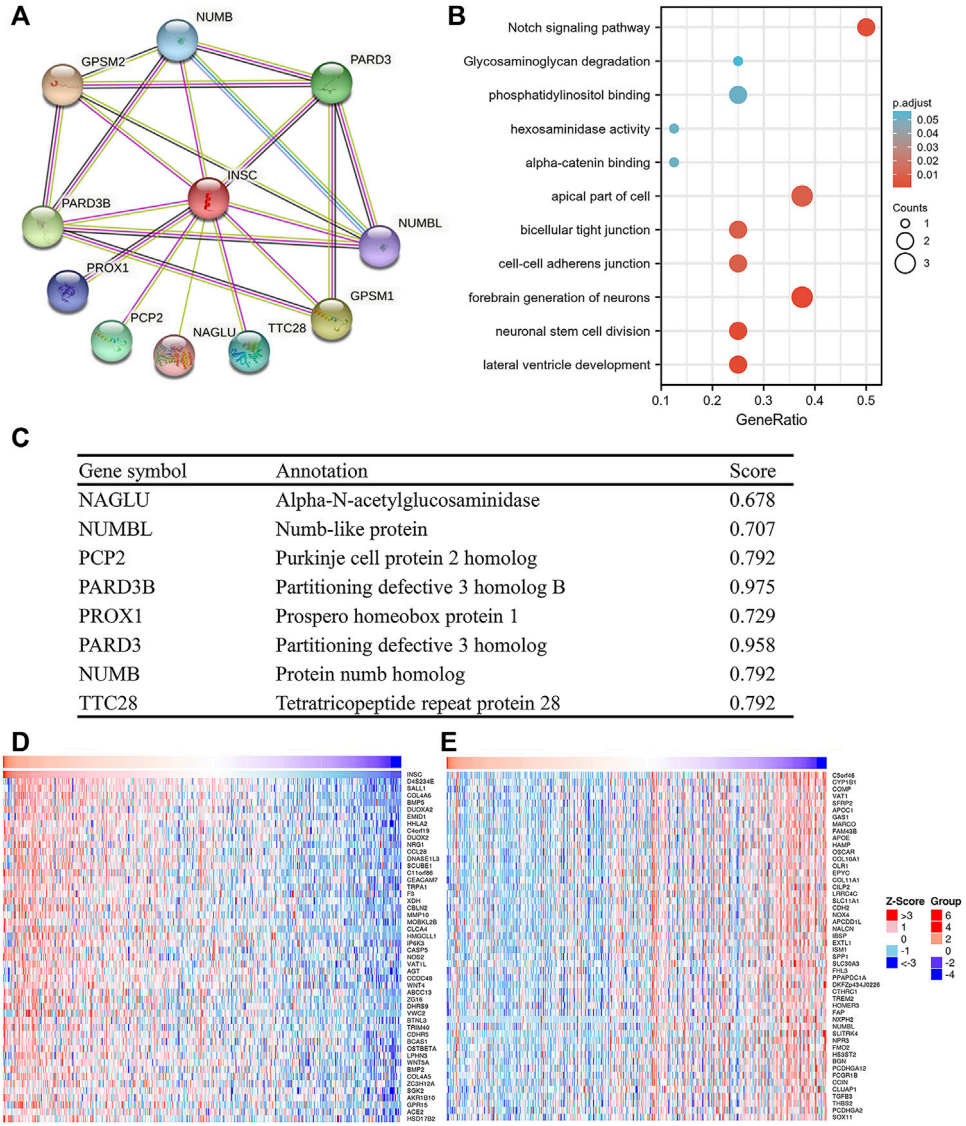


FIGURE 5 | PPI and GO/KEGG analysis of INSC. **(A)** PPI network of INSC. **(B)** Bubble chart showing the enrichment results. **(C)** The detailed information of INSC-related genes. **(D)** Top 50 positively or negatively significant correlated genes with INSC.

INSC and immune infiltrating cells. INSC expression was shown to be substantially linked with the overwhelming majority of B cell and macrophage immunological markers in COAD. As a result, we were able to demonstrate the COAD microenvironment's unique relationship with immune infiltrating cells.

4 DISCUSSION

As described in the background, it is urgent to understand the molecular mechanism of the genesis and progression of COAD and to explore new markers and therapeutic targets in the context of the high mortality rate and the lack of early diagnosis and effective therapeutic targets. This study aims to explore the diagnostic value of the INSC gene in COAD and its influence on tumor immune infiltration.

Studies have confirmed that INSC is mainly involved in cell mitosis. So far, few studies have paid attention to its role in the occurrence and development of colon cancer. In the present study, we investigated the differential expression of INSC in pan-cancer, including COAD. We discovered that INSC was depressed in a variety of tumor tissues compared to normal tissues as well as in COAD. The immunohistochemical results from 76 COAD patients also confirmed this conclusion. Moreover, INSC mRNA levels were markedly related to pathological T and M stages. Next, the ROC and KM survival analyses were employed to illustrate the relationship between

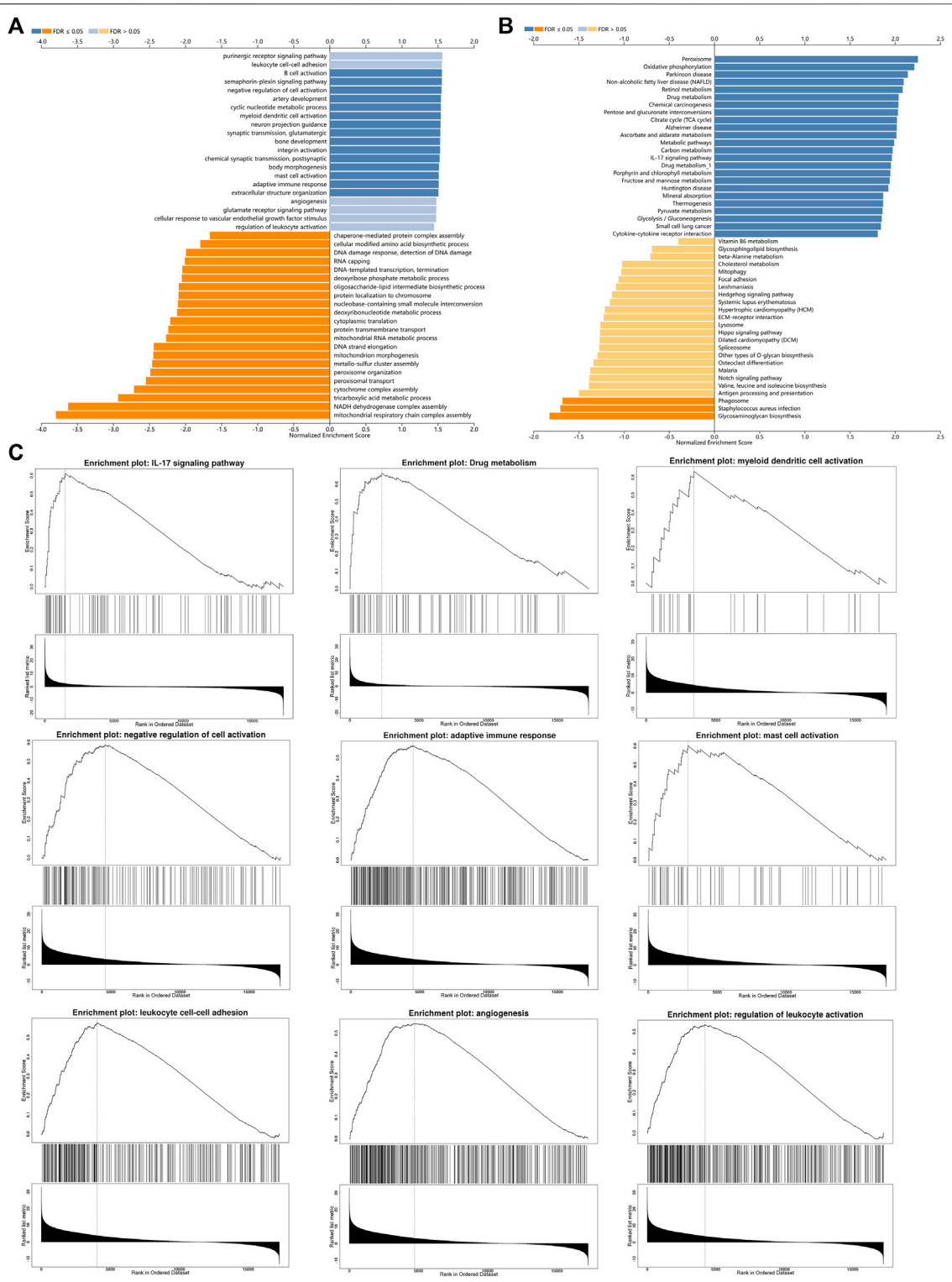


FIGURE 6 | GO **(A)** and KEGG **(B)** pathway analyses from LinkOmics. **(C)** Immune-related biological processes and pathways that related to INSC in COAD.

INSC and the survival rate of COAD patients. To ensure the accuracy of the conclusion, we used the data obtained from TCGA and GEO databases at the same time. We further assessed the relationship between INSC expression and clinicopathological features that were related to OS in COAD by univariate and multivariate Cox regression analyses. It

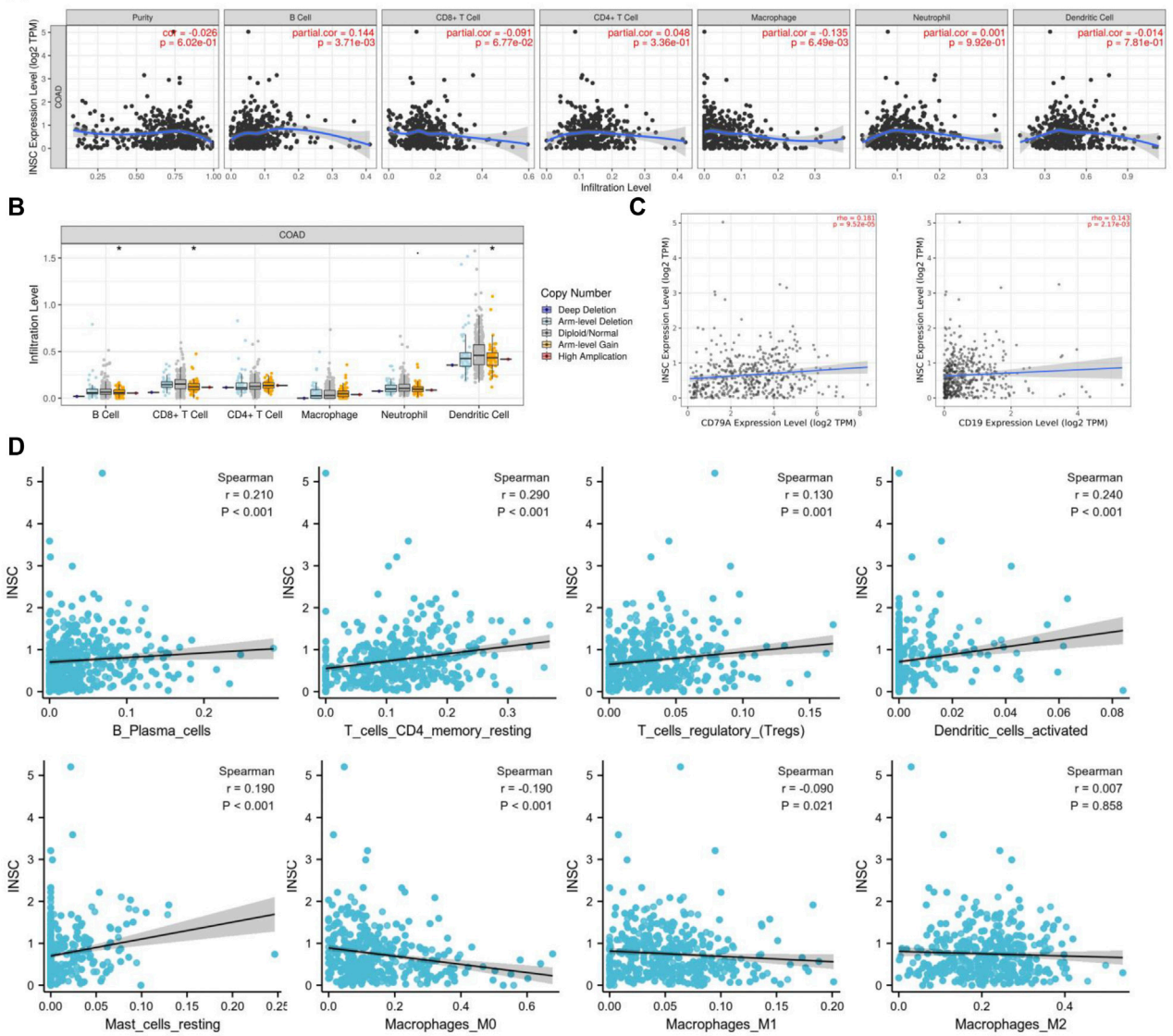


FIGURE 7 | Correlations of INSC expression with TIIC infiltration level in COAD. **(A)** The correlation of INSC expression with tumor purity and TIIC from the TIMER database. **(B)** The effect of INSC CNV on the infiltration levels of immune cells in COAD. **(C)** Relationship between INSC and B cell markers such as CD79A and CD19. **(D)** The effect of INSC on the level of TIIC infiltration in COAD using the CIBERSORT method (*, $p < 0.05$, **, $p < 0.01$, ***, $p < 0.001$).

revealed that low INSC expression ($p < 0.001$) was an important risk factor for the prognosis of COAD. These results illustrate that low INSC expression is related to worse prognosis, and INSC has potential value in predicting prognosis in COAD.

The PPI network was employed in this investigation to find INSC co-regulatory proteins using string tools. INSC-related genes, such as NUMB and NUMBL, were found to be enriched in the Notch signaling pathway. Notch receptors and their ligands are abnormally active in several forms of human malignancies, including COAD, according to recent research (Suliman et al., 2016). Furthermore, in mammalian cells, dysregulation of the Notch system causes disastrous mitosis (Převorovský et al., 2016). The Notch signaling pathway's abnormal activation may be involved in the formation of cancers, particularly in colon carcinoma (Zhang et al., 2017). In addition, INSC has been shown to alter mitosis in previous investigations (Wang et al., 2006), and the results obtained in our study are the same. But how INSC affects the Notch signaling pathway remains to be further studied.

An immune infiltration within the tumor often affect the prognosis of patients (Hu et al., 2021; Zhu et al., 2022) and treatment response in many malignancies (Buisseret et al., 2018; Zhu et al., 2021b). So, we focused on INSC-related immune infiltration levels in COAD to learn more about the latent mechanisms of INSC. According to our findings, INSC and

B cells, $CD4^+$ T cells, macrophages, and dendritic cells showed a substantial difference. INSC expression was positively correlated with B cells, $CD4^+$ T cells, and dendritic cell infiltration in COAD, but negatively correlated with M0 and M1 macrophages. According to publications, B cells and $CD4^+$ T cells have been related to better clinical outcomes in COAD (Yang et al., 2018). B cell differentiation into antibody-secreting cells is facilitated by the interaction of follicular $CD4^+$ T cells with B cells (Wongthida et al., 2020). As the same, contact between $CD4^+$ T cells and follicular B cells enhances $CD4^+$ T cell activation and differentiation into effector and memory cells (Tay et al., 2019). To sum up, low INSC expression indicates a low amount of B cells and CD4 + T cell infiltration, as well as a poor prognosis.

According to further study, monocytes and macrophages M0 and M1 were also connected with colon cancer survival risk in addition to B-cell naive and B-cell memory (Wu et al., 2020). Several studies demonstrated that macrophages enhance colon cancer cell proliferation, which is consistent with the fact that more macrophages are related to a worse prognosis for colon cancer (Wu et al., 2020). As we know, M1 macrophages and M2 macrophages are two types of macrophages (Han et al., 2020). M1-polarized TAM exerts pro-inflammatory and anticancer effects, whereas M2-polarized macrophages boost carcinogenesis and tumor growth through mediating tumor-promoting immune-suppressive actions in colon cancer (Mühlberg et al., 2016). M2 macrophages predominated in tumor-infiltrating macrophages but M1 macrophages predominated in the non-cancerous inflammatory zone around cancer cell infiltrates (Ino et al., 2013). As a consequence, in this study, we can observe the paradoxical but practical results in **Figure 7** and **Supplementary Table S1**, where INSC as a favorable prognostic marker of COAD has a negative connection with M1 macrophages.

However, there were some limitations to this work, such as the small number of normal samples from the TCGA database and the lack of animal models to test the results. These results will very certainly need to be confirmed in future research. Therefore, cell and animal models will be conducted to further confirm our conclusions through experiments.

5 CONCLUSION

Our findings revealed the correlation of INSC expression levels with the prognosis and clinicopathological features of COAD and the association between INSC expression levels and TIIC infiltration. Thus, our findings imply that INSC expression may have predictive relevance in COAD patients and that it might be a novel target for COAD immunotherapy.

DATA AVAILABILITY STATEMENT

Publicly available datasets were analyzed in this study. This data can be found here: https://www.cancer.gov/about-nci/organization/ccg/ research/structural-genomics/tcga and the datasets of GEO can be found at: https://www.ncbi.nlm.nih.gov/geo/. The datasets in the current study are also available from the corresponding authors upon reasonable request in compliance with ethical standards.

ETHICS STATEMENT

The studies were reviewed and approved by the Ethics Committee of Renmin Hospital of Wuhan University.

AUTHOR CONTRIBUTIONS

TY, DL, and ZZ conceived and designed the project, WS, HMZ, and JW acquired the data, HZ and TY analyzed and interpreted the data, and DL and TY wrote the paper, HZ and DL revised the paper.

FUNDING

This work was supported by the project of the National Science Foundation of China (Grant Nos. 81704023, 81803789, and 8160253) and Wu Jieping Medical Foundation (Grant No. 320.6750).

ACKNOWLEDGMENTS

Thanks to Professor Lijuan Gu and Xiaoxing Xiong for their valuable suggestions on the revision of the manuscript.

SUPPLEMENTARY MATERIAL

The Supplementary Material for this article can be found online at: https://www.frontiersin.org/articles/10.3389/fgene.2022.821826/full#supplementary-material

REFERENCES

Barrett, T., Wilhite, S. E., Ledoux, P., Evangelista, C., Kim, I. F., Tomashevsky, M., et al. (2013). NCBI GEO: Archive for Functional Genomics Data Sets-Update. *Nucleic Acids Res.* 41, D991–D995. doi:10.1093/nar/gks1193

Bowman, S. K., Rolland, V., Betschinger, J., Kinsey, K. A., Emery, G., and Knoblich, J. A. (2008). The Tumor Suppressors Brat and Numb Regulate Transit-Amplifying Neuroblast Lineages in Drosophila. *Dev. Cell* 14, 535–546. doi:10.1016/j.devcel.2008.03.004

Bray, F., Ferlay, J., Soerjomataram, I., Siegel, R. L., Torre, L. A., and Jemal, A. (2018). Global Cancer Statistics 2018: GLOBOCAN Estimates of Incidence and

Mortality Worldwide for 36 Cancers in 185 Countries. *CA: A Cancer J. Clinicians* 68, 394–424. doi:10.3322/caac.21492

Buisseret, L., Pommey, S., Allard, B., Garaud, S., Bergeron, M., Cousineau, I., et al. (2018). Clinical Significance of CD73 in Triple-Negative Breast Cancer: Multiplex Analysis of a Phase III Clinical Trial. *Ann. Oncol.* 29, 1056–1062. doi:10.1093/annonc/mdx730

Culurgioni, S., Mari, S., Bonetti, P., Gallini, S., Bonetto, G., Brennich, M., et al. (2018). Insc:LGN Tetramers Promote Asymmetric Divisions of Mammary Stem Cells. *Nat. Commun.* 9, 1025. doi:10.1038/s41467-018-03343-4

Ferlay, J., Soerjomataram, I., Dikshit, R., Eser, S., Mathers, C., Rebelo, M., et al. (2015). Cancer Incidence and Mortality Worldwide: Sources, Methods and Major Patterns in GLOBOCAN 2012. *Int. J. Cancer* 136, E359–E386. doi:10.1002/ijc.29210

GTEx Consortium (2020). The GTEx Consortium Atlas of Genetic Regulatory Effects across Human Tissues. *Science* 369, 1318–1330. doi:10.1126/science.aaz1776

Han, J., Pang, X., Zhang, Y., Peng, Z., Shi, X., and Xing, Y. (2020). Hirudin Protects against Kidney Damage in Streptozotocin-Induced Diabetic Nephropathy Rats by Inhibiting Inflammation via P38 MAPK/NF-κB Pathway. *Drug Des. Devel Ther.* 14, 3223–3234. doi:10.2147/dddt.S257613

Hu, X., Zhu, H., Zhang, X., He, X., and Xu, X. (2021). Comprehensive Analysis of pan-cancer Reveals Potential of ASF1B as a Prognostic and Immunological Biomarker. *Cancer Med.* 10, 6897–6916. doi:10.1002/cam4.4203

Ino, Y., Yamazaki-Itoh, R., Shimada, K., Iwasaki, M., Kosuge, T., Kanai, Y., et al. (2013). Immune Cell Infiltration as an Indicator of the Immune Microenvironment of Pancreatic Cancer. *Br. J. Cancer* 108, 914–923. doi:10.1038/bjc.2013.32

Li, D., Yu, T., Han, J., Xu, X., Wu, J., Song, W., et al. (2021). Prognostic Value and Immunological Role of KIFC1 in Hepatocellular Carcinoma. *Front. Mol. Biosci.* 8, 799651. doi:10.3389/fmolb.2021.799651

Li, D., Yu, T., Hu, J., Wu, J., Feng, S., Xu, Q., et al. (2021). Downregulation of CYP39A1 Serves as a Novel Biomarker in Hepatocellular Carcinoma with Worse Clinical Outcome. *Oxidative Med. Cell Longevity* 2021, 1–18. doi:10.1155/2021/5175581

Mcguire, S. (2016). World Cancer Report 2014. Geneva, Switzerland: World Health Organization, International Agency for Research on Cancer, WHO Press, 2015. *Adv. Nutr.* 7, 418–419. doi:10.3945/an.116.012211

Mühlberg, L., Kühnemuth, B., Costello, E., Shaw, V., Sipos, B., Huber, M., et al. (2016). miRNA Dynamics in Tumor-Infiltrating Myeloid Cells Modulating Tumor Progression in Pancreatic Cancer. *Oncoimmunology* 5, e1160181. doi:10.1080/2162402x.2016.1160181

Poulson, N. D., and Lechler, T. (2010). Robust Control of Mitotic Spindle Orientation in the Developing Epidermis. *J. Cell Biol* 191, 915–922. doi:10.1083/jcb.201008001

Převorovský, M., Oravcová, M., Zach, R., Jordáková, A., Bähler, J., Půta, F., et al. (2016). CSL Protein Regulates Transcription of Genes Required to Prevent Catastrophic Mitosis in Fission Yeast. *Cell Cycle* 15, 3082–3093. doi:10.1080/15384101.2016.1235100

Sanoff, H. K., Bleiberg, H., and Goldberg, R. M. (2007). Managing Older Patients with Colorectal Cancer. *J. Clin. Oncol.* 25, 1891–1897. doi:10.1200/jco.2006.10.1220

Schober, M., Schaefer, M., and Knoblich, J. A. (1999). Bazooka Recruits Inscuteable to orient Asymmetric Cell Divisions in Drosophila Neuroblasts. *Nature* 402, 548–551. doi:10.1038/990135

Suliman, M. A., Zhang, Z., Na, H., Ribeiro, A. L. L., Zhang, Y., Niang, B., et al. (2016). Niclosamide Inhibits colon Cancer Progression through Downregulation of the Notch Pathway and Upregulation of the Tumor Suppressor miR-200 Family. *Int. J. Mol. Med.* 38, 776–784. doi:10.3892/ijmm.2016.2689

Tay, C., Kanellakis, P., Hosseini, H., Cao, A., Toh, B.-H., Bobik, A., et al. (2019). B Cell and CD4 T Cell Interactions Promote Development of Atherosclerosis. *Front. Immunol.* 10, 3046. doi:10.3389/fimmu.2019.03046

Uhlén, M., Fagerberg, L., Hallström, B. M., Lindskog, C., Oksvold, P., Mardinoglu, A., et al. (2015). Tissue-based Map of the Human Proteome. *Science* 347, 1260419. doi:10.1126/science.1260419

Vasaikar, S. V., Straub, P., Wang, J., and Zhang, B. (2018). LinkedOmics: Analyzing Multi-Omics Data within and across 32 Cancer Types. *Nucleic Acids Res.* 46, D956–d963. doi:10.1093/nar/gkx1090

Wang, H., Cai, Y., Chia, W., and Yang, X. (2006). Drosophila Homologs of Mammalian TNF/TNFR-related Molecules Regulate Segregation of Miranda/Prospero in Neuroblasts. *Embo j* 25, 5783–5793. doi:10.1038/sj.emboj.7601461

Wang, K., Xu, C., Smith, A., Xiao, D., Navia, R. O., Lu, Y., et al. (2021). Genome-wide Association Study Identified INSC Gene Associated with Trail Making Test Part A and Alzheimer's Disease Related Cognitive Phenotypes. *Prog. Neuro-Psychopharmacology Biol. Psychiatry* 111, 110393. doi:10.1016/j.pnpbp.2021.110393

Wongthida, P., Schuelke, M. R., Driscoll, C. B., Kottke, T., Thompson, J. M., Tonne, J., et al. (2020). Ad-CD40L Mobilizes CD4 T Cells for the Treatment of Brainstem Tumors. *Neuro Oncol.* 22, 1757–1770. doi:10.1093/neuonc/noaa126

Wu, D., Ding, Y., Wang, T., Cui, P., Huang, L., Min, Z., et al. (2020). Significance of Tumor-Infiltrating Immune Cells in the Prognosis of Colon Cancer. *Ott* 13, 4581–4589. doi:10.2147/ott.S250416

Yang, S. Y. C., Lheureux, S., Karakasis, K., Burnier, J. V., Bruce, J. P., Clouthier, D. L., et al. (2018). Landscape of Genomic Alterations in High-Grade Serous Ovarian Cancer from Exceptional Long- and Short-Term Survivors. *Genome Med.* 10, 81. doi:10.1186/s13073-018-0590-x

Zhang, F., Sun, H., Zhang, S., Yang, X., Zhang, G., and Su, T. (2017). Overexpression of PER3 Inhibits Self-Renewal Capability and Chemoresistance of Colorectal Cancer Stem-like Cells via Inhibition of Notch and β-Catenin Signaling. *Oncol. Res.* 25, 709–719. doi:10.3727/096504016x14772331883976

Zhu, H., Hu, X., Feng, S., Jian, Z., Xu, X., Gu, L., et al. (2022). The Hypoxia-Related Gene COL5A1 Is a Prognostic and Immunological Biomarker for Multiple Human Tumors. *Oxidative Med. Cell Longevity* 2022, 1–42. doi:10.1155/2022/6419695

Zhu, H., Hu, X., Gu, L., Jian, Z., Li, L., Hu, S., et al. (2021). TUBA1C Is a Prognostic Marker in Low-Grade Glioma and Correlates with Immune Cell Infiltration in the Tumor Microenvironment. *Front. Genet.* 12, 759953. doi:10.3389/fgene.2021.759953

Zhu, H., Hu, X., Ye, Y., Jian, Z., Zhong, Y., Gu, L., et al. (2021). Pan-Cancer Analysis of PIMREG as a Biomarker for the Prognostic and Immunological Role. *Front. Genet.* 12, 687778. doi:10.3389/fgene.2021.687778

Conflict of Interest: The authors declare that the research was conducted in the absence of any commercial or financial relationships that could be construed as a potential conflict of interest.

Publisher's Note: All claims expressed in this article are solely those of the authors and do not necessarily represent those of their affiliated organizations, or those of the publisher, the editors, and the reviewers. Any product that may be evaluated in this article, or claim that may be made by its manufacturer, is not guaranteed or endorsed by the publisher.

Copyright © 2022 Yu, Li, Zeng, Xu, Zhang, Wu, Song and Zhu. This is an open-access article distributed under the terms of the Creative Commons Attribution License (CC BY). The use, distribution or reproduction in other forums is permitted, provided the original author(s) and the copyright owner(s) are credited and that the original publication in this journal is cited, in accordance with accepted academic practice. No use, distribution or reproduction is permitted which does not comply with these terms.

frontiers | Frontiers in Genetics

ORIGINAL RESEARCH
published: 22 June 2022
doi: 10.3389/fgene.2022.848926

KIFC3 Promotes Proliferation, Migration, and Invasion in Colorectal Cancer *via* PI3K/AKT/mTOR Signaling Pathway

Huiling Liao[1,2†], *Lan Zhang*[1,2†], *Shimin Lu*[1,2], *Wei Li*[1,2] *and Weiguo Dong*[1*]

[1]Department of Gastroenterology, Renmin Hospital of Wuhan University, Wuhan, China, [2]Central Laboratory, Renmin Hospital of Wuhan University, Wuhan, China

Background: KIFC3, belongs to kinesin superfamily proteins (KIFs), is well known for its role in intracellular cargo movement. KIFC3 has been identified as a docetaxel resistance gene in breast cancer cells, however, the role of KIFC3 and its potential mechanism in colorectal cancer (CRC) remains elusive.

Objectives: We aims to investigate the effects of KIFC3 in proliferation, migration, and invasion in CRC as well as the potential mechanism inside.

Methods: We investigated the expression of KIFC3 in the Oncomine, Gene Expression Profiling Interactive Analysis databases. The KIFC3 protein expression and mRNA level in CRC cells were evaluated by western blot and qRT-PCR. Cell proliferation ability was detected by CCK-8, EdU, colony formation assay and xenograft tumor in nude mice. Flow cytometry was used to detect the cell cycle. The effect of KIFC3 on the epithelial-to-mesenchymal transition (EMT) was investigated by transwell and wound healing assay. The association of KIFC3 with EMT and PI3K/AKT/mTOR signaling pathway were measured by western blot and immunofluorescence staining.

Results: The expression of KIFC3 was higher in CRC tissues than normal colorectal tissue, and was negatively correlated with the overall survival of patients with CRC. KIFC3 silencing inhibited the proliferation, migration and invasion of CRC cells. Meanwhile, it could decrease the number of cells in S phase. KIFC3 silencing inhibited the expression of proliferating cell nuclear antigen, Cyclin A2, Cyclin E1, and CDK2 and increased the expression of p21 and p53. KIFC3 overexpression promoted the G1/S phase transition. KIFC3 silencing inhibited the EMT process, which decreased the level of N-cadherin, Vimentin, SNAIL 1, TWIST, MMP-2, MMP-9 and increased E-cadherin, while KIFC3 overexpression show the opposite results. Furthermore, the knockdown of KIFC3 suppressed the EMT process by modulating the PI3K/AKT/mTOR signaling pathway.

OPEN ACCESS

Edited by:
Alip Ghosh,
University of Maryland, United States

Reviewed by:
Gisela Ceballos,
Instituto Nacional de Medicina Genómica (INMEGEN), Mexico
Olivia Fromigue,
Institut National de la Santé et de la Recherche Médicale (INSERM), France

***Correspondence:**
Weiguo Dong
dongweiguo@whu.edu.cn

[†]*These authors have contributed equally to this work and share first authorship*

Specialty section:
This article was submitted to Cancer Genetics and Oncogenomics, a section of the journal Frontiers in Genetics

Received: *05 January 2022*
Accepted: *06 June 2022*
Published: *22 June 2022*

Citation:
Liao H, Zhang L, Lu S, Li W and Dong W (2022) KIFC3 Promotes Proliferation, Migration, and Invasion in Colorectal Cancer via PI3K/AKT/mTOR Signaling Pathway. Front. Genet. 13:848926. doi: 10.3389/fgene.2022.848926

Abbreviations: CRC, colorectal cancer; KIFs, Kinesin Superfamily Proteins; KIFC3, kinesin family member C3; PI3K, phosphatidylinositol 3-kinase; p-PI3K, phosphorylated phosphatidylinositol 3-kinase; t-PI3K, total phosphatidylinositol 3-kinase; p-AKT, phosphorylated Akt; mTOR, mammalian target of rapamycin; p-mTOR, phosphorylated mammalian target of rapamycin; PCNA, proliferating cell nuclear antigen; MMP, matrix metalloproteinase; GAPDH, glyceraldehyde-3-phosphate dehydrogenase.

KIFC3 silencing decreased the expression of phosphorylated PI3K, AKT, mTOR, but total PI3K, AKT, mTOR have no change. Inversely, the upregulation of KIFC3 increased the expression of phosphorylated PI3K, AKT and mTOR, total PI3K, AKT, mTOR have no change. In a xenograft mouse model, the depletion of KIFC3 suppressed tumor growth. the increased expression levels of KIFC3 could enhance the proliferation, migration and invasion of CRC cells, and enhance the EMT process through the PI3K/AKT/mTOR pathway.

Conclusion: Our study substantiates that KIFC3 can participate in the regulation of CRC progression by which regulates EMT *via* the PI3K/AKT/mTOR axis.

Keywords: KIFC3, proliferation, migration, invasion, epithelial-to-mesenchymal transition, PI3K/Akt/mTOR signal pathway

INTRODUCTION

Colorectal cancer (CRC) is one of the most prevalent malignancies in the digestive system. The incidence of CRC is rising year after year, and CRC ranks third in terms of incidence, but second in terms of mortality (Siegel et al., 2020; Sung et al., 2021). CRC is an important barrier to increasing life expectancy in every country of the world, which seriously threatens human health (Dekker et al., 2019; Sung et al., 2021). Despite that there have been great improvements in CRC treatment in the clinic, and that comprehensive therapy has partly prolonged the survival rate, the prognosis of CRC patients was still not satisfied, as well as that the 5-year survival rate of patients with CRC remains low (Chen et al., 2014; Ishikawa et al., 2019). Most patients are diagnosed at an advanced stage, and accompanied by metastasis, which limits their options for therapeutic strategies (Zhou et al., 2019; Hao et al., 2021). Moreover, the postoperative recurrence rate and metastasis remain high (Li et al., 2020a). Hence, there is an urgent need to seek novel, sensitive and specific biomarkers to improve CRC prognosis and therapeutic targets for CRC.

Intracellular organelle transport is essential for cell morphogenesis, promoting cell survival and maintaining the function of the cell. Among the molecular motors that are involved in intracellular transport, three large superfamilies have been identified—kinesins, dyneins and myosins (Hirokawa and Tanaka, 2015). The Kinesin Superfamily Proteins (KIFs) is a group of proteins that share a highly conserved motor domain, which have been shown to transport organelles, protein complexes, and mRNAs to specific destinations in a microtubule- and ATP dependent manner and also participate in chromosomal and spindle movements during mitosis and meiosis (Miki et al., 2003; Liu et al., 2013). KIFs consist of 45 family members, which play different roles in the genesis and development of tumors (Seog et al., 2004; Hirokawa and Tanaka, 2015). A number of KIFs show aberrant overexpression in various cancer cells, such as KIF4A, which is upregulated in cervical cancer and lung cancer, inhibits the repair of damaged DNA double-strand in lung cancer cells sensitive to cisplatin (Wan et al., 2019). KIF20B is overexpressed in bladder cancer and is considered as a cancer-testis antigen specific to human bladder cancer (Kanehira et al., 2007; Liu et al., 2013). KIF2A is overexpressed in squamous cell carcinoma of the oral tongue, and the downregulation of KIF2A can induce apoptosis in squamous cell carcinoma of the oral tongue through the inhibition of the PI3K/AKT signaling pathway (Wang et al., 2014). KIF18B is highly expressed in colon adenocarcinoma tissues and negatively correlated with patients' prognosis (Zhao et al., 2020).

The kinesin family member C3 (KIFC3) gene, is located on the human chromosome 16q13-q21 (Hoang et al., 1998). KIFC3 has minus end–directed microtubule motor activity and functions in golgi localization, integration and apical transport of epithelial cells (Noda et al., 2001; Xu et al., 2002). KIFC3 has been identified as a docetaxel resistance gene in breast cancer cells (Tan et al., 2012; Li and Bakhoum, 2019). Besides, KIFC3 was also found to be associated with hepatocellular carcinoma. The high expression of KIFC3 suggests shorter survival time, and KIFC3 is associated with migration and invasion of hepatocellular carcinoma (Li et al., 2017). However, our knowledge of its function in CRC is still limited.

In this study, we determined whether KIFC3 will have an effect in the progression of CRC on the proliferation, migration and invasion. Then, we performed subcutaneous tumor formation experiments to verify the effects of KIFC3. Furthermore, we explored the potential mechanism by which KIFC3 is involved in the process with a focus on the regulation of the PI3K/AKT/mTOR signaling pathway.

MATERIALS AND METHODS

Gene Expression Data From Public Databases

We analyzed KIFC3 mRNA levels in CRC and normal colorectal tissues using the Oncomine (http://www.oncomine.org) and GEPIA (http://gepia.cancer-pku.cn/) databases. The GEPIA database was used to analyze the information in The Cancer Genome Atlas (TCGA) database (https://tcga-data.nci.nih.gov/tcga/) to evaluate the prognostic value of KIFC3 level. Raw counts of RNA-sequencing data and corresponding clinical information from KIFC3 in CRC were obtained from International Cancer

Genome Consortium (ICGC) database (https://dcc.icgc.org/releases/current/Projects). The Kaplan–Meier survival analysis with log-rank test were also used to compare the survival difference between above two groups. Time-ROC analysis was performed to compare the predictive accuracy of each gene and risk score. For Kaplan–Meier curves, *p*-values and hazard ratio (HR) with 95% confidence interval (CI) were generated by log-rank tests and univariate Cox proportional hazards regression. All analytical methods above and R packages were performed using R software version v4.0.3 (The R Foundation for Statistical Computing, 2020). $p < 0.05$ was considered as statistically significant. The Kyoto Encyclopedia of Genes and Genomes (KEGG) and Gene Ontology (GO) enrichment analysis was performed with KIFC3-associated genes using the clusterProfiler package in R (https://bioconductor.org/packages/clusterProfiler). FDR $p < 0.05$ is used to distinguish significant enrichment items. Enter the gene and use the "enrichment GO" and "enrichment KEGG" functions for enrichment analysis. The bubble chart, bar chart and network chart are used to show the results of the enrichment analysis.

Cell Culture

Human colorectal cancer cell lines (HT29, HCT116, SW480, DLD-1 cell) and the normal intestinal epithelial cell line (NCM460) were purchased from the China Center for Type Culture Collection (Wuhan, China). These cells were cultured in Roswell Park Memorial Institute (RPMI) 1640 medium (HyClone, United States) containing 10% heat-inactivated fetal bovine serum (FBS, Gibco, United States) and 1% penicillin-streptomycin (Gibco, United States) under a humidified atmosphere incubator of 5% CO_2 at 37°C.

Antibodies and Reagents

Antibodies against KIFC3 were purchased from Abcam (Cambridge, MA, United States). Antibodies against proliferating cell nuclear antigen (PCNA), matrix metalloproteinase (MMP)-2, MMP-9, glyceraldehyde-3-phosphate dehydrogenase (GAPDH), p21, Cyclin A2, Cyclin E1, CDK2, E-cadherin, N-cadherin, Vimentin, Snai1 were purchased from Proteintech (Rosemont, IL, United States). Antibodies against p53, TWIST1 were obtained from Affinity (Cincinnati, United States). Antibodies against total phosphatidylinositol 3-kinase (t-PI3K), phosphorylated phosphatidylinositol 3-kinase (p-PI3K), total AKT (t-AKT), phosphorylated Akt (p-AKT), total mammalian target of rapamycin (t-mTOR), phosphorylated mammalian target of rapamycin (p-mTOR) were obtained from Cell Signaling Technology (Danvers, MA, United States). Antibodies against PCNA, GAPDH, E-cadherin, N-cadherin, Vimentin, were used at a working concentration of 1:5000, and the other antibodies were used at a working concentration of 1:1000 and were stored at 4°C. The secondary antibodies were purchased from Proteintech (Rosemont, IL, United States) and used at a dilution ratio of 1:10,000.

Lentivirus Vectors and Transfection

Three pairs of short hairpin RNA (shRNA) targeting KIFC3 lentivirus vectors (shKIFC3#1, shKIFC3#2, shKIFC3#3) and negative controls (NC) that contain green fluorescent protein (GFP) and purinomycin resistance were purchased from Shanghai Genechem Company (Shanghai, China). The cells were assigned as follows: control group (SW480 or HT29 cells), negative control (NC) group (SW480 or HT29 cell transfected with blank plasmid), shKIFC3 group (SW480 or HT29 cell transfected shKIFC3). SW480 and HT29 cells silenced stably for KIFC3 expression were generated using lentiviral constructs expressing shKIFC3 and negative control. The encoding sequence of KIFC3 was cloned into lentivirus GV248 vector, and the component sequence was hU6-MCS-Ubiquitin-EGFP-IRES-puromycin. Transfection was performed in accordance with the manufacturer's instructions. SW480 and HT29 cells in logarithmic growth phase were collected and inoculated in 6-well plates after digestion with pancreatin. The density of inoculation was 5×10^4 cells/ml, and the cells were cultured overnight in a CO_2 incubator with a volume fraction of 5% at 37°C. According to the instructions, and as growth reached approximately 60%, a RPMI 1640 medium containing lentivirus was added at a multiplicity of infection (MOI) of 100 and mixed with the cells. We use HiTransG A to improve infection efficiency. Also, the overexpression of KIFC3 lentivirus and control vector, which contains red fluorescent protein (RFP) and purinomycin resistance, infected the DLD-1 cell respectively. The KIFC3 lentivirus and control vector were synthesized by Shanghai Genechem Company (Shanghai, China). Similarly, as the procedure described above, DLD-1 cells were transfected with lentivirus vectors carrying OVER or Vector, respectively. We added puromycin (Thermo Fisher Scientific, Waltham, United States) to the medium to screen stable transfected cell lines. The efficiency of knockdown or overexpression were measured at 48 h post-transfection by western blotting and qPCR. The vector with the highest knockdown efficiency was selected for subsequent experiments.

Total RNA Extraction and Quantitative Real-Time PCR

TRIzol reagent (Takara, Japan) was used to extract total RNA from cell lysates, according to the manufacturer's instructions. We used the NanoDrop™ One (Thermo Fisher Scientific, United States) to determine the RNA concentration and purity. Total RNA was reverse transcribed into cDNA using the PrimeScriptTMRT reagent kit with gDNAEraser (Perfect Real Time, Takara, Japan). Target gene mRNA expression levels were detected using TB Green® Premix Ex Taq™ II (TliRNaseH Plus, Takara, Japan). KIFC3 mRNA level was measured by qPCR with CFX Connect Real-Time System (Bio-Rad, United States) and the β-actin was used as an internal reference. The primers sets are as follows: KIFC3 forward, 5′-GCA GATTGCCATGTACGAGTC-3′; reverse, 5′- CGGACGCCTGCT AGATTCTC -3′, β-actin forward, 5′-GCACAGGGTGCTCCT CAG-3′; reverse primer 5′-CTAGGCACCAGGGTGTGATG-3′. The data were calculated by the $2^{-\Delta\Delta Ct}$ method. All qPCR reactions were run in triplicates.

Western Blot Analysis

The proteins in CRC cells lines (HT29, HCT116, SW480, DLD-1 cell) and the NCM460 cell were extracted from the cell lysates

using Radio Immunoprecipitation Assay (RIPA) buffer (Biyotime, China) which containing phosphatase inhibitors and protease inhibitor cocktail, and the concentration of protein was tested with a bicinchoninic acid (BCA) protein assay kit (Biyotime, China) following the instructional manual. Equal mass of protein was separated by SDS-polyacrylamide gel electrophoresis (10% or 8%) and then transferred onto 0.45 μm polyvinylidene difluoride (PVDF, Millipore, United States) membranes. All the PVDF membranes were incubated in Tris-Buffered Saline with 1% TWEEN 20 (TBST, Cell Signaling Technology) blocking solution containing 5% skim milk or 5% Bovine Serum Albumin (BSA) at room temperature for 1–2 h. Next, the membranes were washed on a shaker for 3 × 10 min using TBST. The primary antibodies were added and incubated at 4°C, overnight. Then, after being washed with TBST three times, the membranes were incubated with horseradish peroxidase (HRP)-conjugated secondary antibodies Proteintech (Rosemont, IL, United States) for 1 h at room temperature and washed with TBST again. Finally, the protein bands were detected by ChemiDocTM Touch (Bio-Rad, United States).

Cell Counting Kit-8 Assay

Cell proliferation was examined using the Cell Counting Kit-8 (CCK-8, Beyotime, Shanghai, China) assay. SW480, HT29, and DLD-1 (at 4×10^3 cells/well) were resuspended and seeded in 96-well culture plates, and allowed to attach overnight in complete growth medium at 37°C with 5% CO_2. The supernatant was removed, 10 μl of CCK-8 was added to each well and incubated for 2 h. After 2 h of incubation, the absorbance of the colored formazan reaction product was evaluated at 450 nm by a microplate reader (Perkin Elmer, United States). We measured when the cells were cultured for 24, 36 and 48 h, respectively. All experiments were performed in triplicate to determine their reproducibility.

5-Ethynyl-2-deoxyuridine Assay

According to the operation instructions of the EdU assay kit (Beyotime, Shanghai, China), the transfected cells (at 1×10^4 cells/well) were seeded into 24-well plates for 24 h. Then, add 1 ml culture solution containing EdU to each well, and incubate at 37°C for 2 h. Adding 1 ml of 4% paraformaldehyde solution (Servicebio, China) to fix the fine cells for 15 min; after being washed with Phosphate-buffered saline (PBS), cells were permeabilized with 0.3% TritonX-100 (Biotech, China) for 10 min at room temperature. Cells were washed with PBS three times. Subsequently, cells were reacted with Apollo reaction mixture for 30 min. Then cells were washed 3 times using PBS. Cell nuclei were stained with Hoechst 33,258 to keep away from light for 10 min. After being washed by PBS, the proliferation of cells was visualized under a fluorescence microscope (Olympus BX51, Japan). The percentage of the EdU-positive cells and the average fluorescence intensity were calculated by Image J software (NIH, United States). Each group repeated the process thrice.

Colony Formation Assay

Colony forming ability was detected with colony formation assay. The cell suspensions of SW480, HT29, and DLD-1 (at 1×10^3 cells/well) were plated into 6-well plates and incubated at 37°C and at an atmosphere of 5% CO_2 for 7–10 days. The supernatants were discarded, and the colonies washed with PBS for three times, and fixed in 4% paraformaldehyde solution (Servicebio, China) to fix the cells for 15 min. Next, cells were stained with 0.2% crystal violet at room temperature for 10 min. Finally, the plate was washed moderately with running tap water. The number of colonies containing more than 50 cells was microscopically counted to calculate the colony formation rate as the number of colonies/number of cells × 100% divided by control. The data was analyzed by Prism software 7.0 (GraphPad Software, Inc.). All experiments were performed in triplicate to determine their reproducibility.

Wound Healing Assay

The cell suspensions of SW480, HT29, and DLD-1 (at 1×10^5 cells/well) were placed into a 6-well plates chamber and incubated in RPMI 1640 medium at 37°C with 5% CO_2. When the cells reached 90% confluence, a 200-μl pipette tip was used to scratch shaped wounds consistently on the cell monolayer across each well. Then, PBS was utilized to remove floating cells, and serum-free RPMI 1640 medium was added. The wound was photographed immediately (0 h), using an inverted optical microscope (×200) (Olympus IX51, Japan). The cells were then cultured in the medium. The wounds were photographed at 48 h to measure the extent of wound healing. The change in the scratch area with time and the wound healing percent were calculated as follows: Wound healing (%) = (the initial scratch area—the scratch area after 48 h)/the initial scratch area × 100%. The process above was conducted by Image J. Each experiment was repeated 3 times.

Flow Cytometry

Cell cycle analysis was found using flow cytometry. The cells growing in exponential phase were seeded into 6-well plates cells and treated for 48 h. Next, cells were digested by 0.25% trypsin without EDTA, and then harvested and resuspended in one volume of PBS. Following treatment, cells were fixed with ice-cold 75% ethanol at 4°C overnight. The fixed cell pellets then centrifuged at 1,200 rpm for 10 min. With the removal of the supernatants, cells precipitation was suspended in 1 ml propidium iodide (PI, Antgene, China) staining solution (50 μg/ml PI and 100 μg/ml RNase A in PBS) in darkness before flow cytometric analysis. After incubating for 30 min, the percentages of cells in the G0/G1, S, and G2/M cell cycle phases were analyzed by flow cytometry (FACS Calibur, Becton Dickinson, Franklin Lakes, NJ, United States). Data from at least three independent experiments were analyzed using the Modfit LT^{TM} Software.

Immunofluorescence

Cells were cultured on coverslips (14 mm) in 24-well plates at 37°C with 5% CO_2. After 24 h, the supernatant was removed and PBS was used to wash it. Then, add 1 ml 4% formaldehyde to each well for 15 min. After being washed by PBS, cells were permeabilized with 0.3% Triton X-100 at room temperature for 10 min. Then, blocked with 5% BSA for 30 min and washed by PBS three times. After that, the washed cells were incubated with polyclonal antibodies against E-cadherin (Proteintech, 1: 50), N-cadherin (Proteintech, 1: 50), p-PI3K (Cell Signaling Technology, 1: 400), and p-AKT (Cell Signaling Technology 1: 400), overnight at 4°C in darkness. After

being washed with PBS, add FITC-labeled and Cy3-labeled secondary antibody, 1:500 dilution, for 1 h at dark. DAPI (Biosharp Biotech, Hefei, China, 1: 1000) was used to counterstain the nuclei for 10 min. The slides were mounted on coverslips with an anti-fade mounting medium. All the images were collected by an upright fluorescence microscope (Olympus BX51, Japan). Each experiment was repeated 3 times.

Transwell Migration and Invasion Assay

Cell migration and invasion ability were examined by Corning transwell insert chambers (8 mm pore size, Corning). The transwell chamber was placed into the 24-well culture plate, the chamber was called the upper chamber, and the culture plate was called the lower chamber. In the migration assay, 2×10^5 cells were suspended in 100 μl FBS-free medium and were added to the upper chamber. 600 μl RPMI 1640 with 20% FBS were seeded in the lower compartment of the chamber and the cells were incubated in an environment of 37°C and 5% CO_2. After 24 h, 4% paraformaldehyde (Servicebio, China) was used for fixation. Afterwards, 0.5% crystal violet was dyed for 10 min and the membrane was washed with PBS. The migrated cells on the lower surface were photographed randomly with an Olympus IX51 inverted microscope in five visual fields (× 200 magnification) and the migrated cells were quantified using Image J software. For invasion assay, the upper compartment was precoated with one hundred microliters of matrigel and 5×10^5 cells per invasion well were added to the upper chamber. After incubating for 48 h, the rest of the protocol was similar to the migration assay. Each assay was performed at least three times.

Xenograft Tumor Model

5-week-old male BALB/c nude mice were purchased from Beijing HFK Experimental Animal Center (Beijing, China). SW480 cells stably transfected with shKIFC3 and shNC were suspended in PBS, about 200 μl of cells suspension were subcutaneously injected into the lower right dorsal flank of all mice. Each group included seven mice. Tumor formation was observed and tumor volume was measured by the vernier caliper on day 7 after injection of cell suspension. Then the growth of tumors was monitored for an interval of 1 day. The tumor volume was calculated at the same time intervals, according to the formula: volume (mm^3) = 0.5 × longest diameter × (shortest diameter)^2. When the tumors reached a minimal diameter of 1.0 cm, the subcutaneous tumors were dissected and then measured and weighted after the sacrifice of the mice. The tumor sections were removed from paraffin-embedded blocks of the harvested tissues and we used KIFC3 and ki67 antibodies on the sections for IHC. All animal experiments were performed following the procedures and principles outlined in the National Institutes of Health guidelines for the care and use of laboratory animals, and were approved by the Animal Care and Use Committee of Renmin Hospital of Wuhan University.

Statistical Analysis

All data was expressed as mean ± standard deviation (SD). All statistical analyses were performed using GraphPad Prism 8.0. Comparisons between two groups were determined using Student t-test, while comparisons between multiple groups were analyzed using one-way ANOVA followed by Tukey's post-hoc tests. Overall survival (OS) and disease-free survival (DFS) curves was calculated by Kaplan-Meier method and tested by log-rank test. p values <0.05 were considered statistically significant.

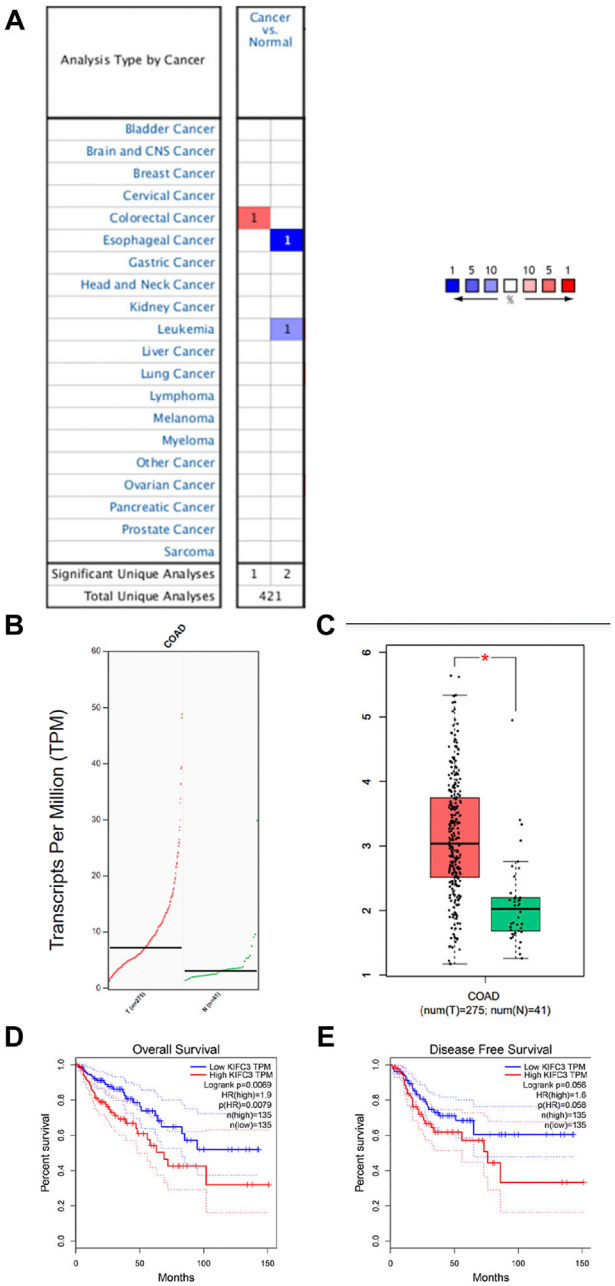


FIGURE 1 | Analysis of KIFC3 mRNA expression in normal colorectal and colorectal cancer (CRC) tissues from public databases. **(A)** Data from the Oncomine databases showed that KIFC3 mRNA expression was upregulated in CRC tissues compared to normal colorectal tissues. **(B,C)** Data from the GEPIA databases showed that KIFC3 mRNA level was higher in CRC tissues compared to normal colorectal tissues. **(D,E)** Data from the GEPIA database showed that the expression level of KIFC3 could affect the OS of CRC ($p = 0.00069$), but did not affect the disease-free survival ($p = 0.056$). The OS of patients with high expression of KIFC3 was shorter than that of patients with low expression of KIFC3.

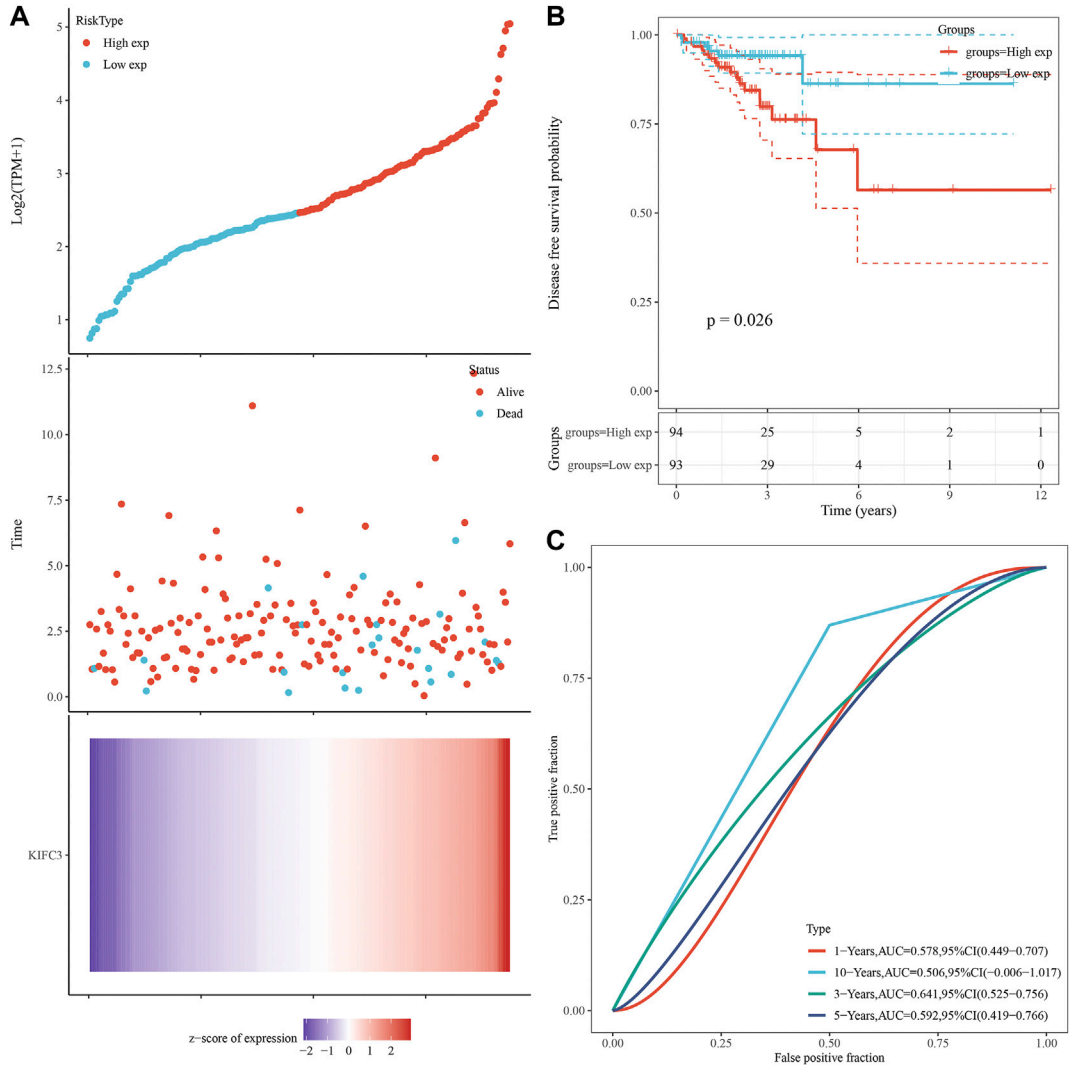


FIGURE 2 | Prognostic analysis of gene signature in the ICGC database. **(A)** KIFC3 expression and survival time and survival status in ICGC data set. **(B)** Kaplan-Meier survival curve distribution of KIFC3 in ICGC data database. **(C)** ROC curve and AUC of KIFC3 at different times. The abscissas of the upper, middle and lower three graphs in **Figure 2A** all represent samples, and the order of the samples is consistent.

RESULTS

Kinesin Family Member C3 mRNA Levels Are Significantly Upregulated in Colorectal Cancer Tissues

We analyzed gene expression data in the Oncomine and GEPIA databases to compare KIFC3 mRNA levels in the tumor and normal tissues from CRC patients. The CRC tissues showed significantly higher KIFC3 mRNA expression than the adjacent tissues (**Figures 1A–C**). Then, we use the GEPIA database to evaluate the prognostic value of KIFC3 level. Kaplan-Meier plotter survival analysis showed that the expression level of KIFC3 could affect the OS of CRC ($p = 0.0069$), but did not affect the disease-free survival ($p = 0.056$). The OS of patients in the group with high KIFC3 expression was shorter than that in the group with low KIFC3 expression, as shown in **Figures 1D,E**. We used ICGC database to analyze the relationship between KIFC3 gene expression and survival time and survival status. As shown in **Figure 2A**, the top represents the scatter plot from low to high expression level of the gene. The middle represents the scatter plot distribution of survival time and survival state corresponding to gene expression in different samples. The image at the bottom represents a heat map of the gene expression. The Kaplan-Meier survival curve distribution of KIFC3 in the ICGC database is shown in the **Figure 2B**, the dotted line represented the median risk score and divided the patients into low-risk and high-risk group, the disease-free survival of patients in the group with high KIFC3 expression was shorter than that in the group with low KIFC3 expression. **Figure 2C** display the ROC curves and AUC of the KIFC3 gene at different times.

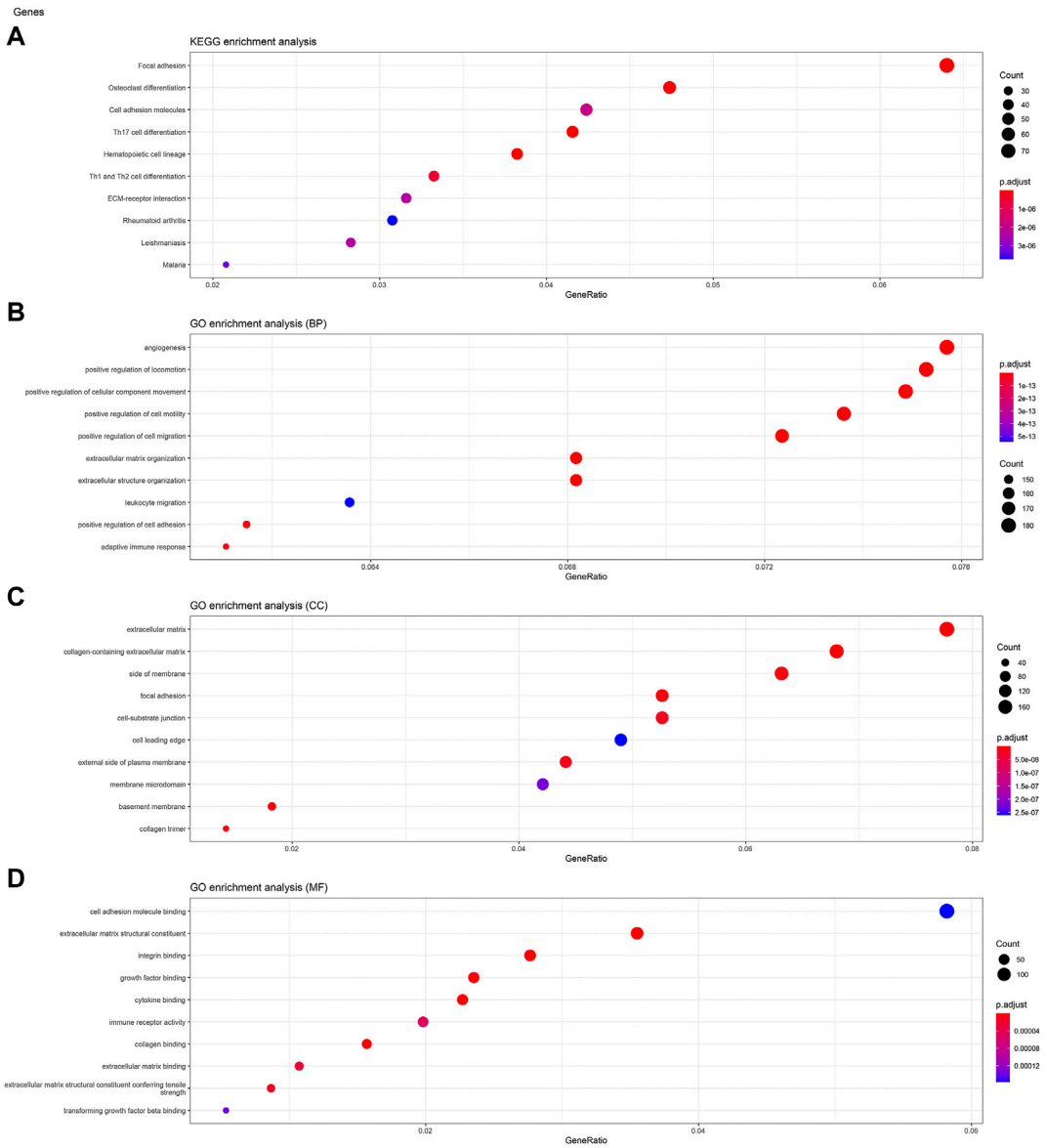


FIGURE 3 | KEGG pathway and GO enrichment analyses of KIFC3-associated genes. **(A)** The bubble chart of KEGG pathway. **(B)** The bubble chart of GO enrichment in biological processes. **(C)** The bubble chart of GO enrichment in cell component. **(D)** The bubble chart of GO enrichment in molecular function.

The results showed that CRC patients with higher KIFC3 mRNA levels were associated with poorer OS than the CRC patients with lower KIFC3 expression.

Kinesin Family Member C3 and Gene Ontology Enrichment Analyses of Kinesin Family Member C3

To analyze the biological classification of KIFC3, function enrichment analyses were performed using clusterProfiler package in R. KEGG pathway analysis revealed that DEGs were mainly enriched in focal adhesion and pathways in cancer (**Figures 3A**, **4A**, **5A**). GO analysis results showed that changes in biological processes (BP) of KIFC3 were significantly enriched in angiogenesis and positive regulation of cellular component movement (**Figures 3B**, **4B**, **5B**) Changes in cell component (CC) of DEGs were mainly enriched in extracellular matrix and collagen-containing extracellular matrix (**Figures 3C**, **4C**, **5C**). Changes in molecular function (MF) were mainly enriched in extracellular matrix structural constituent and cell adhesion-molecule binding (**Figures 3D**, **4D**, **5D**). These result show, KIFC3 may be involved in the process of cell adhesion and tight connection.

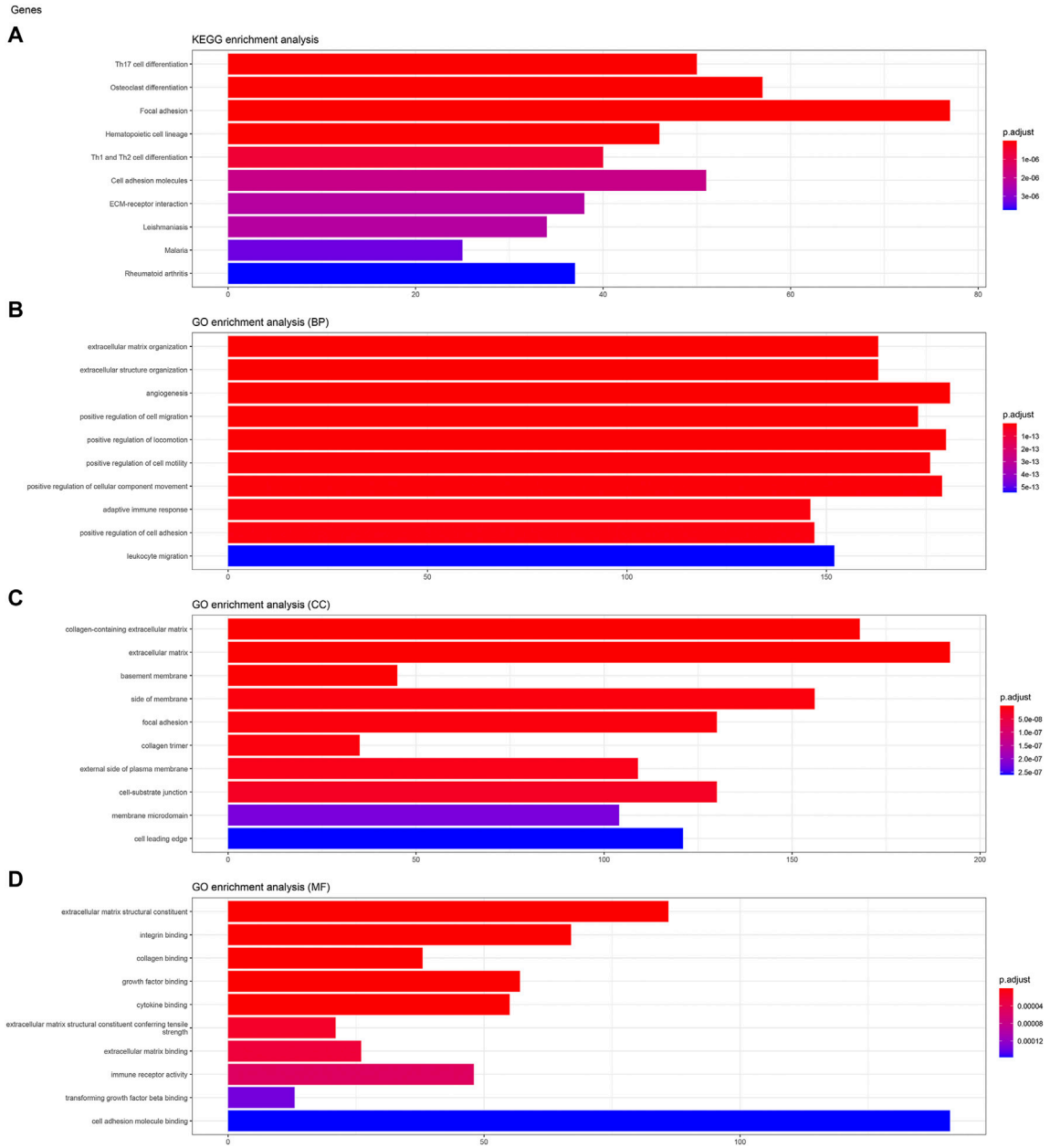


FIGURE 4 | KEGG pathway and GO enrichment analyses of KIFC3-associated genes. **(A)** The bar chart of KEGG pathway. **(B)** The bar chart of GO enrichment in biological processes. **(C)** The bar chart of GO enrichment in cell component. **(D)** The bar chart of GO enrichment in molecular function.

Kinesin Family Member C3 is Expressed at High Levels in Colorectal Cancer Cell Lines

The protein and mRNA levels of KIFC3 in CRC cell lines were validated by western blotting and qRT-PCR. It is confirmed that the protein levels of KIFC3 were significantly higher in CRC cells (HT29, HCT116, SW480, DLD-1) compared with that in the normal colorectal epithelium cell line NCM460 (**Figures 6A,B**). Likewise, the mRNA levels of KIFC3 in CRC cells were also higher than in NCM460 (**Figure 6C**). Among the CRC cell lines, the expression level of the KIFC3 was highest in SW480 cell followed by HT29 cell, while DLD-1 had the lowest level of KIFC3. Based on the above, we established a stable knockdown cell line of SW480 and HT29 cells, and KIFC3-overexpressing in DLD-1 cells. The picture (**Figures 6D–J**) shows the efficiency of knockdown or overexpression at the protein level and mRNA level. We selected the best knockdown effect for subsequent experiments, and a fluorescence microscope showed the transfection efficiency was over 95% (**Figure 7A**).

Kinesin Family Member C3 Promotes Colorectal Cancer Cell Proliferation

To elucidate the function of KIFC3 in cell growth, we performed EdU assay, CCK-8 assay and colony formation assay. Evaluation of EdU

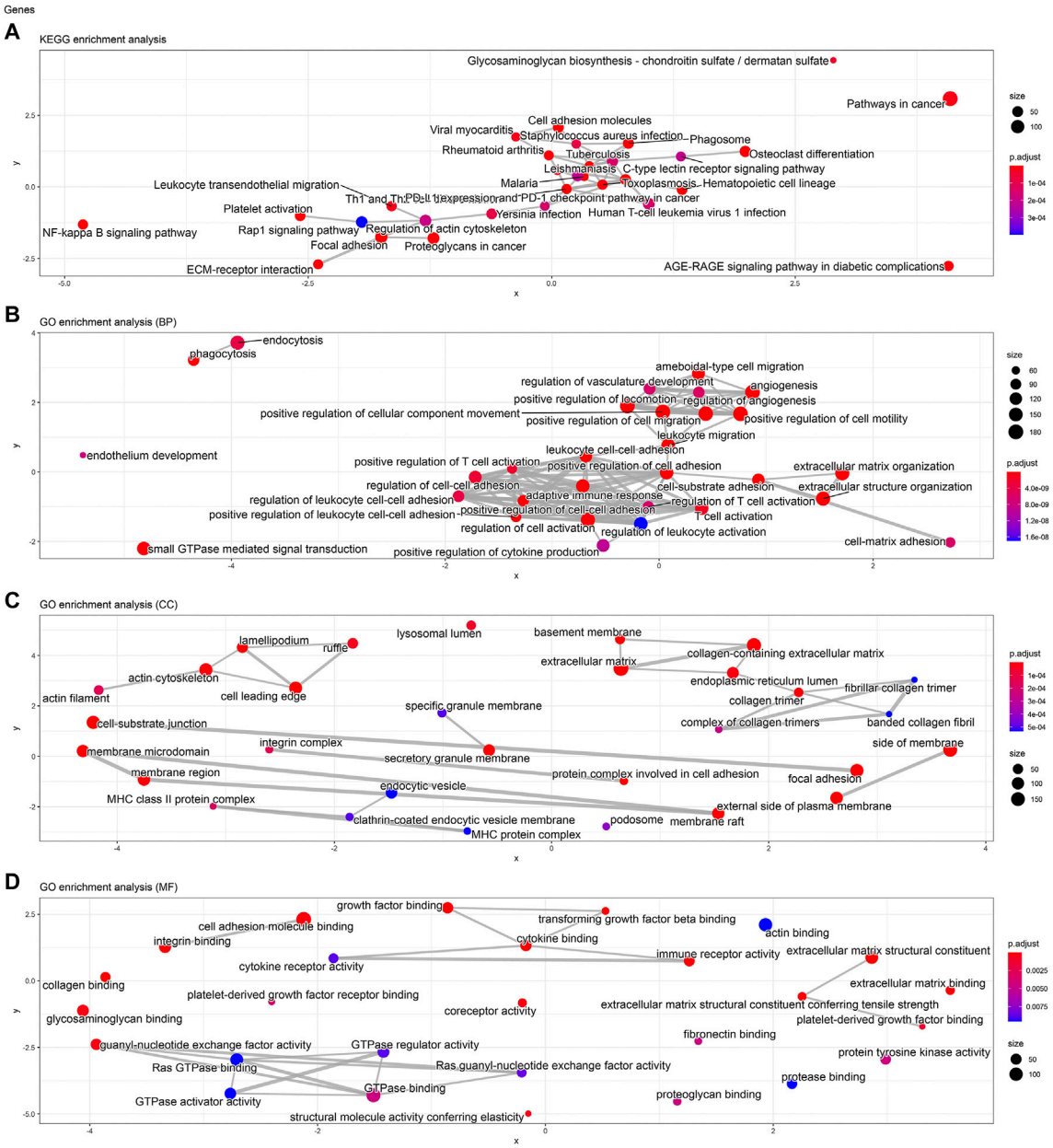


FIGURE 5 | KEGG pathway and GO enrichment analyses of KIFC3-associated genes. **(A)** The network chart of KEGG pathway. **(B)** The network chart of GO enrichment in biological processes. **(C)** The network chart of GO enrichment in cell component. **(D)** The network chart of GO enrichment in molecular function.

staining showed that depleted-KIFC3 in SW480 and HT29 cells gave rise to a decrease in the number of EdU-positive cells (**Figures 7B–E**), while the overexpression of KIFC3 significantly increased the number of EdU labelled cells in contrast with Control and Vector groups (**Figures 7F,G**). CCK-8 assay results demonstrated that the growth of KIFC3-depleted in SW480 cells was slower than the Control and NC group at 24, 36 and 48 h (**Figure 7H**). Similar results were shown when the assay was conducted in the depletion of KIFC3 in HT29 cells (**Figure 7I**). Conversely, KIFC3 overexpression group had a higher proliferation vitality than those transfected with Vector and Control groups (**Figure 7J**). Meanwhile, colony formation assay found that KIFC3 downregulation impaired cell viability in SW480 and HT29 cells (**Figures 7K–N**), whereas KIFC3 upregulation promoted cell viability in DLD-1 cells (**Figures 7O,P**). Due to the observed effects of KIFC3 on CRC cells growth, we assessed the cell cycle assay and found that the knockdown of KIFC3 in SW480 cell lines could increase the number of cells in G1 phase, decrease the number of cells in S phase (**Figures 8A,B**, **Supplementary Figure S1A**). Meanwhile, the knockdown of KIFC3 in HT29 cell lines could increase the number of cells in G1 phase and the number of cells in G1 phase, and decrease the number of cells in S phase (**Figures 8C,D**, **Supplementary Figure S1B**). Next, we evaluated the expression of Cyclin A2, Cyclin E1, and CDK2, which are important and

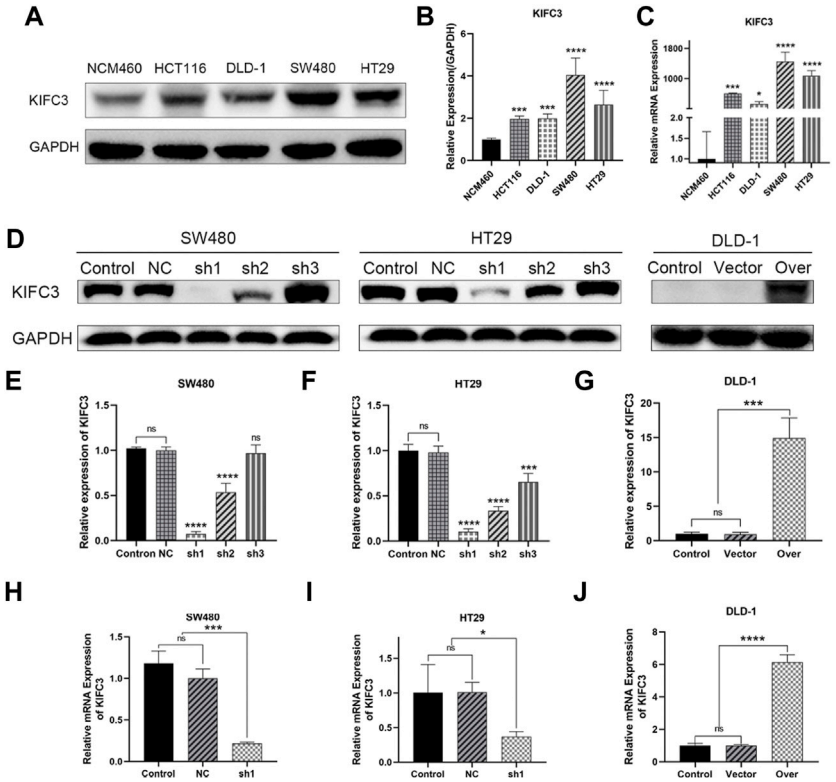


FIGURE 6 | KIFC3 was expressed at higher levels in CRC cell lines. **(A–C)** Western blot and qRT-PCR analysis of KIFC3 expression in CRC cell lines (HT29, HCT116, SW480, DLD-1) and normal colon mucosal epithelial cells (NCM460), and quantification analysis results. **(D–G)** Western blot analysis of the efficiency of sh-KIFC3 and sh-NC transfection compare with Control group in SW480 and HT29 cells, and the efficiency of KIFC3-overexpress and over-Control transfection in DLD-1 cell, and quantification analysis results. **(H–J)** qRT-PCR analysis of the efficiency of the best knockdown effect in SW480 and HT29 cells, and the efficiency of KIFC3-overexpress, NC and Control transfection in DLD-1 cell. The transfected cells above are all stable transfectants. The data are presented as the mean ± standard deviation of triplicate independent experiments and were normalized to the control group. $^{*}p < 0.05$; $^{**}p < 0.01$; $^{***}p < 0.001$; $^{****}p < 0.0001$.

tightly initiate DNA replication in S phase. We also evaluated the expression of p21 and p53. The downregulation of KIFC3 suppress the expression of Cyclin A2, Cyclin E1 and CDK2, enrich the expression of p21 and p53 (**Figures 8E–H**). Moreover, we added the cell cycle assay of KIFC3-overexpression cells to verify whether KIFC3 has an effect on the growth cycle of CRC. The result show that KIFC3 overexpression increase the numbers of cells in S phase, decrease the number of cells in G1 phase, further promoted the G1/S phase transition (**Supplementary Figure S2**). PCNA is a key marker of cell proliferation, which assists in DNA replication. We found that the cells transfected shKIFC3 had lower protein levels of PCNA than those in Control and NC, whereas the protein level of PCNA was enhanced after KIFC3 overexpression compared to the Control and Vector groups (**Figures 9A–F**). Those results indicate that KIFC3 was sufficient to increase the proliferation of CRC cells.

Kinesin Family Member C3 Promotes the Migration and Invasion of Colorectal Cancer Cells

To test the relevance of KIFC3 on cell migration and invasion, we conducted the scratch and transwell assays. We used a wound healing assay to demonstrate the roles of KIFC3 on migration capability of CRC cells. When the cell transfected with shKIFC3, the wound-healing speed was slower than the Control and NC groups and the wound-healing speed was faster in the group of KIFC3 overexpression than the Control and Vector groups (**Figures 9G–L**). Moreover, the transwell assay showed similar results as wound healing assay. From the **Figures 10A–D**, transwell migration assays showed that the downregulation of KIFC3 significantly weakened the migratory ability in SW480 and HT29 cell lines. On the contrary, the cell migratory capability was enhanced after KIFC3 overexpression in DLD-1 cell lines (**Figures 10E,F**). Similarly, the invasion ability of CRC cells through the filter coated with Matrigel were reduced (**Figures 10G–J**). As expected, the results of transwell assay exhibited that the cell invasion rate were increased in KIFC3 overexpression groups compared with the Control and Vector groups (**Figures 10K–L**). The combined data demonstrated that KIFC3 may act as a regulator in promote migration and invasion in CRC cells.

Kinesin Family Member C3 Enhances the Epithelial-to-Mesenchymal Transition Process in Colorectal Cancer Cells

Epithelial cells may develop invasive mesenchymal stem cell-like properties through epithelial-to-mesenchymal transition

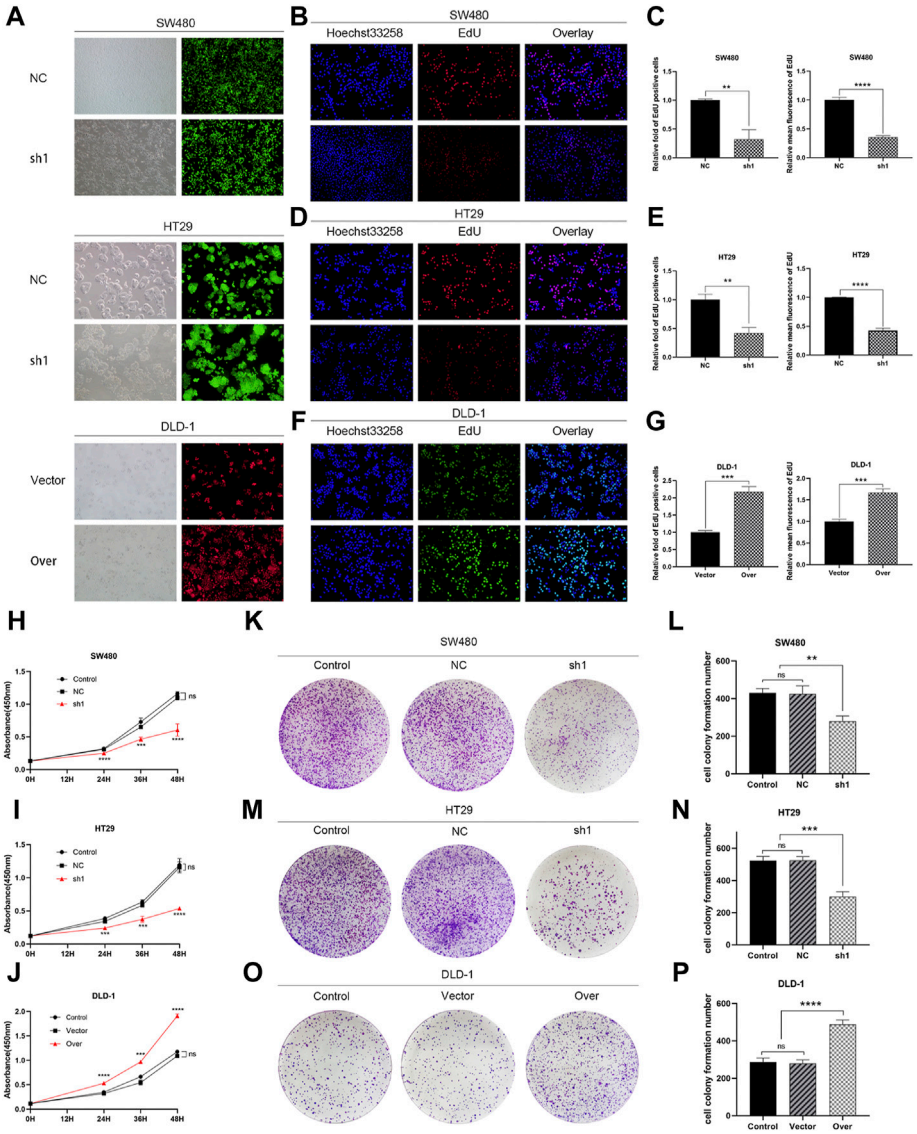


FIGURE 7 | KIFC3 promotes the proliferation of CRC cells. **(A)** The transfection efficiency of SW480, HT29 and DLD-1 were observed under microscope. **(B–G)** EdU assay of KIFC3 silencing or overexpression on CRC cells' proliferation, and quantification analysis results. **(H–J)** The effects of KIFC3 silencing or overexpression on the proliferation ability of SW480, HT29 and DLD-1 cells were measured by the CCK-8 assay. **(K–P)** Colony formation assay of KIFC3 silencing or overexpression on CRC cells' proliferation, and quantification analysis results. The data are presented as the mean ± standard deviation of triplicate independent experiments and were normalized to the control group. *$p < 0.05$; **$p < 0.01$; ***$p < 0.001$; ****$p < 0.0001$.

(EMT). Many researches have revealed that EMT plays a critical role in tumorigenesis and metastasis. MMP-2 and MMP-9, which are proteolytic proteins of the outer membrane, are thought to be involved in cell metastasis and cell invasion. Herein, we found that KIFC3 silencing repressed the protein level of MMP-2 and MMP-9, while the KIFC3 overexpression showed the opposite results (**Figures 11A–F**). To further assess the role of KIFC3 in EMT, we measured the EMT-related marker through western blot analyses after KIFC3 downregulation and overexpression. The results displayed that KIFC3 silencing lead to epithelial marker E-cadherin up-regulated, while the mesenchymal markers including N-cadherin, Vimentin, SNAIL one and TWIST were down-regulated. Yet, after KIFC3 was upregulated in DLD-1 cells, the opposite results were displayed (**Figures 11A–F**). To further investigate the role of KIFC3 in EMT, immunofluorescence staining was conducted, and it showed dramatic upregulation of E-cadherin expression and downregulation of N-cadherin expression when KIFC3-depleted in SW480 and HT29 cells, while the opposite results were investigated when KIFC3 was upregulated in DLD-1 cells, as well (**Figures**

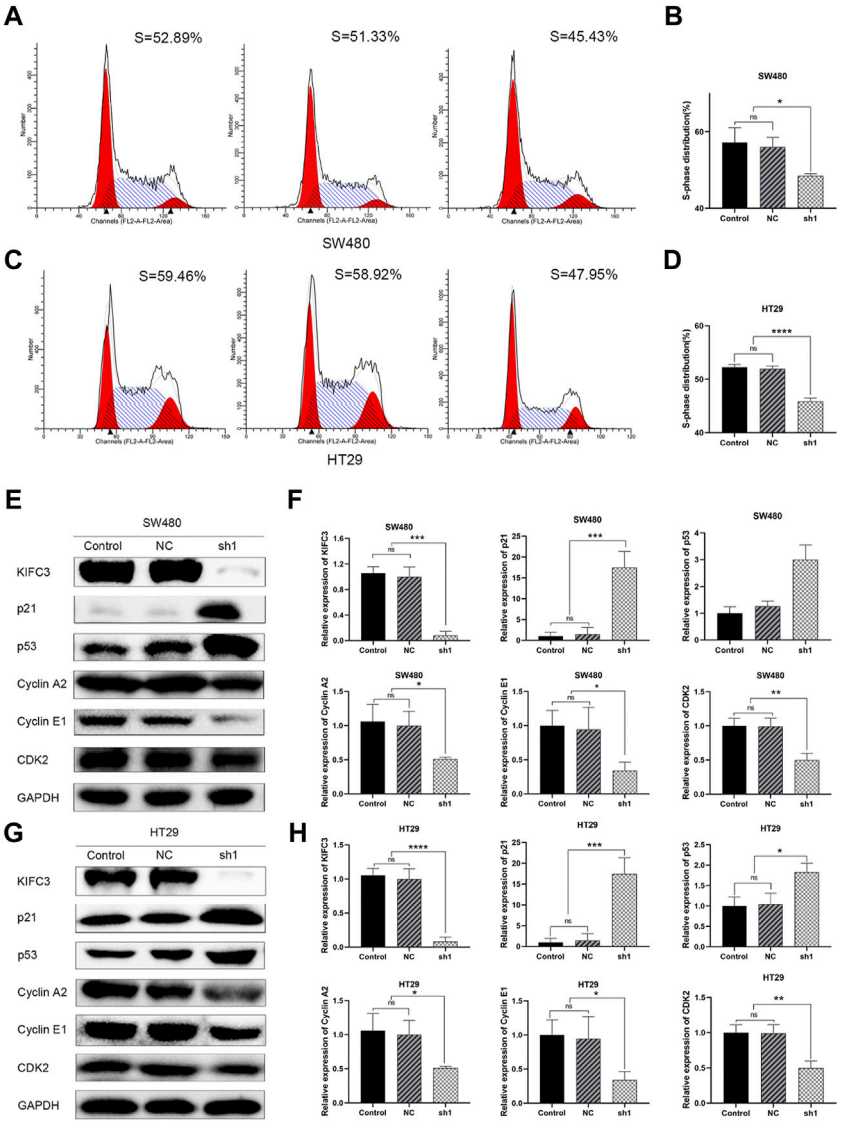


FIGURE 8 | KIFC3 affects the expression of cell cycle-mediated factors. **(A–D)** Effects of KIFC3 silencing on the cell cycle distribution in SW480 and HT29 cells as showed by flow cytometry assay, and quantification analysis results. **(E–H)** Effect of KIFC3 silencing on the expression of cell cycle-mediated factors like p21, p53, Cyclin A2, Cyclin E1, and CDK2, as measured by western blot, and quantification analysis results. The data are presented as the mean ± standard deviation of triplicate independent experiments and were normalized to the control group. *$p < 0.05$; **$p < 0.01$; ***$p < 0.001$; ****$p < 0.0001$.

11G–L). As demonstrated by those experiments, it could be possible that the KIFC3 could enhance the EMT process in CRC cells.

Kinesin Family Member C3 Enhances the PI3K/AKT/mTOR Signaling Pathway in Colorectal Cancer Cells

The PI3K/AKT/mTOR signaling pathway plays a vital role in cancer which regulated cell proliferation, migration and invasion. To further elucidate the possible mechanism of KIFC3 in regulating the EMT process of CRC cells, we inspected the expression of the related proteins in PI3K/AKT/mTOR pathway. As shown by western blot assay, the protein expression levels of p-PI3K, p-AKT, and p-mTOR of KIFC3 silencing cells (SW480-shKIFC3, HT29-shKIFC3) group were notably lower compared with the Control and NC group. At the same time, the total protein levels of PI3K, AKT, and mTOR showed no changes (**Figures 12A,B,D,E**). As displayed in **Figures 12C,F**, when the KIFC3 expression was upregulated in DLD-1 cell, the protein levels of t-P13K, t-AKT and t-mTOR were unchanged, whereas the protein expression level of p-PI3K, p-AKT and p-mTOR were significantly upregulated. What is more, when KIFC3 was knocked down in SW480 and HT29 cells, immunofluorescence staining showed a downregulated expression of p-PI3K and p-AKT, the same as the western blot results, whereas the upregulation of KIFC3 reverted this phenomenon in DLD-1 cell lines (**Figures 12G–L**). The results above showed that the KIFC3 enhances

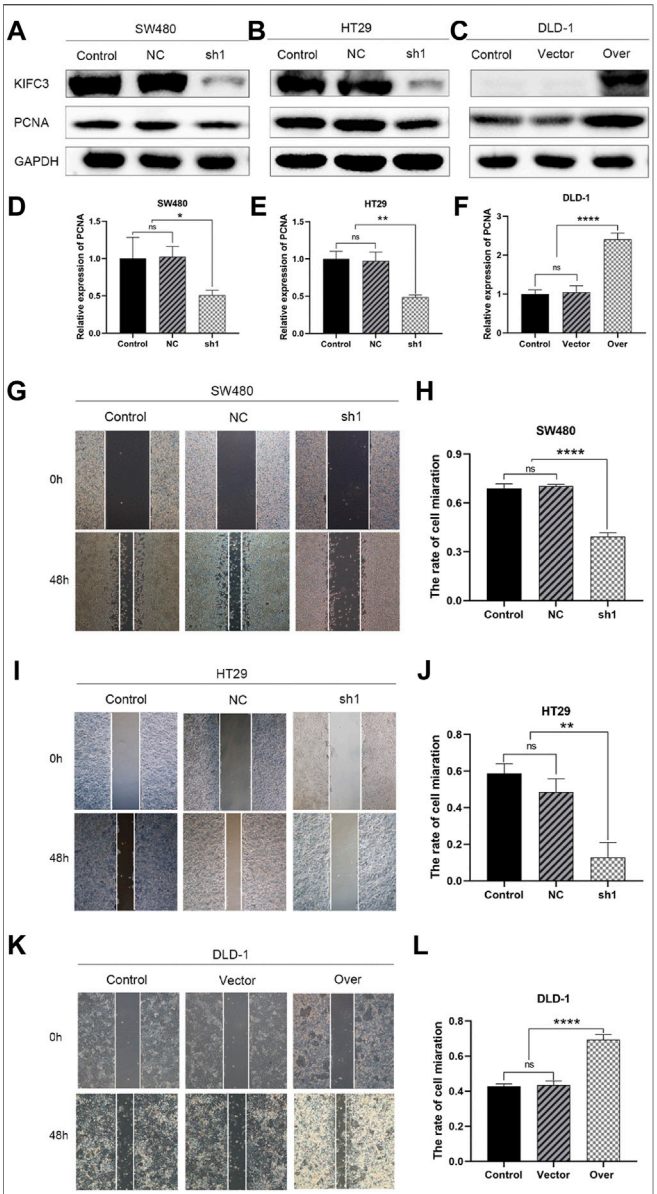


FIGURE 9 | KIFC3 promotes the proliferation and migration of CRC cells. **(A–F)** The expression of PCNA in SW480, HT29 and DLD-1 cells after lentivirus vectors delivery in each group as measured by western blot, and quantification analysis results. **(G–L)** Effects of KIFC3 silencing or overexpression on the wound healing of SW480, HT29 and DLD-1 cells, and quantification analysis results. The data are presented as the mean ± standard deviation of triplicate independent experiments and were normalized to the control group. *$p < 0.05$; **$p < 0.01$; ***$p < 0.001$; ****$p < 0.0001$.

the EMT process by activating the PI3K/AKT/mTOR signaling pathway in CRC cells.

Loss of Kinesin Family Member C3 Inhibits Tumor Growth *in vivo*

Given the significant inhibition of CRC cell survival and EMT through PI3K/AKT/mTOR signaling by the knockdown of KIFC3 *in vitro*, we examined its activity *in vivo*. We established a tumor xenograft model, *via* the subcutaneous injection of the SW480 cells transfected with shKIFC3#1 or transfected with a negative control vector. One week after the tumor cell implantation, apparent subcutaneous tumor formation was observed. We then observed and measured the size of the tumor every 2 days. We found that the growth rate of tumors in the KIFC3 silencing groups were slower than that in the NC groups (**Figures 13A,B**). After 22 days, nude mice were sacrificed and we weighted the tumors. We found that the tumor growth rate was significantly slower in the KIFC3-depletion group than in the NC group (**Figure 13C**, $p < 0.001$). Then, we detected the tumor weight, and we found that the tumors in the knockdown groups were significantly smaller than those in the NC groups (**Figure 13D**). Furthermore, we detected the KIFC3 and ki67 expression on the tumor section. Immunofluorescence staining revealed that the xenograft tumor tissues injected with sh-KIFC3 reduced the expression of KIFC3 and ki67, indicating the decrease of CRC cell proliferation (**Figures 13E,F**). Collectively, these findings elucidated that the down-regulation of KIFC3 could suppress tumor growth in CRC *in vivo*.

Inhibition of the PI3K/AKT/mTOR Pathway Attenuates the Tumorigenic Effect of Kinesin Family Member C3 on Colorectal Cancer Cells

To explore whether the PI3K/AKT/mTOR signaling pathway was related to KIFC3, the DLD-1 cells that transfected with KIFC3 overexpression were preincubated with LY294002 (20 μM, Selleck Chemicals, Shanghai, China) or Triciribine (5 μM, MCE, Shanghai, China). LY294002 is an inhibitor of the PI3K/AKT/mTOR pathway, whereas Triciribine is an AKT inhibitor. As represented in the **Figures 14A–C**, compared with the KIFC3 overexpression group, the phosphorylation levels of PI3K, AKT, and mTOR decreased after using LY294002 or Triciribine, but the total protein levels of P13K, AKT, and mTOR had no changes. Besides, LY294002 reversed the promoting effects of KIFC3 on the proliferation of CRC cells. DLD-1 cells preincubated with Triciribine shows the same trend as LY294002 (**Supplementary Figure S3A**). Moreover, we can find the ability of migration and invasion of CRC cells were restrained after DLD-1 cells culture with LY294002 or Triciribine (**Supplementary Figures S3B,C**). This finding may be attributed to the fact that KIFC3 is indeed related to the PI3K/AKT/mTOR signaling pathway (**Figure 15**).

DISCUSSION

More and more evidences indicate that KIFs play critical roles in the genesis and development of human cancers. Some KIFs are associated with malignancy and drug resistance in solid tumors (Liu et al., 2013). For example, KIF5B plays an important role in determining phenotype and aggressiveness of breast cancer (Moamer et al., 2019), high expression level of KIF11 was associated with unfavorable prognosis in clear cell renal cell

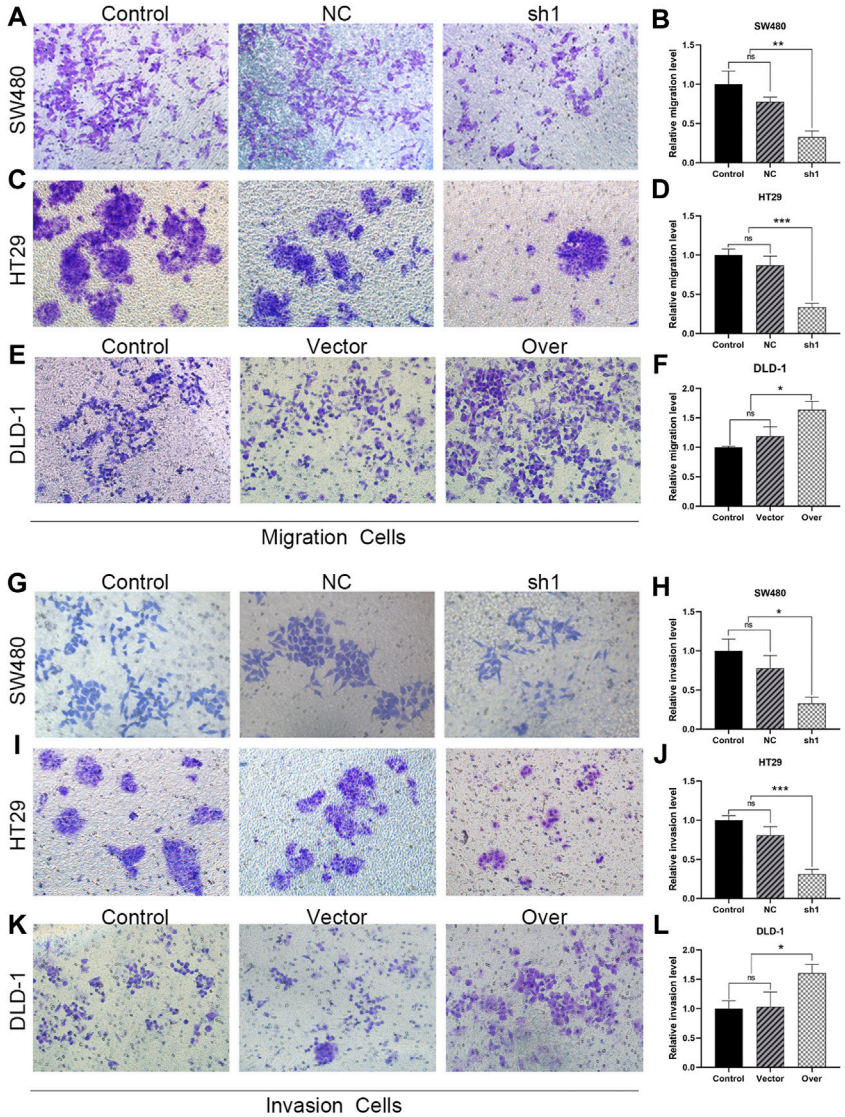


FIGURE 10 | KIFC3 promotes the migration and invasion of CRC cells. **(A–F)** Effects of KIFC3 silencing or overexpression on the migration ability of SW480, HT29 and DLD-1 cells, and quantification analysis results. **(G–L)** Effects of KIFC3 silencing or overexpression on the invasion ability of SW480, HT29 and DLD-1 cells, and quantification analysis results. The data are presented as the mean ± standard deviation of triplicate independent experiments and were normalized to the control group. $^{*}p < 0.05$; $^{**}p < 0.01$; $^{***}p < 0.001$; $^{****}p < 0.0001$.

carcinoma (Jin et al., 2019), KIF2C/4A/10/11/14/18B/20A/23 predict poor prognosis and promote cell proliferation in hepatocellular carcinoma (Li et al., 2020b) and KIF26A could inhibit migration and invasion (Ma et al., 2021). Aside from this, chemotherapeutic drug resistance is the main obstacle in effective tumor treatment, which hinders the efficacy of cytostatic drugs (Li et al., 2019; Tian et al., 2019; Ashar et al., 2020). In breast cancer, the overexpression of KIFC3 increased the resistance of breast cancer cells to docetaxel through opposing the microtubule stabilizing effect of docetaxel (De et al., 2009). In this study, we found that KIFC3 was expressed at higher levels in human CRC tissues and cell lines than in normal colorectal tissues and cells. That means KIFC3 may play a notable role in the occurrence and development of differential expression of the CRC.

Cellular proliferation is essential for normal development and for maintaining tissue homeostasis. Excessive proliferation of cells is closely related to the occurrence of tumors (Shi et al., 2020). Zhao et al. (2020) found that the KIF18B promotes cell proliferation in colon adenocarcinoma and tumor growth *in vitro* and *in vivo*. In our research, we found that the ability and speed of CRC cells proliferation were slower in the KIFC3-depleted groups in the EdU assay, CCK-8 and colony formation assay. The opposite results were observed in the KIFC3 overexpression groups. We further determined whether KIFC3 promotes tumor growth *in vivo*. The results showed that tumor growth rates in nude mice with KIFC3-depleted were significantly lower than in the mice of NC group. The result of the *in vivo* experiment was consistent with that of the *in vitro* experiment. Moreover, an

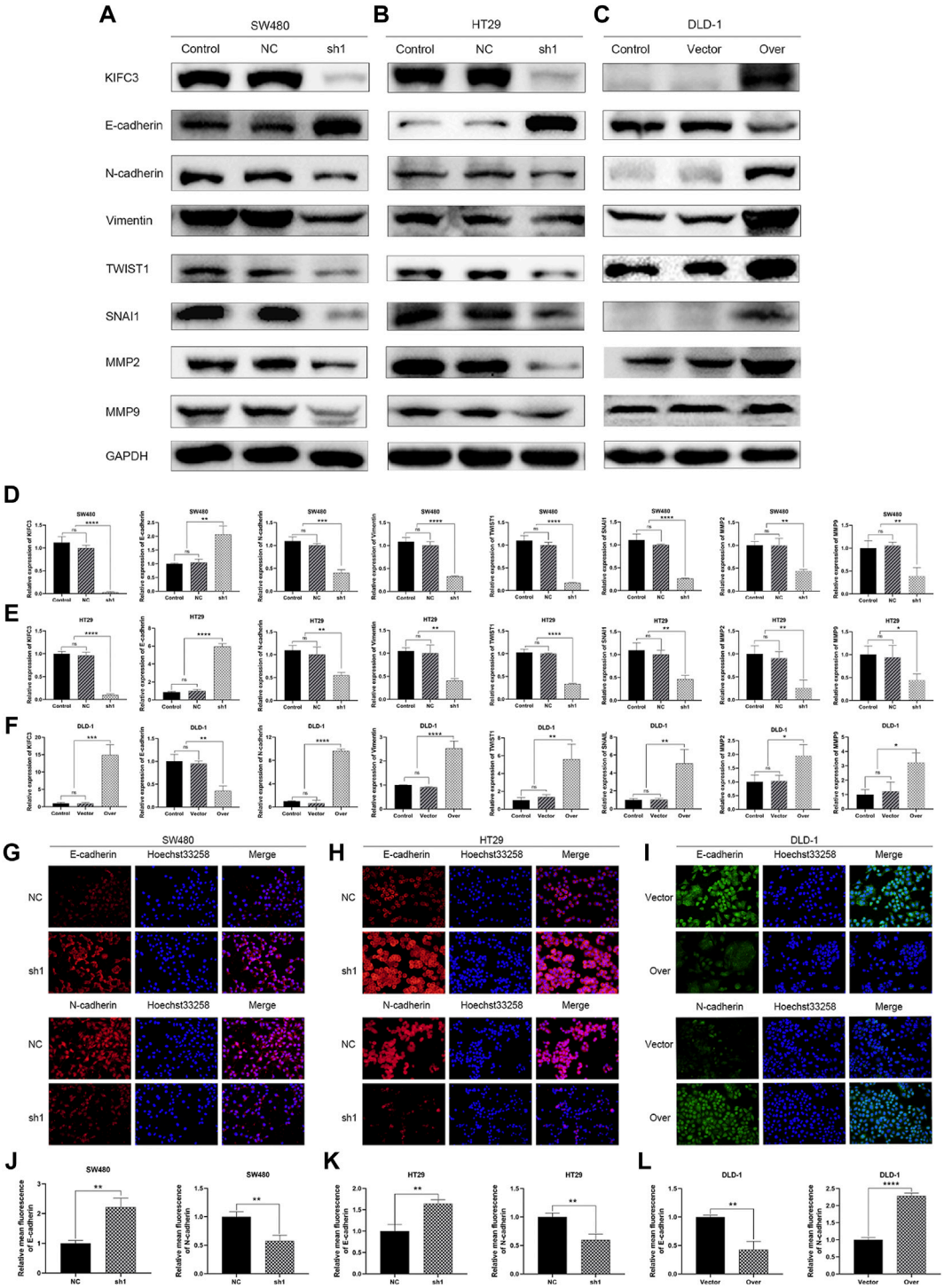


FIGURE 11 | KIFC3 affected the expression of the related factors in the EMT progress. **(A–C)** Effects of KIFC3 silencing or overexpression on the expression of the related factors in the EMT progress like E-cadherin, N-cadherin, Vimentin, TWIST1, SNAI1, MMP-2, and MMP-9, as measured by western blot. **(D–F)** Quantification to the protein level of the related factors in the EMT progress. **(G–I)** Immunofluorescence staining of E-cadherin and N-cadherin. **(J–L)** Statistical analysis of the relative mean fluorescence of E-cadherin and N-cadherin. The data are presented as the mean ± standard deviation of triplicate independent experiments and were normalized to the control group. *$p < 0.05$; **$p < 0.01$; ***$p < 0.001$; ****$p < 0.0001$.

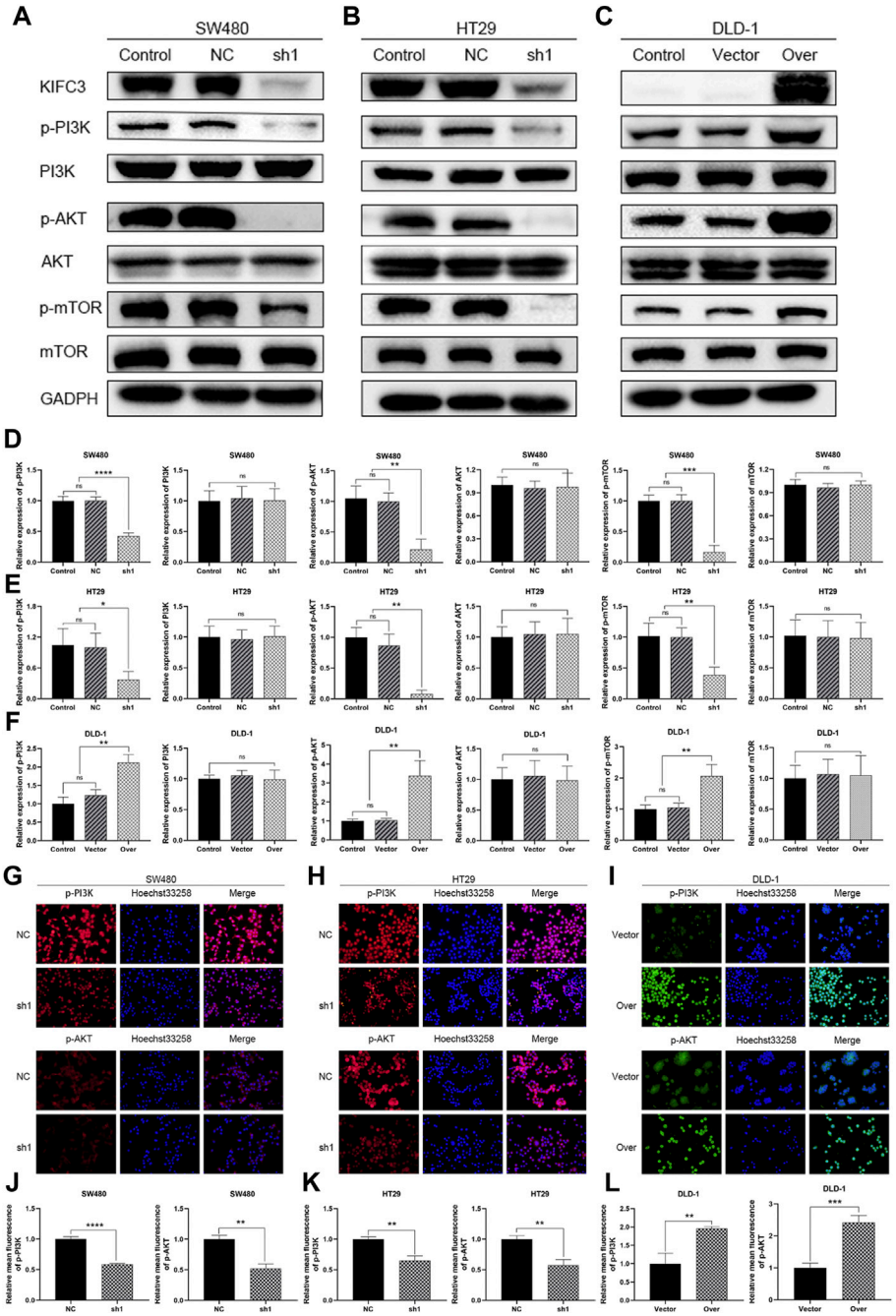


FIGURE 12 | KIFC3 affected the expression of the related factors in the PI3K/AKT/mTOR pathway. **(A–C)** Effects of KIFC3 silencing or overexpression on the expression of the related factors in the PI3K/AKT/mTOR pathway like PI3K, p-PI3K, AKT, p-AKT, mTOR, and p-mTOR, as measured by western blot. **(D–F)** Quantification to the protein level of the related factors in the PI3K/AKT/mTOR pathway. **(G–I)** Immunofluorescence staining of p-PI3K and p-AKT. **(J–L)** Statistical analysis of the relative mean fluorescence of p-PI3K and p-AKT. The data are presented as the mean ± standard deviation of triplicate independent experiments and were normalized to the control group. *$p < 0.05$; **$p < 0.01$; ***$p < 0.001$; ****$p < 0.0001$.

abnormal cell cycle causes carcinogenesis and cancer progression (Kometani et al., 2020). Many studies have proved that the dysregulation of KIFs has been revealed to influence the cell cycle to cause abnormal cell growth and affect cell adhesion to promote EMT in breast, bladder, ovarian and prostate cancer. Wang et al. (2015) found that the silencing of KIF3C by shRNA inhibited epithelial-mesenchymal transition and metastasis by inhibiting TGF-β signaling and suppressed breast cancer cell proliferation through inducing G2/M phase arrest. The cell cycle assay was performed through flow cytometry. We used

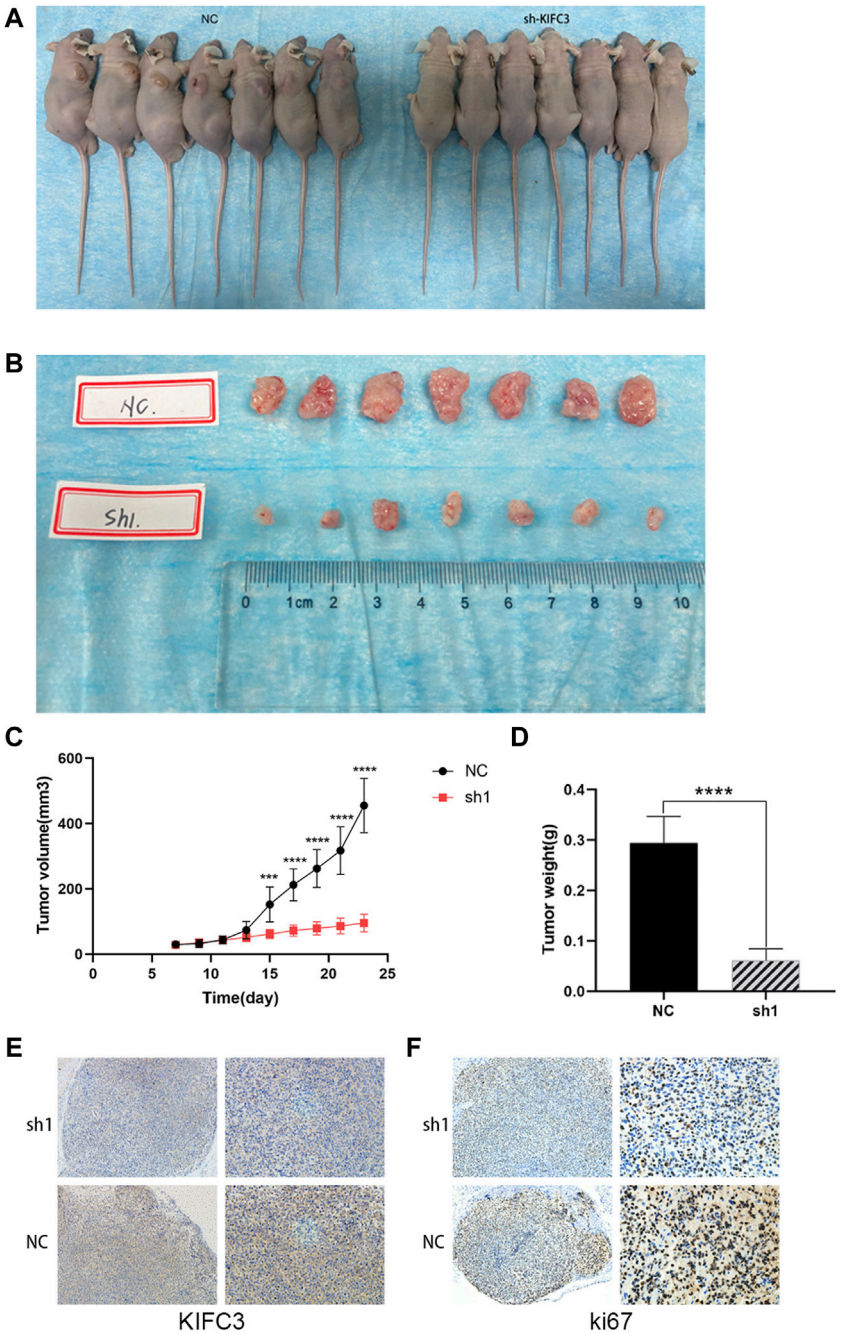


FIGURE 13 | KIFC3 knockdown inhibited tumor growth and proliferation. **(A–D)** Transplanted tumor mice image, tumor xenograft image, tumor xenograft volume, tumor xenograft weight of sh-NC and sh-KIFC3 SW480 cells in nude mice. **(E,F)** Analysis of KIFC3 and Ki67 in tumor xenografts derived from sh-NC and sh-KIFC3 SW480 cells by Immunohistochemistry. The data are presented as the mean ± standard deviation of triplicate independent experiments and were normalized to the control group. *$p < 0.05$; **$p < 0.01$; ***$p < 0.001$; ****$p < 0.0001$.

propidium iodide (PI), a commonly fluorescent dye that is permeable for the cell membrane and intercalates into the nucleic acid. The intensity of the signal is directly proportional to the nucleic acid content. In our study, the knockdown of KIFC3 decreased the expression of PCNA and the number of cells in S phase, whereas the overexpression of KIFC3 increased the expression of PCNA and promoted the G1/S phase transition. S phase is the phase of the cell cycle in which DNA is replicated and represents the proliferation index (Minisy et al., 2020). Cell cycle progression is co-regulated by Cyclin/Cyclin-dependent kinase (CDK) complexes. Different Cyclin-CDK complexes are involved in regulating different cell cycle transitions. Cyclin E-CDK2 plays

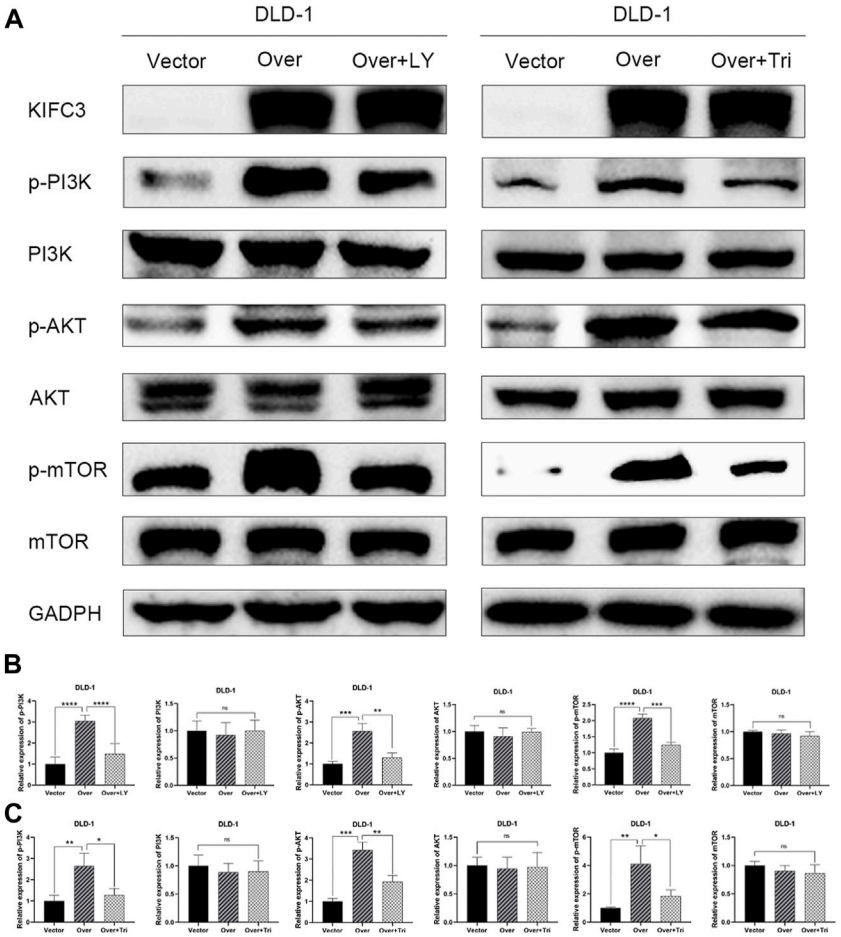


FIGURE 14 | LY294002 and Triciribine attenuates the effect of KIFC3 on PI3K/AKT/mTOR pathway in CRC cells. **(A)** The expression of the related factors in the PI3K/AKT/mTOR pathway was reversed to some extent under the effect of LY294002 and Triciribine. **(B,C)** Quantification to the protein level of the related factors in the PI3K/AKT/mTOR pathway. The data are presented as the mean ± standard deviation of triplicate independent experiments and were normalized to the control group. $^{*}p < 0.05$; $^{**}p < 0.01$; $^{***}p < 0.001$; $^{****}p < 0.0001$.

a key role in the G1-S transition, while Cyclin A-CDK2 palys a key role in S-phase progression (Lee et al., 2013). Defects in many molecules that regulate the cell cycle also contribute to tumor progression. The factor p21, as a CDK inhibitor, is known to be mediated in the regulation of the cell cycle in cancer cells (Park W. et al., 2019). Expression of p21 is mediated by p53 and is essential for DNA-damage-induced cell cycle arrest (Sidor-Kaczmarek et al., 2017). The factor p53, as a tumor suppressor factor, suppresses cell growth, migration, and invasion. Not only does p21 serve as a downstream mediator of p53, but it also cooperates with p53 to suppress cell invasion (Kim et al., 2017). PCNA is a cofactor of DNA polymerases, which is involved in DNA synthesis during genome replication in the S phase of the cell cycle and is used as a marker reflecting the activity of cell proliferation (Lee et al., 2019). Collectively, we hypothesize that the KIFC3 increases the proliferation of CRC cells.

The misregulation of KIFs may contribute to uncontrolled cell growth, highlighting their involvement in tumorigenesis on the course of the cell cycle (Lucanus and Yip, 2018). The resulting daughter cells may exhibit cancerous behavior, including the ability of increased metastasis (Almeida and Maiato, 2018; Lucanus and Yip, 2018). The invasion and migration of tumors are the main reasons leading to the failure of tumor treatment and poor prognosis, which cause low 5-year survival rates (Zhan et al., 2020; Zhao et al., 2020). In tumorigenesis and metastasis, EMT plays a critical role. During EMT, epithelial tumor cells undergo distinct morphological and phenotypic changes, including loss of tight junctions, cell polarity and cytoskeletal reorganization, which renders cells more invasive properties and phenotypes. During metastasis, down-regulation of epithelial-associated marker proteins and up-regulation of mesenchymal marker proteins induce cell adhesion to the stroma and enhance tumor cell invasiveness. Vimentin is an intermediate filament protein and a mesenchymal marker of fibrosis. Snail as a mesenchymal marker protein affects the ability of cancer cells to invade the surrounding tissue. There is an evidence that TWIST1 upregulates vimentin expression in EMT (Meng et al., 2018). The loss of intercellular adhesion makes it easy for tumor cells to migrate and invade,

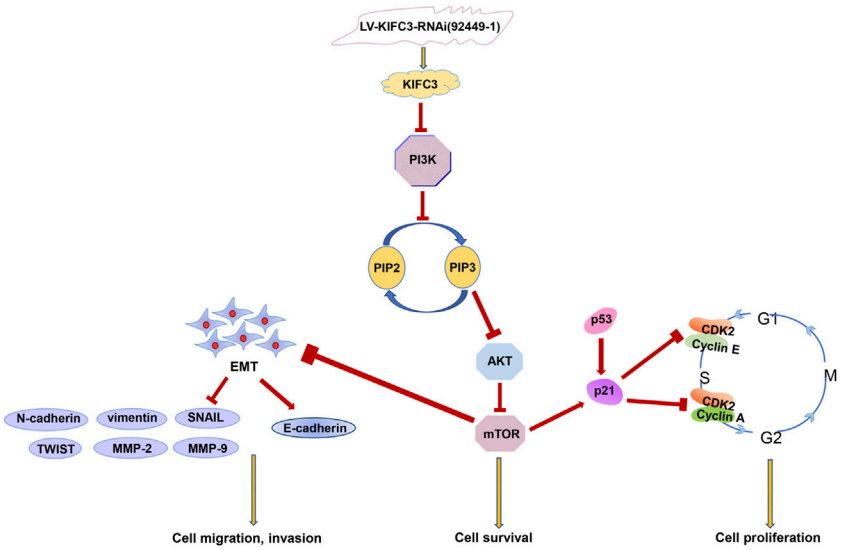


FIGURE 15 | The relationship between KIFC3 and thePI3K/AKT/mTOR pathway.

eventually leading to metastatic dissemination (Liu et al., 2018). In order to penetrate into neighboring tissues and metastasize to distant organs, cancer cells require the motility and degradation of the extracellular matrix (ECM). Under this condition, certain types of ECM-degrading enzymes play a critical role in promoting the migration and subsequent metastasis of cancer cells (Pan et al., 2013). Cancer cells often release matrix metalloproteinase (MMPs), which can degrade ECM proteins. Among them, MMP-2 and MMP-9 are highly-expressed in malignant tumors, and have been proved to have participated in degradation of the ECM, a crucial component of the basal membrane, leading to cancer metastasis (Wu et al., 2019). Increased cell motility, along with the ability to digest ECM, affords cancer cells greater ability to invade tissues, leading to metastasis and diffuse tissue dissemination. Nakamura et al. (2007) established a gastric cancer cell line stably expressing KIF2C, it was found that cells transfected withKIF2C had a high rate of proliferation and increased migratory ability compared to mock-transfected cells. In our study, we found that not only the number of invading cells but also the number of migrating cells were less in the knockdown of KIFC3 group than control and NC groups. Conversely, both the number of invading and migrating cells in the KIFC3 overexpression group was higher than that in the Control and NC groups. As shown by western blot assay, KIFC3 increased the protein content of MMP-2, MMP-9 and mesenchymal associated markers, decreased the protein level of associated markers. These findings may be attributed to the fact that KIFC3 serves a key role in facilitating tumor cell invasiveness and metastasis by regulating MMP-2, MMP-9 and EMT-associated marker proteins expression.

The PI3K/AKT/mTOR pathway not only plays a vital role in physiologically cell biology but has also been identified as a growing target for tumor therapy (Dey et al., 2019; Reddy et al., 2019; Wang et al., 2019; Mannella et al., 2021). Increasing researches have reported that the PI3K/AKT/mTOR molecular signaling pathways play an essential role in the development and progression of CRC which regulate cell survival, growth, proliferation, angiogenesis, invasion, migration and glucose metabolism (Park S. H. et al., 2019; Deng et al., 2019; Jin et al., 2020; Smit et al., 2020). PI3K belongs to lipid kinases family that activated by a large number of RTKs, once stimulated, can produce phosphotidylinositol-4,5-bisphosphate (PIP2) and phosphatidylinositol-3,4,5- trisphosphate (PIP3). PIP3 plays a key role in cell growth and survival by activating downstream signaling pathways through AKT. AKT, also called as protein kinase B (PKB), when the double-phosphorylated AKT separates from the membrane, thus resulting in the activation of mTOR complex, which activates the translation of proteins, enhances cell growth, promotes cell proliferation and cell metabolism. Additionally, the complex of mTOR could exert its positive feedback and then enhance the basal phosphorylation of AKT. It has been reported that Akt plays a critical role on post-transcription of Vimentin, which is involved in the EMT process (Zhuang et al., 2012; Treesuwan et al., 2018). Also, researchers found that KIFs help to cross-link vimentin in microtentacles, which are important for cancer metastasis (Lucanus and Yip, 2018). Current researchers showed that activation of the PI3K/AKT/mTOR pathway could facilitate the process of EMT, thus increasing the metastatic ability of tumor cells. In this study, we evaluated the effects of KIFC3 on the PI3K/AKT/mTOR pathway in CRC cells. Our research data indicate that the phosphorylation levels of PI3K, AKT and mTOR were significantly increased in KIFC3-overexpressing cells, while t-PI3K, t-AKT, and t-mTOR levels had no change. The opposite trend was shown in the KIFC3-depletion groups. In order to further elucidate whether the effect of KIFC3 on CRC cells is related to PI3K/AKT/mTOR pathway, LY294002 (an inhibitor of PI3K/AKT/mTOR pathway) and Triciribine (an inhibitor of AKT) was used to treat KIFC3-overexpressing cells individually. The results showed that LY294002 and Triciribine significantly attenuated the tumor-promoting effect

of KIFC3 on CRC cells. We speculate that overexpress of KIFC3 may promote the proliferation, migration and invasion on CRC cells, by activating the PI3K/AKT/mTOR pathway.

In summary, our study presented here demonstrates, for the first time, that an increased KIFC3 expression is correlated with the proliferation, migration and invasion of CRC cells through regulating the EMT process *via* the PI3K/AKT/mTOR signal transduction pathway. Therefore, we propose that KIFC3 is an important protein in the development of CRC. KIFC3 may be a promising biomarker that provides a new perspective into human CRC treatment, as well as targeting KIFs therapy seems to be a promising anti-cancer strategy.

DATA AVAILABILITY STATEMENT

The original contributions presented in the study are included in the article/**Supplementary Material**, further inquiries can be directed to the corresponding author.

ETHICS STATEMENT

The animal study was reviewed and approved by The Animal Care and Use Committees of Renmin Hospital of Wuhan University (WDRM 20190301).

AUTHOR CONTRIBUTIONS

HL and LZ performed the experiments; SL and WL analyzed the data; HL wrote the manuscript; WD conceived the study design and revised the paper. All the authors read and approved the final manuscript.

FUNDING

A research grant from the National Natural Science Foundation of China (NO. 81870392, NO.82000521) and Key R&D projects in Hubei Province (2020BCA066) supported this research.

ACKNOWLEDGMENTS

The authors thank Qiong Ding from the Central Laboratory, Renmin Hospital of Wuhan University, and Mingxia Fan from the Animal Experiment Center, Renmin Hospital of Wuhan University for their laboratory assistance, help, advice, and support.

SUPPLEMENTARY MATERIAL

The Supplementary Material for this article can be found online at: https://www.frontiersin.org/articles/10.3389/fgene.2022.848926/full#supplementary-material

REFERENCES

Almeida, A. C., and Maiato, H. (2018). Chromokinesins. *Curr. Biol.* 28 (19), R1131–r1135. doi:10.1016/j.cub.2018.07.017

Ashar, Y. V., Zhou, J., Gupta, P., Teng, Q.-X., Lei, Z.-N., Reznik, S. E., et al. (2020). BMS-599626, a Highly Selective Pan-HER Kinase Inhibitor, Antagonizes ABCG2-Mediated Drug Resistance. *Cancers* 12 (9), 2502. doi:10.3390/cancers12092502

Chen, X., Wei, B., Han, X., Zheng, Z., Huang, J., Liu, J., et al. (2014). LGR5 Is Required for the Maintenance of Spheroid-Derived Colon Cancer Stem Cells. *Int. J. Mol. Med.* 34 (1), 35–42. doi:10.3892/ijmm.2014.1752

De, S., Cipriano, R., Jackson, M. W., and Stark, G. R. (2009). Overexpression of Kinesins Mediates Docetaxel Resistance in Breast Cancer Cells. *Cancer Res.* 69 (20), 8035–8042. doi:10.1158/0008-5472.Can-09-1224

Dekker, E., Tanis, P. J., Vleugels, J. L. A., Kasi, P. M., and Wallace, M. B. (2019). Colorectal Cancer. *Lancet* 394 (10207), 1467–1480. doi:10.1016/s0140-6736(19)32319-0

Deng, F., Zhou, R., Lin, C., Yang, S., Wang, H., Li, W., et al. (2019). Tumor-secreted Dickkopf2 Accelerates Aerobic Glycolysis and Promotes Angiogenesis in Colorectal Cancer. *Theranostics* 9 (4), 1001–1014. doi:10.7150/thno.30056

Dey, P., Son, J. Y., Kundu, A., Kim, K. S., Lee, Y., Yoon, K., et al. (2019). Knockdown of Pyruvate Kinase M2 Inhibits Cell Proliferation, Metabolism, and Migration in Renal Cell Carcinoma. *Int. J. Mol. Sci.* 20 (22), 5622. doi:10.3390/ijms20225622

Hao, T., Xu, J., Fang, S., Jiang, J., Chen, X., Wu, W., et al. (2021). Overexpression of ZNF460 Predicts Worse Survival and Promotes Metastasis through JAK2/STAT3 Signaling Pathway in Patient with Colon Cancer. *J. Cancer* 12 (11), 3198–3208. doi:10.7150/jca.55079

Hirokawa, N., and Tanaka, Y. (2015). Kinesin Superfamily Proteins (KIFs): Various Functions and Their Relevance for Important Phenomena in Life and Diseases. *Exp. Cell Res.* 334 (1), 16–25. doi:10.1016/j.yexcr.2015.02.016

Hoang, E. H., Whitehead, J. L., Dosé, A. C., and Burnside, B. (1998). Cloning of a Novel C-Terminal Kinesin (KIFC3) that Maps to Human Chromosome 16q13-Q21 and Thus Is a Candidate Gene for Bardet-Biedl Syndrome. *Genomics* 52 (2), 219–222. doi:10.1006/geno.1998.5431

Ishikawa, K., Kawano, Y., Arihara, Y., Kubo, T., Takada, K., Murase, K., et al. (2019). BH3 Profiling Discriminates the Anti-apoptotic S-tatus of 5-fluorouracil-resistant C-olon C-ancer C-ells. *Oncol. Rep.* 42 (6), 2416–2425. doi:10.3892/or.2019.7373

Jin, G., Zhao, Z., Chakraborty, T., Mandal, A., Roy, A., Roy, S., et al. (2020). Decrypting the Molecular Mechanistic Pathways Delineating the Chemotherapeutic Potential of Ruthenium-Phloretin Complex in Colon Carcinoma Correlated with the Oxidative Status and Increased Apoptotic Events. *Oxidative Med. Cell. Longev.* 2020, 1–24. doi:10.1155/2020/7690845

Jin, Q., Dai, Y., Wang, Y., Zhang, S., and Liu, G. (2019). High Kinesin Family Member 11 Expression Predicts Poor Prognosis in Patients with Clear Cell Renal Cell Carcinoma. *J. Clin. Pathol.* 72 (5), 354–362. doi:10.1136/jclinpath-2018-205390

Kanehira, M., Katagiri, T., Shimo, A., Takata, R., Shuin, T., Miki, T., et al. (2007). Oncogenic Role of MPHOSPH1, a Cancer-Testis Antigen Specific to Human Bladder Cancer. *Cancer Res.* 67 (7), 3276–3285. doi:10.1158/0008-5472.Can-06-3748

Kim, E. M., Jung, C.-H., Kim, J., Hwang, S.-G., Park, J. K., and Um, H.-D. (2017). The P53/p21 Complex Regulates Cancer Cell Invasion and Apoptosis by Targeting Bcl-2 Family Proteins. *Cancer Res.* 77 (11), 3092–3100. doi:10.1158/0008-5472.Can-16-2098

Kometani, T., Arai, T., and Chibazakura, T. (2020). Increased Expression of NPM1 Suppresses p27Kip1 Function in Cancer Cells. *Cancers* 12 (10), 2886. doi:10.3390/cancers12102886

Lee, C. C., Wang, J. W., Leu, W. M., Huang, Y. T., Huang, Y. W., Hsu, Y. H., et al. (2019). Proliferating Cell Nuclear Antigen Suppresses RNA Replication of Bamboo Mosaic Virus through an Interaction with the Viral Genome. *J. Virol.* 93 (22). doi:10.1128/jvi.00961-19

Lee, Y.-S., Choi, K.-M., Kim, W., Jeon, Y.-S., Lee, Y.-M., Hong, J.-T., et al. (2013). Hinokitiol Inhibits Cell Growth through Induction of S-phase Arrest and Apoptosis in Human Colon Cancer Cells and Suppresses Tumor Growth in

a Mouse Xenograft Experiment. *J. Nat. Prod.* 76 (12), 2195–2202. doi:10.1021/np4005135

Li, B., Hong, P., Zheng, C.-C., Dai, W., Chen, W.-Y., Yang, Q.-S., et al. (2019). Identification of miR-29c and its Target FBXO31 as a Key Regulatory Mechanism in Esophageal Cancer Chemoresistance: Functional Validation and Clinical Significance. *Theranostics* 9 (6), 1599–1613. doi:10.7150/thno.30372

Li, G., Chen, J., Li, S., Zhou, S., Cao, S., Lou, Y., et al. (2017). Kinesin Superfamily Protein Expression and its Association with Progression and Prognosis in Hepatocellular Carcinoma. *J. Can. Res. Ther.* 13 (4), 651–659. doi:10.4103/jcrt.JCRT_491_17

Li, J., and Bakhoum, S. F. (2019). Expanding the Role of STING in Cellular Homeostasis and Transformation. *Trends Cancer* 5 (4), 195–197. doi:10.1016/j.trecan.2019.02.001

Li, X., Huang, W., Huang, W., Wei, T., Zhu, W., Chen, G., et al. (2020b). Kinesin Family Members KIF2C/4A/10/11/14/18B/20A/23 Predict Poor Prognosis and Promote Cell Proliferation in Hepatocellular Carcinoma. *Am. J. Transl. Res.* 12 (5), 1614–1639.

Li, X., Wen, D., Li, X., Yao, C., Chong, W., and Chen, H. (2020a). Identification of an Immune Signature Predicting Prognosis Risk and Lymphocyte Infiltration in Colon Cancer. *Front. Immunol.* 11, 1678. doi:10.3389/fimmu.2020.01678

Liu, L., Zhang, Y., Wong, C. C., Zhang, J., Dong, Y., Li, X., et al. (2018). RNF6 Promotes Colorectal Cancer by Activating the Wnt/β-Catenin Pathway via Ubiquitination of TLE3. *Cancer Res.* 78 (8), 1958–1971. doi:10.1158/0008-5472.Can-17-2683

Liu, X., Gong, H., and Huang, K. (2013). Oncogenic Role of Kinesin Proteins and Targeting Kinesin Therapy. *Cancer Sci.* 104 (6), 651–656. doi:10.1111/cas.12138

Lucanus, A. J., and Yip, G. W. (2018). Kinesin Superfamily: Roles in Breast Cancer, Patient Prognosis and Therapeutics. *Oncogene* 37 (7), 833–838. doi:10.1038/onc.2017.406

Ma, R.-R., Zhang, H., Chen, H.-F., Zhang, G.-H., Tian, Y.-R., and Gao, P. (2021). MiR-19a/miR-96-mediated Low Expression of KIF26A Suppresses Metastasis by Regulating FAK Pathway in Gastric Cancer. *Oncogene* 40 (14), 2524–2538. doi:10.1038/s41388-020-01610-7

Mannella, V., Boehm, K., Celik, S., Ali, T., Mirza, A. N., El Hasnaouy, M., et al. (2021). Growth and Viability of Cutaneous Squamous Cell Carcinoma Cell Lines Display Different Sensitivities to Isoform-specific Phosphoinositide 3-Kinase Inhibitors. *Int. J. Mol. Sci.* 22 (7), 3567. doi:10.3390/ijms22073567

Meng, J., Chen, S., Han, J.-X., Qian, B., Wang, X.-R., Zhong, W.-L., et al. (2018). Twist1 Regulates Vimentin through Cul2 Circular RNA to Promote EMT in Hepatocellular Carcinoma. *Cancer Res.* 78 (15), 4150–4162. doi:10.1158/0008-5472.Can-17-3009

Miki, H., Setou, M., and Hirokawa, N. (2003). Kinesin Superfamily Proteins (KIFs) in the Mouse Transcriptome. *Genome Res.* 13 (6b), 1455–1465. doi:10.1101/gr.984503

Minisy, F. M., Shawki, H. H., El Omri, A., Massoud, A. A., Omara, E. A., Metwally, F. G., et al. (2020). Pomegranate Seeds Extract Possesses a Protective Effect against Tramadol-Induced Testicular Toxicity in Experimental Rats. *BioMed Res. Int.* 2020, 1–12. doi:10.1155/2020/2732958

Moamer, A., Hachim, I. Y., Binothman, N., Wang, N., Lebrun, J.-J., and Ali, S. (2019). A Role for Kinesin-1 Subunits KIF5B/KLC1 in Regulating Epithelial Mesenchymal Plasticity in Breast Tumorigenesis. *EBioMedicine* 45, 92–107. doi:10.1016/j.ebiom.2019.06.009

Nakamura, Y., Tanaka, F., Haraguchi, N., Mimori, K., Matsumoto, T., Inoue, H., et al. (2007). Clinicopathological and Biological Significance of Mitotic Centromere-Associated Kinesin Overexpression in Human Gastric Cancer. *Br. J. Cancer* 97 (4), 543–549. doi:10.1038/sj.bjc.6603905

Noda, Y., Okada, Y., Saito, N., Setou, M., Xu, Y., Zhang, Z., et al. (2001). KIFC3, a Microtubule Minus End-Directed Motor for the Apical Transport of Annexin XIIIb-Associated Triton-Insoluble Membranes. *J. Cell Biol.* 155 (1), 77–88. doi:10.1083/jcb.200108042

Pan, G., Zhu, Z., Huang, J., Yang, C., Yang, Y., Wang, Y., et al. (2013). Semaphorin 5A Promotes Gastric Cancer Invasion/metastasis via Urokinase-type Plasminogen Activator/phosphoinositide 3-kinase/protein Kinase B. *Dig. Dis. Sci.* 58 (8), 2197–2204. doi:10.1007/s10620-013-2666-1

Park, S. H., Jo, M. J., Kim, B. R., Jeong, Y. A., Na, Y. J., Kim, J. L., et al. (2019a). Sonic Hedgehog Pathway Activation Is Associated with Cetuximab Resistance and EPHB3 Receptor Induction in Colorectal Cancer. *Theranostics* 9 (8), 2235–2251. doi:10.7150/thno.30678

Park, W., Park, S., Song, G., and Lim, W. (2019b). Inhibitory Effects of Osthole on Human Breast Cancer Cell Progression via Induction of Cell Cycle Arrest, Mitochondrial Dysfunction, and ER Stress. *Nutrients* 11 (11), 2777. doi:10.3390/nu11112777

Reddy, D., Kumavath, R., Ghosh, P., and Barh, D. (2019). Lanatoside C Induces G2/M Cell Cycle Arrest and Suppresses Cancer Cell Growth by Attenuating MAPK, Wnt, JAK-STAT, and PI3K/AKT/mTOR Signaling Pathways. *Biomolecules* 9 (12). doi:10.3390/biom9120792

Seog, D.-H., Lee, D.-H., and Lee, S.-K. (2004). Molecular Motor Proteins of the Kinesin Superfamily Proteins (KIFs): Structure, Cargo and Disease. *J. Korean Med. Sci.* 19 (1), 1–7. doi:10.3346/jkms.2004.19.1.1

Shi, Q., Li, Y., Li, S., Jin, L., Lai, H., Wu, Y., et al. (2020). LncRNA DILA1 Inhibits Cyclin D1 Degradation and Contributes to Tamoxifen Resistance in Breast Cancer. *Nat. Commun.* 11 (1), 5513. doi:10.1038/s41467-020-19349-w

Sidor-Kaczmarek, J., Cichorek, M., Spodnik, J. H., Wójcik, S., and Moryś, J. (2017). Proteasome Inhibitors against Amelanotic Melanoma. *Cell Biol. Toxicol.* 33 (6), 557–573. doi:10.1007/s10565-017-9390-0

Siegel, R. L., Miller, K. D., Goding Sauer, A., Fedewa, S. A., Butterly, L. F., Anderson, J. C., et al. (2020). Colorectal Cancer Statistics, 2020. *CA A Cancer J. Clin.* 70 (3), 145–164. doi:10.3322/caac.21601

Smit, D. J., Cayrefourcq, L., Haider, M.-T., Hinz, N., Pantel, K., Alix-Panabières, C., et al. (2020). High Sensitivity of Circulating Tumor Cells Derived from a Colorectal Cancer Patient for Dual Inhibition with AKT and mTOR Inhibitors. *Cells* 9 (9), 2129. doi:10.3390/cells9092129

Sung, H., Ferlay, J., Siegel, R. L., Laversanne, M., Soerjomataram, I., Jemal, A., et al. (2021). Global Cancer Statistics 2020: GLOBOCAN Estimates of Incidence and Mortality Worldwide for 36 Cancers in 185 Countries. *CA A Cancer J. Clin.* 71 (3), 209–249. doi:10.3322/caac.21660

Tan, M. H., De, S., Bebek, G., Orloff, M. S., Wesolowski, R., Downs-Kelly, E., et al. (2012). Specific Kinesin Expression Profiles Associated with Taxane Resistance in Basal-like Breast Cancer. *Breast Cancer Res. Treat.* 131 (3), 849–858. doi:10.1007/s10549-011-1500-8

Tian, L., Lu, Y., Yang, T., Deng, Z., Xu, L., Yao, W., et al. (2019). aPKCι Promotes Gallbladder Cancer Tumorigenesis and Gemcitabine Resistance by Competing with Nrf2 for Binding to Keap1. *Redox Biol.* 22, 101149. doi:10.1016/j.redox.2019.101149

Treesuwan, S., Sritularak, B., Chanvorachote, P., and Pongrakhananon, V. (2018). Cypripedin Diminishes an Epithelial-To-Mesenchymal Transition in Non-small Cell Lung Cancer Cells through Suppression of Akt/GSK-3β Signalling. *Sci. Rep.* 8 (1), 8009. doi:10.1038/s41598-018-25657-5

Wan, Q., Shen, Y., Zhao, H., Wang, B., Zhao, L., Zhang, Y., et al. (2019). Impaired DNA Double-strand Breaks Repair by Kinesin Family Member 4A Inhibition Renders Human H1299 Non-small-cell Lung Cancer Cells Sensitive to Cisplatin. *J. Cell. Physiology* 234 (7), 10360–10371. doi:10.1002/jcp.27703

Wang, C., Wang, C., Wei, Z., Li, Y., Wang, W., Li, X., et al. (2015). Suppression of Motor Protein KIF3C Expression Inhibits Tumor Growth and Metastasis in Breast Cancer by Inhibiting TGF-β Signaling. *Cancer Lett.* 368 (1), 105–114. doi:10.1016/j.canlet.2015.07.037

Wang, K., Lin, C., Wang, C., Shao, Q., Gao, W., Song, B., et al. (2014). Silencing Kif2a Induces Apoptosis in Squamous Cell Carcinoma of the Oral Tongue through Inhibition of the PI3K/Akt Signaling Pathway. *Mol. Med. Rep.* 9 (1), 273–278. doi:10.3892/mmr.2013.1804

Wang, L.-L., Zhang, L., and Cui, X.-F. (2019). RETRACTED: Downregulation of Long Noncoding RNA LINC01419 Inhibits Cell Migration, Invasion, and Tumor Growth and Promotes Autophagy via Inactivation of the PI3K/Akt1/mTOR Pathway in Gastric Cancer. *Ther. Adv. Med. Oncol.* 11, 175883591987465. doi:10.1177/1758835919874651

Wu, Y. J., Lin, S. H., Din, Z. H., Su, J. H., and Liu, C. I. (2019). Sinulariolide Inhibits Gastric Cancer Cell Migration and Invasion through Downregulation of the EMT Process and Suppression of FAK/PI3K/AKT/mTOR and MAPKs Signaling Pathways. *Mar. Drugs* 17 (12), 668. doi:10.3390/md17120668

Xu, Y., Takeda, S., Nakata, T., Noda, Y., Tanaka, Y., and Hirokawa, N. (2002). Role of KIFC3 Motor Protein in Golgi Positioning and Integration. *J. Cell Biol.* 158 (2), 293–303. doi:10.1083/jcb.200202058

Zhan, K., Liu, R., Tong, H., Gao, S., Yang, G., Hossain, A., et al. (2020). Fetuin B Overexpression Suppresses Proliferation, Migration, and Invasion in Prostate Cancer by Inhibiting the PI3K/AKT Signaling Pathway. *Biomed. Pharmacother.* 131, 110689. doi:10.1016/j.biopha.2020.110689

Zhao, F., Feng, Y., Zhang, X., Liu, X., and Li, A. (2020). Kinesin Superfamily Member 18B (KIF18B) Promotes Cell Proliferation in Colon Adenocarcinoma. *Cancer Manag. Res.* 12, 12769–12778. doi:10.2147/cmar.S261894

Zhou, G., Yang, J., and Song, P. (2019). Correlation of ERK/MAPK Signaling Pathway With Proliferation and Apoptosis of Colon Cancer Cells. *Oncol. Lett.* 17 (2), 2266–2270. doi:10.3892/ol.2018.9857

Zhuang, S., Duan, M., and Yan, Y. (2012). Src Family Kinases Regulate Renal Epithelial Dedifferentiation through Activation of EGFR/PI3K Signaling. *J. Cell. Physiol.* 227 (5), 2138–2144. doi:10.1002/jcp.22946

Conflict of Interest: The authors declare that the research was conducted in the absence of any commercial or financial relationships that could be construed as a potential conflict of interest.

Publisher's Note: All claims expressed in this article are solely those of the authors and do not necessarily represent those of their affiliated organizations, or those of the publisher, the editors and the reviewers. Any product that may be evaluated in this article, or claim that may be made by its manufacturer, is not guaranteed or endorsed by the publisher.

Copyright © 2022 Liao, Zhang, Lu, Li and Dong. This is an open-access article distributed under the terms of the Creative Commons Attribution License (CC BY). The use, distribution or reproduction in other forums is permitted, provided the original author(s) and the copyright owner(s) are credited and that the original publication in this journal is cited, in accordance with accepted academic practice. No use, distribution or reproduction is permitted which does not comply with these terms.

frontiers | Frontiers in Genetics

SYSTEMATIC REVIEW
published: 27 June 2022
doi: 10.3389/fgene.2022.860727

Association Between *GSDMB* Gene Polymorphism and Cervical Cancer in the Northeast Chinese Han Population

Songxue Li[1†], Xiaoying Li[2†], Shuang Zhang[2], Yanan Feng[2], Tianshuang Jia[1], Manning Zhu[1], Lei Fang[2], Liping Gong[2], Shuang Dong[2], Xianchao Kong[3], Zhenzhen Wang[1] and Litao Sun[1]**

[1]Cancer Center, Department of Ultrasound Medicine, Zhejiang Provincial People's Hospital, Hangzhou, China, [2]Department of Ultrasound, The 2nd Affiliated Hospital of Harbin Medical University, Harbin, China, [3]Department of Obstetrics and Gynecology, The 2nd Affiliated Hospital of Harbin Medical University, Harbin, China

Objective: The purpose of this study was to investigate the relationship between *GSDMB* gene polymorphism and genetic susceptibility to cervical cancer in the Han population in Northeast China.

Methods: In this case–control study, the genotypes and alleles of rs8067378 in the *GSDMB* gene were analyzed by multiplex polymerase chain reaction (PCR) and next-generation sequencing methods in 482 cervical cancer (CC) patients, 775 cervical squamous intraepithelial lesion (SIL) patients, and 495 healthy women. The potential relationships between the SNP of the *GSDMB* gene with SIL and CC were analyzed by multivariate logistic regression analysis combined with 10,000 permutation tests.

Results: In the comparison between the SIL group and the control group, the genotype and allele distribution frequencies of rs8067378 SNP of the *GSDMB* gene were statistically significant ($p = 0.0493$ and $p = 0.0202$, respectively). The allele distribution frequencies of rs8067378 were also statistically significant in the comparison between high-grade cervical squamous intraepithelial lesion (HSIL) and low-grade cervical squamous intraepithelial lesion (LSIL) groups with control group ($p = 0.0483$ and $p = 0.0330$, respectively). Logistic regression analysis showed that after adjusting for age, the rs8067378 SNP of the *GSDMB* gene was significantly associated with the reduced risk of SIL under the dominant model ($p = 0.0213$, OR = 0.764, CI = 0.607–0.961) and the additive model ($p = 0.0199$, OR = 0.814, and CI = 0.684–0.968), and its mutant gene G may play a role in the progression of healthy people to LSIL and even HSIL as a protective factor. However, there was no significant association between cervical cancer and its subtypes with the control group ($p > 0.05$). After 10,000 permutations, there was still no correlation that has provided evidence for the accuracy of our study.

Conclusion: The results of this study showed that rs8067378 single nucleotide polymorphism of the *GSDMB* gene may reduce the risk of SIL and protect the susceptibility to cervical precancerous lesions in the Northeast Chinese Han population, but it has no significant correlation with the progression of cervical cancer.

Keywords: cervical cancer, cervical squamous intraepithelial lesion, pyrocytosis, GSDMB, SNP

OPEN ACCESS

Edited by:
Ayan Biswas, University of Alabama at Birmingham, United States

Reviewed by:
Jiajun Shi, Vanderbilt University Medical Center, United States
Juan Carlos Fernandez-Lopez, Instituto Nacional de Medicina Genómica (INMEGEN), Mexico

***Correspondence:**
Litao Sun
litaosun1971@aliyun.com
Zhenzhen Wang
welcomezhen126@126.com

†These authors share first authorship

Specialty section:
This article was submitted to Cancer Genetics and Oncogenomics, a section of the journal Frontiers in Genetics

Received: *23 January 2022*
Accepted: *26 April 2022*
Published: *27 June 2022*

Citation:
Li S, Li X, Zhang S, Feng Y, Jia T, Zhu M, Fang L, Gong L, Dong S, Kong X, Wang Z and Sun L (2022) Association Between GSDMB Gene Polymorphism and Cervical Cancer in the Northeast Chinese Han Population. Front. Genet. 13:860727. doi: 10.3389/fgene.2022.860727

1 INTRODUCTION

Cervical cancer is the fourth most frequently diagnosed cancer and the fourth leading cause of cancer death in women. It is estimated that by 2020, there were 604,000 new cases and 342,000 deaths in the world (Sung et al., 2021). The progression of cervical cancer is a complex process with multiple steps and factors. In addition to the risk factors such as long-term chronic inflammation caused by high-risk human papillomavirus (HPV) persistent infection, long-term oral contraceptives, and fertility and sexual life disorder, the occurrence of cervical cancer also has obvious individual genetic susceptibility (Nkfusai et al., 2019; Olusola et al., 2019; Sadri Nahand et al., 2020; van der Waal et al., 2020; Yang et al., 2020). Single nucleotide polymorphism (SNP) is the most common form of genetic variation, which widely exists in the human genome and is related to the susceptibility to a variety of cancers such as cervical cancer. Therefore, the study of SNP will also contribute to the early diagnosis and treatment of cervical cancer (Shastry, 2009; Tan, 2017).

Gasdermin B (GSDMB) is a member of the GSDM protein superfamily that exists only in vertebrates. The *GSDMB* gene, located on chromosome 17q21.2, has a conserved gasdermin domain, a potential nuclear localization signal, and two nuclear receptor-binding motifs LXX(L/I)L. It is 1518 bp length and encodes 411 amino acids. It is often expressed in normal esophageal and gastrointestinal epithelium and bronchial epithelium of asthmatic lungs (Sun et al., 2008; Zheng et al., 2020). GSDMB has six splice variants, and GSDMB-1 is the longest and most important subtype which is expressed in human cancer cell lines (Feng et al., 2018).

Recently, several studies have identified that the expression of GSDMB has a potential relationship with the occurrence and development of tumors. GSDMB can regulate its lipid binding and pore-forming activity through different mechanisms of the intramolecular domain and then participate in pyrocytosis (Chen et al., 2019; Li et al., 2020). Pyrocytosis is a pro-inflammatory form that regulates cell death. Its essence is a

TABLE 1 | Clinical characteristics in the control group with the CC and SIL groups.

	Control	CC	SIL	P1	P2	P3
Age (years)	39.44 ± 8.22	49.33 ± 9.29	42.22 ± 9.68	**<0.0001**	**<0.0001**	**<0.0001**
Menarche age (years)	--	14.92 ± 1.86	14.61 ± 1.90	--	--	**0.0058**
Amenorrhea n (%)	--	216 (44.8%)	148 (19.1%)	--	--	**<0.0001**
Smoking n (%)	--	30 (6.22%)	23 (2.97%)	--	--	**0.0091**
Drinking n (%)	--	4 (0.83%)	4 (0.52%)	--	--	0.4952

CC, cervical cancer; SIL, cervical squamous intraepithelial lesion.
p-*value (P1, comparison of controls with CC; P2, comparison of controls with SIL; P3, comparison of CC with SIL).*
p *values < 0.05 are considered statistically significant, and shown in bold.*

TABLE 2 | Comparison of genotypes and allele distribution frequencies between the CC group and its subgroups with the healthy control group.

Genotype and allele	Control	Case	P	OR [95% CI]	Statistical model	P′	P′′	OR [95% CI]
	Controls (n= 495)	CC(n = 482)						
AA	259 (52.3%)	235 (48.8%)			Dominant	0.2054	0.2095	0.829[0.620–1.108]
AG	189 (38.2%)	199 (41.3%)			Recessive	0.5305	0.5327	0.852[0.516–1.406]
GG	47 (9.49%)	48 (9.96%)	0.5322		Additive	0.2132	0.2088	0.868[0.696–1.084]
A	707 (71.4%)	669 (69.4%)						
G	283 (28.6%)	295 (30.6%)	0.3290	0.908[0.747–1.102]				
	Controls (n= 495)	SCC (n = 416)						
AA	259 (52.3%)	204 (49.0%)			Dominant	0.2967	0.2968	0.851[0.628–1.152]
AG	189 (38.2%)	169 (40.6%)			Recessive	0.4040	0.4110	0.801[0.476–1.348]
GG	47 (9.49%)	43 (10.3%)	0.6110		Additive	0.2443	0.2437	0.872[0.692–1.098]
A	707 (71.4%)	577 (69.4%)						
G	283 (28.6%)	255 (30.6%)	0.3362	1.104[0.902–1.351]				
	Controls (n= 495)	AUC(n = 36)						
AA	259 (52.3%)	16 (44.4%)			Dominant	0.2542	0.2631	0.659[0.321–1.350]
AG	189 (38.2%)	16 (44.4%)			Recessive	0.5203	0.5204	0.680[0.209–2.207]
GG	47 (9.49%)	4 (11.1%)	0.6589		Additive	0.2441	0.2462	0.727[0.425–1.243]
A	707 (71.4%)	48 (66.7%)						
G	283 (28.6%)	24 (33.3%)	0.3909	0.801[0.481–1.332]				

CC, cervical cancer; SCC, squamous carcinoma of cervical; AUC, adenocarcinoma of the uterine cervical; OR, odds ratio; CI, confidence interval.
P: p-*value (control vs. CC; control vs. SCC; control vs. AUC);* p-*values <0.05 are shown in bold.*
P′: age was adjusted.
P″: the p-*value was calculated using 10,000 permutations for each model to correct the multiple tests.*

TABLE 3 | Comparison of genotypes and allele distribution frequencies between the SIL group and its subgroups with the healthy control group.

Genotype and allele	Control	Case	P	OR [95% CI]	Statistical model	P′	P′′	OR [95% CI]
	Control (n= 495)	SIL (n = 775)						
AA	259 (52.3%)	351 (45.3%)			Dominant	**0.0213**	**0.0228**	0.764[0.607–0.961]
AG	189 (38.2%)	337 (43.5%)			Recessive	0.1861	0.1881	0.773[0.528–1.132]
GG	47 (9.49%)	87 (11.2%)	**0.0493**		Additive	**0.0199**	**0.0208**	0.814[0.684–0.968]
A	707 (71.4%)	1,039 (67.0%)						
G	283 (28.6%)	511 (33.0%)	**0.0202**	0.814[0.684–0.968]				
	Control (n= 495)	HSIL (n = 619)						
AA	259 (52.3%)	283 (45.7%)			Dominant	**0.0356**	**0.0366**	0.773[0.608–0.983]
AG	189 (38.2%)	270 (43.6%)			Recessive	0.3067	0.3102	0.811[0.543–1.211]
GG	47 (9.49%)	66 (10.7%)	0.0903		Additive	**0.0406**	**0.0401**	0.827[0.689–0.992]
A	707 (71.4%)	836 (67.5%)						
G	283 (28.6%)	402 (32.5%)	**0.0483**	0.832[0.694–0.999]				
	Control (n= 495)	LSIL (n = 156)						
AA	259 (52.3%)	68 (43.6%)			Dominant	0.0631	0.0633	0.702[0.484–1.019]
AG	189 (38.2%)	67 (42.9%)			Recessive	0.0928	0.0916	0.614[0.348–1.084]
GG	47 (9.49%)	21 (13.5%)	0.1180		Additive	**0.0308**	**0.0327**	0.740[0.564–0.973]
A	707 (71.4%)	203 (65.1%)						
G	283 (28.6%)	109 (34.9%)	**0.0330**	0.745[0.569–0.977]				

SIL, cervical squamous intraepithelial lesion; HSIL, high-grade cervical squamous intraepithelial lesion; LSIL, low-grade cervical squamous intraepithelial lesion; OR, odds ratio; CI, confidence interval.

P: p-*value (control vs. SIL; control vs. HSIL; control vs. LSIL);* p *values <0.05 are considered statistically significant, and shown in bold.*

P′: age was adjusted.

P″: the p-*value was calculated using 10,000 permutations for each model to correct the multiple tests.*

TABLE 4 | Comparison of genotypes and allele distribution frequencies between the CC group and the SIL group.

Genotype and allele	CC (n = 482)	SIL (n = 775)	P	OR [95% CI]	Statistical model	P′	P′′	OR [95% CI]
AA	235 (48.8%)	351 (45.3%)			Dominant	0.2191	0.2195	1.165[0.913–1.485]
AG	199 (41.3%)	337 (43.5%)			Recessive	0.5878	0.5914	1.116[0.751–1.657]
GG	48 (9.96%)	87 (11.2%)	0.4616		Additive	0.2419	0.2423	1.115[0.929–1.339]
A	669 (69.4%)	1,039 (67.0%)						
G	295 (30.6%)	511 (33.0%)	0.2165	1.115[0.938–1.326]				

CC, cervical cancer; SIL, cervical squamous intraepithelial lesion; OR, odds ratio; CI, confidence interval.

P: p-*value (CC vs. SIL);* p-*values <0.05 are shown in bold.*

P′: age was adjusted.

P″: the p-*value was calculated using 10,000 permutations for each model to correct the multiple tests.*

TABLE 5 | Comparison of genotypes and allele distribution frequencies between the SCC group and AUC group.

Genotype and allele	SCC (n = 416)	AUC (n = 36)	P	OR [95% CI]	Statistical model	P′	P′′	OR [95% CI]
AA	204 (49.0%)	16 (44.4%)			Dominant	0.6073	0.6082	1.197[0.603–2.374]
AG	169 (40.6%)	16 (44.4%)			Recessive	0.8808	0.8827	1.087[0.367–3.222]
GG	43 (10.3%)	4 (11.1%)	0.8690		Additive	0.6495	0.6511	1.123[0.680–1.856]
A	577 (69.4%)	48 (66.7%)						
G	255 (30.6%)	24 (33.3%)	0.6362	0.884[0.530–1.474]				

SCC, squamous carcinoma of cervical; AUC, adenocarcinoma of the uterine cervical; OR, odds ratio; CI, confidence interval.

P: p-*value (SCC vs. AUC);* p-*values <0.05 are shown in bold.*

P′: age was adjusted.

P″: the p-*value was calculated using 10,000 permutations for each model to correct the multiple tests.*

TABLE 6 | Comparison of genotypes and allele distribution frequencies between the HSIL group and LSIL group.

Genotype and allele	HSIL (n = 619)	LSIL (n = 156)	P	OR [95% CI]	Statistical model	P′	P′′	OR [95% CI]
AA	283(45.7%)	68 (43.6%)			Dominant	0.5822	0.5860	1.105[0.774–1.578]
AG	270(43.6%)	67 (42.9%)			Recessive	0.2686	0.2713	1.347[0.794–2.286]
GG	66(10.7%)	21 (13.5%)	0.6043		Additive	0.3525	0.3554	1.132[0.872–1.470]
A	836(67.5%)	203(65.1%)						
G	402(32.5%)	109(34.9%)	0.4080	0.896[0.690–1.163]				

HSIL, high-grade cervical squamous intraepithelial lesion; LSIL, low-grade cervical squamous intraepithelial lesion; OR, odds ratio; CI, confidence interval.
P: p-value (HSIL, vs. LSIL); p-values <0.05 are shown in bold.
P′: age was adjusted.
P″: the p-value was calculated using 10,000 permutations for each model to correct the multiple tests.

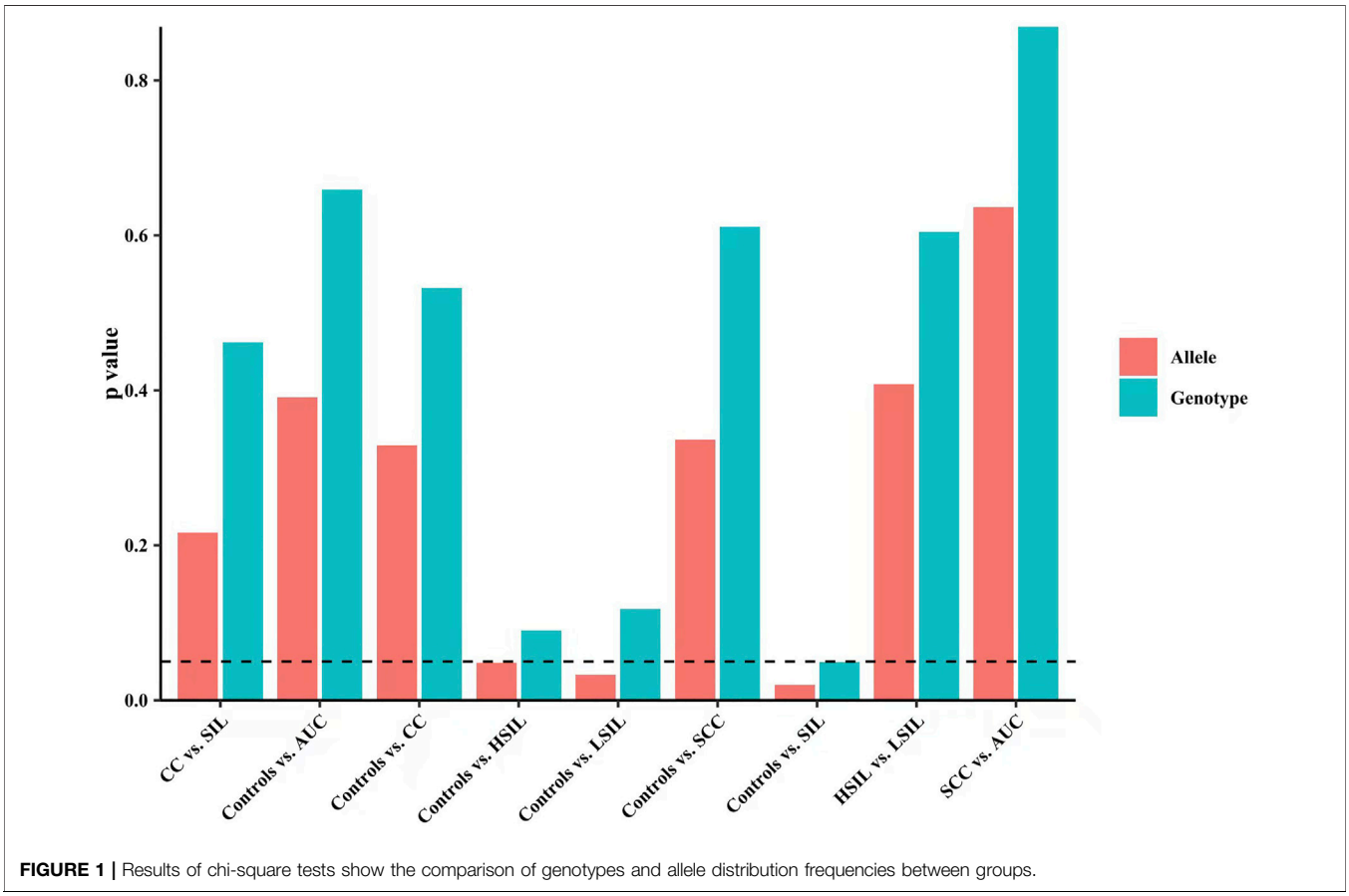


FIGURE 1 | Results of chi-square tests show the comparison of genotypes and allele distribution frequencies between groups.

cascade amplification of inflammatory response. It often participates in the body's immune defense and plays a "double-edged sword" role in the occurrence and development of tumor (Li et al., 2020). In addition, the level of sulfatide on the apical surface of many tumor epithelial cells is significantly increased, and the metastatic ability of tumor cells is related to the specific binding of GSDMB to sulfatide (Chao et al., 2017). Increasingly, a large number of case–control studies have also suggested that the *GSDMB* gene polymorphism is associated with susceptibility to many autoimmune diseases and malignant tumors such as cervical cancer (Hergueta-Redondo et al., 2016; Wiemels et al., 2018; Molina-Crespo et al., 2019; Li et al., 2020; Li et al., 2021). At present, the relationship between *GSDMB* gene polymorphism and the risk of cervical cancer in the Han population in Northeast China has not been reported. Therefore, this study aimed to explore the relationship between rs8067378 polymorphism of the *GSDMB* gene and the risk of cervical cancer in the Northeast Chinese Han population. Since cervical squamous intraepithelial lesions, as a form of precancerous lesions, reflect the continuous development of cervical cancer (de Rycke et al., 2020), we will also study whether rs8067378 polymorphism is associated with cervical squamous intraepithelial lesions in Han women in Northeast China.

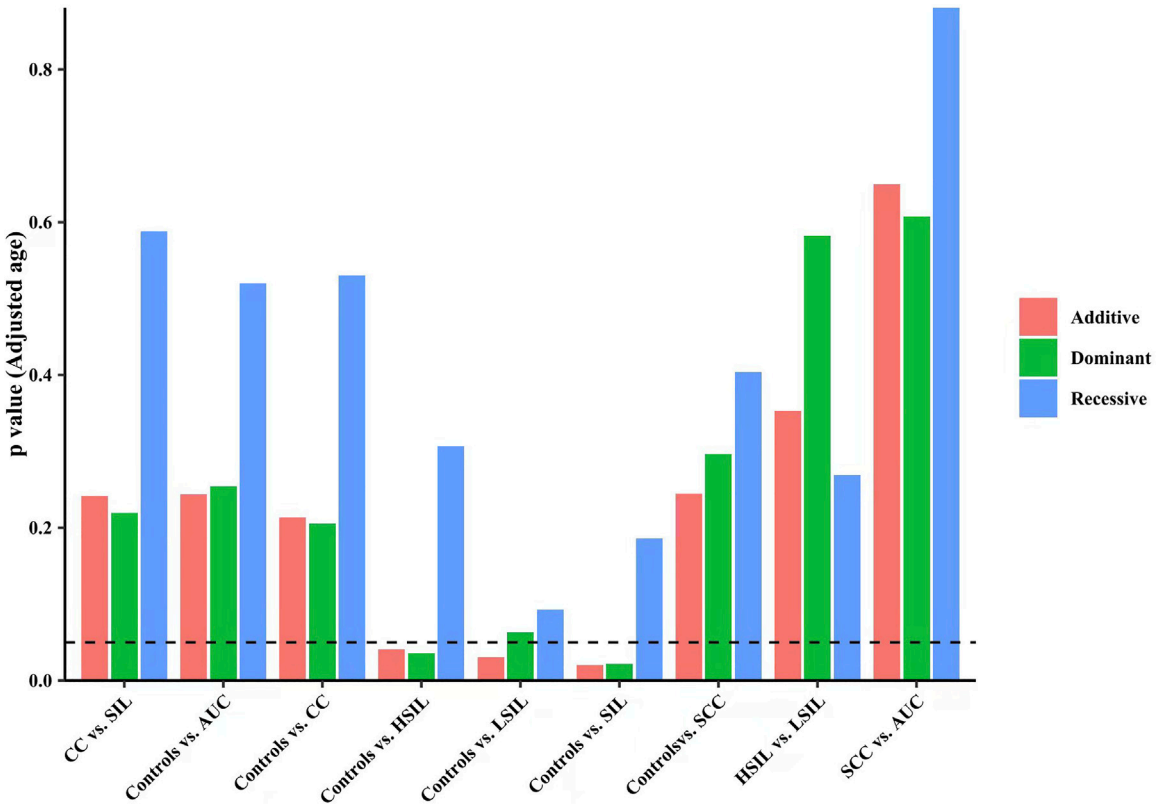


FIGURE 2 | Results of the logistic regression analysis after adjusting for age show the comparison of genotypes and allele distribution frequencies between groups.

2 MATERIALS AND METHODS

2.1 Study Subjects

2.1.1 Case Group

All subjects in this case–control study were recruited from the same center (Department of Obstetrics and Gynecology, Second Affiliated Hospital of Harbin Medical University, Harbin City, Heilongjiang Province, China) from September 2014 to October 2018. The case group included 482 cases of primary cervical cancer without any treatment, among which were 416 cases of SCC, 36 cases of AUC, and 30 cases of other pathological types. Another 775 patients with SIL were recruited, which included 619 patients with HSIL and 156 patients with LSIL. All the patients were confirmed by pathology experts of the Second Affiliated Hospital of Harbin Medical University. Exclusion criteria: cervical benign lesions, cervical benign tumors, other cervical malignant tumors, cervical lesions after preoperative chemoradiotherapy, and patients combined with other cancers.

2.1.2 Control Group

The control group consisted of 496 healthy people from the physical examination center of the same hospital in the same period. Inclusion criteria: there was no abnormality in the ThinPrep cytologic test (TCT), no cancer, or family history of cancer. Exclusion criteria: all gynecological diseases and surgical history of gynecological diseases, hypo-immunity and immune diseases, cervical surgery, skin or genital condyloma, and other cancer history, etc.

All subjects signed informed consent, and all studies in this report were approved by the Ethics Committee of the Second Affiliated Hospital of Harbin Medical University.

2.2 Candidate SNP Selection

Based on the data from the previous literature and combined with the characteristics of the East Asian population in the dbSNP database, the SNP rs8067378 (A > G) at 17q12 identified by previous cervical cancer GWAS (Shi et al., 2013) was selected for the current study.

2.3 Extraction and Genotyping of DNA

After fasting for 12 h, 1 ml peripheral venous blood samples were collected and put into a 2% EDTA-Na_2 anticoagulant tube. The samples were numbered and stored in an −80°C refrigerator until DNA extraction. The genomic DNA of all subjects was extracted from peripheral venous blood samples for genotyping according to the standard steps of the TIANamp Genomic DNA Kit (Tiangen Biotech, Beijing, China). All genotyping experiments for the selected SNP (rs8067378) were performed using two rounds of multiplex PCR combined with next-generation sequencing methods by the Shanghai Biowing Applied Biotechnology Company (Chen et al., 2016). Primer3 online software (v0.4.0) was used to amplify the primer sequences.

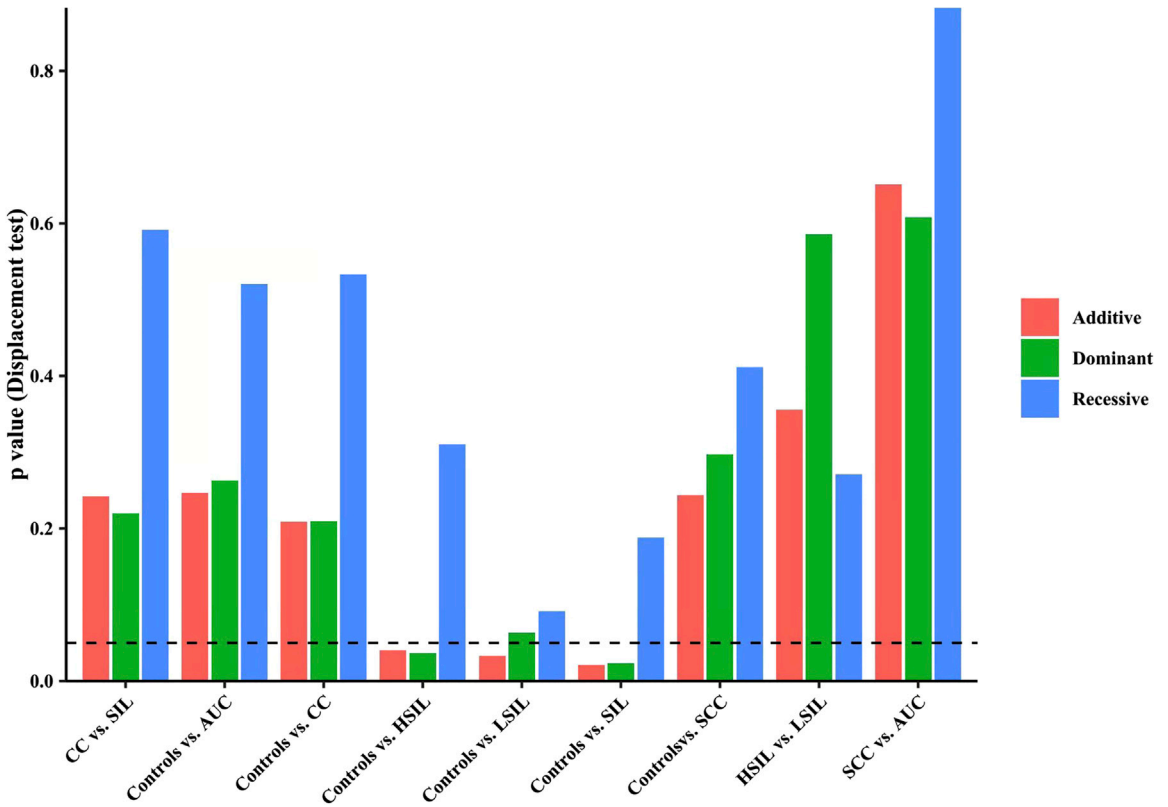


FIGURE 3 | Results after 10,000 permutation tests show the comparison of genotypes and allele distribution frequencies between groups.

PCR was performed for SNP analysis with the following primers: rs8067378 (sense, 5′-GTTGACAGTCAAAACAAAAACCTG-3′). After two rounds of multiplex PCR, the PCR products were mixed into the centrifugal tube, then sealed with the sealing membrane, and placed overnight. The mixture was purified using a TIANgel Midi Purification Kit (Tiangen Biotech, China). The purified PCR products were then paired-end sequenced (2 × 150 bp) by the Illumina HiSeq XTen platform according to the manufacturer's instructions. The read data were compared to the human reference genome using the Burrows–Wheeler (BWA, v0.7.12) (Slater et al., 2009), and SAMtools (v0.1.19) (Li, 2011) was used for SNP calling and genotyping. In total, ninety-one samples were randomly selected for blind DNA replication to control the quality of genotyping.

2.4 Physiological and Biochemical Index Collection and Analysis

The general information and clinical data of each subject in the case group were recorded in detail: age, menstrual history, smoking and drinking history, past disease history, operation history, family history of tumor, relevant laboratory examination results, histopathological diagnosis, clinically confirmed diagnosis, and relevant gynecological examination (ultrasound or colposcopy), etc.

In addition, the general situation and some clinical data of the healthy control population in the physical examination center during the same period were recorded: age, ThinPrep cytologic test (TCT), and HPV, etc. Moreover, due to the influence of traditional Chinese culture, the subjects in this study almost refused to answer questions about sexual life history, so this part of the data could not be collected.

Squamous cell carcinoma (SCC) antigen, carcino-embryonic antigen (CEA), alpha-fetoprotein (AFP), CA125, D-dimer, and other biochemical indicators were detected by the laboratory of the Second Affiliated Hospital of Harbin Medical University. The histopathological diagnosis of cervical tissue samples was confirmed by the pathology department of the Second Affiliated Hospital of Harbin Medical University.

2.5 Allele, Genotypes, and Statistics

SPSS 21.0 software was used to analyze the clinical characteristics of the case group and the control group. Student's *t*-test was used to compare the continuous variables among the groups. The Pearson chi-square test was used to compare the categorical variables between groups (the Fisher exact test was used when the expected value was less than 5). Plink1.9 single nucleotide polymorphism software was used for genotyping analysis. The Hardy–Weinberg equilibrium was analyzed. We established the following three models: dominant model: major allele homozygous vs. heterozygous + minor allele homozygous;

TABLE 7 | Comparison of genotype distribution frequencies with clinical parameters in the CC group.

Parameter	ALL	AA	AG	GG	P		P′	OR [95% CI]
Histology					0.8204			
SCC	416	198	175	43		AG/AA	0.6203	0.834 [0.406–1.712]
AUC	36	19	14	3		GG/AA	0.6206	0.727 [0.206–2.567]
Menarche age					0.7900			
< 15 years	229	113	91	25		AG/AA	0.5695	1.119 [0.760–1.646]
≥15 years	234	111	100	23		GG/AA	0.8370	0.937 [0.502–1.748]
Amenorrhea					0.1083			
Yes	220	96	97	27		AG/AA	0.1336	0.744 [0.506–1.095]
No	246	129	97	20		GG/AA	0.0663	0.551 [0.292–1.041]
Parity					0.2469			
Never	29	10	16	3		AG/AA	0.1002	0.504 [0.222–1.141]
Ever	396	196	158	42		GG/AA	0.6207	0.714 [0.188–2.708]
HPV					0.7248			
(-)	8	5	3	0		AG/AA	0.8795	1.123 [0.250–5.044]
(+)	83	46	31	6		GG/AA	0.9740	78185.319
D-dimer					0.8988			
≤243 ng/ml	392	188	163	41		AG/AA	0.8218	1.086 [0.531–2.217]
>243 ng/ml	36	17	16	3		GG/AA	0.7446	0.809 [0.227–2.890]
SCC					0.4132			
≤1.5 ng/ml	205	99	89	17		AG/AA	0.6246	0.907 [0.613–1.342]
>1.5 ng/ml	245	119	97	29		GG/AA	0.2951	1.419 [0.737–2.733]
CEA					0.6549			
≤5 ng/ml	183	81	80	22		AG/AA	0.8885	0.945 [0.428–2.085]
>5 ng/ml	31	15	14	2		GG/AA	0.3679	0.491 [0.104–2.310]
CA125					0.3928			
≤35 U/ml	197	88	86	23		AG/AA	0.5395	1.302 [0.560–3.028]
>35 U/ml	26	11	14	1		GG/AA	0.3238	0.348 [0.043–2.835]
CA199					0.0898			
≤37 U/ml	194	83	87	24		AG/AA	0.1570	0.477 [0.171–1.330]
>37 U/ml	18	12	6	0		GG/AA	0.9654	0.000

P: p-value; p-values <0.05 are shown in bold.
P′: logistic regression analysis.

recessive model: major allele homozygous + heterozygous vs. minor allele homozygous; and additive model: major allele homozygous vs. heterozygous vs. minor allele homozygous. The 95% confidence interval (CI) and odds ratio (OR) of each genetic model were calculated. Multivariate logistic regression analysis was performed to adjust age to evaluate the association of SNP with cervical cancer, cervical intraepithelial neoplasia, and their subtypes. Moreover, the chi-square test combined with logistic regression analysis was used to analyze the relationship between genotypes and alleles with clinical parameters. All statistical analyses showed that $p < 0.05$ had statistical significance.

3 RESULTS

3.1 SNP Genotype and Quality Controls

The SNP of the *GSDMB* gene was rs8067378, and its genotype distributions in the CC and SIL groups conform to the Hardy–Weinberg equilibrium ($p = 0.9108$ and $p = 0.9508$, respectively). In addition, we controlled the quality of 73 samples in this experiment, and the accuracy rate is 98.5%, and the error rate is within a reasonable range, which ensures the reliability and repeatability of the follow-up research results.

3.2 Clinical Characteristics of the Study Population

The clinical characteristics of all CC patients, SIL patients, and healthy controls in this study were statistically analyzed, as shown in **Table 1**. The results showed that compared with the healthy control group, the average age of CC and SIL patients was old, and the comparison between the control group and CC and SIL groups was statistically significant ($p < 0.0001$). The analysis of other clinical characteristics of the CC group and SIL group showed that there were significant differences in menarche age and amenorrhea between the two groups ($p < 0.05$). In addition, smoking was significantly correlated between the two groups ($p = 0.0091$) while drinking was not ($p = 0.4952$).

3.3 Analysis of Genotypes and Allele Distribution Frequencies

The genotypes and allele distribution frequencies of *GSDMB* gene polymorphism (rs8067378) in the CC group and its subgroups with the healthy control group are shown in **Table 2**. The results of the chi-square test showed that the genotypes and allele frequencies of rs8067378 single nucleotide polymorphism of the *GSDMB* gene had no significant difference between the CC group and healthy

TABLE 8 | Comparison of allele distribution frequencies with clinical parameters in the CC group.

Parameter	ALL	A	G	P	P′	OR [95% CI]
Histology				0.5275	0.5280	0.841[0.492–1.438]
SCC	832	571	261			
AUC	72	52	20			
Menarche age				0.8926	0.8926	1.019[0.772–1.347]
<15 years	458	317	141			
≥15 years	468	322	146			
Amenorrhea				**0.0328**	**0.0330**	0.739[0.559–0.976]
Yes	440	289	151			
No	492	355	137			
Parity				0.2413	0.2428	0.720[0.415–1.250]
Never	58	36	22			
Ever	792	550	242			
HPV				0.5295	0.5320	1.515[0.412–5.573]
(-)	16	13	3			
(+)	166	123	43			
D-dimer				0.9031	0.9036	0.968[0.573–1.634]
≤243 ng/ml	784	539	245			
>243 ng/ml	72	50	22			
SCC				0.5975	0.5981	1.079[0.812–1.435]
≤1.5 ng/ml	410	287	123			
>1.5 ng/ml	490	335	155			
CEA				0.4535	0.4542	0.798[0.443–1.440]
≤5 ng/ml	366	242	124			
>5 ng/ml	62	44	18			
CA125				0.6940	0.6941	0.882[0.472–1.648]
≤35 U/ml	394	262	132			
>35 U/ml	52	36	16			
CA199				**0.0272**	**0.0328**	0.375[0.152–0.923]
≤37 U/ml	388	253	135			
>37 U/ml	36	30	6			

P: p-*value;* p *values <0.05 are considered statistically significant, and shown in bold.*
P′: logistic regression analysis.

control group ($p > 0.05$), and there was no significant difference between the SCC and AUC groups with healthy control group ($p > 0.05$). Logistic regression analysis showed that after adjusting for age, rs8067378 single nucleotide polymorphism was not significantly associated with cervical cancer and its subtypes ($p > 0.05$). After 10,000 permutations, the results were still not statistically significant. The consistency of 10,000 permutations further supports the reliability of our results.

Table 3 shows the comparison of genotypes and allele distribution frequencies between the SIL group and its subgroups with healthy control group. The results of the chi-square test showed that the genotype frequencies of rs8067378 single nucleotide polymorphism of the *GSDMB* gene were statistically significant between the SIL group and healthy control group ($p = 0.0493$), and the A/G allele frequency was also statistically significant between the two groups ($p = 0.0202$). Compared with the healthy control group (28.6%), the G mutation of rs8067378 accounted for 32.5% in the HSIL group and 34.9% in the LSIL group, and the A/G allele frequency was significantly correlated between the HSIL group and LSIL group with the healthy control group ($p = 0.0483$ and 0.0330, respectively). Logistic regression analysis showed that after adjusting for age, rs8067378 SNP was statistically significant between the SIL group and its subgroup (HSIL group) with the healthy control group in the dominant model and additive model ($p = 0.0213$ and 0.0356 in the dominant model, and $p = 0.0199$ and 0.0406 in the additive model, respectively). The difference between the LSIL group and healthy control group was statistically significant in the additive model ($p = 0.0308$). It can be seen that under the additive model, rs8067378 plays a protective role in the progression of healthy people to LSIL and even HSIL ($P2 = 0.0308$, OR = 0.740, CI = 0.564–0.973; $P1 = 0.0406$, OR = 0.827, CI = 0.689–0.992). This correlation still exists after 10,000 permutations.

Table 4 shows the comparison of genotypes and allele distribution frequencies of rs8067378 SNP of the *GSDMB* gene between the CC group and SIL group. The results show that there is no significant difference in genotypes and allele distribution frequencies of rs8067378 SNP between the CC group and SIL group ($p > 0.05$). Logistic regression analysis showed that there was no significant difference in rs8067378 SNP between the CC group and SIL group after adjusting for age ($p > 0.05$). After 10,000 permutations, the results were still not statistically significant.

Finally, we made intra-subgroup comparisons. **Tables 5**, **6** summarized the comparisons of genotypes and allele distribution frequencies of rs8067378 SNP of the *GSDMB* gene between the SCC group and the AUC group, and the HSIL group and the LSIL group, respectively. The results show that there is no significant difference in genotypes and allele distribution frequencies of rs8067378 SNP between the two intra-subgroups ($p > 0.05$). After adjusting for age, there is still no significant difference among the genetic models ($p > 0.05$). After 10,000 permutations, the results were still not statistically significant, which has provided evidence for the accuracy of our study. In addition, in order to more clearly and definitely show the comparison of genotypes and allele distribution frequencies between groups, we drew three graphs: **Figure 1** shows the results of chi-square tests, **Figure 2** shows the results of logistic regression analysis after adjusting for age, and **Figure 3** shows the results after 10,000 permutation tests.

3.4 Analysis of Genotypes and Allele Frequencies With Clinical Parameters

In the CC group and SIL group, the comparisons of genotypes and allele distribution frequencies of *GSDMB* gene rs806778 polymorphism with clinical parameters are shown in **Tables 7**–**10**. It is worth noting that in patients with cervical cancer, allele frequencies are significantly correlated with amenorrhea ($p = 0.0328$). After logistic regression analysis, the correlations still exist ($p = 0.0330$). In addition, no significant correlation was observed between genotypes and allele frequencies with other clinical parameters ($p > 0.05$). Moreover, there was also no significant correlation between genotypes and allele frequencies with clinical parameters in patients with cervical squamous intraepithelial lesions ($p > 0.05$).

4 DISCUSSION

Cervical cancer is characterized by a high incidence rate and high mortality rate, and it is a major public problem affecting the health of middle-aged women, especially in countries with

TABLE 9 | Comparison of genotype distribution frequencies with clinical parameters in the SIL group.

Parameter	ALL	AA	AG	GG	P		P′	OR [95% CI]
Histology					0.4017			
HSIL	619	285	269	65		AG/AA	0.6491	0.916 [0.628–1.336]
LSIL	156	66	68	22		GG/AA	0.1781	0.684 [0.394–1.189]
Menarche age					0.1808			
<15 years	445	201	186	58		AG/AA	0.6156	1.081 [0.798–1.463]
≥15 years	325	148	148	29		GG/AA	0.1244	0.679 [0.414–1.113]
Amenorrhea					0.4376			
Yes	156	68	74	14		AG/AA	0.3993	0.853 [0.589–1.235]
No	607	278	258	71		GG/AA	0.5038	1.240 [0.660–2.332]
Parity					0.5740			
Never	57	29	21	7		AG/AA	0.3058	1.357 [0.756–2.436]
Ever	654	293	288	73		GG/AA	0.9427	1.032 [0.435–2.450]
HPV					0.4522			
(-)	27	10	15	2		AG/AA	0.3170	0.656 [0.288–1.497]
(+)	440	195	192	53		GG/AA	0.6978	1.359 [0.289–6.391]
D-dimer					0.6396			
≤243 ng/ml	743	336	323	84		AG/AA	0.8382	0.892 [0.296–2.681]
>243 ng/ml	16	7	6	3		GG/AA	0.4418	1.714 [0.434–6.770]
SCC					0.5749			
≤1.5 ng/ml	472	211	208	53		AG/AA	0.7599	1.092 [0.620–1.926]
>1.5 ng/ml	58	26	28	4		GG/AA	0.3802	0.612 [0.205–1.831]
CEA					0.7043			
≤5 ng/ml	191	87	84	20		AG/AA	0.9663	1.036 [0.203–5.276]
>5 ng/ml	6	3	3	0		GG/AA	0.9719	0.000
CA125					0.3617			
≤35 U/ml	193	90	82	21		AG/AA	0.3162	1.585 [0.644–3.903]
>35 U/ml	23	9	13	1		GG/AA	0.4929	0.476 [0.057–3.967]
CA199					0.9019			
≤37 U/ml	177	80	79	18		AG/AA	0.8067	0.868 [0.279–2.697]
>37 U/ml	15	7	6	2		GG/AA	0.7765	1.270 [0.243–6.630]

P: p-*value;* p-*values <0.05 are shown in bold.*
P′: logistic regression analysis.

low resources (Hu et al., 2018; Arbyn et al., 2020; Zhang et al., 2020). Persistent infection of high-risk HPV is the most important risk factor associated with cervical cancer (Faridi et al., 2011; Paaso et al., 2019). However, studies have shown that other risk factors associated with HPV may also play important roles in the pathogenesis of cervical cancer, such as immune or genetic factors. SNP has become an important biomarker for locating cancer, such as cervical cancer (Shastry, 2009). Therefore, this case–control study was conducted to research the association between *GSDMB* gene polymorphism and the risk of cervical cancer in the Han population in Northeast China. In this study, we investigated the relationship between rs8067378 SNP of the *GSDMB* gene and susceptibility to cervical cancer in Han population in Northeast China. According to the histopathological classification, CC patients were further divided into the SCC group and AUC group, and the SIL group was divided into the HSIL group and LSIL group. Then, intragroup and intergroup comparisons were performed.

Our results replicated previous studies and showed that the average age of the CC group was 49.33 ± 9.29 years, and the average age of the SIL group was 42.22 ± 9.68 years. This is consistent with the conclusion that the peak of CC in the Chinese mainland is 40–60 years old and the peak of SIL is 30–50 years old (Wang et al., 2018; Liu et al., 2020). This may be related to the fact that women in the 30–40 age group are in the period of sexual activity and childbearing, while most of the women after the age of 50 are postmenopausal (Misra et al., 2018).

In this case–control study, we investigated the relationship between rs8067378 polymorphism of the *GSDMB* gene and the risk of CC in the Han population in Northeast China. The results showed that there was no significant correlation between rs8067378 polymorphism with CC and its subtypes. These are different from the existing research studies. A genome-wide association study on cervical cancer in the Chinese Han population proved that rs8067378 SNP is a susceptible site for cervical cancer (Shi et al., 2013). Miura et al. (2016) showed for the first time that there was a significant correlation between rs8067378 SNP and invasive cervical cancer and further proved that Japanese women with the GG genotype were at high risk of invasive cervical cancer. Lutkowska et al. (2017) studied the relationship between rs8067378 SNP and stage III and IV of cervical cancer in the Polish population, in which the G allele plays a role in the diffusion of tumor cells to adjacent tissues, indicating that rs8067378 SNP increases the risk of occurrence and development of cervical cancer. Such findings have also been confirmed in some parts of southern China. Based on previous studies, the specific mechanism of GSDMB in the occurrence and

TABLE 10 | Comparison of allele distribution frequencies with clinical parameters in the SIL group.

Parameter	ALL	A	G	P	P′	OR [95% CI]
Histology				0.2180	0.2183	0.849[0.655–1.102]
HSIL	1,238	839	399			
LSIL	312	200	112			
Menarche age				0.3557	0.3558	0.903[0.728–1.121]
<15 years	890	588	302			
≥15 years	650	444	206			
Amenorrhea				0.9314	0.9315	1.012[0.776–1.319]
Yes	312	210	102			
No	1,214	814	400			
Parity				0.5893	0.5895	1.121[0.741–1.696]
Never	114	79	35			
Ever	1,308	874	434			
HPV				0.8422	0.8422	0.943[0.530–1.677]
(-)	54	35	19			
(+)	880	582	298			
D-dimer				0.5960	0.5965	1.216[0.590–2.508]
≤243 ng/ml	1,486	995	491			
>243 ng/ml	32	20	12			
SCC				0.6301	0.6302	0.903[0.596–1.369]
≤1.5 ng/ml	944	630	314			
>1.5 ng/ml	116	80	36			
CEA				0.5861	0.5884	0.694[0.185–2.607]
≤5 ng/ml	382	258	124			
>5 ng/ml	12	9	3			
CA125				0.9470	0.9468	1.022[0.532–1.963]
≤35 U/ml	386	262	124			
>35 U/ml	46	31	15			
CA199				0.9242	0.9238	1.039[0.471–2.292]
≤37 U/ml	354	239	115			
>37 U/ml	30	20	10			

P: p-*value;* p-*values <0.05 are shown in bold.*
P′: logistic regression analysis.

development of cervical cancer is not clear. Some studies suppose that GSDMB may participate in the regulation of the estrogen–estrogen receptor-target gene expression pathway under the action of endogenous and exogenous estrogen (Sun et al., 2008). Studies have shown that *GSDMB* containing two nuclear receptor-binding motifs can be used as a nuclear receptor co-activator, recruited in the estrogen receptor to form a complex, provide related enzymatic activity and scaffolding function, promote the high expression of E6/E7 oncogene in patients with high-risk HPV persistent infection, and cause uncontrolled cell proliferation, cervical intraepithelial lesions, and even cervical cancer (Sun et al., 2008). In addition, these differences may be related to the sample size and case determination protocol. Also, the genetic background and lifestyle may also change the genetic susceptibility of the *GSDMB* gene, which explain the differences in the intensity of research correlation between different regions and races. Therefore, we should repeat the study with a larger sample, to determine the relationship between *GSDMB* gene polymorphism with SCC and AUC and even other special types of CC.

GSDMB can participate in pyrocytosis and the production of inflammatory factors, and studies found that GSDMB can be highly expressed in cervical inflammatory lesions and precancerous lesions (Sun et al., 2008). Therefore, in order to further study the role of *GSDMB* gene rs8067378 polymorphism in the development of cervical cancer in healthy women, we also analyzed the susceptibility of SIL. Surprisingly, under the dominant and additive models, the rs8067378 polymorphism of the *GSDMB* gene is significantly correlated with SIL and its subtypes, and rs8067378 single nucleotide polymorphism may reduce the risk of SIL and protect the susceptibility to SIL. This may be related to the dual role of GSDMB-mediated pyrocytosis in tumor, and the occurrence of pyrocytosis is concentration-dependent on GSDMB. Studies have pointed out that (Kayagaki et al., 2015; Tsuchiya, 2020) macrophages and monocytes lacking GSDMB almost completely lose the transmission ability of lipopolysaccharide (LPS) in the cytoplasm and will not activate inflammatory caspases, so they will not induce pyrocytosis. In the process of pyrocytosis, caspases are the inducer and GSDMB is the substrate. Precursor caspases are activated by a variety of inflammatory bodies such as the NOD-like receptor (NLR) and are absent in melanoma 2 (AIM2). Active caspases bind to the cutting site of GSDMB. This process releases the N-terminal and C-terminal, which are inserted into the cell membrane to cause pyrocytosis and release a large number of inflammatory factors such as tumor necrosis factor (TNF), interleukin-1β (IL-1β), and interferon-α (IFN-α). This process can not only directly kill pathological and tumor cells but also further recruit immune cells, so as to expand the inflammatory response. Therefore, some scholars believe that active caspases cutting GSDMB-induced pyrocytosis is a positive feedback mechanism in the immune process, so that most newborn tumor cells are eliminated by the process of pyrocytosis before the formation of tumor. It plays a role in preventing the further development of precancerous lesions (Dinarello, 2009; Guo et al., 2015; Xia et al., 2019; Zhou and Fang, 2019; Ruan et al., 2020). This is consistent with the research results of Zhang WH. The study has shown that after CC cells are infected by HPV, AIM2 can play a tumor inhibitory role by inducing pyrocytosis (So et al., 2018).

The study confirmed for the first time that *GSDMB* gene polymorphism was significantly correlated with cervical squamous intraepithelial lesions, but not with cervical cancer in the Han population in Northeast China. The studies of Miura et al. and Lutkowska et al. have confirmed that *GSDMB* gene polymorphism was significantly associated with cervical cancer. Compared with previous existing studies, the sample size in our study was relatively large, including 482 cases of cervical cancer, 775 cases of cervical squamous intraepithelial lesions, and 495 healthy controls. Moreover, our study was analyzed from multiple perspectives such as cervical cancer subgroups and cervical precancerous lesions. A large sample size is very important for exploring and verifying the potential mechanism of cervical cancer and precancerous lesions in Chinese women and will also play an important role in the research of different pathological types of cervical cancer and precancerous lesions in the future. In addition, we also added the comparison of genotypes and alleles with clinical parameters to understand more clinically related risk factors. However, this study also has some limitations. First, this study adopts a case–control

study, which inevitably has selective bias. Second, our study population is limited to Han women in Northeast China, so it is necessary to conduct a multicenter and large-scale replication study to confirm the results, including people from different regions and races. Finally, cervical cancer is a complex disease affected by multiple genes. This study only discussed the limited loci of the *GSDMB* gene, and other functional genes and loci have not been studied. Therefore, the combined role of the *GSDMB* gene and other genes in the occurrence and development of cervical cancer needs to be further explored.

In conclusion, our study is the first to prove that rs8067378 polymorphism of the *GSDMB* gene is significantly associated with SIL in the Northeast Chinese Han population. Rs8067378 polymorphism may be used as a protective factor to reduce the risk of SIL and even CC in the Han population in Northeast China during the progression of healthy people to LSIL and even HSIL. It is necessary to conduct more in-depth research to understand the specific mechanism of the *GSDMB* gene in the occurrence and development of cervical cancer, so as to provide theoretical support for the diagnosis and treatment of cervical cancer in the future.

DATA AVAILABILITY STATEMENT

The datasets presented in this study can be found in online repositories. The names of the repository/repositories and accession number(s) can be found at: https://doi.org/10.6084/m9.figshare.19351877.

AUTHOR CONTRIBUTIONS

SL and XL: data collection, data analysis, and manuscript writing. SZ, YF, and XK: data analysis. TJ, MZ, LF, LG, and SD: data collection. ZW and LS: project development. All authors contributed to the article and approved the submitted version.

FUNDING

This study was supported by the National Natural Science Foundation of China (No. 82071929).

REFERENCES

Arbyn, M., Weiderpass, E., Bruni, L., de Sanjosé, S., Saraiya, M., Ferlay, J., et al. (2020). Estimates of Incidence and Mortality of Cervical Cancer in 2018: A Worldwide Analysis. *Lancet Glob. Health* 8 (2), e191–e203. doi:10.1016/s2214-109x(19)30482-6

Chao, K. L., Kulakova, L., and Herzberg, O. (2017). Gene Polymorphism Linked to Increased Asthma and IBD Risk Alters Gasdermin-B Structure, a Sulfatide and Phosphoinositide Binding Protein. *Proc. Natl. Acad. Sci. U. S. A.* 114 (7), E1128–E1137. doi:10.1073/pnas.1616783114

Chen, K., Zhou, Y.-x., Li, K., Qi, L.-x., Zhang, Q.-f., Wang, M.-c., et al. (2016). A Novel Three-Round Multiplex PCR for SNP Genotyping with Next Generation Sequencing. *Anal. Bioanal. Chem.* 408 (16), 4371–4377. doi:10.1007/s00216-016-9536-6

Chen, Q., Shi, P., Wang, Y., Zou, D., Wu, X., Wang, D., et al. (2019). GSDMB Promotes Non-Canonical Pyroptosis by Enhancing Caspase-4 Activity. *J. Mol. Cell Biol.* 11 (6), 496–508. doi:10.1093/jmcb/mjy056

de Rycke, Y., Tubach, F., Lafourcade, A., Guillo, S., Dalichampt, M., Dahlab, A., et al. (2020). Cervical Cancer Screening Coverage, Management of Squamous Intraepithelial Lesions and Related Costs in France. *PLoS One* 15 (2), e0228660. doi:10.1371/journal.pone.0228660

Dinarello, C. A. (2009). Immunological and Inflammatory Functions of the Interleukin-1 Family. *Annu. Rev. Immunol.* 27, 519–550. doi:10.1146/annurev.immunol.021908.132612

Faridi, R., Zahra, A., Khan, K., and Idrees, M. (2011). Oncogenic Potential of Human Papillomavirus (HPV) and its Relation with Cervical Cancer. *Virol. J.* 8, 269. doi:10.1186/1743-422x-8-269

Feng, S., Fox, D., and Man, S. M. (2018). Mechanisms of Gasdermin Family Members in Inflammasome Signaling and Cell Death. *J. Mol. Biol.* 430 (18 Pt B), 3068–3080. doi:10.1016/j.jmb.2018.07.002

Guo, H., Callaway, J. B., and Ting, J. P.-Y. (2015). Inflammasomes: Mechanism of Action, Role in Disease, and Therapeutics. *Nat. Med.* 21 (7), 677–687. doi:10.1038/nm.3893

Hergueta-Redondo, M., Sarrio, D., Molina-Crespo, Á., Vicario, R., Bernadó-Morales, C., Martínez, L., et al. (2016). Gasdermin B Expression Predicts Poor Clinical Outcome in HER2-Positive Breast Cancer. *Oncotarget* 7 (35), 56295–56308. doi:10.18632/oncotarget.10787

Hu, L., Jia, M., Zhou, J., Ma, H., Jin, G., Li, N., et al. (2018). Genetic Variants within 17q12 Are Associated with the Risk of Cervical Cancer in the Han Chinese Population. *Gene* 678, 124–128. doi:10.1016/j.gene.2018.08.030

Kayagaki, N., Stowe, I. B., Lee, B. L., O'Rourke, K., Anderson, K., Warming, S., et al. (2015). Caspase-11 Cleaves Gasdermin D for Non-Canonical Inflammasome Signalling. *Nature* 526 (7575), 666–671. doi:10.1038/nature15541

Li, H. (2011). A Statistical Framework for SNP Calling, Mutation Discovery, Association Mapping and Population Genetical Parameter Estimation from Sequencing Data. *Bioinformatics* 27 (21), 2987–2993. doi:10.1093/bioinformatics/btr509

Li, L., Li, Y., and Bai, Y. (2020). Role of GSDMB in Pyroptosis and Cancer. *Cmar* Vol. 12, 3033–3043. doi:10.2147/cmar.s246948

Li, X., Christenson, S. A., Modena, B., Li, H., Busse, W. W., Castro, M., et al. (2021). Genetic Analyses Identify GSDMB Associated with Asthma Severity, Exacerbations, and Antiviral Pathways. *J. Allergy Clin. Immunol.* 147 (3), 894–909. doi:10.1016/j.jaci.2020.07.030

Liu, Y., Ang, Q., Wu, H., Xu, J., Chen, D., Zhao, H., et al. (2020). Prevalence of Human Papillomavirus Genotypes and Precancerous Cervical Lesions in a Screening Population in Beijing, China: Analysis of Results from China's Top 3 Hospital, 2009-2019. *Virol. J.* 17 (1), 104. doi:10.1186/s12985-020-01383-1

Lutkowska, A., Roszak, A., Lianeri, M., Sowińska, A., Sotiri, E., and Jagodziński, P. P. (2017). Analysis of Rs8067378 Polymorphism in the Risk of Uterine Cervical Cancer from a Polish Population and its Impact on Gasdermin B Expression. *Mol. Diagn. Ther.* 21 (2), 199–207. doi:10.1007/s40291-017-0256-1

Misra, J., Srivastava, A., and Zaidi, Z. (2018). Cervical Cytopathological Changes Associated with Onset of Menopause. *J. Mid-life Health* 9 (4), 180–184. doi:10.4103/jmh.jmh_4_18

Miura, K., Mishima, H., Yasunami, M., Kaneuchi, M., Kitajima, M., Abe, S., et al. (2016). A Significant Association Between Rs8067378 at 17q12 and Invasive Cervical Cancer Originally Identified by a Genome-Wide Association Study in Han Chinese Is Replicated in a Japanese Population. *J. Hum. Genet.* 61 (9), 793–796. doi:10.1038/jhg.2016.50

Molina-Crespo, Á., Cadete, A., Sarrio, D., Gámez-Chiachio, M., Martinez, L., Chao, K., et al. (2019). Intracellular Delivery of an Antibody Targeting Gasdermin-B Reduces HER2 Breast Cancer Aggressiveness. *Clin. Cancer Res.* 25 (15), 4846–4858. doi:10.1158/1078-0432.ccr-18-2381

Nkfusai, N. C., Cumber, S. N., Anchang-Kimbi, J. K., Nji, K. E., Shirinde, J., and Anong, N. D. (2019). Assessment of the Current State of Knowledge and Risk Factors of Cervical Cancer Among Women in the Buea Health District, Cameroon. *Pan Afr. Med. J.* 33, 38. doi:10.11604/pamj.2019.33.38.16767

Olusola, P., Banerjee, H. N., Philley, J. V., and Dasgupta, S. (2019). Human Papilloma Virus-Associated Cervical Cancer and Health Disparities. *Cells* 8 (6). doi:10.3390/cells8060622

Paaso, A., Jaakola, A., Syrjänen , S., and Louvanto, K. (2019). From HPV Infection to Lesion Progression: The Role of HLA Alleles and Host Immunity. *Acta Cytol.* 63 (2), 148–158. doi:10.1159/000494985

Ruan, J., Wang, S., and Wang, J. (2020). Mechanism and Regulation of Pyroptosis-Mediated in Cancer Cell Death. *Chemico-Biological Interact.* 323, 109052. doi:10.1016/j.cbi.2020.109052

Sadri Nahand, J., Moghoofei, M., Salmaninejad, A., Bahmanpour, Z., Karimzadeh, M., Nasiri, M., et al. (2020). Pathogenic Role of Exosomes and microRNAs in HPV-Mediated Inflammation and Cervical Cancer: A Review. *Int. J. Cancer* 146 (2), 305–320. doi:10.1002/ijc.32688

Shastry, B. S. (2009). SNPs: Impact on Gene Function and Phenotype. *Methods Mol. Biol.* 578, 3–22. doi:10.1007/978-1-60327-411-1_1

Shi, Y., Li, L., Hu, Z., Li, S., Wang, S., Liu, J., et al. (2013). A Genome-Wide Association Study Identifies Two New Cervical Cancer Susceptibility Loci at 4q12 and 17q12. *Nat. Genet.* 45 (8), 918–922. doi:10.1038/ng.2687

Slater, P. M., Grivell, R., and Cyna, A. M. (2009). Labour Management of a Woman with Carnitine Palmitoyl Transferase Type 2 Deficiency. *Anaesth. Intensive Care* 37 (2), 305–308. doi:10.1177/0310057x0903700211

So, D., Shin, H.-W., Kim, J., Lee, M., Myeong, J., Chun, Y.-S., et al. (2018). Cervical Cancer Is Addicted to SIRT1 Disarming the AIM2 Antiviral Defense. *Oncogene* 37 (38), 5191–5204. doi:10.1038/s41388-018-0339-4

Sun, Q., Yang, J., Xing, G., Sun, Q., Zhang, L., and He, F. (2008). Expression of GSDML Associates with Tumor Progression in Uterine Cervix Cancer. *Transl. Oncol.* 1 (2), 73–IN1. doi:10.1593/tlo.08112

Sung, H., Ferlay, J., Siegel, R. L., Laversanne, M., Soerjomataram, I., Jemal, A., et al. (2021). Global Cancer Statistics 2020: GLOBOCAN Estimates of Incidence and Mortality Worldwide for 36 Cancers in 185 Countries. *CA A Cancer J. Clin.* 71 (3), 209–249. doi:10.3322/caac.21660

Tan, H. (2017). The Association between Gene SNPs and Cancer Predisposition: Correlation or Causality? *EBioMedicine* 16, 8–9. doi:10.1016/j.ebiom.2017.01.047

Tsuchiya, K. (2020). Inflammasome-Associated Cell Death: Pyroptosis, Apoptosis, and Physiological Implications. *Microbiol. Immunol.* 64 (4), 252–269. doi:10.1111/1348-0421.12771

van der Waal, D., Bekkers, R. L. M., Dick, S., Lenselink, C. H., Massuger, L. F. A. G., Melchers, W. J. G., et al. (2020). Risk Prediction of Cervical Abnormalities: The Value of Sociodemographic and Lifestyle Factors in Addition to HPV Status. *Prev. Med.* 130, 105927. doi:10.1016/j.ypmed.2019.105927

Wang, H., Cheng, X., Ye, J., Xu, X., Hong, Y., Sui, L., et al. (2018). Distribution of Human Papilloma Virus Genotype Prevalence in Invasive Cervical Carcinomas and Precancerous Lesions in the Yangtze River Delta Area, China. *BMC Cancer* 18 (1), 487. doi:10.1186/s12885-018-4330-9

Wiemels, J. L., Walsh, K. M., de Smith, A. J., Metayer, C., Gonseth, S., Hansen, H. M., et al. (2018). GWAS in Childhood Acute Lymphoblastic Leukemia Reveals Novel Genetic Associations at Chromosomes 17q12 and 8q24.21. *Nat. Commun.* 9 (1), 286. doi:10.1038/s41467-017-02596-9

Xia, X., Wang, X., Cheng, Z., Qin, W., Lei, L., Jiang, J., et al. (2019). The Role of Pyroptosis in Cancer: Pro-Cancer or Pro-"Host"? *Cell Death Dis.* 10 (9), 650. doi:10.1038/s41419-019-1883-8

Yang, J., Wang, W., Wang, Z., Wang, Z., Wang, Y., Wang, J., et al. (2020). Prevalence, Genotype Distribution and Risk Factors of Cervical HPV Infection in Yangqu, China: A Population-Based Survey of 10086 Women. *Hum. Vaccines Immunother.* 16 (7), 1645–1652. doi:10.1080/21645515.2019.1689743

Zhang, S., Xu, H., Xu, H., Zhang, L., and Qiao, Y. (2020). Cervical Cancer: Epidemiology, Risk Factors and Screening. *Chin. J. Cancer Res.* 32 (6), 720–728. doi:10.21147/j.issn.1000-9604.2020.06.05

Zheng, Z., Deng, W., Lou, X., Bai, Y., Wang, J., Zeng, H., et al. (2020). Gasdermins: Pore-Forming Activities and Beyond. *Acta Biochim. Biophys. Sin. (Shanghai).* 52 (5), 467–474. doi:10.1093/abbs/gmaa016

Zhou, C.-B., and Fang, J.-Y. (2019). The Role of Pyroptosis in Gastrointestinal Cancer and Immune Responses to Intestinal Microbial Infection. *Biochimica Biophysica Acta (BBA) - Rev. Cancer* 1872 (1), 1–10. doi:10.1016/j.bbcan.2019.05.001

Conflict of Interest: The authors declare that the research was conducted in the absence of any commercial or financial relationships that could be construed as a potential conflict of interest.

Publisher's Note: All claims expressed in this article are solely those of the authors and do not necessarily represent those of their affiliated organizations, or those of the publisher, the editors, and the reviewers. Any product that may be evaluated in this article, or claim that may be made by its manufacturer, is not guaranteed or endorsed by the publisher.

Copyright © 2022 Li, Li, Zhang, Feng, Jia, Zhu, Fang, Gong, Dong, Kong, Wang and Sun. This is an open-access article distributed under the terms of the Creative Commons Attribution License (CC BY). The use, distribution or reproduction in other forums is permitted, provided the original author(s) and the copyright owner(s) are credited and that the original publication in this journal is cited, in accordance with accepted academic practice. No use, distribution or reproduction is permitted which does not comply with these terms.

frontiers | Frontiers in Genetics

ORIGINAL RESEARCH
published: 19 July 2022
doi: 10.3389/fgene.2022.838624

Identification and Validation of a Three Pyroptosis-Related lncRNA Signature for Prognosis Prediction in Lung Adenocarcinoma

*Jichang Liu[1†], Qiang Liu[1†], Hongchang Shen[2], Yong Liu[1], Yadong Wang[1], Guanghui Wang[3] and Jiajun Du[1,3]**

[1]*Institute of Oncology, Shandong Provincial Hospital, Cheeloo College of Medicine, Shandong University, Jinan, China,*
[2]*Department of Oncology, Shandong Provincial Hospital Affiliated to Shandong First Medical University, Jinan, China,*
[3]*Department of Thoracic Surgery, Shandong Provincial Hospital, Cheeloo College of Medicine, Shandong University, Jinan, China*

Pyroptosis, defined as programmed cell death, results in the release of inflammatory mediators. Recent studies have revealed that pyroptosis plays essential roles in antitumor immunity and immunotherapy efficacy. Long noncoding RNAs (lncRNAs) are involved in a variety of biological behaviors in tumor cells, although the roles and mechanisms of lncRNAs in pyroptosis are rarely studied. Our study aimed to establish a novel pyroptosis-related lncRNA signature as a forecasting tool for predicting prognosis and ascertaining immune value. Based on lung adenocarcinoma (LUAD) patients from The Cancer Genome Atlas (TCGA), we performed Pearson's correlation analysis to identify pyroptosis-related lncRNAs. After differentially expressed gene analysis and univariate Cox regression analysis, we selected prognosis-related and differentially expressed lncRNAs. Finally, we performed multivariate Cox regression analysis to establish the three pyroptosis-related lncRNA signature. Kaplan–Meier (KM) survival analyses and receiver operating characteristic (ROC) curves indicated the excellent performance for predicting the prognosis of LUAD patients. At the same time, we applied multidimensional approaches to further explore the functional enrichment, tumor microenvironment (TME) landscape, and immunotherapy efficacy among the different risk groups. A nomogram was constructed by integrating risk scores and clinical characteristics, which was validated using calibrations and ROC curves. Three lncRNAs, namely, AC090559.1, AC034102.8, and AC026355.2, were involved in this signature and used to classify LUAD patients into low- and high-risk groups. Overall survival time (OS) was higher in the low-risk group than in the high-risk group, which was also validated in our LUAD cohort from Shandong Provincial Hospital. TME landscape analyses revealed that a higher abundance of infiltrating immune cells and a greater prevalence of immune-related events existed in the low-risk group. Meanwhile, higher expression of immune checkpoint (ICP) genes, higher immunophenoscore (IPSs), and greater T cell dysfunction in the low-risk group demonstrated a better response to immunotherapy than the high-risk group. Combined with predictions from the Tumor Immune Dysfunction and Exclusion (TIDE) website, we found that LUAD patients in the low-risk group significantly benefited from programmed cell death 1 (PD-1) and cytotoxic T-lymphocyte–associated protein 4

OPEN ACCESS

Edited by:
Anton A. Buzdin, European Organisation for Research and Treatment of Cancer, Belgium

Reviewed by:
Leslie Chavez-Galan, Instituto Nacional de Enfermedades Respiratorias-México (INER), Mexico
Bihai Zhao, Changsha University, China

***Correspondence:**
Jiajun Du
dujiajun@sdu.edu.cn

[†]*These authors contributed equally to this work and share first authorship*

Specialty section:
This article was submitted to Cancer Genetics and Oncogenomics, a section of the journal Frontiers in Genetics

Received: *18 December 2021*
Accepted: *15 June 2022*
Published: *19 July 2022*

Citation:
Liu J, Liu Q, Shen H, Liu Y, Wang Y, Wang G and Du J (2022) Identification and Validation of a Three Pyroptosis-Related lncRNA Signature for Prognosis Prediction in Lung Adenocarcinoma. Front. Genet. 13:838624. doi: 10.3389/fgene.2022.838624

(CTLA4) immune checkpoint blockade (ICB) therapy compared with those in the high-risk group. Furthermore, drug susceptibility analysis identified potential sensitive chemotherapeutic drugs for each risk group. In this study, a novel three pyroptosis-related lncRNA signature was constructed, which could accurately predict the immunotherapy efficacy and prognosis in LUAD patients.

Keywords: lung adenocarcinoma, pyroptosis, prognosis, long noncoding RNA, immunotherapy

INTRODUCTION

Lung cancer is currently the leading cause of cancer-related death worldwide, and its 5-year survival rate varies from 4% to 17% depending on stage and regional differences (Hirsch et al., 2017; Siegel et al., 2021). Lung adenocarcinoma (LUAD), as the most common subtype of lung cancer, accounts for approximately 40% of lung cancer cases (Denisenko et al., 2018). Despite the tremendous progress in a variety of treatment strategies, the survival rate of LUAD remains low. Therefore, there is an urgent need of developing accurate and reliable biomarkers for effective prognosis prediction of LUAD.

Pyroptosis is a novel programmed inflammatory cell death mediated by gasdermin proteins (GSDMs) (Yu P. et al., 2021; Deets and Vance, 2021). The activation of caspases-1/4/5/11 by inflammasomes mediates the cleavage of GSDMs, which results in the rupture of cell membranes and release of intracellular proinflammatory substances such as interleukin-1 β (IL-1 β) and interleukin-18 (IL-18). This is followed by a strong inflammatory response that is triggered in the immune microenvironment (Rathinam and Fitzgerald, 2016). In cancer, the complex effects of pyroptosis are dependent on genetic characteristics, which vary across different tissues. Several studies have reported that pyroptosis can suppress tumorigenesis, and even if only a few tumor cells undergo pyroptosis, a strong inflammatory response is triggered to recruit immune cells and enhance T cell-mediated antitumor immunity (Wang et al., 2020; Zhang et al., 2020). Another study has reported that pyroptosis also creates a tumor microenvironment (TME), which was a requirement of tumor growth (Zhang et al., 2021). Nevertheless, the mechanisms of action and effects of pyroptosis are still largely unknown in LUAD.

Long noncoding RNAs (lncRNAs) are transcripts longer than 200 nucleotides that are encoded by the genome but usually not translated into proteins (Bhan et al., 2017). Recent studies have reported that lncRNAs can regulate pyroptosis in a variety of ways such as targeting microRNAs (miRNA) and directly or indirectly binding to pyroptosis-associated proteins (Evavold, Hafner-Bratkovic et al., 2021). As lncRNAs can remain stable in the blood, which is easily collected from patients, they have good prospects as prognostic or predictive markers that are radiosensitive, chemosensitive, and sensitive to target therapy (Chen et al., 2021).

With the development of next-generation sequencing, various biomarkers have been identified to construct signatures for subgroup classification and prognosis prediction (Seijo et al., 2019; Lazzari et al., 2020). However, due to the lack of effective subgroup classification and prognostic prediction models, LUAD patients remain to be undertreated. Therefore, the construction of accurate subgroup classification and prognostic prediction models is urgently needed to guide clinicians on chemotherapy and immunotherapy.

In this study, we aimed to develop a prognostic risk model based on pyroptosis-related lncRNAs in LUAD patients. Based on LUAD patients from The Cancer Genome Atlas (TCGA), we constructed and validated a prognostic risk model to accurately predict the prognosis and overall survival (OS) of LUAD patients, which consisted of three pyroptosis-related lncRNAs. The risk score was significantly associated with tumor-infiltrating immune cells, immune function, and immunotherapy response. Our study revealed the potential connection and mechanism of action between pyroptosis, TME, and immunotherapy response.

MATERIALS AND METHODS

Collection and Processing of Data Sets

Gene transcriptome profiling data, mutation data, and corresponding clinical information of LUAD patients were downloaded from (https://portal.gdc.cancer.gov/). Fragments per kilobase of exon model per million mapped fragments (FPKM) were converted to $log_2\ (FPKM + 1)$ as a reflection of the gene expression level to visually display the results when constructing the figures. The dataset from TCGA served as a training cohort to construct the pyroptosis-related lncRNA prognostic model.

Clinical LUAD Patient Specimens

A total of 45 LUAD patient specimens were recruited at Shandong Provincial Hospital, Shandong, China. The biomedical research ethic committee of Shandong Provincial Hospital approved this study (SWYX: NO. 2021-433).

Differential Gene Expression and Mutation Analyses of Pyroptosis-Related Genes

We identified 33 pyroptosis-related genes from the literature, as listed in **Supplementary Table S1** (Deets and Vance, 2021; Liu et al., 2021; Ye et al., 2021). The R software (R, vision 4.1.0) package "limma" (Ritchie et al., 2015) was used to determine the differently expressed pyroptosis-related genes with the absolute log2-fold change ($|log_2FC|$) > 1 and adjusted p value <0.05. In addition, copy number variations (CNVs), mutation frequencies, and location analyses of pyroptosis-related genes were performed

using "maftools" (Mayakonda et al., 2018) and "RCircos" with R software (Zhang et al., 2013).

Identification of Pyroptosis-Related lncRNAs

Pyroptosis-related lncRNAs were extracted using Pearson's correlation analysis between pyroptosis-related genes and lncRNAs (correlation coefficient >0.60, $p < 0.001$, and false-discovery rate (FDR) < 0.05).

Construction of an mRNA–lncRNA Network

We extracted differently expressed pyroptosis-related lncRNAs with an $|log_2\mathbf{FC}| > 1$ and an adjusted p value <0.05 using R package "limma". Subsequently, 17 prognostic pyroptosis-related lncRNAs were identified by applying univariate Cox regression analysis ($p < 0.05$). A hazard ratio (HR) < 1 represented that lncRNAs were protective factors. To explore the regulatory mechanism of the selected pyroptosis-related lncRNAs, an mRNA–lncRNA regulatory network was constructed based on the 17 lncRNAs and two co-expressed mRNAs.

Survival Analysis and Differential Expression Analysis of Co-expressed mRNAs by the Website

The Kaplan–Meier plotter (https://kmplot.com/analysis/) was used to analyze the impact of co-expressed mRNAs, while TIMER2.0 (Li et al., 2020) (http://timer.cistrome.org/) and gene expression profiling integrative analysis (Tang et al., 2017) (GEPIA, http://gepia.cancer-pku.cn/) were used for differential expression analysis of co-expressed mRNAs.

Construction of a Risk Score

According to the prognostic-related lncRNAs, multivariate Cox regression analysis was performed to identify the best prognostic signature, which consisted of three lncRNAs, namely, AC090559.1, AC026355.2, and AC034102.8. We calculated the risk score as follows: risk score = (−0.2603×AC090559.1) + (−0.0974×AC026355.2) + (−0.9235×AC034102.8). Based on the median of risk score, the LUAD patients from the TCGA database were divided into high- and low-risk groups for further analysis. Subsequently, risk score distribution maps, survival status maps, and lncRNA expression heat maps were plotted. Kaplan–Meier analysis was applied to compare the overall survival (OS) of the two groups. The time receiver operating characteristic (ROC) curve was plotted using the "timeROC" package with R software, which was used to evaluate the predictive capability of the risk model. The area under the curve (AUC) of the constructed risk model in predicting the OS of LUAD patients was compared with several previously published lncRNA signatures, including the ferroptosis-related lncRNA signature of Lu (Lu et al., 2021), hypoxia-associated lncRNA signature of Shao (Shao et al., 2021), autophagy-related lncRNA signature of Liu (Liu and Yang, 2021), and six-lncRNA-based prognostic signatures of Yang (Yang et al., 2021).

Establishment of the Nomogram

The prognostic significance of the risk score and other clinical characteristics was evaluated by using univariate and multivariate Cox regression analyses. A nomogram was established to predict the 1-, 3-, and 5-year OS, which consisted of the risk score, age, and stage. Calibration curves were plotted to assess the accuracy of the risk model.

Functional Enrichment Analysis

GO enrichment analysis was applied to investigate the potential pathways of the differentially expressed pyroptosis genes using "org.Hs.eg.db," "clusterProfiler," and "enrichplot" modules within the R package. By applying the "GSVA" tool, GSVA enrichment analysis was performed based on hallmark gene sets extracted from the MSigDB database (Hänzelmann et al., 2013).

TME Landscape Analyses

Single-sample gene set enrichment analysis (ssGSEA) was performed to compare the difference in abundance of 28 types of infiltrating immune cells, 13 immune functions, and 13 other tumor-related biological processes, which were extracted from previous articles (Şenbabaoğlu et al., 2016; Charoentong et al., 2017; Mariathasan et al., 2018). In addition, we used computational methods to assess the infiltrating immune cells, including the TIMER (Li et al., 2020), CIBERSORT (Chen et al., 2018), quanTIseq (Finotello et al., 2019), MCP-counter (Becht et al., 2016), xCell (Aran et al., 2017), EPIC (Racle et al., 2017), and TIDE (Jiang et al., 2018) algorithms. Immune score and tumor purity were calculated using the "ESTIMATE" tool within the R package (Chakraborty and Hossain, 2018). In addition, correlation analysis was performed using the correlation heat map tool in HiPlot (https://hiplot.com.cn), a comprehensive web platform for scientific data visualization.

Prediction of Response to Immune Checkpoint Blockade (ICB) Therapy

The immunophenoscore (IPS) was obtained from The Cancer Immunome Atlas (https://tcia.at/). Information on the dysfunction and exclusion of infiltrating cytotoxic T lymphocytes (CTLs) was downloaded from the Tumor Immune Dysfunction and Exclusion (TIDE) website (http://tide.dfci.harvard.edu/). In addition, TIDE was used to evaluate patients who received a benefit or no benefit from ICB therapy through the comprehensive biomarkers of the ICB response in different groups (Fu et al., 2020).

RNA Extraction and Real-Time PCR

Following the manufacturer's protocol, total RNA was extracted from clinical specimens using AG RNAex Pro Reagent (Accurate Biotechnology (Hunan) Co., Ltd., China). The Evo M-MLVRT Master Mix kit (Accurate Biotechnology (Hunan) Co., Ltd., China) was used for reverse transcription to obtain cDNA. Relative gene expression was detected using the SYBR Premix Ex Tap kit (Accurate Biotechnology (Hunan) Co., Ltd., China) and normalized to the expression using 18S. The primers are listed in **Supplementary Table S1**.

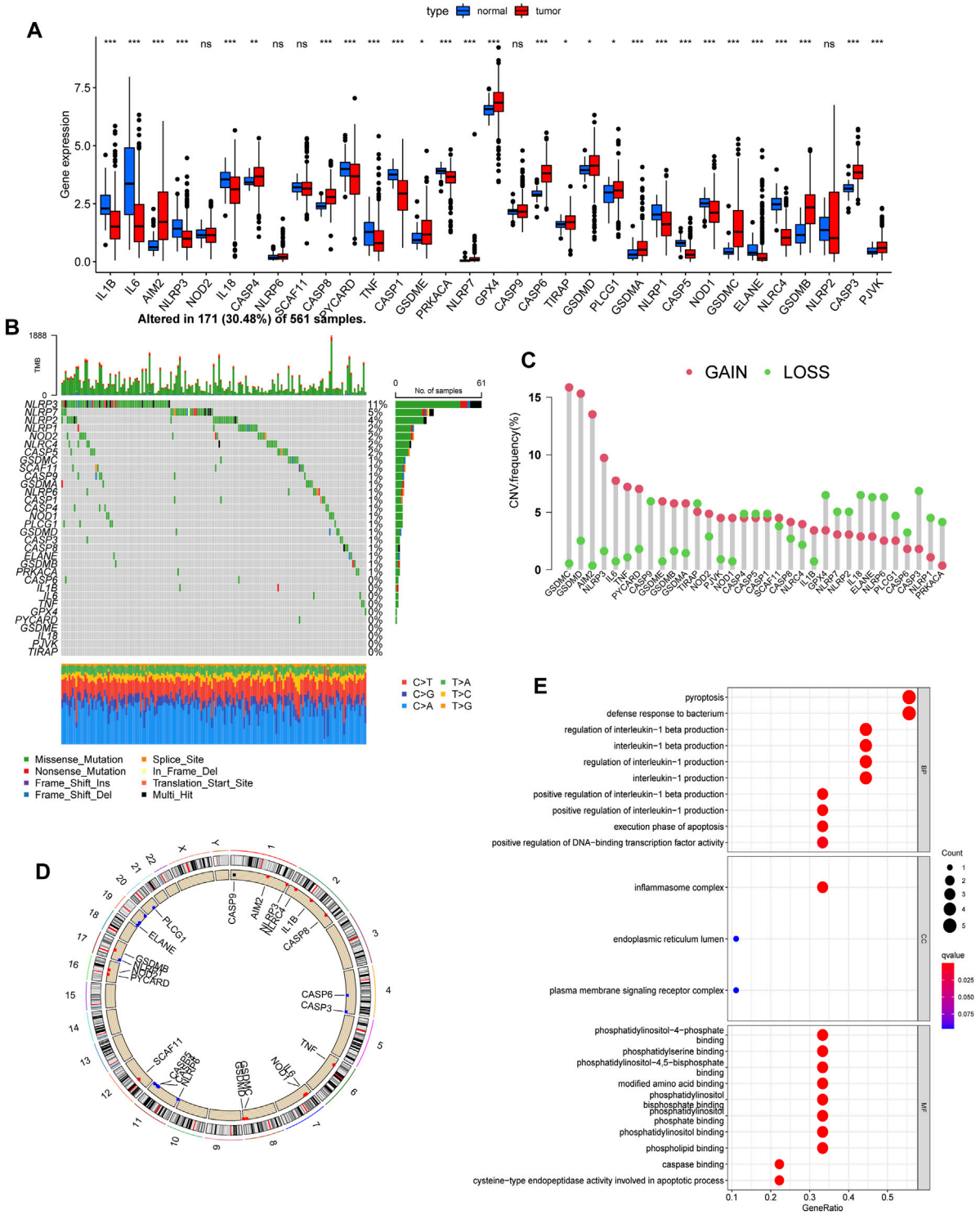


FIGURE 1 | Landscape of expression, genetic variation, and functional enrichment of pyroptosis-related genes in LUAD. **(A)** Expression of pyroptosis-related genes between normal tissues and LUAD tissues (Wilcoxon test, $*p < 0.05$; $**p < 0.01$; $***p < 0.001$; ns, not statistically significant). **(B)** Landscape of mutation profiles in LUAD patients from the TCGA cohort. **(C)** CNV frequency of 33 pyroptosis-related genes. **(D)** Location of CNV alternation of pyroptosis-related genes in the chromosome. The red dots represent more samples with increased copy number gains than samples with copy number losses, while the blue dots are the opposite. The black dot means the two are equal. **(E)** Enrichment analysis of GO biological process, cellular component, and molecular function. LUAD, lung adenocarcinoma; CNV, copy number variation.

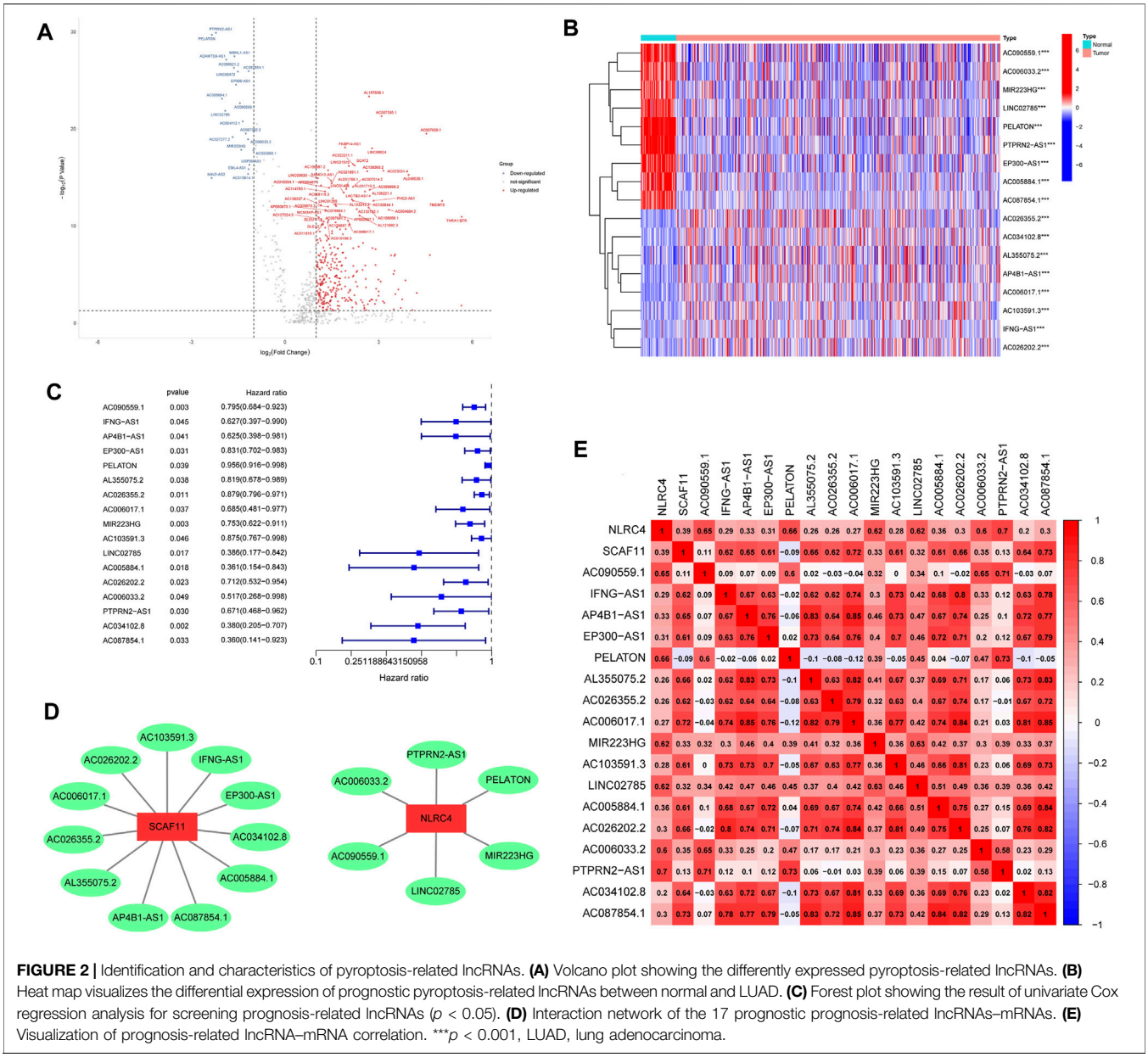


FIGURE 2 | Identification and characteristics of pyroptosis-related lncRNAs. **(A)** Volcano plot showing the differently expressed pyroptosis-related lncRNAs. **(B)** Heat map visualizes the differential expression of prognostic pyroptosis-related lncRNAs between normal and LUAD. **(C)** Forest plot showing the result of univariate Cox regression analysis for screening prognosis-related lncRNAs ($p < 0.05$). **(D)** Interaction network of the 17 prognostic prognosis-related lncRNAs–mRNAs. **(E)** Visualization of prognosis-related lncRNA–mRNA correlation. ***$p < 0.001$, LUAD, lung adenocarcinoma.

Statistical Analysis

Student's t test was used to compare the differences between the two groups. Pearson's correlation test was used for correlation analysis. Survival analysis was performed by the Kaplan–Meier method and compared with the log-rank test. All statistical analyses were performed using R software (vision 4.1.0), and $p < 0.05$ was considered statistically significant.

RESULTS

Landscape of Pyroptosis-Related Genes in LUAD

We identified 33 pyroptosis-related genes and performed differential gene expression analysis between LUAD and normal lung tissues. A total of 15 genes, namely, AIM2, CASP4, CASP8, GSDME, NLRP7, GPX4, CASP6, TIRAP, GSDMD, PLCG1, GSDMA, GSDMC, GSDMB, CASP3, and PJVK were highly expressed in LUAD, while the expression of IL1B, IL6, NLRP3, IL18, PYCARD, TNF, CASP1, PRKACA, NLRP1, CASP5, NOD1, ELANE, and NLRC4 was decreased (**Figure 1A**). Subsequently, we developed a panorama of the somatic mutations of pyroptosis-related genes. A total of 30.48% of the samples had mutations, and the three genes with the highest mutation rates were NLRP3 (11%), NLRP7 (5%), and NLRP2 (4%) (**Figure 1B**). **Figures 1C and D** show the frequency of the CNV alterations of the 33 pyroptosis-related genes and their locations on the chromosome. The frequency of copy number mutations in pyroptosis-related genes was greater

TABLE 1 | Results of univariate Cox regression.

ID	HR	HR.95L	HR.95H	*p*-Value
AC090559.1	0.79477	0.68402	0.923452	0.002699
IFNG-AS1	0.626928	0.396886	0.990309	0.045315
AP4B1-AS1	0.624799	0.397789	0.98136	0.041187
EP300-AS1	0.831072	0.702447	0.983248	0.031015
PELATON	0.955892	0.915806	0.997732	0.039035
AL355075.2	0.818529	0.677601	0.988767	0.037789
AC026355.2	0.879216	0.79625	0.970827	0.010915
AC006017.1	0.685354	0.48061	0.97732	0.036918
MIR223HG	0.752638	0.622047	0.910645	0.003471
AC103591.3	0.874798	0.767129	0.997579	0.045919
LINC02785	0.386337	0.17719	0.842352	0.016787
AC005884.1	0.360554	0.154291	0.842556	0.018495
AC026202.2	0.712373	0.532036	0.953836	0.022767
AC006033.2	0.517374	0.268118	0.99835	0.049427
PTPRN2-AS1	0.671347	0.4684	0.962225	0.030035
AC034102.8	0.380262	0.204576	0.706823	0.002236
AC087854.1	0.360318	0.140624	0.923239	0.033476

than the frequency of copy number deletions. To clarify the functions of the pyroptosis-related genes, we conducted GO functional enrichment analyses. Apart from the pyroptosis pathway, pyroptosis-related genes were also enriched in defense response to bacterium, regulation of interleukin-1 or interleukin-1β production, and inflammasome complex (**Figure 1E**).

Identification of Prognostic Pyroptosis–Related lncRNAs

We first performed correlation analysis (correlation coefficients >0.60, $p < 0.001$, FDR<0.05) between 14,057 lncRNAs and 33 pyroptosis-related genes in LUAD samples, and 1,070 pyroptosis-related lncRNAs were identified. Subsequently, 320 differently expressed pyroptosis-related lncRNAs were identified and exhibited in a volcano map after differential expression analysis (**Figure 2A**). Finally, 17 lncRNAs related to LUAD prognosis were identified after applying univariate COX regression analysis (**Table 1**). A heat map was plotted to show the differential expression of the 17 lncRNAs between normal and tumor tissues (**Figure 2B**). The forest map indicated that the hazard ratios of these 17 lncRNAs were all <1, suggesting that they were protective factors for prognosis (**Figure 2C**). In addition, we used Cytoscope to construct a co-expression network for the 17 pyroptosis-related lncRNAs and two corresponding genes (**Figure 2D**). The correlation scores between NLRC4, SCAF11, and 17 lncRNAs are shown in **Figure 2E**, suggesting that these lncRNAs may perform functions through NLRC4 and SCAF11. Next, we analyzed the impact of NLRC4 and SCAF11 on survival by applying the Kaplan–Meier plotter, which indicated that high expression was significantly associated with high overall survival (**Supplementary Figure S1A**). TIMER2.0 and GEPIA were used for differential gene expression analysis, and the results showed a significant downregulation of NLRC4 in LUAD but no change in SCAF11 (**Supplementary Figure S1B–D**).

Establishment of a Risk Model

We subsequently performed multivariate COX regression analysis on the previously obtained 17 lncRNAs and three lncRNAs were identified (**Figure 3A**). A risk score was established based on the multivariate regression coefficients (**Table 2**). According to the median risk score, LUAD patients were divided into high- and low-risk groups. Most pyroptosis-related genes were significantly upregulated in the low-risk group, suggesting a more active involvement of pyroptosis (**Figure 3B**). By contrast, survival analysis revealed that patients in the low-risk group showed a better prognosis, indicating that pyroptosis was associated with survival advantages (**Figure 3C**). Principal component analysis (PCA) indicated significant distinction in transcription profiles between the two groups (**Figure 3D**). The risk score, survival status, and lncRNA expression are shown in **Figure 3E**, revealing that mortality was significantly related to risk score. Moreover, a higher risk score was significantly related to advanced stage (**Figure 3F**). These results indicated that a lower risk score was associated with active pyroptosis and better clinical outcome. The areas under the curves (AUCs) of the 1-year, 3-year, and 5-year ROC curve were 0.775, 0.730, and 0.705, respectively, revealing a high accuracy in the prognosis prediction of the risk model (**Figure 3G**). Compared with four published lncRNA signatures, the risk model we constructed had higher accuracy in predicting 1-, 3-, and 5-year survival for TCGA–LUAD patients (**Figure 3H**).

Construction of a Predictive Nomogram

After incorporating the risk scores and clinical features, univariate and multivariate COX regression analyses were performed, and the results indicated that the risk score could serve as an independent factor affecting the survival of LUAD patients, similar to stage and age (**Figures 4A,B**). To better predict the 1-, 3-, and 5-year OS of LUAD patients, we constructed a nomogram by incorporating risk score, age, and stage (**Figure 4C**), and calibration curves were constructed to assess the accuracy of nomogram (**Figure 4D**).

Differences in Landscape of the TME Between the High- and Low-Risk Groups

To further understand the significance of the risk score, we conducted GSVA analysis. Several immune-related pathways and events, including interferon (IFN) gamma/alpha response, IL-6–JAK-STAT3 signaling, allograft rejection, and inflammatory response, were upregulated in the low-risk group, while in the high-risk group, metabolic and cancer-promoting pathways, such as oxidative phosphorylation, glycolysis, MYC signaling, E2F signaling, and MTORC1 signaling, were activated (**Figure 5A**).

We investigated the differences in various immune-related functions, immune-infiltrating cells, and other tumor-related functions between high- and low-risk groups using ssGSEA. As expected, the low-risk group, with a higher level of pyroptosis, was more involved in immune-related functions such as antigen-presenting cell (APC) co-stimulation/inhibition, inflammation, cytolytic activity, human leukocyte antigen (HLA) function, T cell co-stimulation/inhibition, and type I/II IFN responses,

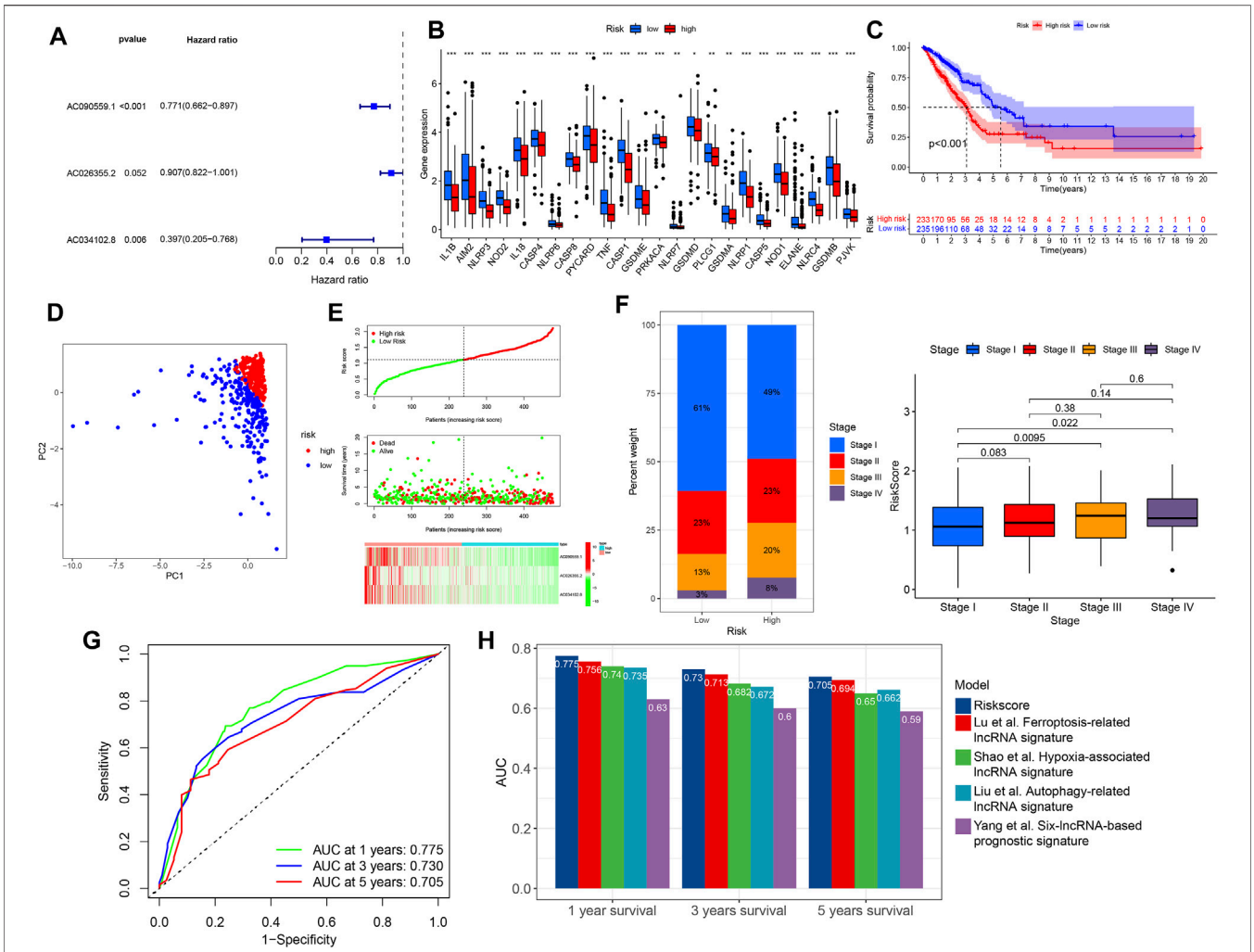


FIGURE 3 | Construction of risk model and clinical correlation of high- and low-risk groups. **(A)** Three lncRNAs were identified in multivariate Cox regression analysis for model construction. **(B)** Differential expression of pyroptosis-related genes between high- and low-risk groups (Wilcoxon test, $*p < 0.05$; $**p < 0.01$; $***p < 0.001$). **(C)** Kaplan–Meier curve of high- and low-risk groups. **(D)** PCA of high and low-risk groups. **(E)** Risk curve based on the risk score of each sample. Scatterplot showing the survival status of LUAD patients. Heat map showing the expression of identified lncRNAs in high- and low-risk groups. **(F)** Relationship between tumor stage and risk score. **(G)** Time-dependent ROC curves of OS at 1, 3, and 5 years. **(H)** Comparison of the risk model with four published lncRNA signatures. OS, overall survival; PCA, principal component analysis.

TABLE 2 | Results of multivariate Cox regression.

ID	Coef	HR	HR.95L	HR.95H	*p*-Value
AC090559.1	−0.26027	0.77084	0.662457	0.896955	0.000761
AC026355.2	−0.09742	0.907175	0.822133	1.001013	0.052403
AC034102.8	−0.9235	0.397127	0.205362	0.76796	0.006058

indicative of active immune functions (**Figure 5B**). Consistently, the higher abundance of most infiltrating immune cells existed in the low-risk group, including activated B cells, activated $CD8^+$ T cells, dendritic cells, eosinophils, MDSCs, and macrophages (**Figure 5C**, **Supplementary Figure S2**). In addition, several tumor-related pathways and events, including immune checkpoint, angiogenesis, antigen processing machinery, and $CD8^+$ T effector function, were also upregulated in the low-risk group. By contrast, DNA damage repair, mismatch repair, nucleotide excision repair, and DNA replication were upregulated in the high-risk group, which may play roles in genome stability and LUAD progression (**Figure 5D**). In addition, HLA-related genes were significantly upregulated in the low-risk group, indicative of antigen presentation (**Figure 5E**). Finally, tumor purity, immune score, ESTIMATE score, and stromal score were calculated using the "estimate" tool within the R package (**Figure 5F**). Significantly upregulated immune and stromal scores were features of the low-risk group, while the high-risk group was characterized by higher tumor purity.

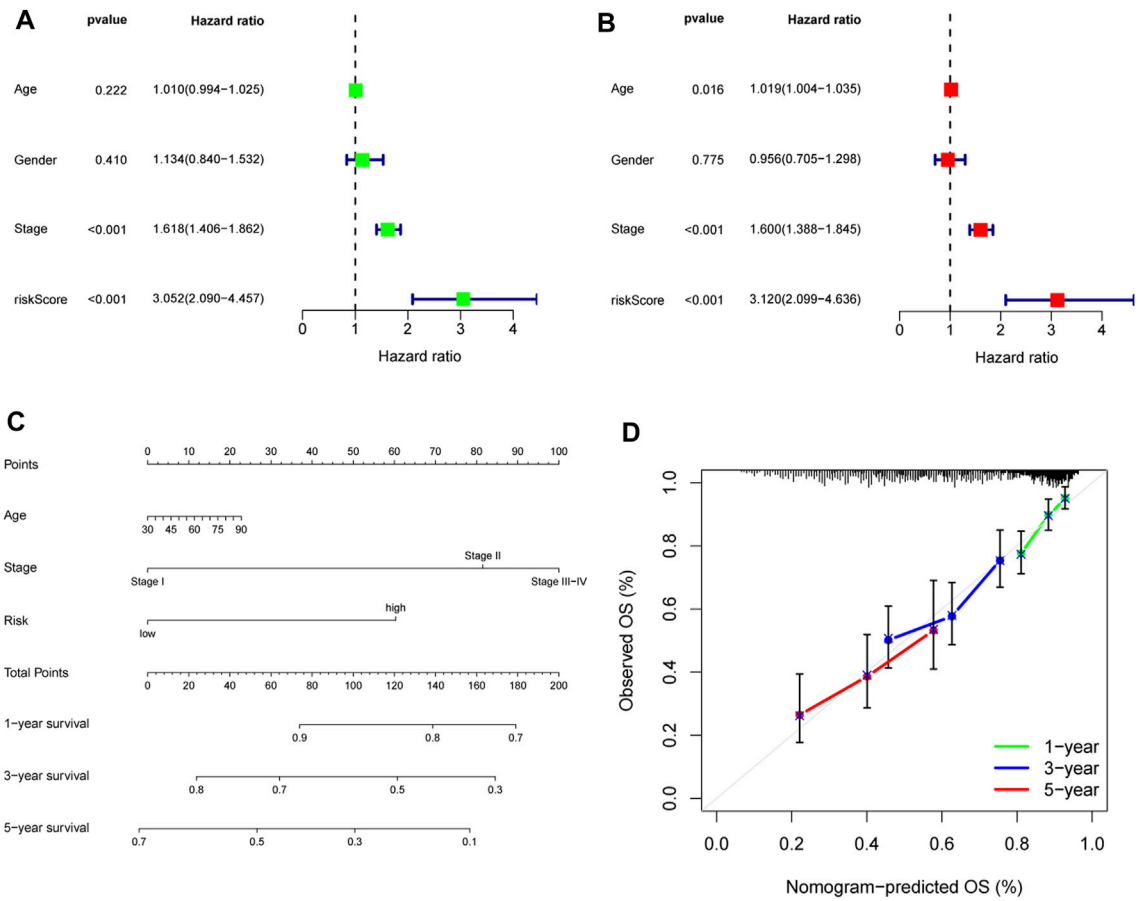


FIGURE 4 | Construction and validation of a nomogram. Univariate **(A)** and multivariate **(B)** Cox regression analyses of age, gender, stage, and risk score. **(C)** Nomogram for predicting the OS of LUAD patients at 1, 3, and 5 years. **(D)** Calibration curves of the nomogram for OS prediction at 1, 3, and 5 years. OS, overall survival; LUAD, lung adenocarcinoma.

Prediction of Response to ICB Therapy

Considering the significant differences in the TME landscape, we identified several ICPs and performed differential expression analysis between low- and high-risk groups. As shown in **Figure 6A**, all 39 selected ICPs were upregulated in the low-risk group, indicating the potential benefit of ICI therapy. Furthermore, we used IPS obtained from TIDE as a predictor of the response to anticytotoxic T lymphocyte antigen-4 (CTLA-4) and antiprogrammed cell death protein 1 (anti-PD-1) antibodies (Charoentong et al., 2017). The results showed a higher IPS level in the low-risk group, revealing a better response to combined PD1 and CTLA4 blockade therapy or PD1 monotherapy (**Figures 6B,C**). Considering the upregulation of immune checkpoints and infiltration of Treg cells in the low-risk group, which could suppress the effect of $CD8^+$ T cells, we further investigated the status of T cells in the TME. Consistently, the low-risk group was characterized by higher T cell dysfunction and lower exclusion, suggesting a potential advantage to ICI therapy (**Figures 6D,E**). To further investigate the response to ICIs, we utilized the TIDE website to predict the "responder" and "nonresponders" of PD1 and CTLA4 blockade therapy in TCGA–LUAD patients, which were constructed by integrating TIDE score, IFNG, MSI, MDSC, CAFs, and other published modules. We found that 44% of patients in the low-risk group were identified as responders to PD1 and CTLA4 blockade therapy, while only 31% in the high-risk group were classified as responders (**Figure 6F**). In further analysis, only 4% of patients in the low-risk group showed no benefit from ICB compared with 13% in the high-risk group (**Figure 6G**). In addition, patients who were not responders or showed no benefit from PD1 and CTLA4 blockade therapy had significantly higher risk scores (**Figures 6H,I**).

In conclusion, the low-risk group could be clarified as an immune "hot" phenotype, with a high abundance of infiltrating immune cells and better efficacy for PD1 and CTLA4 blockade therapy, while the high-risk group represented the immune "cold" phenotype which was characterized by less sensitivity to ICB.

To explore whether the risk score affected immune function through NLRC4 or SCAF11, we performed a correlation analysis between NLRC4 or SCAF11 and infiltrating immune cells. The heat map showed that lncRNA AC090559.1 and its corresponding mRNA NLRC4 were closely correlated with infiltrating immune cells, suggesting that AC090559.1 may

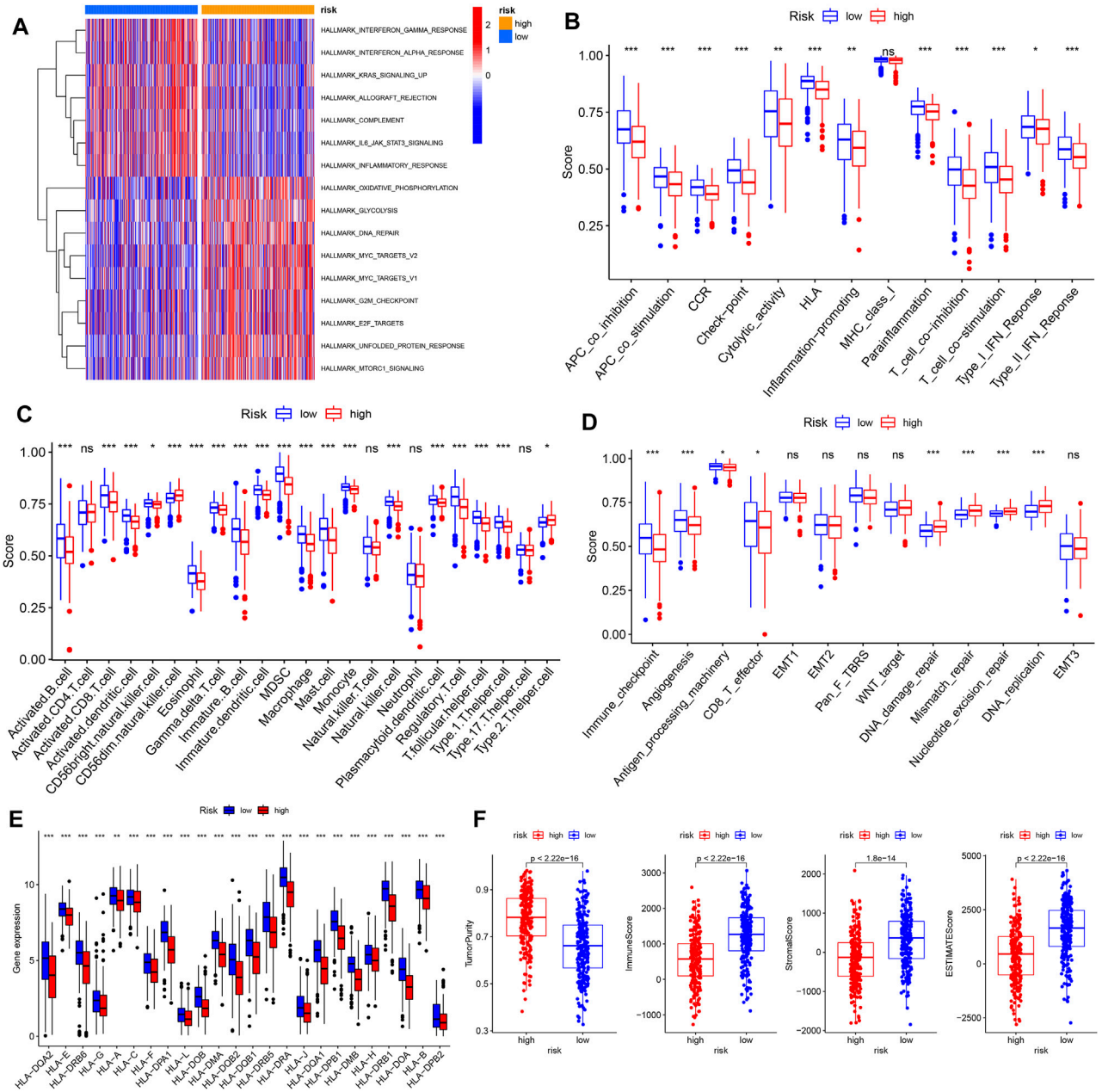


FIGURE 5 | Differences in landscape of the TME between high- and low-risk groups. **(A)** GSVA enrichment analysis of tumor hallmark pathways. **(B–E)** Differences in immune-related functions, TME infiltrating immune cells, other tumor-related functions, and HLA-related gene expression in the high- and low-risk groups. **(F)** Comparison of tumor purity, immune score, stromal score, and ESTIMATE score between high- and low-risk groups. TME, tumor microenvironment, $^{*}p < 0.05$; $^{**}p < 0.01$; $^{***}p < 0.001$; ns, not statistically significant.

exert its regulatory function by targeting NLRC4 (**Supplementary Figure S3**). The scatter plots of NLRC4, SCAF11, and various infiltrating immune cells downloaded from TIMER indicated that NLRC4 was highly correlated with a variety of immune cells (**Supplementary Figure S4**). Finally, we predicted the sensitivity of several common chemotherapy drugs in high- and low-risk groups. The high-risk group was more sensitive to doxorubicin, sorafenib, docetaxel, and erlotinib but less sensitive to gefitinib (**Supplementary Figure S5**).

Validation of the Risk Model With the Clinical Cohort

We detected the relative expression levels of the three lncRNAs in LUAD specimens by using qRT-PCR. The risk score was

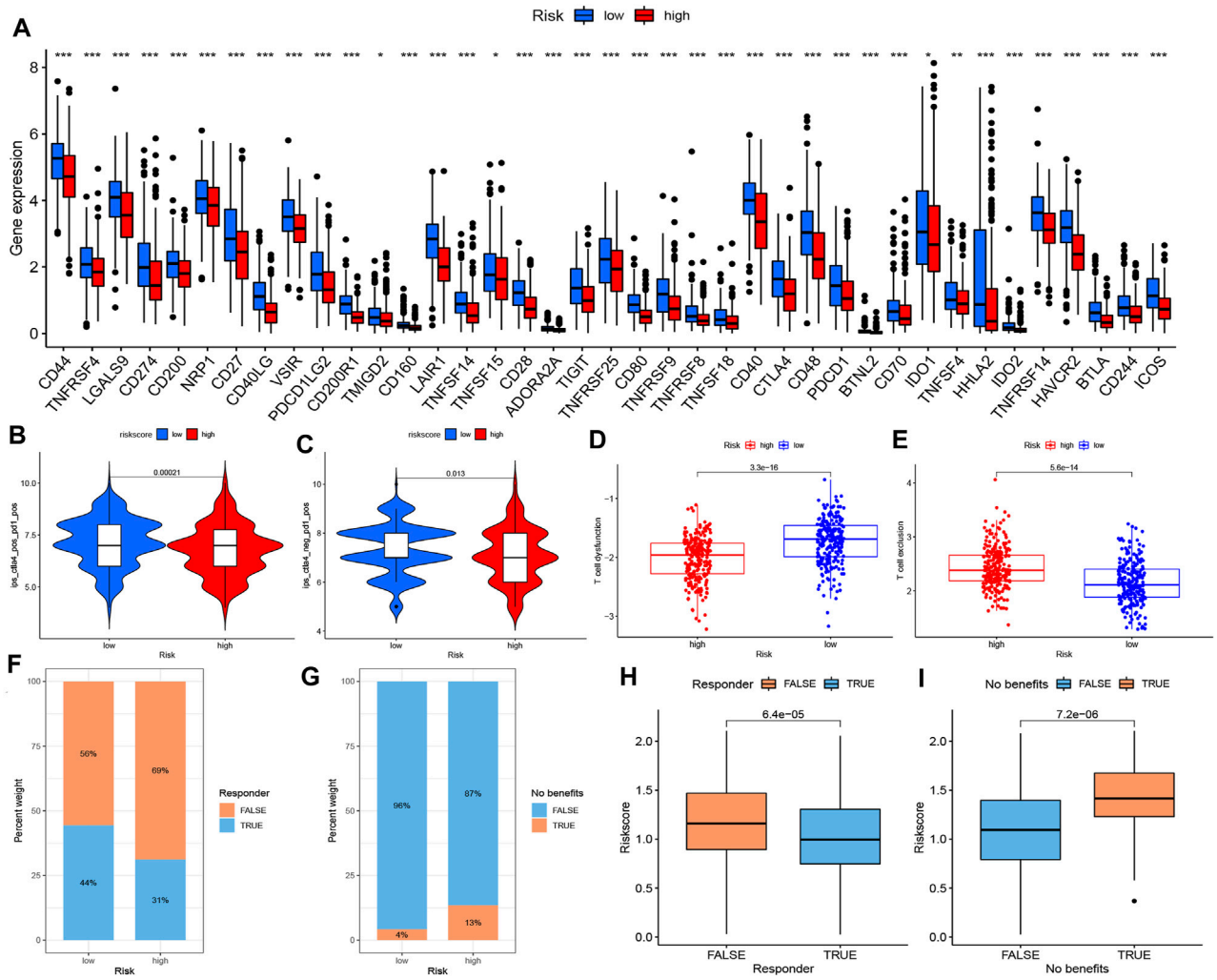


FIGURE 6 | Prediction of response to ICB therapy. **(A)** The expression of ICPs between high- and low-risk groups (Wilcox test, $*p < 0.05$; $**p < 0.01$; $***p < 0.001$). The response to combined PD1 and CTLA4 blockade therapy **(B)** and PD1 monotherapy **(C)** between high- and low- risk groups. Differences in T cell status, including T cell dysfunction **(D)** and T cell exclusion **(E)**, in high and low risk groups. **(F–I)** Prediction of the "responder" and "no benefit" of PD1 and CTLA4 blockade therapy in TCGA- LUAD patients from TIDE website. ICB immune checkpoint blockade, ICP immune checkpoint, PD1 programmed cell death protein 1, TCGA The Cancer Genome Atlas, LUAD lung adenocarcinoma.

subsequently calculated, and the patients were divided into high- and low-risk groups based on the median value. The overall survival of the low-risk group was significantly better, consistent with previous results (**Figure 7A**). The AUC values of 3 year, 5 year and 7 year were 0.599, 0.671, and 0.704, respectively (**Figure 7B**). By correlation analysis of the three identified lncRNAs and immune checkpoint genes in LUAD specimens, we found a strong correlation between risk score and CTLA4, indicative of a better response to anti-CTLA4 immunotherapy (**Figures 7C,D**).

DISCUSSION

In recent years, the development of immunotherapy and chemotherapy has brought about a paradigm shift in the treatment of LUAD patients. However, only some patients can benefit from immunotherapy due to drug resistance (Boumahdi and de Sauvage, 2020). Furthermore, it is still difficult to identify patients who may benefit from immunotherapy. Therefore, it is important to identify novel therapeutic targets.

Pyroptosis is a type of GSDM-mediated programmed cell death that is accompanied by the release of damaged-associated molecular pattern (DAMP) and mature IL-1 proteins, which can lead to recruitment of immune cells (Rathinam and Fitzgerald, 2016; Liu et al., 2021). Pyroptosis plays distinct roles in tumor microenvironments, and thus, tumorigenesis. On the one hand, long-term chronic inflammation induced by pyroptosis can stimulate and promote tumorigenesis. On the other hand, pyroptosis can also alter the abundance of infiltrating immune cells and

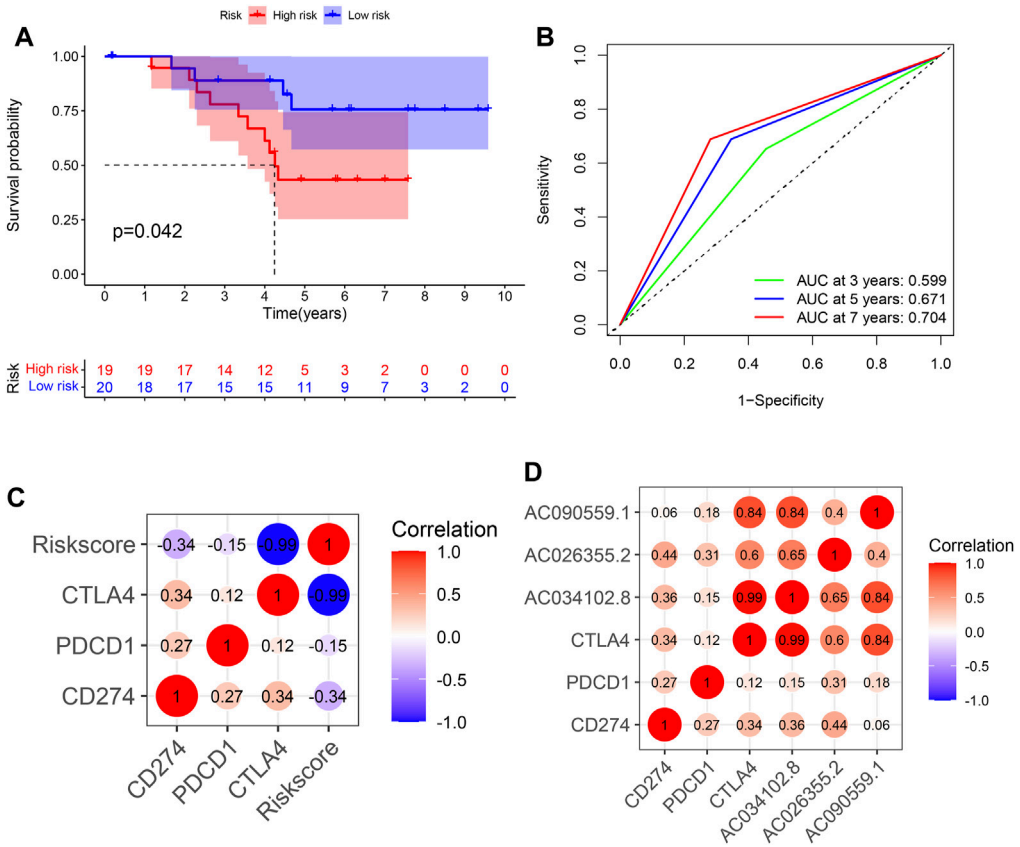


FIGURE 7 | Validation of risk score using clinical specimens of LUAD patients. **(A)** Kaplan–Meier curve of high- and low-risk groups in clinical LUAD patients. **(B)** Time-dependent ROC curves of OS at 1, 3, and 5 years. **(C)** The correlation between 3 identified lncRNAs, risk score and immune checkpoints. LUAD, lung adenocarcinoma; OS, overall survival.

transform "cold" tumors into "hot" tumors, which could enhance the antitumor immune response (Du et al., 2021; Zhang et al., 2021). Moreover, pyroptosis plays important roles in activating antitumor immunity. Granzyme A, which is released by CTLs and natural killer cells, can directly cleave GSDMB to mediate tumor cell pyroptosis (Zhou et al., 2020). Meanwhile, the inflammatory response triggered by pyroptosis in a small proportion of tumor cells can trigger a strong antitumor immune response (Wang et al., 2020). Similarly, GSDME also converts apoptosis, a noninflammatory programmed cell death, into pyroptosis, and exerts antitumor functions while enhancing CTL and natural killer cell infiltration (Zhang et al., 2020). Therefore, we speculate that pyroptosis can improve the prognosis and efficacy of immunotherapy in LUAD patients. In addition, abnormally expressed lncRNAs in tumors can be detected in plasma, urine, or saliva specimens, which indicates that they have potential value as biomarkers of lncRNAs (Chandra Gupta and Nandan Tripathi, 2017). Therefore, we aimed to develop a pyroptosis-related lncRNA-based signature to accurately predict the immunotherapy efficacy and prognosis of LUAD patients.

In this study, we first extracted pyroptosis-related genes from previously published articles, and 17 prognostic-related lncRNAs were identified after correlation analysis, differential expression analysis, and univariate Cox regression analysis. After multivariate regression analysis, we developed a risk model consisting of three pyroptosis-related lncRNAs. Based on the median risk score, we divided patients into high- and low-risk groups and analyzed the differences in prognosis and immune microenvironment. ROC curves were used to verify the accuracy of the risk score. In addition, 39 LUAD patients from Shandong Provincial Hospital were used as a test cohort to verify the risk score.

The risk score served as an independent factor, which was significantly associated with stage and survival. A better prognosis was observed in the low-risk group, accompanied by highly expressed pyroptosis-related genes. Consistent with previous studies, active pyroptosis was associated with better prognosis. GSVA enrichment analysis showed that a greater inflammatory response existed in the low-risk group, which involved interferon γ/α and IL6/JAK/STAT3 pathways, allograft rejection, complement, and inflammatory response. By contrast, the high-risk group was more related to MYC, E2F, MTORC1, and glycolytic pathways, which are essential for tumorigenesis. Similarly, the abundance of infiltrating immune cells was generally higher in the low-risk group. Considering the results

of ssGSEA (**Figure 5C**) and correlation analysis (**Supplementary Figure S3**), we noticed that the significantly enriched infiltrating immune cells were mainly associated with inflammation and antigen presentation (eosinophils, mast cells, monocytes, macrophages, immature dendritic cells, and activated dendritic cells) and immunomodulatory events (regulatory T cell and various T helper cells) in the low-risk group. As shown in **Figure 5E**, HLA function was significantly activated in the low-risk group, further confirming antigen presentation.

Interestingly, activated $CD8^+$ T cells highly infiltrated the low-risk group, accompanied by the high abundance of immunosuppressive cells such as Treg and MDSCs (**Figure 5C**). Considering simultaneous T cell co-stimulation and co-inhibition, we examined whether T cells could exercise their conventional function of antitumor immunity in the low-risk group (**Figure 5B**). As such, we analyzed the dysfunction and exclusion of T cells, which revealed significant T cell dysfunction in the low-risk group (**Figures 6D,E**). A previous study has reported that a broad spectrum of dysfunctional states can exist in intratumoral T cells, which essentially blocks the durable clinical benefits of patients (Thommen and Schumacher, 2018). The upregulation of ICPs mediated by PD-1 was the main manifestation of T cell dysfunction, accompanied by a variety of other inhibitory factors such as Treg cell infiltration, cytokine production, and metabolic stress (Speiser et al., 2016; Zarour, 2016; Gajewski et al., 2013). According to previous reports on the simultaneous blockade of PD-1, other inhibitory receptors such as CTLA-4, Tim-3, Lag-3, and TIGIT have been shown to reactivate dysfunctional T cells and provide benefit from ICBs, which was also verified in our results (**Figures 6F–I**).

Therefore, the low-risk group was considered an immune "hot" phenotype, indicative of a beneficial response to immunotherapy. Alternatively, the high-risk group was identified as an immune "cold" phenotype, whose efficacy of immunotherapy was poor.

In our study, the constructed risk score consisted of only three pyroptosis-related lncRNAs, namely, AC090559.1, AC034102.8, and AC026355.2, which have been rarely mentioned in previous studies. Nevertheless, AC090559.1 was also identified as an independent risk factor related to autophagy and ferroptosis, suggesting that it may be a key regulator in programmed cell death (Guo et al., 2021; Wu et al., 2021). We also found that AC090559.1 may have a potential regulatory relationship with NLRC4. NLRC4 is the core component of NLRC4 inflammasomes, which was composed of a trigger (e.g., cytosolic flagellin), sensor (NAIP), nucleator (NLRC4), adapter (ASC), and effector (CASP1) (Duncan and Canna, 2018). The activation of NLRC4 inflammasomes can activate caspase-1, which cleaves pro-IL-1β and pro-IL-18 and simultaneously cleaves and activates gasdermin-D, thereby activating pyroptosis (Kay et al., 2020). Similar to pyroptosis, the effects of NLRC4 depend on the type and genomic background of the tumor. Continuously aberrant activation of chronic inflammation mediated by NLRC4 can promote the malignant progression of tumor cells. A previous study revealed that obesity-associated NLRC4 inflammasomes mediated IL-1β release, which promotes the growth of breast cancer by triggering VEGF production and angiogenesis (Kolb et al., 2016). Similarly, in nonalcoholic fatty liver, IL-1 signaling promoted metastasis (Ohashi et al., 2019). Consistent with our research, NLRC4 could also suppress tumor development while inducing antitumor immunity. In another study, Flagrp170, an artificially designed immunomodulator, showed protective antitumor immunity in an NLRC4-dependent manner (Yu X. et al., 2021). Sutterwala et al. demonstrated that NLRC4 enhanced inflammation in tumor-associated macrophages (TAMs) in a noninflammasome-dependent manner and the antimelanoma effects of IFN-γ produced by CD4 + and CD8 + T cells (Janowski et al., 2016). Moreover, NLRC4/NAIP5 also participated in the antigen recognition of flagellin-expressing tumor cells to facilitate antigen presentation to T cells, thereby activating $CD4^+$ and $CD8^+$ T cells and exerting antitumor effects (Garaude et al., 2012). However, studies on NLRC4 in lung cancer are still limited.

We found that NLRC4 was highly associated with immune cells such as activated/immature/plasmacytoid dendritic cells, γ delta T cells, MDSCs, macrophages, natural killer cells, regulatory T cells, T follicular helper cells, and type 1 T helper cells. Interestingly, AC090559.1 showed a similar effect compared with NLRC4 in the aforementioned immune cells (**Supplementary Figure S3**), suggesting that AC090559.1 may affect the extent of pyroptosis and the abundance of immune cells through NLRC4. Here, we performed correlation analysis of the three identified lncRNAs and several immune checkpoints and observed that these three lncRNAs were highly correlated with CTLA4 expression, suggesting that the risk model may reveal more significant effects on CTLA4 blockade; regardless of this, there were some limitations. Presently, there are few studies supporting the mechanisms of action of NLRC4 and AC090559.1, and thus, further studies are needed to clarify these mechanisms.

CONCLUSION

In conclusion, we constructed a prognostic model based on pyroptosis-related lncRNAs. In addition to prognosis prediction, this model was significantly associated with pyroptosis extent and immune phenotype. We believe that these lncRNAs may serve as new targets for inducing pyroptosis, and stimulating pyroptosis-mediated antitumor immunity may provide new insights for the treatment of LUAD patients.

DATA AVAILABILITY STATEMENT

The original contributions presented in the study are included in the article/**Supplementary Material**; further inquiries can be directed to the corresponding author.

ETHICS STATEMENT

Written informed consent was obtained from the individuals for the publication of any potentially identifiable images or data included in this article. Our research obtained approval from the

Biomedical Research Ethic Committee of Shandong Provincial Hospital (SWYX:NO. 2021-433).

AUTHOR CONTRIBUTIONS

JD contributed to design and supervised the study and correspondence. Co-authors JL and QL collected and analyzed the data and completed the manuscript. HS, YL, YW, and GW helped search for references and offered guidelines of statistical methods. All authors have read and approved the final version to be published.

FUNDING

This study is supported by the Natural Science Foundation of Shandong Province (grant number ZR2019PH002) and Clinical Medicine Science and Technology Innovation Plan of Jinan (grant number 202019058).

ACKNOWLEDGMENTS

We express our sincere thanks to the LUAD patients from Shandong Provincial Hospital, TCGA–LUAD for providing data. We thank openbiox community and HiPlot team (https://hiplot.com.cn) for providing technical assistance and valuable tools for data analysis and visualization.

SUPPLEMENTARY MATERIAL

The Supplementary Material for this article can be found online at: https://www.frontiersin.org/articles/10.3389/fgene.2022.838624/full#supplementary-material.

Supplementary Figure S1 | Expression and prognosis analysis of NLRC4 and SCAF11/SIP1. **(A)** KM curves of NLRC4 and SCAF11/SIP1 in LUAD patients obtained from the KMPlot. Differential expression of NLRC4 and SCAF11 in GEPIA websites **(B)** and TIMER2.0 **(C)**. NLRC4 nod-like receptor family CARD domain containing 4, SCAF11/SIP1 SR-related CTD associated factor 11, LUAD lung adenocarcinoma.

Supplementary Figure S2 | Differential abundance of infiltrating immune cells between high- and low-risk groups in LUAD. TME: tumor microenvironment, LUAD: lung adenocarcinoma.

Supplementary Figure S3 | Correlation analysis between risk score, interacted mRNAs, identified lncRNAs, and TME infiltrating immune cells. TME: tumor microenvironment.

Supplementary Figure S4 | Correlation between NLRC4 or SCAF11 and TME immune cell infiltration in LUAD from TIMER website. NLRC4: nod-like receptor family CARD domain containing 4, SCAF11: SR-related CTD associated factor 11, TME: tumor microenvironment, LUAD lung adenocarcinoma.

Supplementary Figure S5 | Prediction of drug sensitivity.

REFERENCES

Aran, D., Hu, Z., and Butte, A. J. (2017). xCell: Digitally Portraying the Tissue Cellular Heterogeneity Landscape. *Genome Biol.* 18 (1), 220. doi:10.1186/s13059-017-1349-1

Becht, E., Giraldo, N. A., Lacroix, L., Buttard, B., Elarouci, N., Petitprez, F., et al. (2016). Estimating the Population Abundance of Tissue-Infiltrating Immune and Stromal Cell Populations Using Gene Expression. *Genome Biol.* 17 (1), 218. doi:10.1186/s13059-016-1070-5

Bhan, A., Soleimani, M., and Mandal, S. S. (2017). Long Noncoding RNA and Cancer: A New Paradigm. *Cancer Res.* 77 (15), 3965–3981. doi:10.1158/0008-5472.can-16-2634

Boumahdi, S., and de Sauvage, F. J. (2020). The Great Escape: Tumour Cell Plasticity in Resistance to Targeted Therapy. *Nat. Rev. Drug Discov.* 19 (1), 39–56. doi:10.1038/s41573-019-0044-1

Chakraborty, H., and Hossain, A. (2018). R Package to Estimate Intracluster Correlation Coefficient with Confidence Interval for Binary Data. *Comput. Methods Programs Biomed.* 155, 85–92. doi:10.1016/j.cmpb.2017.10.023

Chandra Gupta, S., and Nandan Tripathi, Y. (2017). Potential of Long Non-Coding RNAs in Cancer Patients: From Biomarkers to Therapeutic Targets. *Int. J. Cancer* 140 (9), 1955–1967. doi:10.1002/ijc.30546

Charoentong, P., Finotello, F., Angelova, M., Mayer, C., Efremova, M., Rieder, D., et al. (2017). Pan-Cancer Immunogenomic Analyses Reveal Genotype-Immunophenotype Relationships and Predictors of Response to Checkpoint Blockade. *Cell Rep.* 18 (1), 248–262. doi:10.1016/j.celrep.2016.12.019

Chen, B., Khodadoust, M. S., Liu, C. L., Newman, A. M., and Alizadeh, A. A. (2018). Profiling Tumor Infiltrating Immune Cells with CIBERSORT. *Methods Mol. Biol.* 1711, 243–259. doi:10.1007/978-1-4939-7493-1_12

Chen, Y., Zitello, E., Guo, R., and Deng, Y. (2021). The Function of LncRNAs and Their Role in the Prediction, Diagnosis, and Prognosis of Lung Cancer. *Clin. Transl. Med.* 11 (4), e367. doi:10.1002/ctm2.367

Deets, K. A., and Vance, R. E. (2021). Inflammasomes and Adaptive Immune Responses. *Nat. Immunol.* 22 (4), 412–422. doi:10.1038/s41590-021-00869-6

Denisenko, T. V., Budkevich, I. N., and Zhivotovsky, B. (2018). Cell Death-Based Treatment of Lung Adenocarcinoma. *Cell Death Dis.* 9 (2), 117. doi:10.1038/s41419-017-0063-y

Du, T., Gao, J., Li, P., Wang, Y., Qi, Q., Liu, X., et al. (2021). Pyroptosis, Metabolism, and Tumor Immune Microenvironment. *Clin. Transl. Med.* 11 (8), e492. doi:10.1002/ctm2.492

Duncan, J. A., and Canna, S. W. (2018). The NLRC4 Inflammasome. *Immunol. Rev.* 281 (1), 115–123. doi:10.1111/imr.12607

Evavold, C. L., Hafner-Bratkovič, I., Devant, P., D'Andrea, J. M., Ngwa, E. M., Boršić, E., et al. (2021). Control of Gasdermin D Oligomerization and Pyroptosis by the Ragulator-Rag-mTORC1 Pathway. *Cell* 184 (17), 4495–4511. doi:10.1016/j.cell.2021.06.028

Finotello, F., Mayer, C., Plattner, C., Laschober, G., Rieder, D., Hackl, H., et al. (2019). Molecular and Pharmacological Modulators of the Tumor Immune Contexture Revealed by Deconvolution of RNA-Seq Data. *Genome Med.* 11 (1), 34. doi:10.1186/s13073-019-0638-6

Fu, J., Li, K., Zhang, W., Wan, C., Zhang, J., Jiang, P., et al. (2020). Large-Scale Public Data Reuse to Model Immunotherapy Response and Resistance. *Genome Med.* 12 (1), 21. doi:10.1186/s13073-020-0721-z

Garaude, J., Kent, A., van Rooijen, N., and Blander, J. M. (2012). Simultaneous Targeting of Toll- and Nod-Like Receptors Induces Effective Tumor-Specific Immune Responses. *Sci. Transl. Med.* 4 (120), 120ra16. doi:10.1126/scitranslmed.3002868

Guo, Y., Qu, Z., Li, D., Bai, F., Xing, J., Ding, Q., et al. (2021). Identification of a Prognostic Ferroptosis-Related lncRNA Signature in the Tumor Microenvironment of Lung Adenocarcinoma. *Cell Death Discov.* 7 (1), 190. doi:10.1038/s41420-021-00576-z

Hänzelmann, S., Castelo, R., and Guinney, J. (2013). GSVA: Gene Set Variation Analysis for Microarray and RNA-Seq Data. *BMC Bioinforma.* 14, 7. doi:10.1186/1471-2105-14-7

Hirsch, F. R., Scagliotti, G. V., Mulshine, J. L., Kwon, R., Curran, W. J., Wu, Y.-L., et al. (2017). Lung Cancer: Current Therapies and New Targeted Treatments. *Lancet* 389 (10066), 299–311. doi:10.1016/s0140-6736(16)30958-8

Janowski, A. M., Colegio, O. R., Hornick, E. E., McNiff, J. M., Martin, M. D., Badovinac, V. P., et al. (2016). NLRC4 Suppresses Melanoma Tumor

Progression Independently of Inflammasome Activation. *J. Clin. Invest.* 126 (10), 3917–3928. doi:10.1172/jci86953

Jiang, P., Gu, S., Pan, D., Fu, J., Sahu, A., Hu, X., et al. (2018). Signatures of T Cell Dysfunction and Exclusion Predict Cancer Immunotherapy Response. *Nat. Med.* 24 (10), 1550–1558. doi:10.1038/s41591-018-0136-1

Kay, C., Wang, R., Kirkby, M., and Man, S. M. (2020). Molecular Mechanisms Activating the NAIP-NLRC4 Inflammasome: Implications in Infectious Disease, Autoinflammation, and Cancer. *Immunol. Rev.* 297 (1), 67–82. doi:10.1111/imr.12906

Kolb, R., Phan, L., Borcherding, N., Liu, Y., Yuan, F., Janowski, A. M., et al. (2016). Obesity-Associated NLRC4 Inflammasome Activation Drives Breast Cancer Progression. *Nat. Commun.* 7, 13007. doi:10.1038/ncomms13007

Lazzari, C., Bulotta, A., Cangi, M. G., Bucci, G., Pecciarini, L., Bonfiglio, S., et al. (2020). Next Generation Sequencing in Non-Small Cell Lung Cancer: Pitfalls and Opportunities. *Diagn. (Basel)* 10 (12), 1092. doi:10.3390/diagnostics10121092

Li, T., Fu, J., Zeng, Z., Cohen, D., Li, J., Chen, Q., et al. (2020). TIMER2.0 for Analysis of Tumor-Infiltrating Immune Cells. *Nucleic Acids Res.* 48 (W1), W509–W514. doi:10.1093/nar/gkaa407

Liu, B., and Yang, S. (2021). A Five Autophagy-Related Long Non-Coding RNA Prognostic Model for Patients with Lung Adenocarcinoma. *Int. J. General Med.* 14, 7145–7158. doi:10.2147/ijgm.s334601

Liu, X., Xia, S., Zhang, Z., Wu, H., and Lieberman, J. (2021). Channelling Inflammation: Gasdermins in Physiology and Disease. *Nat. Rev. Drug Discov.* 20 (5), 384–405. doi:10.1038/s41573-021-00154-z

Lu, L., Liu, L.-P., Zhao, Q.-Q., Gui, R., and Zhao, Q.-Y. (2021). Identification of a Ferroptosis-Related LncRNA Signature as a Novel Prognosis Model for Lung Adenocarcinoma. *Front. Oncol.* 11, 675545. doi:10.3389/fonc.2021.675545

Mariathasan, S., Turley, S. J., Nickles, D., Castiglioni, A., Yuen, K., Wang, Y., et al. (2018). TGFβ Attenuates Tumour Response to PD-L1 Blockade by Contributing to Exclusion of T Cells. *Nature* 554 (7693), 544–548. doi:10.1038/nature25501

Mayakonda, A., Lin, D.-C., Assenov, Y., Plass, C., and Koeffler, H. P. (2018). Maftools: Efficient and Comprehensive Analysis of Somatic Variants in Cancer. *Genome Res.* 28 (11), 1747–1756. doi:10.1101/gr.239244.118

Ohashi, K., Wang, Z., Yang, Y. M., Billet, S., Tu, W., Pimienta, M., et al. (2019). NOD-Like Receptor C4 Inflammasome Regulates the Growth of Colon Cancer Liver Metastasis in NAFLD. *Hepatology* 70 (5), 1582–1599. doi:10.1002/hep.30693

Racle, J., de Jonge, K., Baumgaertner, P., Speiser, D. E., and Gfeller, D. (2017). Simultaneous Enumeration of Cancer and Immune Cell Types from Bulk Tumor Gene Expression Data. *Elife* 6, e26476. doi:10.7554/eLife.26476

Rathinam, V. A. K., and Fitzgerald, K. A. (2016). Inflammasome Complexes: Emerging Mechanisms and Effector Functions. *Cell* 165 (4), 792–800. doi:10.1016/j.cell.2016.03.046

Ritchie, M. E., Phipson, B., Wu, D., Hu, Y., Law, C. W., Shi, W., et al. (2015). Limma Powers Differential Expression Analyses for RNA-Sequencing and Microarray Studies. *Nucleic Acids Res.* 43 (7), e47. doi:10.1093/nar/gkv007

Seijo, L. M., Peled, N., Ajona, D., Boeri, M., Field, J. K., Sozzi, G., et al. (2019). Biomarkers in Lung Cancer Screening: Achievements, Promises, and Challenges. *J. Thorac. Oncol.* 14 (3), 343–357. doi:10.1016/j.jtho.2018.11.023

Şenbabaoğlu, Y., Gejman, R. S., Winer, A. G., Liu, M., Van Allen, E. M., de Velasco, G., et al. (2016). Tumor Immune Microenvironment Characterization in Clear Cell Renal Cell Carcinoma Identifies Prognostic and Immunotherapeutically Relevant Messenger RNA Signatures. *Genome Biol.* 17 (1), 231. doi:10.1186/s13059-016-1092-z

Shao, J., Zhang, B., Kuai, L., and Li, Q. (2021). Integrated Analysis of Hypoxia-Associated lncRNA Signature to Predict Prognosis and Immune Microenvironment of Lung Adenocarcinoma Patients. *Bioengineered* 12 (1), 6186–6200. doi:10.1080/21655979.2021.1973874

Gajewski, T. F., Schreiber, H., and Fu, Y. X. (2013). Innate and Adaptive Immune Cells in Tumor Microenvironment. *Nature immunology* 14 (10), 1014–1022. doi:10.1038/ni.2703

Siegel, R. L., Miller, K. D., Fuchs, H. E., and Jemal, A. (2021). Cancer Statistics, 2021. *CA A Cancer J. Clin.* 71 (1), 7–33. doi:10.3322/caac.21654

Speiser, D. E., Ho, P.-C., and Verdeil, G. (2016). Regulatory Circuits of T Cell Function in Cancer. *Nat. Rev. Immunol.* 16 (10), 599–611. doi:10.1038/nri.2016.80

Tang, Z., Li, C., Kang, B., Gao, G., Li, C., and Zhang, Z. (2017). GEPIA: A Web Server for Cancer and Normal Gene Expression Profiling and Interactive Analyses. *Nucleic Acids Res.* 45, W98–W102. doi:10.1093/nar/gkx247

Thommen, D. S., and Schumacher, T. N. (2018). T Cell Dysfunction in Cancer. *Cancer Cell* 33 (4), 547–562. doi:10.1016/j.ccell.2018.03.012

Wang, Q., Wang, Y., Ding, J., Wang, C., Zhou, X., Gao, W., et al. (2020). A Bioorthogonal System Reveals Antitumour Immune Function of Pyroptosis. *Nature* 579 (7799), 421–426. doi:10.1038/s41586-020-2079-1

Wu, L., Wen, Z., Song, Y., and Wang, L. (2021). A Novel Autophagy-Related lncRNA Survival Model for Lung Adenocarcinoma. *J. Cell Mol. Med.* 25 (12), 5681–5690. doi:10.1111/jcmm.16582

Yang, L., Wu, Y., Xu, H., Zhang, J., Zheng, X., Zhang, L., et al. (2021). Identification and Validation of a Novel Six-lncRNA-Based Prognostic Model for Lung Adenocarcinoma. *Front. Oncol.* 11, 775583. doi:10.3389/fonc.2021.775583

Ye, Y., Dai, Q., and Qi, H. (2021). A Novel Defined Pyroptosis-Related Gene Signature for Predicting the Prognosis of Ovarian Cancer. *Cell Death Discov.* 7 (1), 71. doi:10.1038/s41420-021-00451-x

Yu, P., Zhang, X., Liu, N., Tang, L., Peng, C., and Chen, X. (2021a). Pyroptosis: Mechanisms and Diseases. *Sig Transduct. Target Ther.* 6 (1), 128. doi:10.1038/s41392-021-00507-5

Yu, X., Liu, W., Chen, S., Cheng, X., Paez, P. A., Sun, T., et al. (2021b). Immunologically Programming the Tumor Microenvironment Induces the Pattern Recognition Receptor NLRC4-Dependent Antitumor Immunity. *J. Immunother. Cancer* 9 (1), e001595. doi:10.1136/jitc-2020-001595

Zarour, H. M. (2016). Reversing T-Cell Dysfunction and Exhaustion in Cancer. *Clin. Cancer Res.* 22 (8), 1856–1864. doi:10.1158/1078-0432.ccr-15-1849

Zhang, H., Meltzer, P., and Davis, S. (2013). RCircos: An R Package for Circos 2D Track Plots. *BMC Bioinforma.* 14, 244. doi:10.1186/1471-2105-14-244

Zhang, Z., Zhang, Y., and Lieberman, J. (2021). Lighting a Fire: Can We Harness Pyroptosis to Ignite Antitumor Immunity? *Cancer Immunol. Res.* 9 (1), 2–7. doi:10.1158/2326-6066.cir-20-0525

Zhang, Z., Zhang, Y., Xia, S., Kong, Q., Li, S., Liu, X., et al. (2020). Gasdermin E Suppresses Tumour Growth by Activating Anti-Tumour Immunity. *Nature* 579 (7799), 415–420. doi:10.1038/s41586-020-2071-9

Zhou, Z., He, H., Wang, K., Shi, X., Wang, Y., Su, Y., et al. (2020). Granzyme A from Cytotoxic Lymphocytes Cleaves GSDMB to Trigger Pyroptosis in Target Cells. *Science* 368 (6494), eaaz7548. doi:10.1126/science.aaz7548

Conflict of Interest: The authors declare that the research was conducted in the absence of any commercial or financial relationships that could be construed as a potential conflict of interest.

Publisher's Note: All claims expressed in this article are solely those of the authors and do not necessarily represent those of their affiliated organizations, or those of the publisher, the editors, and the reviewers. Any product that may be evaluated in this article, or claim that may be made by its manufacturer, is not guaranteed or endorsed by the publisher.

Copyright © 2022 Liu, Liu, Shen, Liu, Wang, Wang and Du. This is an open-access article distributed under the terms of the Creative Commons Attribution License (CC BY). The use, distribution or reproduction in other forums is permitted, provided the original author(s) and the copyright owner(s) are credited and that the original publication in this journal is cited, in accordance with accepted academic practice. No use, distribution or reproduction is permitted which does not comply with these terms.

GLOSSARY

AUC Area under the curve
APC Antigen-presenting cell
CCR C-C chemokine receptor
ceRNA Competing endogenous RNA
CNV Copy number variations
CTL Cytotoxic lymphocyte
CTLA-4 Cytotoxic T lymphocyte antigen-4
DAMP Damaged-associated molecular pattern
FDR False-discovery rate
FPKM Fragments per kilobase of exon model per million reads mapped
GEPIA Gene Expression Profiling Integrative Analysis
GSDMs Gasdermins
HLA Human leukocyte antigen
HR Hazard ratio
ICB Immune checkpoint blockade
ICP Immune checkpoint
IFN Interferon
IL Interleukin
IPS Immunophenoscore
KM Kaplan–Meier
lncRNA long noncoding RNA
LUAD Lung adenocarcinoma
miRNA MicroRNA
NK cell Natural killer cell
OS Overall survival
PCA Principal component analysis
PCD Programmed cell death
PD-1 Programmed cell death 1
ROC Receiver operating characteristic
ssGSEA Single-sample gene set enrichment analysis
TAM Tumor-associated macrophage
TCGA The Cancer Genome Atlas
TIDE Tumor Immune Dysfunction and Exclusion
TME Tumor microenvironment

frontiers | Frontiers in Genetics

ORIGINAL RESEARCH
published: 19 July 2022
doi: 10.3389/fgene.2022.891744

Identification and Validation of an m6A Modification of JAK-STAT Signaling Pathway–Related Prognostic Prediction Model in Gastric Cancer

Fei Jiang[1,2], *Xiaowei Chen*[1,2], *Yan Shen*[1,2] *and Xiaobing Shen*[1,2,3]*

[1]*Key Laboratory of Environmental Medical Engineering and Education Ministry, Nanjing Public Health College, Southeast University, Nanjing, China,* [2]*Department of Epidemiology and Health Statistics, School of Public Health, Southeast University, Nanjing, China,* [3]*Department of Occupational and Environmental Health, School of Public Health, Southeast University, Nanjing, China*

Background: Gastric cancer (GC) is one of the malignant tumors worldwide. Janus (JAK)–signal transduction and activator of transcription (STAT) signaling pathway is involved in cellular biological process and immune function. However, the association between them is still not systematically described. Therefore, in this study, we aimed to identify key genes involved in JAK-STAT signaling pathway and GC, as well as the potential mechanism.

Methods: The Cancer Genome Atlas (TCGA) database was the source of RNA-sequencing data of GC patients. Gene Expression Omnibus (GEO) database was used as the validation set. The predictive value of the JAK-STAT signaling pathway-related prognostic prediction model was examined using least absolute shrinkage and selection operator (LASSO); survival, univariate, and multivariate Cox regression analyses; and receiver operating characteristic curve (ROC) analyses to examine the predictive value of the model. Quantitative real-time polymerase chain reaction (qRT-PCR) and chi-square test were used to verify the expression of genes in the model and assess the association between the genes and clinicopathological parameters of GC patients, respectively. Then, Gene Ontology (GO), Kyoto Encyclopedia of Genes and Genomes (KEGG), gene set enrichment analysis, version 3.0 (GSEA), sequence-based RNA adenosine methylation site predictor (SRAMP) online websites, and RNA immunoprecipitation (RIP) experiments were used to predict the model-related potential pathways, m6A modifications, and the association between model genes and m6A.

Results: A four-gene prognostic model (GHR, PIM1, IFNA8, and IFNB1) was constructed, namely, riskScore. The Kaplan–Meier curves suggested that patients with high riskScore expression had a poorer prognosis than those with low riskScore expression ($p = 0.006$). Multivariate Cox regression analyses showed that the model could be an independent predictor ($p < 0.001$; HR = 3.342, 95%, CI = 1.834–6.088). The 5-year area under time-dependent ROC curve (AUC) reached 0.655. The training test set verified these results. Further analyses unveiled an enrichment of cancer-related pathways, m6A modifications, and the direct interaction between m6A and the four genes.

OPEN ACCESS

Edited by:
Ayan Biswas,
University of Alabama at Birmingham, United States

Reviewed by:
Ziyi Chen,
Nanjing Medical University, China
Zhouxiao Li,
Ludwig Maximilian University of Munich, Germany

***Correspondence:**
Xiaobing Shen
xb.shen@seu.edu.cn

Specialty section:
This article was submitted to Cancer Genetics and Oncogenomics, a section of the journal Frontiers in Genetics

Received: *08 March 2022*
Accepted: *13 June 2022*
Published: *19 July 2022*

Citation:
Jiang F, Chen X, Shen Y and Shen X (2022) Identification and Validation of an m6A Modification of JAK-STAT Signaling Pathway–Related Prognostic Prediction Model in Gastric Cancer. Front. Genet. 13:891744. doi: 10.3389/fgene.2022.891744

Conclusion: This four-gene prognostic model could be applied to predict the prognosis of GC patients and might be a promising therapeutic target in GC.

Keywords: gastric cancer, TCGA, prognosis, mRNA, M6A

INTRODUCTION

Gastric cancer (GC) is a malignant tumor that occurs worldwide. According to the latest global cancer statistics from 2020, globally, the incidence of GC ranks fifth and the mortality ranks fourth (Sung et al., 2021). At present, the commonly used methods for the treatment of GC include surgery, radiotherapy, and chemotherapy or combination (Song et al., 2017). Although these methods have improved the survival rate of patients, surgery is invasive, radiotherapy is nontargeted, chemotherapy has toxic side effects (Shao et al., 2021a), and the 5-year survival rate of patients is not high (Zhao et al., 2021). Therefore, a prognostic model that can predict the prognosis of GC and provide a new effective target for the treatment of GC should be urgently established.

The Janus (JAK)–signal transduction and activator of transcription (STAT) signaling pathway is involved in gene expression, inflammation, transcriptional programs, and immune response (Meng et al., 2020). Previous research has confirmed that the activation of the JAK-STAT signaling pathway is closely related to many diseases (Yue et al., 2020), including ovarian cancer (Gao et al., 2022), nonsmall cell lung cancer (Prabhu et al., 2021), breast cancer (Chen et al., 2021), and cardiovascular diseases (Baldini et al., 2021).

Some reports regarding the JAK-STAT signaling pathway and GC also exist. Li et al. (2022) found that STAT1 is activated in human *H. pylori*-positive gastritis, whereas STAT1 and its target gene programmed death ligand-1 (PD-L1) are significantly elevated in GC. Bei et al. (2022) found that apatinib enhances GC cell sensitivity to paclitaxel by inhibiting the JAK/STAT3 signaling pathway. Yang et al. (2021) observed that STAM2 knockdown may inhibit malignant processes by targeting the JAK2/STAT3 signaling pathway in GC. These are reports on the association between this pathway and GC, and there are also reports on genes associated with GC that are associated with this pathway. Huang et al. (2022) found that gamma-glutamyltransferase 5 could be a potential prognostic molecular predictor in GC and is involved in the JAK-STAT signaling pathway. Similarly, Lysyl oxidase is also a potential molecular predictor in prognostic GC and also participates in the JAK-STAT signaling pathway (2021).

However, few studies have directly analyzed the effect of genes related to both this pathway and GC on the prognosis of GC and explored the underlying mechanism, and we must learn more about the influential genes and related mechanisms to explore effective therapeutic targets for GC.

Thus, in this study, we aimed to identify and explore the key genes involved in the JAK-STAT signaling pathway and GC based on TCGA and GEO databases. Differentially expressed genes were identified to construct a GC prognosis-related model by following a series of bioinformatic analyses to ensure the predictive value of the model, as well as training test set verification. Moreover, we verified the gene expression and assessed the association between genes and the clinicopathological parameters of GC patients in our samples. Afterward, we explored the mechanism of the genes in the model, which plays a role in the progression of GC via Gene Ontology (GO); Kyoto Encyclopedia of Genes and Genomes (KEGG); gene set enrichment analysis, version 3.0 (GSEA); and sequence-based RNA adenosine methylation site predictor (SRAMP) online websites and RNA immunoprecipitation (RIP)–quantitative real-time polymerase chain reaction (qRT-PCR) experiments. Our results may provide additional evidence about the prognostic biomarkers and therapeutic targets for GC.

METHODS AND MATERIALS

Data Collection

The training RNA-seq data were obtained from the Cancer Genome Atlas Stomach Adenocarcinoma (TCGA STAD) database; the testing RNA-seq data were obtained from GEO (GSE84437). JAK-STAT signaling pathway–related genes were acquired from the GSEA online websites.

Tissue Samples

A total of 25 pairs of GC tissues and adjacent normal tissues were acquired from GC patients, who were treated in the Department of General Surgery, Nanjing No. 1 City Hospital, from 2015 to 2016 following the Helsinki Declaration. Informed consent was obtained from each patient before they participated in this study. This project was approved by the Ethics Committee of Nanjing Medical University.

Cell Samples

Gastric cancer cell lines AGS, HGC-27, and gastric epithelial cells GES-1 used in this study were purchased from Saiku Biological Company (Guangzhou, China). All the cells were cultured in Roswell Park Memorial Institute (RPMI) 1640 medium. Both media were supplemented with 10% fetal bovine serum (Gibco, USA) and 1% streptomycin and penicillin (Gibco, USA). Cells were incubated at 37℃ and 5% CO_2.

LASSO Cox Regression Analysis and Identification of Different Expression Genes

The glmnet and survival packages were used to construct the LASSO Cox regression analysis. First, the glmnet package was applied to determine the penalty parameter lambda via cross-validation and identify the optimal lambda value that corresponded to the minimum value of the cross-validation error mean. Then, the best gene group was selected to

construct a risk model (riskScore model), and the results were categorized into high-risk and low-risk groups based on the median curve. The calculation of the risk score was based on the linear combination of the coefficients obtained from the LASSO Cox regression model multiplied by the expression value of each selected gene. We created a heat map that shows gene expression using the PheatMap software package in R.

Furthermore, the analysis of differentially expressed genes in the GC tissues and adjacent cancer tissues was identified using the limma package. The selection criteria: | log2 fold change| > 1 and $p < 0.05$.

Survival Analysis, ROC Curve Analysis, and Univariate and Multivariate Cox Regression Analyses

We used the Survival and Survminer packages in R to analyze patient survival and prognosis in the high-risk or low-risk group. The survival curve was plotted using the Kaplan–Meier method, and the log-rank test was used to assess statistical significance.

The survival ROC package was used to perform ROC analysis to analyze the prediction effectiveness of the constructed assessment model. Moreover, the area under the ROC curve was calculated. An area under the curve of more than 0.5 indicated that the model could accurately predict patient survival.

Then, using the survival package in R, we performed univariate and multivariate Cox regression analyses to analyze the independent prognostic role of the riskScore model, which also included age, sex, grade, stage, T stage, M stage, and N stage.

Quantitative Reverse Transcription Polymerase Reaction

TRIzol reagent was used to extract total RNA from tissues and cells according to the manufacturer's protocol (GenStar, China). RNA was then reverse-transcribed using a reverse transcription kit (Takara Bio, Japan, RR036A). Quantification of mRNA was performed using an SYBR Green PCR Kit (Yeasen Biotech Co., Ltd., China). GAPDH was used to normalize mRNA levels. The primers were presented in **Supplementary Table S1A**.

Functional Annotation, Protein–Protein Interaction, m6A Modification of Genes, and Correlation Between Genes

ClusterProfiler package was performed to visualize and compare multiple GO and KEGG] enrichment results. In addition, protein–protein interaction (PPI) analyses were performed to investigate the potential molecular mechanisms using STRING V11.5.

GSEA was used to explore the signaling pathways related to GHR of the model in GC. GSEA was carried out between datasets with low or high GHR mRNA expression in TCGA. The low expression group was selected as the reference. Gene set permutations were performed 1,000 times for each analysis to identify significantly different pathways. The normalized enrichment score, nominal *p*-value, and false discovery rate q-value indicated the importance of the association between gene sets and pathways.

SRAMP online website (http://www.cuilab.cn/sramp) was used to predict whether the gene contains m6A modifications.

Corrplot package was used to analyze the correlation between m6A regulators and genes of the model.

RNA Immunoprecipitation Experiment

According to the manufacturer's instructions, first, AGS cells (approximately 1×10^7) were lysed with RIP lysis buffer (EMD Millipore, Billerica, MA, USA). Then, the cell lysates were incubated with RIP immunoprecipitation buffer containing magnetic beads conjugated with rabbit N6-methyladenosine (m6A) antibody (ABclonal, China) and negative control rabbit immunoglobulin G (IgG) (Millipore, Billerica, MA, USA). Samples were incubated with Proteinase K, and then, immunoprecipitated RNA was isolated. Extracted RNAs were analyzed using qRT-PCR to determine whether GHR, PIM1, IFNA8, and IFNB1 could be pulled down by m6A protein significantly.

Statistical Analysis

R software and Prism 6 were used to analyze all data. Perl language was used to merge all datasets. The Wilcox test or paired *t*-test was used to assess the difference in mRNA expression between GC tissues and adjacent cancer tissues. The difference in overall survival in the low- or high-risk score group patients was analyzed using Kaplan–Meier and log-rank tests. The correlation between risk scores and patients' clinicopathological characteristics was examined using the Kruskal–Wallis test. The association between gene expression and clinicopathological parameters was analyzed using the χ^2 test. Univariate and multivariate analyses were conducted based on a Cox proportional hazard regression model. Statistical significance was set at $p < 0.05$.

RESULTS

Identification of Different Jak-STAT Signaling Pathway–Related Expression Genes in TCGA

Through the GSEA online website http://www.gsea-msigdb.org/gsea/msigdb/collections.jsp, we obtained 155 genes on the Jak-STAT signaling pathway (**Supplementary Table S1B**).

Then, we identified 98 different expression genes with the Wilcoxon test from the STAD dataset in TCGA (The criterion is $p < 0.05$, **Figure 1**, **Supplementary Table S1C**).

Acquisition of the Shared Different JAK-STAT Signaling Pathway–Related Expression Genes via GEO Dataset and TCGA

We obtained a total of 74 species of human results when we used "gastric cancer" and "survival" as the search keywords. In our

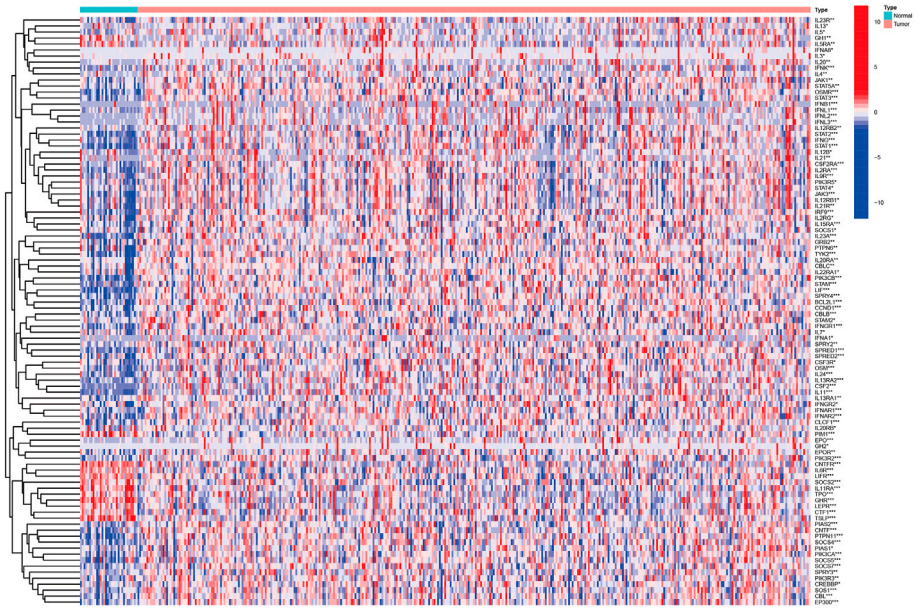


FIGURE 1 | Heatmap identified different expression Jak-STAT pathway-related mRNAs in GC based on TCGA.

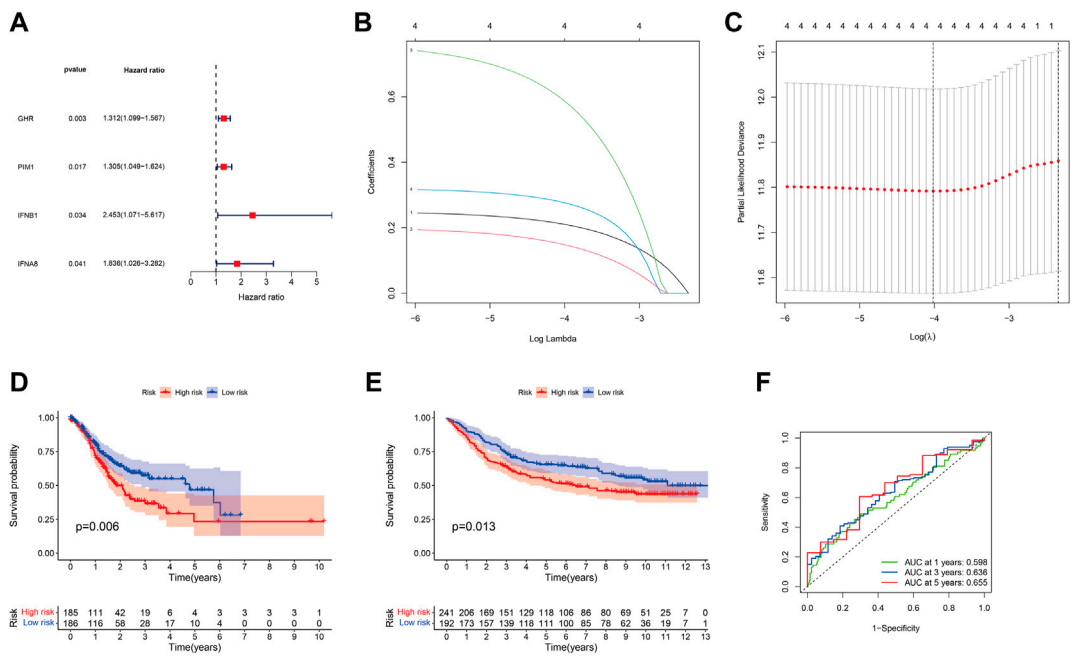


FIGURE 2 | Prognostic ability of the DJSEGs model. **(A)**. Univariate Cox regression analysis identified mRNAs with prognostic values. Hazard ratios were visualized in forest plots. **(B)**. LASSO regression analysis was used to build the final prediction model based on the optimal gene. The number on top of the plot represents the total number of genes. Partial likelihood deviance is plotted against log lambda. Dotted vertical lines were drawn at the optimal values. The optimal gene group was chosen by 10-fold cross-validation and the minimal value of lambda. **(C)**. LASSO coefficient profiles of the four shared genes. The number on top of the plot represents the total number of genes. Each curve represents the corresponding shared gene, and the number next to it is the serial number of each gene; **(D,E)**. Kaplan–Meier survival curves for patients with GC in the training set (TCGA) and the testing set (GEO) stratified by high- and low-risk scores, and high-risk patients had shorter overall survival than low-risk ones. **(F)**. Accuracy of the riskScore model in predicting 1-, 3-, and 5-year overall survival of GC patients, according to the training set (TCGA).

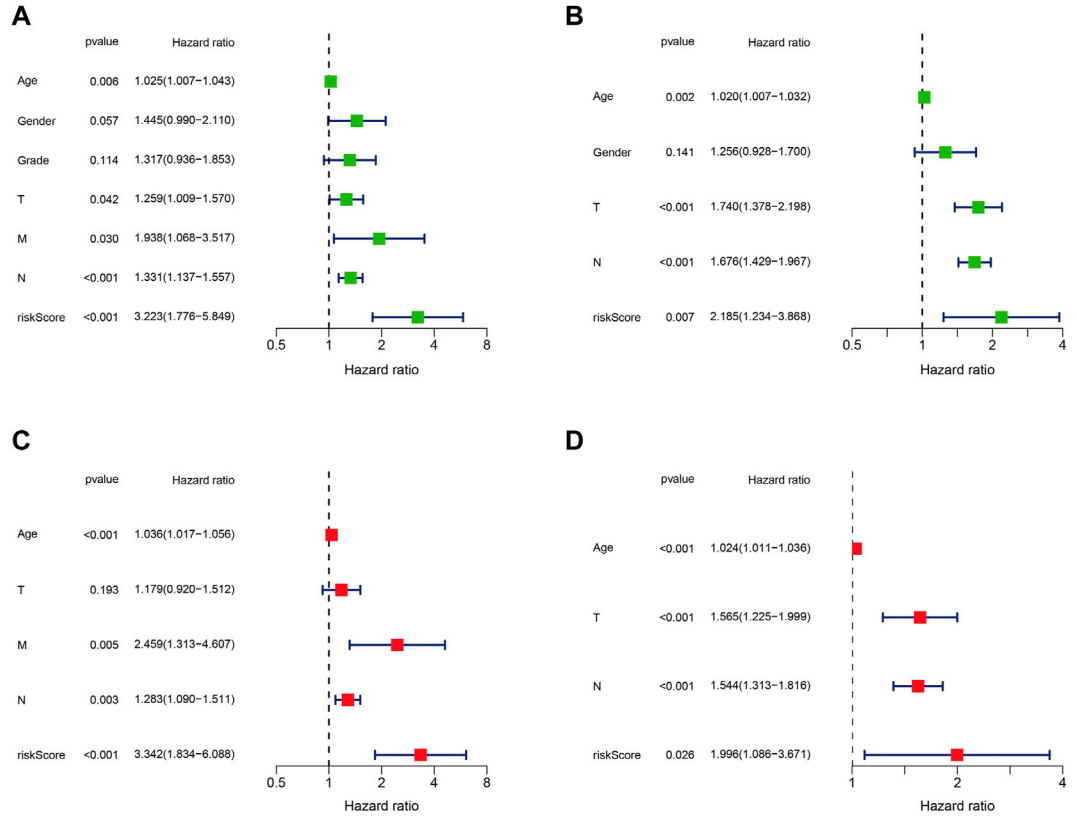


FIGURE 3 | The prognostic model could be an independent prognostic factor in GC. **(A,B)**. Univariate Cox risk ratio analysis of the training set (TCGA) and the testing set (GEO) revealed that the risk model could predict GC prognosis. **(C,D)**. Multivariate Cox risk ratio analysis of the training set (TCGA) and the testing set (GEO) revealed that the risk model could predict GC prognosis independently.

further analysis of the title and abstract, we selected the GSE84437 data set because of its large sample size (433 samples) and because each sample has the survival index.

When we used $p < 0.05$ and $|FC| > 2$ as our criterion for screening (according to **Supplementary Table S1C**, there were 32 genes with $p < 0.05$ and $|FC| > 2$), 28 DJSEGs were finally obtained, which were shared both in GEO and TCGA (**Supplementary Tables S2A,B**). At the same time, we used the surrogate variable analysis package for batch correction of data in two datasets. Furthermore, the data used in our subsequent analysis are all normalized data.

Construction and Validation of the Prognostic Model of DJSEGs

To investigate the effect of shared DJSEGs on GC prognosis, univariate Cox regression analysis was used first. Furthermore, we found that four DJSEGs had prognostic value (**Figure 2A**; $p < 0.05$). Then, the LASSO Cox regression analysis results suggested that the model worked best when all four DJSEGs were included (**Figures 2B,C**). The computation of the risk score is elucidated in terms of the expression level of each gene: riskScore = GHR×0.21087289828517 + PIM1×0.149236426661109 + IFNB1×0.589611733452815 + IFNA8×0.277049597016476. The median risk score was applied to categorize patients into high-risk (TCGA: n = 185, GEO: $n = 241$) and low-risk (TCGA: $n = 186$; GEO = 192) groups.

We found that the low-risk group patients had a lower probability of mortality than the high-risk group patients, both in the training set (TCGA normalized data set, **Figure 2D**) and the testing set (GEO normalized data set, **Figure 2E**). Thereafter, the area under the ROC curve (AUC) result of the training set was 0.598 at 1 year, 0.636 at 3 years, and 0.655 at 5 years (**Figure 2F**); the AUC of the testing set was 0.558 at 1 year, 0.565 at 3 years, and 0.572 at 5 years (**Supplementary Figure S2A**), which indicated that this model could be an indicator for patients' prognosis.

The Prognostic Model Was an Independent Prognostic Factor in GC

Given the predictive power of the prognostic model, we were interested in determining whether the model could be used as an independent prognostic factor for GC patients. Therefore, univariate and multivariate Cox regression analyses were

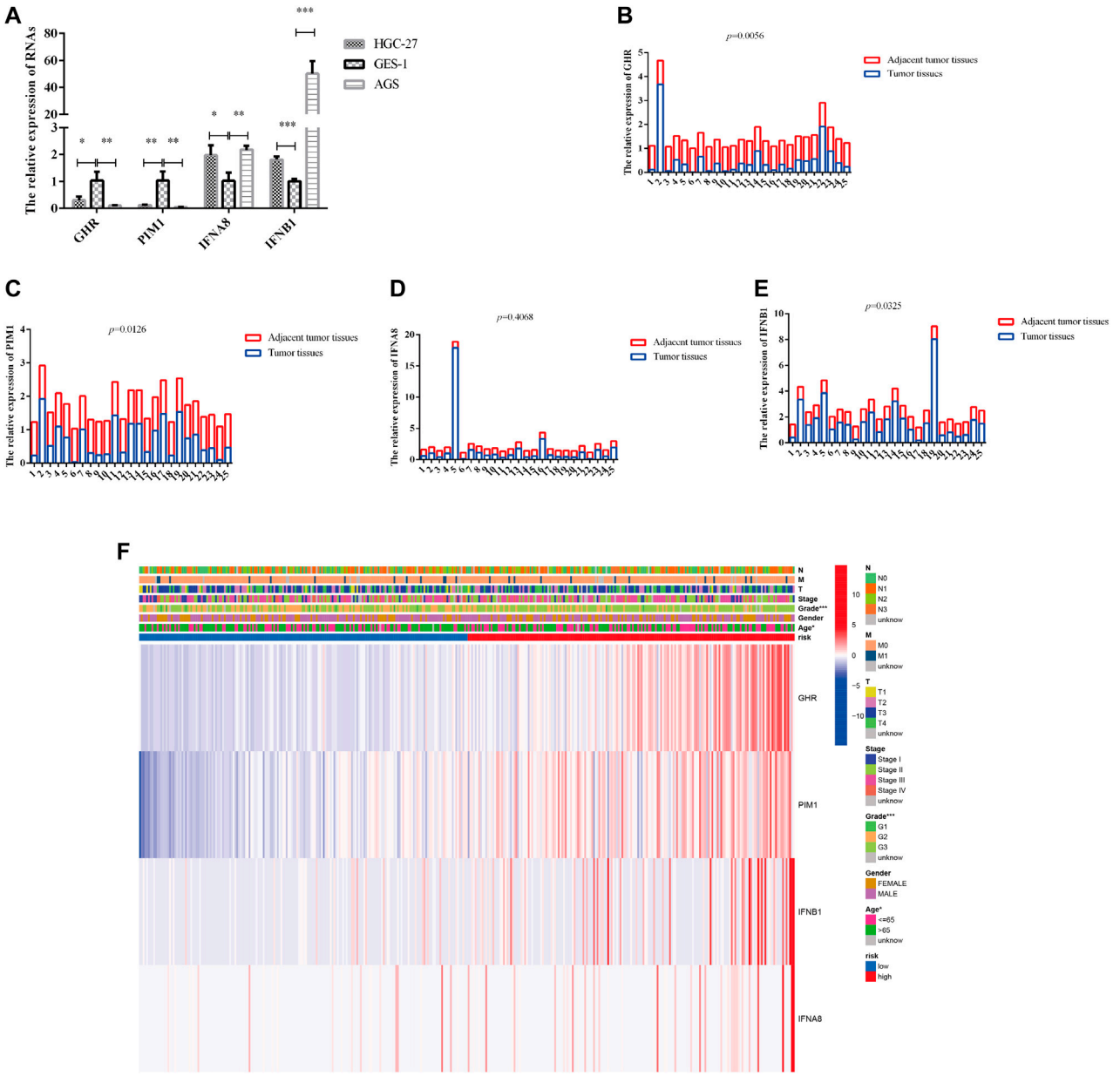


FIGURE 4 | The expression of four DJSEGs in cells, tissues, and the association between four DJSEGs and clinicopathological characteristics in GC patients. **(A)**. The expression of GHR, PIM1, IFNA8, and IFNB1 in HGC-27, AGS, and GES-1. **(B–E)**. The expression of GHR, PIM1, IFNA8, and IFNB1 in 25 pairs of GC tissues and adjacent tumor tissues (the paired sample *t*-test was performed using the $2^{-\Delta\Delta CT}$ value of each pair of samples). **(F)**. The expression of four DJSEGs and the correlation of clinicopathological parameters with different risk groups are shown in the heatmap. Red indicates overexpression, and green indicates low expression.

applied to elucidate the independence of the model. Univariate Cox regression analysis showed that the model of four DJSEGs was significantly related to the overall survival of GC patients. The HR of training set was 3.223 ($p < 0.001$, 95% CI = 1.776–5.849), and the HR of testing set was 2.185 ($p = 0.007$, 95% CI = 1.234–3.868) (**Figures 3A,B**). Multivariate analyses indicated that this model could be an independent predictor for predicting the prognosis of GC patients (training set: HR = 3.342, 95% CI = 1.834–6.088, $p < 0.001$; testing set: HR = 1.996, 95% CI = 1.086–3.671, $p = 0.026$) (**Figures 3C,D**).

TABLE 1 | Correlation between the four DJEGs expression and clinicopathological parameters.

Characteristics	Variable	Number(25)	GHR expression		$p(\chi^2 test)$	PIM1 expression		$p(\chi^2 test)$	IFNA8 expression		$p(\chi^2 test)$	IFNB1 expression		$p(\chi^2 test)$
			low	high		low	high		low	high		low	high	
Age (years)	≤65	9	6	3	0.1612	3	6	0.2709	5	4	0.5706	4	5	0.7896
	>65	16	6	10	—	9	7	—	7	9	—	8	8	—
Gender	male	17	7	10	0.3195	7	10	0.3195	8	9	0.8908	8	9	0.8908
	female	8	5	3	—	5	3	—	4	4	—	4	4	—
AJCC (version type 7th)	stage I + II	1 + 13	0 + 5	1 + 8	0.0977	1 + 6	0 + 7	1	1 + 7	6	0.4076	1 + 6	0 + 7	1
	stage III + IV	10 + 0	7	3	—	5	5	—	4	6	—	5	5	—
	NA	1	—	—	—	—	—	—	—	—	—	—	—	—
Tumor size (cm)	≤4.5	13	5	8	0.2191	6	7	0.682	7	6	0.682	7	6	0.682
	>4.5	11	7	4		6	5	—	5	6	—	5	6	—
	NA	1	—	—	—	—	—	—	—	—	—	—	—	—
Blood type	A	5	2	3	0.526	5	0	0.0345	2	3	0.1234	3	2	0.2801
	AB	1	1	0	—	1	0	—	1	0	—	1	0	—
	B	4	1	3	—	1	3	—	0	4	—	3	1	—
	O	15	8	7	—	5	10	—	9	6	—	5	10	—

The Relationship Between the Expression of Four DJSEGs and Clinicopathologic Characteristics in GC patients

Our bioinformatic results had shown that the four DJSEGs constructed model could predict the prognosis of GC patients, independently. Therefore, we intended to conduct further studies on the expression of these four DJSEGs in our GC cells, patient samples, and their relationship with the clinicopathological data of patients.

According **Supplementary Table S1B**, GHR and PIM1 were downregulated in TCGA GC patients (GHR: FC = −3.502462468, $p < 0.001$; PIM1: FC = −2.23633752, $p < 0.001$), whereas IFNA8 and IFNB1 were upregulated mRNAs (IFNA8: FC = 20.16667288, $p = 0.031718147$; IFNB1: FC = 3.31414108, $p < 0.001$), in comparison with normal tissues. In our experimental results, we found that the expression trends of GHR and PIM1 were downregulated in HGC-27 and AGS compared with that in GES-1; IFNA8 and IFNB1 were upregulated in HGC-27 and AGS, compared with the expression trend in GES-1 (**Figure 4A**). Next, we detect all of them in our patients' sample; the results indicated that the expression trends of GHR, PIM1, and IFNA8 were consistent with TCGA results (**Figures 4B,C,E**), while there was no difference in the expression trend in IFNA8 between tumor tissues and adjacent tumor tissues (**Figure 4D**). The results in **Table 1** show that only the high- and low-PIM1 groups had different expression trends in different blood types, whereas the rest had no significant statistical differences (In this study, genes were divided into high and low expression groups based on median gene expression levels). Nevertheless, when the model composed of these four genes was analyzed with the clinicopathological data of TCGA patients, it was found that the high- and low-risk groups of the model were significantly correlated with the patient's age and pathological grade (**Figure 4F**). These results indicated that four DJSEGs might be involved in the development of GC.

The Four DJSEGs Function Analysis Through GO, KEGG, and GSEA

Next, we explored the four DJSEGs function by performing GO and KEGG analyses. The GO analysis revealed that the four DJSEGs were mainly enriched in extracellular matrix organization, external encapsulating structure organization, cell-substrate adhesion, and Wnt-protein binding (**Figure 5A**). The KEGG analysis revealed that the four DJSEGs were mainly enriched in vascular smooth muscle contraction, focal adhesion, and Wnt signaling pathway (**Figure 5B**). Then, the STRING database was used to explore the interactions of the four DJSEGs, with a confidence score of more than 0.400 (medium confidence). The PPI network showed that GHR, IFNA8, and IFNB1 protein could interact with each other, except for PIM1 protein (**Figure 5C**). Because the confidence score of GHR interacting with other proteins was higher (**Supplementary Table S3A**) and the different expression of GHR in our GC patient samples was most significant, we further explored the potential pathways of

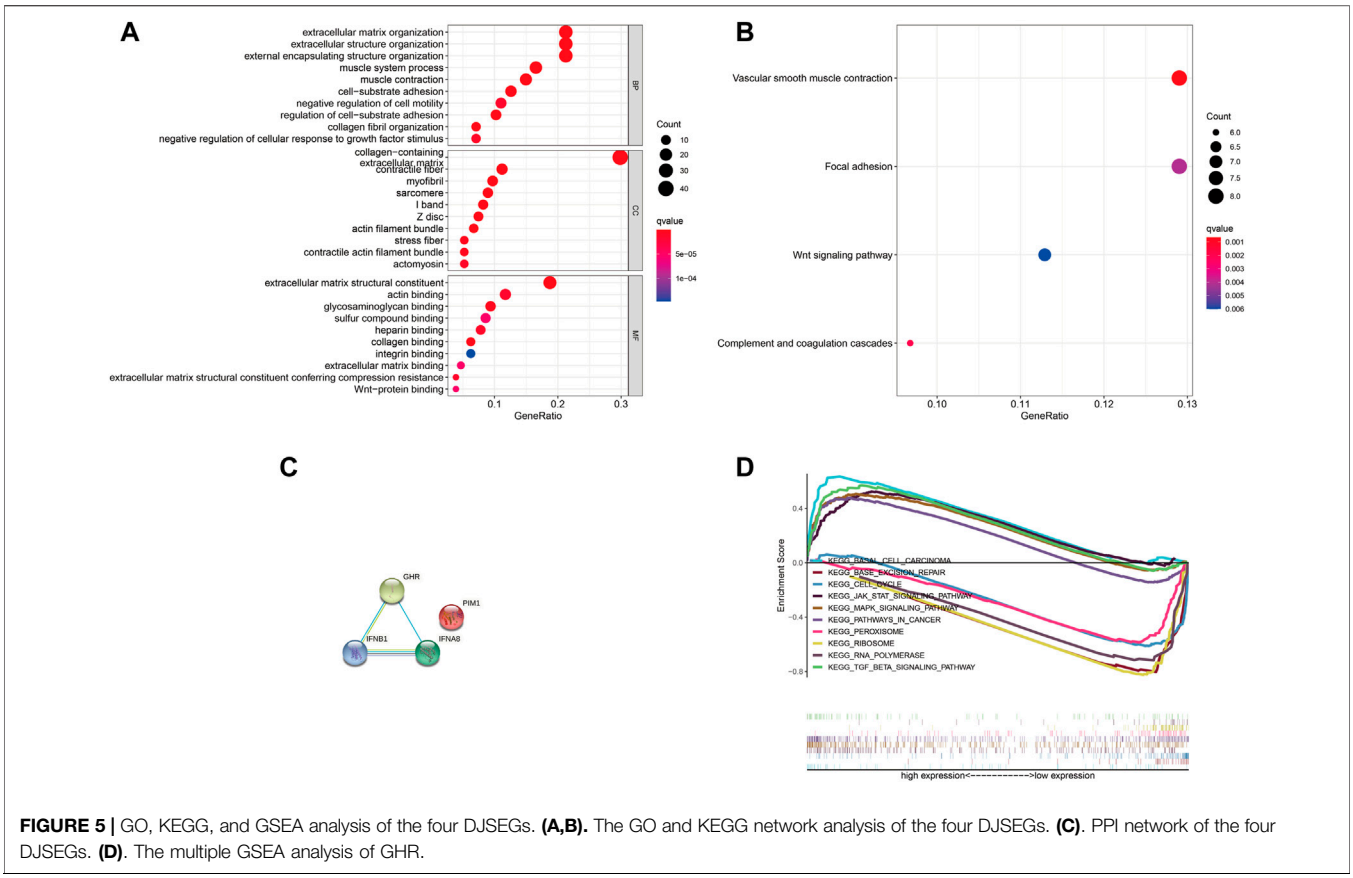


FIGURE 5 | GO, KEGG, and GSEA analysis of the four DJSEGs. **(A,B).** The GO and KEGG network analysis of the four DJSEGs. **(C)**. PPI network of the four DJSEGs. **(D)**. The multiple GSEA analysis of GHR.

GHR by regulating the development of GC with the GSEA database. The results showed that "base excision repair," "RNA polymerase," "peroxisome," "ribosome," and "cell cycle" signaling pathways were enriched in the GHR low expression group; "pathways in cancer," "basal cell carcinoma," "mapk signaling pathway," "TGF beta signaling pathway," and "Jak-stat signaling pathway" were enriched in the GHR high expression group (**Figure 5D**). All of these pathways were related to the occurrence and development of GC.

Therefore, it is reasonable to infer that the four DJSEGs model does play a role in the progression of GC and is likely to play the role through these signaling pathways.

The Four DJSEGs Had Enrichment m6A Modifications

In recent years, the m6A modification of noncoding RNA has become a research focus, but m6A modification is more common on mRNA, which plays important regulatory roles in a variety of physiological processes and disease progression (Wu et al., 2021). Therefore, we performed m6A site prediction via the SRAMP online website (http://www.cuilab.cn/sramp), which achieves promising performance both in cross-validation tests on its training dataset and in the rigorous independent tests. The thresholds for very high/high/moderate/low-confidence m6A sites correspond to the thresholds that achieved 99%/95%/90%/85% specificities (in other words, had a 5%/10%/15% false-positive rate) on cross-validation tests, respectively. As shown in **Figures 6A–D**, very high confidence m6A sites universally existed in the four DJSEGs—GHR, PIM1, IFNA8, and IFNB1.

RIP-qRT-PCR results showed that the m6A antibody could significantly pull down these four genes, indicating that they had direct interaction with the m6A protein (**Figure 6E**).

To gain further insight into the role of m6A on the four DJSEGs in GC, we studied the correlation between the four DJSEGs (GHR, PIM1, IFNA8, and IFNB1) and m6A writer (KIAA1429, METTL3, METTL14, RBM15, WTAP, and ZC3H13), reader (HNRNPC, YTHDC1, YTHDC2, YTHDF1, and YTHDF2), and eraser proteins (ALKBH5 and FTO) based on TCGA STAD data. The results showed that GHR is strongly positively correlated with FTO and negatively correlated with YTHDF1, YTHDF2, and HNRNPC, whereas PIM1 is weakly negatively correlated with HNRNPC, KIAA429, and METTL3 (**Figure 6F**). Our RIP experiment results also show that GHR and PIM1 have stronger interaction effects on m6A than IFNA8 and IFNB1.

Thus, we speculated that the function of four DJSEGs on GC progression may also be correlated with m6A modification or m6A regulators.

DISCUSSION

At present, endoscopic mucosal resection and endoscopic submucosal dissection are the preferred treatments in the early stages of GC (Simić et al., 2019; Min et al., 2021). However, the disease progresses rapidly

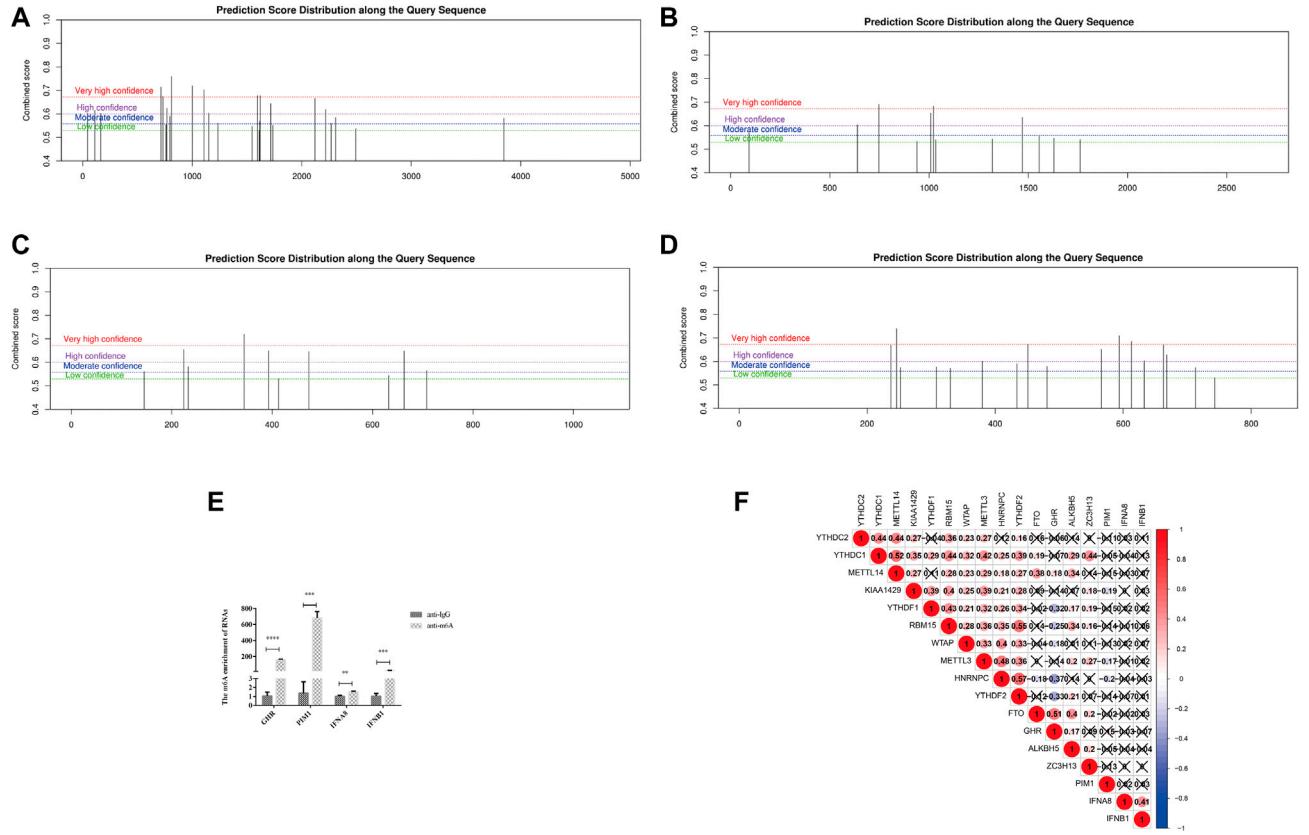


FIGURE 6 | m6A modifications on the four DJSEGs. **(A–D)** M6A modifications of GHR, PIM1, IFNA8, and IFNB1. **(E)**. The RIP-qRT-PCR results of the four DJSEGs. Results indicated that GHR, PIM1, IFNA8, and IFNB1 had enrichment m6A modification than the IgG group. **(F)**. Spearman correlation analysis clarified the association between m6A regulators and four DJSEGs.

when patients are diagnosed with GC that are already beyond the early stages; so, the 5-year disease survival rates of GC patients remain low (Li et al., 2018). Chemotherapy regimens, such as SOX (oxaliplatin + S1)/CapeOX (oxaliplatin + capecitabine), FOLFOX (oxaliplatin + leucovorin + 5-fluorouracil), and DCF (docetaxel + cisplatin + 5-fluorouracil)/DOF (docetaxel + oxaliplatin + 5-fluorouracil), are commonly used in patients with advanced GC (Zhang et al., 2020); however, their efficacy is limited. Many current studies suggest the combination of chemotherapy with surgery, radiotherapy, or targeted therapy as a first-line treatment strategy to improve patient survival (Digklia, 2016; Ruan et al., 2020; Mocan, 2021). However, because of the toxicity of chemotherapeutic drugs, the difficulty in screening beneficiaries of targeted therapy drugs, and the tendency of drug resistance, the prognosis of GC patients has not significantly improved (Li et al., 2021; Sun et al., 2021).

However, immunotherapy offers new hope for some cancer patients, and a breakthrough has been made (Li et al., 2021; Liang et al., 2021). In recent years, research on immune checkpoint inhibitors, such as programmed cell death protein-1/PD-L1 inhibitors and anti-cytotoxic T lymphocyte-associated antigen 4 (CTLA-4) inhibitors, has become important for identifying key roles in tumor-induced immunosuppression (Van Limbergen et al., 2017). Nevertheless, some studies have pointed out that not all patients can benefit from immunotherapy. Some researchers have pointed out that tumor mutation burden (Guo et al., 2021), microsatellite instability, and Epstein–Barr virus positivity (Muti et al., 2021) are all correlated with the extent to which patients benefit from immunotherapy, which means that patients need an effective marker to assess their response to immunotherapy. We aimed to identify the key genes related to GC that can be effective independent predictors of immune pathways in GC patients. Thus, we aimed to identify a potential target for the treatment of GC or a biomarker that can reflect the immune response in GC.

In this study, we identified 155 key genes in the JAK-STAT signaling pathway. Thus, we established a refined model that included four different expression genes (GHR, PIM1, IFNA8, and IFNB1). To our knowledge, few studies have reported the function of the JAK-STAT signaling pathway–related key genes in GC. After a PubMed search, we found that only a few pieces of literature reported the role of GHR (Yan et al., 2021; Meng et al., 2022) and PIM1 (Yan et al., 2012; Kim et al., 2020) in GC, whereas there is no relevant report of IFNA8 and IFNB1 in GC at present. In addition, we found that in the four DJSEGs model, the low-risk group patients had a lower probability of mortality than the high-risk group patients, both in training (**Figure 2D**) and testing (**Figure 2E**) sets. In the further ROC diagnosis of the

constructed model, this study found that the AUC result of the training set was 0.598 at 1 year, 0.636 at 3 years, and 0.655 at 5 years (**Figure 2F**), whereas the AUC of the testing set was at 0.55–0.58 (**Supplementary Figure S2A**). In the analysis of related studies on prognostic models, it is found that the AUC of most models is between 0.7 and 0.9, for example, Kunfu Dai et al. found that the AUC of their risk scoring model was 0.75–0.78 for predicting the 1-, 3-, and 5-year overall survival (Dai et al., 2022). In contrast, there are also AUCs below 0.7, for example, Qiansan Zhu et al. found the AUC of the prognosis model was 0.641and 0.677 in forecasting the 2- and 3-year prognosis of rectal cancer, respectively (Zhu et al., 2022). It is generally thought that AUC 0.5 = noninformative; AUC 0.5–0.7 = less accurate; AUC 0.7–0.9 = moderate accuracy; AUC 0.1–1 = high accuracy; and AUC 1 = perfect test (Park and Cho, 2022). Therefore, the model we constructed this time has the predictive ability, but the accuracy is not very high.

In addition, this model was significantly correlated with the patient's age and pathological grade based on TCGA data, although no statistically significant correlation was found in the clinicopathological parameters of GC patients in our laboratory. When we further analyzed GRHR-related pathways, we found that GHR was highly expressed in a large number of cancer-related pathways and related to some m6A regulators, as well as PIM1. We also found that the m6A antibody could directly interact with GHR, PIM1, IFNB1and IFNA8, suggesting that the function mechanism of four DJSEGs may be related to m6A modifications or m6A regulators.

In recent years, circRNAs have been continuously studied as targets for cancer diagnosis or treatment (Zhang et al., 2017; Arnaiz et al., 2019; Zhou et al., 2019a; Wang et al., 2021). Some researchers have revealed that circRNAs can regulate the expression or function of their parental genes; for example, circEIF3J and circPAIP2 can regulate their parental gene transcription by binding to U1snRNP and RNA Pol II (Li et al., 2015). Other studies suggested that circRNAs could also regulate parental gene expression by acting as miRNA sponges (Zhou et al., 2019b; Kong et al., 2019) and mRNA traps or through translational modulation and posttranslational modification processes (Shao et al., 2021b). In addition, we should consider the influence of miRNA, because miRNA usually regulates the expression or function of its target genes (Zhou et al., 2013; Ho et al., 2017). Such that GHR was regulated by miR-139 (Cui et al., 2017), miR-33a decreased PIM1 expression to inhibit GC cell proliferation (Wang et al., 2015). Therefore, we speculate that the mechanism of the four DJSEGs model influences GC, which may be regulated by upstream circRNAs or miRNAs; however, we still need to verify this through experiments, such as the double luciferase experiment.

According to the above results, the four DJSEGs model could be used as a prognostic indicator of GC patients. Furthermore, they could co-function or be affected by their related pathway genes or proteins, upstream circRNA, miRNA, or their own m6A modification. This study has carried out a comparatively comprehensive prediction and analysis of these four aspects. Thus, this study could be used as a reference basis for future research. In addition, we have to consider the influence of the tumor microenvironment because chronic inflammation and immune cell damage in the tumor microenvironment are also key factors in the development and progression of GC (Zhao et al., 2021).

Nevertheless, this paper has its own limitations. The biggest problem is that the above prediction analysis results lack sufficient experimental verification. We only verified the expression levels of the four genes in GC cells, patient tissues, and their association with m6A, which undoubtedly affected the certainty of the research conclusions.

CONCLUSION

Through predictive analysis, we found that GHR, PIM1, IFNA8, and IFNB1 could effectively predict the prognosis of GC, and this predictive ability may be related to their m6A modifications. Overall, our study provides a basis for relevant experimental transformation.

DATA AVAILABILITY STATEMENT

The datasets presented in this study can be found in online repositories. The names of the repository/repositories and accession number(s) can be found in the article/**Supplementary Material**.

ETHICS STATEMENT

This project was reviewed and approved by the Ethics Committee of Nanjing Medical University (No.2019669). The patients/participants provided their written informed consent to participate in this study.

AUTHOR CONTRIBUTIONS

XS was responsible for experimental design and paper modification; XC and YS were responsible for literature collection and part of data collation; FJ was in charge of all data collation, operation, and paper writing.

FUNDING

This work was supported by a grant from the National Science Foundation of China (No. 81472940).

ACKNOWLEDGMENTS

We are thankful to Chuang Chen for his technical support and guidance.

SUPPLEMENTARY MATERIAL

The Supplementary Material for this article can be found online at: https://www.frontiersin.org/articles/10.3389/fgene.2022.891744/full#supplementary-material

REFERENCES

Arnaiz, E., Sole, C., Manterola, L., Iparraguirre, L., Otaegui, D., and Lawrie, C. H. (2019). CircRNAs and Cancer: Biomarkers and Master Regulators. *Seminars Cancer Biol.* 58, 90–99. doi:10.1016/j.semcancer.2018.12.002

Baldini, C., Moriconi, F. R., Galimberti, S., Libby, P., and De Caterina, R. (2021). The JAK-STAT Pathway: an Emerging Target for Cardiovascular Disease in Rheumatoid Arthritis and Myeloproliferative Neoplasms. *Eur. Heart J.* 42, 4389–4400. doi:10.1093/eurheartj/ehab447

Bei, Y., Chen, X., Xu, Q., Lv, J., Hu, J., and Yang, S. (2022). Apatinib Weakens Resistance of Gastric Cancer Cells to Paclitaxel by Suppressing JAK/STAT3 Signaling Pathway. *Drug Dev. Res.* 83 (2022), 379–388. doi:10.1002/ddr.21867

Chen, J., Cheng, L., Zou, W., Wang, R., Wang, X., and Chen, Z. (2021). ADAMTS9-AS1 Constrains Breast Cancer Cell Invasion and Proliferation via Sequestering miR-301b-3p. *Front. Cell Dev. Biol.* 9, 719993. doi:10.3389/fcell.2021.719993

Cui, Y., Sun, X., Jin, L., Yu, G., Li, Q., Gao, X., et al. (2017). MiR-139 Suppresses β-casein Synthesis and Proliferation in Bovine Mammary Epithelial Cells by Targeting the GHR and IGF1R Signaling Pathways. *BMC Vet. Res.* 13, 350. doi:10.1186/s12917-017-1267-1

Dai, K., Liu, C., Guan, G., Cai, J., and Wu, L. (2022). Identification of Immune Infiltration-Related Genes as Prognostic Indicators for Hepatocellular Carcinoma. *BMC Cancer* 22, 596. doi:10.1186/s12885-022-09587-0

Digklia, A. (2016). Advanced Gastric Cancer: Current Treatment Landscape and Future Perspectives. *World J. Gastroenterol.* 22, 2403. doi:10.3748/wjg.v22.i8.2403

Gao, A. H., Hu, Y. R., and Zhu, W. P. (2022). IFN-γ Inhibits Ovarian Cancer Progression via SOCS1/JAK/STAT Signaling Pathway. *Clin. Transl. Oncol.* 24 (2022), 57–65. doi:10.1007/s12094-021-02668-9

Guo, X., Liang, X., Wang, Y., Cheng, A., Zhang, H., Qin, C., et al. (2021). Significance of Tumor Mutation Burden Combined with Immune Infiltrates in the Progression and Prognosis of Advanced Gastric Cancer. *Front. Genet.* 12, 642608. doi:10.3389/fgene.2021.642608

Ho, K.-H., Chen, P.-H., Hsi, E., Shih, C.-M., Chang, W.-C., Cheng, C.-H., et al. (2017). Identification of IGF-1-Enhanced Cytokine Expressions Targeted by miR-181d in Glioblastomas via an Integrative miRNA/mRNA Regulatory Network Analysis. *Sci. Rep.* 7, 732. doi:10.1038/s41598-017-00826-0

Huang, Y., Zhou, H., Zou, J., and Wang, D. (2022). GGT5 Is an Independent Prognostic Biomarker in Stomach Adenocarcinoma. *Can. J. Gastroenterology Hepatology* 2022 (2022), 1–14. doi:10.1155/2022/9983351

Kim, S., Kim, W., Kim, D.-H., Jang, J.-H., Kim, S.-J., Park, S.-A., et al. (2020). Resveratrol Suppresses Gastric Cancer Cell Proliferation and Survival through Inhibition of PIM-1 Kinase Activity. *Archives Biochem. Biophysics* 689, 108413. doi:10.1016/j.abb.2020.108413

Kong, P., Yu, Y., Wang, L., Dou, Y.-Q., Zhang, X.-H., Cui, Y., et al. (2019). circ-Sirt1 Controls NF-κB Activation via Sequence-specific Interaction and Enhancement of SIRT1 Expression by Binding to miR-132/212 in Vascular Smooth Muscle Cells. *Nucleic Acids Res.* 47, 3580–3593. doi:10.1093/nar/gkz141

Li, K., Zhang, A., Li, X., Zhang, H., and Zhao, L. (2021). Advances in Clinical Immunotherapy for Gastric Cancer. *Biochimica Biophysica Acta (BBA) - Rev. Cancer* 1876, 188615. doi:10.1016/j.bbcan.2021.188615

Li, P., Huang, C.-M., Zheng, C.-H., Russo, A., Kasbekar, P., Brennan, M. F., et al. (2018). Comparison of Gastric Cancer Survival after R0 Resection in the US and China. *J. Surg. Oncol.* 118, 975–982. doi:10.1002/jso.25220

Li, X., Pan, K., Vieth, M., Gerhard, M., Li, W., and Mejiías-Luque, R. (2022). JAK-STAT1 Signaling Pathway Is an Early Response to *Helicobacter pylori* Infection and Contributes to Immune Escape and Gastric Carcinogenesis. *Int. J. Mol. Sci.* 23, 4147. doi:10.3390/ijms23084147

Li, Z., Huang, C., Bao, C., Chen, L., Lin, M., Wang, X., et al. (2015). Exon-intron Circular RNAs Regulate Transcription in the Nucleus. *Nat. Struct. Mol. Biol.* 22, 256–264. doi:10.1038/nsmb.2959

Liang, C., Wu, H.-M., Yu, W.-M., and Chen, W. (2021). Research Status on Immunotherapy Trials of Gastric Cancer. *Wjcc* 9 (2021), 5782–5793. doi:10.12998/wjcc.v9.i21.5782

Meng, L., Ding, L., Yu, Y., Li, W., and Huang, T. (2020). JAK3 and TYK2 Serve as Prognostic Biomarkers and Are Associated with Immune Infiltration in Stomach Adenocarcinoma. *BioMed Res. Int.* 2020, 1–15. doi:10.1155/2020/7973568

Meng, Y., Zhou, B., Pei, Z., Chen, Y., and Chang, D. (2022). The Nuclear-Localized GHR Is Involved in the Cell Proliferation of Gastric Cancer, and Pegvisomant May Be an Important Potential Drug to Inhibit the Proliferation of Gastric Cancer Cells. *Biochem. Cell Biol.* 100 (2022), 125–135. doi:10.1139/bcb-2021-0386

Min, J.-S., Seo, K. W., and Jeong, S.-H. (2021). Choice of LECS Procedure for Benign and Malignant Gastric Tumors. *J. Gastric Cancer* 21, 111. doi:10.5230/jgc.2021.21.e21

Mocan, L. (2021). Surgical Management of Gastric Cancer: A Systematic Review. *J. Clin. Med.* 10, 2557. doi:10.3390/jcm10122557

Muti, H. S., Heij, L. R., Keller, Gisela, Kohlruss, Meike, Langer, Rupert, Dislich, Bastian, et al. (2021). Development and Validation of Deep Learning Classifiers to Detect Epstein-Barr Virus and Microsatellite Instability Status in Gastric Cancer: A Retrospective Multicentre Cohort Study. *Lancet Digital Health* 3, e654–e664. doi:10.1016/S2589-7500(21)00133-3

Park, S-H., and Cho, Y. S. (2022). Predictive Validity of the Cornell Scale for Depression in Dementia Among Older Adults with and without Dementia: A Systematic Review and Meta-Analysis. *Psychiat. Res.* 310, 114445. doi:10.1016/j.psychres.2022.114445

Prabhu, K. S., Bhat, A. A., Siveen, K. S., Kuttikrishnan, S., Raza, S., Raheed, T., et al. (2021). Sanguinarine Mediated Apoptosis in Non-Small Cell Lung Cancer via Generation of Reactive Oxygen Species and Suppression of JAK/STAT Pathway. *Biomed. Pharmacother.* 144, 112358. doi:10.1016/j.biopha.2021.112358

Ruan, T., Liu, W., Tao, K., and Wu, C. (2020). A Review of Research Progress in Multidrug-Resistance Mechanisms in Gastric Cancer. *Onco Targets Ther.* 13, 1797–1807. doi:10.2147/OTT.S239336

Shao, J., Liang, R., Ding, D., Zheng, X., Zhu, X., Hu, S., et al. (2021). A Smart Multifunctional Nanoparticle for Enhanced Near-Infrared Image-Guided Photothermal Therapy Against Gastric Cancer. *Int. J. Nanomedicine* 16, 2897–2915. doi:10.2147/ijn.s289310

Shao, T., Pan, Y.-h., and Xiong, X.-d. (2021). Circular RNA: an Important Player with Multiple Facets to Regulate its Parental Gene Expression. *Mol. Ther. - Nucleic Acids* 23, 369–376. doi:10.1016/j.omtn.2020.11.008

Simić, A. P., Skrobić, O. M., and Peško, P. M. (2019). A Surgeon's Role in the Management of Early Esophageal, EGJ and Gastric Lesions. *Dig. Dis.* 37, 355–363. doi:10.1159/000500120

Song, Z., Wu, Y., Yang, J., Yang, D., and Fang, X. (2017). Progress in the Treatment of Advanced Gastric Cancer. *Tumour Biol.* 39, 101042831771462. doi:10.1177/1010428317714626

Sun, W., Jiang, C., Ji, Y., Xiao, C., and Song, H. (2021). Long Noncoding RNAs: New Regulators of Resistance to Systemic Therapies for Gastric Cancer. *BioMed Res. Int.* 2021 (2021), 1–14. doi:10.1155/2021/8853269

Sung, H., Ferlay, J., Siegel, R. L., Laversanne, M., Soerjomataram, I., Jemal, A., et al. (2021). Global Cancer Statistics 2020: GLOBOCAN Estimates of Incidence and Mortality Worldwide for 36 Cancers in 185 Countries. *CA A Cancer J. Clin.* 71, 209–249. doi:10.3322/caac.21660

Van Limbergen, E. J., De Ruysscher, D. K., Olivo Pimentel, V., Marcus, D., Berbee, M., Hoeben, A., et al. (2017). Combining Radiotherapy with Immunotherapy: the Past, the Present and the Future. *Br. J. Radiol.* 90, 20170157. doi:10.1259/bjr.20170157

Wang, Y.-W., Xu, Y., Wang, Y.-Y., Zhu, J., Gao, H.-D., Ma, R., et al. (2021). Elevated circRNAs Circ_0000745, Circ_0001531 and Circ_0001640 in Human Whole Blood: Potential Novel Diagnostic Biomarkers for Breast Cancer. *Exp. Mol. Pathology* 121, 104661. doi:10.1016/j.yexmp.2021.104661

Wang, Y., Zhou, X., Shan, B., Han, J., Wang, F., Fan, X., et al. (2015). Downregulation of microRNA-33a Promotes Cyclin-dependent Kinase 6, Cyclin D1 and PIM1 Expression and Gastric Cancer Cell Proliferation. *Mol. Med. Rep.* 12, 6491–6500. doi:10.3892/mmr.2015.4296

Wu, J., Guo, X., Wen, Y., Huang, S., Yuan, X., Tang, L., et al. (2021). N6-Methyladenosine Modification Opens a New Chapter in Circular RNA Biology. *Front. Cell Dev. Biol.* 9, 709299. doi:10.3389/fcell.2021.709299

Yan, B., Yau, E. X., Samanta, S., Ong, C. W., Yong, K. J., et al. (2012). Clinical and Therapeutic Relevance of PIM1 Kinase in Gastric Cancer. *Gastric Cancer* 15, 188–197. doi:10.1007/s10120-011-0097-2

Yan, H. Z., Wang, H. F., Yin, Y., Zou, J., Xiao, F., Yi, L. N., et al. (2021). GHR is Involved in Gastric Cell Growth and Apoptosis via PI3K/AKT Signalling. *J. Cell. Mol. Medi* 25, 2450–2458. doi:10.1111/jcmm.16160

Yang, Y., Zhang, Q., Liang, J., Yang, M., Wang, Z., Tang, D., et al. (2021). STAM2 Knockdown Inhibits Proliferation, Migration, and Invasion by Affecting the JAK2/STAT3 Signaling Pathway in Gastric Cancer. *Acta Bioch. Bioph. Sin.* 53, 697–706. doi:10.1093/abbs/gmab038

Yue, Y., Zhang, Q., Wu, S., Wang, S., Cui, C., Yu, M., et al. (2020). Identification of Key Genes Involved in JAK/STAT Pathway in Colorectal Cancer. *Mol. Immunol.* 128, 287–297. doi:10.1016/j.molimm.2020.10.007

Zhang, J., Liu, H., Hou, L., Wang, G., Zhang, R., Huang, Y., et al. (2017). Circular RNA_LARP4 Inhibits Cell Proliferation and Invasion of Gastric Cancer by Sponging miR-424-5p and Regulating LATS1 Expression. *Mol. Cancer* 16, 151. doi:10.1186/s12943-017-0719-3

Zhang, L., Wang, Z., Xiao, J., Zhang, Z., Li, H., Wang, Y., et al. (2020). Prognostic Value of Fibrinogen-to-albumin R-atio in P-atients with G-astric C-ancer R-eceiving F-irst-line C-hemotherapy. *Oncol. Lett.*, 20. 10. doi:10.3892/ol.2020.11871

Zhao, W., Liu, M., Zhang, M., Wang, Y., Zhang, Y., Wang, S., et al. (2021). Effects of Inflammation on the Immune Microenvironment in Gastric Cancer. *Front. Oncol.* 11, 690298. doi:10.3389/fonc.2021.690298

Zhou, J., Zhang, S., Chen, Z., He, Z., Xu, Y., and Li, Z. (2019). CircRNA-ENO1 Promoted Glycolysis and Tumor Progression in Lung Adenocarcinoma through Upregulating its Host Gene ENO1. *Cell Death Dis.* 10, 885. doi:10.1038/s41419-019-2127-7

Zhou, P., Xu, W., Peng, X., Luo, Z., Xing, Q., Chen, X., et al. (2013). Large-scale Screens of miRNA-mRNA Interactions Unveiled that the 3'UTR of a Gene Is Targeted by Multiple miRNAs. *PLoS One* 8, e68204–12. doi:10.1371/journal.pone.0068204

Zhou, Y., Zheng, X., Xu, B., Chen, L., Wang, Q., Deng, H., et al. (2019). Circular RNA Hsa_circ_0004015 Regulates the Proliferation, Invasion, and TKI Drug Resistance of Non-small Cell Lung Cancer by miR-1183/PDPK1 Signaling Pathway. *Biochem. Biophysical Res. Commun.* 508, 527–535. doi:10.1016/j.bbrc.2018.11.157

Zhu, J., Luo, C., Zhao, J., Zhu, X., Lin, K., Bu, F., et al. (2021). Expression of LOX Suggests Poor Prognosis in Gastric Cancer. *Front. Med.* 8, 718986. doi:10.3389/fmed.2021.718986

Zhu, Q., Wu, X., Ma, L., and Xue, H. (2022). Apoptosis-Associated Gene Expression Profiling Is One New Prognosis Risk Predictor of Human Rectal Cancer. *Dis. Markers* 2022 (2022), 1–16. doi:10.1155/2022/4596810

Conflict of Interest: The authors declare that the research was conducted in the absence of any commercial or financial relationships that could be construed as a potential conflict of interest.

Publisher's Note: All claims expressed in this article are solely those of the authors and do not necessarily represent those of their affiliated organizations or those of the publisher, the editors, and the reviewers. Any product that may be evaluated in this article or claim that may be made by its manufacturer is not guaranteed or endorsed by the publisher.

Copyright © 2022 Jiang, Chen, Shen and Shen. This is an open-access article distributed under the terms of the Creative Commons Attribution License (CC BY). The use, distribution or reproduction in other forums is permitted, provided the original author(s) and the copyright owner(s) are credited and that the original publication in this journal is cited, in accordance with accepted academic practice. No use, distribution or reproduction is permitted which does not comply with these terms.

frontiers | Frontiers in Genetics

TYPE Original Research
PUBLISHED 16 August 2022
DOI 10.3389/fgene.2022.898474

Check for updates

OPEN ACCESS

EDITED BY
Alip Ghosh,
University of Maryland, Baltimore, United States

REVIEWED BY
Giovanni Martinelli,
University of Bologna, Italy
Adán Guerrero,
National Autonomous University of Mexico, Mexico

*CORRESPONDENCE
Feng Li,
lifeng1982315@163.com
Kai-Lin Xu,
lihmd@163.com
Qing-Yun Wu,
qywu82@163.com

†These authors have contributed equally to this work

SPECIALTY SECTION
This article was submitted to Cancer Genetics and Oncogenomics, a section of the journal Frontiers in Genetics

RECEIVED 17 March 2022
ACCEPTED 18 July 2022
PUBLISHED 16 August 2022

CITATION
Mu X-R, Ma M-M, Lu Z-Y, Liu J, Xue Y-T, Cao J, Zeng L-Y, Li F, Xu K-L and Wu Q-Y (2022), Effects of the PLK4 inhibitor Centrinone on the biological behaviors of acute myeloid leukemia cell lines.
Front. Genet. 13:898474.
doi: 10.3389/fgene.2022.898474

COPYRIGHT
© 2022 Mu, Ma, Lu, Liu, Xue, Cao, Zeng, Li, Xu and Wu. This is an open-access article distributed under the terms of the Creative Commons Attribution License (CC BY). The use, distribution or reproduction in other forums is permitted, provided the original author(s) and the copyright owner(s) are credited and that the original publication in this journal is cited, in accordance with accepted academic practice. No use, distribution or reproduction is permitted which does not comply with these terms.

Effects of the PLK4 inhibitor Centrinone on the biological behaviors of acute myeloid leukemia cell lines

Xing-Ru Mu[1†], Meng-Meng Ma[1†], Zi-Yi Lu[1†], Jun Liu[1], Yu-Tong Xue[1], Jiang Cao[2], Ling-Yu Zeng[2], Feng Li[3*], Kai-Lin Xu[1,2*] and Qing-Yun Wu[1,2*]

[1]Blood Diseases Institute, Xuzhou Medical University, Xuzhou, Jiangsu, China, [2]Department of Hematology, the Affiliated Hospital of Xuzhou Medical University, Xuzhou, Jiangsu, China, [3]Department of Cell Biology and Neurobiology, Xuzhou Medical University, Xuzhou, China

Polo-like kinase 4 (PLK4), a key regulator of centriole biogenesis, is frequently overexpressed in cancer cells. However, roles and the mechanism of PLK4 in the leukemiagenesis of acute myeloid leukemia (AML) remain unclear. In this study, the PLK4 inhibitor Centrinone and the shRNA knockdown were used to investigate roles and the mechanism of PLK4 in the leukemiagenesis of AML. Our results indicated that Centrinone inhibited the proliferation of AML cells in a dose- and time-dependent manner *via* reduced the expression of PLK4 both in the protein and mRNA levels. Moreover, colony formation assay revealed that Centrinone reduced the number and the size of the AML colonies. Centrinone induced AML cell apoptosis by increasing the activation of Caspase-3/poly ADP-ribose polymerase (PARP). Notably, Centrinone caused the G2/M phase cell cycle arrest by decreasing the expression of cell cycle-related proteins such as Cyclin A2, Cyclin B1, and Cyclin-dependent kinase 1 (CDK1). Consistent with above results, knockdown the expression of PLK4 also inhibited cell proliferation and colony formation, induced cell apoptosis, and caused G2/M phase cell cycle arrest without affecting cell differentiation. All in all, this study suggested that PLK4 inhibited the progression of AML *in vitro*, and these results herein may provide clues in roles of PLK4 in the leukemiagenesis of AML.

KEYWORDS

acute myeloid leukemia, PLK4, small molecule inhibitors, centrinone, biological behaviors

Introduction

Acute myeloid leukemia (AML) is a malignant proliferative disease of bone marrow hematopoietic stem cells with a high mortality rate (Siegel et al., 2020). Continuing for nearly four decades, the treatment of AML is still dominated by induction chemotherapy combined with allogeneic hematopoietic stem cell transplantation, with low cure rates and certain limitations (Vakiti and Mewawalla. 2021). AML patients often have genetic

abnormalities which were associated with the poor prognosis. Targeted therapy for AML with the therapeutic advantages of selective removal of leukemia cells and the ability to overcome drug resistance has received increasing attention in recent years (Kayser and Levis. 2018). Although many inhibitors were used in the clinical trials, the therapeutic effect was still unsatisfactory. Thus, it is necessary to explore new therapeutic strategies for AML, particularly individualized molecularly targeted therapies.

Polo-like kinases (PLKs) are a family of serine/threonine kinases, which are involved in the centrosome replication and cell cycle regulation (Archambault and Glover. 2009; de Carcer et al., 2011). PLK family members feature similar structures with an N-terminal kinase catalytic domain and C-terminal Polo-box structural domains (PBDs) (Strebhardt. 2010; Archambault et al., 2015). PLK4, also known as serine/threonine kinase (SAK), contrasts with other PLKs in that it contains only a PBD structural domain (Leung et al., 2002; Sillibourne and Bornens. 2010). PLK4 high expression contributes to excessive centriole formation, which causes genomic instability and tumorigenesis (Holland et al., 2010).

The aberrant expression of PLK4 has a close relationship with a variety of malignancies. Although many studies have been done on roles of PLK4, there was a controversy in whether PLK4 promoted or suppressed the progression of cancers. A series of studies indicated that PLK4 promoted the progression of cancers. PLK4 was prevailing high expressed in the breast cancer, with only 2.6% samples being negative (Li et al., 2016). Similarly, over half of the gastric cancer cell lines showed significantly elevated PLK4 mRNA levels (Shinmura et al., 2014). Kawakami et al. also demonstrated that the PLK4 was high expressed in lung adenocarcinoma tissues compared to normal lung tissues which indicated a low overall survival and progression-free survival (Kawakami et al., 2018a). Besides, PLK4 was also overexpressed and promoted the progression of melanoma, hepatocellular carcinoma and brain tumors (Denu et al., 2018). Similar to roles of PLK4 in the solid tumors, in 80% of classical Hodgkin's lymphoma were high expressed and promoted its progression (Ward et al., 2015). But the expression of PLK4 was decreased in some hematologic malignancies compared to normal tissues, such as in 82.0% of lymphomas, 80.5% of myelodysplastic syndromes (MDS) and 60% of acute lymphoblastic leukemia (ALL) and did not display oncogene roles. In our previous study, the RNA-Seq analysis revealed that PLK4 was highly expressed in AML and had a close relationship with the overall survival of AML patients. However, roles and mechanisms of PLK4 in the leukemiagenesis of AML were still unclear. In this study, effects of PLK4 inhibitor Centrinone and lentivirus-mediated PLK4 knockdown on the biological behaviors of AML cell lines were used to investigate roles and mechanisms of PLK4 in the pathology of AML.

In recent years, due to key roles of PLK4 in the progression of cancers, several PLK4 inhibitors have been identified, but the clinical therapeutic effects on cancers were still unsatisfactory (Holland and Cleveland. 2014; Mason et al., 2014; Liu et al., 2017; Lei et al., 2018). Thus, to elucidate roles and mechanisms of PLK4 in the progression of cancers was important for the new drug design and screen. In this study, effects of PLK4 inhibitor Centrinone and lentivirus mediated knockdown the expression of PLK4 on the AML cell lines' biological behaviors such as cell proliferation, apoptosis, cell cycle, and colony formation were investigated to clarify roles and mechanisms of PLK4 in the leukemiagenesis of AML. Our results suggested that PLK4 inhibited AML cell proliferation, colony formation, induced AML cell apoptosis and caused the G2/M cell cycle arrest by affecting the activation of Caspase-3/PARP and the expression of cell cycle-related proteins such as Cyclin A2, Cyclin B1 and CDK1. Thus, these results herein may provide clues in roles and mechanisms of PLK4 in the leukemiagenesis of AML.

Materials and methods

Cell culture and reagents

Human AML cell lines MOLM-13, KG-1 and OCI-AML3 were cultured in RPMI-1640/IMDM (HyClone, United States) medium, supplemented with 10% fetal bovine serum (FBS; Gibco, United States) and 1% penicillin/streptomycin mixture. All cells were incubated at 37°C with 5% CO_2 in a humidified atmosphere. Centrinone (MCE, China) was dissolved in the dimethyl sulfoxide (DMSO; Sigma, United States) to a storage concentration of 50 mM.

Cell viability assays

AML cells were seeded into a 96-well plate at a density of 20,000 cells/well for cell viability assay. Cells were treated with different Centrinone concentrations or the vehicle DMSO for 24–96 h, then 10 μL/well Cell Counting Kit-8 (CCK-8; Absin, China) was added to the medium and incubated at 37°C for 3 h, followed by measuring absorbance at 450 nm by Spectra Max M2 Microplate Reader (Molecular Devices, United States).

Cell apoptosis assay

AML cells with the designed treatment were collected and incubated with Annexin V-APC and 7-Aminoactinomycin D (7-AAD; BD, United States) for 15 min. Then, cells were subjected to flow cytometry. The rates of apoptotic cells were acquired on the Navios flow cytometer (Beckman Coulter, United States).

Cell cycle assay

AML cells were treated with a serum-free medium to synchronize cells. Then cells were treated with Centrinone at different concentrations for 48 h. Cells were collected and fixed with 70% ethanol overnight at 4°C, then stained with propidium iodide (PI)/RNase staining buffer (BD, United States) for 15 min. The DNA content was monitored by the Navios flow cytometer (Beckman Coulter, United States), and the data was analyzed using FlowJo Version 7.6 software (TreeStar, United States).

Cell differentiation assay

AML cells were treated with different concentrations of Centrinone and incubated with fluorescein isothiocyanate (FITC) CD 11b (BD, United States) for 30 min. Then cells were subjected to flow cytometry and acquired on Navios flow cytometer (Beckman Coulter, United States).

colony formation assay

AML cells (300 cells/well) were inoculated in the 6-well plates filled with methylcellulose, treated with different concentrations of Centrinone, and incubated in an incubator at 37°C, 5% CO_2 for 2 weeks. Colonies were observed and counted with an inverted microscope, stained with Giemsa (Beyotime, China), and photographed.

RNA Isolation and quantitative real-time PCR

Total RNA was extracted using Trizol reagent (Invitrogen, United States), and cDNA was synthesized by reverse transcription with OligodT as a primer and M-MLV reverse transcriptase (Invitrogen, United States). PLK4 and GAPDH were amplified by real-time PCR on the Light Cycler480 II system (Roche, United States) using Platinum SYBR Green qPCR Super Mix-UDG kit (Roche, United States), and the relative expression levels of each group of genes were calculated by relative gene quantification ($2^{-\Delta\Delta Ct}$) using GAPDH expression levels as an internal reference. The primer sequences were as follows:

PLK4 forward: 5′-GTGGGGAAATCAAGAAACCA-3′;
PLK4 reverse: 5′-GGTGGCTCCATACCCCTAGT-3′;
GADPH forward: 5′-CGAGATCCCTCCAAAATCAA-3′;
GADPH reverse: 5′-TGTGGTCATGAGTCCTTCCA-3′.

western blot analysis

Total protein was extracted using radio immunoprecipitation assay (RIPA) lysis buffer (Beyotime, China) containing protease inhibitor cocktail tablets (KeyGen, China) and phosphatase inhibitor cocktail (KeyGen, China), according to operating instructions. Protein concentrations were measured using a bicinchoninic acid (BCA) assay (Beyotime, China), and then equal amounts of total protein were separated by electrophoresis on a 10% polyacrylamide gel (Bio-Rad, United States). The protein extracts were transferred onto polyvinylidene fluoride (PVDF) membranes (Millipore, Billerica, United States), and then membranes were blocked in Tris-buffered saline (contained 0.05% Tween) with 5% defatted milk for 1.5 h. Then membranes were incubated with primary antibodies at 4°C overnight. The primary antibodies were used with a concentration of 1: 1,000 as follows: PLK4 (Proteintech, China), Caspase-3, PARP, Cyclin A2, Cyclin B1, CDK1, signal transducers and activators of transcription 3 (STAT3), and p-STAT3 (Cell Signaling Technology, United States). GAPDH (Bioworld, United States) was used as the endogenous control. Goat anti-rabbit or goat anti-mouse secondary antibodies labeled with horseradish peroxidase (HRP) (1: 5,000, Bioworld, United States) were hybrid bindings at room temperature for 1.5 h, and signals were detected with the AI600 Imaging System (General Electric, United States) using an enhanced chemiluminescence (ECL) kit (Bio-Rad, United States).

Construction of lentiviral interference vector and transfection

The specific shRNA sequence of the *PLK4* was annealed and ligated with the pLV-shRNA-EGFP linear vector after double digestion with *EcoR*I and *BamH*I to construct the recombinant interfering vector OCI-AML3-sh-PLK4-1/2, which was sent to Invitrogen for sequencing. The virus particles were packaged using a triple plasmid system, and ultracentrifugation was used to concentrate the virus and stored at −80°C. 1 day before transfection, OCI-AML3 cells were seeded into 24-well plates at a concentration of 5×10^4 cells per well. Appropriate doses of lentivirus and transfection enhancers were co-cultured with cells. Both empty vector and PLK4 knockdown lentivirus vectors expressed green fluorescent protein (GFP) and puromycin resistance genes. 2 days later, 8 μg/ml puromycin (VICMED, China) was added to the culture medium to screen stably transfected cells. Infection efficiency was determined by GFP and then validated by RT-PCR and Western blot.

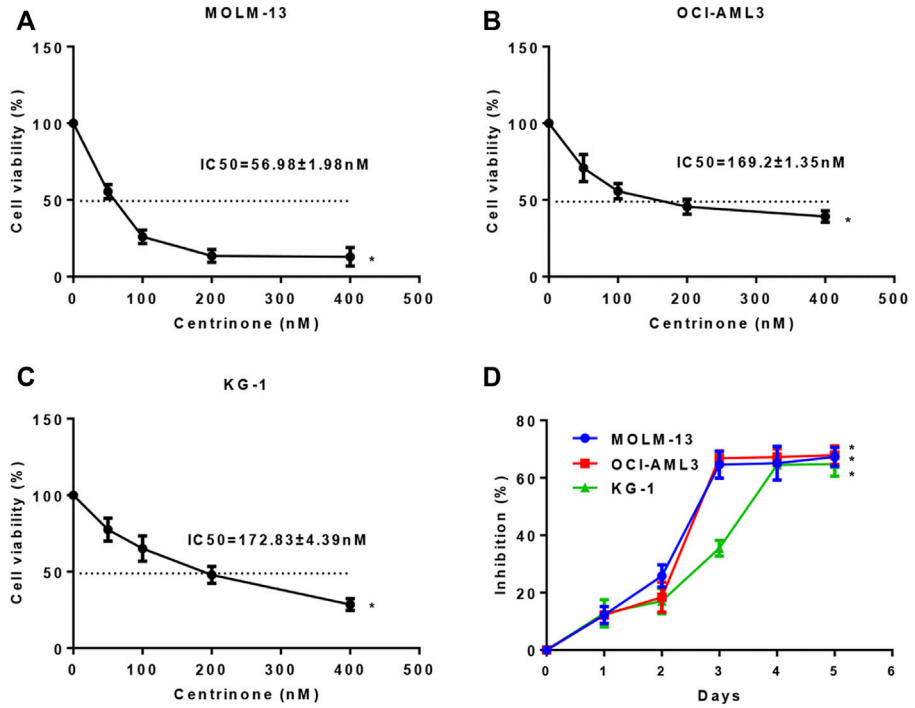


FIGURE 1
Centrinone inhibited the proliferation of AML cells in a dose- and time-dependent manner. **(A–C)** Effects of different Centrinone concentrations (0, 50, 100, 200, 400 nM) on the proliferation of AML cells were determined by treatment MOLM-13, OCI-AML3, and KG-1 cells for 72 h, then CCK-8 was added, incubated for 3 h, finally the OD450 absorbance was detected. **(D)** The indicated Centrinone concentrations was used to treat MOLM-13 (54.26 nM), OCI-AML3 (177.7 nM), and KG-1 (189.9 nM) cells for 1-5 days to detect the effect of Centrinone on the proliferation of AML cells at different treatment times. Columns, means ($n \geq 3$); bars, *SD*. *$p < 0.05$ versus the control group.

Statistical analysis

All experiments were repeated at least three times, and the data were statistically analyzed and processed with SPSS16.0 software or GraphPad Prism7.03 software. The measurement data were expressed as mean ± standard deviation, and *t*-test was used for comparison of two sample means, and one-way ANOVA was used for comparison of more than two sample means. The test level was $\alpha = 0.05$, and *$p < 0.05$ indicated that the difference was statistically significant.

Results

Centrinone inhibited the proliferation of AML cells in a dose- and time-dependent manner

In order to investigate effects of Centrinone on the proliferation of MOLM-13, OCI-AML3, and KG-1 AML cell lines, CCK-8 assay was done. AML cells were inoculated in 96-well plates at a density of 2×10^4 cells/well, and different Centrinone concentrations (50, 100, 200 and 400 nM) were used to treat AML cells for 24, 48 and 72 h. Our results indicated that the proliferation of OCI-AML3, and KG-1 AML cells gradually decreased with Centrinone concentrations increased compared with the control group (Figures 1A–C), while the proliferation of MOLM-13 gradually decreased when the Centrinone concentrations were between 50–200 nM, and no obvious changes were observed when the Centrinone concentrations between 200–400 nM which might be caused by the high drug concentrations (Figures 1A–C). Similarly, the proliferation of MOLM-13, OCI-AML3, and KG-1 AML cells gradually decreased with the Centrinone treatment time increased compared with the control group (Figure 1D). These results suggested that Centrinone inhibited the proliferation of AML cell lines in a dose- and time-dependent manner.

Centrinone inhibited the expression of PLK4 in AML Cell lines

In order to elucidate effects of Centrinone concentrations (0, 100, 200 nM) on the expression of PLK4 in the MOLM-13, OCI-AML3, and KG-1 cells, the RT-PCR and Western blot

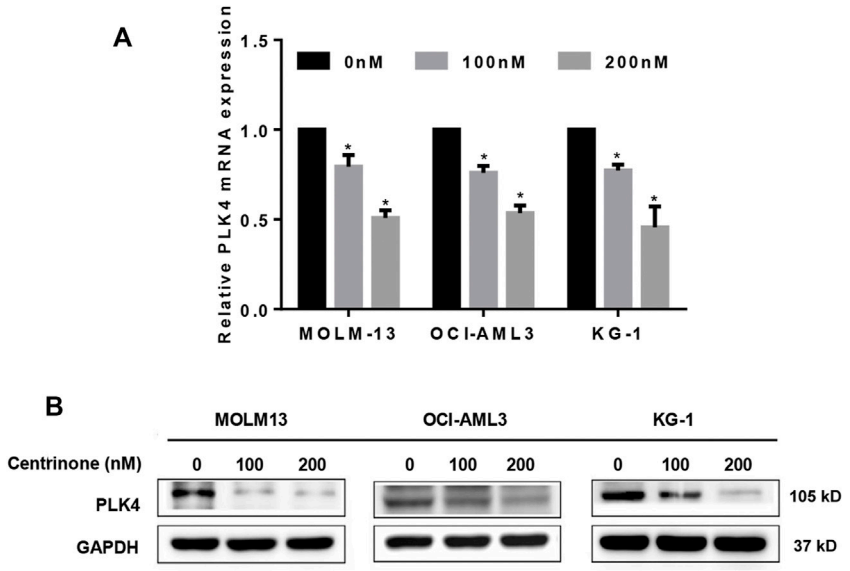


FIGURE 2
Centrinone inhibited the expression of PLK4. **(A)** The mRNA expression levels of PLK4 were detected by RT-PCR after AML cells treated with different concentrations of Centrinone for 72 h. Compared with the control group, *$p < 0.05$. **(B)** The expression of PLK4 were detected by Western blot in AML cells treated with diverse concentrations of Centrinone for 72 h and the expression of GAPDH was used as an internal control.

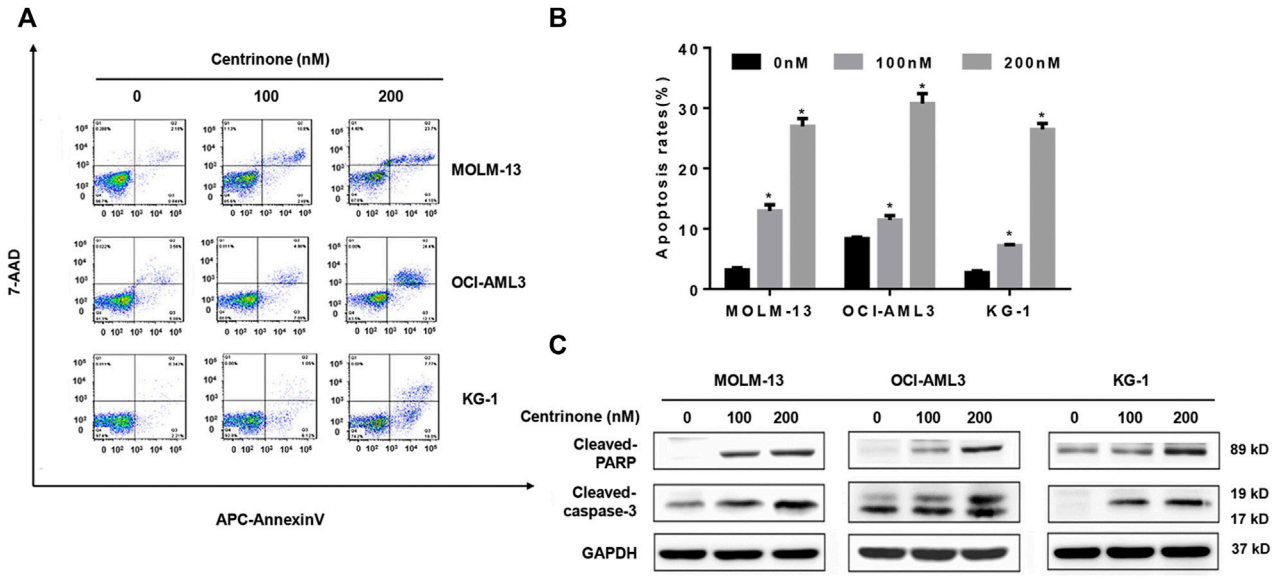


FIGURE 3
Centrinone induced the apoptosis of AML cells *via* increasing the expression of cleaved Caspase-3 and cleaved PARP. **(A)** The apoptosis of AML cells treated with different Centrinone concentrations after 72 h was analyzed by flow cytometry with Annexin V/7-AAD double staining. **(B)** Statistical analysis of apoptosis of AML cells treated by Centrinone (compared with the control group, *$p < 0.05$). **(C)** The expression of cleaved Caspase-3 and cleaved PARP were detected by Western blot.

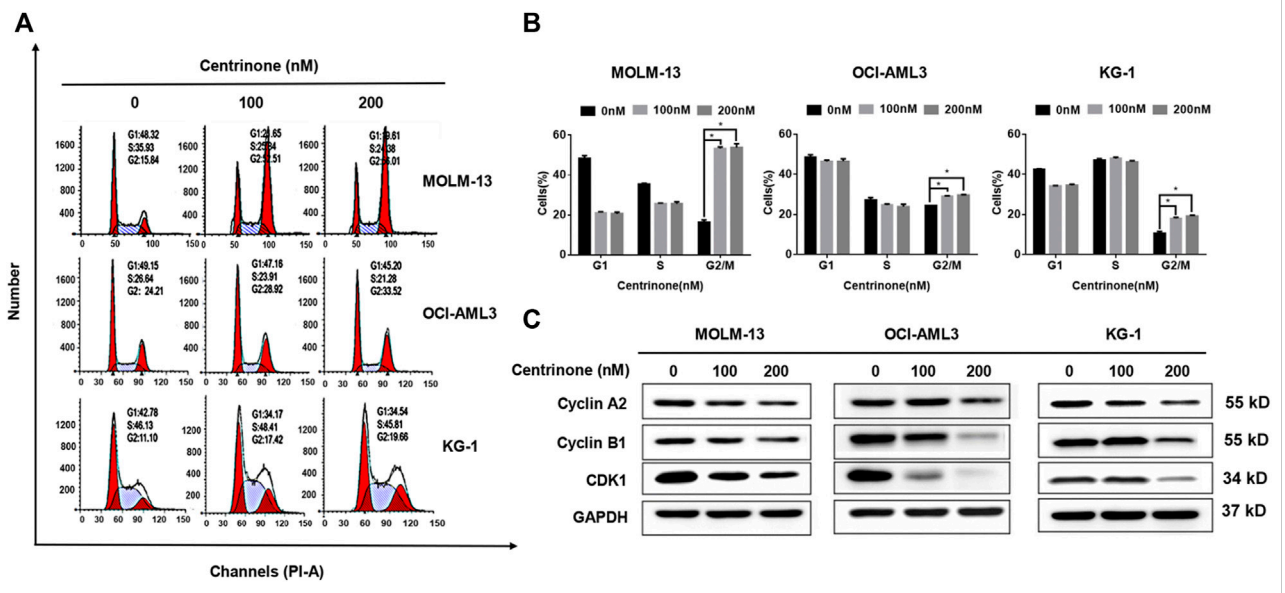


FIGURE 4
Centrinone caused AML cells in the G2/M phase cell cycle arrest by reducing the expression of Cyclin A2, Cyclin B1, and CDK1. **(A)** AML cells were treated by Centrinone for 48 h, and the cell cycle of ethanol-fixed cells with PI staining was analyzed by flow cytometry. **(B)** Statistical analysis of the distribution of G1, S and G2/M phase AML cells treated by Centrinone (compared with the control group, $*p < 0.05$). **(C)** The expression of Cyclin A2, Cyclin B1, and CDK1 were detected by Western blot.

experiments were done. Our results indicated that Centrinone inhibited the expression of PLK4 both in the mRNA and protein levels with the increased Centrinone concentrations in the MOLM-13, OCI-AML3 and KG-1 cells (Figures 2A,B).

Centrinone induced the apoptosis of AML cells

In order to investigate effects of Centrinone on the apoptosis of AML cells, flow cytometry was used to detect the number of double staining cells with Annexin V and 7-AAD. The early apoptotic cells were defined as Annexin V^+/7-AAD^-, late apoptotic cells were defined as Annexin V^+/7-AAD^+ and the total percentage of apoptotic cells was the sum of early apoptotic cells and late apoptotic cells. Our results suggested that the percentage of apoptotic cells in all three AML cell lines increased with the elevated Centrinone concentrations (0, 100, 200 nM) after 72 h treatment (Figures 3A,B). The expression of apoptosis-related proteins was also detected to clarify the mechanism of Centrinone led to the AML cell apoptosis. As shown in Figure 3C, the expression of cleaved Caspase-3 and cleaved PARP were significantly increased in AML cells after Centrinone treatment. Thus, these observations suggested that Centrinone induced the apoptosis of AML cells *via* the activation of Caspase-3 and PARP pathway.

Centrinone induced AML cells in the G2/M phase cell cycle arrest

In order to clarify effects of the Centrinone on the cell cycle of AML cell lines, the PI stain experiments were done. MOLM-13, OCI-AML3, and KG-1 cells were treated with different Centrinone concentrations (0, 100, 200 nM) for 48 h. DNA from ethanol-fixed cells was stained with PI, and the DNA content was measured by flow cytometry. The number of cells in the G2/M phase increased continuously with Centrinone concentrations increased (Figures 4A,B). At the same time, the expressions of cell cycle-related proteins were detected to explore the mechanism of Centrinone caused the cell cycle arrest of AML cells. As shown in Figure 4C, the expression of Cyclin A2, Cyclin B1 and CDK1 were significantly reduced in AML cells after Centrinone treatment. This result suggested that Centrinone arrested the cell cycle in the G2/M phase by reducing the expression of Cyclin A2, Cyclin B1, and CDK1.

Centrinone suppressed the colony formation of AML cells

The colony formation assay was conducted to evaluate effects of Centrinone on colony formation ability of AML cell lines. MOLM-13, OCI-AML3, and KG-1 cells were seeded in methylcellulose medium and treated with different Centrinone concentrations (0, 100, and 200 nM) for 14 days, and the number

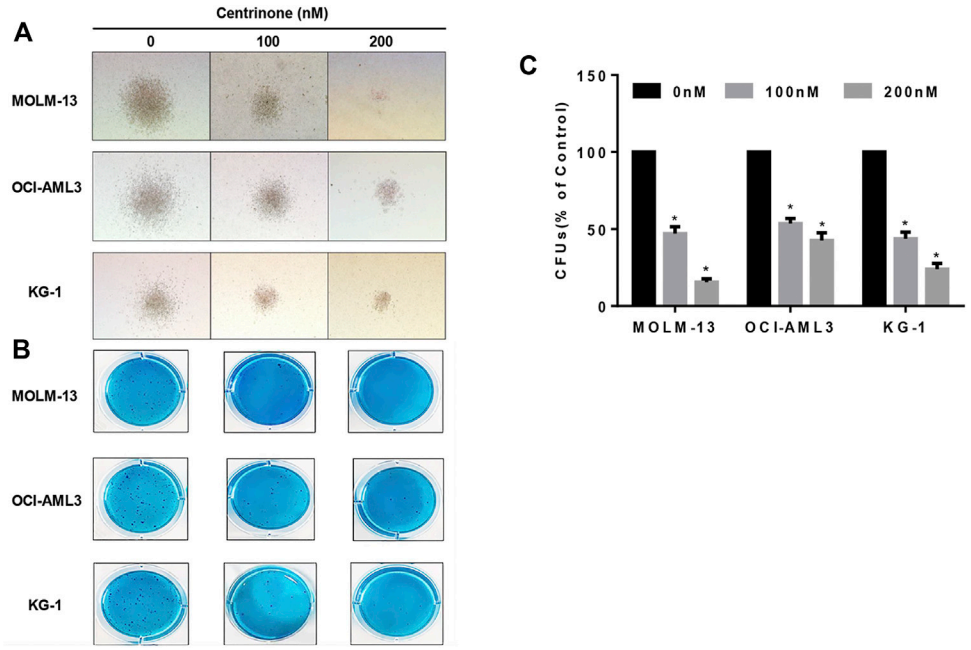


FIGURE 5
Centrinone reduced the clonogenic ability of AML cell lines. AML cells were co-incubated with Centrinone for 14 days. Single colonies were observed and counted under the microscope. **(A)** Microscopic observation of cell colony generation size (100×). **(B)** The number of colony generations was observed after Giemsa staining. **(C)** Statistical analysis of the number of colony formation of MOLM-13, OCI-AML3, and KG-1 AML cells (Compared with the control group, $*p < 0.05$).

of colonies was counted under the microscope. Compared with the control group, the quantity and size of cell colonies markedly decreased and significantly reduced after Centrinone treatment for 14 days (Figures 5A–C).

Centrinone had no effect on the differentiation of AML cells

The blockage of cell differentiation was one reason for the pathology of AML (Denu et al., 2018). In order to elucidate whether Centrinone affected the differentiation of AML cell lines, the expression of myeloid differentiation maker CD 11b was determined. MOLM-13, OCI-AML3, and KG-1 cells were treated with different Centrinone concentrations (0, 100, 200 nM) for 48 h. Then, cells were collected, stained with FITC CD11b, and detected by flow cytometry. No significant cell differentiation changes were observed compared with the control group (Figure 6A).

Centrinone inhibited the activation of STAT3 in AML cells

Previous study indicated that STAT3 was involved in the regulation of centrosome clustering in cancer cells (Morris et al., 2017). In order to investigate whether Centrinone affected the activation of STAT3, the expression of STAT3 and p-STAT3 in AML cells was detected by Western blot. MOLM-13, OCI-AML3, KG-1 cells were treated with different Centrinone concentrations (0, 100, 200 nM) for 72 h, and then cell harvest, protein extraction and the Western blot experiment was done. As shown in Figure 6B, the expression of STAT3 and p-STAT3 significantly decreased with the Centrinone concentrations increased, which suggested that PLK4 inhibited the progression of AML *via* reducing the activation of STAT3.

Knockdown the expression of PLK4 inhibited the Cell proliferation and suppressed the clonogenic ability of OCI-AML3 cells

The OCI-AML3 cells that stably knockdown the expression of PLK4 were obtained by the lentivirus-mediated transduction and sorted by the flow cytometry. The expression of PLK4 was significantly decreased both in the mRNA and protein levels in the knockdown groups compared with the control group (Figures 7A,B). In order to investigate effects of knockdown the expression of PLK4 on the proliferation of OCI-AML3 cells, CCK-8 assay was done. OCI-AML3-sh-EGFP, OCI-AML3-sh-

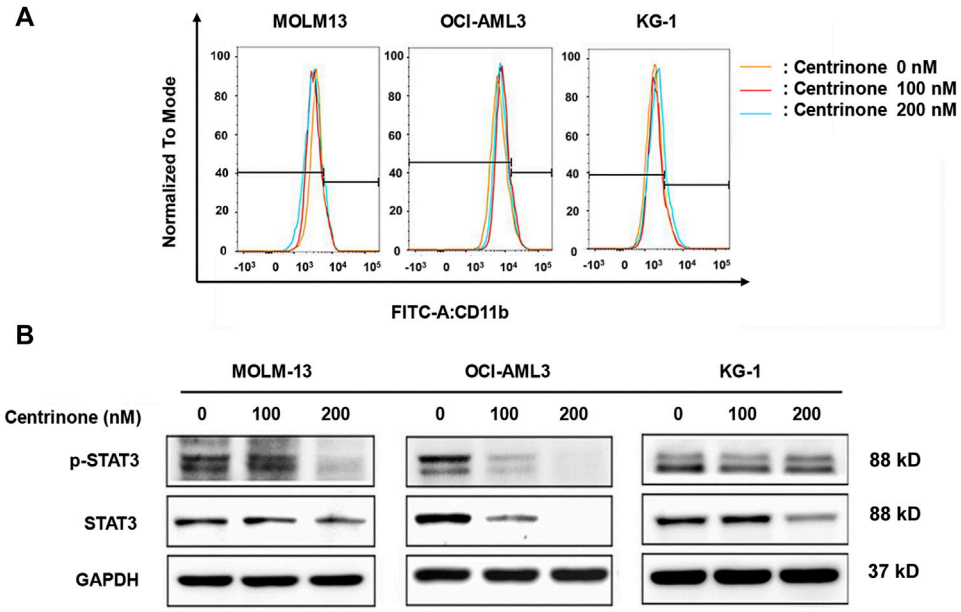


FIGURE 6
Effects of Centrinone on the expression of CD11b and the activation of STAT3 in AML cell lines. **(A)** Effects of Centrinone on the expression of myeloid cell differentiation marker CD11b in AML cell lines. AML cells were treated with Centrinone for 48 h, and the expression of CD11b was analyzed by flow cytometry. **(B)** Centrinone inhibited the activation of STAT3. AML cells treated with different concentrations of Centrinone for 72 h, and then the expression of STAT3 and p-STAT3 were detected by Western blot. The expression of GAPDH was used as an internal control.

PLK4-1 and OCI-AML3-sh-PLK4-2 cells were inoculated uniformly in 96-well plates at a density of 2×10^4 cells/well, at 24, 48 and 72 h, CCK-8 was added and incubated for 3 h, and then the OD450 was detection. Similar to results of Centrinone inhibition experiments, knockdown the expression of PLK4 significantly suppressed the proliferation of OCI-AML3 cells compared with the control group (Figure 7C). At the same time, effects of knockdown the expression of PLK4 on the clonogenic ability of OCI-AML3 cells were investigated by colony formation assay. As shown in Figures 7D,E, knockdown the expression of PLK4 reduced the number and the size of colonies compared to the control group.

Knockdown the expression of PLK4 promoted the apoptosis, arrested Cell cycle, while had no effect on the differentiation of OCI-AML3 cells

The blockage of cell apoptosis and cell differentiation were important for the leukemiagenesis of AML. In order to detect effects of knockdown the expression of PLK4 on cell apoptosis and cell differentiation, the cell numbers with Annexin V and 7-AAD double stain, the expression of apoptosis related proteins and the myeloid differentiation maker CD11b was determined by flow cytometry and Western blot. As shown in Figures 8A,B, the proportion of apoptotic cells was significantly higher in the PLK4 knockdown groups than that of the control group. At the same time, knockdown the expression of PLK4 promoted the expression of cleaved Caspase-3 and cleaved PARP (Figure 8C). Similar to the result of Centrinone inhibition, knockdown the expression of PLK4 significantly reduced the expression of cell cycle-related proteins Cyclin A2, Cyclin B1 and CDK1 (Figure 8D), which indicated the cell cycle arrested. No significant cell differentiation changes were observed between the PLK4 knockdown groups and the control group, since the expression of CD 11b in the knockdown groups was almost similar to that of control group as detected by flow cytometry (Figure 8E).

Discussion

In recent years, the impact of centrosome abnormalities on human cancers has been attracting attention (Anderhub et al., 2012; Denu et al., 2016; Levine et al., 2017). Centrosomes played vital roles in accurate chromosome segregation during mitosis, making precisely per copy during each cell division and helping to maintain genomic integrity (Neben et al., 2004). Centrosome abnormalities caused spindle formation and dysfunction, chromosome segregation imbalance, triggering subsequent genomic instability and promoting tumorigenesis (Cosenza

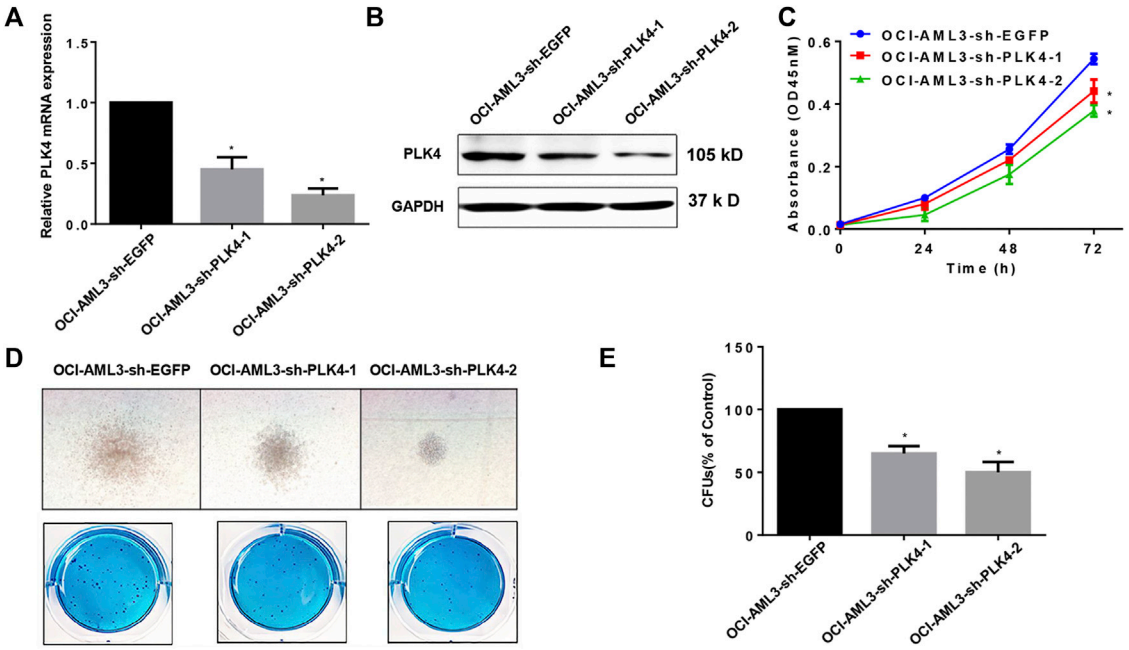


FIGURE 7
Knockdown the expression of PLK4 inhibited the proliferation and the colony formation of OCI-AML3 cells. **(A)** Relative mRNA expression levels of PLK4 in the OCI-AML3 cells after lentivirus medicated transduction, *$p < 0.05$, compared with OCI-AML3-sh-EGFP group. **(B)** Expression of PLK4 in transfected OCI-AML3 cells was detected by Western blot. **(C)** Knockdown the expression of PLK4 inhibited the proliferation of OCI-AML3 cells. *$p < 0.05$, compared with OCI-AML3-sh-EGFP group. **(D)** Knockdown the expression of PLK4 inhibited the size and the numbers of the colony formation. Microscopic observation of cell colony generation size (100×) and the number of colony generations was observed after Giemsa staining. **(E)** Statistical analysis of the number of cell-forming colonies (compared with control, *$p < 0.05$).

et al., 2017). Genetic instability was one of the common features of AML. Neben et al. revealed that centrosomal aberrations as a possible cause of aneuploidy in AML and the proportion of cells carrying abnormal centrosomes was associated with increased cytogenetic risk status and poor prognosis (Neben et al., 2004). PLK4 is a regulator of centrosome replication and plays important roles in centriole replication (Maniswami et al., 2018). PLK4 dysregulation led to abnormal number of centrosomes, mitotic defects, chromosomal instability and consequently tumorigenesis. Therefore, inhibition of PLK4 might be a new strategy for the treatment of many cancers, including AML (Zhao and Wang. 2019). The PLK4 high expression always leads to defective cell mitosis, which triggers tumorigenesis (Bettencourt-Dias et al., 2005; Habedanck et al., 2005). Although roles of PLK4 in solid cancers have been studied, there was a controversy in whether PLK4 as an oncogene or tumor suppressor. Our previous RNA-Seq analysis indicated that PLK4 was high expressed in the AML cells, but roles and mechanisms of PLK4 in the leukemiagenesis of AML were still unclear. So, to inhibit the expression of PLK4 either by the PLK4 inhibitor or lentivirus-mediated knockdown in the AML cell lines would help us to clarify roles and mechanisms of PLK4 in the leukemiagenesis of AML, and thus provide clues in whether PLK4 was a potential target for AML clinical treatment and therapy. In this study, lentivirus-mediated PLK4 interference and PLK4 inhibitor Centrinone was used to investigate roles and mechanisms of PLK4 in the pathology of AML. Our results suggested that knockdown the expression of PLK4 inhibited the cell proliferation, colony formation of AML cell lines, promoted the cell apoptosis, and caused the G2/M phase cell cycle arrest of AML cell lines. These observations herein may provide clues in roles of PLK4 in the leukemiagenesis of AML.

Previous studies indicated that PLK4 was high expressed in several human cancers, including hepatocellular carcinoma, colorectal cancer, gastric cancer, glioblastoma, neuroblastoma, breast cancer, and lung cancer (Zhang et al., 2021), and had a close relationship with the progression of cancers. Due to the vital roles of PLK4 in the regulation of centrosome replication and the pathology of cancers, more and more PLK4 inhibitors were developed, such as Centrinone, Centrinone-B, CFI-400495 and YLT-11 (Mason et al., 2014; Wong et al., 2015; Kawakami et al., 2018b; Denu et al., 2018; Lei et al., 2018; Kerschner-Morales et al., 2020; Zhao et al., 2021; Singh et al., 2022). The already known studies information about above PLK4 inhibitors, such as structures, mainly studied cancer cells and effects of these inhibitors on the biological behaviors have been summarized in Table 1. Since the Centrinone was a selective and reversible

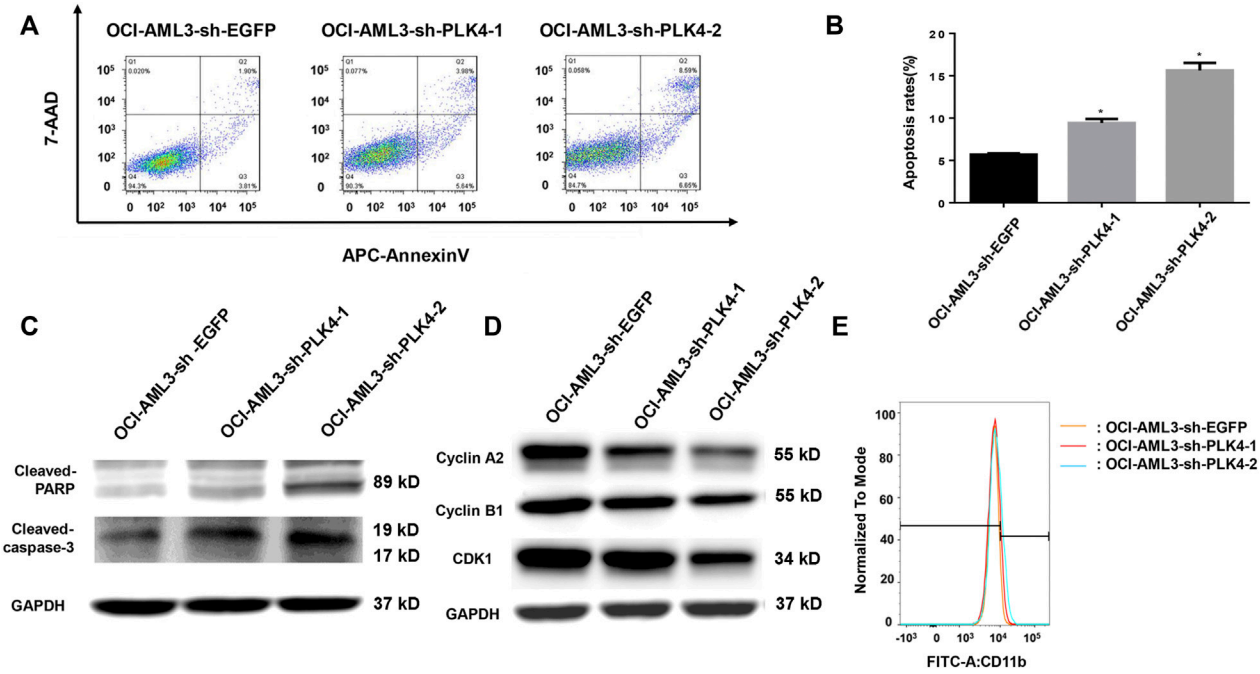
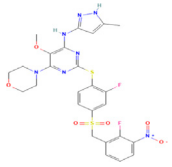
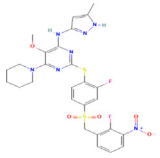
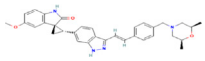
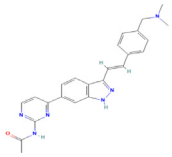


FIGURE 8
Knockdown the expression of PLK4 induced the apoptosis and the cell cycle arrest of OCI-AML3, while had no effect on the differentiation of OCI-AML3 cells. **(A)** The apoptosis of each group was analyzed by flow cytometry with Annexin V/7-AAD double stain. **(B)** Statistical analysis of the apoptosis of PLK4 knockdown OCI-AML3 cells (compared with the control group, $*p < 0.05$). **(C)** The expression of cleaved Caspase-3 and cleaved PARP was detected by Western blot. **(D)** The expression of Cyclin A2, Cyclin B1 and CDK1 was detected by Western blot. **(E)** Effect of PLK4 on the differentiation of OCI-AML3 cells were stained with FITC CD11b and analyzed by flow cytometry.

TABLE 1 The summary of the structure, studied cancer cells and roles of the inhibitors of PLK4.

Inhibitors	Structure	Target	Mainly studied cancer cells	Effects	References
Centrinone		PLK4	Ewing's sarcoma cells; Cervical carcinoma cells	Cell proliferation inhibition; cell cycle arrest; cell apoptosis induction; colony formation inhibition	Kerschner-Morales et al. (2020); Wong et al. (2015)
Centrinone-B		PLK4	Melanoma cells; Prostate cancer cells	Cell proliferation inhibition; cell apoptosis induction; colony formation inhibition	Denu et al. (2018); Singh et al. (2022)
CFI-400495		PLK4	Breast cancer cells; Lung cancer cells; Prostate cancer cells; Diffuse large B-cell lymphoma cells	Cell proliferation inhibition; cell cycle arrest; cell apoptosis induction; colony formation inhibition	Mason et al. (2014); Kawakami et al. (2018a); Singh et al. (2022); Zhao et al. (2021)
YLT-11		PLK4	Breast cancer cells	Cell proliferation inhibition; colony formation inhibition; cell apoptosis induction	Lei et al. (2018)

The structures of inhibitors were taken from database PubChem.

PLK4 inhibitor with the lowest Ki values among all known inhibitors, in this study the Centrinone was used to treat AML cell lines to explore roles and mechanisms of PLK4 in the pathology of AML. Our results suggested that Centrinone inhibited the proliferation of AML cells in a dose- and time-dependent manner. This observation was consistent with previous studies which indicated that PLK4 promoted the progression of cancers (Zhang et al., 2021). Moreover, our study revealed that Centrinone induced the apoptosis of AML cells in a dose-dependent manner. Mechanismly, Centrinone induced the apoptosis of AML cells *via* increased the expression of cleaved Caspase-3 and cleaved PARP. This result implied that Centrinone induced the apoptosis of AML cells by activating the Caspase signaling pathway.

The cell cycle engine is located downstream of the confluence of oncogenic signaling networks and it is an important target for cancer diagnosis and therapy. The cell cycle dysregulation was responsible for the aberrant cell proliferation of cancer cells (Williams and Stoeber. 2012). Previous studies showed that PLK4 was involved in the regulation of the cell cycle and stress response, and its abnormal expression levels were associated with the progression of tumors (Raab et al., 2021). In this study, our results indicated that knockdown or Centrinone inhibited the expression of PLK4 caused AML cells in the G2/M phase cell cycle arrest by decreasing the expression of Cyclin A2, Cyclin B1, and CDK1. This result was consistent with previous studies which suggested that PLK4 was involved in the regulation of the cell cycle and promoted the development of cancers (Raab et al., 2021).

The leukemia stem cell (LSC) was the source of leukemia relapse and the death of AML patients (Knorr and Goldberg. 2020). In this study, effects of PLK4 on the stemness maintenance of LSC were detected by the colony formation assay. Our results suggested that the colony size and the number of colonies were significantly decreased when the expression of PLK4 was downregulated. Thus, our results suggest that downregulation of PLK4 reduces the stemness maintenance of LSC.

All in all, our results suggested that either the Centrinone or the lentivirus-mediated interference the expression of PLK4 inhibited cell proliferation, induced cell apoptosis and suppressed cell colony formation of AML cells. This study provided an experimental basis for PLK4 in the leukemiagenesis of AML. However, our understanding of PLK4 aberrant expression in cancer development is far from adequate, and more research is needed to investigate the novel mechanisms of their involvement in maintaining genomic stability and new strategies for AML targeted therapies.

Data availability statement

The original contributions presented in the study are included in the article/Supplementary Material, further inquiries can be directed to the corresponding authors.

Author contributions

Conceptualization, Q-YW, K-LX, and FL; data curation, X-RM, M-MM, and Z-YL; formal analysis, JL, Y-TX, and JC; methodology, X-RM, M-MM, and Z-YL; supervision, Q-YW, K-LX, and FL; writing- original draft, Q-YW, K-LX, and FL; writing-review and editing, X-RM, M-MM, and Z-YL. All authors have read and agreed to the published version of the manuscript.

Funding

The present investigation was supported by grants from the National Natural Science Foundation of China (82070156 and 81570136), “Outstanding Youth” Talents Foundation of Jiangsu Province (BK20160054), Jiangsu Provincial Medical Youth Talent (QNRC2016777) and Jiangsu Provincial research and development program (BE2020639).

Conflict of interest

The authors declare that the research was conducted in the absence of any commercial or financial relationships that could be construed as a potential conflict of interest.

Publisher’s note

All claims expressed in this article are solely those of the authors and do not necessarily represent those of their affiliated organizations, or those of the publisher, the editors and the reviewers. Any product that may be evaluated in this article, or claim that may be made by its manufacturer, is not guaranteed or endorsed by the publisher.

Supplementary material

The Supplementary Material for this article can be found online at: https://www.frontiersin.org/articles/10.3389/fgene.2022.898474/full#supplementary-material

References

Anderhub, S. J., Krämer, A., and Maier, B. (2012). Centrosome amplification in tumorigenesis. *Cancer Lett.* 322, 8–17. doi:10.1016/j.canlet.2012.02.006

Archambault, V., and Glover, D. M. (2009). Polo-like kinases: Conservation and divergence in their functions and regulation.. *Nat. Rev. Mol. Cell Biol.* 10, 265–275. doi:10.1038/nrm2653

Archambault, V., Lepine, G., and Kachaner, D. (2015). Understanding the polo kinase machine. *Oncogene* 34, 4799–4807. doi:10.1038/onc.2014.451

Bettencourt-Dias, M., Rodrigues-Martins, A., Carpenter, L., Riparbelli, M., Lehmann, L., Gatt, M. K., et al. (2005). SAK/PLK4 is required for centriole duplication and flagella development. *Curr. Biol.* 15, 2199–2207. doi:10.1016/j.cub.2005.11.042

Cosenza, M. R., Cazzola, A., Rossberg, A., Schieber, N. L., Konotop, G., Bausch, E., et al. (2017). Asymmetric centriole numbers at spindle Poles cause chromosome missegregation in cancer. *Cell Rep.* 20, 1906–1920. doi:10.1016/j.celrep.2017.08.005

de Carcer, G., Manning, G., and Malumbres, M. (2011). From Plk1 to Plk5: Functional evolution of polo-like kinases. *Cell Cycle* 10, 2255–2262. doi:10.4161/cc.10.14.16494

Denu, R. A., Shabbir, M., Nihal, M., Singh, C. K., Longley, B. J., Burkard, M. E., et al. (2018). Centriole overduplication is the predominant mechanism leading to centrosome amplification in melanoma. *Mol. Cancer Res.* 16, 517–527. doi:10.1158/1541-7786.Mcr-17-0197

Denu, R. A., Zasadil, L. M., Kanugh, C., Laffin, J., Weaver, B. A., and Burkard, M. E. (2016). Centrosome amplification induces high grade features and is prognostic of worse outcomes in breast cancer. *Bmc Cancer* 16, 47. ARTN 4710. doi:10.1186/s12885-016-2083-x

Habedanck, R., Stierhof, Y. D., Wilkinson, C. J., and Nigg, E. A. (2005). The Polo kinase Plk4 functions in centriole duplication. *Nat. Cell Biol.* 7, 1140–1146. doi:10.1038/ncb1320

Holland, A. J., and Cleveland, D. W. (2014). Polo-like kinase 4 inhibition: A strategy for cancer therapy? *Cancer Cell* 26, 151–153. doi:10.1016/j.ccr.2014.07.017

Holland, A. J., Lan, W., Niessen, S., Hoover, H., and Cleveland, D. W. (2010). Polo-like kinase 4 kinase activity limits centrosome overduplication by autoregulating its own stability. *J. Cell Biol.* 188, 191–198. doi:10.1083/jcb.200911102

Kawakami, M., Mustachio, L. M., Zheng, L., Chen, Y. L., Rodriguez-Canales, J., Mino, B., et al. (2018b). Abstract 1948: Polo-like kinase 4 inhibition produces polyploidy and apoptotic death of lung cancers. *Cancer Res.* 78, 1948. doi:10.1158/1538-7445.Am2018-1948

Kawakami, M., Mustachio, L. M., Zheng, L., Chen, Y., Rodriguez-Canales, J., Mino, B., et al. (2018a). Polo-like kinase 4 inhibition produces polyploidy and apoptotic death of lung cancers. *Proc. Natl. Acad. Sci. U. S. A.* 115, 1913–1918. doi:10.1073/pnas.1719760115

Kayser, S., and Levis, M. J. (2018). Advances in targeted therapy for acute myeloid leukaemia. *Br. J. Haematol.* 180, 484–500. doi:10.1111/bjh.15032

Kerschner-Morales, S. L., Kuhne, M., Becker, S., Beck, J. F., and Sonnemann, J. (2020). Anticancer effects of the PLK4 inhibitors CFI-400945 and centrinone in Ewing's sarcoma cells. *J. Cancer Res. Clin. Oncol.* 146, 2871–2883. doi:10.1007/s00432-020-03346-z

Knorr, K. L. B., and Goldberg, A. D. (2020). Leukemia stem cell gene expression signatures contribute to acute myeloid leukemia risk stratification. *Haematologica* 105, 533–536. doi:10.3324/haematol.2019.241117

Lei, Q., Xiong, L., Xia, Y., Feng, Z. Z., Gao, T. T., Wei, W., et al. (2018). YLT-11, a novel PLK4 inhibitor, inhibits human breast cancer growth via inducing maladjusted centriole duplication and mitotic defect. *Cell Death Dis.* 9, 1066. ARTN. doi:10.1038/s41419-018-1071-2

Leung, G. C., Hudson, J. W., Kozarova, A., Davidson, A., Dennis, J. W., and Sicheri, F. (2002). The Sak polo-box comprises a structural domain sufficient for mitotic subcellular localization. *Nat. Struct. Biol.* 9, 719–724. doi:10.1038/nsb848

Levine, M. S., Bakker, B., Boeckx, B., Moyett, J., Lu, J., Vitre, B., et al. (2017). Centrosome amplification is sufficient to promote spontaneous tumorigenesis in mammals. *Dev. Cell* 40, 313–322. doi:10.1016/j.devcel.2016.12.022

Li, Z., Dai, K., Wang, C., Song, Y., Gu, F., Liu, F., et al. (2016). Expression of polo-like kinase 4(PLK4) in breast cancer and its response to taxane-based neoadjuvant chemotherapy. *J. Cancer* 7, 1125–1132. doi:10.7150/jca.14307

Liu, Z. H., Lei, Q., Wei, W., Xiong, L., Shi, Y. J., Yan, G. Y., et al. (2017). Synthesis and biological evaluation of (E)-4-(3-arylvinyl-1H-indazol-6-yl) pyrimidin-2-amine derivatives as PLK4 inhibitors for the treatment of breast cancer. *RSC Adv.* 7, 27737–27746. doi:10.1039/c7ra02518a

Maniswami, R. R., Prashanth, S., Karanth, A. V., Koushik, S., Govindaraj, H., Mullangi, R., et al. (2018). PLK4: A link between centriole biogenesis and cancer. *Expert Opin. Ther. Targets* 22, 59–73. doi:10.1080/14728222.2018.1410140

Mason, J. M., Lin, D. C. C., Wei, X., Che, Y., Yao, Y., Kiarash, R., et al. (2014). Functional characterization of CFI-400945, a polo-like kinase 4 inhibitor, as a potential anticancer agent. *Cancer Cell* 26, 163–176. doi:10.1016/j.ccr.2014.05.006

Morris, E. J., Kawamura, E., Gillespie, J. A., Balgi, A., Kannan, N., Muller, W. J., et al. (2017). Stat3 regulates centrosome clustering in cancer cells via Stathmin/PLK1. *Nat. Commun.* 8, 15289. ARTN 1528910. doi:10.1038/ncomms15289

Neben, K., Tews, B., Wrobel, G., Hahn, M., Kokocinski, F., Giesecke, C., et al. (2004). Gene expression patterns in acute myeloid leukemia correlate with centrosome aberrations and numerical chromosome changes. *Oncogene* 23, 2379–2384. doi:10.1038/sj.onc.1207401

Raab, C. A., Raab, M., Becker, S., and Strebhardt, K. (2021). Non-mitotic functions of polo-like kinases in cancer cells. *Biochim. Biophys. Acta. Rev. Cancer* 1875, 188467. doi:10.1016/j.bbcan.2020.188467

Shinmura, K., Kurabe, N., Goto, M., Yamada, H., Natsume, H., Konno, H., et al. (2014). PLK4 overexpression and its effect on centrosome regulation and chromosome stability in human gastric cancer. *Mol. Biol. Rep.* 41, 6635–6644. doi:10.1007/s11033-014-3546-2

Siegel, R. L., Miller, K. D., and Jemal, A. (2020). Cancer statistics, 2020. *CA. Cancer J. Clin.* 70, 7–30. doi:10.3322/caac.21590

Sillibourne, J. E., and Bornens, M. (2010). Polo-like kinase 4: The odd one out of the family. *Cell Div.* 5, 25. doi:10.1186/1747-1028-5-25

Singh, C. K., Denu, R. A., Nihal, M., Shabbir, M., Garvey, D. R., Huang, W., et al. (2022). PLK4 is upregulated in prostate cancer and its inhibition reduces centrosome amplification and causes senescence. *Prostate* 82, 957–969. doi:10.1002/pros.24342

Strebhardt, K. (2010). Multifaceted polo-like kinases: Drug targets and antitargets for cancer therapy. *Nat. Rev. Drug Discov.* 9, 643–660. doi:10.1038/nrd3184

Vakiti, A., and Mewawalla, P. (2021). "Acute myeloid leukemia," in *StatPearls* (Treasure Island (FL): StatPearls Publishing Copyright © 2021, StatPearls Publishing LLC.).

Ward, A., Sivakumar, G., Kanjeekal, S., Hamm, C., Labute, B. C., Shum, D., et al. (2015). The deregulated promoter methylation of the Polo-like kinases as a potential biomarker in hematological malignancies. *Leuk. Lymphoma* 56, 2123–2133. doi:10.3109/10428194.2014.971407

Williams, G. H., and Stoeber, K. (2012). The cell cycle and cancer. *J. Pathol.* 226, 352–364. doi:10.1002/path.3022

Wong, Y. L., Anzola, J. V., Davis, R. L., Yoon, M., Motamedi, A., Kroll, A., et al. (2015). Cell biology. Reversible centriole depletion with an inhibitor of Polo-like kinase 4. *Science* 348, 1155–1160. doi:10.1126/science.aaa5111

Zhang, X., Wei, C., Liang, H., and Han, L. (2021). Polo-like kinase 4's critical role in cancer development and strategies for plk4-targeted therapy. *Front. Oncol.* 11, 587554. doi:10.3389/fonc.2021.587554

Zhao, Y., and Wang, X. (2019). PLK4: A promising target for cancer therapy. *J. Cancer Res. Clin. Oncol.* 145, 2413–2422. doi:10.1007/s00432-019-02994-0

Zhao, Y., Yang, J., Liu, J. R., Cai, Y. Q., Han, Y., Hu, S. F., et al. (2021). Inhibition of Polo-like kinase 4 induces mitotic defects and DNA damage in diffuse large B-cell lymphoma. *Cell Death Dis.* 12, 640. ARTN 64010. doi:10.1038/s41419-021-03919-x

frontiers | Frontiers in Genetics

TYPE Review
PUBLISHED 09 September 2022
DOI 10.3389/fgene.2022.886170

Check for updates

OPEN ACCESS

EDITED BY
Alip Ghosh,
University of Maryland, Baltimore,
United States

REVIEWED BY
Giovanna Damia,
Mario Negri Pharmacological Research Institute (IRCCS), Italy
Nicholas Pavlidis,
University of Ioannina, Greece

*CORRESPONDENCE
Clare L. Scott,
scottc@wehi.edu.au

SPECIALTY SECTION
This article was submitted to Cancer Genetics and Oncogenomics, a section of the journal Frontiers in Genetics

RECEIVED 28 February 2022
ACCEPTED 05 August 2022
PUBLISHED 09 September 2022

CITATION
Bound NT, Vandenberg CJ, Kartikasari AER, Plebanski M and Scott CL (2022), Improving PARP inhibitor efficacy in high-grade serous ovarian carcinoma: A focus on the immune system.
Front. Genet. 13:886170.
doi: 10.3389/fgene.2022.886170

COPYRIGHT
© 2022 Bound, Vandenberg, Kartikasari, Plebanski and Scott. This is an open-access article distributed under the terms of the Creative Commons Attribution License (CC BY). The use, distribution or reproduction in other forums is permitted, provided the original author(s) and the copyright owner(s) are credited and that the original publication in this journal is cited, in accordance with accepted academic practice. No use, distribution or reproduction is permitted which does not comply with these terms.

Improving PARP inhibitor efficacy in high-grade serous ovarian carcinoma: A focus on the immune system

Nirashaa T. Bound[1,2], Cassandra J. Vandenberg[1,3], Apriliana E. R. Kartikasari[2], Magdalena Plebanski[2] and Clare L. Scott[1,3,4,5]*

[1]Cancer Biology and Stem Cells, Walter and Eliza Hall Institute of Medical Research, Parkville, VIC, Australia, [2]Cancer Ageing and Vaccines (CAVA), Translational Immunology & Nanotechnology Research Program, School of Health & Biomedical Sciences, RMIT University, Bundoora, VIC, Australia, [3]Department of Medical Biology, University of Melbourne, Parkville, VIC, Australia, [4]Peter MacCallum Cancer Centre, Parkville, VIC, Australia, [5]Royal Women's Hospital, Parkville, VIC, Australia

High-grade serous ovarian carcinoma (HGSOC) is a genomically unstable malignancy responsible for over 70% of all deaths due to ovarian cancer. With roughly 50% of all HGSOC harboring defects in the homologous recombination (HR) DNA repair pathway (e.g., *BRCA1/2* mutations), the introduction of poly ADP-ribose polymerase inhibitors (PARPi) has dramatically improved outcomes for women with HR defective HGSOC. By blocking the repair of single-stranded DNA damage in cancer cells already lacking high-fidelity HR pathways, PARPi causes the accumulation of double-stranded DNA breaks, leading to cell death. Thus, this synthetic lethality results in PARPi selectively targeting cancer cells, resulting in impressive efficacy. Despite this, resistance to PARPi commonly develops through diverse mechanisms, such as the acquisition of secondary *BRCA1/2* mutations. Perhaps less well documented is that PARPi can impact both the tumour microenvironment and the immune response, through upregulation of the stimulator of interferon genes (STING) pathway, upregulation of immune checkpoints such as PD-L1, and by stimulating the production of pro-inflammatory cytokines. Whilst targeted immunotherapies have not yet found their place in the clinic for HGSOC, the evidence above, as well as ongoing studies exploring the synergistic effects of PARPi with immune agents, including immune checkpoint inhibitors, suggests potential for targeting the immune response in HGSOC. Additionally, combining PARPi with epigenetic-modulating drugs may improve PARPi efficacy, by inducing a BRCA-defective phenotype to sensitise resistant cancer cells to PARPi. Finally, invigorating an immune response during PARPi therapy may engage anti-cancer immune responses that potentiate efficacy and mitigate the development of PARPi resistance. Here, we will review the emerging PARPi literature with a focus on PARPi effects on the immune response in HGSOC, as well as the potential of epigenetic combination therapies. We highlight the potential of transforming HGSOC from a lethal to a chronic disease and increasing the likelihood of cure.

KEYWORDS

high-grade serous ovarian carcinoma, poly ADP-ribose polymerase inhibitors, epigenetics, immunotherapy, combination (combined) therapy, clinical trials, checkpoint inhibition, PARPi combinations

1 Introduction

Even with years of research and the development of a new effective therapy, high-grade serous ovarian carcinoma (HGSOC) remains, to this day, one of the most lethal gynaecological malignancies. HGSOC belongs to the type II class of epithelial ovarian cancers (EOC) and mostly develops from fallopian tube secretory cells into aggressive high-grade tumours with early metastatic potential (Pavlidis. et al., 2021). In contrast, type 1 EOC, such as endometrioid OC, is relatively indolent and genetically stable, with a better prognosis, arising from precursors such as endometriosis (McCluggage, 2011). Responsible for over 70% of all ovarian cancer (OC) deaths, only 30% of women affected with HGSOC are expected to survive five years (Dion et al., 2020). Current treatment for HGSOC includes a complete resection of the cancer and platinum/taxane chemotherapy, however, only 30% of women will remain in remission following this, with the remainder undergoing more chemo-resistant relapse occurring within 4–16 months (Agarwal and Kaye, 2003; Cooke and Brenton, 2011; Vaughan et al., 2011; Korkmaz et al., 2016). This high mortality rate is largely due to late-stage diagnosis and disease recurrence (Dion et al., 2020). The intra-tumoral heterogeneity that arises within HGSOC, enables the acquisition of resistance mechanisms to first-line treatments (Milanesio et al., 2020). Thus, there have been efforts to improve the first-line regimen, to introduce additional therapies, particularly in the maintenance setting, to combat recurrence, in order to improve outcomes for women with HGSOC.

Women who have received first-line therapy can be stratified into having platinum-resistant or platinum-sensitive HGSOC/OC (defined as women whose cancer progresses within six months or after six months respectively) (Lee and Matulonis, 2020). However, the fifth Ovarian Cancer Consensus Conference (OCCC) convened by the Gynecologic Cancer Intergroup (GCIG) in Tokyo, Japan in 2015 concurred that, "as time since last platinum chemotherapy represents a continuum of probability of response to further chemotherapy, a fixed 6-month cut-off decision on platinum sensitivity was neither sensible nor biologically relevant" suggesting a greater degree of flexibility should be taken into account when considering a patient's treatment options (Colombo et al., 2019). Upon recurrence, platinum-sensitive OC continues to be treated with a platinum-based chemotherapy regimen, with combination platinum regimens having a better OS when compared with single-agent carboplatin, with a median overall survival (OS) of around 30 months (Lendermann et al., 2003; Lee and Matulonis, 2020; Vanacker et al., 2021). In the ICON7 trial (NCT00262847), the addition of the anti-angiogenic drug, bevacizumab (BV), to the platinum/taxane chemotherapy combination offered a slight extension of progression-free survival (PFS) for these women and of OS in those at high-risk for disease progression (Perren et al., 2011). However, regardless of treatment, most HGSOC patients relapse, with the degree of benefit derived from treatment and duration of remission decreasing with each subsequent line of treatment (Lee and Matulonis, 2020). Women with platinum-resistant OC are treated with non-platinum chemotherapies such as pegylated liposomal doxorubicin (PLD), weekly paclitaxel, gemcitabine, topotecan or oral cyclophosphamide. These non-platinum-containing regimens are comparable in terms of efficacy and typically have poor response rates, as low as 10%–15% with median OS of 12 months (Lheureux et al., 2019a; McMullen et al., 2020). In the AURELIA trial (NCT00976911), the addition of BV, to these second-line and beyond lines of chemotherapy increased the PFS of patients from 3.4 months to 6.7 months, however, there was no significant improvement in OS compared with chemotherapy alone (Pujade-Lauraine et al., 2014; Lee and Matulonis, 2020).

In 2014, the use of poly(ADP-ribose) polymerase inhibitors (PARPi) was approved for the treatment of recurrent, advanced *BRCA1/2*-mutant HGSOC (George et al., 2017). Within four years, phase III clinical trials of PARPi in the relapsed setting (SOLO2/ENGOT-Ov21 (NCT01874353), ARIEL3 (NCT01968213) and NOVA/ENGOT-OV16 (NCT01847274)) demonstrated improved PFS for women with either mutated or wild-type *BRCA1/2* (Tomao et al., 2019; Banerjee and Lord, 2020). This led to the use of PARPi as a maintenance therapy regardless of *BRCA* status in recurrent OC, and subsequent phase III first-line trials (SOLO1 (NCT01844986), PAOLA-1/ENGOT-ov25 (NCT02477644), PRIMA/ENGOT-OV26/GOG-3012 trial (NCT026555016) and VELIA/GOG-3005 (NCT02470585)) led to PARPi's more recent use as a front-line maintenance therapeutic for women with mutant *BRCA1/2* (both germline and somatic) and then in the setting of platinum-responsive or HR defective (HRD) HGSOC (HRD status determined through tests such as the Myriad MyChoice™ test) (Banerjee and Lord, 2020).

This was a major advance, as PARPi was the first targeted treatment approved for women with HGSOC which was dependent on certain genetic mutations being present in the cancer itself. However, the presence of specific HRD gene mutations have been concluded by recent phase III trials to not be essential, rather to predict which women will benefit from experiencing the strongest responses to PARPi therapy and summarised in a meta-analysis of a trial in relapsed OC

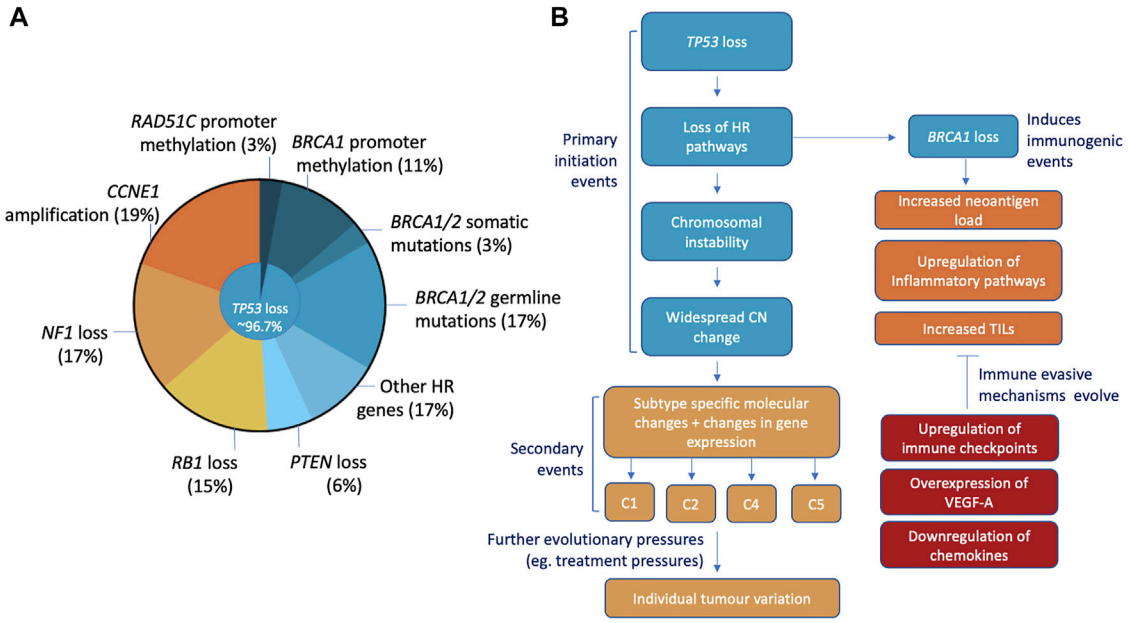


FIGURE 1
Characteristics, initiation, and molecular progression of HGSOC. **(A)** Most common mutations include ubiquitous loss of *TP53* (96.7% of cases), loss of *BRCA1/2* (somatic/germline mutations, promoter methylation), *CCNE1* amplification, *NF1*, *RB1* and *PTEN* mutations. **(B)** The loss of *TP53* is thought to be the initiating event that with subsequent loss of HR pathways stimulates the chromosomal instability and widespread copy number changes seen in HGSOC. This causes changes in gene expression and promotes the development of specific molecular changes that define the 4 HGSOC subtypes (C1, C2, C4, and C5). Loss of HR, specifically *BRCA1,* can elicit immune responses through increased neoantigen loads and upregulation of inflammatory pathways. Additionally, HRD and *BRCA* mutant tumours have been associated with elevated levels of TILs. Common immune evasion mechanisms that HGSOC develop to negate these innate immunogenic traits include the upregulation of immune checkpoints, overexpression of angiogenesis factor VEGF-A and the downregulation of immune-stimulating molecules.

(Coleman et al., 2017; Lee et al., 2019; Ray-Coquard et al., 2019; Matulonis et al., 2021). Treatment with PARPi offers a significant benefit to women, however acquired resistance has driven the requirement for the development of combinatorial therapeutic approaches, as women treated with single agent PARPi may develop recurrence which is resistant to both subsequent PARPi and to chemotherapy (Park et al., 2022). Extensive research has been performed to characterize the effects and mechanisms of action of PARPi. This has better defined which women with HGSOC would derive the most benefit from PARPi, including as single agent therapy, and continues to improve the likelihood that more women who are more likely to need PARPi combination therapy will be identifiable so that they can receive it. Additionally, this characterisation has demonstrated the effects of PARPi beyond its role as a DNA repair inhibitor, such as in inflammation and checkpoint expression, illuminating new pathways for combinatorial therapeutic approaches (Shen et al., 2019). This review summarizes the actionable mechanisms of PARPi in relation to HGSOC, highlighting effects on immune responses and epigenetic modulation, as well as relevant combinatorial clinical trials of PARPi.

2 Genomic and immune characteristics of HGSOC

In order to improve outcomes for PARPi, we must first understand the disease. HGSOC are chromosomally unstable malignancies characterised by widespread genomic structural variation and copy number aberrations (Bowtell et al., 2015; Wang et al., 2017). Aside from mutations in *TP53* and *BRCA1/BRCA2*, driver mutations in other tumour suppressor or oncogenes are less common (Figure 1) (Kurman and Shih, 2016). Instead, structural change through DNA gains and losses are the main mechanisms for the inactivation of tumour suppressor genes (Wang et al., 2017). Pathogenic *TP53* mutations were identified in 96.7% of HGSOC cases and are believed to be an early mutational event essential for pathogenesis (Ahmed et al., 2010; Bowtell, 2010). Roughly 50% of HGSOC have defects in DNA repair and are a result of somatic/germline mutations and/or epigenetic silencing *via* methylation of HR related genes (Bowtell, 2010; Bowtell et al., 2015).

Mutations in *BRCA1/2* account for 10%–18% of hereditary OC cases, with somatic mutations in *BRCA1/2* accounting for another ~4% of cases (Alsop et al., 2012; Cunningham et al., 2014). *BRCA1* and *BRCA2* are essential components of the HR

pathway and are required for the repair of DNA double-stranded breaks (DSB) in DNA (Bowtell, 2010). In normal tissue, loss of BRCA1/2 triggers an apoptotic response involving p53. However, in HGSOC with loss or dysfunction of p53 as an initiating event, *BRCA1/2* loss leads to chromosomal instability and widespread copy number changes (Bowtell, 2010). G (Bowtell, 2010). Apart from *BRCA1/2* mutations, hypermethylation of the *BRCA1* or *RAD51C* gene promoters resulting in gene silencing is the next most common event, occurring in another 14% of cases (11% and 3% of cases respectively) (Network, 2011; Nesic et al., 2018). The remaining HRD HGSOC can be attributed to alterations in the Fanconi Anemia genes and other genes also involved in genome stability and DNA damage repair (*RAD51C, RAD51D, PALB2, ATM, ATR,* and *EMSY*) (Network, 2011). Loss of HR pathways requires tumours to rely on alternative, low fidelity mechanisms to repair DNA damage (Strickland et al., 2016). These error-prone pathways accumulate point mutations and random insertions/deletions resulting in the increase in mutational load, of potential relevance for immune therapies, as well as a distinct mutational signature (Patch et al., 2015; Strickland et al., 2016). This HRD signature has also been observed in carcinomas without known mutations in *BRCA1/2* or other HR genes, so it is possible there are more HRD HGSOC than currently hypothesised (Strickland et al., 2016). This HRD cohort likely contributes to the sensitivity of HGSOC to platinum and other DNA damaging agents, with an improvement of PFS and OS for HRD HGSOC compared to HR proficient cohorts.

Gene expression analysis has allowed the identification and validation of four subtypes of HGSOC: C1 (mesenchymal), C2 (immunoreactive), C4 (differentiated), and C5 (proliferative) (Tothill et al., 2008; Leong et al., 2015). Each subtype has distinct patterns of gene expression and clinical outcomes (Tothill et al., 2008). The C1 subtype displays a mesenchymal gene expression signature, extensive myofibroblast infiltration and poor survival rates (Tothill et al., 2008; Leong et al., 2015). In contrast, the C2 subtype is characterized by the presence of tumour infiltrating lymphocytes (TILs) and a more favourable prognosis (Zhang et al., 2003). Similarly, the presence of TILs has been noted in the C4 differentiated subtype along with a low stromal response and high expression of *MUC16/CA125* and *MUC1* (Tothill et al., 2008; Network, 2011). Thus, compared with C1 and C5 subtypes, C2 and C4 subtypes have a better prognosis, and may benefit from the use of immunotherapies in combination with chemotherapy or other DNA damaging agents such as PARPi (Tothill et al., 2008; Network, 2011). The C5 subtype is driven by the suppression of the *Let7* family of microRNAs, leading to the amplification of stem-cell associated factors *MYCN* and *LIN28B, and the* low expression of differentiation markers including *MUC-16/CA-125* and other immune cell markers (Tothill et al., 2008; Helland et al., 2011; Leong et al., 2015). C1, C2 and C4 HGSOC displayed multiple subtype signatures, with most samples having a dominant signature (Zhang et al., 2014). The C5 subtype did not display a more dominant subtype, attributed to its stem-cell like, de-differentiated state (Zhang et al., 2014; Leong et al., 2015).

HRD positive and *BRCA*-mutant HGSOC have improved prognoses compared with their HR proficient counterparts, especially *BRCA2*-mutant HGSOC (Yang et al., 2011; Bolton et al., 2012; Strickland et al., 2016). This has been attributed to increased platinum sensitivity, however, the increased immunogenicity of these tumours could be an important contributing factor. A robust anti-tumour immune response relies on a cascade of interactions from the presentation of tumour-specific antigens, activation and trafficking of cytotoxic lymphocytes and the recognition and killing of tumour cells (Dunn et al., 2004a; Dunn et al., 2004b; Li et al., 2019). Specifically, the *BRCA1/2* mutant subset of HGSOC are associated with higher neoantigen loads, elevated levels of tumour infiltrating lymphocytes (TILs), and increased expression of immune pathway genes (Strickland et al., 2016).

Different lymphocyte subsets present in the tumour microenvironment (TME) can affect prognosis and tumour progression (Hendry et al., 2017). Most notably for HGSOC, the presence of $CD8^+$ T cells, $CD3^+$ T cells, and $CD20^+$ B cells positively correlates with an improved overall survival (Hwang et al., 2012; Preston et al., 2013; Nelson, 2015; Hendry et al., 2017). Particularly, a higher ratio of $CD8^+$ T cells to $CD4^+$ $CD25^+$ $FOXP3^{+/-}$ regulatory T cells (Tregs) is associated with a better prognosis (Barnett et al., 2010; Preston et al., 2013). The mechanisms that define TIL attraction to these tumours continue to be studied but part could be attributed to the generation of tumour-specific antigens or neoantigens (Patch et al., 2015). Neoantigens are a class of human leukocyte antigen (HLA)-bound peptides that arise from tumour-specific mutations that elicit anti-tumour T-cell responses (Brown et al., 2014; Ott et al., 2017). HR-deficient HGSOC have a significant increase in neoantigen load compared to their HR proficient counterparts, correlating with the elevated level of TILs observed in HR-deficient carcinomas (Patch et al., 2015; Strickland et al., 2016). An additional mechanism of TIL attraction can be attributed to the activation of cyclic GMP-AMP synthase (cGAS) and STING pathways. The chromosomal instability that arises from BRCA1/2 loss in HGSOC lends to an increase in cytosolic DNA (ctDNA) fragments that bind to and stimulate the DNA-sensing cGAS/STING pathways and subsequently activates interferon (IFN) responses (Härtlova et al., 2015; Harding et al., 2017; Heijink et al., 2019; Reisländer et al., 2019). These pathways are an important part of the innate immune response and critical for dendritic cell (DC) activation and subsequent T cell priming against tumour cells (Flood et al., 2019).

A recent study demonstrated that *BRCA1* mutant HGSOC are prone to maintaining an obligatory inflammatory state through the upregulation of cGAS/STING signalling and producing an abundance of ctDNA fragments (Bruand et al.,

2021). The loss of BRCA1 facilitated the enrichment of enhancers and the transcriptional upregulation of key genes in inflammatory pathways, DNA sensing pathways and IFN responses, committing tumour cells to an inflammatory state that promotes TIL recruitment (Bruand et al., 2021). To combat these immune responses, *BRCA1/2* mutant cells commonly downregulated CCL5 which significantly reduced T cell infiltration and attenuated inflammatory responses. This was supported by the prevalence of HGSOC with a methylated CCL5 locus lacking $CD8^+$ TILs (Dangaj et al., 2019). Additionally, deletions of NFKB1 and IFNB1 alongside CCL5 were the most common in HRD HGSOC lacking immune activation and signalling (Bruand et al., 2021). Other immune evasion mechanisms included the upregulation of immune checkpoints such as programmed cell death-1 (PD-1) and the overexpression of vascular endothelial growth factor A (VEGF-A) an inducer of tumour angiogenesis, commonly seen in *BRCA1/2*-mutant HGSOC (Ruscito et al., 2018; Bruand et al., 2021). These evasion mechanisms present potential targets for treatment, as inhibiting these mechanisms may invigorate anti-tumour immune responses for more effective tumour clearance.

3 PARP inhibitor therapy in HGSOC

3.1 The PARP family and PARP inhibitors

PARPs are a family of proteins that are essential for several cellular processes including DNA repair, replication fork stability and genomic stability (Schreiber et al., 2006; Lord and Ashworth, 2017; Forment and O'Connor, 2018). PARP-1 and 2 act as DNA damage sensors, rapidly binding to breaks in DNA strands to hydrolyse NAD^+ and produce linear and branched PAR chains in a process called poly(ADP-ribosyl)ation (PARylation) (Krishnakumar and Kraus, 2010; Rouleau et al., 2010; Murai et al., 2012). PARylation of chromatin proteins recruits DNA repair proteins to sites of damage causing PARP-1/2 to then dissociate from DNA *via* auto-PARylation (El-Khamisy et al., 2003; Schreiber et al., 2006; Murai et al., 2012). The PARylation by PARP is not only important in DNA repair but chromatin modulation, regulation of DNA transcription and replication, protein degradation and cell cycle (Schreiber et al., 2006; Martí et al., 2020).

PARPi bind to the catalytic domains of PARP-1/2 and compete with NAD^+, inhibiting PARylation, effectively disrupting recruitment of DNA repair proteins and PARP dissociation, thereby "trapping" PARP-1/2 on damaged DNA, and further reviewed in (D'Andrea, 2018; Wakefield et al., 2019). The trapping of PARP proteins on DNA stalls replication forks leading them to become dysregulated and collapse (Murai et al., 2012; Wakefield et al., 2019). Active PARP-1 regulates replication fork progression and when inhibited, replication fork stalling leads to a majority of single-stranded breaks (SSBs) being processed into double-stranded breaks (DSBs) (Berti et al., 2013). In healthy cells, these DSBs are repaired by the high-fidelity homologous recombination (HR) DNA repair pathway to successfully repair the damage (Ter Brugge et al., 2016).The HR DNA repair pathway is pivotal in accurate repair of DSBs and restarting stalled/collapsed replication forks, with BRCA1 and BRCA2 being crucial for the protection of replication forks during replication stress (Chen et al., 2018). In HGSOC cells with mutant *BRCA1/2* or other defective HR genes, the inhibition of PARP forces cancer cells to rely on error-prone repair DNA pathways or otherwise unrepaired damage persist into mitosis, leading to the rapid accumulation of mutations, genomic instability, and eventual cell death. The dual loss of the HR pathway and PARP function is synthetically lethal, in that the simultaneous inhibition of the two pathways leads to cell death, whereas loss of only one does not (Ashworth and Lord, 2018). It is within this realm of synthetic lethality that PARPi works best, as seen in the treatment of women with *BRCA*-mutant HGSOC experiencing sustained and profound responses to PARPi, compared with women with HR proficient carcinomas.

3.2 PARPi mechanisms of action

There are currently several PARPi available including olaparib, rucaparib, niraparib, veliparib, pamiparib and talazoparib being tested in phase III trials, with the first three mentioned having both Food and Drug Administration (FDA) and European Medicines Agency (EMA) approval for use in OC in the clinic (Pilié et al., 2019; Lee and Matulonis, 2020). A key feature of all PARPi molecules is a benzamide moiety that binds to the catalytic center of PARP, disrupting enzymatic activity. However, the disruption of catalytic activity alone is not enough to explain the vastly different outcomes in anti-tumour responses and efficacy in the clinic (Sun et al., 2018; Kim et al., 2021). The most effective PARPi trap PARP at sites of DNA damage and this could be due to difference in size and flexibility of each molecule influencing how PARPi bind and effect conformational changes. Allosteric destabilization of a critical helical regulatory domain neighboring the catalytic domain was crucial for cytotoxic and PARP-trapping effects with this being most prominent for rucaparib, niraparib and veliparib compared with olaparib and talazoparib (Zandarashvili et al., 2020). Talazoparib was reported to trap PARP roughly 100-fold more than niraparib, olaparib and rucaparib (Murai et al., 2014). However, the capacity for PARPi trapping does not relate to overall clinical benefit, as talazoparib is also noted for having increased toxicity in the clinic (Murai et al., 2014).

Additionally, another aspect of PARPi to consider is substrate selectivity and specificity. Most PARPi are highly selective toward PARP-1/2 although, computational in-silico analyses have uncovered 58 potential interactions with kinases

of which only 10 were previously known (Thorsell et al., 2017; Antolin et al., 2020). Supporting this is evidence of rucaparib inhibiting the activity of kinases CDK16, PIM3 and DYRK1B in catalytic inhibition assays and additionally niraparib inhibiting the activity of two others, DYRK1A and DYRK1B (Antolin et al., 2020). Additional research in deciphering the specific mechanisms unique to each PARPi may elucidate novel pathways for clinical benefit. Investigation into improving PARPi specificity, tolerability and pharmacokinetic properties continues, with several PARPi in phase I/II clinical trials; including senaparib, which is 20-fold more potent than olaparib, and the highly selective, PARP-1 specific, PARP-1-DNA-trapper, AZD5305 (Cao, 2019; Johannes et al., 2021).

3.3 PARPi as a monotherapy in HGSOC

The PARPi olaparib and niraparib have been approved by both the EMA and FDA for use as maintenance therapy after response to first-line treatment with chemotherapy for women with germline or somatic *BRCA1/2* mutations or platinum-sensitive HGSOC respectively (Veneris et al., 2020). Additionally, olaparib, rucaparib, and niraparib are approved for use as a maintenance treatment for recurrent platinum-sensitive HGSOC patients and in some additional recurrent OC settings.

The phase III SOLO-1 trial evaluated the efficacy of olaparib in women with advanced *BRCA*-mutant platinum-sensitive HGSOC and demonstrated a 67% decrease in risk of disease progression or death (hazard ratio [HR] 0.33; 95% confidence interval [CI]: 0.25–0.43). Strikingly, at 5-year of follow-up, the PFS for the placebo arm was 13.8 months compared with the olaparib arm, on which women had achieved an unprecedented 56.0 months PFS, a 4-fold improvement, and 48% of women on olaparib remained disease free at this time, compared with only 20.5% of women on the placebo arm (Banerjee et al., 2021). Similarly, the phase III PRIMA/ENGOT-OV26/GOG-3012 trial (NCT026555016) examined responses to niraparib in platinum-sensitive advanced HGSOC and high grade endometrioid OC, regardless of *BRCA* mutation and/or HRD status (González-Martín et al., 2019). A significant improvement in PFS on niraparib maintenance was observed in the overall population with a median PFS of 13.8 months compared with 8.2 months for the placebo (HR 0.62, CI 0.50–0.76, $p < 0.001$). Roughly 50% of women were classified as having HGSOC with HRD and the greatest benefit derived from niraparib was seen in the subset of these with *BRCA*-mutations (median PFS 22.1 versus 10.9 months, HR 0.40, CI 0.27–0.62); followed by that observed in the non-*BRCA* HRD HGSOC subset (19.6 versus 8.2 months, HR 0.50, CI 0.31–0.83); lastly the remaining ~50% of women had HGSOC which was HR proficient and responded the least well to PARPi (8.1 versus 5.4 months, HR 0.68, CI 0.49–0.94) (González-Martín et al., 2019). As seen in both clinical trials, response rates in women with HR proficient and platinum-resistant HGSOC were modest in comparison to HRD and platinum-sensitive HGSOC, thus a spectrum to the benefits derived from PARPi was observed. The combination of PARPi with other drugs to induce HRD in HR proficient disease or targeting other pathways that PARP-deficient tumours rely on, may be the answer to improving response further in HGSOC.

3.4 PARPi resistance

Regardless of the efficacy of PARPi as a monotherapy, a growing concern is the development of resistance with the prolonged use of PARPi. There are five main classes of resistance that have been characterised; drug efflux, changes in PAR metabolism, mutational changes of binding sites or target proteins, rewiring of stalled fork replication and restoration of the HR pathways (Wakefield et al., 2019). Several articles have reviewed these mechanisms in detail (Noordermeer and van Attikum, 2019; Wakefield et al., 2019; Kubalanza and Konecny, 2020), however the relevance of the different resistance mechanisms will need to be studied in large clinical cohorts for a better understanding of the selective pressures from PARPi in tumour evolution. The resistance landscape in patients is likely more diverse than what has been observed in research settings to date, thus developing a better understanding of the diversity could better inform therapeutic strategies moving forward. New technologies, including in proteomics (e.g., mass spectrometry and protein array analysis), that allow for the dissection of underlying molecular signaling events, could reveal clinically relevant biomarkers and new therapeutic choices for HGSOC, especially in the setting of the prediction and analysis of acquired PARPi resistance (Ghose et al., 2022). However, with our current knowledge, instigating early treatment with PARPi, rapid retreatment upon relapse and use of PARPi in combination therapies are important tools in maximizing PARPi efficacy. Treating early in the upfront maintenance setting, having first performed molecular analysis during first-line chemotherapy in order to match the HGSOC to appropriate combination PARPi therapy, may yield the most success in the treatment of highly heterogenous HGSOC.

4 PARP inhibitor effects beyond DNA repair

Studies of PARPi initially focused on DNA damage repair and *BRCA1/2* mutations. However, since then, the field of PARPi has expanded to include the roles PARP-1 has in chromatin structure, gene expression, and innate and adaptive immune responses.

4.1 Function of PARP-1 in chromatin remodeling and DNA methylation

In a normal state, DNA is wound around histones and non-histone proteins to form highly compact structures known as chromatin. When access to DNA is required, chromatin structures relax, unravelling bound DNA to allow protein complexes to bind and function, this reorganization of bound DNA is called chromatin remodelling (Sinha et al., 2021). Chromatin remodelling is important for maintaining genomic stability and is important in processes like DNA transcription, replication, and repair. PARP-1 plays an important role in these processes, by regulating chromatin remodelling *via* PARylation of the histones. In its latent state, PARP-1 is found bound to linker DNA and/or histone proteins, resulting in the condensed structure of chromatin called heterochromatin. In this state, no transcription machinery can access the DNA, repressing gene transcription. In the presence of DNA damage however, PARP-1 becomes active (Kim et al., 2004; Muthurajan et al., 2014). Active PARP-1 PARylates itself and histones, promoting the remodelling of chromatin to become euchromatin as the addition of negatively charged PARs on the histones repels DNA. At sites of DNA damage, histone PARylation causes its eviction from DNA strands, facilitating the recruitment of other chromatin remodelers and further loosening of chromatin for subsequent recruitment of DNA repair proteins (Quénet et al., 2009). More specifically, PARP-1 PARylates and then binds to chromatin remodelers at their PAR-binding domain for subsequent alteration of chromatin structures (Andronikou and Rottenberg, 2021). For example, PARylation of the lysine specific demethylase 4D (KDM4D) at its C-terminal promotes demethylation of the methylated forms of H3K9, reducing chromatin compaction, and allowing gene transcription (Khoury-Haddad et al. 2014). However, PARylation of KDM4D at its N-terminal inhibits the action of this enzyme at the promoter of retinoic acid receptor-dependent genes and represses gene transcription (Le May et al., 2012). In this case, the use of PARPi may abolish this specific PARP activity in chromatin remodelling machinery. Particularly, PARPi interferes with the recruitment of KDM4D to double stranded breaks and thus inhibits the repair process (Khoury-Haddad et al. 2014).

There are several natural inhibitors that can counteract PARP-1's involvement in chromatin remodelling machinery, one of them is poly-ADP-ribose glycohydrolase (PARG). PARG counteracts the action of PARP-1 by cleaving the PAR on PARylated PARP-1, rendering it inactive (Kim et al., 2004). Amplified in liver cancer protein 1 (ALC1) is a chromatin remodeler that is rapidly recruited to DNA-damage and binds to PARylated PARP-1 (Pines et al., 2012; Ahel et al., 2009). When ALC1 binds to PARylated PARP-1, it not only activates the protein but secondarily protects PAR on PARP-1 from PARG hydrolysis (Ahel et al., 2009; Gottschalk et al., 2012; Singh et al., 2017). Loss of ALC1, and subsequent loss of PAR protection by ALC1, was found to enhance PARP-1/2 trapping on DNA by PARPi, effectively sensitising cells to PARPi (Blessing et al., 2020; Juhász et al., 2020).

Another natural inhibitor of PARP-1 activity is macroH2A1.1 which binds to autoPARylated PARP-1 to prevent PAR hydrolysis, which can promote chromatin recondensation to interfere with transcriptional processes (Timinszky et al., 2009). MacroH2A1.1 is a splice variant of macroH2A1, which is recruited to DSBs and is implicated in regulating PAR metabolism and NAD + turnover (Ruiz et al., 2019). The alternative splice variant, macroH2A1.2, interacts with other enzymes to recondense chromatin through the production of H3K9 methylation marks (Khurana et al., 2014; Alagoz et al., 2015). These compact chromatin marks attract BRCA1, promoting the use of the HR pathway to repair DNA damage (Lee et al., 2013; Alagoz et al., 2015). Loss of macroH2A1.1 has been noted in several cancers and, due to its roles in chromatin condensation and BRCA1 recruitment, depletion of this histone may increase PARPi sensitivity (Ruiz et al., 2019).

DNA methylation is another major epigenetic modification which occurs at the fifth carbon of cytosine when followed by guanine (CpG) in eukaryotic genomes. The methylated cytosine (5 mC) is induced and maintained by DNA methyltransferase (DNMT). Promoter hypermethylation commonly promotes gene silencing. This epigenetic silencing has been observed in HR genes, including *BRCA1* or *RAD51C*, occurring as an early clonal event, contributing to the development of OC cases (Alsop et al., 2012) *BRCA1* can in fact partially predict BRCAness in OC (Aref-Eshghi et al., 2020). Homozygous methylation (of all copies present) of the *BRCA1* promoter can predict sensitivity to PARPi therapy. On the other hand, heterozygous methylation, (loss of methylation of any copy of the gene present in the cancer), correlates with PARPi resistance (Kondrashova et al., 2018). Similarly, for *RAD51C,* complete gene silencing correlates with PARPi response whilst loss of methylation of even one allele of *RAD51C* drives resistance to PARPi (Nesic et al., 2021).

PARP-1 interaction with DNMT1 contributes to the regulation of DNA methylation. PARylation has been shown to maintain unmethylated CpG at specific sites of the genome, while blockade of PARylation increases DNA methylation levels in the genome (DE CAPOA et al., 1999; Zampieri et al., 2012). Interestingly, the modulation of DNA methylation by PARP-1 can be counteracted by CCCTC-binding factor (CTCF), that can induce the auto-modification of PARP-1 (Guastafierro et al., 2008; Zampieri et al., 2012). Pharmacological inhibition of PARP-1 has been shown to change the genome-wide DNA methylation profile, confirming PARP involvement in DNA methylation processes (Nalabothula et al., 2015). Besides inducing more DNA methylation, PARPi has been shown to induce the expression of enhancer of zeste homolog 2 (EZH2), a histone methyltransferase that catalyses trimethylation of the

lysine residue on histone3 (Martin et al., 2015). This in turns results in a genome-wide increase of H3K27me3 and thus chromatin compaction (Martin et al., 2015). Both increases in DNA methylation and H3K27me3 in the genome result in increased heterochromatin structure and further silencing of various genes.

4.1.1 Exploiting the epigenome with PARPi

In BRCA1/2 defective cancer cells, when the backup DNA repair pathways are disrupted, PARPi can induce synthetic lethality. Thus, inducing the complete loss of DNA repair capability has been strategized to kill BRCA-proficient cancer cells, by combining PARPi with epigenetic drugs that can induce a BRCA defective-like phenotype (DE CAPOA et al., 1999; Caiafa et al., 2009; Abbotts et al., 2019). Combining PARPi with epigenetic drugs can also sensitize PARPi-resistant cancer cells, thus overcoming resistance to treatment (DE CAPOA et al., 1999; Abbotts et al., 2019; Caiafa et al., 2009; Cimmino et al., 2017; Eckschlager et al, 2017). Several epigenetic-targeting drugs have been suggested for use in combination therapy with PARPi for not only BRCA-defective cancers, but also BRCA-proficient cancers, for which therapy choices are more limited (Abbotts et al., 2019; Cimmino et al., 2017; Eckschlager et al, 2017).

Several studies have demonstrated the use of low doses of DNMT inhibitors (DNMTi) in combination with PARPi to target HR pathways in BRCA-proficient triple-negative breast cancer, ovarian cancer, acute myeloid leukemia, and non-small cell lung cancer (Muvarak et al., 2016; Pulliam et al., 2018; Abbotts et al., 2019). DNMTi are cytidine analogs that, following their incorporation into DNA, covalently entrap the methylation maintenance enzyme, DNMT1 (Santi et al., 1984). Several DNMTi are currently in clinical trials, and two of them, decitabine and 5-azacytidine, have been approved for the treatment of myelodysplastic syndrome and acute myeloid leukemia (Hu et al., 2021). PARP-1 is in fact crucial for DNMT1 to function properly by protecting the *DNMT1* promoter from being methylated, and also by non-covalently interacting with DNMT1 to promote its methylating activity (Reale et al., 2005; Caiafa et al., 2009; Zampieri et al., 2009). A combination of PARPi and DNMTi has been shown to promote cytotoxicity, as DNMTi creates a BRCA-defective-like phenotype through repression of HR and nonhomologous end-joining (NHEJ) genes, while PARPi inhibits HR and thus enhances DNMTi functionality (Abbotts et al., 2019). Additionally, Muvarak et al. (2016) shows that a combination of a DNMTi, 5-azacytidine, and PARPi, talazoparib, increased the trapping time of PARP at DNA damage sites from 30 min to up to six hours, preventing PARP from fixing DNA damage for a longer period, providing a potential therapeutic strategy.

A genome-wide RNAi screen by Kharat et al. (2020) associated loss of TET2 with the development of resistance to PARPi. Depletion of TET2 reduces the conversion of DNA methylation mark 5-methylcytosine, to 5-hydroxymethycytosine (5 hmC), the first step in the demethylation process. Subsequently, replication forks in cancer cells fail to degrade and in turn, this promotes resistance to PARPi in cancer cells. When cells were treated chemically to increase 5 hmC abundance, the replications forks were degraded by the recruited base excision repair-associated apurinic/apyrimidinic endonuclease (APE1), independent of BRCA status (Kharat et al., 2020). These findings suggest that exposure to epigenetic drugs that induce TET2 activity or increase 5 hmC abundance may induce PARPi sensitivity. Indeed, Sajadian et al. (2015) showed that the active demethylation by anti-cancer DNMTi, 5-azacytidine, is TET2 dependent, while Cimmino et al. (2017)restored sensitivity of TET2-deficient cancer cells to PARPi by increasing the abundance of 5 hmC using ascorbic acid.

Another type of epigenetic drug that could augment the effect of PARPi is the histone deacetylase inhibitors (HDACi). HDAC removes acetyl groups from the lysine residues of histone tails and has been shown to play various roles in cancer initiation, progression, metastasis and angiogenesis, thus it has emerged as anticancer drug (Eckschlager et al, 2017). Several HDACi have entered clinical trials, and four have been approved by the FDA. These include vorinostat, romidepsin and belinostat for T-cell lymphoma and panobinostat for multiple myeloma (Eckschlager et al, 2017). In prostate cancer, HDAC inhibition by HDACi results in downregulation of HR DNA repair genes by reduction of the recruitment of the activating transcription factor, E2F1 to the promoter of these genes (Kachhap et al., 2010). Several *in vitro* studies show an augmented efficacy of PARPi at targeting HR pathways when combined with HDACi (Adimoolam et al., 2007; Ha et al., 2014; Liu et al., 2015). Here, the HDACi induces a BRCA defective-like phenotype, by depleting the expression and reducing the recruitment of HR proteins thus increasing the sensitivity of the cancer cells towards PARPi (Ha et al., 2014; Liu et al., 2015). Since a monotherapy with HDACi alone has not resulted in an effective treatment, a combination of HDACi with PARPi therapy is now under investigation for OC in the clinic (NCT03924245) (Mackay et al., 2010). The induction of BRCAness by HDACi may allow the combination therapy to effectively treat OC, independent of their BRCA status.

5 Immuno-modulatory effects of PARPi

5.1 Extra-tumoural effects of PARPi in immune cell subsets

With important roles in DNA regulation, PARP-1/2 play a role in T-cell development, differentiation, and function. The development of T-cells is a complex and highly regulated process that begins in the thymus with bone marrow-derived lymphoid precursors and through well-characterized maturation steps give rise to mature T-cells (Koch and Radtke, 2011). PARP-1 modulates activity of nuclear factor of activated T-cells

(NFAT) which drives CD4+ T-cell differentiation (Olabisi et al., 2008; Valdor et al., 2008). A reduction in the expression of NFAT reliant cytokines was observed in PARP-1 deficient T-cells and furthermore PARP-1 deficiency creates a bias for CD4+ T-cell differentiation to a Th1 phenotype (Macian, 2005; Olabisi et al., 2008; Sambucci et al., 2013). The Th1 subset of CD4+ T-cells is associated with the production of cytokines such as IFN- γ, IL-2 and TNF -β that induce inflammation and cell-mediated immune responses (Constant and Bottomly, 1997). The Th2 subset promotes B-cell proliferation and differentiation through IL-4 and IL-5 cytokine production and is associated with humoral-type immune responses (Constant and Bottomly, 1997). There is conflicting data on PARP-1 deficiency driving Th1 differentiation of CD4+ T-cells, with one study in a model of airway inflammation observing olaparib promoting the Th1 phenotype whereas a model of inflammatory arthritis observed PARP inhibition associated with a suppression of Th-1-associated cytokines. Thus, PARP driven Th1 differentiation is likely mediated by other context-specific factors.

During early T-cell development, PARP2 is essential for the development of CD4/CD8 double positive thymocytes and PARP-1 regulates expression of Foxp3 in CD4+ T-cells (Zhang et al., 2013; Luo et al., 2015; Navarro et al., 2017). *In-vitro* studies show that PARP-1 and PARP2 deficient T cells have a decrease in total CD8+ and CD4+ populations (Navarro et al., 2017). This observation was prevalent in singular deficiencies and with the dual loss of both PARP-1 and PARP2, with the dual loss having a more dramatic reduction suggesting a, and there was prevalent amounts of DNA damage detected suggesting the reduction in these T-cell populations are a result of accumulating DNA damage and genomic instability and not entirely a block in maturation (Navarro et al., 2017). In the circumstance of PARP-1 deficiency, populations of CD4+ T-cells expressing Foxp3 increases due to the lack of Foxp3 PARylation for subsequent degradation (Luo et al., 2015). Expression of Foxp3 on CD4+ T-cells causes differentiation into Tregs which are immunosuppressive through their production of inhibitory cytokines, mediation of cytolysis and modulation of DC maturation or function (Vignali et al., 2008; Zhang et al., 2013; Luo et al., 2015). *In vivo* models studying olaparib in BRCA1-deficient ovarian cancer observed significantly increased proportions of CD4+ and CD8+ effector T-cells infiltrating intratumorally and peripherally and, notably, an increase in intra-tumoral CD4/Foxp3+ Tregs was not seen (Ding et al., 2018). Suggesting that treatment with PARPi in an *in vivo* setting does not disrupt T-cell development and function to the extent of tumour benefit. Additionally, olaparib-treated CD8+ T-cells showed reduced expression of immune receptors, such as PD-L1, that are associated with T-cell inhibition and exhaustion and produced higher levels of TNFα and IFNγ (Ding et al., 2018).

The recruitment of DC to the tumour microenvironment is an important step in the anti-tumour immune response as they play roles in activating and inducing the differentiation of T-cells (Patente et al., 2019). There is evidence PARPi has an indirect effect in activating DC though its DNA-damaging abilities and creation of cytosolic DNA fragments. Cytosolic DNA activates the cGAS/STING pathway within the cell but can also be exocytosed to activate STING pathways in neighbouring DC (Mouw et al., 2017; Pantelidou et al., 2019). The activation of cGAS/STING was noted in a PARPi treated BRCA1-deficient mouse model of TNBC, but not in DC treated with PARPi alone (Pantelidou et al., 2019). This suggests that DC cGAS/STING activation is not induced by PARPi alone. This notion was supported in a BRCA1 deficient model of OC, with activation of cGAS/STING observed upon treatment with olaparib (Ding et al., 2018). To confirm the paracrine effect of PARPi on DC activation, PARPi treated ovarian cells were co-cultured with naïve DC. Increased levels of TBK-1, IRF3, CXCL10 and IFNβ were observed, confirming cGAS/STING activation and expression of downstream genes, further supporting the indirect activation of DC upon treatment with PARPi (Ding et al., 2018). Furthermore, treatment with PARPi increased DC populations with increased antigen presentation machinery, specifically upregulated costimulatory CD80 and CD86 and antigen presenting major histocompatibility complex class II (MHC II) (Ding et al., 2018; Pantelidou et al., 2019).

Natural killer (NK) cells are effector lymphocytes utilized in the innate immune response against “non-self” cells and “self” cells undergoing stress in the form of infections or malignant transformations (Vivier et al., 2004). When activated, NK cells either have direct cytotoxic attacks on targets or produce large arrays of cytokines and chemokines to initiate antigen-specific immune responses. Specifically, NK cells can directly interact with cells through TNF-related apoptosis-inducing ligand (TRAIL) and the Fas ligand to induce apoptosis or indirectly through secretion of IFNγ and TNFα (Barrow and Colonna, 2017; Souza-Fonseca-Guimaraes et al., 2019). In tumour cells, TRAIL stimulates PARP-1 activation and subsequently the PARylation of high-mobility group box protein 1 (HMGB1) which results in HMGB1 localisation to the cytoplasm. This localisation from nucleus to cytoplasm promotes an autophagic response and protects the tumour cells from TRAIL mediated apoptosis (Yang et al., 2015). Treatment with PARPi suppressed the PARP-1/HMGB1 pathway and re-sensitized tumour cells to TRAIL induced cell death suggesting PARPi can sensitize tumours to NK-cell mediated apoptosis (Yang et al., 2015). Treatment with PARPi has also been shown to upregulate death receptors Fas and death receptor 5 in several cancer cell lines (Meng et al., 2014). Upregulation of these receptors sensitized cells to TRAIL induced apoptosis. This was further supported by a study observing NK cell killing in prostate cancer cells with and without PARPi treatment independent of BRCA status (Fenerty et al., 2018). They found treating tumour cells with olaparib upregulated death receptor TRAIL-2 and significantly increase tumour cell sensitivity to NK cell killing

in both BRCA-wildtype and BRCA-mutant cells. Additionally, they replicated these results in additional tumour cell lines, including breast, chordoma, non-small cell lung carcinoma (Fenerty et al., 2018). It is important to note that the presence of NK cells has a favourable impact on OS for HGSOC patients and these findings suggest that PARPi can recruit and sensitize tumour cells to NK cells, and that NK cells contribute to PARPi anti-tumour effects (Henriksen et al., 2020).

5.2 Intra-tumoural effects of PARPi on inflammation, the cGAS-STING pathway, and immune checkpoint expression

Tumours with existing DNA repair defects initially stimulate inflammation and T_H1 immune responses, however, maintaining a constant level of DNA damage and subsequent chronic inflammatory responses encourages the infiltration of immune-suppressive cells (Schreiber et al., 2011; Crusz and Balkwill, 2015; Fridman et al., 2017). Chronic inflammation promotes immunosuppression and in cancer this promotes tumour progression. However, studies suggest PARPi has the potential to counteract this and reinvigorate the anti-tumour immune response (Fridman et al., 2017).

Inflammatory responses can be promoted by PARP-1 through its regulation of several transcription factors, cytokines and chemokines (Pazzaglia and Pioli, 2020). Nuclear factor κB (NF-κB) is a transcription factor that is important in the regulation of genes for inflammatory, apoptotic and cell proliferative responses, and for complete NF-κB-dependent gene transcription PARP-1 acetylation is required (Hassa et al., 2005). Additionally, PARP-1 can activate NF-κB through several mechanisms including through the mono-ubiquitination of NF-κB essential modulator (NEMO) for NF-κB nuclear translocation and sustaining toll-like receptor (TLR) induced NF-κB activation (Stilmann et al., 2009; Hinz et al., 2010; Ji et al., 2016). To study whether treatment with PARPi affects inflammatory responses, Alvarado-Cruz et al. (2021) interrogated *BRCA1*-mutant triple negative breast cancer (TNBC) cell lines and tumours samples after treatment with veliparib for three weeks. Upregulation of hallmark inflammatory TNFα pathways were observed after treatment with PARPi specifically in the BRCA1-deficient cells, and the mechanistic basis for this upregulation was through the cGAS/STING pathways. Separately, a study using genetically engineered mouse models (GEMM) of HGSOC investigated the effects of olaparib in *BRCA1* deficient and *BRCA1* wildtype settings. Treatment with olaparib elicited an increase in $CD4^+$ and $CD8^+$ T-cells as well as a pronounced increase in IFNγ and TNFα (Ding et al., 2018). The increase in $CD4^+$ and $CD8^+$ T-cells was also associated with the increased presence of DC with a potent antigen presenting capacity, and a decrease in MDSCs in the tumour, spleen and blood (Ding et al., 2018). These responses seen were restricted to the *BRCA1* deficient GEMM and mechanistically were associated with the stimulation of the STING pathway. It was proposed that PARPi induced DSBs creating cytosolic DNA fragments that are bound by cGAS, activating STING, and subsequently the production of pro-inflammatory cytokines and IFN responses (Pantelidou et al., 2019; Shen et al., 2019). The recent study by Bruand et al.(2021) suggests that *BRCA* mutant cells are intrinsically programmed for the cGAS/STING/IFN signalling seen in HGSOC and that PARPi enhances this signalling by increasing the amount of ctDNA present. This potentially explains why the immune responses observed after treatment with PARPi were isolated to *BRCA1* deficient GEMM models.

Another study interrogated the role of STING in relation to PARPi in both *in vitro* and *in vivo* experiments regardless of *BRCA1/2* status (Shen et al., 2019). Treating OC cells with talazoparib markedly elevated the phosphorylation of two key components along the STING pathway, IRF3 and TBK1. An increase of total IRF3 and TBK1 translocation from the cytoplasm to the nucleus was observed, suggesting functional signaling of STING (Shen et al., 2019). Additionally, CCL5 and CXCL10, which are two major chemokines activated by STING that positively correlate with the presence of $CD8^+$ T-cells, were seen to be upregulated post PARPi treatment. The knockdown of STING, TBK1, IRF3 or cGAS significantly reduced the upregulation of CCL5 and CXCL10 in PARPi treatment in OC cell lines. Further work in mouse models validated these findings showing treatment with PARPi elicited the expression of CCL5 and CXCL10 and induced higher percentages of $CD8^+$ T-cells and PD-L1+ cells infiltrating the TME. Treatment with PARPi had no therapeutic effects in immunodeficient mice but prolonged survival and limited tumour growth in immune competent mice (Shen et al., 2019). Additionally, knockout of STING abolished the anti-tumour effects of PARPi establishing PARPi efficacy is based in an immunogenic response. These results do not correlate with the previous studies mentioned thus further work to determine the role of BRCA-loss in STING and IFN responses in HGSOC is needed, which will hopefully further elucidate mechanisms by which PARPi invigorates immune responses.

Both studies also noted the increased expression of programmed cell death-ligand 1 (PD-L1) in cells when treated with PARPi (Ding et al., 2018; Shen et al., 2019). Programmed death-ligand 1 is the ligand of PD-1, which is an immune receptor expressed on $CD4^+$/CD8+ T-cells and B cells, and mediates the inhibition of T-cell proliferation and IFNγ production (Iwai et al., 2017). The role of PD-1/PD-L1 is to mediate autoimmune responses, however in cancer, the upregulation of immune checkpoints can be used to suppress the anti-tumour immune response. Upregulation of PD-L1 expression can occur through several mechanisms including PD-L1 promotor binding by NF-kB, JAK1/2 activation and IFNγ secretion following type I IFN response (Bellucci et al.,

2015; Chabanon et al., 2019; Cai et al., 2020). All of these effects can be stimulated through the cGAS/STING pathway that is activated upon treatment with PARPi. Shen et al., found treatment with PARPi increased percentages of PD-L1+ cells and explored the effects of combining talazoparib and an anti-PD-L1 antibody. Tumours treated with the combination therapy significantly reduced tumour burden compared to either monotherapy, and had the most significant increase in $CD8^+$ cell recruitment (Shen et al., 2019). Additionally Jiao et al. (2017) demonstrated that PARPi induced PD-L1 expression regardless of BRCA-status, and effectively reduced the efficacy of active cytotoxic T-cells. Combination of olaparib and an anti-PD-L1 antibody desensitised PARPi treated cells and found the combination more effective than either agent alone (Jiao et al., 2017). Due to the encouraging results of PARPi and checkpoint inhibitor combinations in research, this combination is being explored in several clinical trials.

5.2.1 Combining PARPi with immune checkpoint inhibitors

Currently, the most promising immunotherapy for HGSOC are immune checkpoint inhibitors (ICI), which are monoclonal antibodies that disrupt signalling that would promote effector T-cell deactivation. Most common ICI for HGSOC are antibodies that target PD-1 and Cytotoxic T-Lymphocyte Antigen 4 (CTLA-4), as a monotherapy they have had some efficacy in patients but few durable responses (Cortez et al., 2018; Färkkilä et al., 2020). The phase II KEYNOTE-100 clinical trial of pembrolizumab (an anti-PD-1) as a monotherapy in EOC had an objective response rate (ORR) of only 8% and median progression free survival (PFS) of 2.1 months (Matulonis et al., 2018). Similarly, results from the clinical trial JAVELIN in recurrent OC with avelumab (anti-PD-L1) yielded an ORR of 9.6% and median PFS of 2.6 months (Disis et al., 2019). This could be, in part, due to the low expression of PD-L1 on tumour cells or the highly immunosuppressive TME that develops during a prolonged immune response (Gashi, 2022). Offering ICI early in the treatment of EOC could improve poor responses rates by treating before an immunosuppressive TME develops, potentially delaying the development of immune evasion. Alternatively, the combination of ICI therapy with other therapeutics such as PARPi could mitigate issues of timing of delivery, by driving immunogenicity and reviving immune responses through accumulative DNA damage and tumour specific mutations.

In the phase I/II clinical trial TOPACIO/KEYNOTE-162 (NCT02657889) investigating the combination of niraparib/pembrolizumab (anti-PD-1) in recurrent OC and TNBC, an ORR of 25% was achieved in the general cohort which was an improvement compared to response rates of PARPi or IC as a monotherapy (Konstantinopoulos et al., 2018; Konstantinopoulos et al., 2019). Additionally, the study highlighted the importance of using predictive biomarkers to identify patients who will benefit most from this combination therapy and found that tumours with a mutational signature 3 (HRD signature) and a positive immune-score for exhausted $CD8^+$ T cells were associated with an improved response (Färkkilä et al., 2020). The phase II MEDIOLA (NCT02734004) trial evaluating the combination of olaparib/durvalumab in recurrent platinum-sensitive EOC observed a median PFS of 11.1 months (95% CI: 8.2, 15.9) and ORR of 71.9% (95% CI: 53.25%, 86.25%) with a partial response (PR) rate of 53% (17/32) and complete response (CR) rate of 21.8% (7/32). To date, the median overall survival (OS) for all patients has not been reached, with 87% of patients alive at 24 months (Drew et al., 2019). The combination treatment was well tolerated with the most common adverse events (AE) being anaemia (17.6%), elevated lipase (11.8%), neutropenia (8.8%) and lymphopenia (8.8%), and only eight out of 32 patients discontinuing olaparib or durvalumab due to an AE. Currently there are several clinical trials ongoing, looking at PARPi and ICI in the frontline maintenance setting and the results should further define the benefits to be derived from this combination (Table 1). However, the response rates from available clinical trial data in platinum-sensitive HGSOC look promising and exploring the potential of ICI in other combinations may also be beneficial. There are other clinical trials investigating triple combinations of PARPi and ICI with other drugs commonly used in the treatment of HGSOC with varying success and these will be discussed below.

5.2.2 Anti-angiogenics and PARPi

Bevacizumab (BV) is an anti-VEGFR antibody already in use for the treatment of HGSOC in combination with standard chemotherapies. It targets the cytokine VEGF-A which is secreted by tumour cells and binds to VEGFR-1 and VEGFR-2 receptors, promoting angiogenesis (the formation of blood vessels that allow for tumour growth) and metastasis. VEGF-A has been shown to be overexpressed in *BRCA1* mutant HGSOC and its inhibition increases hypoxia and subsequent downregulation of HR genes (specifically *BRCA1/2* and *RAD51C*) as a result (Bindra et al., 2004; Bindra et al., 2005; Ruscito et al., 2018; Bruand et al., 2021). This decrease in DNA-repair potential could sensitise tumours to PARPi, thus providing a rationale for combining PARPi plus BV therapy in clinical trials. Inhibition of VEGF has also been shown to reduce MDSC, Treg and TAM populations and increase T-cell activation and priming, enhance DC antigen presentation and encourage TIL presence (Goel et al., 2011; Hegde et al., 2018). It has been studied in combination with both olaparib and niraparib in phase I studies, with both showing tolerability without dose-limiting toxicities (Dean et al., 2012). The phase II clinical trial NSGO-AVANOVA2/ENGOT-ov24 studied BV and niraparib compared to niraparib monotherapy in platinum-sensitive recurrent HGSOC or endometrioid ovarian cancer. The combined treatment of BV and niraparib significantly improved patient outcomes compared to niraparib alone with

TABLE 1 Clinical trials combining PARP inhibitors with chemotherapy or with therapeutics with relevance for the immune system. This includes immune checkpoint inhibitors and/or angiogenesis agents in order to attempt to elicit more robust and durable responses.

Study and Phase	Drugs	Cohort	Outcomes	Side effects
TOPACIO/KEYNOTE-162 Phase I/II (NCT02657889)	Niraparib + Pembrolizumab	Recurrent platinum-resistant HGSOC	ORR 18%; DCR 68%; overall ORR 45%; DCR 73% in *BRCAmut* pts	Common grade ≥ 3 AEs; anemia (19%) and thrombocytopenia (9%)
MEDIOLA Phase II (NCT02734004)	Olaparib + Durvalumab	Recurrent platinum-sensitive EOC	28-wk DCR 65.6%; ORR 71.9%; mPFS 11.1 mos; mOS for all pts not yet reached	Common ≥ Grade 3 AEs; anaemia (17.6%), elevated lipase (11.8%), neutropenia (8.8%), and lymphopenia (8.8%).
Phase I/II (NCT02571725)	Olaparib + Tremelimumab	Recurrent *BRCA* mutant OC	Awaiting results	N/A
Phase I/II (NCT02953457)	Olaparib + Durvalumab + Tremelimumab	Recurrent platinum-sensitive/resistant/refractory EOC, Fallopian Tube, or Primary Peritoneal Cancer	Awaiting results	N/A
NSGO-AVANOVA2/ENGOT-ov24 Phase II	Niraparib + Bevacizumab	HGSOC or endometrioid platinum-sensitive recurrent OC	mPFS 11.9 mos; mPFS 14.4 mos in *BRCAmut* pts; mPFS 11.9 mos in HRD pts; mPFS 11.3 mos in non-*BRCAmut* pts;	Common ≥ Grade 3 AEs; anaemia (15%), thrombocytopenia (10%) and hypertension (21%)
PAOLA-1/ENGOT-ov25 Phase III (NCT02477644)	Olaparib + Bevacizumab	Recurrent HGSOC	mPFS 36.5 mos; mPFS 50.3 mos in HRD positive pts; mPFS 24.4 mos in HRD negative pts; mPFS 34.0 mos in HRD unknown pts	Common Grade ≥3 AEs; hypertension (19%) and anaemia (17%). Five treatment emergent AEs of death (olaparib, $n = 1$; placebo, $n = 4$)
MITO25 Phase II (NCT03462212)	Rucaparib + Bevacizumab	HRD and HR HGSOC	Ongoing and awaiting results	N/A
Phase II trial	Olaparib + Cediranib	Recurrent platinum-sensitive, HGSOC or endometrioid OC	mPFS 16.5 mos; overall No significance in OS; mPFS 16.4 vs. 16.5 mos (control arm) in *BRCAmut* pts; mPFS 23.7 vs. 5.7mos (control arm) in *BRCA*-wildtype pts	Grade 3 and 4 AEs; fatigue (12 pts), diarrhoea (10 pts), and hypertension (18 pts)
NRG- GY004 phase III trial (NCT02446600)	Olaparib + Cediranib vs. Olaparib vs. Chemo	Recurrent platinum-sensitive HGSOC or high-grade endometrioid ovarian, primary peritoneal, or fallopian tube cancers.	mPFS 13.7 mos in HR-deficient pts; mPFS 8.3 mos in HR proficient pts; mPFS 20.4 vs. 12.3 vs. 13.1 mos (combo vs. chemo vs. PARPi) in HR-deficient pts	N/A
Single arm trial EVOLVE Phase II	Olaparib + Cediranib	PARPi-resistant HGSOC	16-week PFS rates 55% (platinum-sensitive after PARPi), 50% (platinum-resistant after PARPi), and 39% (exploratory cohort)	Grade 3 toxicities; diarrhea (12%) and anemia (9%)
ICON9 Phase III (NCT03278717)	Olaparib + Cediranib	Recurrent platinum-sensitive OC	Ongoing	N/A
COCOS Phase II/III (NCT02502266)	Olaparib + Cediranib	Recurrent Platinum-Resistant or -Refractory Ovarian, Fallopian Tube, or Primary Peritoneal Cancer	Ongoing	N/A
Phase II open-label study (NCT03574779)	Niraparib + Dostarlimab + Bevacizumab	Recurrent platinum-resistant EOC	mPFS 7.6 mos; DCR 76.9%	Common grade ≥3 TEAEs; hypertension (22.0%), fatigue (17.1%), and anemia (17.1%). Common serious TEAEs; thrombocytopenia (7.3%), anemia (4.9%), and hypertension (4.9%).
MEDIOLA Phase II (NCT02734004)	Olaparib + Durvalumab + Bevacizumab	Recurrent platinum-sensitive non-germline *BRCA* mutant OC	24-week DCR 77.4%; ORR 77.4%; mPFS 14.7	Common grade ≥ 3 AEs in O + D; anaemia, lipase increased and neutropenia and anaemia, hypertension, fatigue, lipase increased, and neutropenia
Phase I trial (NCT00516724)	Olaparib + Carboplatin +/or paclitaxel	Advanced solid tumours refractory to standard treatments	Increased hematologic toxicities, made establishing a dosing regimen difficult	Grade 1/2 DLTs; thrombocytopenia and neutropenia. Non-hematologic grade 1/2 AEs; fatigue (70%), nausea (40%), neutropenia (51%) , thrombocytopenia (25%)

(Continued on following page)

TABLE 1 (*Continued*) Clinical trials combining PARP inhibitors with chemotherapy or with therapeutics with relevance for the immune system. This includes immune checkpoint inhibitors and/or angiogenesis agents in order to attempt to elicit more robust and durable responses.

Study and Phase	Drugs	Cohort	Outcomes	Side effects
VELIA/GOG-3005 Phase III	Veliparib + carboplatin-paclitaxel	Newly diagnosed HGSOC	mPFS 29.3 mos vs. 19.2 mos (veliparib combo vs. placebo)	Nausea and fatigue common in overall cohort. Veliparib combo had higher incidence of anemia and thrombocytopenia
Phase II clinical trial (NCT01306032)	Veliparib + Oral cyclophosphamide	Recurrent *BRCA*-mutant OC	mPFS 2.3 mos vs. 2.1 mos (combo vs. cyclophosphamide alone)	Common grade 2/3 AEs; leucopenia and lymphopenia
Phase II clinical trial (NCT02853318)	Pembrolizumab + Bevacizumab + Oral cyclophosphamide	Recurrent OC	ORR 47.5%; mPFS 10 mos	Common AEs fatigue; [18 (45.0%)], diarrhea [13 (32.5%)], and hypertension [11 (27.5%)].

ORR, overall respone rate; DCR, disease control rate; *BRCA*mut, *BRCA*mutant; mos, months; pts, patients; mPFS, median progression free survival; mOS, median overall survival; AEs, adverse events; TEAEs, treatment emergent adverse events; N/A, not available; HRD, homologous repair deficient; HGSOC, high grade serous ovarian carcinoma; EOC, epithelial ovarian cancer; OC, ovarian cancer; PARPi, PARP inhibitor

a median PFS of 11.9 versus 5.5 months (HR: 0.35, CI 0.21–0.57, $p < 0.001$) (Mirza et al., 2019). The *BRCA*-mutant patient cohort derived the most benefit with a PFS of 14.4 versus 9.0 months, (HR 0.49, CI 0.21–1.15), followed by the HR-deficient subgroup with a PFS of 11.9 vs. 4.1 months (HR 0.19, CI 0.06–0.59 and then the non-*BRCA*-mutant patients with a PFS of 11.3 versus 4.2 months (HR 0.32, CI 0.17–0.58) (Mirza et al., 2019). Overall, patients on the combination of BV and PARPi did significantly better regardless of HR-status.

In phase III PAOLA-1 clinical trial (ENGOT OV25, NCT02477644), the olaparib and BV combination was studied in a maintenance setting after first-line chemotherapy in HGSOC patients. In the overall cohort, the combination of BV and olaparib resulted in a median PFS of 36.5 months compared to the 32.6 months in the placebo and BV combination [HR 0.78, CI (0.64–0.95), $p = 0.0125$]. The biggest benefit gained was in the *BRCA*-mutant cohort where the median PFS has not been reached versus 45 months for placebo and BV (HR 0.53, CI 0.34–0.83). The next best group to benefit was the HRD cohort at 50.3 versus 35.3 months for placebo (HR 0.56, CI 0.41–0.77) comparatively the HRD negative cohort performed the worst at 24.4 vs. 26.4 months (HR 1.04, CI 0.77–1.42) (Martín et al., 2020). The combination of PARPi and BV offers a benefit in extending PFS, especially in *BRCA*-mutant and HRD HGSOC, however the magnitude of clinical benefit in HR proficient cohorts is less clear. The phase II MITO25 study (NCT03462212) investigating rucaparib and BV in a maintenance setting in HRD and HR proficient newly diagnosed HGSOC and endometrioid patients is currently recruiting and results may confirm the benefit of this combination in the HR proficient setting.

The pan-VEGFR and PDGFR tyrosine kinase inhibitor Cediranib is another antiangiogenic agent being investigated with PARPi. In a phase II trial with olaparib and cediranib in relapsed platinum-sensitive HGSOC or endometrioid ovarian cancer, a PFS advantage was observed in the combination arm with a median PFS of 16.5 months compared to the olaparib only arm with 8.2 months (HR 0.50, CI 0.30–0.83, $p = 0.006$) (Liu et al., 2014; Liu et al., 2019). The overall cohort did not show a significant OS difference between treatment arms (44.2 versus 33.3 months, HR 0.64, CI 0.36–1.11, $p = 0.11$), and similarly the *BRCA*-mutant cohort did not have a significant difference in PFS (16.4 versus 16.5 months, HR 0.76, CI 0.38–1.49, $p = 0.42$) or OS (44.2 versus 40.1 months, HR 0.86, CI 0.41–1.82, $p = 0.70$) between combination and olaparib only arms. Comparatively, women in the *BRCA*-wildtype cohort had a significant improvement in the combination arm versus the olaparib only with PFS at 23.7 versus 5.7 months (HR.0.31, CI 0.15–0.66, $p = 0.0013$). The OS for this cohort was also significantly improved at 37.8 versus 23.0 months (HR 0.44, CI 0.19–1.01, $p = 0.047$) (Liu et al., 2014; Liu et al., 2019). This phase II trial suggested that women with *BRCA*-wildtype HGSOC derived the most benefit from this regimen.

However, this combination was also studied in the randomised NRG-GY004 phase III trial (NCT02446600) comparing patients with platinum sensitive recurrent high-grade serous or high-grade endometrioid ovarian, primary peritoneal, or fallopian tube cancers. Patients were screened for HR and LOH status with the BROCA-HR targeted next generation sequencing assay on germline and tumour DNA in 491 of 565 patients and compared across treatment arms of olaparib only, chemotherapy only and combination cediranib and olaparib. The HR-deficient cohort did the best compared to the HR proficient cohort, with a median PFS of 13.7 vs. 8.3 months (HR 0.41, $p < 0.0001$). When compared across treatment arms the cediranib and olaparib combination extended PFS to 20.4 months (HR 0.55, 95% CI 0.32–0.95) compared to 12.3 months in the chemotherapy arm and 13.1 months in olaparib only arm (HR 0.78, 95% CI 0.48–1.27). There was no difference between treatments in the HR proficient cohort, with a median PFS of 8.5 months in the cediranib and olaparib combination arm (HR 0.93 m, CI 0.68–1.27), and 9.0 months in the chemotherapy arm and

6.4 months in the olaparib only arm (HR 1.56, CI 1.15–2.12). This study also looked at LOH as a prognostic factor and found it was not predictive of response to olaparib, combination cediranib/olaparib or chemotherapy possibly suggesting that the HRD assay used was not sufficiently discriminatory (Swisher et al., 2021).

The phase II single arm trial EVOLVE interrogated PARPi-resistant HGSOC patients with a combination of cediranib and olaparib to identify objective response rates in PARPi-sensitive (PS), PARPi resistant (PR) and in patients who had chemotherapy post-PARPi progression (PE). A total of 34 patients were enrolled, with 9/11 PS, 8/10 PR and 7/13 PE patients with *BRCA1/2* mutations. Additionally, out of the 34 patients, four had a partial response to treatment and 18 patients were noted with stable disease. Of the cohorts 54.5% of PS patients (31.8–93.6), 50% of PR patients (26.9–92.9) and 36% of PE patients (15.6–82.8) reached the 16-weeks PFS with OS at 1 year 81.8% (61.9–100) in PS, 64.8% (39.3–100) in PR and 39.1% (14.7–100) in PE (Lheureux et al., 2019b). This study establishes that using patient response to PARPi could determine patient response to cediranib and PARPi combinations and suggests that this combination could have potential in PARPi-resistant disease.

Overall, the results from these clinical trials establish that there may be an OS benefit to be gained from the combination of cediranib and PARPi in the treatment of HGSOC, however results are inconclusive and are being investigated further in the phase III ICON9 trial assessing cediranib and olaparib vs. olaparib alone as a maintenance therapy in platinum sensitive recurrent OC currently enrolling and the phase II/III GY005 platinum-resistant relapsed OC cediranib PARPi combination therapy clinical trial (NCT02502266) (Lee, 2018; Elyashiv et al., 2021).

The triple combination of PARPi, bevacizumab and anti-PD-L1 therapy has also been trialed in the clinic. The phase II open-label study (NCT03574779) of dostarlimab, BV and niraparib in platinum-resistant recurrent EOC resulted in a median PFS of 7.6 months, disease control rate (DCR) of 76.9% with 23 patients with stable disease, seven patients with PRs and no CRs (Liu et al., 2021). The clinical side effects were tolerable however 34.1% of patients discontinued one of the three drugs due to adverse events. Other trials ongoing include the phase II DUO-O study investigating durvalumab, olaparib and BV after treatment with carboplatin, paclitaxel and BV (AGO-OVAR23/ENGOT-OV46, NCT3737643) and the phase II study combining nivolumab, rucaparib and BV in recurrent ovarian cancer. The MEDIOLA study also compared treatment of olaparib and durvalumab (O + D) to O + D and BV (O + D + BV). The O + D + BV cohort had better a ORR at 77% (95% CI 58.9%–90.4%) compared to 31.3% (95% CI 16.1%–50.0%) in the O + D cohort. This was reflected in the PFS with the triple combination eliciting a PFS of 14.7 months compared to 5.5 months. Both treatments were tolerable however the triplet combination had a higher rate of patients discontinuing treatment, 17% versus 6% in the O + D cohort (Drew et al., 2020). The triplet therapy of PARPi, bevacizumab and CI seems to elicit more durable responses compared to PARPi and CI alone, however the tolerability of this treatment long term is unclear.

5.2.3 PARPi and chemotherapy

In recent years, studies have demonstrated platinum compounds can act as immune modulators effectively inducing immunogenic cell death alongside their DNA-damaging characteristics (de Biasi et al., 2014; Rébé et al., 2020). Platinum chemotherapies were primarily known as DNA-damaging agents that HR-deficient tumours readily respond to as they interfere with DNA transcription and replication. This leads to DNA damage and subsequent activation of DNA repair pathways which in HR-deficient cells, induces cell death (Martin et al., 2008). However, there is variation between platinum agents in their ability to augment immune responses, some can promote anti-tumour immune responses through the recruitment of effector cells, upregulation of MHC molecules and downregulation of immunosuppressive factors (de Biasi et al., 2014). The use of PARPi in combination with platinum chemotherapy has the potential to sensitise tumour cells to DNA-damaging agents and potentially the anti-tumour immune response (Nguewa et al., 2006; Cheng et al., 2013). However, PARPi effects on DNA repair enhances chemotherapy-induced myelosuppression, creating a major concern in patient tolerability to this combination therapy (Dent et al., 2013). The overlapping toxicities affect dosing and scheduling, resulting in attenuated doses of either or both PARPi and platinum therapeutics, potentially affecting the efficacy of either drug, due to the use of concentrations below the recommended monotherapy dose. The recent development of PARP-1-specific PARPi may provide new opportunities (Johannes et al., 2021).

A phase I study (NCT00516724) trialled olaparib with paclitaxel or carboplatin or carboplatin or the paclitaxel (CP) combination in advanced solid tumours refractory to standard treatments (van der Noll et al., 2020a). Patients treated with daily olaparib continuously in combination with CP experienced hematologic toxicities resulting in the attenuated scheduling (van der Noll et al., 2020a). Patients receiving intermittent olaparib increased tolerability but still experienced significant myelosuppression (van der Noll et al., 2020b). However, results from this trial did identify two olaparib treatment schedules that were tolerable in patients. Further interrogation of the olaparib and CP combination in study 41(NCT01081951) in platinum sensitive recurrent ovarian cancer achieved a significant improvement in PFS in the combination arm compared to chemotherapy alone (12.2 versus 9.6 months; HR 0.51, CI 0.34–0.77, $p = 0.0012$). The combination was well tolerated with only 15% reporting adverse events in the combinational group versus the 21% in the chemotherapy group alone. Most benefit was assumed derived from the maintenance phase of olaparib and specifically in the

BRCA1/2 mutant cohort. Regardless, the ORR was 64% versus 58% between the different treatment arms.

Veliparib is a relatively weaker PARP trapper therefore potentially better tolerated for combination studies. Veliparib has been trialed with the standard carboplatin and paclitaxel (CP) chemotherapy combination in the phase III VELIA study in women with newly diagnosed HGSOC (Coleman et al., 2019; Aghajanian et al., 2021). Patients were to receive 6 cycles of CP following primary cytoreduction or with an interval cytoreduction. Veliparib or placebo was administered during CP at an attenuated dose of 150 mg twice daily and subsequently a full dose at 400 mg twice daily after CP treatment. Of the 1,140 patients enrolled, 26% were *BRCA*-mutant and 55% noted as HRD. Overall, the addition of Veliparib significantly improved PFS with median PFS of 23.5 months vs. 17.3 (HR 0.68%, 95% CI [0.56,0.83], $p < 0.001$] for Veliparib vs. placebo. The greatest PFS benefit was seen in *BRCA*-mutant and HRD cohorts at 34.7 months vs. 22.0 months (HR 0.44, 95% CI [0.28,0.68], $p > 0.001$) and 31.9 months vs. 20.5 months (HR 0.57, 95% CI [0.43,0.76], $p > 0.001$) respectively. Veliparib has currently not been approved for use in the treatment of OC.

Another chemotherapy agent that has been generating interest is low-dose cyclophosphamide (LDCy), it is a potent immunostimulant when delivered at low doses and is well tolerated, eliciting clinically beneficial responses in roughly 44% of recurrent OC cases (Handolias et al., 2016). Studies have shown that LDCy promotes anti-tumour immunity through the selective depletion of Tregs and enhancing the function of effector T cells (Handolias et al., 2016; Madondo et al., 2016). A phase II clinical trial (NCT01306032) explored the combination of veliparib and cyclophosphamide in recurrent *BRCA*-mutant OC and HGSOC (Kummar et al., 2015). The addition of the low dose or 60 mg of veliparib to 50 mg of LDCy had no improvement in ORR or median PFS compared to LDCy monotherapy. Stratifying patients according to BRCA status and DNA repair defects also did not predict response to either monotherapy or combination. But, two patients from this trial had a prolonged clinical benefit from the combination treatment, receiving over two years of treatment, which was still ongoing at the time of data analysis (Kummar et al., 2015). This trial encompassed not only HGSOC but primary peritoneal, fallopian tube or *BRCA*-mutant OC which could have affected the ability to decipher characteristics that determine patient responses. Additionally, the doses of veliparib used were below the standard 250–400 mg, thus higher doses of veliparib may yield more significant results or alternatively the addition of a third drug could potentially boost responses. Although their correlative studies could not identify characteristics that determine patient prognosis to treatment further studies could possibly interrogate features of patients that respond to this combination to broaden treatment cohorts.

The NCT02853318 phase II clinical trial observed the effects of pembrolizumab (anti-PD1), bevacizumab and LDCy in recurrent OC (Zsiros et al., 2021). The triple combination had an ORR of 47.5% and a median PFS of 10 months, with 100% of platinum-sensitive patients meeting the 6-month PFS rate compared to only 59% of the platinum-resistant patients ($p = 0.024$). Combining LDCy with PARPi and CI could elicit similar responses, targeting cancer cells and invigorating immune responses, particularly in platinum-sensitive/HRD patients that derive the most benefit from these drugs.

The combination of olaparib and LDCy has been examined in recurrent OC and triple negative breast cancer to determine its safety and tolerability (Lee et al. Br J Cancer). A tolerable regimen was identified and in HGSOC and the *gBRCAm* subset, the unconfirmed objective RR was 48% and 64% respectively.

6 Conclusion

The treatment of HGSOC provides an ongoing challenge, due to the heterogenous and metastatic nature of this disease rendering women susceptible to disease relapse. Extensive research performed to characterise the disease has led to a better understanding of which characteristics correlate with clinical benefit from current therapeutic regimens. However, monotherapies do not effectively target the multiple aspects of HGSOC tumours that can occur simultaneously, in the vast majority of cases. The development of drug resistance is a growing concern, especially following treatment with PARPi and thus the use of combination regimens has garnered increasing interest. The characterisation of PARPi has elucidated its myriad roles in DNA repair and regulation, including roles in chromatin remodelling and methylation. Additionally, effects of PARPi on immune cells and immune responses offer alternative pathways for therapeutic exploitation. To date we have seen PARPi combined with chemotherapy, angiogenesis agents, immune checkpoint inhibitors and more recently novel therapeutics including epigenetic drugs and other DNA repair inhibitors, with some trials investigating triple combination treatments. The benefit of these therapies for women with platinum-resistant and HR proficient OC are still unclear when compared to their platinum-sensitive and HRD OC counterparts. One of the most challenging aspects of combination therapy is tolerability. Investigating alternative treatment sequencing and scheduling could result in triple-combination therapies becoming more tolerable and in prolongation of survival if successfully matched to the molecular characteristics of the HGSOC. Additionally, clinical trials involving correlative studies to investigate outcomes are essential to establish ideal biospecimen cohorts to enable the most complete understanding of a trial outcome and for further research. Understanding the characteristics that drive responses could improve strategies for driving prolonged remissions and

ultimately improve the survival outcomes for women with HGSOC.

Author contributions

NB wrote the body of work excluding Sections 4.1, 4.1.1 which was written by AK. CS, MP, and CV guided structure and content. CS and CV edited the work.

Funding

The authors are supported by fellowships and grants from the Stafford Fox Medical Research Foundation (CV and CLS); Cancer Council Victoria (Sir Edward Dunlop Fellowship in Cancer Research to CLS); the Victorian Cancer Agency (Clinical Fellowships to CLS CRF10-20, CRF16014). National Health and Medical Research Council (NHMRC) ideas grant No. 2011747 (to MP and AK). MP is an Australian NHMRC Senior Research Fellow, grant No.1154850. NB is supported by a PhD scholarship funded by RMIT.

Conflict of interest

CLS reports membership in advisory boards for AstraZeneca, Clovis Oncology, Roche, Eisai, Sierra Oncology, Takeda, and Merck Sharp and Dohme (no honoraria were received for any advisory boards); grant/research support from Clovis Oncology, Eisai, Sierra Oncology, Roche, BeiGene, AstraZeneca, drug in kind support from Clovis Oncology, Eisai, Sierra Oncology, Roche, and BeiGene).

The remaining authors declare that the research was conducted in the absence of any commercial or financial relationships that could be construed as a potential conflict of interest.

Publisher's note

All claims expressed in this article are solely those of the authors and do not necessarily represent those of their affiliated organizations, or those of the publisher, the editors and the reviewers. Any product that may be evaluated in this article, or claim that may be made by its manufacturer, is not guaranteed or endorsed by the publisher.

Reference

Abbotts, R., Topper, M. J., Biondi, C., Fontaine, D., Goswami, R., Stojanovic, L., et al. (2019). DNA methyltransferase inhibitors induce a BRCAness phenotype that sensitizes NSCLC to PARP inhibitor and ionizing radiation. *Proc. Natl. Acad. Sci. U. S. A.* 116 (45), 22609–22618. doi:10.1073/pnas.1903765116

Adimoolam, S., Sirisawad, M., Chen, J., Thiemann, P., Ford, J. M., and Buggy, J. J. (2007). HDAC inhibitor PCI-24781 decreases RAD51 expression and inhibits homologous recombination. *Proc. Natl. Acad. Sci. U. S. A.* 104 (49), 19482–19487. doi:10.1073/pnas.0707828104

Agarwal, R., and Kaye, S. B. (2003). Ovarian cancer: Strategies for overcoming resistance to chemotherapy. *Nat. Rev. Cancer* 3 (7), 502–516. doi:10.1038/nrc1123

Aghajanian, C., Bookman, M. A., Fleming, G. F., Swisher, E. M., Steffensen, K. D., Friedlander, M., et al. (2021). Progression-free survival by investigator versus blinded independent central review in newly diagnosed patients with high-grade serous ovarian cancer: Analysis of the VELIA/GOG-3005 trial. *Gynecol. Oncol.* 162 (2), 375–381. doi:10.1016/j.ygyno.2021.05.031

Ahel, D., Horejsi, Z., Wiechens, N., Polo, S. E., Garcia-Wilson, E., Ahel, I., et al. (2009). Poly (ADP-ribose)–dependent regulation of DNA repair by the chromatin remodeling enzyme ALC1. *science* 325 (5945), 1240–1243. doi:10.1126/science.1177321

Ahmed, A. A., Etemadmoghadam, D., Temple, J., Lynch, A. G., Riad, M., Sharma, R., et al. (2010). Driver mutations in TP53 are ubiquitous in high grade serous carcinoma of the ovary. *J. Pathol.* 221 (1), 49–56. doi:10.1002/path.2696

Alagoz, M., Katsuki, Y., Ogiwara, H., Ogi, T., Shibata, A., Kakarougkas, A., et al. (2015). SETDB1, HP1 and SUV39 promote repositioning of 53BP1 to extend resection during homologous recombination in G2 cells. *Nucleic Acids Res.* 43 (16), 7931–7944. doi:10.1093/nar/gkv722

Alsop, K., Fereday, S., Meldrum, C., deFazio, A., Emmanuel, C., George, J., et al. (2012). BRCA mutation frequency and patterns of treatment response in BRCA mutation–positive women with ovarian cancer: A report from the Australian ovarian cancer study group. *J. Clin. Oncol.* 30 (21), 2654–2663. doi:10.1200/JCO.2011.39.8545

Alvarado-Cruz, I., Mahmoud, M., Khan, M., Zhao, S., Oeck, S., Meas, R., et al. (2021). Differential immunomodulatory effect of PARP inhibition in BRCA1 deficient and competent tumor cells. *Biochem. Pharmacol.* 184, 114359. doi:10.1016/j.bcp.2020.114359

Andronikou, C., and Rottenberg, S. (2021). Studying PAR-dependent chromatin remodeling to tackle PARPi resistance. *Trends Mol. Med.* 27, 630–642. doi:10.1016/j.molmed.2021.04.010

Antolin, A. A., Ameratunga, M., Banerji, U., Clarke, P. A., Workman, P., and Al-Lazikani, B. (2020). The kinase polypharmacology landscape of clinical PARP inhibitors. *Sci. Rep.* 10 (1), 1–14. doi:10.1038/s41598-020-59074-4

Aref-Eshghi, E., McGee, J. D., Pedro, V. P., Kerkhof, J., Stuart, A., Ainsworth, P. J., et al. (2020). Genetic and epigenetic profiling of BRCA1/2 in ovarian tumors reveals additive diagnostic yield and evidence of a genomic BRCA1/2 DNA methylation signature. *J. Hum. Genet.* 65 (10), 865–873. doi:10.1038/s10038-020-0780-4

Ashworth, A., and Lord, C. J. (2018). Synthetic lethal therapies for cancer: what's next after PARP inhibitors? *Nat. Rev. Clin. Oncol.* 15 (9), 564–576. doi:10.1038/s41571-018-0055-6

Banerjee, S. N., and Lord, C. J. (2020). First-line PARP inhibition in ovarian cancer—Standard of care for all? *Nat. Rev. Clin. Oncol.* 17 (3), 136–137. doi:10.1038/s41571-020-0335-9

Banerjee, S., Moore, K. N., Colombo, N., Scambia, G., Kim, B. G., Oaknin, A., et al. (2021). Maintenance olaparib for patients with newly diagnosed advanced ovarian cancer and a BRCA mutation (SOLO1/GOG 3004): 5-year follow-up of a randomised, double-blind, placebo-controlled, phase 3 trial. *Lancet. Oncol.* 22, 1721–1731. doi:10.1016/S1470-2045(21)00531-3

Barnett, J. C., Bean, S. M., Whitaker, R. S., Kondoh, E., Baba, T., Fujii, S., et al. (2010). Ovarian cancer tumor infiltrating T-regulatory (Treg) cells are associated with a metastatic phenotype. *Gynecol. Oncol.* 116 (3), 556–562. doi:10.1016/j.ygyno.2009.11.020

Barrow, A. D., and Colonna, M. (2017). Tailoring Natural Killer cell immunotherapy to the tumour microenvironment. *Semin. Immunol.* 31, 30–36. doi:10.1016/j.smim.2017.09.001

Bellucci, R., Martin, A., Bommarito, D., Wang, K., Hansen, S. H., Freeman, G. J., et al. (2015). Interferon-γ-induced activation of JAK1 and JAK2 suppresses tumor cell susceptibility to NK cells through upregulation of PD-L1 expression. *Oncoimmunology* 4 (6), e1008824. doi:10.1080/2162402X.2015.1008824

Berti, M., Ray Chaudhuri, A., Thangavel, S., Gomathinayagam, S., Kenig, S., Vujanovic, M., et al. (2013). Human RECQ1 promotes restart of replication forks reversed by DNA topoisomerase I inhibition. *Nat. Struct. Mol. Biol.* 20 (3), 347–354. doi:10.1038/nsmb.2501

Bindra, R. S., Gibson, S. L., Meng, A., Westermark, U., Jasin, M., Pierce, A. J., et al. (2005). Hypoxia-induced down-regulation of BRCA1 expression by E2Fs. *Cancer Res.* 65 (24), 11597–11604. doi:10.1158/0008-5472.CAN-05-2119

Bindra, R. S., Schaffer, P. J., Meng, A., Woo, J., Maseide, K., Roth, M. E., et al. (2004). Down-regulation of Rad51 and decreased homologous recombination in hypoxic cancer cells. *Mol. Cell. Biol.* 24 (19), 8504–8518. doi:10.1128/MCB.24.19.8504-8518.2004

Blessing, C., Mandemaker, I. K., Gonzalez-Leal, C., Preisser, J., Schomburg, A., and Ladurner, A. G. (2020). The oncogenic helicase ALC1 regulates PARP inhibitor potency by trapping PARP2 at DNA breaks. *Mol. Cell* 80 (5), 862–875. e6. doi:10.1016/j.molcel.2020.10.009

Bolton, K. L., Chenevix-Trench, G., Goh, C., Sadetzki, S., Ramus, S. J., Karlan, B. Y., et al. (2012). Association between BRCA1 and BRCA2 mutations and survival in women with invasive epithelial ovarian cancer. *Jama* 307 (4), 382–390. doi:10.1001/jama.2012.20

Bowtell, D. D., Bohm, S., Ahmed, A. A., Aspuria, P. J., Bast, R. C., Beral, V., et al. (2015). Rethinking ovarian cancer II: Reducing mortality from high-grade serous ovarian cancer. *Nat. Rev. Cancer* 15 (11), 668–679. doi:10.1038/nrc4019

Bowtell, D. D. (2010). The genesis and evolution of high-grade serous ovarian cancer. *Nat. Rev. Cancer* 10 (11), 803–808. doi:10.1038/nrc2946

Brown, S. D., Warren, R. L., Gibb, E. A., Martin, S. D., Spinelli, J. J., Nelson, B. H., et al. (2014). Neo-antigens predicted by tumor genome meta-analysis correlate with increased patient survival. *Genome Res.* 24 (5), 743–750. doi:10.1101/gr.165985.113

Bruand, M., Barras, D., Mina, M., Ghisoni, E., Morotti, M., Lanitis, E., et al. (2021). Cell-autonomous inflammation of BRCA1-deficient ovarian cancers drives both tumor-intrinsic immunoreactivity and immune resistance via STING. *Cell Rep.* 36 (3), 109412. doi:10.1016/j.celrep.2021.109412

Cai, H., Yan, L., Liu, N., and Xu, M. (2020). IFI16 promotes cervical cancer progression by upregulating PD-L1 in immunomicroenvironment through STING-TBK1-NF-kB pathway. *Biomed. Pharmacother.* 123, 109790. doi:10.1016/j.biopha.2019.109790

Caiafa, P., Guastafierro, T., and Zampieri, M. (2009). Epigenetics: Poly (ADP-ribosyl) ation of PARP-1 regulates genomic methylation patterns. *FASEB J.* 23 (3), 672–678. doi:10.1096/fj.08-123265

Cao, J. (2019). "Pooled analysis of phase I dose-escalation and dose cohort expansion studies of IMP4297, a novel PARP inhibitor," in *Chinese and Australian patients with advanced solid tumors* (American Society of Clinical Oncology).

Chabanon, R. M., Muirhead, G., Krastev, D. B., Adam, J., Morel, D., Garrido, M., et al. (2019). PARP inhibition enhances tumor cell–intrinsic immunity in ERCC1-deficient non–small cell lung cancer. *J. Clin. Invest.* 129 (3), 1211–1228. doi:10.1172/JCI123319

Chen, C.-C., Feng, W., Lim, P. X., Kass, E. M., and Jasin, M. (2018). Homology-directed repair and the role of BRCA1, BRCA2, and related proteins in genome integrity and cancer. *Annu. Rev. Cancer Biol.* 2, 313–336. doi:10.1146/annurev-cancerbio-030617-050502

Cheng, H., Zhang, Z., Borczuk, A., Powell, C. A., Balajee, A. S., Lieberman, H. B., et al. (2013). PARP inhibition selectively increases sensitivity to cisplatin in ERCC1-low non-small cell lung cancer cells. *Carcinogenesis* 34 (4), 739–749. doi:10.1093/carcin/bgs393

Cimmino, L., Dolgalev, I., Wang, Y., Yoshimi, A., Martin, G. H., Wang, J., et al. (2017). Restoration of TET2 function blocks aberrant self-renewal and leukemia progression. *Cell* 170 (6), 1079–1095. e20. doi:10.1016/j.cell.2017.07.032

Coleman, R., Fleming, G., Brady, M., Swisher, E., Steffensen, K., Friedlander, M., et al. (2019). VELIA/GOG-3005: Integration of veliparib (V) with front-line chemotherapy and maintenance in women with high-grade serous carcinoma of ovarian, fallopian tube, or primary peritoneal origin (HGSC). *Ann. Oncol.* 30, v895–v896. doi:10.1093/annonc/mdz394.054

Coleman, R. L., Oza, A. M., Lorusso, D., Aghajanian, C., Oaknin, A., Dean, A., et al. (2017). Rucaparib maintenance treatment for recurrent ovarian carcinoma after response to platinum therapy (ARIEL3): A randomised, double-blind, placebo-controlled, phase 3 trial. *Lancet* 390 (10106), 1949–1961. doi:10.1016/S0140-6736(17)32440-6

Colombo, N., Sessa, C., du Bois, A., Ledermann, J., McCluggage, W. G., McNeIsh, I., et al. (2019). ESMO–ESGO consensus conference recommendations on ovarian cancer: Pathology and molecular biology, early and advanced stages, borderline tumours and recurrent disease. *Ann. Oncol.* 30 (5), 672–705. doi:10.1093/annonc/mdz062

Constant, S. L., and Bottomly, K. (1997). Induction of Th1 and Th2 CD4+ T cell responses: The alternative approaches. *Annu. Rev. Immunol.* 15 (1), 297–322. doi:10.1146/annurev.immunol.15.1.297

Cooke, S. L., and Brenton, J. D. (2011). Evolution of platinum resistance in high-grade serous ovarian cancer. *Lancet. Oncol.* 12 (12), 1169–1174. doi:10.1016/S1470-2045(11)70123-1

Cortez, A. J., Tudrej, P., Kujawa, K. A., and Lisowska, K. M. (2018). Advances in ovarian cancer therapy. *Cancer Chemother. Pharmacol.* 81 (1), 17–38. doi:10.1007/s00280-017-3501-8

Crusz, S. M., and Balkwill, F. R. (2015). Inflammation and cancer: Advances and new agents. *Nat. Rev. Clin. Oncol.* 12 (10), 584–596. doi:10.1038/nrclinonc.2015.105

Cunningham, J. M., Cicek, M. S., Larson, N. B., Davila, J., Wang, C., Larson, M. C., et al. (2014). Clinical characteristics of ovarian cancer classified by BRCA1, BRCA2 and RAD51C status. *Sci. Rep.* 4 (1), 4026–4027. doi:10.1038/srep04026

D'Andrea, A. D. (2018). Mechanisms of PARP inhibitor sensitivity and resistance. *DNA repair* 71, 172–176. doi:10.1016/j.dnarep.2018.08.021

Dangaj, D., Bruand, M., Grimm, A. J., Ronet, C., Barras, D., Duttagupta, P. A., et al. (2019). Cooperation between constitutive and inducible chemokines enables T cell engraftment and immune attack in solid tumors. *Cancer cell* 35 (6), 885–900. doi:10.1016/j.ccell.2019.05.004

de Biasi, A. R., Villena-Vargas, J., and Adusumilli, P. S. (2014). Cisplatin-induced antitumor immunomodulation: A review of preclinical and clinical evidence. *Clin. Cancer Res.* 20 (21), 5384–5391. doi:10.1158/1078-0432.CCR-14-1298

DE Capoa, A., de CApoA, A., GiovannelliF.NiveleAu, A., Zardo, G., Marenzi, S., et al. (1999). Reduced levels of poly (ADP-ribosyl) ation result in chromatin compaction and hypermethylation as shown by cell-by-cell computer-assisted quantitative analysis. *FASEB J.* 13 (1), 89–93. doi:10.1096/fasebj.13.1.89

Dean, E., Middleton, M. R., PwinT, T., Swaisland, H., Carmichael, J., Goodege-Kunwar, P., et al. (2012). Phase I study to assess the safety and tolerability of olaparib in combination with bevacizumab in patients with advanced solid tumours. *Br. J. Cancer* 106 (3), 468–474. doi:10.1038/bjc.2011.555

Dent, R. A., Lindeman, G. J., Clemons, M., Wildiers, H., Chan, A., McCarthy, N. J., et al. (2013). Phase I trial of the oral PARP inhibitor olaparib in combination with paclitaxel for first-or second-line treatment of patients with metastatic triple-negative breast cancer. *Breast Cancer Res.* 15 (5), R88–8. doi:10.1186/bcr3484

Ding, L., Kim, H. J., Wang, Q., Kearns, M., Jiang, T., Ohlson, C. E., et al. (2018). PARP inhibition elicits STING-dependent antitumor immunity in Brca1-deficient ovarian cancer. *Cell Rep.* 25 (11), 2972–2980. e5. doi:10.1016/j.celrep.2018.11.054

Dion, L., Carton, I., Jaillard, S., Nyangoh Timoh, K., Henno, S., Sardain, H., et al. (2020). The landscape and therapeutic implications of molecular profiles in epithelial ovarian cancer. *J. Clin. Med.* 9 (7), 2239. doi:10.3390/jcm9072239

Disis, M. L., Taylor, M. H., Kelly, K., Beck, J. T., Gordon, M., Moore, K. M., et al. (2019). Efficacy and safety of avelumab for patients with recurrent or refractory ovarian cancer: Phase 1b results from the JAVELIN solid tumor trial. *JAMA Oncol.* 5 (3), 393–401. doi:10.1001/jamaoncol.2018.6258

Drew, Y., Kaufman, B., Banerjee, S., Lortholary, A., Hong, S., Park, Y., et al. (2019). Phase II study of olaparib+ durvalumab (MEDIOLA): Updated results in germline BRCA-mutated platinum-sensitive relapsed (PSR) ovarian cancer (OC). *Ann. Oncol.* 30, v485–v486. doi:10.1093/annonc/mdz253.016

Drew, Y., Penson, R., O'Malley, D., Kim, J. W., Zimmermann, S., Roxburgh, P., et al. (2020). 814MO Phase II study of olaparib (O) plus durvalumab (D) and bevacizumab (B)(MEDIOLA): Initial results in patients (pts) with non-germline BRCA-mutated (non-gBRCAm) platinum sensitive relapsed (PSR) ovarian cancer (OC). *Ann. Oncol.* 31, S615–S616. doi:10.1016/j.annonc.2020.08.953

Dunn, G. P., Old, L. J., and Schreiber, R. D. (2004). The immunobiology of cancer immunosurveillance and immunoediting. *Immunity* 21 (2), 137–148. doi:10.1016/j.immuni.2004.07.017

Dunn, G. P., Old, L. J., and Schreiber, R. D. (2004). The three Es of cancer immunoediting. *Annu. Rev. Immunol.* 22, 329–360. doi:10.1146/annurev.immunol.22.012703.104803

Eckschlager, T., Plch, J., Stiborova, M., and Hrabeta, J. (2017). Histone deacetylase inhibitors as anticancer drugs. *Int. J. Mol. Sci.* 18 (7), 1414. doi:10.3390/ijms18071414

Elyashiv, O., Ledermann, J., Parmar, G., Farrelly, L., Counsell, N., Feeney, A., et al. (2021). ICON 9—An international phase III randomized study to evaluate the efficacy of maintenance therapy with olaparib and cediranib or olaparib alone in patients with relapsed platinum-sensitive ovarian cancer following a response to platinum-based chemotherapy. *Int. J. Gynecol. Cancer* 31 (1), 134–138. doi:10.1136/ijgc-2020-002073

El-Khamisy, S. F., Masutani, M., Suzuki, H., and Caldecott, K. W. (2003). A requirement for PARP-1 for the assembly or stability of XRCC1 nuclear foci at sites of oxidative DNA damage. *Nucleic Acids Res.* 31 (19), 5526–5533. doi:10.1093/nar/gkg761

Färkkilä, A., Gulhan, D. C., Casado, J., Jacobson, C. A., Nguyen, H., Kochupurakkal, B., et al. (2020). Immunogenomic profiling determines responses to combined PARP and PD-1 inhibition in ovarian cancer. *Nat. Commun.* 11 (1), 1–13. doi:10.1038/s41467-020-15315-8

Fenerty, K. E., Padget, M., Wolfson, B., Gameiro, S. R., Su, Z., Lee, J. H., et al. (2018). Immunotherapy utilizing the combination of natural killer–and antibody dependent cellular cytotoxicity (ADCC)–mediating agents with poly (ADP-ribose)

polymerase (PARP) inhibition. *J. Immunother. Cancer* 6 (1), 1–14. doi:10.1186/s40425-018-0445-4

Flood, B. A., Higgs, E. F., Li, S., Luke, J. J., and Gajewski, T. F. (2019). STING pathway agonism as a cancer therapeutic. *Immunol. Rev.* 290 (1), 24–38. doi:10.1111/imr.12765

Forment, J. V., and O'Connor, M. J. (2018). Targeting the replication stress response in cancer. *Pharmacol. Ther.* 188, 155–167. doi:10.1016/j.pharmthera.2018.03.005

Fridman, W. H., Zitvogel, L., Sautes-Fridman, C., and Kroemer, G. (2017). The immune contexture in cancer prognosis and treatment. *Nat. Rev. Clin. Oncol.* 14 (12), 717–734. doi:10.1038/nrclinonc.2017.101

Gashi, A. M. (2022). Expression of PD/PD-L1 as a prognostic bio-marker in ovarian serous carcinoma carcinoma-A. *immunity* 16, 18.

George, A., Kaye, S., and Banerjee, S. (2017). Delivering widespread BRCA testing and PARP inhibition to patients with ovarian cancer. *Nat. Rev. Clin. Oncol.* 14 (5), 284–296. doi:10.1038/nrclinonc.2016.191

Ghose, A., Gullapalli, S. V. N., Chohan, N., Bolina, A., Moschetta, M., Rassy, E., et al. (2022). Applications of proteomics in ovarian cancer: Dawn of a new era. *Proteomes* 10 (2), 16. doi:10.3390/proteomes10020016

Goel, S., Duda, D. G., Xu, L., Munn, L. L., Boucher, Y., Fukumura, D., et al. (2011). Normalization of the vasculature for treatment of cancer and other diseases. *Physiol. Rev.* 91 (3), 1071–1121. doi:10.1152/physrev.00038.2010

González-Martín, A., Pothuri, B., Vergote, I., DePont Christensen, R., Graybill, W., Mirza, M. R., et al. (2019). Niraparib in patients with newly diagnosed advanced ovarian cancer. *N. Engl. J. Med.* 381 (25), 2391–2402. doi:10.1056/NEJMoa1910962

Gottschalk, A. J., Trivedi, R. D., Conaway, J. W., and Conaway, R. C. (2012). Activation of the SNF2 family ATPase ALC1 by poly (ADP-ribose) in a stable ALC1· PARP1· nucleosome intermediate. *J. Biol. Chem.* 287 (52), 43527–43532. doi:10.1074/jbc.M112.401141

Guastafierro, T., Cecchinelli, B., Zampieri, M., Reale, A., Riggio, G., Sthandier, O., et al. (2008). CCCTC-binding factor activates PARP-1 affecting DNA methylation machinery. *J. Biol. Chem.* 283 (32), 21873–21880. doi:10.1074/jbc.M801170200

Ha, K., Fiskus, W., Choi, D. S., Bhaskara, S., Cerchietti, L., Devaraj, S. G. T., et al. (2014). Histone deacetylase inhibitor treatment induces 'BRCAness' and synergistic lethality with PARP inhibitor and cisplatin against human triple negative breast cancer cells. *Oncotarget* 5 (14), 5637–5650. doi:10.18632/oncotarget.2154

Handolias, D., Quinn, M., Foo, S., Mileshkin, L., Grant, P., Dutu, G., et al. (2016). Oral cyclophosphamide in recurrent ovarian cancer. *Asia. Pac. J. Clin. Oncol.* 12 (1), e154–e160. doi:10.1111/ajco.12074

Harding, S. M., Benci, J. L., Irianto, J., Discher, D. E., Minn, A. J., and Greenberg, R. A. (2017). Mitotic progression following DNA damage enables pattern recognition within micronuclei. *Nature* 548 (7668), 466–470. doi:10.1038/nature23470

Härtlova, A., Erttmann, S. F., Raffi, F. A., Schmalz, A. M., Resch, U., Anugula, S., et al. (2015). DNA damage primes the type I interferon system via the cytosolic DNA sensor STING to promote anti-microbial innate immunity. *Immunity* 42 (2), 332–343. doi:10.1016/j.immuni.2015.01.012

Hassa, P. O., Haenni, S. S., Buerki, C., Meier, N. I., Lane, W. S., Owen, H., et al. (2005). Acetylation of poly(ADP-ribose) polymerase-1 by p300/CREB-binding protein regulates coactivation of NF-kappaB-dependent transcription. *J. Biol. Chem.* 280 (49), 40450–40464. doi:10.1074/jbc.M507553200

Hegde, P. S., Wallin, J. J., and Mancao, C. (2018). Predictive markers of anti-VEGF and emerging role of angiogenesis inhibitors as immunotherapeutics. *Semin. Cancer Biol.* 52, 117–124. doi:10.1016/j.semcancer.2017.12.002

Heijink, A. M., Talens, F., Jae, L. T., van Gijn, S. E., Fehrmann, R. S. N., Brummelkamp, T. R., et al. (2019). BRCA2 deficiency instigates cGAS-mediated inflammatory signaling and confers sensitivity to tumor necrosis factor-alpha-mediated cytotoxicity. *Nat. Commun.* 10 (1), 100–114. doi:10.1038/s41467-018-07927-y

Helland, Å., Anglesio, M. S., George, J., Cowin, P. A., Johnstone, C. N., House, C. M., et al. (2011). Deregulation of MYCN, LIN28B and LET7 in a molecular subtype of aggressive high-grade serous ovarian cancers. *PloS one* 6 (4), e18064. doi:10.1371/journal.pone.0018064

Hendry, S., Salgado, R., Gevaert, T., Russell, P. A., John, T., Thapa, B., et al. (2017). Assessing tumor infiltrating lymphocytes in solid tumors: A practical review for pathologists and proposal for a standardized method from the international immuno-oncology biomarkers working group: Part 2: TILs in melanoma, gastrointestinal tract carcinomas, non-small cell lung carcinoma and mesothelioma, endometrial and ovarian carcinomas, squamous cell carcinoma of the head and neck, genitourinary carcinomas, and primary brain tumors. *Adv. Anat. Pathol.* 24 (6), 311–335. doi:10.1097/PAP.0000000000000161

Henriksen, J. R., Donskov, F., Waldstrom, M., Jakobsen, A., Hjortkjaer, M., Petersen, C. B., et al. (2020). Favorable prognostic impact of Natural Killer cells and T cells in high-grade serous ovarian carcinoma. *Acta Oncol.* 59 (6), 652–659. doi:10.1080/0284186X.2019.1711173

Hinz, M., Stilmann, M., Arslan, S. C., Khanna, K. K., Dittmar, G., and Scheidereit, C. (2010). A cytoplasmic ATM-TRAF6-cIAP1 module links nuclear DNA damage signaling to ubiquitin-mediated NF-κB activation. *Mol. Cell* 40 (1), 63–74. doi:10.1016/j.molcel.2010.09.008

Hu, C., Liu, X., Zeng, Y., Liu, J., and Wu, F. (2021). DNA methyltransferase inhibitors combination therapy for the treatment of solid tumor: Mechanism and clinical application. *Clin. Epigenetics* 13 (1), 1–16. doi:10.1186/s13148-021-01154-x

Hwang, W.-T., Adams, S. F., Tahirovic, E., Hagemann, I. S., and Coukos, G. (2012). Prognostic significance of tumor-infiltrating T cells in ovarian cancer: A meta-analysis. *Gynecol. Oncol.* 124 (2), 192–198. doi:10.1016/j.ygyno.2011.09.039

Lendermann, J. A., N. Colombo, A. Du Bois, V. Torri, I. Floriani, W. Qian, H. P. Adams et al. (2003). Paclitaxel plus platinum-based chemotherapy versus conventional platinum-based chemotherapy in women with relapsed ovarian cancer: The ICON4/AGO-OVAR-2.2 trial. *Lancet* 361 (9375), 2099–2106. doi:10.1016/s0140-6736(03)13718-x

Iwai, Y., Hamanishi, J., Chamoto, K., and Honjo, T. (2017). Cancer immunotherapies targeting the PD-1 signaling pathway. *J. Biomed. Sci.* 24 (1), 26–11. doi:10.1186/s12929-017-0329-9

Ji, Y., Thomas, C., Tulin, N., Lodhi, N., Boamah, E., Kolenko, V., et al. (2016). Charon mediates immune deficiency–driven PARP-1–dependent immune responses in Drosophila. *J. Immunol.* 197 (6), 2382–2389. doi:10.4049/jimmunol.1600994

Jiao, S., Xia, W., Yamaguchi, H., Wei, Y., Chen, M. K., Hsu, J. M., et al. (2017). PARP inhibitor upregulates PD-L1 expression and enhances cancer-associated immunosuppression. *Clin. Cancer Res.* 23 (14), 3711–3720. doi:10.1158/1078-0432.CCR-16-3215

Johannes, J. W., Balazs, A., Barratt, D., Bista, M., Chuba, M. D., Cosulich, S., et al. (2021). Discovery of 5-{4-[(7-Ethyl-6-oxo-5, 6-dihydro-1, 5-naphthyridin-3-yl) methyl] piperazin-1-yl}-N-methylpyridine-2-carboxamide (AZD5305): A PARP1–DNA trapper with high selectivity for PARP1 over PARP2 and other PARPs. *J. Med. Chem.* 64 (19), 14498–14512. doi:10.1021/acs.jmedchem.1c01012

Juhász, S., Smith, R., Schauer, T., Spekhardt, D., Mamar, H., Zentout, S., et al. (2020). The chromatin remodeler ALC1 underlies resistance to PARP inhibitor treatment. *Sci. Adv.* 6 (51), eabb8626. doi:10.1126/sciadv.abb8626

Kachhap, S. K., Rosmus, N., Collis, S. J., Kortenhorst, M. S. Q., Wissing, M. D., Hedayati, M., et al. (2010). Downregulation of homologous recombination DNA repair genes by HDAC inhibition in prostate cancer is mediated through the E2F1 transcription factor. *PloS one* 5 (6), e11208. doi:10.1371/journal.pone.0011208

Kharat, S. S., Ding, X., Swaminathan, D., Suresh, A., Singh, M., Sengodan, S. K., et al. (2020). Degradation of 5hmC-marked stalled replication forks by APE1 causes genomic instability. *Sci. Signal.* 13 (645), eaba8091. doi:10.1126/scisignal.aba8091

Khoury-Haddad, H., Guttmann-Raviv, N., Ipenberg, I., Huggins, D., Jeyasekharan, A. D., and Ayoub, N. (2014). PARP1-dependent recruitment of KDM4D histone demethylase to DNA damage sites promotes double-strand break repair. *Proc. Natl. Acad. Sci. U. S. A.* 111 (7), E728–E737. doi:10.1073/pnas.1317585111

Khurana, S., Kruhlak, M. J., Kim, J., Tran, A. D., Liu, J., Nyswaner, K., et al. (2014). A macrohistone variant links dynamic chromatin compaction to BRCA1-dependent genome maintenance. *Cell Rep.* 8 (4), 1049–1062. doi:10.1016/j.celrep.2014.07.024

Kim, D.-S., Camacho, C. V., and Kraus, W. L. (2021). Alternate therapeutic pathways for PARP inhibitors and potential mechanisms of resistance. *Exp. Mol. Med.* 53 (1), 42–51. doi:10.1038/s12276-021-00557-3

Kim, M. Y., Mauro, S., Gevry, N., Lis, J. T., and Kraus, W. L. (2004). NAD+-dependent modulation of chromatin structure and transcription by nucleosome binding properties of PARP-1. *Cell* 119 (6), 803–814. doi:10.1016/j.cell.2004.11.002

Koch, U., and Radtke, F. (2011). Mechanisms of T cell development and transformation. *Annu. Rev. Cell Dev. Biol.* 27, 539–562. doi:10.1146/annurev-cellbio-092910-154008

Kondrashova, O., Topp, M., Nesic, K., Lieschke, E., Ho, G. Y., Harrell, M. I., et al. (2018). Methylation of all BRCA1 copies predicts response to the PARP inhibitor rucaparib in ovarian carcinoma. *Nat. Commun.* 9 (1), 1–16. doi:10.1038/s41467-018-05564-z

Konstantinopoulos, P. A., Waggoner, E., and Vidal, G. (2018). TOPACIO/Keynote-162 (NCT02657889): A phase 1/2 study of niraparib+ pembrolizumab in patients (pts) with advanced triple-negative breast cancer or recurrent ovarian cancer (ROC)—results from ROC cohort. *J. Clin. Oncol.* 36. doi:10.1200/JCO.2018.36.15

Konstantinopoulos, P. A., Waggoner, S., Vidal, G. A., Mita, M., Moroney, J. W., Holloway, R., et al. (2019). Single-arm phases 1 and 2 trial of niraparib in

combination with pembrolizumab in patients with recurrent platinum-resistant ovarian carcinoma. *JAMA Oncol.* 5 (8), 1141–1149. doi:10.1001/jamaoncol.2019.1048

Korkmaz, T., Seber, S., and Basaran, G. (2016). Review of the current role of targeted therapies as maintenance therapies in first and second line treatment of epithelial ovarian cancer; in the light of completed trials. *Crit. Rev. Oncol. Hematol.* 98, 180–188. doi:10.1016/j.critrevonc.2015.10.006

Krishnakumar, R., and Kraus, W. L. (2010). The PARP side of the nucleus: Molecular actions, physiological outcomes, and clinical targets. *Mol. Cell* 39 (1), 8–24. doi:10.1016/j.molcel.2010.06.017

Kubalanza, K., and Konecny, G. E. (2020). Mechanisms of PARP inhibitor resistance in ovarian cancer. *Curr. Opin. Obstet. Gynecol.* 32 (1), 36–41. doi:10.1097/GCO.0000000000000600

Kummar, S., Oza, A. M., Fleming, G. F., Sullivan, D. M., Gandara, D. R., Naughton, M. J., et al. (2015). Randomized trial of oral cyclophosphamide and veliparib in high-grade serous ovarian, primary peritoneal, or fallopian tube cancers, or BRCA-mutant ovarian cancer. *Clin. Cancer Res.* 21 (7), 1574–1582. doi:10.1158/1078-0432.CCR-14-2565

Kurman, R. J., and Shih, I.-M. (2016). The dualistic model of ovarian carcinogenesis: Revisited, revised, and expanded. *Am. J. Pathol.* 186 (4), 733–747. doi:10.1016/j.ajpath.2015.11.011

Le May, N., Iltis, I., Ame, J. C., Zhovmer, A., Biard, D., Egly, J. M., et al. (2012). Poly (ADP-ribose) glycohydrolase regulates retinoic acid receptor-mediated gene expression. *Mol. Cell* 48 (5), 785–798. doi:10.1016/j.molcel.2012.09.021

Lee, C. K., Scott, C., Lindeman, G. J., Hamilton, A., Lieschke, E., Gibbs, E., et al. (2019). Phase 1 trial of olaparib and oral cyclophosphamide in BRCA breast cancer, recurrent BRCA ovarian cancer, non-BRCA triple-negative breast cancer, and non-BRCA ovarian cancer. *Br. J. Cancer* 120 (3), 279–285. doi:10.1038/s41416-018-0349-6

Lee, E. K., and Matulonis, U. A. (2020). Emerging drugs for the treatment of ovarian cancer: A focused review of PARP inhibitors. *Expert Opin. Emerg. Drugs* 25 (2), 165–188. doi:10.1080/14728214.2020.1773791

Lee, J., Cediranib maleate and olaparib or standard chemotherapy in treating patients with recurrent platinum-resistant or-refractory ovarian, fallopian tube, or primary peritoneal cancer. 2018.

Lee, Y.-H., Kuo, C. Y., Stark, J. M., Shih, H. M., and Ann, D. K. (2013). HP1 promotes tumor suppressor BRCA1 functions during the DNA damage response. *Nucleic Acids Res.* 41 (11), 5784–5798. doi:10.1093/nar/gkt231

Leong, H. S., Galletta, L., Etemadmoghadam, D., George, J., Köbel, M., Ramus, S.J., and Bowtell, D. (2015). Efficient molecular subtype classification of high-grade serous ovarian cancer. *J. Pathol.* 236 (3), 272–277. doi:10.1002/path.4536

Lheureux, S., Gourley, C., Vergote, I., and Oza, A. M. (2019). Epithelial ovarian cancer. *Lancet* 393 (10177), 1240–1253. doi:10.1016/S0140-6736(18)32552-2

Lheureux, S., Oaknin, A., Garg, S., Bruce, J. P., Madariaga, A., Dhani, N. C., et al. (2019). Evolve: A multicenter open-label single-arm clinical and translational phase II trial of cediranib plus olaparib for ovarian cancer after PARP inhibition progression. *Clin. Cancer Res.* 26, 4206–4215. doi:10.1158/1078-0432.CCR-19-4121

Li, A., Yi, M., Qin, S., Chu, Q., Luo, S., and Wu, K. (2019). Prospects for combining immune checkpoint blockade with PARP inhibition. *J. Hematol. Oncol.* 12 (1), 98–12. doi:10.1186/s13045-019-0784-8

Liu, J., Barry, W. T., BirrerM.Lee, J. M., Buckanovich, R. J., Fleming, G. F., et al. (2019). Overall survival and updated progression-free survival outcomes in a randomized phase II study of combination cediranib and olaparib versus olaparib in relapsed platinum-sensitive ovarian cancer. *Ann. Oncol.* 30 (4), 551–557. doi:10.1093/annonc/mdz018

Liu, J. F., Barry, W. T., Birrer, M., Lee, J. M., Buckanovich, R. J., Fleming, G. F., et al. (2014). Combination cediranib and olaparib versus olaparib alone for women with recurrent platinum-sensitive ovarian cancer: A randomised phase 2 study. *Lancet. Oncol.* 15 (11), 1207–1214. doi:10.1016/S1470-2045(14)70391-2

Liu, J., Gaillard, S., Hendrickson, A. W., Moroney, J., Yeku, O., Diver, E., et al. (2021). An open-label phase II study of dostarlimab (TSR-042), bevacizumab (bev), and niraparib combination in patients (pts) with platinum-resistant ovarian cancer (PROC): Cohort A of the OPAL trial. *Gynecol. Oncol.* 162, S17–S18. doi:10.1016/s0090-8258(21)00680-6

Liu, Y., Martin-Trevino, R., Shang, L., Davis, A., Wicha, M., Liu, S., et al. (2015). Abstract 4226: Histone deacetylase inhibitors sensitize cancer stem cells to PARP inhibitors in triple-negative breast cancer. *Cancer Res.* 75, 4226. doi:10.1158/1538-7445.AM2015-4226

Lord, C. J., and Ashworth, A. (2017). PARP inhibitors: Synthetic lethality in the clinic. *Science* 355 (6330), 1152–1158. doi:10.1126/science.aam7344

Luo, X., Nie, J., Wang, S., Chen, Z., Chen, W., Li, D., et al. (2015). Poly (ADP-ribosyl) ation of FOXP3 protein mediated by PARP-1 protein regulates the function of regulatory T cells. *J. Biol. Chem.* 290 (48), 28675–28682. doi:10.1074/jbc.M115.661611

Macian, F. (2005). NFAT proteins: Key regulators of T-cell development and function. *Nat. Rev. Immunol.* 5 (6), 472–484. doi:10.1038/nri1632

Mackay, H. J., Hirte, H., Colgan, T., Covens, A., MacAlpine, K., Grenci, P., et al. (2010). Phase II trial of the histone deacetylase inhibitor belinostat in women with platinum resistant epithelial ovarian cancer and micropapillary (LMP) ovarian tumours. *Eur. J. Cancer* 46 (9), 1573–1579. doi:10.1016/j.ejca.2010.02.047

Madondo, M. T., Quinn, M., and Plebanski, M. (2016). Low dose cyclophosphamide: mechanisms of T cell modulation. *Cancer Treat. Rev.* 42, 3–9. doi:10.1016/j.ctrv.2015.11.005

Martí, J. M., Fernandez-Cortes, M., Serrano-Saenz, S., Zamudio-Martinez, E., Delgado-Bellido, D., Garcia-Diaz, A., et al. (2020). The multifactorial role of PARP-1 in tumor microenvironment. *Cancers* 12 (3), 739. doi:10.3390/cancers12030739

Martín, A. G., Tazi, Y., Heitz, F., Montane, L., Gargiulo, P., Berger, R., et al. (2020). LBA33 maintenance olaparib plus bevacizumab (bev) in patients (PTS) with newly diagnosed advanced high-grade ovarian carcinoma (HGOC): Final analysis of second progression-free survival (Pfs2) in the phase III PAOLA-1/ENGOT-ov25 trial. *Ann. Oncol.* 31, S1163–S1164. doi:10.1016/j.annonc.2020.08.2263

Martin, K. A., Cesaroni, M., Denny, M. F., Lupey, L. N., and Tempera, I. (2015). Global transcriptome analysis reveals that poly (ADP-ribose) polymerase 1 regulates gene expression through EZH2. *Mol. Cell. Biol.* 35 (23), 3934–3944. doi:10.1128/MCB.00635-15

Martin, L. P., Hamilton, T. C., and Schilder, R. J. (2008). Platinum resistance: The role of DNA repair pathways. *Clin. Cancer Res.* 14 (5), 1291–1295. doi:10.1158/1078-0432.CCR-07-2238

Matulonis, U. A., Shapira-Frommer, R., and Santin, A. D. (2018). Antitumor activity and safety of pembrolizumab in patients with advanced recurrent ovarian cancer: Interim results from the phase 2 KEYNOTE-100 study. *Ann. Oncol.* 30. doi:10.1093/annonc/mdz135

Matulonis, U., Herrstedt, J., Oza, A., Mahner, S., Redondo, A., Berton, D., et al. (2021). Long-term safety and secondary efficacy endpoints in the ENGOT-OV16/NOVA phase III trial of niraparib in recurrent ovarian cancer. *Gynecol. Oncol.* 162, S24–S25. doi:10.1016/s0090-8258(21)00693-4

McCluggage, W. G. (2011). Morphological subtypes of ovarian carcinoma: A review with emphasis on new developments and pathogenesis. *Pathology* 43 (5), 420–432. doi:10.1097/PAT.0b013e328348a6e7

McMullen, M., Madariaga, A., and Lheureux, S. (2020). "New approaches for targeting platinum-resistant ovarian cancer," in *Seminars in cancer biology* (Elsevier).

Meng, X. W., Koh, B. D., Zhang, J. S., Flatten, K. S., Schneider, P. A., Billadeau, D. D., et al. (2014). Poly (ADP-ribose) polymerase inhibitors sensitize cancer cells to death receptor-mediated apoptosis by enhancing death receptor expression. *J. Biol. Chem.* 289 (30), 20543–20558. doi:10.1074/jbc.M114.549220

Milanesio, M. C., Giordano, S., and Valabrega, G. (2020). Clinical implications of DNA repair defects in high-grade serous ovarian carcinomas. *Cancers* 12 (5), 1315. doi:10.3390/cancers12051315

Mirza, M. R., Avall Lundqvist, E., Birrer, M. J., dePont Christensen, R., Nyvang, G. B., Malander, S., et al. (2019). Niraparib plus bevacizumab versus niraparib alone for platinum-sensitive recurrent ovarian cancer (NSGO-AVANOVA2/ENGOT-ov24): A randomised, phase 2, superiority trial. *Lancet. Oncol.* 20 (10), 1409–1419. doi:10.1016/S1470-2045(19)30515-7

Mouw, K. W., Goldberg, M. S., Konstantinopoulos, P. A., and D'Andrea, A. D. (2017). DNA damage and repair biomarkers of immunotherapy response. *Cancer Discov.* 7 (7), 675–693. doi:10.1158/2159-8290.CD-17-0226

Murai, J., Huang, S. y. N., Das, B. B., Renaud, A., Zhang, Y., Doroshow, J. H., et al. (2012). Trapping of PARP1 and PARP2 by clinical PARP inhibitors. *Cancer Res.* 72 (21), 5588–5599. doi:10.1158/0008-5472.CAN-12-2753

Murai, J., Huang, S. Y. N., Renaud, A., Zhang, Y., Ji, J., Takeda, S., et al. (2014). Stereospecific PARP trapping by BMN 673 and comparison with olaparib and rucaparib. *Mol. Cancer Ther.* 13 (2), 433–443. doi:10.1158/1535-7163.MCT-13-0803

Muthurajan, U. M., Hepler, M. R. D., Hieb, A. R., Clark, N. J., Kramer, M., Yao, T., et al. (2014). Automodification switches PARP-1 function from chromatin architectural protein to histone chaperone. *Proc. Natl. Acad. Sci. U. S. A.* 111 (35), 12752–12757. doi:10.1073/pnas.1405005111

Muvarak, N. E., Chowdhury, K., Xia, L., Robert, C., Choi, E. Y., Cai, Y., et al. (2016). Enhancing the cytotoxic effects of PARP inhibitors with DNA demethylating agents–a potential therapy for cancer. *Cancer cell* 30 (4), 637–650. doi:10.1016/j.ccell.2016.09.002

Nalabothula, N., Al-jumaily, T., Eteleeb, A. M., Flight, R. M., Xiaorong, S., Moseley, H., et al. (2015). Genome-wide profiling of PARP1 reveals an interplay

with gene regulatory regions and DNA methylation. *PloS one* 10 (8), e0135410. doi:10.1371/journal.pone.0135410

Navarro, J., Gozalbo-Lopez, B., Mendez, A. C., Dantzer, F., Schreiber, V., Martinez, C., et al. (2017). PARP-1/PARP-2 double deficiency in mouse T cells results in faulty immune responses and T lymphomas. *Sci. Rep.* 7 (1), 1–14. doi:10.1038/srep41962

Nelson, B. H. (2015). New insights into tumor immunity revealed by the unique genetic and genomic aspects of ovarian cancer. *Curr. Opin. Immunol.* 33, 93–100. doi:10.1016/j.coi.2015.02.004

Nesic, K., Kondrashova, O., Hurley, R. M., McGehee, C. D., Vandenberg, C. J., Ho, G. Y., et al. (2021). Acquired RAD51C promoter methylation loss causes PARP inhibitor resistance in high-grade serous ovarian carcinoma. *Cancer Res.* 81 (18), 4709–4722. doi:10.1158/0008-5472.CAN-21-0774

Nesic, K., Wakefield, M., Kondrashova, O., Scott, C. L., and McNeish, I. A. (2018). Targeting DNA repair: The genome as a potential biomarker. *J. Pathol.* 244 (5), 586–597. doi:10.1002/path.5025

Network, C. G. A. R. (2011). Integrated genomic analyses of ovarian carcinoma. *Nature* 474 (7353), 609–615. doi:10.1038/nature10166

Nguewa, P. A., Fuertes, M. A., Cepeda, V., Alonso, C., Quevedo, C., Soto, M., et al. (2006). Poly (ADP-ribose) polymerase-1 inhibitor 3-aminobenzamide enhances apoptosis induction by platinum complexes in cisplatin-resistant tumor cells. *Med. Chem.* 2 (1), 47–53. doi:10.2174/157340606775197697

Noordermeer, S. M., and van Attikum, H. (2019). PARP inhibitor resistance: A tug-of-war in BRCA-mutated cells. *Trends Cell Biol.* 29 (10), 820–834. doi:10.1016/j.tcb.2019.07.008

Olabisi, O. A., Soto-Nieves, N., Nieves, E., Yang, T. T. C., Yang, X., Yu, R. Y. L., et al. (2008). Regulation of transcription factor NFAT by ADP-ribosylation. *Mol. Cell. Biol.* 28 (9), 2860–2871. doi:10.1128/MCB.01746-07

Ott, P. A., Hu, Z., Keskin, D. B., Shukla, S. A., Sun, J., Bozym, D. J., et al. (2017). An immunogenic personal neoantigen vaccine for patients with melanoma. *Nature* 547 (7662), 217–221. doi:10.1038/nature22991

Pantelidou, C., Sonzogni, O., De Oliveria Taveira, M., Mehta, A. K., Kothari, A., Wang, D., et al. (2019). PARP inhibitor efficacy depends on CD8+ T-cell recruitment via intratumoral STING pathway activation in BRCA-deficient models of triple-negative breast cancer. *Cancer Discov.* 9 (6), 722–737. doi:10.1158/2159-8290.CD-18-1218

Park, J., Kim, S. I., Jeong, S. Y., Kim, Y., Bookman, M. A., Kim, J. W., et al. (2022). Second-line olaparib maintenance therapy is associated with poor response to subsequent chemotherapy in BRCA1/2-mutated epithelial ovarian cancer: A multicentre retrospective study. *Gynecol. Oncol.* 165 (1), 97–104. doi:10.1016/j.ygyno.2022.02.002

Patch, A.-M., Christie, E. L., Etemadmoghadam, D., Garsed, D. W., George, J., Fereday, S., et al. (2015). Whole–genome characterization of chemoresistant ovarian cancer. *Nature* 521 (7553), 489–494. doi:10.1038/nature14410

Patente, T. A., Pinho, M. P., Oliveira, A. A., Evangelista, G. C. M., Bergami-Santos, P. C., and Barbuto, J. A. M. (2019). Human dendritic cells: Their heterogeneity and clinical application potential in cancer immunotherapy. *Front. Immunol.* 9, 3176. doi:10.3389/fimmu.2018.03176

Pavlidis., N., Rassy, E., Vermorken, J. B., Assi, T., Kattan, J., Boussios, S., et al. (2021). The outcome of patients with serous papillary peritoneal cancer, fallopian tube cancer, and epithelial ovarian cancer by treatment eras: 27 years data from the SEER registry. *Cancer Epidemiol.* 75, 102045. doi:10.1016/j.canep.2021.102045

Pazzaglia, S., and Pioli, C. (2020). Multifaceted role of PARP-1 in DNA repair and inflammation: Pathological and therapeutic implications in cancer and non-cancer diseases. *Cells* 9 (1), 41. doi:10.3390/cells9010041

Perren, T. J., Swart, A. M., Pfisterer, J., Ledermann, J. A., Pujade-Lauraine, E., Kristensen, G., et al. (2011). A phase 3 trial of bevacizumab in ovarian cancer. *N. Engl. J. Med.* 365 (26), 2484–2496. doi:10.1056/NEJMoa1103799

Pilié, P. G., Gay, C. M., Byers, L. A., O'Connor, M. J., and Yap, T. A. (2019). PARP inhibitors: Extending benefit beyond BRCA-mutant cancers. *Clin. Cancer Res.* 25 (13), 3759–3771. doi:10.1158/1078-0432.CCR-18-0968

Pines, A., Vrouwe, M. G., Marteijn, J. A., Typas, D., Luijsterburg, M. S., Cansoy, M., et al. (2012). PARP1 promotes nucleotide excision repair through DDB2 stabilization and recruitment of ALC1. *J. Cell Biol.* 199 (2), 235–249. doi:10.1083/jcb.201112132

Preston, C. C., Maurer, M. J., Oberg, A. L., Visscher, D. W., Kalli, K. R., Hartmann, L. C., et al. (2013). The ratios of CD8+ T cells to CD4+ CD25+ FOXP3+ and FOXP3-T cells correlate with poor clinical outcome in human serous ovarian cancer. *PloS one* 8 (11), e80063. doi:10.1371/journal.pone.0080063

Pujade-Lauraine, E., Hilpert, F., Weber, B., Reuss, A., Poveda, A., Kristensen, G., et al. (2014). Bevacizumab combined with chemotherapy for platinum-resistant recurrent ovarian cancer: The AURELIA open-label randomized phase III trial. *Obstetrical Gynecol. Surv.* 69 (7), 402–404. doi:10.1097/01.ogx.0000452705.82050.e4

Pulliam, N., Fang, F., Ozes, A. R., Tang, J., Adewuyi, A., Keer, H., et al. (2018). An effective epigenetic-PARP inhibitor combination therapy for breast and ovarian cancers independent of BRCA mutations. *Clin. Cancer Res.* 24 (13), 3163–3175. doi:10.1158/1078-0432.CCR-18-0204

Quénet, D., El Ramy, R., Schreiber, V., and Dantzer, F. (2009). The role of poly (ADP-ribosyl) ation in epigenetic events. *Int. J. Biochem. Cell Biol.* 41 (1), 60–65. doi:10.1016/j.biocel.2008.07.023

Ray-Coquard, I., Pautier, P., Pignata, S., Perol, D., Gonzalez-Martin, A., Berger, R., et al. (2019). Olaparib plus bevacizumab as first-line maintenance in ovarian cancer. *N. Engl. J. Med.* 381 (25), 2416–2428. doi:10.1056/NEJMoa1911361

Reale, A., Matteis, G. D., Galleazzi, G., Zampieri, M., and Caiafa, P. (2005). Modulation of DNMT1 activity by ADP-ribose polymers. *Oncogene* 24 (1), 13–19. doi:10.1038/sj.onc.1208005

Rébé, C., Demontoux, L., Pilot, T., and Ghiringhelli, F. (2020). Platinum derivatives effects on anticancer immune response. *Biomolecules* 10 (1), 13. doi:10.3390/biom10010013

Reisländer, T., Lombardi, E. P., Groelly, F. J., Miar, A., Porru, M., Di Vito, S., et al. (2019). BRCA2 abrogation triggers innate immune responses potentiated by treatment with PARP inhibitors. *Nat. Commun.* 10 (1), 1–13. doi:10.1038/s41467-019-11048-5

Rouleau, M., Patel, A., Hendzel, M. J., Kaufmann, S. H., and Poirier, G. G. (2010). PARP inhibition: PARP1 and beyond. *Nat. Rev. Cancer* 10 (4), 293–301. doi:10.1038/nrc2812

Ruiz, P. D., Hamilton, G. A., Park, J. W., and Gamble, M. J. (2019). MacroH2A1 regulation of poly (ADP-ribose) synthesis and stability prevents necrosis and promotes DNA repair. *Mol. Cell. Biol.* 40 (1), e00230–19. doi:10.1128/MCB.00230-19

Ruscito, I., Cacsire Castillo-Tong, D., Vergote, I., Ignat, I., Stanske, M., Vanderstichele, A., et al. (2018). Characterisation of tumour microvessel density during progression of high-grade serous ovarian cancer: Clinico-pathological impact (an OCTIPS consortium study). *Br. J. Cancer* 119 (3), 330–338. doi:10.1038/s41416-018-0157-z

Sajadian, S. O., Ehnert, S., Vakilian, H., Koutsouraki, E., Damm, G., Seehofer, D., et al. (2015). Induction of active demethylation and 5hmC formation by 5-azacytidine is TET2 dependent and suggests new treatment strategies against hepatocellular carcinoma. *Clin. Epigenetics* 7 (1), 98–14. doi:10.1186/s13148-015-0133-x

Sambucci, M., LaudisiF.NovelliF.BEnnici, E., Rosado, M. M., and Pioli, C. (2013). Effects of PARP-1 deficiency on Th1 and Th2 cell differentiation. *ScientificWorldJournal.* 2013, 375024. doi:10.1155/2013/375024

Santi, D. V., Norment, A., and Garrett, C. E. (1984). Covalent bond formation between a DNA-cytosine methyltransferase and DNA containing 5-azacytosine. *Proc. Natl. Acad. Sci. U. S. A.* 81 (22), 6993–6997. doi:10.1073/pnas.81.22.6993

Schreiber, R. D., Old, L. J., and Smyth, M. J. (2011). Cancer immunoediting: Integrating immunity's roles in cancer suppression and promotion. *Science* 331 (6024), 1565–1570. doi:10.1126/science.1203486

Schreiber, V., Dantzer, F., Ame, J. C., and de Murcia, G. (2006). Poly (ADP-ribose): Novel functions for an old molecule. *Nat. Rev. Mol. Cell Biol.* 7 (7), 517–528. doi:10.1038/nrm1963

Shen, J., Zhao, W., Ju, Z., Wang, L., Peng, Y., Labrie, M., et al. (2019). PARPi triggers the STING-dependent immune response and enhances the therapeutic efficacy of immune checkpoint blockade independent of BRCAness. *Cancer Res.* 79 (2), 311–319. doi:10.1158/0008-5472.CAN-18-1003

Singh, H. R., Nardozza, A. P., Moller, I. R., Knobloch, G., Kistemaker, H. A. V., Hassler, M., et al. (2017). A poly-ADP-ribose trigger releases the auto-inhibition of a chromatin remodeling oncogene. *Mol. Cell* 68 (5), 860–871.e7. e7. doi:10.1016/j.molcel.2017.11.019

Sinha, S., Molla, S., and Kundu, C. N. (2021). PARP1-modulated chromatin remodeling is a new target for cancer treatment. *Med. Oncol.* 38 (10), 1–16. doi:10.1007/s12032-021-01570-2

Souza-Fonseca-Guimaraes, F., Cursons, J., and Huntington, N. D. (2019). The emergence of natural killer cells as a major target in cancer immunotherapy. *Trends Immunol.* 40 (2), 142–158. doi:10.1016/j.it.2018.12.003

Stilmann, M., Hinz, M., Arslan, S. C., Zimmer, A., Schreiber, V., and Scheidereit, C. (2009). A nuclear poly(ADP-ribose)-dependent signalosome confers DNA damage-induced IkappaB kinase activation. *Mol. Cell* 36 (3), 365–378. doi:10.1016/j.molcel.2009.09.032

Strickland, K. C., Howitt, B. E., Shukla, S. A., Rodig, S., Ritterhouse, L. L., Liu, J. F., et al. (2016). Association and prognostic significance of BRCA1/2-mutation status

with neoantigen load, number of tumor-infiltrating lymphocytes and expression of PD-1/PD-L1 in high grade serous ovarian cancer. *Oncotarget* 7 (12), 13587–13598. doi:10.18632/oncotarget.7277

Sun, K., Mikule, K., Wang, Z., Poon, G., Vaidyanathan, A., Smith, G., et al. (2018). A comparative pharmacokinetic study of PARP inhibitors demonstrates favorable properties for niraparib efficacy in preclinical tumor models. *Oncotarget* 9 (98), 37080–37096. doi:10.18632/oncotarget.26354

Swisher, E., Miller, A., Kohn, E., Brady, M., Radke, M., Pennil, C., et al. (2021). LBA34 Association of homologous recombination deficiency (HRD) with clinical outcomes in a phase III study of olaparib or cediranib and olaparib compared to platinum-based chemotherapy in recurrent platinum-sensitive ovarian cancer (PSOC): Biomarker analyses from NRG-GY004. *Ann. Oncol.* 32, S1309. doi:10.1016/j.annonc.2021.08.2111

Ter Brugge, P., Kristel, P., van der Burg, E., Boon, U., de Maaker, M., Lips, E., et al. (2016). Mechanisms of therapy resistance in patient-derived xenograft models of BRCA1-deficient breast cancer. *J. Natl. Cancer Inst.* 108 (11), djw148. doi:10.1093/jnci/djw148

Thorsell, A.-G., Ekblad, T., Karlberg, T., Low, M., Pinto, A. F., Tresaugues, L., et al. (2017). Structural basis for potency and promiscuity in poly (ADP-ribose) polymerase (PARP) and tankyrase inhibitors. *J. Med. Chem.* 60 (4), 1262–1271. doi:10.1021/acs.jmedchem.6b00990

Timinszky, G., Till, S., Hassa, P. O., Hothorn, M., Kustatscher, G., Nijmeijer, B., et al. (2009). A macrodomain-containing histone rearranges chromatin upon sensing PARP1 activation. *Nat. Struct. Mol. Biol.* 16 (9), 923–929. doi:10.1038/nsmb.1664

Tomao, F., Bardhi, E., Di Pinto, A., Sassu, C. M., Biagioli, E., Petrella, M. C., et al. (2019). Parp inhibitors as maintenance treatment in platinum sensitive recurrent ovarian cancer: An updated meta-analysis of randomized clinical trials according to BRCA mutational status. *Cancer Treat. Rev.* 80, 101909. doi:10.1016/j.ctrv.2019.101909

Tothill, R. W., Tinker, A. V., George, J., Brown, R., Fox, S. B., Lade, S., et al. (2008). Novel molecular subtypes of serous and endometrioid ovarian cancer linked to clinical outcome. *Clin. Cancer Res.* 14 (16), 5198–5208. doi:10.1158/1078-0432.CCR-08-0196

Valdor, R., Schreiber, V., Saenz, L., Martinez, T., Munoz-Suano, A., Dominguez-Villar, M., et al. (2008). Regulation of NFAT by poly (ADP-ribose) polymerase activity in T cells. *Mol. Immunol.* 45 (7), 1863–1871. doi:10.1016/j.molimm.2007.10.044

van der Noll, R., Jager, A., Ang, J. E., Marchetti, S., Mergui-Roelvink, M. W. J., de Bono, J. S., et al. (2020). Phase I study of intermittent olaparib capsule or tablet dosing in combination with carboplatin and paclitaxel (part 2). *Invest. New Drugs* 38 (4), 1096–1107. doi:10.1007/s10637-019-00857-6

van der Noll, R., Jager, A., Ang, J. E., Marchetti, S., Mergui-Roelvink, M. W. J., Lolkema, M. P., et al. (2020). Phase I study of continuous olaparib capsule dosing in combination with carboplatin and/or paclitaxel (Part 1). *Invest. New Drugs* 38 (4), 1117–1128. doi:10.1007/s10637-019-00856-7

Vanacker, H., Harter, P., Labidi-Galy, S. I., Banerjee, S., Oaknin, A., Lorusso, D., et al. (2021). PARP-inhibitors in epithelial ovarian cancer: Actual positioning and future expectations. *Cancer Treat. Rev.* 99, 102255. doi:10.1016/j.ctrv.2021.102255

Vaughan, S., Coward, J. I., Bast, R. C., Berchuck, A., Berek, J. S., Brenton, J. D., et al. (2011). Rethinking ovarian cancer: Recommendations for improving outcomes. *Nat. Rev. Cancer* 11 (10), 719–725. doi:10.1038/nrc3144

Veneris, J. T., Matulonis, U. A., Liu, J. F., and Konstantinopoulos, P. A. (2020). Choosing wisely: Selecting PARP inhibitor combinations to promote anti-tumor immune responses beyond BRCA mutations. *Gynecol. Oncol.* 156 (2), 488–497. doi:10.1016/j.ygyno.2019.09.021

Vignali, D. A., Collison, L. W., and Workman, C. J. (2008). How regulatory T cells work. *Nat. Rev. Immunol.* 8 (7), 523–532. doi:10.1038/nri2343

Vivier, E., Nunès, J. A., and Vély, F. (2004). Natural killer cell signaling pathways. *Science* 306 (5701), 1517–1519. doi:10.1126/science.1103478

Wakefield, M. J., Nesic, K., Kondrashova, O., and Scott, C. L. (2019). Diverse mechanisms of PARP inhibitor resistance in ovarian cancer. *Biochim. Biophys. Acta. Rev. Cancer* 1872 (2), 188307. doi:10.1016/j.bbcan.2019.08.002

Wang, Y. K., Bashashati, A., Anglesio, M. S., Cochrane, D. R., Grewal, D. S., Ha, G., et al. (2017). Genomic consequences of aberrant DNA repair mechanisms stratify ovarian cancer histotypes. *Nat. Genet.* 49 (6), 856–865. doi:10.1038/ng.3849

Yang, M., Liu, L., Xie, M., Sun, X., Yu, Y., Kang, R., et al. (2015). Poly-ADP-ribosylation of HMGB1 regulates TNFSF10/TRAIL resistance through autophagy. *Autophagy* 11 (2), 214–224. doi:10.4161/15548627.2014.994400

Yang, D., Khan, S., Sun, Y., Hess, K., Shmulevich, I., Sood, A. K., et al. (2011). Association of BRCA1 and BRCA2 mutations with survival, chemotherapy sensitivity, and gene mutator phenotype in patients with ovarian cancer. *Jama* 306 (14), 1557–1565. doi:10.1001/jama.2011.1456

Zampieri, M., Guastafierro, T., Calabrese, R., Ciccarone, F., Bacalini, M. G., Reale, A., et al. (2012). ADP-ribose polymers localized on Ctcf–Parp1–Dnmt1 complex prevent methylation of Ctcf target sites. *Biochem. J.* 441 (2), 645–652. doi:10.1042/BJ20111417

Zampieri, M., Passananti, C., Calabrese, R., Perilli, M., Corbi, N., De Cave, F., et al. (2009). Parp1 localizes within the Dnmt1 promoter and protects its unmethylated state by its enzymatic activity. *PloS one* 4 (3), e4717. doi:10.1371/journal.pone.0004717

Zandarashvili, L., Langelier, M. F., Velagapudi, U. K., Hancock, M. A., Steffen, J. D., Billur, R., et al. (2020). Structural basis for allosteric PARP-1 retention on DNA breaks. *Science* 368 (6486), eaax6367. doi:10.1126/science.aax6367

Zhang, L., Conejo-Garcia, J. R., Katsaros, D., Gimotty, P. A., Massobrio, M., Regnani, G., et al. (2003). Intratumoral T cells, recurrence, and survival in epithelial ovarian cancer. *N. Engl. J. Med.* 348 (3), 203–213. doi:10.1056/NEJMoa020177

Zhang, P., Maruyama, T., Konkel, J. E., Abbatiello, B., Zamarron, B., Wang, Z. q., et al. (2013). PARP-1 controls immunosuppressive function of regulatory T cells by destabilizing Foxp3. *PloS one* 8 (8), e71590. doi:10.1371/journal.pone.0071590

Zhang, Q., Burdette, J. E., and Wang, J.-P. (2014). Integrative network analysis of TCGA data for ovarian cancer. *BMC Syst. Biol.* 8 (1), 1338. doi:10.1186/s12918-014-0136-9

Zsiros, E., Lynam, S., Attwood, K. M., Wang, C., Chilakapati, S., Gomez, E. C., et al. (2021). Efficacy and safety of pembrolizumab in combination with bevacizumab and oral metronomic cyclophosphamide in the treatment of recurrent ovarian cancer: A phase 2 nonrandomized clinical trial. *JAMA Oncol.* 7 (1), 78–85. doi:10.1001/jamaoncol.2020.5945

frontiers | Frontiers in Genetics

TYPE Original Research
PUBLISHED 30 September 2022
DOI 10.3389/fgene.2022.907058

Check for updates

OPEN ACCESS

EDITED BY
Zuquan Hu,
Guizhou Medical University, China

REVIEWED BY
Feng Jiang,
Fudan University, China
Zhitong Bing,
Institute of Modern Physics (CAS), China

*CORRESPONDENCE
Yang Wang,
wangyang19920209@qq.com

†These authors contributed equally to the work

SPECIALTY SECTION
This article was submitted to Cancer Genetics and Oncogenomics, a section of the journal Frontiers in Genetics

RECEIVED 29 March 2022
ACCEPTED 31 August 2022
PUBLISHED 30 September 2022

CITATION
Huang Q, Yang S, Yan H, Chen H, Wang Y and Wang Y (2022), Development and validation of a combined glycolysis and immune prognostic signature for lung squamous cell carcinoma.
Front. Genet. 13:907058.
doi: 10.3389/fgene.2022.907058

COPYRIGHT
© 2022 Huang, Yang, Yan, Chen, Wang and Wang. This is an open-access article distributed under the terms of the Creative Commons Attribution License (CC BY). The use, distribution or reproduction in other forums is permitted, provided the original author(s) and the copyright owner(s) are credited and that the original publication in this journal is cited, in accordance with accepted academic practice. No use, distribution or reproduction is permitted which does not comply with these terms.

Development and validation of a combined glycolysis and immune prognostic signature for lung squamous cell carcinoma

Qiang Huang[1†], Shan Yang[2†], Hao Yan[1], Hong Chen[1], Yuzhu Wang[1] and Yang Wang[3*]

[1]Department of Respiratory and Critical Care Medicine, Chengdu Second People's Hospital, Chengdu, China, [2]Department of Rehabilitation Medicine, Chengdu Sixth People's Hospital, Chengdu, China, [3]National Cancer Center, Cancer Hospital, Chinese Academy of Medical Sciences and Peking Union Medical College, Beijing, China

Background: The involvement of glycolysis in the regulation of the tumor immune microenvironment has become a novel research field. In this study, the specific functions and clinical significance of glycolysis-related genes (GRGs) and immune-related genes (IRGs) were systematically characterized in lung squamous cell carcinoma (LUSC).

Methods: We evaluated the prognostic value, interactions, somatic mutations, and copy-number variations of GRGs and IRGs in LUSC from a dataset of The Cancer Genome Atlas (TCGA). An integrated glycolysis–immune score (GIS) model was generated by random forest algorithm and stepwise Cox regression analysis. The predictive power of the GIS was examined by survival analysis, receiver operating characteristics, univariate and multivariate analyses, and subgroup analysis. The correlations between GIS and biological functions, glycolysis, immune activity, immune cell infiltration, and genomic changes were analyzed, and the potential of GIS to guide clinical treatment decisions was evaluated.

Results: A total of 54 prognostic GRGs and IRGs were identified, and a strong correlation was noted among them. However, most of them had somatic mutations and a high incidence of CNV. The GIS model that contained two GRGs (*PYGB* and *MDH1*) and three IRGs (*TSLP*, *SERPIND1*, and *GDF2*) was generated and a high GIS indicated poor survival. Moreover, we found that low GIS was associated with immune pathway activation, M1 macrophage infiltration, and higher immune scores. Finally, patients with low GIS were more sensitive to chemotherapy and immunotherapy.

Conclusion: An integrated model based on glycolysis and immune genes can distinguish the biological functions and immune infiltration patterns of individual tumors, quantitatively estimate the prognosis of patients with LUSC, and guide chemotherapy and immunotherapy decisions.

KEYWORDS
lung squamous cell carcinoma, glycolysis, immune, gene signature, prognosis

Introduction

Lung cancer is one of the leading causes of cancer-related deaths worldwide and is the most common type of cancer (Siegel et al., 2020). Overall, 80%–85% of human lung cancers are non-small cell lung cancers (NSCLCs), and most NSCLCs contain two major histological subtypes, namely, lung adenocarcinoma (LUAD) and lung squamous cell carcinoma (LUSC), which account for approximately 25–30% of all lung cancers (Chen et al., 2014). Recent advances in targeted therapies have greatly benefitted patients with LUAD. However, little progress has been made in the development of LUSC-targeted therapies; as a result, traditional chemotherapy remains the first-line treatment of LUSC for decades. The 5-years survival rates of patients with advanced LUSC treated with currently used chemotherapy were less than 5% (Sun et al., 2007; Drilon et al., 2012), which appears overwhelmingly discouraging. Thus, there is an urgent need to determine prognostic biomarkers to identify patients who are sensitive to treatment. This will enable clinicians to predict clinical outcomes of LUSC timely and accurately and initiate personalized treatment regimens.

Abnormal tumor immune microenvironment (TIME) and tumor metabolic reprogramming are two important features of tumors (Hanahan and Weinberg, 2011). Cancer cells have traditional oxidative metabolism and glycolysis anaerobic metabolism. However, their proliferation is characterized by increased glycolysis metabolism, even in the presence of oxygen (Warburg effect) (Icard et al., 2018). Previous studies have focused on the Warburg effect, supporting the aggressiveness and drug resistance of cancer cells (Lu et al., 2015; Icard and Lincet, 2016), whereas the involvement of glycolysis and its product, lactic acid, in the regulation of TIME has recently become a research area. Studies have reported that lactic acid leads to tumor immune escape and inhibits the activity of T cells and natural killer (NK) cells while being up-taken by regulatory T (Treg) cells and maintaining their immunosuppressive ability (Brand et al., 2016; Watson et al., 2021). It can also inhibit monocyte activation and dendritic cell differentiation (Colegio et al., 2014). Moreover, it induces the M2 polarization of macrophages and promotes tumor growth through mechanisms by involving the hypoxia-inducible factor 1-alpha (HIF-1α) (Colegio et al., 2014). Although glycolysis has a clear inhibitory effect on the TIME, few studies have focused on this relationship comprehensively.

In this study, we integrated glycolysis-related genes (GRGs) and immune-related genes (IRGs) and constructed a systematic glycolysis–immune score (GIS) model. This GIS model showed stable prognostic efficacy in different datasets and clinical subgroups of LUSC. We also demonstrated the relationship of the GIS model to glycolysis and immune status and systematically explored the biological mechanisms of GIS from the perspectives of pathway activity, immune infiltration, and genomic changes. Finally, the study presents that GIS can identify patients with LUSC who are susceptible to chemotherapy and immunotherapy.

Methods

Genomic data and clinical information

RNA-sequencing data and clinical follow-up data from TCGA-LUSC patients were downloaded from the database of The Cancer Genome Atlas (TCGA). A total of 492 patients with LUSC were enrolled after excluding patients who had missing clinical information (such as stage, sex, and age) and who were lost to follow-up. In addition, three datasets, namely, GSE29013, GSE30219, and GSE37745, from the same chip platform (GPL570) were downloaded from the Gene Expression Omnibus (GEO) database. We enrolled patients whose pathological diagnosis was squamous cell carcinoma and excluded patients without detailed clinical information. Finally, 166 patients with LUSC were enrolled and used as a validation queue. The R Package ComBat was used to remove batch effects among datasets.

The corresponding MAF data of TCGA-LUSC patients on the Mutect2 platform were downloaded by the "TCGAbiolinks" package. Then, we used the R package maftools to process the MAF data, calculate the mutation load of samples, and draw the mutation map of genes.

Copy-number variation (CNV) data of patients were downloaded from the UCSC Xena Data Center (https://xena.ucsc.edu/) and preprocessed by GISTIC 2.0. Amplifications and deletions are defined with a threshold of 0.3.

The GRGs were collected from the MSIGDB database (www.gsea-msigdb.org), and the IRGs were collected from the ImmPort database (www.immport.org). The detailed gene list is provided in Supplementary Table S1.

Construction of the GIS model

Initially, we screened the independent prognostic factors in GRGs and IRGs by univariate Cox regression. For significant independent prognostic factors ($p < 0.05$), we then used the random forest algorithm to identify the 10 most important prognostic genes within them. Then, we summarized all possible gene combinations of these 10 genes and determined the *p*-values of all combinations through Kaplan–Meier (KM) analysis. Based on the *p*-values, the gene combinations with the

best prognostic efficiency were screened out. Then, the prognostic genes were used to construct a GIS model, as provided below:

$$\text{GI Score} = \sum \text{iCoefficient}(\text{mRNA}_i) \times \text{Expression}(\text{mRNA}_i)$$

The "servcomp" R package was used to calculate the consistency of the C index, and a larger C-index indicated that the prediction ability of the model was more accurate (Schröder et al., 2011). The high- and low-risk groups were divided based on the median GIS, and the prognostic value of the risk model was evaluated by the KM survival curve, univariate and multivariate Cox regression analyses, and time-dependent receiver operating characteristics (ROC) curve system.

Functional enrichment analysis

The relative abundance of 22 immune cells per patient in the TCGA-LUSC cohort was calculated using the cibersortR package and LM22 feature. The ESTIMATE algorithm was used to calculate the immune score and matrix score of the samples. The R package gsva was used for single-sample gene set enrichment analysis (ssGSEA) to evaluate the pathway enrichment scores of the samples. The related pathway activity was collected from previously published references (Liberzon et al., 2011; Ayers et al., 2017; Gibbons and Creighton, 2018; McDermott et al., 2018; Liang et al., 2020). In addition, we collected the homologous recombination defect (HRD) score, neoantigens, and microsatellite instability (MSI) score (Thorsson et al., 2018) of samples from the study by Thorsson et al. to evaluate patient response to immunotherapy. Detailed gene sets are provided in Supplementary Table S2.

Prediction of chemotherapy and immunotherapy responses

The R package "pRRophetic" can evaluate patients' response to chemotherapy based on the Genomics of Drug Sensitivity in Cancer database. Five first-line agents for treating LUSC (namely, cisplatin, docetaxel, gemcitabine, paclitaxel, and vinorelbine) were selected, and the median maximum inhibitory concentration (IC50) for each patient was calculated using ridge regression to assess the sensitivity to chemotherapy in high- and low-risk groups. Then, the 10-fold cross-validation was used to enhance the predictive accuracy. The Tracking of Indels by Decomposition (TIDE) algorithm was used to assess patient response to anti-programmed death-1 (PD1) and anti-cytotoxic T-lymphocyte-associated protein 4 (CTLA4) therapy. Then, we matched the genome data of the high and low subgroups to a publicized cohort of 47 patients who can react to anti-PD1 and anti-CTLA4 therapy by using unsupervised subclass mapping (https://cloud.genepattern.org/gp/) and thus predict the response of high and low subtypes to immunotherapy.

Finally, we constructed a GIS model of a PD1-treated NSCLC cohort (GSE135222) and a mature PDL1-treated urothelial carcinoma cohort (IMvigor210) to evaluate the predictive power of GIS for immunotherapy response rates. GSE135222 included 27 patients with NSCLC treated with PD1, and the IMvigor210 cohort included 298 patients with melanoma treated with PDL1 and has integrated clinical information.

Bioinformatics and statistical analysis

All statistical analyses and mappings were performed using R software version 4.04 (R Foundation for Statistical Computing, Vienna, Austria). The time-dependent area under the curve (AUC) was calculated using the R package "survivalROC" to evaluate the predictive power of variables. Univariate and multivariate COX regression analyses were performed using the R package "Survival." A nomogram was drawn using the "rms" package. The R package "DCA" was used to draw decision curve analysis (DCA) curves. The Kruskal–Wallis test was used to compare more than two groups and the Wilcoxon test to compare two groups. The proportion differences were compared by the chi-square test. KM plotters were used to generate survival curves for subgroups in each dataset. Pearson correlation was used for correlation tests.

Results

Preliminary screening of prognostic GRGs and IRGs in LUSC

We screened for independent prognostic factors in GRGs and IRGs in the training dataset (i.e., TCGA-LUSC cohort) and performed univariate Cox regression analysis to select genes that are significantly associated with prognosis. A total of 54 prognostic factors were identified, which included 48 risk factors and six protective factors (Figure 1A). Figure 1B displays their correlation network; six protective genes were negatively correlated with other genes, and 48 risk genes were positively correlated with other genes. Oncoplot presented mutation maps of prognostic factors in LUSC (Figure 1C). Specifically, the most common mutation of prognostic factors was a nonsense mutation, the most common change in base started from cytosine to thymine, and the *HGF* gene had the highest mutation frequency (Figure 1D). Fifty-four prognostic factors had extensive CNV events in LUSC (Figure 1E). The circle diagram presents their overall CNV status on chromosomes

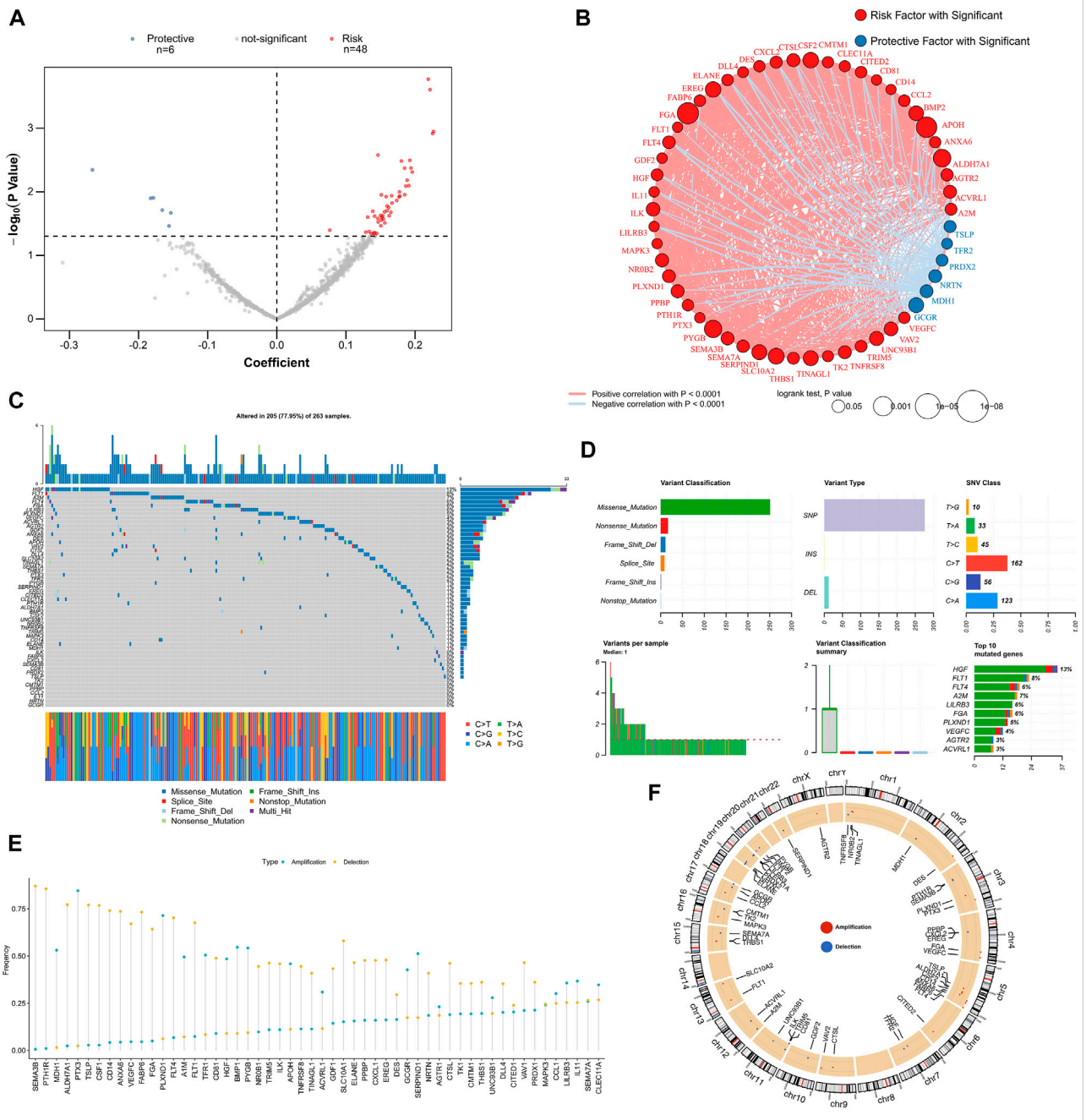


FIGURE 1
Identify prognostic-related GRGs and IRGs. **(A)** The volcano map illustrates the results of the univariate Cox analysis. **(B)** Correlation network of prognostic GRGs and IRGs. **(C)** Oncoplot displays mutation maps of prognostic GRGs and IRGs. **(D)** Summary of prognostic GRGs and IRGs mutation events in TCGA-LUSC. **(E)** Summary of CNV events for prognostic GRGs and IRGs in TCGA-LUSC. **(F)** The circle diagram presents the CNV maps of prognostic GRGs and IRGs on chromosomes. CNV, copy number variation; IRGs, immune-related genes; GRGs, glycolysis and immune score; TCGA-LUSC, The Cancer Genome Atlas Lung Squamous Cell Carcinoma.

(Figure 1F). Most of the mutations in prognostic genes were nonsense mutations, whereas CNV events occurred extensively, suggesting that prognostic genes were mainly regulated by CNV than by single nucleotide variation.

Generation and evaluation of GIS models

We used the random forest algorithm to identify the 10 most important genes among the 54 prognostic factors

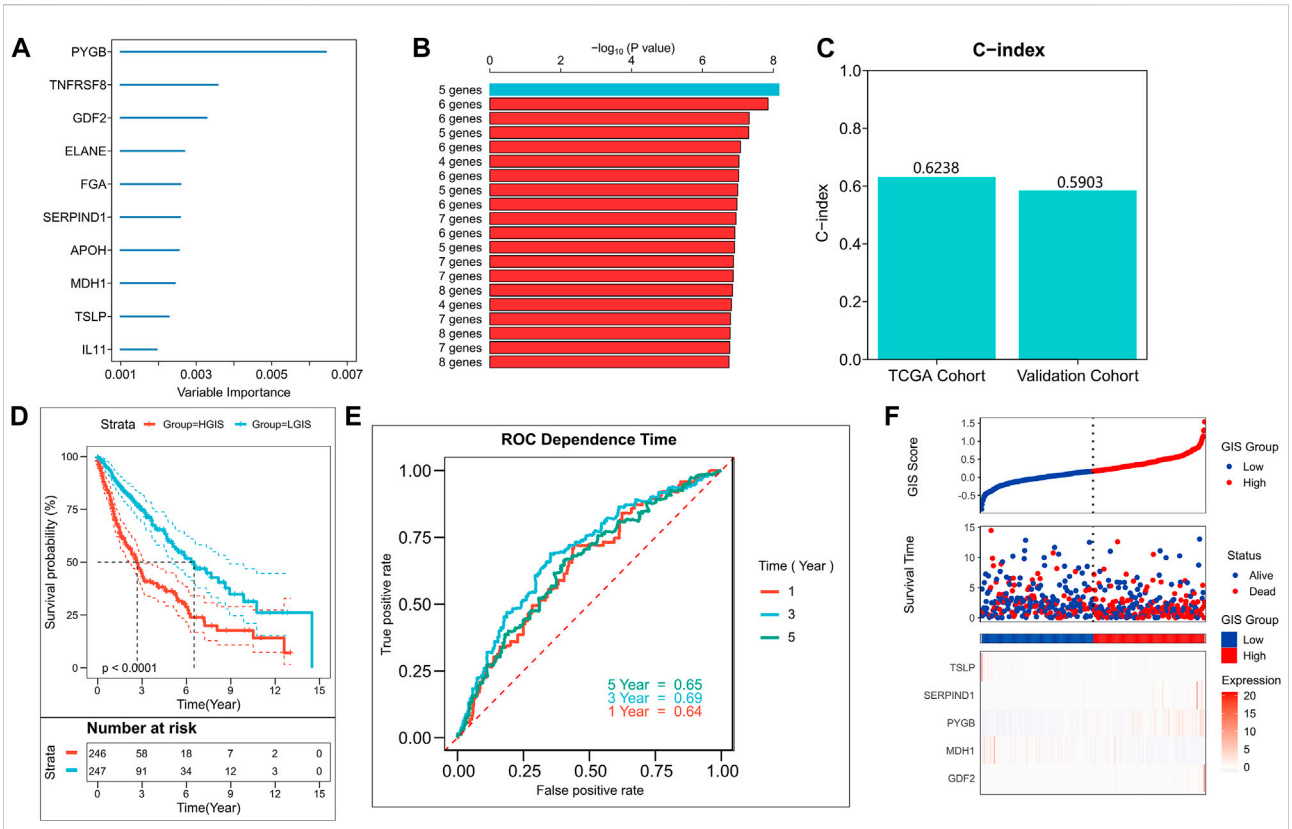


FIGURE 2
Construction of the GIS risk model. **(A)** Random forest screening of top10 important prognostic genes. **(B)** Log-rank test of *p*-value for each gene model. **(C)** C-index of the best model in TCGA and GEO queues. **(D)** KM survival curves of high and low GIS groups in the TCGA cohort. **(E)** ROC curves of GIS in the TCGA cohort at 1, 3, 5, and 8 years **(F)** Survival status and model gene expression of patients in the TCGA cohort. GEO, Gene Omnibus Expression; KM, Kaplan–Meier; ROC, receiver operating characteristics curve; GIS, glycolysis–immune score; TCGA, The Cancer Genome Atlas.

(Figure 2A). Then, we used the exhaustion method to find all combinations of the 10 genes and found 1,023 of them. A Cox regression model was constructed by gene combination, and the *p*-value of each model was evaluated by KM analysis. Finally, a five-gene model was selected to be the best prognostic model (Figure 2B), and detailed results are provided in Supplementary Table S3. The model contains two GRGs (*PYGB* and *MDH1*) and three IRGs (*TSLP*, *SERPIND1*, and *GDF2*), and the gene coefficients are listed in Supplementary Table S4. The C-index display model demonstrated good predictive performance in TCGA queues and external validation queues (Figure 2C). In the survival analysis, the survival rate of the high GIS group was significantly lower than that of the low GIS group (Figure 2D, $p < 0.0001$). The AUC values of the model at 1, 3, and 5 years were 0.64, 0.69, and 0.65, respectively (Figure 2E). Figure 2F presents the distribution of GIS in the TCGA cohort and the transcription map of the model genes. We also evaluated the effectiveness of GIS in an external validation queue. In the survival analysis, the survival of patients with high GIS was significantly worse (Supplementary Figure S1A, $p = 0.013$). In the ROC analysis, the AUC values of GIS in 1, 3, and 5 years were 0.61, 0.61, and 0.63, respectively (Supplementary Figure S1B). Supplementary Figure S1C illustrates the distribution of GIS in the GEO queue and the transcription map of the model genes.

Evaluation of the predictive independence of GIS models

We firstly used univariate Cox and multivariate Cox regressions to analyze the relationship between the risk score, clinical characteristics, and prognosis. Univariate Cox regression was an independent prognostic indicator in both training and validation sets (Figure 3A, $p < 0.01$). Multivariate Cox regression indicated that GIS was still an independent prognostic factor of overall survival in both training and validation cohorts after correcting other clinical features (Figure 3B, $p < 0.01$). The subgroup analysis also revealed

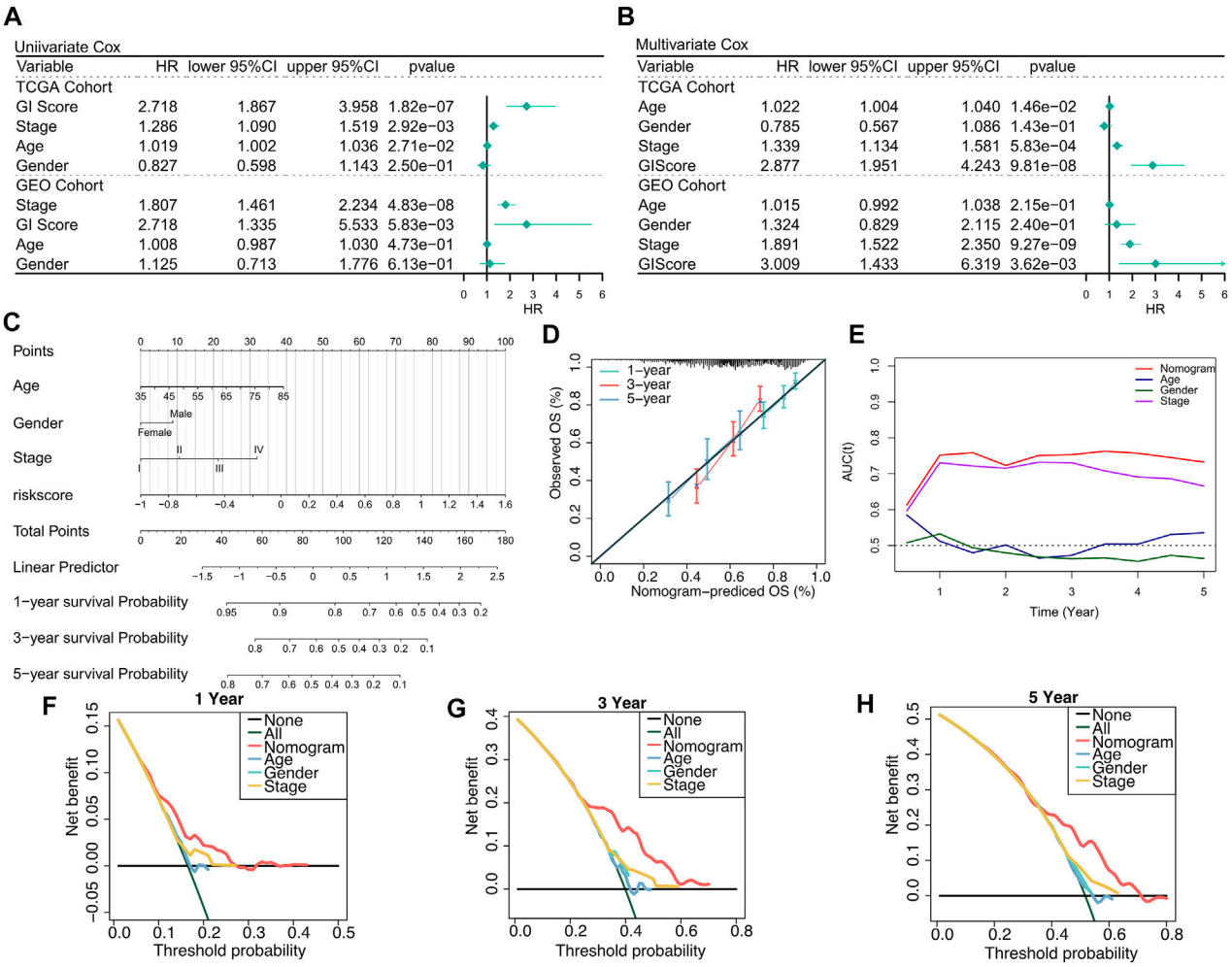


FIGURE 3
Verifying the GIS-related risk model. **(A)** Univariate Cox regression analysis of GIS and clinical features in the TCGA and GEO datasets. **(B)** Multivariate Cox regression analysis of GIS and clinical features in the TCGA and GEO datasets. **(C)** Nomogram based on the GIS model to quantify individual patient risk. **(D)** Nomogram calibration curve. **(E)** tROC curves of nomogram and clinical features. Nomogram DCA curves at 1 **(F)**, 3 **(G)**, and 5 **(H)** years. DCA, decision curve analysis; GEO, Gene Omnibus Expression; ROC, receiver operating characteristics curve; GIS, glycolysis–immune score; TCGA, The Cancer Genome Atlas.

that GIS remained a reliable prognostic factor in different clinical subgroups (Supplementary Figure S2). The GIS model proved to be a promising prognostic indicator for predicting the survival of patients with LUSC, and we subsequently constructed a nomogram to better quantify the risk assessment for these patients (Figure 3C). The nomogram correction curves reflected that the nomogram model had good stability and accuracy at 1, 3, and 5 years (Figure 3D). The TROC analysis revealed that the nomogram model was the best predictor when compared with clinical features (Figure 3E). We subsequently performed DCA to evaluate the decision benefits of the nomogram model and found that the nomogram is suitable for risk assessment of patients with LUSC at 1, 3, and 5 years (Figures 3F–H).

Functional enrichment analysis and glycolysis spectrum of GIS

Furthermore, we quantified the activity of some typical biological pathways using the ssGSEA algorithm and assessed the correlation between GIS and pathways. The heat map illustrates the relationship among GIS, biological pathway activity, classical glycolysis, and immune gene expression (Figure 4A). The corresponding correlation analysis is given on the right side of the heat map (Figure 4B). We found that EMT, hypoxia, and some immune-related pathways (such as the CCR, major histocompatibility complex [MHC] class 1, and type II interferon [IFN] response) GIS was significantly negatively correlated and significantly upregulated in the low

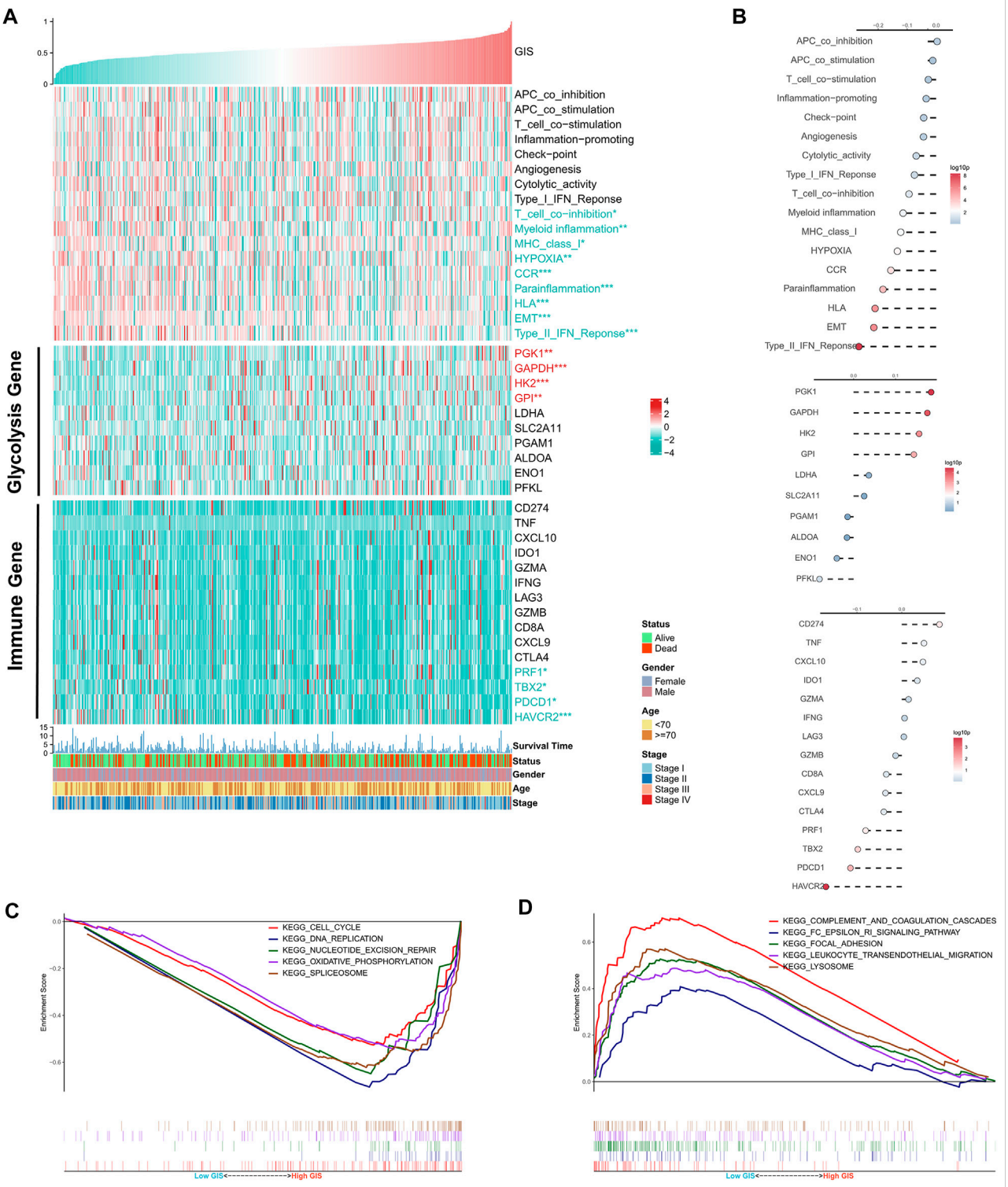


FIGURE 4
Functional analysis of the GIS risk model. **(A)** Heat maps of the correlations among GIS, biological pathway activity, glycolysis gene expression, immune gene expression, and clinical features. Red name with * represents upregulation in the high GIS group, and green name with * represents upregulation in the low GIS group; *$p < 0.05$, **$p < 0.01$, ***$p < 0.001$. **(B)** Correlation analysis of GIS and biological pathway activity, glycolysis gene expression, and immune gene expression (top to bottom). **(C)** GSEA enrichment map shows the five pathways of interest within the high GIS group. **(D)** GSEA enrichment map shows the five pathways of interest within the low GIS group. GIS, glycolysis–immune score; GSEA, gene set enrichment analysis.

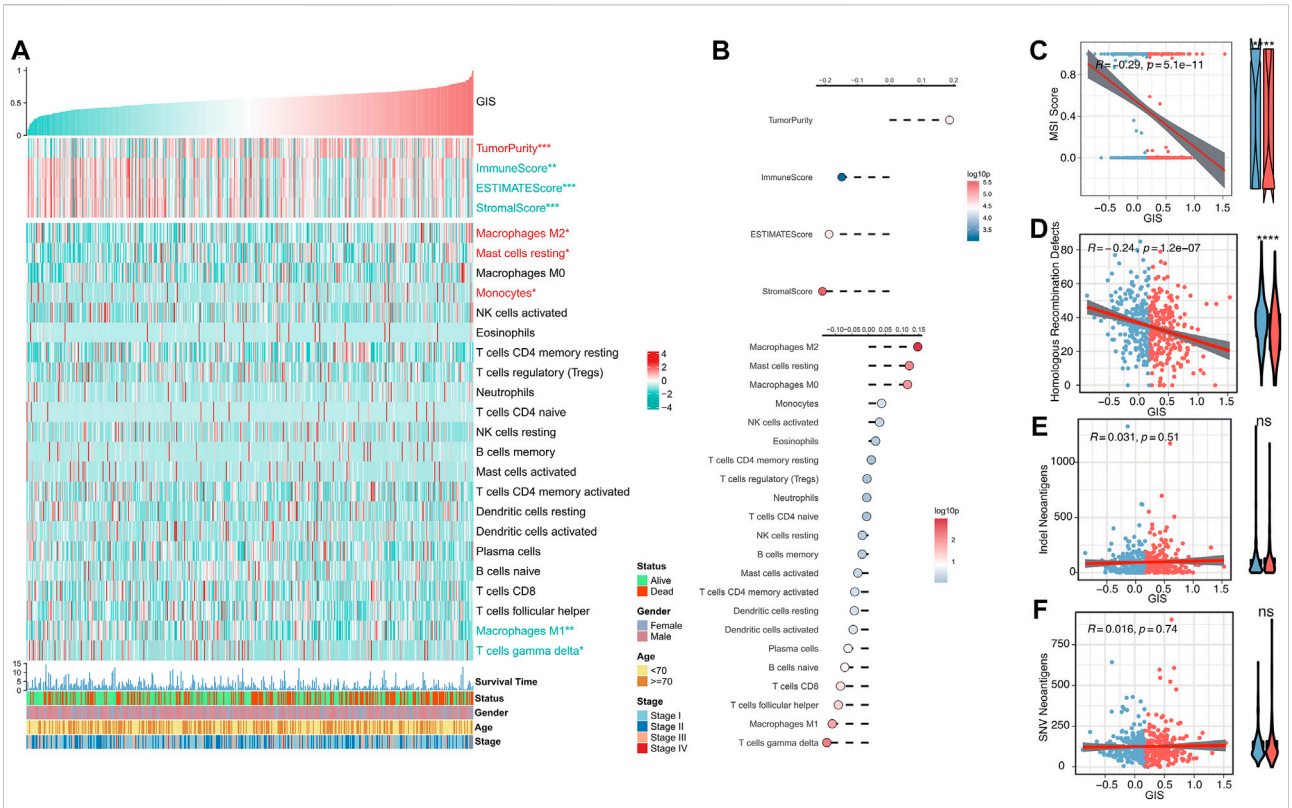


FIGURE 5
Immune landscape of the GIS risk model. **(A)** Heat maps of the correlations among GIS, estimate score, immune cell infiltration abundance, and clinical features. Red name with * represents upregulation in the high GIS group, and green name with * represents upregulation in the low GIS group; $^{*}p < 0.05$, $^{**}p < 0.01$, $^{***}p < 0.001$. **(B)** Correlation analysis of GIS, estimate score, and immune cell infiltration abundance (top to bottom). Scatter and box plots of the correlation between GIS and **(C)** MSI score, **(D)** HRD score, **(E)** indel neoantigens, and **(F)** SNV neoantigens. Indel, insertion and deletion; GIS, glycolysis–immune score; MSI, microsatellite instability; HRD, homologous recombination deficiency; SNV, single-nucleotide variant.

GIS group. In addition, four glycolysis genes were positively correlated with GIS and upregulated in high GIS, whereas four immunity genes were negatively correlated with GIS and upregulated in low GIS. GSEA revealed that cell cycle, oxidative stress, and DNA replication activity were significantly increased in the high GIS group (Figure 4C), whereas lysosome and lymphocyte migration pathways were significantly enriched in the low GIS group (Figure 4D). In summary, these results suggest increased glycolysis activity and active tumor replication and proliferation in the high GIS group, whereas increased immune and cytotoxic activity in the low GIS group.

Immune infiltration analysis of GIS

We further evaluated the correlation between GIS and immune landscape in detail. The heat map illustrates the correlation of GIS, estimate score, and abundance of immune-infiltrating cells (Figure 5A). The corresponding correlation analysis results are provided on the right side of the heat map (Figure 5B). The results revealed that patients with high GIS had higher tumor purity, whereas patients with low GIS had increased immune scores and estimate scores. Immune cell infiltration analysis also indicated that GIS was positively correlated with M2 macrophages and mast cells and increased in the high GIS group, whereas M1 macrophages and gamma delta T cells were negatively correlated with GIS and increased in the low GIS group. These results further suggest that antitumor immunity is suppressed in patients with high GIS, whereas antitumor immunity is active in patients with low GIS. Furthermore, we analyzed four indexes that affect the response to immunotherapy. Accordingly, the MSI and HRD scores were significantly negatively correlated with GIS and increased in the low GIS group (Figure 5C,D). This suggests that patients with low GIS have more chromosomal instability, leading to more tumor-specific neoantigen generation (Ganesh et al., 2019; Eso et al., 2020; Shi et al., 2021). However, no difference was found in insertion and deletion (indel) neoantigens and single-nucleotide variant (SNV) neoantigens between the high and low GIS groups (Figure 5E,F).

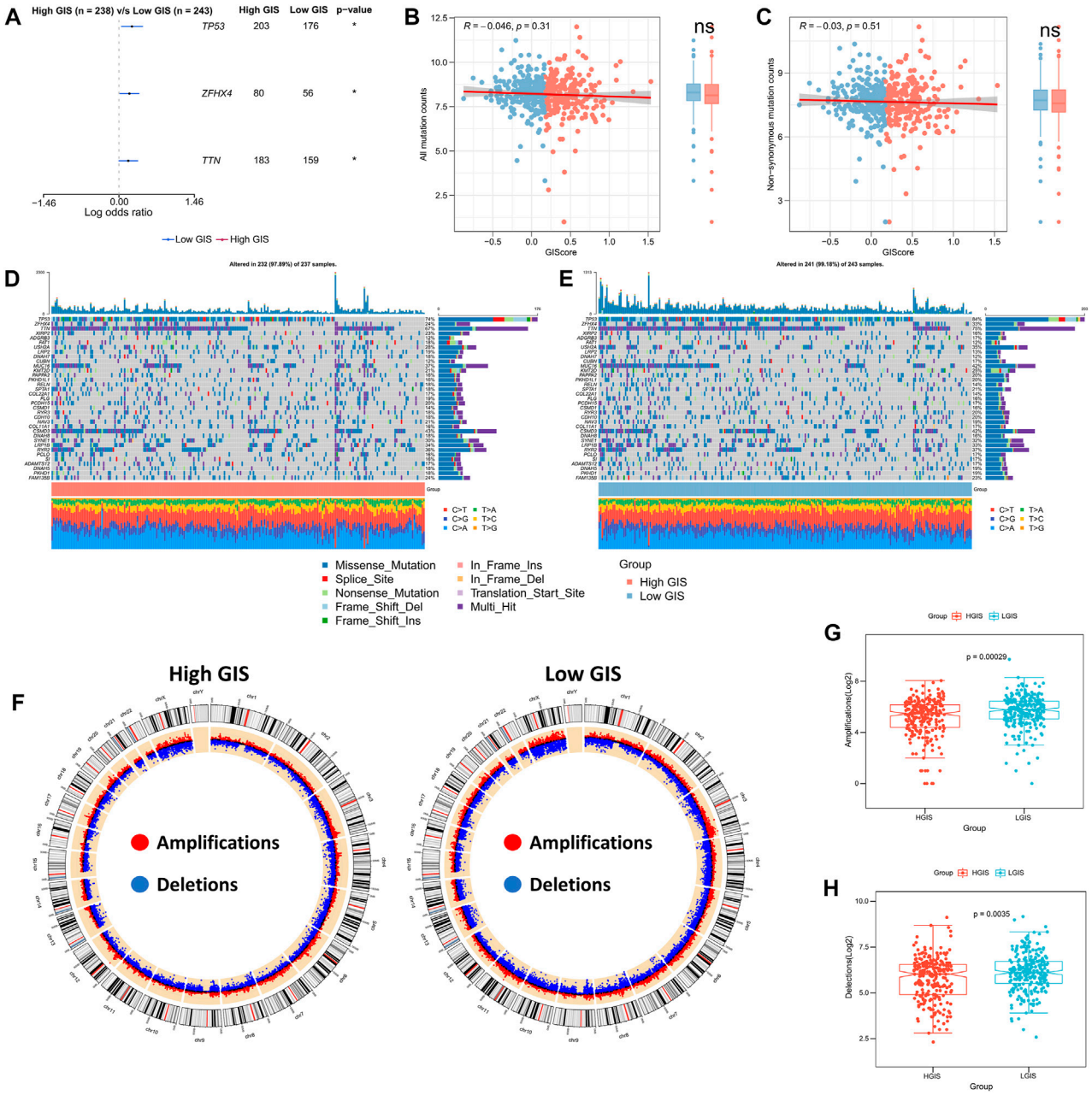


FIGURE 6
Genomic mutation landscapes of GIS models. **(A)** Forest map of the high-frequency mutated genes with significant mutation differences between the high GIS and low GIS groups. **(B)** Correlation between GIS and all mutant loads. **(C)** Correlation between GIS and non-synonymous mutation load. **(D)** Oncoplot of the high-frequency mutated genes in the high GIS group. **(E)** Oncoplot of the high-frequency mutated genes in the low GIS group. **(F)** Circle diagram summarizing CNV events on different chromosome arms in the high and low GIS groups. **(G)** Box plot of the difference in chromosome amplification between the high GIS and low GIS groups. **(H)** Box plot of the difference in chromosome deletions between the high GIS group and the low GIS group. GIS, glycolysis–immune score; CNV, copy number variation.

Correlation between GIS and genome changes

Recent studies have proposed using the tumor mutation burden (TMB) as a novel indicator in predicting immunotherapy response and prognosis, as more mutated genes may generate new antigenic peptides that can be recognized by the immune system. Antigens containing mutated peptides can activate the immune system and enhance anti-tumor immunity (Matsushita et al., 2012; Rizvi

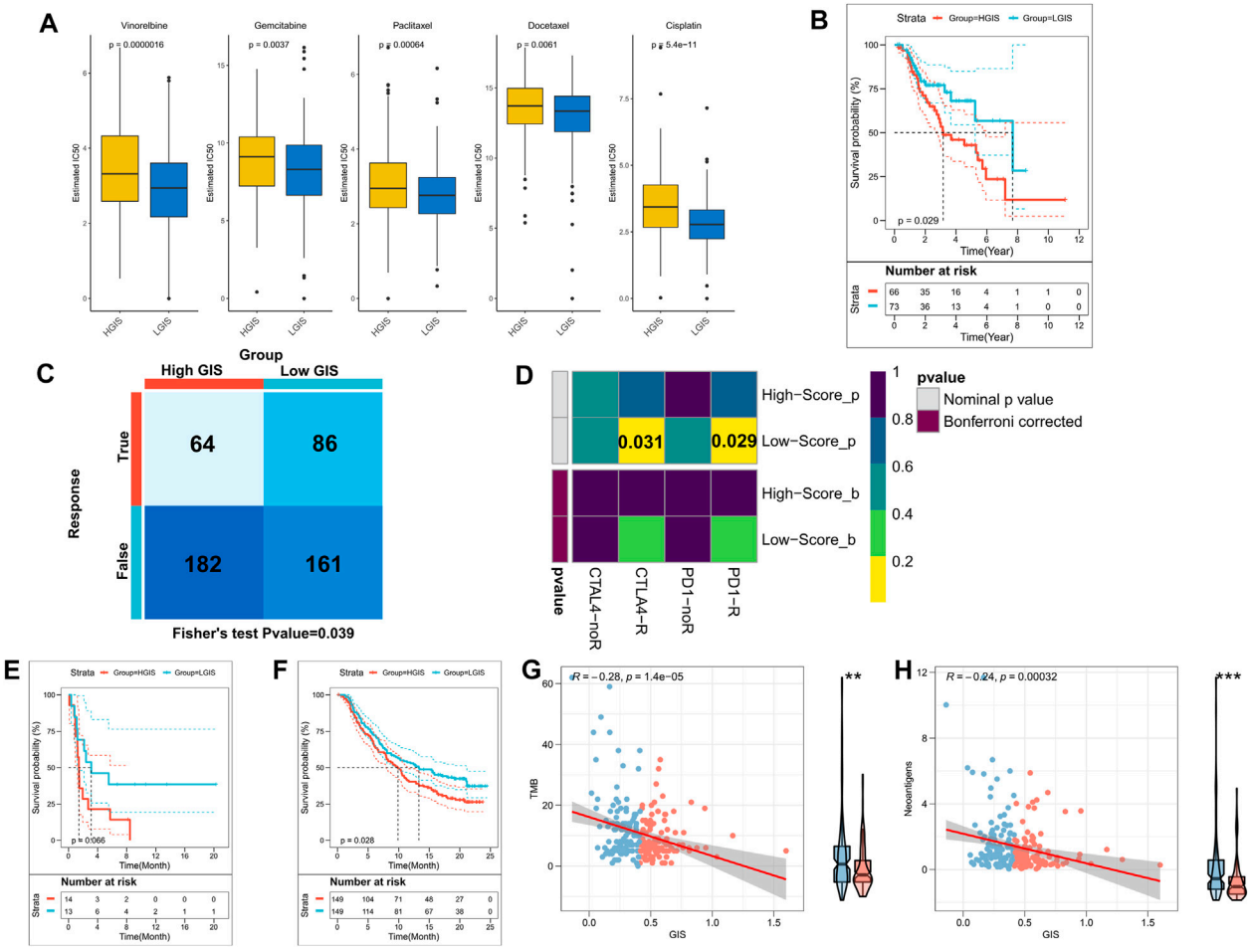


FIGURE 7
The GIS model guides the clinical treatment decision. **(A)** Box plot of the predicted IC50 values of five commonly used lung cancer drugs in the high and low GIS groups. **(B)** KM survival curves of patients receiving chemotherapy in the TCGA cohorts with high and low GIS. **(C)** The TIDE algorithm was used to predict the overall response rate to immunotherapy in the high and low GIS groups. **(D)** Subclass mapping was used to predict the sensitivity of patients in the high and low GIS groups to anti-PD1 and anti-CTLA4 therapy. **(E)** KM survival curves of high and low GIS groups in the GSE135222 cohort. **(F)** KM survival curves of the high and low GIS groups in the IMvigor210 cohort. **(G)** Correlation between GIS and TMB in the IMvigor210 cohort. **(H)** Correlation between GIS and neoantigens in the IMvigor210 cohort. GIS, glycolysis–immune score; GSEA, gene set enrichment analysis; TMB, tumor mutation burden; KM, Kaplan–Meier; TCGA, The Cancer Genome Atlas; TIDE, Tracking of Indels by Decomposition.

et al., 2015; Chan et al., 2019). Therefore, we explore the correlation between TMB and GIS. Through Fisher's test, we identified three high-frequency mutated genes with significant mutation differences, namely, *TP53*, *ZFHX4*, and *TTN*, with increased mutation frequency in the low GIS group (Figure 6A). However, the number of mutation techniques and non-synonymous mutations demonstrated an increasing trend in the low GIS group, but it was not significant (Figures 6B,C). The waterfall diagram illustrates the mutation maps of high-frequency mutated genes in the high and low GIS groups (Figures 6D,E). CNV caused genomic changes in patients as chromosome segment changes, and we subsequently analyzed the correlation between CNV and GIS. The circle graph presents the overall CNV landscape of patients with high and low GIS, and the results revealed that patients with low GIS have more CNV events (Figure 6F). The box plot illustrates that both amplification and missing events in the low GIS group were significantly higher than those in the high GIS group (Figures 6G,H).

The GIS model can guide clinical treatment decision

We firstly assessed the sensitivity of patients to five commonly used chemotherapy agents for lung cancer, namely,

cisplatin, docetaxel, gemcitabine, paclitaxel, and vinorelbine. Accordingly, patients with low GIS were more sensitive to these five chemotherapeutic agents (Figure 7A). In the validation cohort, the low GIS group was more sensitive to the other four drugs, except for gemcitabine (Supplementary Figure S1D). The survival analysis revealed that among patients receiving chemotherapy in the TCGA cohort, survival was better in patients with low GIS (Figure 7B, $p = 0.029$). Previous results suggested that patients with low GIS may be more sensitive to immunotherapy; thus, we subsequently assessed patient response to immunotherapy. In the TIDE analysis, patients with low GIS were more sensitive to immunotherapy (Figure 7C), although not significant in the validation cohort (Supplementary Figure S1E). Subclass mapping indicated that patients with low GIS were more sensitive to anti-PD-1 and anti-CTLA-4 therapy, and the same results were observed in the validation cohort (Figure 7D, Supplementary Figure S1F). Subsequently, we validated GIS in an NSCLC cohort that received anti-PD-1 therapy, and the results presented poorer survival in patients with high GIS (Figure 7E, $p = 0.066$). The efficacy of GIS was also evaluated in IMvigor210, a large immunotherapy cohort, which exhibited significantly worse survival in patients with high GIS (Figure 7F). Further analysis revealed that TMB and neoantigens were negatively correlated with GIS in the IMvigor210 cohort and significantly increased in the low GIS group (Figures 7G,H). This may explain the high benefit of immunotherapy in patients with low GIS.

Discussion

With the limited success of LUSC-related targeted therapies, traditional chemotherapy remains the first-line treatment for decades; thus, patients with advanced LUSC treated with current chemotherapy show poor 5-years survival rates, that is, less than 5%. Therefore, there is an urgent need to identify prognostic biomarkers to accurately and timely predict clinical outcomes of LUSC and initiate personalized treatment programs. Glycolysis not only plays an important role in tumor invasion and drug resistance but also has a strong inhibitory effect on the TIME (Brand et al., 2016; Watson et al., 2021). The complex role of glycolysis and TIME reflects great promise in immunotherapy and targeted cancer therapy (Ganapathy-Kanniappan and Geschwind, 2013; Ganapathy-Kanniappan, 2017). In this study, we constructed a GIS model based on GRGs and IRGs and demonstrated that this model has satisfactory predictive efficacy in different clinical subgroups of datasets. Therefore, it can be used as an independent prognostic factor for patients with LUSC. Furthermore, we explored the relationship between the GIS model and biological function, immune cell infiltration, and genome changes. Several transcriptomic models are proved to have promising applications in lung cancer and have surprising potential in predicting prognosis (Wang et al., 2021a; Gao et al., 2021; Feng et al., 2022; Guo et al., 2022; Jiang et al., 2022). Compared with these models, our model not only has good performance in predicting prognosis but also can distinguish between "cold" and "hot" tumors and provide a reference for clinical treatment decisions of patients with LUSC.

Immunotherapy has developed rapidly in LUSC in recent years (Lazzari et al., 2017). LUSC tends to be highly immunogenic and has higher TMB. Therefore, LUSC is an ideal indication for immunotherapy (Li et al., 2018). However, the overall response rate to immunotherapy is relatively low, and only a subset of patients with LUSC can benefit from immunotherapy (Forde et al., 2018). Therefore, the identification of patients with LUSC having "hot" tumors is expected to enhance treatment response to immunotherapy. Through functional enrichment analysis, we found that low GIS was associated with increased activity of some immune-related pathways, such as CCR, MHC class 1, and type II IFN response, and lysosome and lymphocyte migration, suggesting that the low GIS group was a "hot" tumor with anti-tumor immunoactivity (Ivashkiv, 2018; Dersh et al., 2021). We also analyzed the immune cell infiltration in the low GIS group and we found that the low GIS group had higher immune scores and increased M1 macrophages and gamma delta T cells, suggesting that low GIS tumors are immuno-activated "hot" tumors with antitumor activity (Chanmee et al., 2014; Kabelitz et al., 2020; Yazdanifar et al., 2020). The cell cycle and DNA replication pathway were enriched in the high GIS group, indicating that tumor proliferation was active in this group. Furthermore, oxidative stress activity increased in the high GIS group, and oxidative stress stimulates tumorigenesis and supports tumor cell proliferation (Hayes et al., 2020; Kotsafti et al., 2020). Moreover, high GIS was associated with increased glycolysis activity, and low GIS was associated with increased immune gene activity. Furthermore, we analyzed the immune cell infiltration in the TIME of high GIS group, and the results revealed that a high GIS was associated with higher tumor purity and M2 macrophages, which may lead to immunosuppression and tumor-promoting TIME (Chanmee et al., 2014) in the high GIS group. These results suggest that high GIS could identify patients with "cold" tumors, high glycolysis, metabolically active tumors, and suppressed antitumor immunity. Subsequently, we found that the HRD and MSI scores were negatively correlated with GIS and significantly increased in the low GIS group, indicating that tumors with low GIS may be more sensitive to chemotherapy, have high immunogenicity, and are more sensitive to immunotherapy (Le et al., 2017; Overman et al., 2017; Hoppe et al., 2018; Silva et al., 2022). However, no significant difference was found in the number of neoantigens between the two groups.

We subsequently found that *TP53*, *ZFHX4,* and *TTN* mutated more frequently in the low GIS group. *TP53* is

generally considered a tumor-suppressor gene (Bykov et al., 2018; Skoulidis and Heymach, 2019), whereas the *TP53* gene in the low GIS group shows a better survival rate and more mutations, which may be caused by the active immune function of low GIS. Recent studies have reported that genomic changes are closely related to neoantigen formation and immunotherapy response (Anagnostou et al., 2017). Our results indicate that TMB differences between low and high GIS groups are not significant, and GIS can better reflect patients' immune activity than TMB. We also found that both CNV amplification and deletion events were significantly higher in the low GIS group, and the chromosomal changes were more closely related to GIS than the single nucleotide variation. Studies have shown that chromosomal somatic rearrangement events actively promote carcinogenesis and lead to immunosuppression. However, our analysis showed that immunoactivity was stronger in the low GIS group than in the high GIS group. These results suggest that GIS can better reflect tumor immune status and predict immunotherapy response than TMB and CNV.

In summary, low GIS appears to indicate "hot" tumors with an immunoactivated phenotype that may be more sensitive to treatment. We then systematically assessed patient response to chemotherapy and immunotherapy. Accordingly, we found that the low GIS group was more sensitive to chemotherapy than the high GIS group. In addition, TIDE and subclass mapping algorithms predicted that patients with low GIS would be more sensitive to immunotherapy. More convincingly, we found that a low GIS was associated with better outcomes in the immunotherapy cohort of NSCLC. In a further large-scale immunotherapy cohort, IMvigor210, better survival was observed in patients with low GIS. A negative correlation was noted between GIS and TMB and neoantigens in the IMvigor210 cohort. Immunotherapy mainly relies on $CD8^+$ T cells to recognize tumor-specific mutant antigens to induce antitumor immunity (Wang et al., 2021b; Jhunjhunwala et al., 2021). In addition, more somatic mutations will lead to the formation of more potential new antigens (Matsushita et al., 2012; Rizvi et al., 2015). Therefore, more neoantigens and TMB in the low GIS group may lead to the increased sensitivity of patients with low GIS to immunotherapy. Taken together, these results demonstrate that the GIS model is a powerful tool for guiding the treatment of patients with LUSC and that patients with low GIS have a higher sensitivity to chemotherapy and immunotherapy.

Despite its findings, this study has some limitations. First, this study was based on high-throughput sequencing and only considered inter-patient heterogeneity, but there was no intra-tumor heterogeneity. Second, immunotherapy and chemotherapy sensitivity predictions are based on computations and should be validated in further clinical cohorts. Thus, additional *in vivo* and *in vitro* experiments are needed to explore the specific biological functions of GIS in LUSC.

In conclusion, the results of this study suggest a close relationship between glycolysis and immune activity. Moreover, the integrated model based on glycolysis and immune genes can distinguish "cold and hot" patterns of individual tumors from biological function and immune infiltrating system, can quantitatively estimate the prognosis of patients LUSC, and guide chemotherapy and immunotherapy decisions.We thank all the participants who supported our study. In particular, thanks to the TCGA database and GEO database for the analytical data.

Data availability statement

The raw data mentioned in this study can be downloaded from online databases. More detailed information can be provided by the corresponding author upon reasonable request.

Author contributions

QH analyzed the data and wrote the manuscript. SY and HY provided specialized expertise and collaboration in data analysis. HC and YuW carried out data interpretations and helped data discussion. YaW conceived and designed the whole project and drafted the manuscript. All authors read and approved the final manuscript.

Acknowledgments

We thank all the participants who supported our study. In particular, thanks to the TCGA database and GEO database for the analytical data.

Conflict of interest

The authors declare that the research was conducted in the absence of any commercial or financial relationships that could be construed as a potential conflict of interest.

Publisher's note

All claims expressed in this article are solely those of the authors and do not necessarily represent those of their affiliated organizations, or those of the publisher, the editors and the reviewers. Any product that may be evaluated in this article, or claim that may be made by its manufacturer, is not guaranteed or endorsed by the publisher.

Supplementary material

The Supplementary Material for this article can be found online at: https://www.frontiersin.org/articles/10.3389/fgene.2022.907058/full#supplementary-material

SUPPLEMENTARY FIGURE S1
External validation of GIS **(A)** KM survival curves of high and low GIS groups in the GEO cohort. **(B)** ROC curves of GIS in the GEO cohort at 1, 3, 5, and 8 years **(C)** GIS, survival status, and model gene expression profile of patients in the GEO cohort. **(D)** Box plot of the predicted IC50 values of five commonly used lung cancer drugs in the high and low GIS groups of the GEO cohort. **(E)** The TIDE algorithm was used to predict the response of high and low GIS groups to immunotherapy in the GEO cohort. **(F)** Subclass mapping was used to predict the sensitivity of patients in the high and low GIS groups to anti-PD1 and anti-CTLA4 treatment in the GEO cohort. GIS, glycolysis–immune score; KM, Kaplan–Meier; GEO, Gene Omnibus Expression; TIDE, Tracking of Indels by Decomposition; PD1, programmed death-1 (PD1); CTLA4, anti-cytotoxic T-lymphocyte-associated protein 4.

SUPPLEMENTARY FIGURE S2
Subgroup Cox analysis of GIS Subgroup Cox regression analysis of GIS in the TCGA queue (A) and GEO queue (B). GIS, glycolysis–immune score; GEO, Gene Omnibus Expression; TCGA, The Cancer Genome Atlas.

References

Anagnostou, V., Smith, K. N., Forde, P. M., Niknafs, N., Bhattacharya, R., White, J., et al. (2017). Evolution of neoantigen landscape during immune checkpoint blockade in non-small cell lung cancer. *Cancer discovery. Cancer Discov.* 7 (3), 264–276. doi:10.1158/2159-8290.Cd-16-0828

Ayers, M., Lunceford, J., Nebozhyn, M., Murphy, E., Loboda, A., Kaufman, D. R., et al. (2017). IFN-γ-related mRNA profile predicts clinical response to PD-1 blockade. *J. Clin. Invest.* 127 (8), 2930–2940. doi:10.1172/jci91190

Brand, A., Singer, K., Koehl, G. E., Kolitzus, M., Schoenhammer, G., Thiel, A., et al. (2016). LDHA-associated lactic acid production blunts tumor immunosurveillance by T and NK cells. *Cell metabolism. Cell Metab.* 24 (5), 657–671. doi:10.1016/j.cmet.2016.08.011

Bykov, V. J. N., Eriksson, S. E., Bianchi, J., and Wiman, K. G. (2018). Targeting mutant p53 for efficient cancer therapy. *Nat. Rev. Cancer* 18 (2), 89–102. doi:10.1038/nrc.2017.109

Chan, T. A., Yarchoan, M., Jaffee, E., Swanton, C., Quezada, S. A., Stenzinger, A., et al. (2019). Development of tumor mutation burden as an immunotherapy biomarker: Utility for the oncology clinic. *Ann. Oncol.* 30 (1), 44–56. doi:10.1093/annonc/mdy495

Chanmee, T., Ontong, P., Konno, K., and Itano, N. (2014). Tumor-associated macrophages as major players in the tumor microenvironment. *Cancers* 6 (3), 1670–1690. doi:10.3390/cancers6031670

Chen, Z., Fillmore, C. M., Hammerman, P. S., Kim, C. F., and Wong, K. K. (2014). Non-small-cell lung cancers: A heterogeneous set of diseases. *Nat. Rev. Cancer* 14 (8), 535–546. doi:10.1038/nrc3775

Colegio, O. R., Chu, N. Q., Szabo, A. L., Chu, T., Rhebergen, A. M., Jairam, V., et al. (2014). Functional polarization of tumour-associated macrophages by tumour-derived lactic acid. *Nature* 513 (7519), 559–563. doi:10.1038/nature13490

Dersh, D., Hollý, J., and Yewdell, J. W. (2021). A few good peptides: MHC class I-based cancer immunosurveillance and immunoevasion. *Nature reviews immunology. Nat. Rev. Immunol.* 21 (2), 116–128. doi:10.1038/s41577-020-0390-6

Drilon, A., Rekhtman, N., Ladanyi, M., and Paik, P. (2012). Squamous-cell carcinomas of the lung: Emerging biology, controversies, and the promise of targeted therapy. *Lancet. Oncol.* 13 (10), e418–26. doi:10.1016/s1470-2045(12)70291-7

Eso, Y., Shimizu, T., Takeda, H., Takai, A., and Marusawa, H. (2020). Microsatellite instability and immune checkpoint inhibitors: Toward precision medicine against gastrointestinal and hepatobiliary cancers. *Journal of gastroenterology. J. Gastroenterol.* 55 (1), 15–26. doi:10.1007/s00535-019-01620-7

Feng, S., Zhang, X., Gu, X., Zhou, M., Chen, Y., and Wang, C. (2022). Identification of six novel prognostic gene signatures as potential biomarkers in Small Cell Lung Cancer. *Comb. Chem. High. Throughput Screen.* 25. doi:10.2174/1386207325666220427121619

Forde, P. M., Chaft, J. E., Smith, K. N., Anagnostou, V., Cottrell, T. R., Hellmann, M. D., et al. (2018). Neoadjuvant PD-1 blockade in resectable lung cancer. *N. Engl. J. Med.* 378 (21), 1976–1986. doi:10.1056/NEJMoa1716078

Ganapathy-Kanniappan, S., and Geschwind, J. F. (2013). Tumor glycolysis as a target for cancer therapy: Progress and prospects. *Mol. Cancer* 12, 152. doi:10.1186/1476-4598-12-152

Ganapathy-Kanniappan, S. (2017). Linking tumor glycolysis and immune evasion in cancer: Emerging concepts and therapeutic opportunities. *Biochim. Biophys. Acta. Rev. Cancer* 1868 (1), 212–220. doi:10.1016/j.bbcan.2017.04.002

Ganesh, K., Stadler, Z. K., Cercek, A., Mendelsohn, R. B., Shia, J., Segal, N. H., et al. (2019). Immunotherapy in colorectal cancer: Rationale, challenges and potential. *Nature reviews gastroenterology & hepatology. Nat. Rev. Gastroenterol. Hepatol.* 16 (6), 361–375. doi:10.1038/s41575-019-0126-x

Gao, C., Gu, X., Chen, Y., Zhou, M., Jiang, F., and Zheng, S. (2021). Identification of potential prognostic and predictive biomarkers for immune-checkpoint inhibitor response in small cell lung cancer. *Med. Sci. Monit.* 27, e932275. doi:10.12659/msm.932275

Gibbons, D. L., and Creighton, C. J. (2018). Pan-cancer survey of epithelial-mesenchymal transition markers across the cancer genome Atlas. *Developmental dynamics : An official publication of the American Association of anatomists. Dev. Dyn.* 247 (3), 555–564. doi:10.1002/dvdy.24485

Guo, C. R., Mao, Y., Jiang, F., Juan, C. X., Zhou, G. P., and Li, N. (2022). Computational detection of a genome instability-derived lncRNA signature for predicting the clinical outcome of lung adenocarcinoma. *Cancer Med.* 11 (3), 864–879. doi:10.1002/cam4.4471

Hanahan, D., and Weinberg, R. A. (2011). Hallmarks of cancer: The next generation. *Cell* 144 (5), 646–674. doi:10.1016/j.cell.2011.02.013

Hayes, J. D., Dinkova-Kostova, A. T., and Tew, K. D. (2020). Oxidative stress in cancer. *Cancer Cell* 38 (2), 167–197. doi:10.1016/j.ccell.2020.06.001

Hoppe, M. M., Sundar, R., Tan, D. S. P., and Jeyasekharan, A. D. (2018). Biomarkers for homologous recombination deficiency in cancer. *J. Natl. Cancer Inst.* 110 (7), 704–713. doi:10.1093/jnci/djy085

Icard, P., and Lincet, H. (2016). The reduced concentration of citrate in cancer cells: An indicator of cancer aggressiveness and a possible therapeutic target. *Drug resistance updates : Reviews and commentaries in antimicrobial and anticancer chemotherapy. Drug resist. updat.* 29, 47–53. doi:10.1016/j.drup.2016.09.003

Icard, P., Shulman, S., Farhat, D., Steyaert, J. M., Alifano, M., and Lincet, H. (2018). How the Warburg effect supports aggressiveness and drug resistance of cancer cells? *Drug resist. updat.* 38, 1–11. doi:10.1016/j.drup.2018.03.001

Ivashkiv, L. B. (2018). IFNγ: Signalling, epigenetics and roles in immunity, metabolism, disease and cancer immunotherapy. *Nat. Rev. Immunol.* 18 (9), 545–558. doi:10.1038/s41577-018-0029-z

Jhunjhunwala, S., Hammer, C., and Delamarre, L. (2021). Antigen presentation in cancer: Insights into tumour immunogenicity and immune evasion. *Nat. Rev. Cancer* 21 (5), 298–312. doi:10.1038/s41568-021-00339-z

Jiang, F., Hu, Y., Liu, X., Wang, M., and Wu, C. (2022). Methylation pattern mediated by m(6)A regulator and tumor microenvironment invasion in lung adenocarcinoma. *Oxid. Med. Cell. Longev.* 2022, 2930310. doi:10.1155/2022/2930310

Kabelitz, D., Serrano, R., Kouakanou, L., Peters, C., and Kalyan, S. (2020). Cancer immunotherapy with γδ T cells: Many paths ahead of us. *Cellular & molecular immunology. Cell. Mol. Immunol.* 17 (9), 925–939. doi:10.1038/s41423-020-0504-x

Kotsafti, A., Scarpa, M., Castagliuolo, I., and Scarpa, M. (2020). Reactive oxygen species and antitumor immunity-from surveillance to evasion. *Cancers* 12 (7), E1748. doi:10.3390/cancers12071748

Lazzari, C., Karachaliou, N., Gregorc, V., Bulotta, A., Gonzalez-Cao, M., Verlicchi, A., et al. (2017). Second-line therapy of squamous non-small cell lung cancer: An evolving landscape. *Expert Rev. Respir. Med.* 11 (6), 469–479. doi:10.1080/17476348.2017.1326822

Le, D. T., Durham, J. N., Smith, K. N., Wang, H., Bartlett, B. R., Aulakh, L. K., et al. (2017). Mismatch repair deficiency predicts response of solid tumors to PD-1 blockade. *Sci. (New York, NY)* 357 (6349), 409–413. doi:10.1126/science.aan6733

Li, X., Shao, C., Shi, Y., and Han, W. (2018). Lessons learned from the blockade of immune checkpoints in cancer immunotherapy. *J. Hematol. Oncol.* 11 (1), 31. doi:10.1186/s13045-018-0578-4

Liang, J. Y., Wang, D. S., Lin, H. C., Chen, X. X., Yang, H., Zheng, Y., et al. (2020). A novel ferroptosis-related gene signature for overall survival prediction in patients with hepatocellular carcinoma. *Int. J. Biol. Sci.* 16 (13), 2430–2441. doi:10.7150/ijbs.45050

Liberzon, A., Subramanian, A., Pinchback, R., Thorvaldsdóttir, H., Tamayo, P., and Mesirov, J. P. (2011). Molecular signatures database (MSigDB) 3.0. *Bioinforma. Oxf. Engl.* 27 (12), 1739–1740. doi:10.1093/bioinformatics/btr260

Lu, J., Tan, M., and Cai, Q. (2015). The Warburg effect in tumor progression: Mitochondrial oxidative metabolism as an anti-metastasis mechanism. *Cancer Lett.* 356 (2), 156–164. doi:10.1016/j.canlet.2014.04.001

Matsushita, H., Vesely, M. D., Koboldt, D. C., Rickert, C. G., Uppaluri, R., Magrini, V. J., et al. (2012). Cancer exome analysis reveals a T-cell-dependent mechanism of cancer immunoediting. *Nature* 482 (7385), 400–404. doi:10.1038/nature10755

McDermott, D. F., Huseni, M. A., Atkins, M. B., Motzer, R. J., Rini, B. I., Escudier, B., et al. (2018). Clinical activity and molecular correlates of response to atezolizumab alone or in combination with bevacizumab versus sunitinib in renal cell carcinoma. *Nature medicine. Nat. Med.* 24 (6), 749–757. doi:10.1038/s41591-018-0053-3

Overman, M. J., McDermott, R., Leach, J. L., Lonardi, S., Lenz, H. J., Morse, M. A., et al. (2017). Nivolumab in patients with metastatic DNA mismatch repair-deficient or microsatellite instability-high colorectal cancer (CheckMate 142): An open-label, multicentre, phase 2 study. *Lancet. Oncol.* 18 (9), 1182–1191. doi:10.1016/s1470-2045(17)30422-9

Rizvi, N. A., Hellmann, M. D., Snyder, A., Kvistborg, P., Makarov, V., Havel, J. J., et al. (2015). Cancer immunology. Mutational landscape determines sensitivity to PD-1 blockade in non-small cell lung cancer. *Sci. (New York, NY)* 348 (6230), 124–128. doi:10.1126/science.aaa1348

Schröder, M. S., Culhane, A. C., Quackenbush, J., and Haibe-Kains, B. (2011). survcomp: an R/Bioconductor package for performance assessment and comparison of survival models. *Bioinforma. Oxf. Engl.* 27 (22), 3206–3208. doi:10.1093/bioinformatics/btr511

Shi, Z., Zhao, Q., Lv, B., Qu, X., Han, X., Wang, H., et al. (2021). Identification of biomarkers complementary to homologous recombination deficiency for improving the clinical outcome of ovarian serous cystadenocarcinoma. *Clin. Transl. Med.* 11 (5), e399. doi:10.1002/ctm2.399

Siegel, R. L., Miller, K. D., and Jemal, A. (20202020). Cancer statistics, 2020. *Ca. Cancer J. Clin.* 70 (1), 7–30. doi:10.3322/caac.21590

Silva, S. B., Wanderley, C. W. S., and Colli, L. M. (2022). Immune checkpoint inhibitors in tumors harboring homologous recombination deficiency: Challenges in attaining efficacy. *Front. Immunol.* 13, 826577. doi:10.3389/fimmu.2022.826577

Skoulidis, F., and Heymach, J. V. (2019). Co-occurring genomic alterations in non-small-cell lung cancer biology and therapy. *Nat. Rev. Cancer* 19 (9), 495–509. doi:10.1038/s41568-019-0179-8

Sun, S., Schiller, J. H., Spinola, M., and Minna, J. D. (2007). New molecularly targeted therapies for lung cancer. *J. Clin. Invest.* 117 (10), 2740–2750. doi:10.1172/jci31809

Thorsson, V., Gibbs, D. L., Brown, S. D., Wolf, D., Bortone, D. S., Ou Yang, T. H., et al. (2018). The immune landscape of cancer. *Immunity* 48 (4), 812–830. e14. doi:10.1016/j.immuni.2018.03.023

Wang, C., Gu, X., Zhang, X., Zhou, M., and Chen, Y. (2021). Development and validation of an E2F-related gene signature to predict prognosis of patients with lung squamous cell carcinoma. *Front. Oncol.* 11, 756096. doi:10.3389/fonc.2021.756096

Wang, Y., Tan, H., Yu, T., Chen, X., Jing, F., and Shi, H. (2021). Potential immune biomarker candidates and immune subtypes of lung adenocarcinoma for developing mRNA vaccines. *Front. Immunol.* 12, 755401. doi:10.3389/fimmu.2021.755401

Watson, M. J., Vignali, P. D. A., Mullett, S. J., Overacre-Delgoffe, A. E., Peralta, R. M., Grebinoski, S., et al. (2021). Metabolic support of tumour-infiltrating regulatory T cells by lactic acid. *Nature* 591 (7851), 645–651. doi:10.1038/s41586-020-03045-2

Yazdanifar, M., Barbarito, G., Bertaina, A., and Airoldi, I. (2020). Γδ T cells: The ideal tool for cancer immunotherapy. *Cells* 9 (5), E1305. doi:10.3390/cells9051305

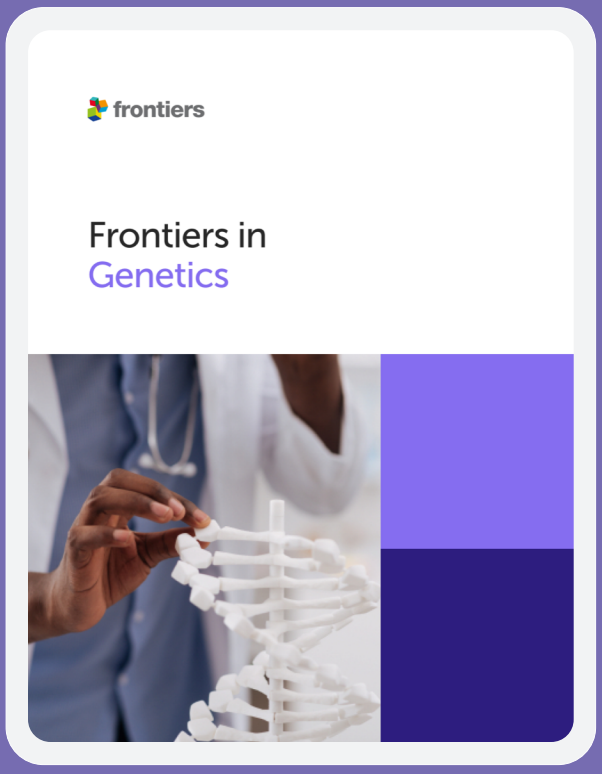
Frontiers in Genetics

Highlights genetic and genomic inquiry relating to all domains of life

The most cited genetics and heredity journal, which advances our understanding of genes from humans to plants and other model organisms. It highlights developments in the function and variability of the genome, and the use of genomic tools.

Discover the latest Research Topics

See more →



Frontiers

Avenue du Tribunal-Fédéral 34
1005 Lausanne, Switzerland
frontiersin.org

Contact us

+41 (0)21 510 17 00
frontiersin.org/about/contact